

Synthesis and Characterisation of Some Novel Banana and Discotic Liquid Crystals

By

Ashwathanarayana Gowda. M

Thesis submitted to Jawaharlal Nehru University, New Delhi for the
award of the degree of

DOCTOR OF PHILOSOPHY



Raman Research Institute

Bengaluru-560080

DEDICATED TO

My mother, family members, teachers and
the memory of my father

CERTIFICATE

This is to certify that the thesis entitled “**Synthesis and Characterisation of Some Novel Banana and Discotic Liquid Crystals**” submitted by **Mr. Ashwathanarayana Gowda. M**, for the award of the degree of DOCTOR OF PHILOSOPHY of Jawaharlal Nehru University, New Delhi, is his original experimental investigation and conclusions. The subject matter of this thesis has not been previously published or submitted to any other university for the award of any other degree or diploma.

Prof. Ravi Subrahmanyam

Director

Raman Research Institute

Bengaluru –560080

Prof. Sandeep Kumar

(Thesis Supervisor)

DECLARATION

I hereby declare that the entire work embodied in this thesis is the result of the experimental investigation carried out by me independently at Raman Research Institute, Bangalore, under the guidance and supervision of Prof. Sandeep Kumar. The experimental work and conclusions presented in this thesis work have not been previously submitted and no part of this thesis work has formed the basis for the award of any other degree, diploma, fellowship or any other similar title. Further, I declare that I have checked this thesis through the antiplagiarism software Turnitin.

Prof. Sandeep Kumar

Ashwathanarayana Gowda. M

(Thesis Supervisor)

Raman Research Institute

Bengaluru-560080

Date:

Place: Bengaluru

Acknowledgements

I wish to express deepest sense of gratitude to my honored supervisor Prof. Sandeep Kumar for his endless support inspired me at every stage of my research work. There are no adequate words to explain his keen interest, immense patience, kind advice, constant help, sustained encouragement and thought provoking discussions that I had with him during this time. He has given an extraordinary amount of freedom to execute the research problems. It was a rich experience to work with him and learn so many things from him both as a scientist and as a human being. Without his patience and guidance, I would not have finished my thesis. He has always encouraged not only becoming a good researcher but also a good human being as well. It has been a great pleasure and I really admired working with him.

I would like to express my earnest gratitude to Dr. Arun Roy for his valuable discussions that I had with him, Prof. Reji Phillip and his students Nithin, Agnes & Anitta for their kind help in nonlinear optical studies and photophysical studies. Prof. Pratibha for her help in characterisation of mesophase. I also thank Prof. V. A. Raghunathan for valuable discussions related to the X-ray diffraction studies. I wish to thank Dr. Vijayaraghavan for the help in acquiring NMR data.

I also express my gratefulness to Prof. V. Lakshminarayanan, Prof. N. V. Madhusudana for their support and wishes. I sincerely thank to Prof. Wei Lee, National Chiao Tung University, Taiwan, for allowing me to visit his lab and helping me to learn new techniques. I would not miss this opportunity to thank all the soft condensed matter group faculty members for their help in various ways and suggestions.

My sincere thanks to Dr. Mahuya De Ghosh (HOD of chemistry) & Latha V at IADC, Bengaluru for introducing me to organic chemistry during my master degree course. I also thank Dr. Ajeesh Kumar for helping me to learn research skills and constant support. It was a great experience to work with him at Anthem Bioscience Pvt. Ltd, Bengaluru.

I take this opportunity to thank Dr. Srinivas H.T for his kind help during my stay and TGA studies. Mrs. K. N. Vasudha for recording IR, DSC, XRD & elemental analysis, Mr. Venkatesh for his support in the lab. I also thank Mr. K. Radhakrishna for his time and valuable support

throughout my research work. I would like to express my sincere thanks to Mr. Dhason for his help in SEM and AFM imaging and fabricating glass apparatus. Mr. Mani for his help in making accessories for our lab. I take this opportunity to thank my friend, Mr. Yatheendran for his kind help in TEM, SEM, EDAX, AFM and Raman studies.

I also thank my seniors Dr. Mahesh Varia, Dr. Avinash, for their suggestions and support. I thank my labmates Dr. Yuvaraj, Swamynathan, Mari, Irla, Vinay, Pruthvi, Litwin, Jaggu, Alaka, Vanishree and Samarjith for their support, cooperation and friendly working atmosphere in the lab. I sincerely thank to my friends Manish Kumar and Shalaka Varshney for their cheerful companionship, their timely encouragement and valuable inputs regarding the research work. I thank our collaborator Dr. Dharmendra and Dr. Manish Pandey, for their constant support and suggestions.

I would like to thank all my batchmates Santanu, Sanjay, Sreeja, Deepshika, Ashutosh, Rajarshi for their best companionship during my course work. I also thank my seniors at RRI Dr. Arnab, Dr. Debasish, Dr. Chaitra, Dr. Deepak, Dr. Neha and Prutha for their suggestions and wishes during my stay. I must thank to VSP's Shreemala, Himamshu, Prathiba, Kavitha, Swasthika, Viditha, Krishna, Anu and Dhanya who worked with me during my research work. Also, I would like to express my sincere thanks to my junior Subhadip Ghosh for his help in learning origin and other software techniques. I wish to thank my friends Monica, Veerabhadraswamy, Madhu Babu, Sachin Bhat from CeNS, Bengaluru, for their help in photophysical studies, Dr, Hemant (BHU), Dr. Sumit (IISc) for their help in DFT calculations. I wish to thank all my friends and research colleagues in the institute who made my stay enjoyable.

I would like to acknowledge RRI library staff members Dr. B. M. Meera, Dr. Manjunath, Dr. Nagaraj, Manjunath Kaddipujar and Vani for providing me an excellent opportunity to use library facility during my research work. The ever smiling staff always kind helpful.

I would like to express my sincere thanks to RRI director Prof. Ravi Subrahmanyam, Administrative Officer Mr. C.S.R. Murthy, Ex-AO Mr. Krishnamaraju K, AAO Mr. Naresh and Account Officer Mr. Suresh Varadarajan for their constant support. I also thank Radha and Vidya for their kind help in administrative work. I especially thank various other departments of

RRI, the administration, computer section, accounts, workshop, transport, security, canteen, hostel and clinic for their constant support during my Ph.D life.

My gratitude to all my previous teachers from Govt. Higher Primary School (Mindhalli), JSS High School (Malur), JSS Pre-University College (Malur), Cricks Institute of Advanced Sciences (Devanahalli), Indian Academy Degree College (IADC-Bengaluru) for giving me an extraordinary amount of knowledge about subject.

My deep gratitude to my thesis supervisor's wife Navita Rani for her kind suggestions, encouragements & tasty food, his granddaughter Shubhangi Varshney, for her ever smiling face & her great respect, his sons Navdeep Kumar & Sudeep Kumar and daughter-in-laws Shivani Varshney & Swati Varshney for their constant support and wishes throughout my Ph.D life.

I wish to thank to all my well wishers Mr. Paramesh (Assistant Deputy Director of Horticulture, Kolar), Mr. Chowdegowda (Manager, Red Hat Inc.), Dr. Madhu Chandra, Dr. Ravi, Dr.Nethra, Dr. Raghu, Vinutha, Pallavi, Tejaswini, Manjunath, Nagesh, Bharath Kumar, Somanatha, Ramesh, Kallesh, Hema, Sumalatha, Bhavya, Kavitha, Chaithra, Mala, Sindhu, Shabana, Sagar, Soma Ghosh, Banu, Manjunath Reddy for their encouragement during my PhD life.

I am honestly obliged Raman Research Institute for providing me the wonderful opportunity to pursue my doctoral research work, research facilities, travel grant to attend national and international conferences and fellowship. I also thank Department of Science and Technology, Govt. of India for providing travel grant award to participate conference in USA. I also thank Ministry of Education, Taiwan for providing me Taiwan Experience Education Program (TEEP) fellowship to visit Prof. Wei Lee's lab, NCTU, Taiwan.

Finally, I would like to mention my deep gratitude to my sisters Channamari, Rathnamma, Shantha, Lakshmi, Savithri, Padma, Manjula, brother-in-laws Nagaraj Gowda, Kempanna, Ravi, Munegowda, Suresh, Mohan, CK Srinivas, My uncles Channarayappa, Narayanaswami and my elder brother Chandra Shekara, younger brothers Venkat, Prathap, Bharath, family members, relatives and my village friends for their love, support, care and constant source of encouragement throughout my study and research work. I have greatly benefited by their valuable suggestions and thought provoking advice. I finally wish to thank my Father and Mother for everything they have been.

Table of Content

Chapter 1:

1.1 Part A. Introduction	1
1.1.1 Liquid crystals	2
1.1.2 History of liquid crystals	3
1.2 Classification of liquid crystals	5
1.3 Lyotropic liquid crystals	6
1.4 Thermotropic liquid crystals	7
1.4.1 Calamitic liquid crystals	7
1.4.1.1 Nematic phase	9
1.4.1.2 Smectic phase	9
1.5 Banana liquid crystals	10
1.6 Discotic liquid crystals	12
1.6.1 Self-assembly of mesophases formed by discotic mesogens	14
1.6.2 Nematic phases of discotic mesogens	14
1.6.3 Columnar phases of discotic mesogens	15
1.6.3.1 Columnar hexagonal phase (Col_h)	16
1.6.3.2 Columnar rectangular phase (Col_r)	16
1.6.3.3 Columnar oblique phase (Col_{ob})	17
1.6.3.4 Columnar plastic phase (Col_p)	18

1.6.3.5 Columnar helical phase (H)	19
1.6.3.6 Columnar tetragonal phase (Col _{tet})	19
1.6.3.7 Columnar lamellar phase (Col _L)	20
1.6.4 Cubic phase of discotic mesogens	21
1.6.5 Smectic phases of discotic mesogens	21
1.7 Mesophase structure of discotic liquid crystals	22
1.8 Structural template and synthesis of DLCs	23
1.9 Characterization of liquid crystalline phases	24
1.10 DLCs as materials for a new generation of organic electronics	25

References

1.2 Part B. Statement of the problem	30
---	-----------

Chapter 2: Synthesis and mesomorphic properties of bent-core mesogens derived from naturally occurring curcumin

2.1 Introduction	32
2.2 Objective	35
2.3 Results and discussion	36
2.3.1 Synthesis	36
2.3.2 Density functional theory calculations	38
2.3.3 Thermal behaviour	38

2.3.4 X-ray diffraction studies	42
2.4 Thermogravimetric analysis	42
2.5 Conclusions	43
2.6 Experimental section	43
2.6.1 General information	43

References

Chapter 3: Novel EDOT- based bent-core and hockey stick mesogens

3.1 Part A. Synthesis and characterisation of EDOT-based bent-core liquid crystals containing alkyne-linkage

3.1.1 Introduction	60
3.1.2 Objective	64
3.1.3 Results and discussion	64
3.1.3.1 Density functional theory calculations	64
3.1.3.2 Synthesis	65
3.1.3.3 Thermal properties	67
3.1.3.4 X-ray diffraction studies	69
3.1.4 Photophysical properties	69
3.1.5 Raman spectroscopy	70
3.1.6 Thermogravimetric analysis	70
3.1.7 Conclusions	70

3.1.8 Experimental section	71
3.1.8.1 General information	71
3.1.8.2 General procedure for the synthesis of intermediates and final compounds	71
3.2 Part B. Synthesis and characterisation of EDOT-based bent-core liquid crystals containing Schiff-base linkage	
3.2.1 Introduction	86
3.2.2 Objective	87
3.2.3 Results and discussion	88
3.2.3.1 Density functional theory calculations	88
3.2.3.2 Synthesis	89
3.2.3.3 Mesomorphic properties	91
3.2.3.4 X-ray scattering measurements	94
3.2.4 Raman spectroscopy	94
3.2.5 Thermogravimetric analysis	95
3.2.6 Conclusions	95
3.2.7 Experimental section	96
3.2.7.1. General methods	96
3.2.7.2 General procedure for the synthesis of intermediates and final compounds	96
3.3 Part C. Synthesis, characterization and physical studies of EDOT based bent-core and hockey-stick like liquid crystals	
3.3.1 Introduction	117
3.3.2 Objective	120

3.3.3 Results and discussion	120
3.3.3.1 Density functional theory calculations	120
3.3.3.2 Synthesis	122
3.3.3.3 Mesomorphic properties	123
3.3.3.4 X-ray scattering measurements	126
3.3.4 Photophysical properties	126
3.3.5 Raman spectroscopy	128
3.3.6 Thermogravimetric analysis	129
3.3.7 Nonlinear optical transmission measurements	130
3.3.8 Conclusions	132
3.3.9 Experimental section	132
3.3.9.1 General procedure for the synthesis of intermediate and final compounds	132

References

Chapter 4: Phenazine fused triphenylene discotic liquid crystals

4.1 Part A. Synthesis, characterization and charge transport properties of thiol-substituted phenazine fused triphenylene supramolecular systems

4.1.1 Introduction	154
4.1.2 Objective	157
4.1.3 Results and discussion	157
4.1.3.1 Synthesis	157

4.1.3.2 Thermal properties	159
4.1.3.3 X-ray diffraction studies	161
4.1.4 Photophysical properties	164
4.1.5 Density functional theory calculations	165
4.1.6 Thermogravimetric analysis	166
4.1.7 Charge carrier mobility	166
4.1.8 Conclusions	168
4.1.9 Experimental section	168
4.1.9.1. General procedure for synthesis of intermediate and final compounds	168
4.2 Part B. Alkyl and alkoxy phenylacetylene containing phenazine fused triphenylene discotic liquid crystals	
4.2.1 Introduction	182
4.2.2. Objective	184
4.2.3 Results and discussion	185
4.2.3.1 Synthesis	185
4.2.3.2 Mesomorphic properties	187
4.2.3.3 Thermogravimetric analysis	188
4.2.3.4 X-ray scattering measurements	189
4.2.4 Photophysical properties	191
4.2.5 Nonlinear optical studies	192
4.2.6 Conclusions	194

4.2.7 Experimental section	195
4.2.7.1. General procedure for the synthesis of final compounds	195
4.3 Part C. Monomeric ester containing phenazine fused triphenylene discotic liquid crystals	
4.3.1. Objective	204
4.3.2 Results and discussion	205
4.3.2.1. Synthesis	205
4.3.2.2 Thermal properties	207
4.3.2.3 X-ray diffraction studies	208
4.3.3 Photophysical properties	211
4.3.4 Nonlinear optical transmission studies	212
4.3.5 Conclusions	214
4.3.6 Experimental section	214
4.3.6.1. General procedure for synthesis of intermediate and final compounds	214
4.4 Part D. Synthesis, mesomorphic and photophysical properties of π-extended dibenzophenazine based discotic liquid crystals	
4.4.1 Introduction	223
4.4.2 Objective	225
4.4.3 Results and discussion	226
4.4.3.1 Synthesis	226
4.4.3.2 Thermal properties	228
4.4.3.3 X-ray diffraction measurements	230

4.4.4 Photophysical properties	233
4.4.5 Thermogravimetric analysis	235
4.4.6 Conclusions	235
4.4.7 Experimental section	236

References

Chapter 5: Self-assembly of metal nanoparticles in a metal-free phthalocyanine discotic liquid crystalline material

5.1 Introduction	257
5.2 Objective	260
5.3 Results and discussion	260
5.3.1 Synthesis of 2,3,9,10,16,17,23,24-octakis (3,7-dimethyloctoxy) phthalocyanine	260
5.3.2 Synthesis and characterization of alkanethiol–capped metal nanoparticles	260
5.3.3 Preparation of nanocomposites	262
5.3.4 Characterization of nanocomposites	262
5.3.4.1. Polarising optical microscopy studies	262
5.3.4.2. Differential scanning calorimetry studies	263
5.3.4.3 Small angle X-ray scattering studies	264
5.3.4.4 FE-SEM and absorption studies	266
5.3.5 DC conductivity measurements	266
5.3.6 Thermogravimetric analysis	267

5.3.7 Nonlinear optical transmission measurements	267
5.3.8 Conclusions	270
5.3.9 Experimental section	271
5.3.9.1 Materials and methods	271
5.3.9.2 Synthesis of metal free phthalocyanine DLC	271
5.3.9.3 Synthesis of metal nanoparticles	272

References

Chapter 6: Summary

List of abbreviations

LC	Liquid Crystal
LCD	Liquid Crystal Display
BC LC	Bent Core Liquid Crystal
LLC	Lyotropic Liquid Crystals
DLC	Discotic Liquid Crystal
ILCC	International Liquid Crystal Conference
Cr	Crystal
Sm	Smectic
SmA	Smectic A phase
SmC	Smectic C phase
N	Nematic
Col	Columnar
Col _h	Hexagonal Columnar phase
Col _{rect}	Rectangular Columnar phase
I	Isotropic
DNA	Deoxyribonucleic Acid
1D	One Dimension
UV-Vis	Ultraviolet–Visible
FT-IR	Fourier Transform Infrared
NMR	Nuclear Magnetic Resonance
POM	Polarized Optical Microscopy
DSC	Differential Scanning Calorimetry
XRD	X-ray Diffraction

SAXS	Small Angle X-ray Scattering
SEM	Scanning Electron Microscopy
FE-SEM	Field Emission Scanning Electron Microscopy
TEM	Transmission Electron Microscopy
STEM	Scanning Transmission Electron Microscopy
EDAX	Energy-Dispersive X-ray spectroscopy
SPR	Surface Plasmon Resonance
ToF	Time of Flight
DFT	Density Functional Theory
NLO	Nonlinear Optics
J	Coupling Constant
EDOT	3,4-ethylenedioxythiophene
TP	Triphenylene
Pc	Phthalocyanine
NP	Nanoparticle
AuNP	Gold Nanoparticles
AgNP	Silver Nanoparticles
MNPs	Metal Nanoparticles
TGA	Thermo Gravimetric Analysis
ppm	parts per million
TLC	Thin Layer Chromatography
TMS	Tetra Methyl Silane
CHCl ₃	Chloroform
DMF	Dimethylformamide
THF	Tetrahydrofuran

$(\text{PdCl}_2(\text{PPh}_3)_2)$	Bis(triphenylphosphine)palladium (II) dichloride
CuI	Copper (I) Iodide
CuCN	Copper (I) Cyanide
TEA	Triethylamine
DCC	N, N'-Dicyclohexylcarbodiimide
DMAP	4-Dimethylaminopyridine
NBS	N-Bromosuccinimide
$\text{Pd}(\text{OAc})_2$	Palladium acetate
PPh_3	Triphenylphosphine
Cs_2CO_3	Cesium carbonate
Na_2SO_4	Sodium sulphate
CAN	Ceric Ammonium Nitrate
DC	Direct Current
ΔH	Enthalpy change

Synopsis

Synthesis and Characterisation of Some Novel Banana and Discotic Liquid Crystals

Introduction

Liquid crystals are observed in between ordered crystalline phase and disordered isotropic liquid phase and generally referred to as mesophases [1]. They display both the order and mobility at molecular, supramolecular and macroscopic levels. Liquid crystals have been accepted as the fourth state of matter after the three classical states of matter, solid, liquid and gas [2,3]. The self-healing and self-aligning ability of LCs can be smoothly constructed through weak interactions such as hydrogen bonding, van der Waals forces, π - π stacking, dipolar or quadrupolar interactions, charge transfer interactions, molecular shape anisotropy, microsegregation of incompatible subunits, etc. The constituent molecules, referred to as mesogens, could be organic, inorganic or organometallic which form mesophases under appropriate conditions [4]. Liquid crystals are important class of functional materials which find immense applications in fundamental and applied sciences.

Liquid crystals can be broadly classified into two classes; (i) lyotropic, which are obtained by adding a solvent to a solute and, therefore, concentration and temperature dependent and (ii) thermotropic, which are obtained only by varying the temperature. Many surface active agents in water form lyotropic liquid crystal phases. Lyotropic liquid crystals are key component in cleaning process (soaps, detergent, etc), cosmetics and food products. They are used as template for the preparation of mesoporous materials and acts authentic systems for biomembranes. LLCs have essential role in living system such as biological membranes, DNA, etc [5]. The anisotropic liquid crystalline polymers are presently used for making high-strength fibers, for examples Kevlar (utilized for bullet proof vests, defensive garments, and superior composites for aircraft and car ventures), encapsulation of microelectronic circuits, making micro-electromechanical and micro-fluidic devices. There are also increasing interest in their biomedical applications such as controlled drug delivery, protein binding, phospholipid labeling, microbe detection and gene therapy [6].

On the other hand, thermotropic LCs play a vital role in electro-optic displays, temperature sensors and selective reflecting pigments, etc. Although LCs have diverse commercial applications, they are primarily known for their extensive exploitation in electro-optical display devices such as watches, calculators, telephones, laptops, flat panel televisions, etc. The lightweight, flat and low power consumption LCD is one of the key components present in the electronic display devices, which changed the human life style in the world.

The most important requirement for a molecule to exhibit thermotropic mesomorphism is a structure consisting of a central core (often aromatic) and flexible peripheral chain(s). The geometric shape anisotropy, interaction anisotropy, self-assembly, self-organization, and microsegregation are the driving parameters for mesophase formation. Based on the shape of the mesogen, thermotropic LCs are classified into three main groups: (i) calamitic (rod-like); (ii) bent-core (bad rods, boomerang, banana-like), and (iii) discotic (disk-like) LCs. This thesis work deals only with bent-core and disk-like molecules.

Bent-core or banana liquid crystals show interesting properties which cannot be envisioned in calamitic LCs, particularly in the aspects of polarity and chirality. Bent-shaped molecules furnish access to polar order and spontaneous symmetry breaking to form macroscopic chiral structures despite the molecules being achiral [7]. Typically, the molecular structure of bent-core mesogens composed of three units: an angular central core, two linear rod-like rigid cores, and terminal flexible chains. The bent in the rigid cores of banana LCs prompts diminishment of rotational order of the molecules about their long axis and directed packing of molecules within the layers. The vital outcome of the directed packing of such molecules is the occurrence of polar order parallel to the smectic layers, provided that the molecules possess a lateral dipole moment. BC LCs opens the new era in novel complex types of molecular self-organization and to the new field of supramolecular stereochemistry. Various potential applications of these bent-core LCs include nonlinear optics, flexoelectricity, photoconductivity and the design of biaxial nematic phase, etc.

Among all types of thermotropic liquid crystals, discotic liquid crystalline materials are unique supramolecular nanostructured materials with remarkable electronic and optoelectronic properties. They find significant role as functional materials for device applications such as one-dimensional conductors, photoconductors, photovoltaic solar cells, light emitting diodes, gas

sensors and thin film transistors etc [8,9]. The negative birefringence films formed by polymerized discotic nematic liquid crystals have been commercialized as optical compensation film to enlarge the viewing angle in commonly used twisted nematic liquid crystal displays [10].

Apart from materials science and bioscience, liquid crystals are now moving rapidly into forefront of nanoscience and nanotechnology. For example, the synthesis of various anisotropic nanoparticles with tunable shape, size and controllable polydispersity using LCs as templates medium. LC nanostructures have been utilized for encapsulation and drug delivery. Processing of nanomaterials using LC medium yields high performance materials and devices [11]. Nanoparticles are unique in their physical and chemical properties which depend on their size and shape [12]. Confinement of nanomaterials in liquid crystal phases exhibits new and exciting phenomenon compared to bulk LC phases. LCs are emerging as a viable system for the self-assembly of nanomaterials in LC phases as well as self assembly of LC molecules themselves. The incorporation of nanomaterials into LCs media usually doesn't impart much distortion of mesomorphic properties but alters the electro-optical properties significantly. Nanomaterials of various shape and size have been dispersed in the LCs matrix to enhance the photophysical and optical properties of LCs. Moreover, alignment and self-assembly of nanomaterials themselves can be smoothly achieved in LC phases. Dispersion of various NPs in DLCs and evaluation of their physical properties is currently a very active research field.

This thesis deals with the synthesis and characterization of novel banana liquid crystals derived from central isoxazole and central EDOT core; discotic liquid crystals derived from appropriate substituted phenazine fused triphenylene core and the uniform dispersion of metal nanoparticle into metal free phthalocyanine discotic liquid crystals. The thesis work begins from the synthesis of five membered BC LCs prepared from naturally available curcumin and investigated their mesophase structure. Similarly, novel bent-core liquid crystals synthesised from central EDOT unit exhibit wide range of stable mesophases. We have also designed and synthesised hockey stick compounds obtained from EDOT and they exhibit good photophysical and nonlinear optical properties. Later part of thesis describes the modern synthetic efforts for the preparation of phenazine fused triphenylene discotic for the effect of π -extended conjugation. We have also investigated charge transport properties of representative thiol substituted phenazine fused TP DLCs using time of flight experiment. Last part of thesis

includes the dispersion of zero-dimensional gold and silver nanoparticles into the metal free phthalocyanine and investigated the conductivity and nonlinear optical properties. The molecular structures of all the intermediate and final compounds have been characterized by nuclear magnetic resonance spectroscopy, infrared spectroscopy, ultraviolet spectroscopy, Raman spectroscopy and elemental analysis. The thermotropic behaviour of all the mesogenic compounds were investigated using polarizing optical microscopy and differential scanning calorimetry. The self-assembly of mesophase structure was characterized by using X-ray diffraction studies. Thermal stability of mesogens was studied using thermogravimetric analysis. The self-assembly of metal nano-composited and conductivity measurements were carried out using scanning electron microscopy, transmission electron microscopy and conductivity studies etc.

Herein, this thesis describes novel approaches to functional bent-core liquid crystals, discotic liquid crystals and discotic nanocomposites and shows how the molecular engineering of liquid crystals lead to the formations of various self-organized soft functional materials. In what follows, we have briefly described some of the significant results and conclusions derived from our experimental work.

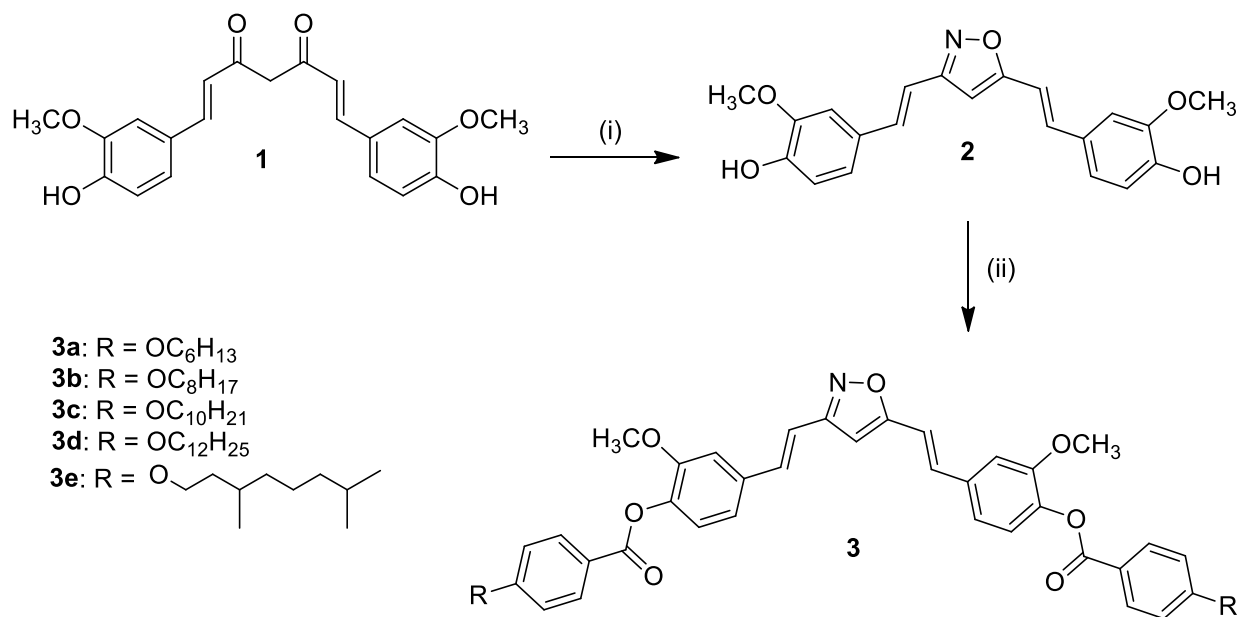
Chapter 1

This is an introductory chapter to liquid crystals and nano composites in general like their classification and their important role in material science, nanoscience, life science, and their dominance in electro optical display devices. Beginning with an over view of thermotropic liquid crystals and their brief history, this chapter mainly focuses the major classes of nematic and smectic phases formed by banana liquid crystals, columnar mesophases formed by discotic liquid crystals and discotic nano-composites and finally, some applications and perspectives in material science, nanoscience and molecular electronics.

Chapter 2

This chapter illustrates the synthesis of novel isoxazole based bent core liquid crystal. Here, we adopted naturally occurring inexpensive curcumin as a starting precursor for the

synthesis of banana liquid crystals (**Scheme 1**). Curcumin is a medicinal natural product which can be isolated from the rhizome of *Curcuma longa L.* (Zingiberaceae family). Because of its biological activities, a number of curcumin derivatives have been prepared and studied [13]. Curcumin belongs to the family of β -diketone, which is stabilized by six membered cyclic keto-enol form through hydrogen bonding. Curcumin bears an ethylene spacer between guaiacol ring and β -diketone moiety. The phenyl ring having free hydroxyl group at para position to the ethylene spacer can be further modified through simple esterification with various acids. β -diketones are key precursors for the synthesis of various five membered heterocyclic and metallomesogenic derivatives [4]. A new series of five BC LCs derived from isoxazole central unit is prepared from curcumin and investigated for their liquid crystalline properties (**Scheme 1**). While lower homologous show only enantiotropic nematic phase, higher homologous displays a tilted smectic C phase with a fairly large tilt angle of 51° , in addition to the higher-temperature nematic phase. Replacing normal alkyl chain by a branched chain reduces the isotropic temperature significantly. Five new BC nematic LCs have been added to the growing list of BC nematic LCs, which are currently gaining considerable research interest due to their remarkable properties.

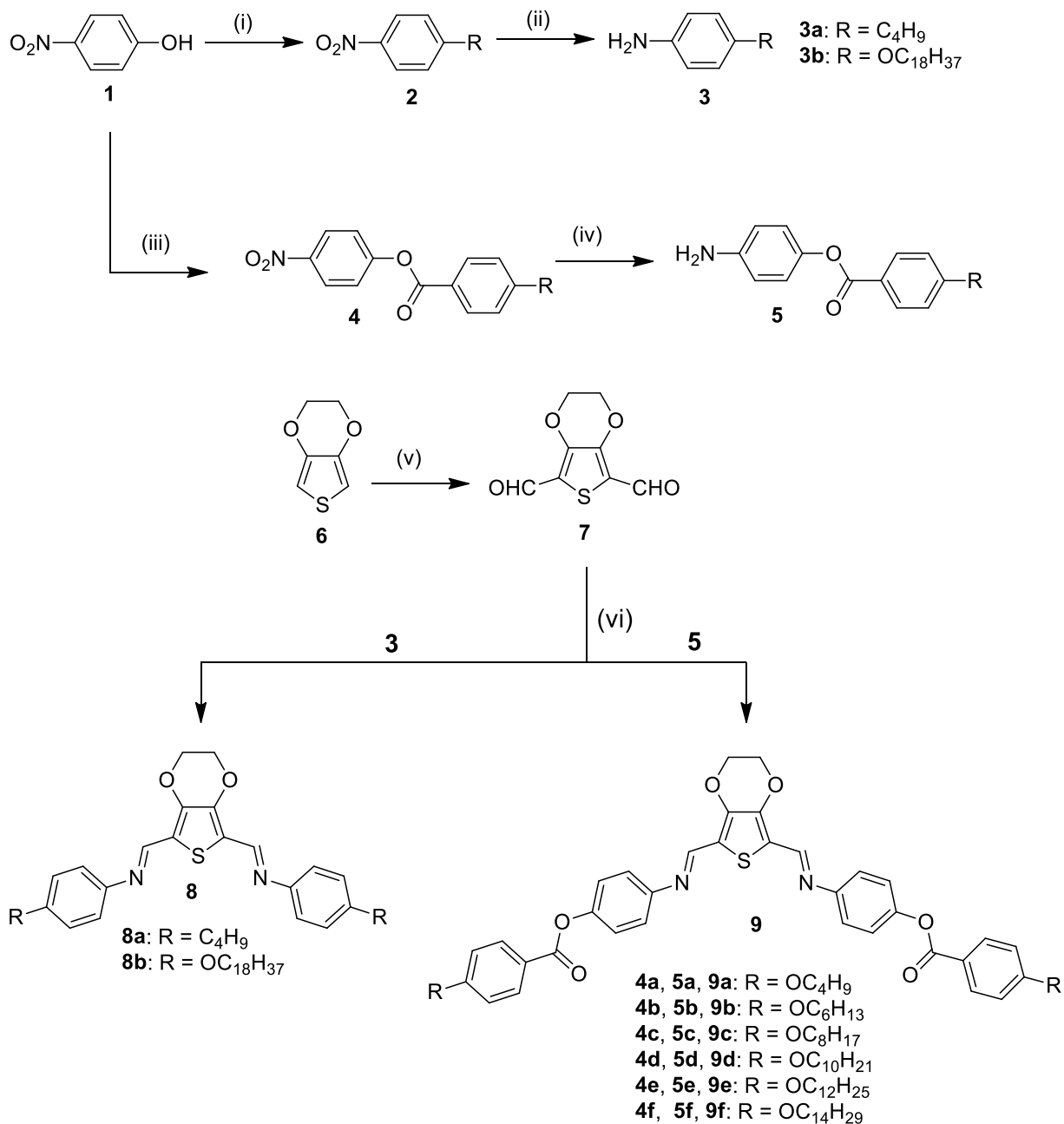


Scheme 1. Synthesis of isoxazole-based BC LCs; (i) $\text{NH}_2\text{OH}\cdot\text{HCl}$, abs. EtOH, cat. CH_3COOH , 16 h, reflux; (ii) 4-alkoxybenzoyl chloride, pyridine, CH_2Cl_2 , 24 h, r.t.

Chapter 3

This chapter deals with synthesis, characterisation, photophysical properties and nonlinear optical properties of some novel BC LCs derived from EDOT. Three different series of BC LCs were designed and synthesised from EDOT central core. EDOT is a thiophene based heterocyclic electron-rich compound and key precursor to many advanced conducting polymer materials. In addition to that, EDOT acts as excellent candidate for assorted building blocks of π -electron conjugated functional materials. EDOT undergoes rapid polymerisation at ambient conditions and these conducting polymers find applications in fabrication of various kinds of electronic and optoelectronic devices such as field-effect transistors, photovoltaic devices, nonlinear optical materials, light-emitting diodes etc. In chapter 3, we have adopted the synthesis of three different series of BC LCs derived from EDOT central unit as shown in **Scheme 2, 3 and 4** respectively.

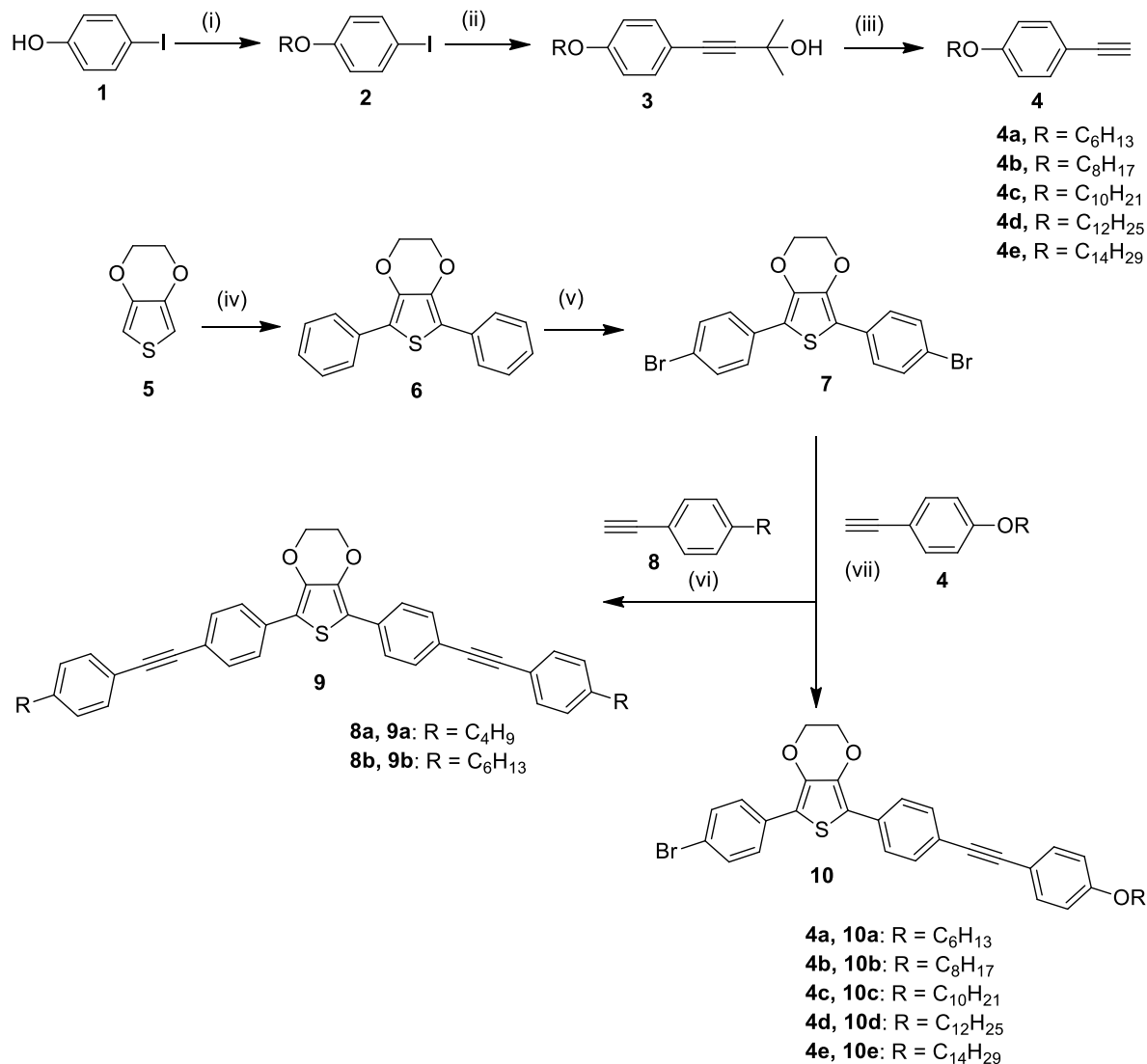
Herein, we reported for the first time, the synthesis and characterization of BC LCs derivatives from EDOT central core. Initially, we designed and synthesized EDOT based three-ring bent-core molecules (**Scheme 2**), where the central EDOT core is flanked by alkyl or alkoxy substituted phenyl rings. These compounds were found to be non-LC, which is not much surprising as three ring structures are usually not conducive for BC LCs [14]. To enhance the length: width ratio, we added one phenyl ring each side to generate five ring structure. The additional rings were coupled via ester bridge on both wings as shown in **Scheme 2**. The 2,5-disubstituted EDOT with acetylene linkage groups promotes greater stability of mesophase and provide a moderate bent-angle in between $152\text{--}155^\circ$ depending on substitution. We synthesized four five ring EDOT derivatives (**9a–9d**), including one racemic mixture of branched alkoxy chain derivative in order to understand structure-property relationship between these compounds. The molecular structures of intermediate and final compounds were investigated using spectral and elemental analysis. The detail mesophase behavior and phase transitions temperature of all the novel compounds were investigated and exhibit enantiotropic nematic phase only.



Scheme 3. Synthesis of EDOT-based BC LCs. (i) 1-bromooctadecane, K₂CO₃, dry. DMF, 80 °C 12 h; (ii) 10% Pd/C, (1:1) EtOH:THF, r.t, 6 h; (iii) 4-alkoxybenzoic acid, DCC, DMAP, DCM, r.t, 12 h; (iv) 10% Pd/C, (1:1) EtOH:THF, r.t, 6 h; (v) *n*-BuLi (1.6 M), dry DMF, dry THF, -78 °C, 2 h; (vi) 3-4 drops glacial acetic acid, EtOH, reflux, 4 h.

Furthermore, to increase length: width ratio, we added one more phenyl ring on each side by ester linkage to generate five-membered BC LCs bearing Schiff base as shown in **Scheme 3**. The 2,5-disubstituted EDOT with imine linkage exhibits the bent-angle of about 155°. To understand the structure–property relationship and to develop novel BC LCs of EDOT central unit, we prepared six novel derivatives in which EDOT was converted into EDOT-2,5-dialdehyde as the key intermediate for the synthesis of Schiff base containing three- and five-ring compounds. The influence of terminal chains on mesophase transition temperatures is studied by varying the length of the flexible alkyl chains. All the five-membered mesogens in the series (**9a–9f**) were found to exhibit enantiotropic mesophase behaviour. Higher homologous of the series show nematic phase along with SmC phase at lower temperature.

The later part of this chapter deals with the synthesis, characterisation, thermal and optical study of BC LCs and hockey-stick LCs derived from EDOT core as shown in **Scheme 4**. While five membered BC LCs are obtained by direct C-H bond arylation of EDOT with bromobenzene using palladium. Bromination of compound **6** gives key intermediate compound **7**. Sonogashira coupling reaction of 4-alkyl phenylacetylene derivatives with intermediated compound **7** gives final BC mesogens (**Scheme 4**). Two compounds (**9a–9b**) with variation in terminal alkyl chains were prepared and their mesomorphic behaviour was characterized. Both the compounds exhibit wide range of enantiotropic mesophases. The compounds **9a** shows wide range nematic phase only while compound **9b** exhibits a SmA phase at lower temperature along with the nematic phase at higher temperature. Similarly, hockey stick like liquid crystals obtained by Sonogashira coupling reaction of 4-alkoxy phenylacetylene with key intermediate compound **7**. All the compounds (**10a–10e**) in the series show wide range nematic phase and SmA phase for longer alkyl chains at a lower temperature. Further, the photophysical properties and non-linear optical studies were also investigated for all the novel mesogens.



Scheme 4. Synthesis of novel bent-core and hockey stick compounds: (i) alkyl halide, anhydrous K₂CO₃, dry DMF, reflux, 24 h; (ii) 2-methyl-3-butyn-2-ol, PdCl₂(PPh₃)₂, CuI, TEA, reflux, 24 h; (iii) NaOH, toluene, reflux, 3 h; (iv) bromobenzene, Pd(OAc)₂, PPh₃, Cs₂CO₃, toluene, 110 °C, 24 h; (v) Br₂, dry. DCM, 6 h, r.t; (vi) 1-ethyl-4-alkynylbenzene, PdCl₂(PPh₃)₂, CuI, TEA, reflux, 24 h; (vii) 1-ethyl-4-alkoxybenzene, PdCl₂(PPh₃)₂, CuI, TEA, reflux, 24 h.

Chapter 4

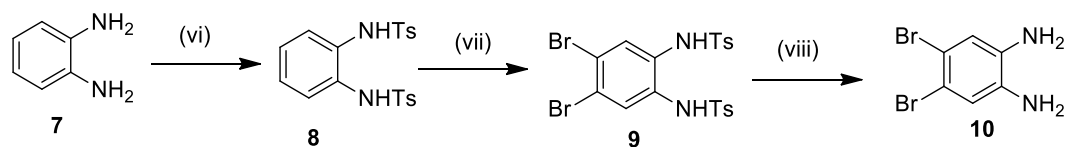
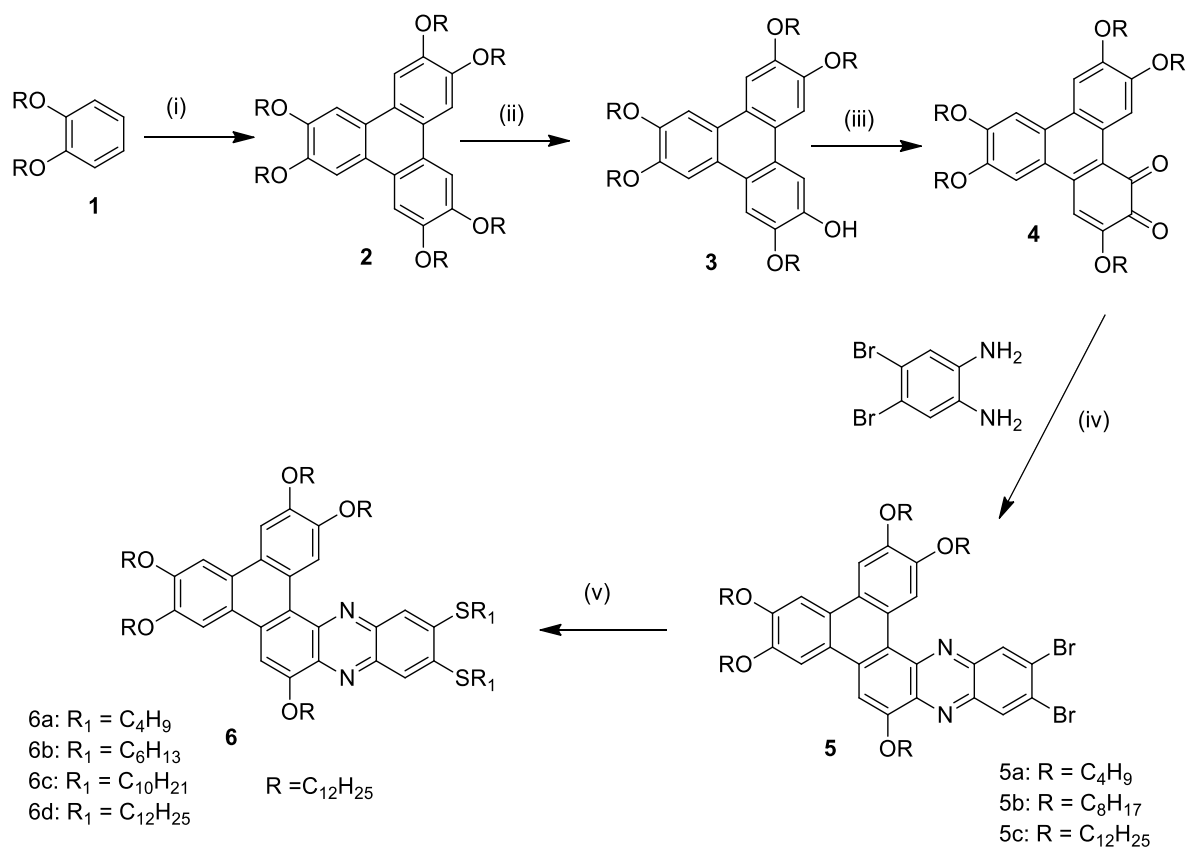
This chapter focused on synthesis and characterisation of heterocyclic discotic liquid crystals derived from phenazine fused triphenylene to look the effect of π -extended conjugation on thermal and photophysical properties. As mentioned in the introduction, discotic liquid crystals are renowned for their one dimensional transportation of charge, energy and ions. Owing to their unique electronic and self healing properties, DLCs also been considered as potential materials for various device applications apart from energy and charge migration properties. Currently, a number of DLCs derived from triphenylene exist and they show rich mesomorphism at elevated temperature as well as at ambient temperature. Appropriately functionalized TP derivatives are known for hole-transporting properties and their charge carrier mobility is ranged from $10^{-5} \text{ cm}^2 \text{ V}^{-1} \text{ s}^{-1}$ to $10^{-1} \text{ cm}^2 \text{ V}^{-1} \text{ s}^{-1}$ in the highly ordered columnar phases [15]. The electron rich nature of TP derivatives are typically known as hole transport materials and are suitable for doping with electron acceptors to serve as a *p*-type semiconductor. Extension of triphenylene discotic core leads to an extension of π -orbitals and thus increases π - π overlapping of neighbouring discotic cores along the columnar direction which enhances the charge carrier mobility and overwhelming semiconducting properties of discotic liquid crystals for device applications. Therefore, the design of appropriate functionalized π -conjugation or substitution of DLC materials may finds an immense interest for electronic devices. With this idea, we have designed and synthesised new extended π -conjugated phenazine fused triphenylene DLCs.

The initial part of this chapter deals with the design and synthesis of novel extended triphenylene based phenazine heterocyclic DLCs containing alkanethiols and alkoxy chains (**Scheme 5**). The π -extended intermediate dibrominated phenazine derivatives and final alkanethiols containing phenazine fused TP derivatives were self organized into hexagonal columnar mesophase over a broad temperature range. The mesomorphic properties of all the compounds were confirmed by POM and DSC. Hexagonal columnar structure of the liquid crystalline compounds was further investigated using X-ray diffraction studies. All these phenazine derivatives exhibit excellent photophysical properties in anhydrous chloroform solvent. Charge carrier mobility of representative compound (**6b**) was measured by the ToF technique, which reveals that compound (**6b**) exhibits *p*-type (hole) mobility of the order of $10^{-4} \text{ cm}^2 \text{ V}^{-1} \text{ s}^{-1}$. The mobility of charge carriers increases with increase in temperature following to a

power law. This behavior of synthesized LC material is similar to single crystalline materials. The current-voltage characteristics follow ohmic behavior. The π -extended phenazine fused triphenylene based columnar DLCs may play a significant role in organic optoelectronic devices and solar cells applications.

The second part of this chapter address the synthesis, mesomorphic properties and nonlinear optical studies of alkyl and alkoxy phenylacetylene containing phenazine fused extended triphenylene DLCs (**Scheme 6**). A new class of triphenylene based discotic liquid crystals were synthesised using Sonogashira coupling reaction between alkoxy phenylacetylene or alkyl phenylacetylene with intermediate dibrominated phenazine fused triphenylene. All the extended mesogens were self-assembled into hexagonal columnar mesophase over wide temperature and retains liquid crystalline properties upto room temperature upon cooling from isotropic liquid. The liquid crystalline properties were investigated using POM and DSC. The mesophase structure of all the mesogens were investigated using X-ray diffraction studies. All the extended discotic compounds exhibit strong photoluminescence properties in the anhydrous chloroform solvent. The π -extended heteroaromatic triphenylene discotic mesogens enhance nonlinear optical properties and are suitable materials for electro-optical applications.

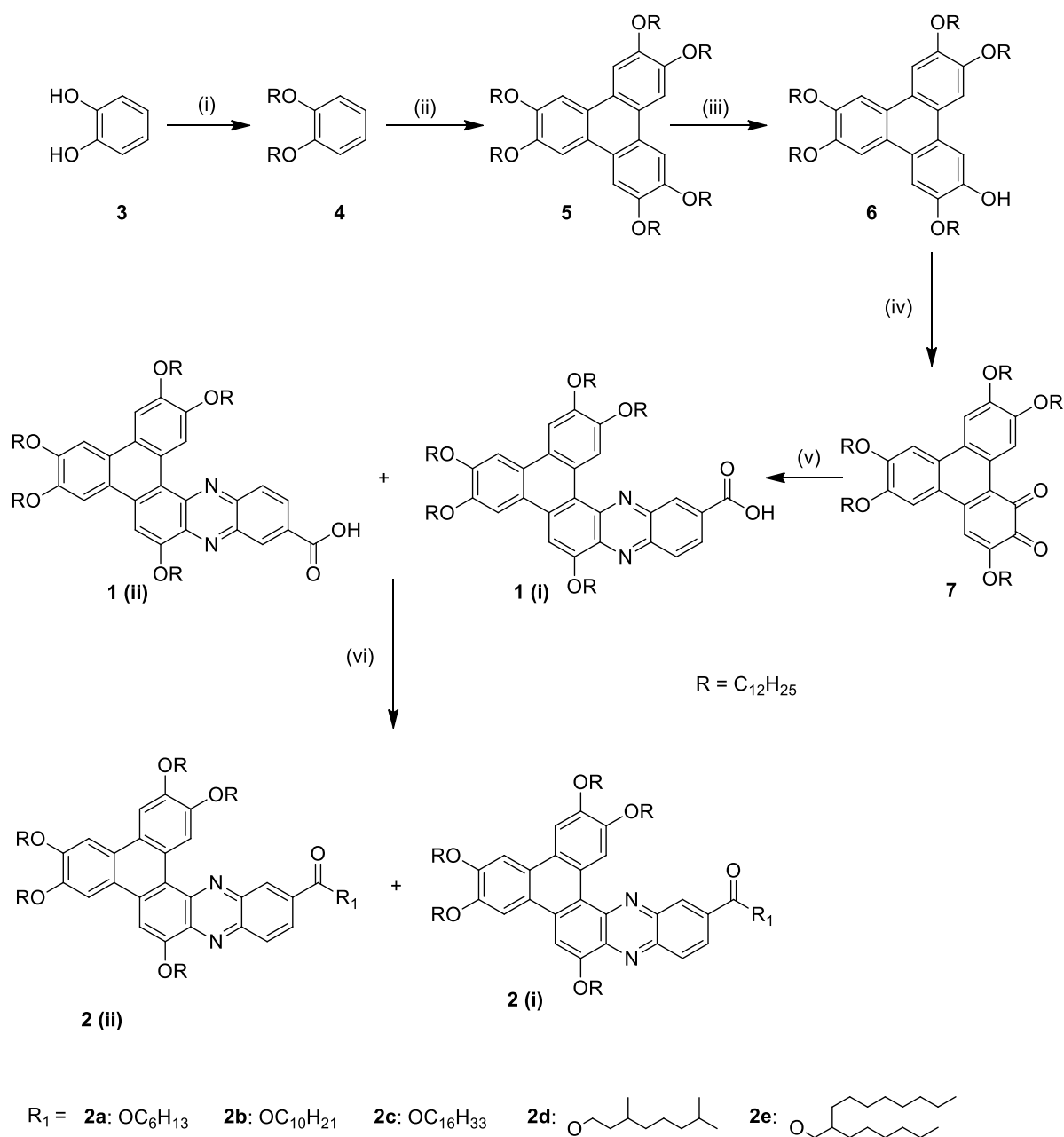
The third part of this chapter represents the synthesis, mesomorphic and optical properties of monomeric acid and ester derivatives of phenazine fused triphenylene DLCs (**Scheme 7**). The synthesis and characterisation of five novel extended π -conjugated monomeric ester containing phenazine fused triphenylene DLCs are reported. The intermediate inseparable acid derivatives **1(i)** and its regioisomer **1(ii)** exhibits a rectangular columnar phase (Col_r) over broad temperature range, while monomeric ester derivatives exhibit hexagonal columnar phase which remains stable till room temperature upon cooling from isotropic phase. All the ester derivatives exhibit strong photoluminescence properties in anhydrous chloroform solvent upon excitation at 474 nm. The intermediate monomeric acid derivative exhibits gelation properties in non-polar solvents. The π -extended conjugation in triphenylene fused phenazine based DLCs enhances the nonlinear optical properties. Such ordered supramolecular structures may find applications in various semiconducting devices.



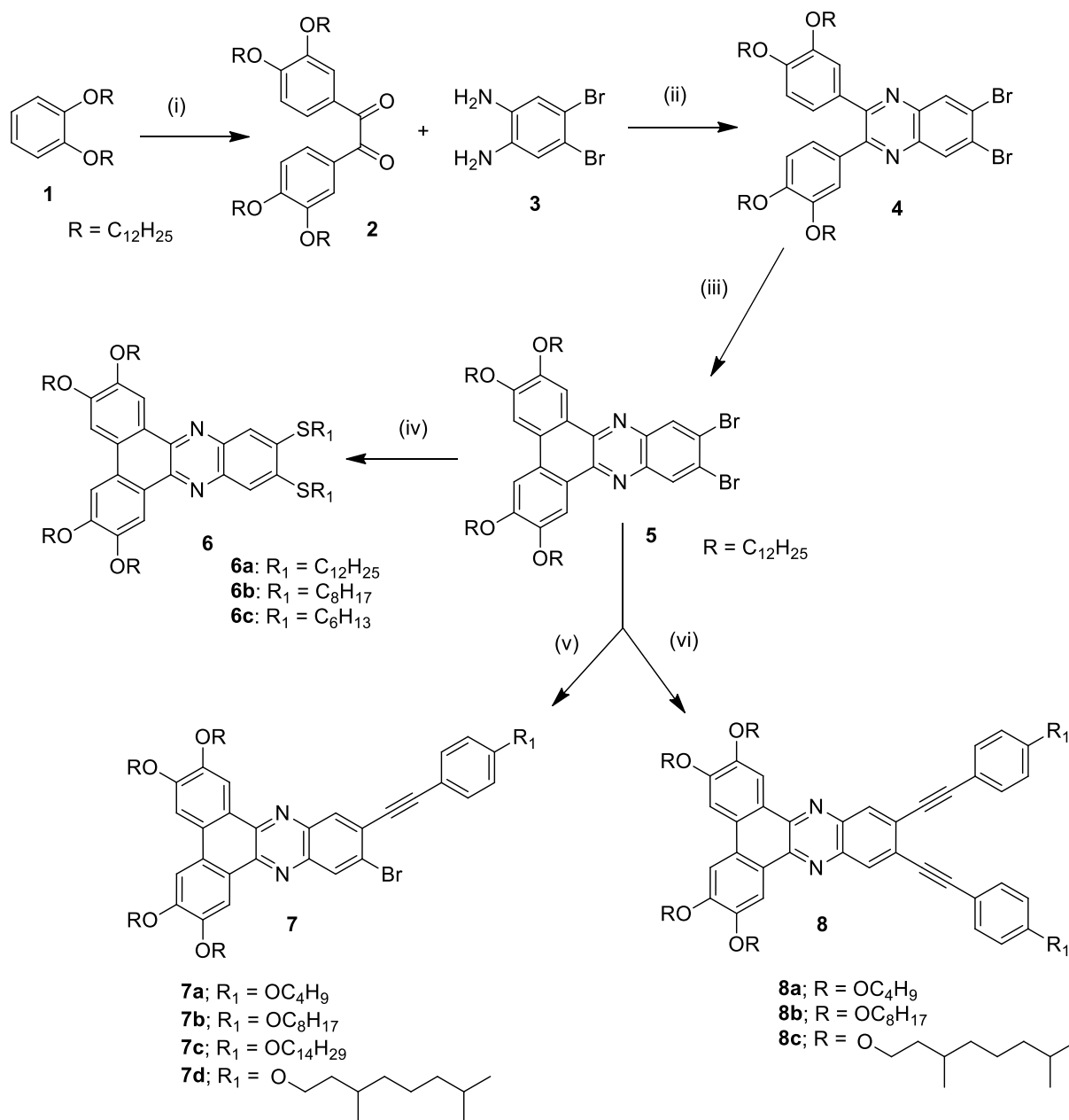
Scheme 5. (i) FeCl₃, CH₂Cl₂, r.t, 30 min; (ii) catechol boron bromide, CH₂Cl₂, r.t, 24 h; (iii) CAN, CH₃CN, r.t, 30 min; (iv) CH₃COOH: toluene (7:3), reflux, 6 h; (v) alkanethiol, Cs₂CO₃, DMAC, reflux, 24 h; (vi) *p*-TosCl, pyridine, r.t, 24 h; (vii) Br₂, NaOAc, acetic acid, 110 °C, 3 h; (viii) Con. H₂SO₄, 110 °C, 15 min

FeCl₃, CH₂Cl₂, r.t, 30 min; (viii) catechol boron bromide, CH₂Cl₂, r.t, 24 h; (ix) CAN, CH₃CN, r.t, 30 min; (x) acetic acid: toluene (7:3), reflux, 6 h; (xi) 4-alkyl phenylacetylene or 4-alkoxy phenylacetylene, PdCl₂(PPh₃)₂, CuI, TEA, reflux, 24 h.

The last part of this chapter deals with the synthesis and mesomorphic properties of heterocyclic DLCs derived from dibenzophenazines (**Scheme 8**). We have synthesised three different series of dibenzophenazines based DLCs containing alkylthiol, symmetrical and unsymmetrical 4-alkoxy phenylacetylene derivatives. All the synthesised compounds exhibit hexagonal columnar phase over broad temperature range. They show good photophysical properties recorded in anhydrous chloroform solvent. The liquid crystalline properties of all the mesogens were studied using POM and DSC measurements. The columnar structure was investigated using X-ray diffraction studies. Molecular structures of all the compounds were characterised using spectral and elemental analysis.



Scheme 7. (i) alkyl halide, anhy. K₂CO₃, DMF, reflux, 24 h; (ii) anhy. FeCl₃, DCM, 15 min, r.t.; (iii) B-bromocatecholborane, DCM, 24 h, r.t.; (iv) ceric ammonium nitrate, acetonitrile, r. t, 30 min; (v) 3,4-diaminobenzoic acid, acetic acid: toluene (7:3), 100 °C, 8 h; (vi) alkyl alcohol, EDCl.HCl, HOBt, DMAP, DCM, 24 h, r.t.



Scheme 8. (i) Oxalyl chloride, anhy. $AlCl_3$, DCM, r.t. 3 h; (ii) glacial acetic acid, reflux, 6 h; (iii) $FeCl_3$, DCM, r.t., 3 h; (iv) alkyl thiol, anhy. K_2CO_3 , DMF, reflux, 12 h; (v) and (vi) 4-alkoxy phenylacetylene, $PdCl_2(PPh_3)_2$, CuI , TEA, reflux, 24 h.

Chapter 5

As stated in the introduction part, nanoparticles possess unique physical and chemical properties which rely upon their morphology [16]. The dispersion of zero-, one- and two-dimensional nanomaterials in DLCs and evaluation of their physical properties is currently a very active research field [17]. Doping of functionalized gold nanoparticles in to metal phthalocyanine liquid crystals improve the photosensitizers in photodynamic therapy, photophysical, photochemical and optical properties [18]. The dispersion of metal nanoparticles in metal-free phthalocyanine DLC may improve their electro-optical properties; with this idea, we synthesized small sized hexanethiol-functionalized metallic–nanoparticles of gold and silver using reported procedure with slight modification. Similarly, metal–free phthalocyanine discotic liquid crystal bearing eight branched alkoxy chains are also synthesized (**Scheme 9**). This compound **6** exhibits room temperature hexagonal columnar phase over broad temperature range. We then dispersed hexanethiol functionalized gold and silver nanoparticles in metal free phthalocyanine DLC and investigated the effects of the dispersion of these MNPs (Au & Ag) on nonlinear optical, electrical, thermal properties and supramolecular order of the phthalocyanine discotic liquid crystal (Pc-DLC). Thermal and structural properties were investigated by POM and DSC measurements. The self assembly of metal nanoparticles in the hexagonal columnar phase structure was investigated using X-ray diffraction studies. The POM, DSC and SAXS studies revealed that the doping of MNPs into discotic liquid crystals does not disturb the nature of mesophase with different concentration variations, except for a minor shift in the transition temperature. The size distribution and morphology of MNPs were estimated using SEM and TEM. The DC conductivity measurements show enhanced electrical conductivity upon increasing concentration of MNPs in columnar DLC matrix.

The doping of metal nanoparticles into Pc liquid crystals leads to an enhancement of the nonlinear optical absorption response. Between Au and Ag doping, Au results in a higher enhancement. The enhanced conductivity and NLO properties make MNPs doped Pc DLC a potential candidate for optoelectronics and photonics applications. A graphical representation of dispersion of MNPs in DLC matrix is shown in **Figure 1**.

Chapter 6

The thesis is concluded with this chapter which summarizes important results and conclusions derived from this thesis work entitled “**Synthesis and Characterisation of Some Novel Banana and Discotic Liquid Crystals**”. We briefly discuss the diverse possibilities and scope for future work based on the results obtained from our experimental work. Some of the findings of this thesis have been published/communicated in the international journals.

References

- [1] Collings P.J. Liquid crystals: nature's delicate phase of matter. Bristol: Princeton University Press; **2002**
- [2] (a) Demus D, Goodby J, Gray G. W, Spiess H. W, and Vill V (eds.). Physical Properties of Liquid Crystals, Wiley VCH, Weinheim, Germany, **1999**; (b) Bahadur B. (ed.). Liquid Crystals: Applications and Uses, Vols. 1–3, World Scientific, Singapore, **1990**; (c) Chandrasekhar, S. Liquid Crystals, Cambridge University Press, Cambridge, U.K., **1992**; (d) Collings P. J. and Hird M. Introduction to Liquid Crystals: Chemistry and Physics, Taylor & Francis, London, U.K., **1997**.
- [3] (a) Vertogen G and de Jeu W. H. Thermotropic Liquid Crystals, Fundamentals, Springer-Verlag, Berlin, Germany, **1988**; (b) Singh, S. Liquid Crystals: Fundamentals, World Scientific, Singapore, **2002**; (c) Gray G. W and Luckhurst G. R. (eds.). The Molecular Physics of Liquid Crystals, Academic Press, London, U.K., **1979**; (d) Kumar S. (ed.). Liquid Crystals: Experimental Study of Physical Properties and Phase Transitions, Cambridge University Press, Cambridge, U.K., **2001**.
- [4] (a) Gray G. W. Thermotropic Liquid Crystals, John Wiley, New York, **1987**; (b) Fisch M. R. Liquid Crystals, Laptops and Life, World Scientific, Singapore, **2004**; (c) Crawford G. P. and Zumer S. (eds.). Liquid Crystals in Complex Geometries: Formed by Polymers and Porous Networks, Taylor & Francis, London, U.K., **1996**; (d) Serrano J. L. Metallomesogens-Synthesis, Properties and Application, VCH Weinheim, **1996**.

- [5] (a) Koltover I, Salditt T, Radler J. O, Safinya C. R. *Science.*, **1998**, 281, 78–81; (b) Nakata M, Zanchetta G, Chapman D. B. et. al. *Science.*, **2007**, 318, 1276–1279; (c) Zanchetta G, Nakata M, Buscaglia M, Bellini T, Clark N. A. *Proc. Natl. Acad. Sci. USA.*, **2008**, 105, 1111–1117.
- [6] (a) O'Connor I, Hayden H, O'Connor S, Coleman J. N, Gunko Y. K. *J. Mater. Chem.*, **2008**, 18, 5585–5588; (b) Kato T, Yasuda T, Kamikawa Y, Yoshio M. *Chem. Commun.*, **2009**, 729–739; (c) Woltman S. J, Jay G. D, Crawford G. P. (eds.). *Liquid Crystals: Frontiers in Biomedical Applications*, World Scientific, Singapore, **2007**.
- [7] (a) Pelzl G, Diele S and Weissflog W. *Adv. Mater.*, **1999**, 11, 707–724; (b) Tschierske C, Dantlgraber G. *Pramana.*, **2003**, 61, 455–481; (c) Link D. R, Natale G, Shao R, MacLennan J. E, et. al. *Science.*, **1997**, 278, 1924–1927.
- [8] (a) Bushby R. J, Lozman O. R. *Curr. Opin. Solid State and Mater. Sci.* **2002**, 6, 569–578; (b) Bushby R. J, Kawata K. *Liq. Cryst.*, **2011**, 38, 1415–1426; (c) Chen S, Eichhorn S. H. *Isr. J. Chem.*, **2012**, 52, 830–843; (d) Pisula W, Feng X, Mullen K. *Chem. Mater.*, **2011**, 23, 554–567.
- [9] (a) Kumar S. *Liq. Cryst.*, **2009**, 36, 607–638; (b) Goodby J. W, Saez M, Cowling S. J, Gortz V, et al. *Angew. Chem. Int. Ed.*, **2008**, 47, 2754–2787; (c) Sergeyevev S, Pisula W, Geerts Y. H. *Chem. Soc. Rev.*, **2007**, 36, 1902–1929; (d) Wu J, Pisula W, Mullen K. *Chem. Rev.* **2007**, 107, 718–747.
- [10] (a) Kumar S, *Chem. Soc. Rev.*, **2006**, 35, 83; (b) Kato T, Yasuda Y, Kamikawa, Yoshio M. *Chem. Commun.*, **2009**, 729; (c) Laschat S, Baro A, Steinke N, Giesselmann F, Hagele C, Scalia G, Judele R et al. *Angew. Chem. Int. Ed.*, **2007**, 46, 4832; (d) Sergeyevev S, Pisula W, Geerts Y. H, *Chem. Soc. Rev.*, **2007**, 36, 1902; (e) Wu J, Pisula W, Mullen K, *Chem. Rev.*, **2007**, 107, 718; (f) Kawata k. *Chem. Rec.*, **2002**, 2, 59.
- [11] (a) Hegmann T, Qi H, Marx V. M. J. *Inorg. Organomet. Polym. Mater.*, **2007**, 17, 483–508; (b) Cseh L, Mehl G. H. *J. Mater. Chem.*, **2007**, 17, 311–315; (c) Kumar S, Pal S. K, Kumar P. S, Lakshminarayanan V. *Soft Matter.*, **2007**, 3, 896–900.
- [12] (a) Kumar S, *Synth. React. Inorg., Met.-Org., Nano-Met. Chem.*, **2007**, 37, 327–331; (b) Cseh L, Mehl G. H, *J. Mater. Chem.*, **2007**, 17, 311–315; (c) Qi H, Hegmann T, *J. Mater. Chem.*, **2008**, 18, 3288–3294; (d) Shen Z, Yamada M, Miyake M, *J. Am. Chem. Soc.*, **2007**, 129, 14271–14280.

- [13] Sharma RA, Gescher AJ, Steward WP. *Eur J Cancer.*, **2005**, 41, 1955–1968.
- [14] (a) Weissflog W. *Liq Cryst.*, **2011**, 38, 1081–1083; (b) Weissflog W, Baumeister U, Tamba MG, et al. *Soft Matter.*, **2012**, 8, 2671–2685.
- [15] (a) Simmerer J, Glusen B, Paulus W, Kettner A, Schuhmacher P, et al. *Adv. Mater.*, **1996**, 8, 815–819; (b) Adam D, Schuhmacher P, Simmerer J, Haussling L, Paulus W, Siemensmeyer K, Eitzbach k. H, Ringsdorf H, Haarer D, *Adv. Mater.*, **1995**, 7, 276–280.
- [16] (a) Schwerdtfeger P. *Angew. Chem. Int. Ed.*, **2003**, 42, 1892–1895; (b) Rao C. N. R, Muller A, Cheetham A. K. *The chemistry of nanomaterials: synthesis, properties and applications.* John Wiley & Sons, **2006**; (c) Schmid G. *Clusters and Colloids, From Theory to Applications;* Wiley-VCH: Weinheim, Germany, **1994**.
- [17] (a) Kumar S, Lakshminarayanan V, *Chem. Commun.*, **2004**, 1600–1601; (b) Kumar S, Pal S.K, Kumar P. S, Lakshminarayanan V, *Soft Matter.*, **2007**, 3, 896–900; (c) Kumar S, Sagar I. K, *Chem. Commun.*, **2011**, 47, 12182–12184; (d) Kumar M, Kumar S, *RSC Adv.*, **2015**, 5, 1262–1267; (e) Kumar S, Bisoyi H. K, *Angew. Chem. Int. Ed.*, **2007**, 46, 1501–1503; (f) Bisoyi H. K, Kumar S. *J. Mater. Chem.*, **2008**, 18, 3032–3039; (g) Shivanandareddy A. B, Krishnamurthy S, Lakshminarayanan V, Kumar S, *Chem. Commun.* **2014**;50:710–712.(h) Kumar, Kumar S. *RSC Adv.*, **2015**, 5, 14871–14878.
- [18] (a) Nombona N, Maduray K, Antunes E, Karsten A, Nyokong T, *J. Photochem. Photobiol. B.*, **2012**, 107, 35–44; (b) Basova T.V, Parkhomenko R. G, Igumenov I. K, Hassan A, Durmus M, Gurek A. G, Ahsen V, *Dyes and Pigments.*, **2014**, 111, 58–63.

Signature of the Research Fellow

Ashwathanarayana Gowda. M

Signature of the Research Guide

Prof. Sandeep Kumar

List of Publications

1. Synthesis and characterisation of novel isoxazole based banana liquid crystals from naturally occurring curcumin.

A. Gowda, A. Roy and S. Kumar. *Liq. Cryst.*, **2016**, 43, 175–182.

2. Self-Assembly of Silver and Gold Nanoparticles in a Metal-Free Phthalocyanine Liquid Crystalline Matrix: Structural, Thermal, Electrical and Nonlinear Optical Characterization.

A. Gowda, M. Kumar, A. R. Thomas, R. Philip and S. Kumar. *ChemistrySelect.*, **2016**, 1, 1361–1370.

3. Ethylenedioxythiophene as a novel central unit for bent-core liquid crystals.

A. Gowda and S. Kumar. *Liq. Cryst.*, **2016**, 43, 1721–1731.

4. Synthesis and mesomorphic properties of novel Schiff base liquid crystalline EDOT derivatives.

A. Gowda, A. Roy and S. Kumar. *J. Mol. Liq.*, **2016**, 225, 840–847.

5. Thermal and nonlinear optical studies of newly synthesized EDOT based bent-core and hockey-stick like liquid crystals.

A. Gowda, L. Jacob, N. Joy, R. Philip, Prathiba R and S. Kumar. *New J. Chem.*, **2018**, 42, 2047–2057.

6. Charge Transport in Novel Phenazine Fused Triphenylene Supramolecular Systems.

A. Gowda, L. Jacob, D. P. Singh, R. Douali, and S. Kumar. *ChemistrySelect.*, **2018**, 3, 6551–6560.

7. Synthesis, mesomorphic properties and nonlinear optical studies of alkyl and alkoxy phenylacetylene containing phenazine fused extended triphenylene discotic liquid crystal dyes.

A. Gowda, L. Jacob, A. Patra, A. George, R. Philip and S. Kumar. *Dyes and Pigment.*, **2019**, 160, 128–135.

8. Novel Phenazine Fused Triphenylene Discotic Liquid Crystals: Synthesis, Characterisation, Thermal, Optical and Nonlinear Optical Properties.

A. Gowda, L. Jacob, N. Joy, R. Philip and S. Kumar. *New J. Chem.*, **2018**. DOI: 10.1039/C8NJ03024.C. Accepted, in press.

9. Dibenzophenazines based discotic liquid crystals: Synthesis, thermal and optical properties.

A. Gowda†, L. Jacob† and Sandeep Kumar. (Manuscript under preparation, † equal contribution to this work)

Article/review articles which are not included in this thesis:

10. The chemistry of bent-core molecules forming nematic liquid crystals

S. Kumar and **A. Gowda**. *Liq. Cryst. Rev.*, **2015**, 3, 99–145.

11. Discotic Liquid Crystals with Graphene: Supramolecular Self-assembly to Applications.

M. Kumar, **A. Gowda**, S. Kumar. *Part. Part. Syst. Charact.*, **2017**, 1700003.

12. Discotic liquid crystals derived from polycyclic aromatic cores: from the smallest benzene to the utmost graphene cores.

A. Gowda, M. Kumar, S. Kumar. *Liq. Cryst.*, **2017**, 44, 1990–2017.

- 13.** Soft discotic matrix with 0-D silver nanoparticles: Impact on molecular ordering and conductivity.
S. Varshney, M. Kumar, **A. Gowda** and S. Kumar. *J. Mol. Liq.*, **2017**, 238, 290–295.
- 14.** Silver nanodisks in soft discotic forest: Impact on self-assembly, conductivity and molecular packing.
M. Kumar, S. Varshney, **A. Gowda** and S. Kumar. *J. Mol. Liq.*, **2017**, 241, 666–674.
- 15.** Trapping of inorganic nanowires in supramolecular organic nanoribbons.
A. B. Shivanandareddy, M. Kumar, **A. Gowda** and Sandeep Kumar. *J. Mol. Liq.*, **2017**, 244, 1–6.
- 16.** Rapid Formation and Macroscopic Self-Assembly of Liquid-Crystalline, High-Mobility, Semiconducting Thienothiophene.
M. Pandey, **A. Gowda**, S. Nagamatsu, S. Kumar, W. Takashima, S. Hayase, and S. S. Pandey. *Adv. Mater. Interfaces.*, **2018**, 5, 1700875.
- 17.** Recent Advances in Discotic Liquid Crystal-Assisted Nanoparticles.
A. Gowda and Sandeep Kumar. *Materials.*, **2018**, 11, 382
- 18.** Laser Beam Deflection Study of Diffusion in Bovine Serum Albumin and Green Synthesised Gold Nano-Particle-Conjugate.
N. P. Dhanya, A. **Gowda**, P. K. Bindu Sharmila, A. S. Shanu, and P. R. Sasikumar. *J. Bionanosci.*, **2018**, DOI: 10.1166/jbns.2018.1582. Accepted

Conferences /Workshops Attended

Oral presentations:

1. Oral presentation on “*Novel synthesis and characterisation of Banana, Discotic liquid crystals and Nano-Composites*” Hosted by Prof. David Walba, **Chemistry and Biochemistry department, University of Colorado, Boulder, USA**. From 07-08-2016 to 10-08-2016.
2. Oral presentation on “*Ethylenedioxythiophene: Novel central unit for bent-core liquid crystals*” at **23rd National Conference on Liquid Crystal-2016 (NCLC), IIT-ISM Dhanbad, India**. From 07-12-2016 to 09-12-2016
3. Oral presentation on “*Self-assembly of metal nanoparticles (0-D and 2-D) in discotic liquid crystals: Next generation energy materials*” at **Nanomaterials and Nanoelectronic devices for Energy applications-2017, Indian Academy Center for PG and Research Studies, Bengaluru, India**. From 28/07/2017 to 29/07/2017.
4. Oral presentation on “*Novel Discotic Liquid Crystals from Triphenylene*” at **CHEMPOSIUM -2017, Indian Academy Degree College, Bengaluru, India**. 08/08/2017.
5. Oral presentation on “*Ethylenedioxythiophene: Novel central unit for bent-core and hockey-stick like liquid crystals*” at **17th Optic of Liquid Crystal Conference (OLC), Sao Paulo, Brazil**. From 24/08/2017 to 29/08/2017.
6. Oral presentation on “*Extension of Triphenylene Discotic Liquid Crystal Core*” at **24th National Conference on Liquid Crystal, IISER-Mohali, India**. From 11/09/2017 to 13/09/2017.

Poster presentations:

1. *Attended “21st National Conference on Liquid Crystals- 2014”.* Kanpur. India.
2. Poster presentation on "Synthesis and characterisation of novel isoxazole based banana liquid crystals from naturally occurring curcumin" and received best poster award at **22nd National Conference on Liquid Crystals- 2015.** DIT University, Dehradun. India.
(Best poster presentation award)
3. Poster presentation on "Self-assembly of silver and gold nanoparticles in a metal-free phthalocyanine liquid crystalline matrix" at **Winter School-2015 Jawaharlal Nehru Centre for Advanced Scientific Research (JNCASR) Bengaluru. India.**
4. Poster presentation on "Ethylenedioxythiophene as a novel central unit for bent-core liquid crystals" at **26th International Liquid Crystal Conference (ILCC-2016), Kent state university, USA, 2016.**
5. Poster presentation on "Self-assembly of metal nanoparticles (Au & Ag) in discotic crystalline dye matrix: thermal and non-linear optical studies" at **Annual 2017-Meeting of Taiwan Liquid Crystal Society, Tunghai University, Taichung, Taiwan, December 15, 2017.**
6. Attended **2018 Taiwan-Japan Bilateral Symposium in Optics for Intelligent Information Science and Technology: Biophotonics & Agricultural Photonics** held on **April 15th – 19th 2018** at **Tainan Science Park. Tainan, Taiwan.**

Chapter 1

1.1 Part A. Introduction

1.2 Part B. Statement of the problem

1.1 Part A. Introduction

1.1.1 Liquid crystals

Liquid crystals (LCs) are dynamic functional soft materials which retains both order and mobility at molecular, supramolecular as well as macroscopic levels [1]. Hierarchical self-assembly in LCs forms phases in between highly ordered crystalline solid and disordered isotropic liquid phase. For this reason they are called mesophases or intermediate phases (**Figure 1**). These intermediate phases are true thermodynamic stable state of matter. Hence, liquid crystals are accepted as the fourth state of matter after the three classical states of matter; solid, liquid and gas. The constituent molecules responsible for the formation of mesophases are called *mesogens* and can be organic, inorganic or organometallic [2].

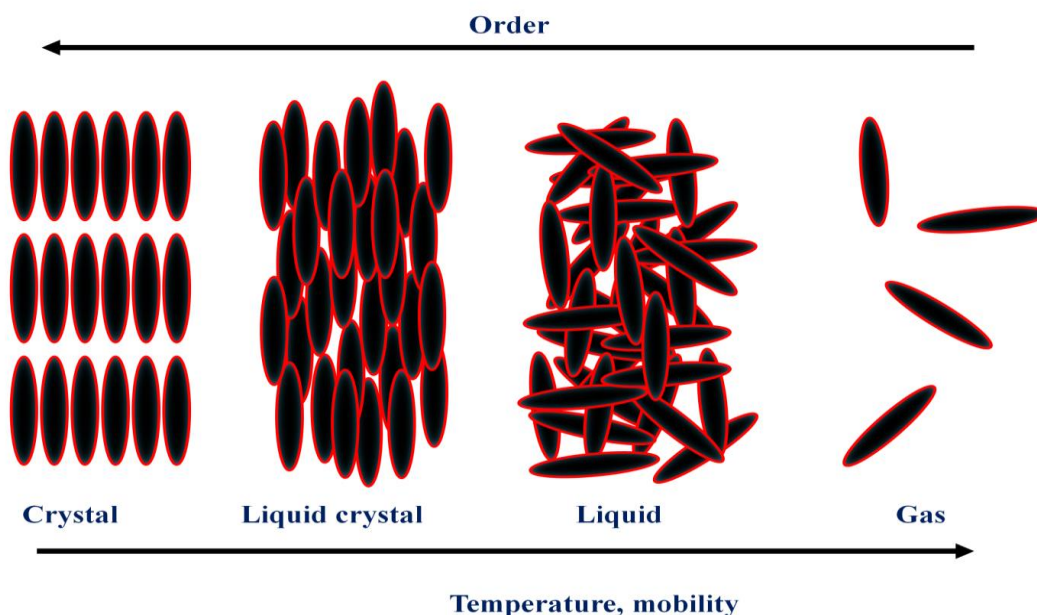


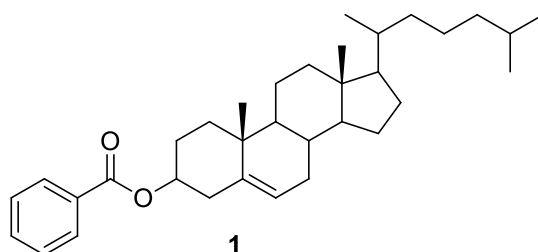
Figure 1. The structural difference and molecular ordering between different states of matter.

Molecules in the crystalline state are generally arranged in a specific location, having three dimensional long range positional and orientational orders. Their anisotropic properties are direction dependent. When a solid transforms to liquid phase upon heating, the molecules loose

its positional and orientational orders. In this state, the molecules randomly diffused in all the directions. However, in liquid crystalline phases, molecules possess at least long range orientational order in one dimension and may or may not have positional order. Eventually, the least ordered LC phase has no long range positional order but has long range orientational order in one dimension (nematic phase), while the most ordered LC phases have two-dimensional long range positional and orientational order [3–5].

1.1.2 History of liquid crystals

The foundation of liquid crystal science is traditionally goes back to the year 1888, when Austrian botanist-cum-chemist Friedrich Richard Reinitzer synthesised several ester derivatives of cholesterol, a naturally occurring compound in plants and animal cell membranes. Reinitzer found that cholesteryl benzoate (**1**) exhibits “*dual melting*” behaviour [6]. It melts at 145.5 °C from solid to cloudy liquid that goes to a completely isotropic liquid at 178.5 °C [6]. He also observed some unusual behaviour upon cooling the clear liquid.



Cholesteryl benzoate

Later, Reinitzer sought help from Otto Lehmann, a German physicist and well known crystallographer to understand this phenomena using polarised optical microscopy designed by himself [7]. He initially referred this phase as “soft crystals” and later as “crystalline fluids”, once he was convinced that the opaque phase was an uniform phase of matter sharing properties of both liquids and solids; later he called them “liquid crystals”. It may be noted that though in

1850s researchers have dealt with liquid crystal materials yet they didn't understand the uniqueness of this phenomena [8]. During the first half of twentieth century, the progress was mainly made by chemist, who tried to find new types of liquid crystalline materials. Daniel Vorlander, a professor of chemistry at university of Halle, started working on the synthesis of liquid crystalline materials in his laboratory [9]. By the end of 1935, he synthesised around 1100 liquid crystal compounds and systematically investigated the structure–mesophase relationship. Vorlander remarked that liquid crystal phases are exhibited by the molecules having elongated (rod-like) molecular shape, now commonly called as “*calamitic liquid crystals*”. In 1965, the first application of liquid crystalline compounds in thermography was presented at International Liquid Crystal Conference (ILCC). Subsequently, in 1968 ILCC, Heilmeyer’s group gave first sign for use of liquid crystals in electrooptical display technology. This report drove serious research activities in liquid crystals exponentially. Till date, more than 1,00,000 liquid crystalline compounds are known in the literature.

In September 1977, Chandrasekhar and his co-workers at the Raman Research Institute, Bangalore reported that not only the rod-shape molecules but also compounds with disc-like molecular shape are able to form LC phases [10]. These are commonly referred to as discotic LCs. Currently more than 3000 discotic liquid crystals are known in the literature.

About two decades later, in 1996, Niori et al. discovered ferroelectricity in non-chiral banana shaped molecules [11]. This has led to a very intense research activity involving bent-shaped molecules which provide access to mesophases with polar order and supramolecular chirality despite the molecules being achiral. It is noteworthy that the first banana shaped LCs were prepared by Vorlander et al. in 1929, but the type of mesophase was not reported at that time [12]. Vorlander asserted that a bend in the molecular long axes of calamitic molecules reduces or nullifies liquid crystalline properties and such molecules were termed as ‘*bad*’ molecules for forming LC phases; because if such molecules freely rotate about their long molecular axes, the excluded volume becomes large and violates the ability to form mesophase. Matsunaga and co-workers have also synthesized bent-core mesogens in the early 1990s, [13,14] but they did not realize the unique mesophases in these banana compounds. However, with the present stage of knowledge, the mesomorphic behavior of these compounds have been reinvestigated and found that some of them form banana phases.

1.2 Classification of liquid crystals

Liquid crystals can be broadly classified by a number of ways e.g., based on molecular weight of constituent molecules such as low molecular mass (monomers and oligomers) and high molecular mass (polymers) LCs; based on how mesophase formed, that is by adding particular solvent (lyotropic) and by changing the temperature (thermotropic); based on nature of constituent molecules (organic, inorganic and organometallic); based on molecular shape of the constituent molecules (rod-like, bent-like, disc-like); and based on self assembly of constitute molecules in the mesophase (nematic, smectic, columnar, B-phases, etc). The classification of liquid crystal is shown in **Figure 2** flow chart. However, most commonly, LCs are recognized into two major categories:

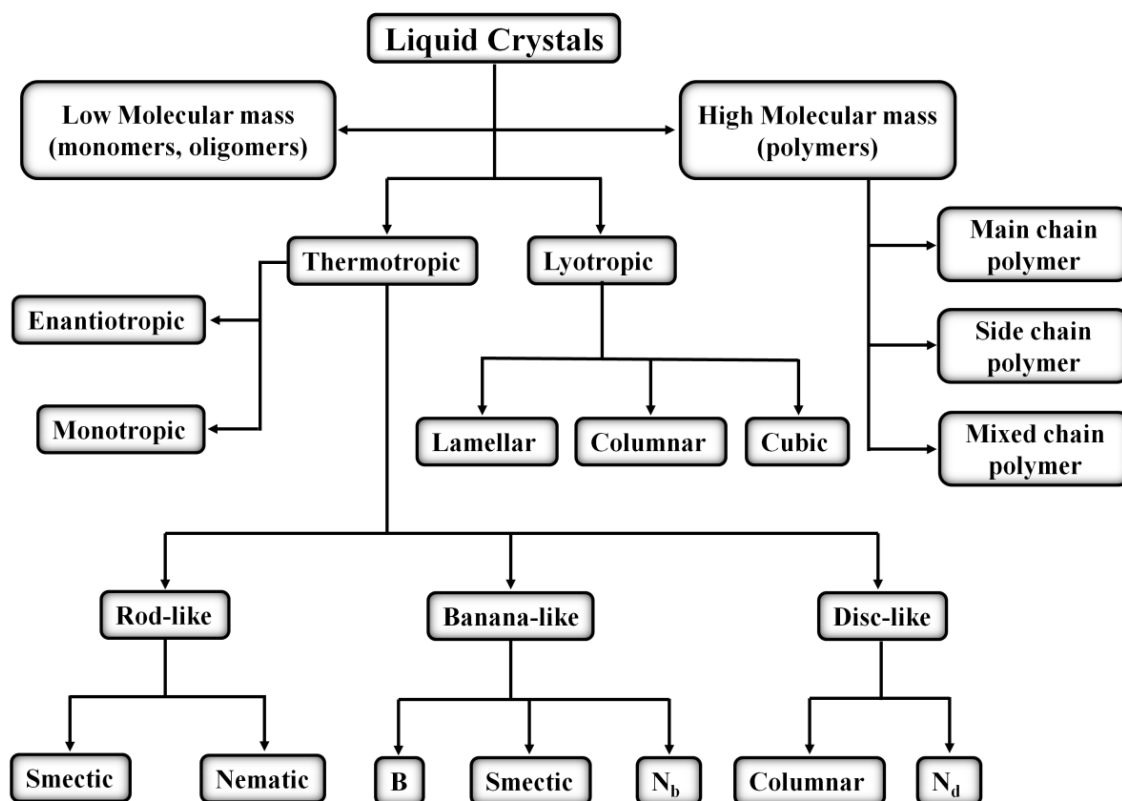


Figure 2. Classification of liquid crystals.

(i) Thermotropic liquid crystals – mesophase formation is temperature dependent.

(ii) Lyotropic liquid crystals – mesophase formation is solvent and concentration dependent.

If the constituent molecules displays both thermotropic and lyotropic liquid crystalline phases, they are called *amphotropic liquid crystals* [15].

Though this thesis is concerned only with **thermotropic liquid crystals**, a very brief introduction about lyotropic liquid crystals is given below owing to their significant role in living systems [16].

1.3 Lyotropic liquid crystals

Some amphiphilic molecules when added in a solvent, form lyotropic liquid crystals. Lyotropic liquid crystals are composed of two distinct parts of contrasting characters, a hydrophilic part (polar head) and a hydrophobic part (nonpolar tail). The mesophase formation is essentially depends on temperature, concentration of solute and solvent (most often water). Typical examples of lyotropic liquid crystals are surfactant (soaps, detergents) in water and various phospholipids (cell membranes, DNA). The structural modification of amphiphilic molecules exhibits various phase structures depending on molecular ordering within the solvent matrix, similar to thermotropic liquid crystals. These are lamellar, hexagonal columnar and cubic phases (**Figure 3**), and their structures have been classified by X-ray diffraction techniques.

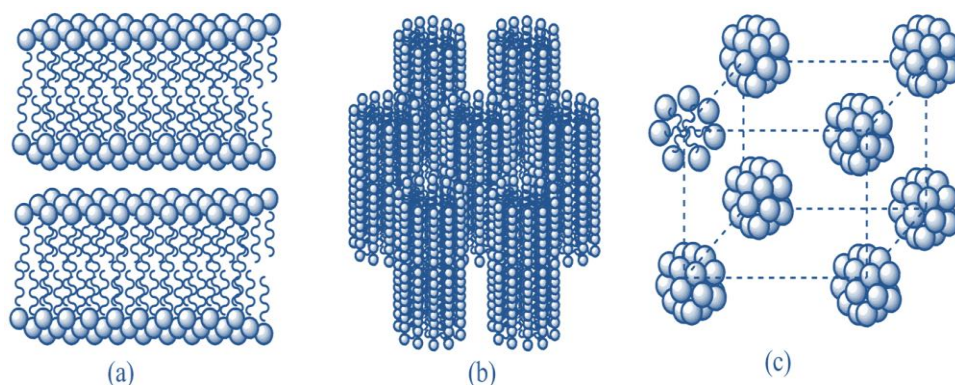


Figure 3. Lyotropic liquid crystalline phases: (a) lamellar; (b) hexagonal columnar and (c) cubic.

1.4 Thermotropic liquid crystals

When the thermodynamically stable mesophases are obtained upon changing temperature of the compounds then they are called *thermotropic liquid crystals*. When mesophases are obtained both on heating and subsequent cooling then the phases are known as *enantiotropic*. If the liquid crystalline phase is obtained only while cooling from isotropic liquid i.e., the mesophase transition occurs below the melting point then it is called *monotropic* phase and, therefore, it is a metastable mesophase. The transition from crystal phase to mesophase is termed as *melting point*, while the phase transition occurs from liquid crystalline phase to isotropic liquid is named as *clearing point*. The quintessential requirement for a molecule to be a thermotropic liquid crystal is a molecular structure consisting of a central core (often aromatic ring) and a flexible peripheral moiety (generally aliphatic chains). The geometric anisotropy, interaction anisotropy and microsegregation of noncompatible subunits are the driving parameters for mesophase formation. Based on the shape of the mesogenic molecules, thermotropic liquid crystals are classified into three main groups:

- (a) Calamitic (rod-like) liquid crystals
- (b) Discotic (disc-like) liquid crystals
- (c) Bent-core (banana-like) liquid crystals

1.4.1 Calamitic (rod-like) liquid crystals

Appropriate molecular designing of rod-shape molecules exhibit calamitic liquid crystals. These molecules possess elongated molecular shape, that is, the molecular length (l) is significantly greater than the molecular breadth (b) as shown in **Figure 4**. Calamitic liquid crystals often consist of two or more aromatic rings bonded directly or via linking groups, terminal aliphatic chains and sometime lateral substitution.

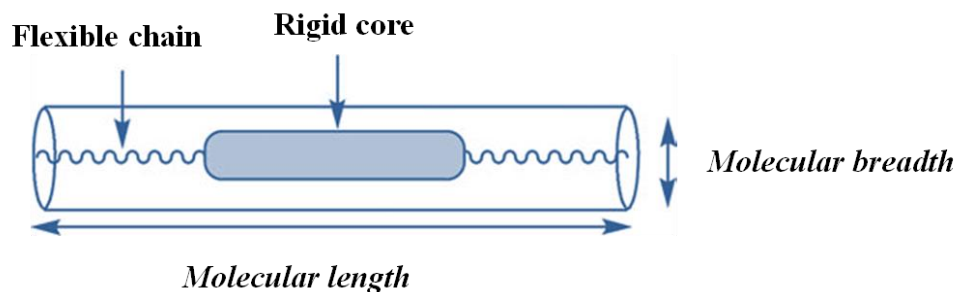


Figure 4. Schematic representation of a calamitic liquid crystal where $l > b$.

The general template for molecular structure of calamitic mesogens is represented in **Figure 5**, where A and B corresponds to aromatic rings (usually benzene, naphthalene, biphenyl, etc.), R and R' indicates flexible aliphatic chains, M and N are lateral substituents such as halides, nitro, methyl, methoxy, cyano etc. Y is the linking group to the aromatic core units. X and Z are linking groups of terminal chains and core units. The nature of the central core, linking groups, and lateral substituents impart significant effect on the mesophase morphology and physical properties of calamitic LCs.

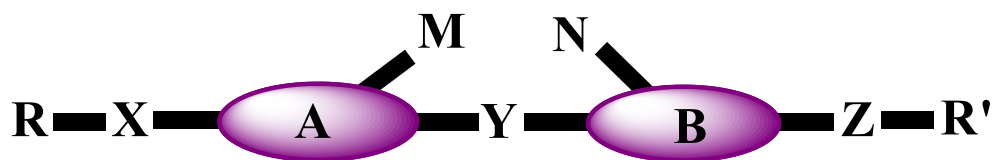


Figure 5. The general template of calamitic liquid crystals.

Calamitic LCs generally exhibit two types of mesophases:

- (a) Nematic (from the Greek word *nematos* meaning “thread”) phase
- (b) Smectic (from the Greek word *smectos* meaning “soap”) phase

1.4.1.1 Nematic phase

Nematic phase shows high degree of long-range orientational order of the mesogens, but it lacks long-range positional order, it is the least ordered mesophase, closest to isotropic liquid. It differs from the isotropic liquid state, where the molecules are oriented in preferred direction with their long molecular axes approximately parallel to each other. The nematic phase is denoted by symbol 'N'. The preferred axes of orientation of molecules, depicted as a long arrow, is called the *director* (Figure 6).

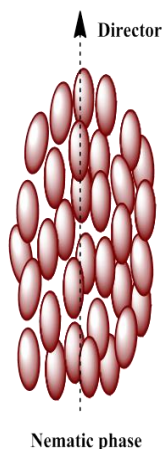


Figure 6. Schematic representation of calamitic nematic phase

1.4.1.2 Smectic phase

Calamitic molecules also exhibit mesomorphic properties where in addition to their orientational order, they also possess positional order. These molecules self-assembled in layers having well-defined layer spacing or periodicity. The smectic phase is denoted by symbol 'Sm'. There are number of smectic mesophases characterised by a variety of molecular orientation within the layers. The smectic LCs can be classified based on whether the director is parallel or tilted with respect to the layer normal. Rod-like molecules freely rotate about their long molecular axes (C_{∞}). Although number of smectic phases cannot be specified, the following types have been defined: SmA, SmB_{hex}, SmC, SmF, and SmI. Among them, SmA and SmC phases are most commonly observed mesophases (Figure 7).

In SmA phase, the rod-like mesogens arranged in layers with their main axes parallel to the director. In case of SmC, the molecules arranged similar to SmA, but the molecules are tilted at an angle to the layer plane. Hence, director is tilted from the normal axes. Both the phases lack positional order between molecules within the layers. SmB, SmF and SmI form more ordered smectic phases. The molecules here possess hexagonal order within the layers. They are called hexatic smectic liquid crystals. Disordered crystals having layer-like structures are often referred to as SmE, SmH, SmK, SmG and SmJ phases but they are more appropriately defined as lamellar plastic crystals. Tilted smectic mesophases formed by chiral compounds or containing chiral mixtures are designated by star symbol (*) (ex. SmC*, SmF*, etc.).

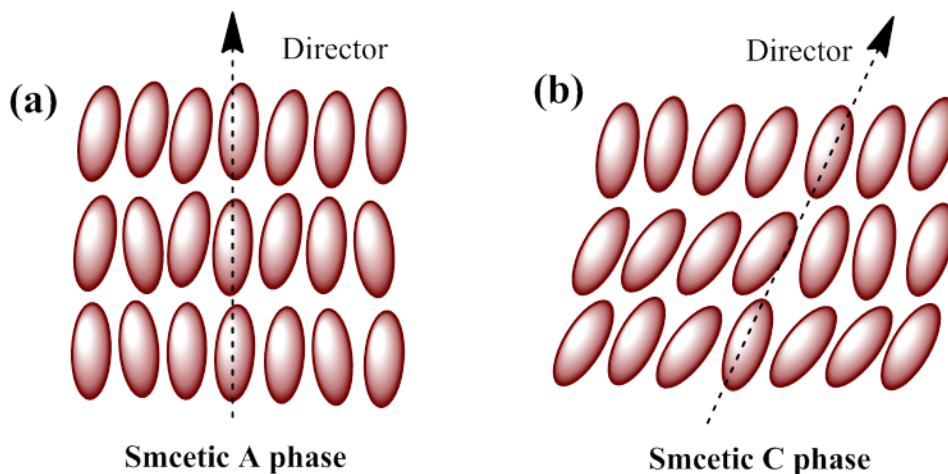


Figure 7. Schematic representation of smectic A and smectic C phases of rod-like liquid crystals.

1.5 Banana liquid crystals

Bent in the molecular structures or deviation from rod-shape molecules forms a new subclass of thermotropic liquid crystals, known as bent-core liquid crystals or banana liquid crystals. Typically, bent-shaped liquid crystalline molecules are composed of three units: an angular central core, two linear rigid arms, and terminal chains (**Figure 8**). The bent-angle is around 120–140° in these molecules. The bent in the central rigid core of banana liquid crystals substantially reduces the free rotation about their long molecular axes. The reduction in the symmetry of the molecules leads to a directed packing of the molecules within layers. The

important consequence of the directed packing of such molecules is the occurrence of a polar order parallel to the smectic layers. In order to escape from polar packing of bent-shape mesogens, layered structures are modified, and this gives new types of mesophase structures. Bent core molecules are the first examples which have experimentally shown that antiferroelectric switching with large spontaneous polarization is indeed possible in a liquid crystal phase composed of non-chiral materials.

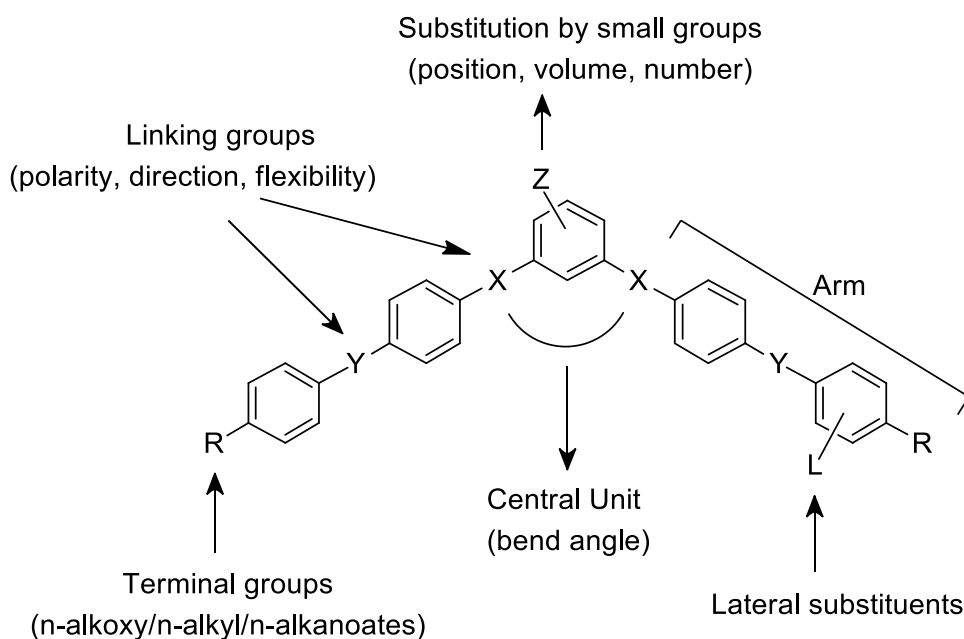


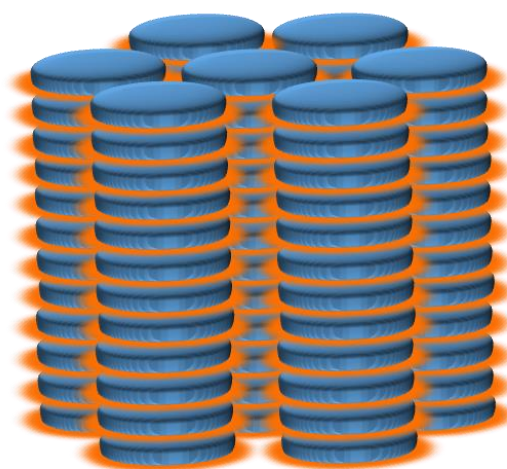
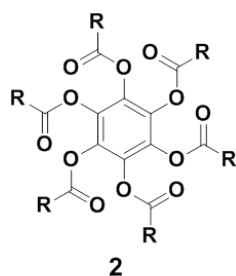
Figure 8. General template of banana LC molecules.

Numerous new mesophases which are different from conventional calamitic LCs have been detected in bent core mesogens. The phases are designated as B1, B2, . . . , B8 according to the sequence of their discovery, where B stands for ‘bent-core’, ‘banana’, ‘bow’, etc. The distinctions between the phases are made on the basis of optical textures, X-ray diffraction studies, and electro-optical responses. Furthermore, it has been reported that some of the B phases have several sub-phases, that is, these phases actually represent families of related

mesophases. Moreover, a number of mesophases formed by bent-core molecules have not yet been unambiguously characterized. In addition to the fascinating B phases, bent-core mesogens also form conventional nematic and smectic phases (SmA, SmC etc.). LCs formed by bent-core molecules open the door to novel complex types of molecular self-organization and to the new field of supramolecular stereochemistry. A number of applications of these materials such as nonlinear optics, flexoelectricity, photoconductivity, and the design of biaxial nematic phase, and so on have been envisaged [17–19].

1.6 Discotic liquid crystals

Sivaramakrishna Chandrasekhar et. al. in 1977 reported “...*what is probably the first observation of thermotropic mesomorphism in pure, single component systems of relatively simple plate like, or more appropriately disc-like molecules*” [10]. They prepared a number of benzene hexa-*n*-alkanoates (**2**) and investigated from polarized optical microscopy, differential scanning calorimetry and X-ray studies. It was revealed that these materials form a new class of liquid crystals in which molecules are stacked one on the top of other in columns that constitute a hexagonal arrangement. This opened a whole new field of fascinating liquid crystal research.



Hexagonal columnar phase

It may be noted that in 1924 Vorländer had predicted the possibility of observing liquid crystalline properties in leaf-shaped molecules [20] but he failed to obtain mesophase behaviour in these molecules probably because the studied molecules did not have flexible aliphatic chains. He thus concluded that leaf-shaped molecules did not form any liquid crystalline phases. It was later realised that the same molecules showed columnar phase upon substitution with flexible alkyl chains. Further to be noted that in the early 1960s Taylor et al. observed that anisotropic mesophases with nematic texture are formed during pyrolysis process of graphitizable substances (carbonaceous mesophase) [21]. These mesophases were considered to be built up of disc like flat aromatic molecules. They were not homogeneous and unstable mesophase in nature. Therefore, it was not fully characterised mesophase structure.

Self-assembly of disc-like mesogens lead to the formation of columnar liquid crystals which are entirely new sub-class of liquid crystals, quite different from rod-like liquid crystals. The disc-like molecules spontaneously self-assemble in one-dimensional (1D) columns, which in turn, self-organize into various two-dimensional (2D) lattices (**Figure 9**).

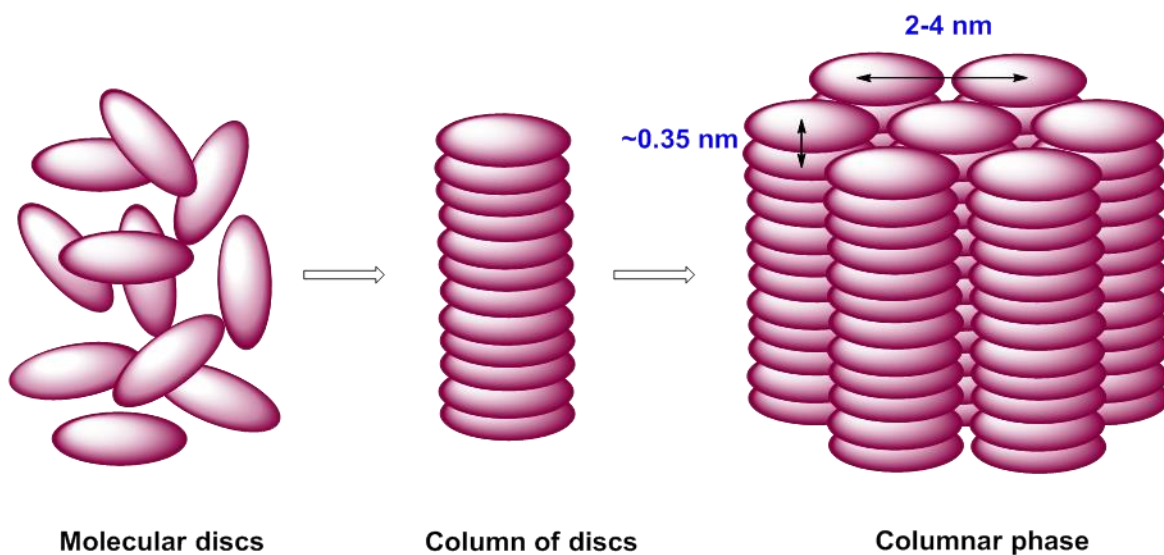


Figure 9. Self assembly of discotic liquid crystals into columnar phase.

1.6.1 Self-assembly of mesophases formed by discotic mesogens

Most of discotic mesogens exhibit columnar phases but there are a few examples which show polymorphism [22–35]. The mesophases formed by discotic mesogens are mainly four types:

(i) Nematic phase; (ii) Columnar phase; (iii) Cubic phase and (iv) Smectic phase

1.6.2 Nematic phases of discotic mesogens

Discotic nematic phase is the least ordered phase, where the mesogens are parallel to one another. They have orientational order but no positional order. The symmetry of the nematic phase formed by rod-shaped molecules is similar to that of phase formed by disc-shaped molecules. But the nematic phases of rod-like molecules are not miscible with discotic nematic host. The discotic nematic phases are further sub classified into four different types depending on molecular arrangement of discotic molecules. (1) Discotic nematic (N_D), (2) chiral discotic nematic (N_{D^*}), (3) nematic columnar (N_{Col}), and (4) nematic lateral (N_L). The structure of these nematic phases is shown in **Figure 10**. In N_D phase the director is along the short molecular axes of the molecule since the disc normals are orientationally ordered. Chiral discotic nematic phase is obtained by introducing chiral groups or by doping with chiral dopant in N_D host. Chiral nematic phase is characterised by a helical structures (**Figure 10b**). In the N_{Col} phase, discotic mesogens self-assemble into small columnar stacks with short-range positional order and long-range orientational order of the columns. They do not form two dimensional (2D) lattice structures (**Figure 10c**). Recently, it has been observed that discotic mesogens self-assembled into disc-shape super structures and these aggregates exhibit nematic arrangements. This nematic arrangement is driven by the strong lateral interaction and thus it is called as nematic lateral phase (N_L) [30–36].

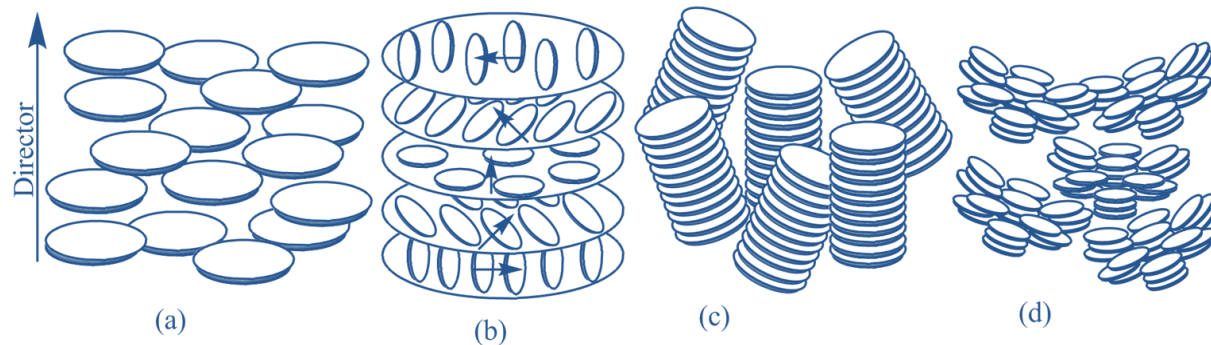


Figure 10. Nematic phases observed in discotic liquid crystals: (a) discotic nematic, (b) chiral discotic nematic, (c) nematic columnar, (d) nematic lateral.

1.6.3 Columnar phases of discotic mesogens

In the columnar phase, discotic mesogens self-assemble one on the top of other in columns. These columns in turn self-organize into various two-dimensional lattice structures. The discotic mesogens in columnar mesophase may be arranged in ordered or disordered fashion. Columnar mesophase can be classified into seven sub classes based on molecular order in the columnar staking, orientation of molecules along the columnar axis (orthogonal, tilted, helical, etc.), molecular motions within the columns and the two-dimensional lattice symmetry of the columnar packing.

- | | |
|--|--|
| (1) Columnar hexagonal phase (Col_h) | (2) Columnar rectangular phase (Col_r) |
| (3) Columnar oblique phase (Col_{ob}) | (4) Columnar plastic phase (Col_p) |
| (5) Columnar helical phase (H) | (6) Columnar tetragonal phase (Col_{tet}) |
| (7) Columnar lamellar phase (Col_L) | |

1.6.3.1 Columnar hexagonal phase (Col_h)

In the columnar hexagonal mesophase, discotic mesogens self-assemble into hexagonal lattice. Hexagonal columnar mesophase often represented as Col_{ho} or Col_{hd} (**Figure 11**), where, ‘h’ indicate hexagonal phase, o and d represent ordered or disordered arrangements of discotic mesogens. Both ordered or disordered phases exhibit fluidity; only the correlation lengths are different and, therefore, it is recommended to discontinue o and d subscripts. The most common abbreviation for columnar hexagonal phase is “ Col_h ”.

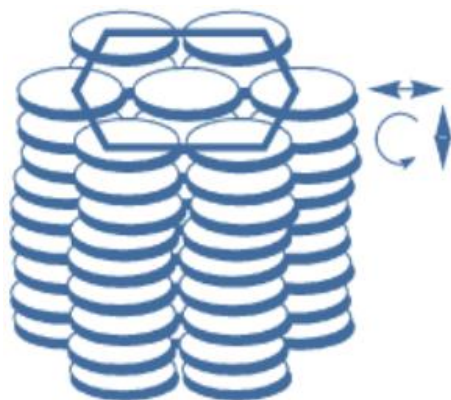


Figure 11. Schematic representation of hexagonal columnar phase structure.

1.6.3.2 Columnar rectangular phase (Col_r)

In the rectangular columnar phase, discotic columns self-assemble into rectangular fashion as shown in **Figure 12**. Three different types of molecular ordering are observed in the columnar rectangular mesophase (**Figure 13a–c**). The discotic mesogens are often oriented at an angle with respect to columnar axes [37]. An orthogonal cross section to the columnar axes is elliptic. Depending upon number of columns per unit cell and mutual orientation of the mesogens (ellipses), columnar rectangular mesophases have been sub divided into three different types. The symmetry of the 2D lattices are specified by three different planar space group i.e. $P21/a$, $P2/a$ and $C2/m$ (**Figure 13a–c**). They belong to the subset of space groups which lack any translational order in the direction of the principal symmetry axis i.e. the direction of the columns.

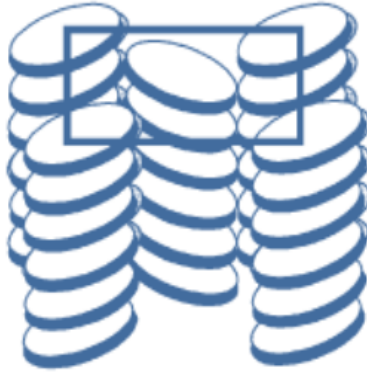


Figure 12. Schematic representation of rectangular columnar phase structure.

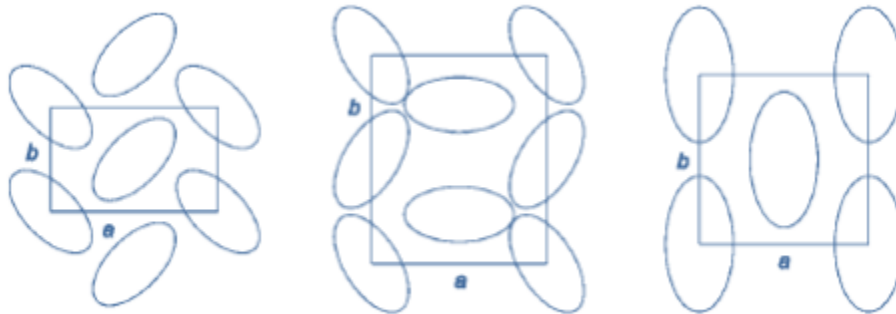


Figure 13. Different types of rectangular columnar phases: (a) Col_r ($P21/a$); (b) Col_r ($P2/a$) and (c) Col_r ($C2/m$).

1.6.3.3 Columnar oblique phase (Col_{ob})

A schematic representation of discotic columns in columnar oblique phase is shown in **Figure 14**. Each tilted columns are represented by elliptic cross sections. The symmetry of columnar oblique phase of 2D lattice belongs to the space group $P1$, strong core-core interaction gives Col_{ob} phase and it is not commonly observed [38].

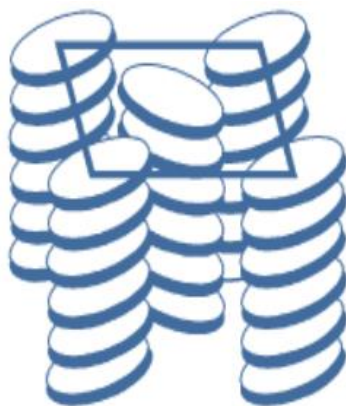


Figure 14. Schematic representation of columnar oblique phase structure

1.6.3.4 Columnar plastic phase (Col_p)

The columnar plastic phase has been recently identified in addition to other columnar phases of discotic mesogens [39]. This mesophase is determined by highly crystal-like order in a hexagonal lattice, while the aromatic discotic mesogens like to have the freedom of rotation about their columnar axes (**Figure 15**). Columnar plastic phase are devoid of structural disorders like non-parallel stacking of discs, lateral or longitudinal displacements, unlike columnar hexagonal phase. The motional freedom of discs in the Col_p phase is restricted.

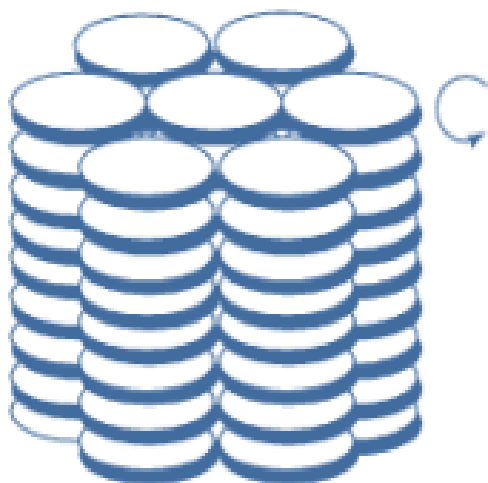


Figure 15. Schematic representation of columnar plastic phase structure.

1.6.3.5 Columnar helical phase (H)

Hexahexylthiotriphenylene (HHTT) discotic mesogen exhibit an exceptional mesophase structure with helical order [40]. In this H phase helical columns form which interdigitate in a set of three columnar stacks. From X-ray investigation reveals that helical phase is unique to HHTT and certain mixture of compounds having average chain length close to six carbons [41]. The molecular ordering in H phase found is illustrated in **Figure 16**.

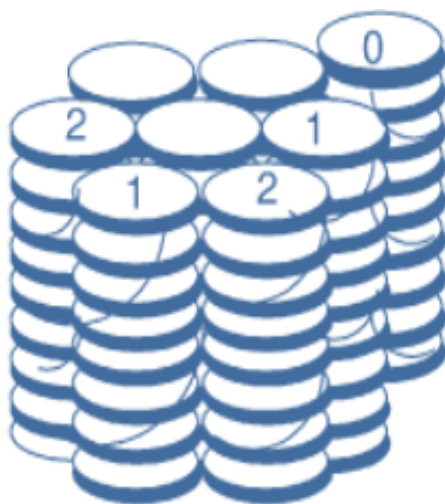


Figure 16. Schematic representation of columnar helical phase structure.

1.6.3.6 Columnar tetragonal phase (Col_{tet})

The columnar tetragonal phase (Col_{tet}) otherwise known as the columnar square phase is shown in **Figure 17**. Here, the columns are upright and they are arranged in a square lattice. Like columnar hexagonal phase, this phase also exhibit spontaneous homeotropic alignment of the columns. This phase is often exhibited by sugar molecules, phthalocyanines and supramolecular fluorinated liquid crystals, etc [42].

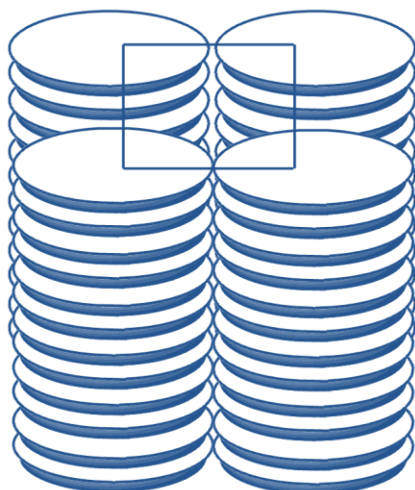


Figure 17. Schematic representation of columnar tetragonal phase structure.

1.6.3.7 Columnar lamellar phase (Col_L)

In columnar lamellar phase, columns arrange themselves in layers. The columns present in lamellar layers can slide in the mesophase. The columns in layer have no positional (translational) correlation with the neighbouring layer. Lamellar structure is observed in the mesophases of certain discotic compounds e.g. bis(*p*-*n*-decylbenzoyl)methanato copper(II), some perylene derivatives, etc. [43].

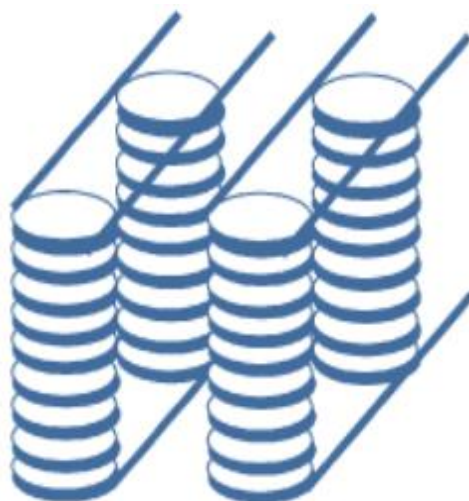


Figure 18. Schematic representation of columnar lamellar phase structure.

Columnar lamellar mesophase is assigned the symbol Col_L and a layered ordering of molecules is shown in **Figure 18**.

1.6.4 Cubic phase of discotic mesogens

Cubic phases are very common in lyotropic liquid crystals, but some columnar phthalocyanine derivatives [44] exhibit bicontinuous cubic phase which consist of interwoven but not connected branched columns.

1.6.5 Smectic phases of discotic mesogens

If any unequal distribution of peripheral alkyl chains or reduced number of peripheral alkyl chains on discotic mesogens, smectic phases are formed as shown in the **Figure 19**. In the discotic smectic phases, the molecular discs are arranged in a layered fashion, each layer is separated by sub layers of alkyl chains, similar to smectic phase of rod-like molecules [45]. They are also known as discotic lamellar (D_L) phases.

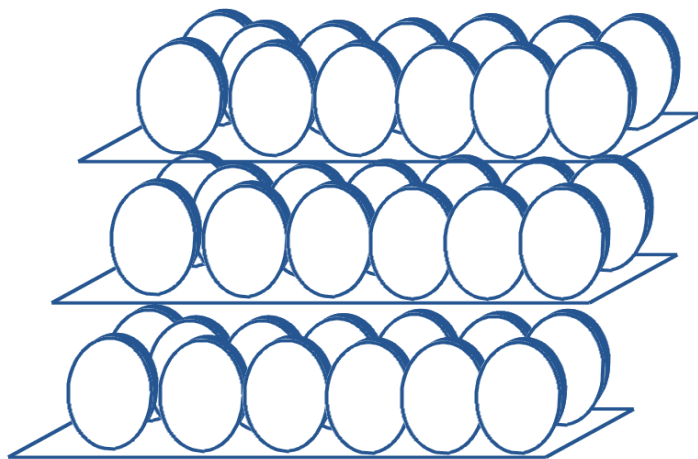


Figure 19. Smectic phase of discotic liquid crystals.

The molecular rotations about their long molecular axes are restricted in layers; they tend to be expected to show biaxial smectic phases. The discotic smectic phases are not very common unlike columnar phase.

1.7 Mesophase structure of discotic liquid crystals

Since the first discovery of discotic liquid crystals, scientists around the globe have attempted to understand the nature of molecular parameters that leads to the formation of various columnar mesophase, and control their transition temperature. In a columnar mesophase the spontaneous self-assembly of functional disc-shaped molecules firmly packed very close similar to molecular packing in the crystalline solid, which prompt to the formation of one-dimensional columns. In the columnar structure, owing to strong intracolumnar interactions, the core-core separation is quite low (~ 0.35 nm) while the columns-to-columns separation is very high (2–4 nm). The π -electron interactions associated with the aromatic cores allow molecules to stack one on the top of other, where central aromatic cores act as conducting part and encompassing flexible aliphatic chains act as insulating part. Thus these columns can be considered as molecular wires, where charge and energy migration occur in an organized manner (**Figure 20**) [46–47].

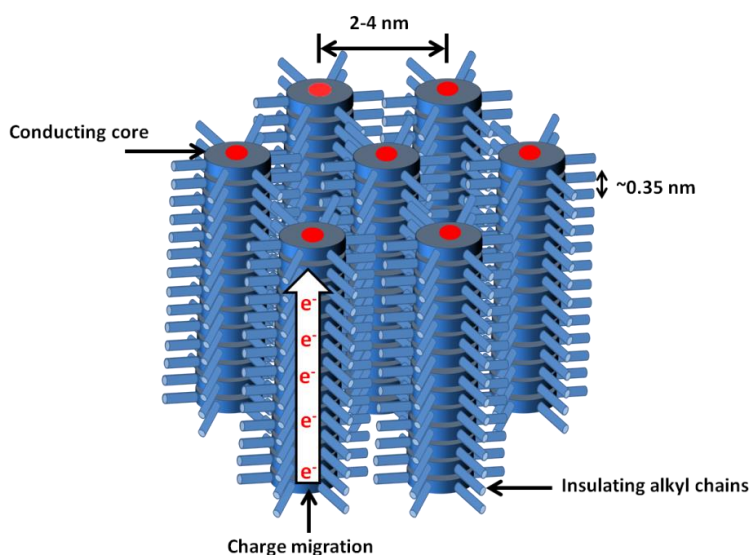


Figure 20. Schematic illustration of columnar hexagonal arrangement of discotic cores in 1-D semiconductor and charge migration.

The central aromatic core is substituted with more than four molten aliphatic chains. These flexible alkyl chains are disorder in nature, which induces mobility to the central aromatic cores. Discotic mesogens often have two, three, four or six-fold rotational symmetry. However, a number of discotic materials having non-planar, non-aromatic core with shorter number of chains are also known to form columnar phases. The microsegregation of two non-compatible units (rigid core and flexible chains) leads to mesomorphism. Discotic molecules self-assemble into one-dimensional columns; they possess self-healing properties, i.e. the capacity to repair the structural defects.

1.8 Structural template and synthesis of DLCs

A general template for discotic mesogens is shown in **Figure 21**. Usually, they consist of a central rigid core surrounded by plural number of flexible aliphatic chains. These chains can be connected to the core directly or via linking atoms or groups. Discotic liquid crystals are commonly synthesized from appropriate chemical modification of polycyclic aromatic cores. Assembling of aromatic core followed by nucleophilic or electrophilic aromatic substitution reactions is most often used for the synthesis of discotic liquid crystals. The chemistry of general methods for their synthesis has been covered in many books and review articles [27, 42–50].

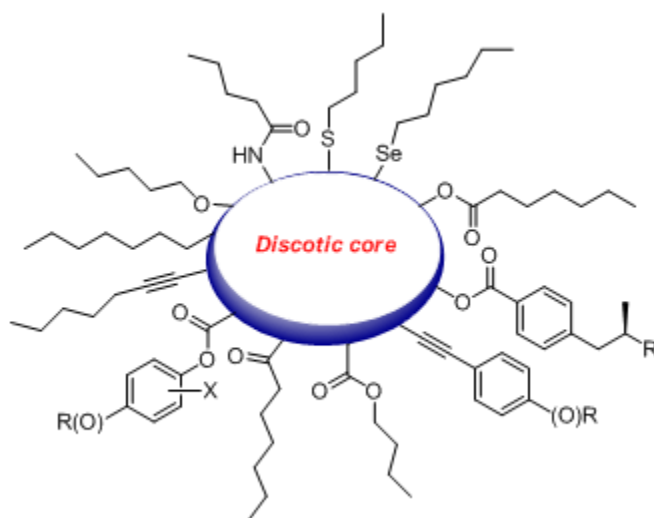


Figure 21. The general molecular approach for designing discotic liquid crystals

Most of the DLCs are derived from polycyclic aromatic cores. Therefore, it is obvious that during the formation of mesomorphism the aromaticity passes from the smallest benzene core to the utmost graphene core. While preparation of these materials is often but not always simple, their purification is usually difficult and tedious. This is primarily because of incomplete substitution of all the functional groups. Partial substitution of polyfunctional groups gives a mixture of structurally similar products having almost identical R_f values as that of pure mesogen on a chromatographic plate. Their separation is often difficult even by HPLC. In order to obtain pure product in greater yields, the reaction is pushed towards completion by taking small excess of the reagent and carrying out the reaction little longer. Sometimes, this could lead to side reactions and further complicate the synthesis. Most important part of the synthesis is finding optimum reaction conditions. The chemistry involved in synthesis of discotic liquid crystals has been improved significantly in last two decades. Highly regio-selective and high yielding methods have been mastered particularly for the synthesis of triphenylene based discotic liquid crystals.

1.9 Characterization of liquid crystalline phases

The thermotropic liquid crystalline mesophase structure is primarily characterised using polarized optical microscopy, differential scanning calorimetry and X-ray diffraction experimental techniques.

POM observation is the key step to understand the existence of mesophase. When an LC compound observed under POM in its isotropic phase, the transmitted light is completely extinguished i.e. no light leakage. If it is in mesophase, the transmitted light is not completely extinguished and an optical texture appears because of the alternation of orientation of the polarized light. This is due to birefringent nature of liquid crystal samples. Various liquid crystal samples show different textures under POM, which gives information about structural arrangement of the mesophase. DSC studies give information about the exact phase transition temperature and associated enthalpy values obtained from both heating and cooling scan of liquid crystal sample. The main advantage of DSC measurement is fast, accurate and convenient to measure temperature and transitions enthalpies to understand the phase diagram and to study

the kinetic of phase transition during heating and cooling scan. We can determine the glass transition temperature of LC samples, which is not possible in POM. The self-assembly of mesophase structure and corresponding packing parameters in each phase can be studied in detail using X-ray diffraction studies. The XRD measurement is the final conclusion for existence of mesophases in the liquid crystalline materials. The diffraction peaks in the small angle and wide angle region gives information about existence of particular mesophase structure.

1.10 DLCs as materials for a new generation of organic electronics

In recent years, the potential use of π -conjugated aromatic compounds as functional components in electronic devices, has led to an increase interest in scientific research in this area. Such fields of research activities are referred as Organic Electronics. This new field has found very interesting applications in electronic devices like, organic solar cells, organic field effect transistors (OFET), organic light-emitting diodes (OLED), sensors, memory materials, etc [22–24]. This has resulted in detailed studies into structure-property relationships of organic molecules, which are determined by the physical and chemical properties of these novel materials. This challenge creates the need of new novel organic materials with semiconducting properties. Two of the potential systems for application in organic (opto) electronic devices are π -conjugated conducting polymers and π - π stacked columnar discotic materials. Mesogens with hierarchical self-assembly into supramolecular structures, like discotic liquid crystals, which form two-dimensional ordered structures and has dynamics (ability to self-healing of structural defects) are considered potential candidates for organic semiconductor devices. The low molecular weight of discotic liquid crystals allows the synthesis of defect-free chemical structures. These small molecular systems have upper hand over conducting polymers, due to the fact that possess very high purity and low molecular mass materials can be conveniently synthesized [27–36,46,47].

References

- [1] (a) Kato T, Mizoshita N, Kishimoto K, *Angew. Chem. Int. Ed.*, **2006**, 45, 38–68; (b) Goodby JW, Saez IM, Cowling SJ, et. al. *Angew. Chem. Int. Ed.*, **2008**, 47, 2754–2787; (c) Tschierske C, *Chem. Soc. Rev.*, **2007**, 36, 1930–1970.
- [2] (a) Gray GW. *Thermotropic Liquid Crystals*, John Wiley, New York, **1987**; (b) Fisch MR. *Liquid Crystals, Laptops and Life*, World Scientific, Singapore, **2004**; (c) Crawford GP, Zumer S. (eds.). *Liquid Crystals in Complex Geometries: Formed by Polymers and Porous Networks*, Taylor & Francis, London, U.K., **1996**; (d) Serrano JL. *Metallomesogens-Synthesis, Properties and Application*, VCH Weinheim, **1996**.
- [3] (a) Bahadur B., *Liquid Crystals Applications and Uses*. World Scientific **1991**, 3, pp. 68–199; (b) Chandrasekhar S., *Liquid Crystals*. Cambridge University Press **1977**; (c) Collings J., *Liquid Crystals: Nature's Delicate Phase of Matter*. Princeton University Press., **2002**; (d) Collings J, Hird M. *Introduction to Liquid Crystals Chemistry and Physics*. Taylor & Francis **1997**.
- [4] (a) Collings J, Patel JS., *Handbook of Liquid Crystal Research*. Oxford University Press **1997**; (b) Demus D., *Types and Classification of Liquid Crystals*. In *Liquid Crystals — Applications and Uses*, World Scientific **2012**, pp 1–36; (c) Demus D, Goodby JW, Gray GW. *Handbook of Liquid Crystals*, Four Volume Set. **1998**; (d) Doane JW, *Polymer Dispersed Liquid Crystal Displays*. In *Liquid Crystals— Applications and Uses*, World Scientific, **2012**, pp 361–395.
- [5] (a) Gennes PG. *The Physics of Liquid Crystals*. Clarendon Press **1974**; (b) Kelker H, Hatz R, Schumann C. *Handbook of Liquid Crystals*. Verlag Chemie **1980**; (d) Pohl L, Merck E. Physical Properties of Liquid Crystals. In *Liquid Crystals – Applications and Uses*, World Scientific **2012**, pp 139–170.
- [6] Reinitzer F, *Monatsh Chem.*, **1988**, **9**, 421; for English translation see *Liq. Cryst.*, **1989**, 5, 7.
- [7] Lehmann O. *Zeitschrift für Physikalische Chemie.*, **1889**, 4, 462.
- [8] Heintz W, *J. Prakt. Chem.*, **1855**, 66, 1.
- [9] Vorlander D, *Kristallinisch-flussige Substanzen*, Enke, Stuttgart., **1905**.
- [10] Chandrasekhar S, Sadashiva BK, Suresh KA, *Pramana.*, **1977**, 9, 471.
- [11] Niori T, Sekine T, Watanabe J, et al. *J. Mater. Chem.*, **1996**, 6, 1231–1233.

- [12] Vorlander D, Fuchs K, Katscher EE. Über die Einwirkung von Chlorsulfonsäure auf Aldehyde. *Ber. Dtsch. Chem. Ges.*, **1929**, 62, 2381–2386.
- [13] Matsunaga Y, Miyamoto S. *Mol. Cryst. Liq. Cryst.*, **1993**, 237, 311–317.
- [14] Matsuzaki H, Matsunaga Y. *Liq. Cryst.*, **1993**, 14, 105–120
- [15] Tschierske C. *Curr. Opin. Colloid Interface Sci.*, **2002**, 7, 355–370
- [16] Koltover I, Salditt T, Radler JO, et al. *Science.*, **1998**, 281, 78
- [17] (a) Link DR, Natale G, Shao R, et al. *Science.*, **1997**, 278, 1924–1927; (b) Pelzl G, Diele S, Weissflog W. *Adv. Mater.*, **1999**, 11, 707–724; (c) Tschierske C, Dantlgraber G. *Pramana.*, **2003**, 61, 455–481; (d) Ros MB, Serrano JL, Fuente MR, et al. *J. Mater. Chem.*, **2005**, 15, 5093–5098.
- [18] (a) Takezoe H, Takanishi Y. *Jpn. J. Appl. Phys.*, **2006**, 45, 597–625; (b) Reddy R, Tschierske C. *J. Mater. Chem.*, **2006**, 16, 907–961; (c) Weissflog W, Murthy SNH, Diele S, et al. *Phil Trans R Soc A.*, **2006**, 364, 2657–2679.
- [19] (a) Etxebarria J, Ros MB. *J. Mater. Chem.*, **2008**, 18, 2919–2926; (b) Lin SC, Ho RM, Chang C-Y, et al. *Chem. Eur. J.*, **2012**, 18, 9091–9098; (c) Eremin A, Jakli A., *Soft Matt.*, **2012**, 9, 615–637.
- [20] Vorländer D., *Chemische Kristallographie Der Flüssigkeiten: Kurze Anleitung Zur Synthese Und Untersuchung Polymorpher Und Kristallinflüssiger Substanzen*; Akademische Verlagsgesellschaft, **1924**.
- [21] Brooks JD, Taylor GH. *Nature.*, **1965**, 206, 697–699.
- [22] Bushby RJ, *J. Mater. Chem.*, **1999**, 9, 2081–2086.
- [23] Bushby RJ, Lozman OR. *Curr. Opin. Coll. Iinter. Sci.*, **2002**, 7, 343.
- [24] Bushby RJ, Lozman OR. *Curr. Opin. Solid State and Mater. Sci.*, **2002**, 6, 769.
- [25] Chandrasekhar S. *Liq. Cryst.*, **1993**, 14, 1.
- [26] Chandrasekhar S, Ranganath GS. *Recent Progress in Physics* **1990**, 53, 1.
- [27] Kato T, Yasuda T, Kamikawa Y, et al. *Chem. Commun.*, **2009**, 729–739.
- [28] Kazuchika O, Kazuaki H, Makiko S, et al. *Mol. Cryst. Liq. Cryst.*, **2003**, 397.
- [29] Kouwer PHJ, Jager WF, Mijs WJ, et al. *Macromolecules.*, **2001**, 34, 7582.
- [30] Kumar S. *Chem. Soc. Rev.*, **2006**, 35, 83–109.
- [31] Laschat S. et al., *Angew. Chemie.*, **2007**, 46, 4832–4887.
- [32] Sergeyeve S, Pisula W, Geerts YH. *Chem. Soc. Rev.*, **2007**, 36, 1902–1929.

- [33] Shimizu Y, Oikawa K, Nakayama K. *J. Mater. Chem.*, **2007**, 17, 4223–4229.
- [34] Takezoe H, Kishikawa K, Gorecka E. *J. Mater. Chem.*, **2006**, 16, 2412–2416.
- [35] Wu J, Pisula W, Mullen K. *Chem. Rev.*, **2007**, 107, 718–747.
- [36] (a) Bisoyi HK, Kumar S. *Chem. Soc. Rev.*, **2010**, 39, 264–285
- [37] (a) Frank FC, Chandrasekhar S. *J. Phys. France.*, **1980**, 41, 1285–1288; (b) Levelut A. *Journal de chimie physique.*, **1983**, 80, 149–161.
- [38] (a) Destrade C, Foucher P, Esparoux H, et. al. *Mol. Cryst. Liq. Cryst.*, **1984**, 106, 121; (b) Morale F, Date RW, Guillon D, et. al. *Chem. Eur. J.*, **2003**, 9, 2484.
- [39] Glusen B, Heitz W, Kettner A, J. H. Wendorff, *Liq. Cryst.*, **1996**, 20, 627.
- [40] (a) Fontes E, Heiney PA, et. al. *Phys. Rev. Lett.*, **1988**, 61, 1202; (b) Heiney PA, Fontes E, Jeu DWH. *J. Phys. France.*, **1989**, 50, 461–483.
- [41] Idziak SHJ, Heiney PA, Mccauley Jr JP, et. al. *Mol. Cryst. Liq. Cryst.*, **1993**, 231, 271–215.
- [42] (a) Vlad-Bubulak T, Buchs J, Kohlmeier A, et. al. *Chem. Mater.*, **2007**, 19, 4460; (b) Ohta K, Watanabe T, Hasebe H, et. al. *Mol. Cryst. Liq. Cryst.*, **1991**, 196, 13; (c) Hatsusaka K, Ohta K, Yamamoto I, et. al. *J. Mater. Chem.*, **2001**, 11, 423; (d) Ichihara M, Suzuki A, Hatsusaka K, et. al. *Liq. Cryst.*, **2007**, 34, 555; (e) Praefcke K, Marquard P, Kohne B, et. al. *Mol. Cryst. Liq. Cryst.*, **1991**, 203, 149.
- [43] (a) Ohta K, Muroki H, Takagi A, et. al. *Mol. Cryst. Liq. Cryst.*, **1986**, 140, 131; (b) Sakashita H, Nishitani A, Sumiya Y, et. al. *Mol. Cryst. Liq. Cryst.*, **1988**, 163, 211.
- [44] Hatsusaka K, Ohta K, Yamamoto I. *J. Mater. Chem.*, **2001**, 11, 423–433.
- [45] (a) Alameddine B, Aebischer OF, Amrein W, et. al. *Chem. Mater.*, **2005**, 17, 4798–4807; (b) Bruce DW, Dunmur DA, Santa LS, et. al. *J. Mater. Chem.*, **1992**, 2, 363–364.
- [46] (a) Pisula W, Feng X, Mullen K. *Adv. Mater.*, **2010**, 22, 3634–3649; (b) Arikainen EO, Boden N, Bushby RJ. *J. Mater. Chem.*, **1995**, 5, 2161–2165; (c) Boden N, Bushby RJ, Clements J. *J. Chem. Phys.*, **1993**, 98, 5920–5931; (d) Haverkate LA, Zbiri M, Johnson MR, et. al. *J. Phys. Chem. B* **2011**, 115, 13809–13816; (e) Adam D, Closs F, Frey T. *Phys. Rev. Lett.*, **1993**, 70, 457–460; (f) Olivier Y, Muccioli L, Lemaire V. et. al. *J. Phys. Chem. B* **2009**, 113, 14102–14111

- [47] (a) Adam D, Schuhmacher P, Simmerer J, et. al. *Nature.*, **1994**, 371, 141–143; (b) Demenev A, Eichhorn SH, Taerum T. et. al. *Chem. Mater.*, **2010**, 22, 1420–1428; (c) Iino H, Hanna J, Haarer D, et. al. *Jpn. J. Appl. Phys.*, **2006**, 45, 430–433; (d) Li L, Tang Q, Li H. et. al. *Pure Appl. Chem.*, **2008**, 80, 2231–2240; (e) Bunk O, Nielsen MM, Solling TI, et. al. *J. Am. Chem. Soc.*, **2003**, 125, 2252–2258; (f) Lee JH, Choi SM, Pate. Et. et. al. *J. Mater. Chem.*, **2006**, 16, 2785–2791.
- [48] (a) Kumar S. *Chemistry of Discotic Liquid Crystals: From Monomers to Polymers*; CRC press: Boca Raton, FL, USA, **2010**; (b) Bisoyi HK, Kumar S. *Chem. Soc. Rev.*, **2011**, 40, 306–319; (c) Bushby RJ, Lozman OR. *Curr. Opin. Solid State and Mater. Sci.* **2002**, 6, 569–578; (d) Bushby RJ, Kawata K. *Liq. Cryst.*, **2011**, 38, 1415–1426; (e) Chen S, Eichhorn SH. *Isr. J. Chem.*, **2012**, 52, 830–843.
- [49] (a) Takezoe H, Araoka F. *Liq. Cryst.*, **2014**, 41, 393–401; (b) Roy B, De N, Majumdar K. C. *Chem. Eur. J.*, **2012**, 18, 14560–14588; (c) Kumar S. *Liq. Cryst.*, **2009**, 36, 607–638; (d) Praefcke K, Singer D, Kohne B. et. al. *Liq. Cryst.*, **1991**, 10, 147–159
- [50] (a) Kumar S. *NPG Asia Materials.*, **2014**, 6, e82; (b) Kumar S. *Isr. J. Chem.*, **2012**, 52, 820–829; (c) Bisoyi H. K, Kumar S. *Liq. Cryst.*, **2011**, 38, 1427–1449; (d) Kaafarani B. R. *Chem. Mater.*, **2011**, 23, 378–396. (e) Pisula W, Feng X, Mullen K. *Chem. Mater.*, **2011**, 23, 554–567; (f);

1.2 Part B. Statement of the problem

Liquid crystal display devices (LCDs) are now part and parcel of our life. Currently, there are more number of LCDs than number of people on the Earth. The LCD industry is well over 100 billion dollar per year industry. Most of these devices are based on calamitic liquid crystals. Accordingly, the chemistry and physics of calamitic liquid crystals have been well established. However, recently discovered discotic and banana LCs have not yet been well explored for their structure-property relationship and device applications. New materials are required to understand the structure-property relationship of these intriguing materials and to look their application potential. Therefore, the primary objectives of this thesis work are:

1. Search for new central bent core to generate novel banana LCs
2. Synthesis and characterization of novel discotic liquid crystals and their nanocomposites

The search has resulted in the discovery of:

1. Novel isoxazole bent core liquid crystals derived from naturally occurring curcumin
2. Ethylenedioxythiophene as a new central core for a variety of novel banana LCs
3. A number of phenazine fused triphenylene discotic liquid crystals
4. Novel phthalocyanine nanocomposites

The results are presented in the following four chapters of this thesis.

Note: All the **Figures** are appended at the end of experimental section.

Chapter 2

Synthesis and mesomorphic properties of bent-core mesogens derived from naturally occurring curcumin

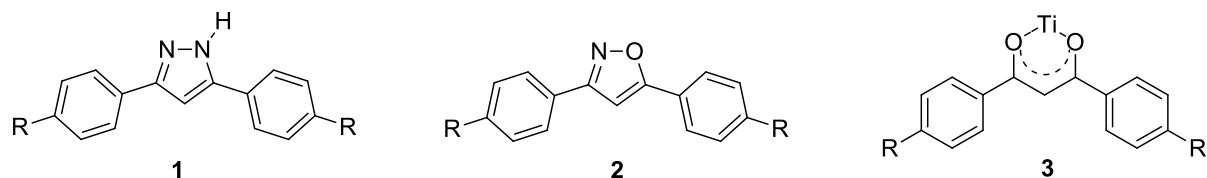
2.1 Introduction

Over the past two decades, liquid crystal research on bent-shaped molecules has provoked considerable attention because of their remarkable electronic properties. In 1929 Vorlander, who is pioneer in the liquid crystals synthesis, prepared several banana-shaped LCs forming mesophase and he observed that the thermal stability of mesophase is low compared with that of straight-core analogous. At that time, they did not realize the type of mesophase observed in the liquid crystal materials [1]. In 1990, Matsunaga and co-workers also synthesised several achiral bent-shaped mesogens but they did not realize the physical importance of these bent-shape molecules before the discovery of polar switching in these mesogens [2].

Later, in 1996, Niori et al. reinvestigated the liquid crystalline properties of an achiral bent-core mesogen, that is “1,3-phenylene-bis-[4-(4-n-octylphenylimino)methyl] benzoates”, originally synthesised by Matsunaga and reported the first distinct example of ferroelectric switching in these banana-shape molecules, ascribing polar order packing of the molecules with C_{2v} symmetry [3]. Subsequently, the first observation of spontaneous formation of opposite chirality by tilting smectic phases of achiral bent-core mesogens in the opposite direction in a smectic layers was reported in 1997 by Link et al. and followed by Heppak et al.[4]. Further, Weissflog et al. reported that ferroelectricity could be achieved for some achiral banana-shaped molecules by chemical modification of linking groups (spacers) and substitution of functional groups in the molecular structure [5]. The discovery of polar order in the achiral molecules laid focal point of intensive research in the LC community. Subsequently, a number of bent-shaped achiral molecules have been synthesised and characterised to access mesophase with polar order and supramolecular chirality [6–10]. Most of the bent-core liquid crystals were synthesised from 1,3-disubstituted benzene ring that gives 120° bent in the middle of the aromatic core which is commonly referred to as bent-angle/bond angle. However, a number of BC LCs derived from five membered heterocycles such as oxazole, oxadiazole, isoxazole, thiophene, etc., are also reported. In such molecules, the bent-angle is around $130\text{--}157^\circ$, depending on substitutions. They have attracted significant attention as a core unit in designing of bent-core molecules. The bend angle of these central heterocyclic aromatic core unit places borderline between classical rod-like LCs and bent-core mesogens [11–20].

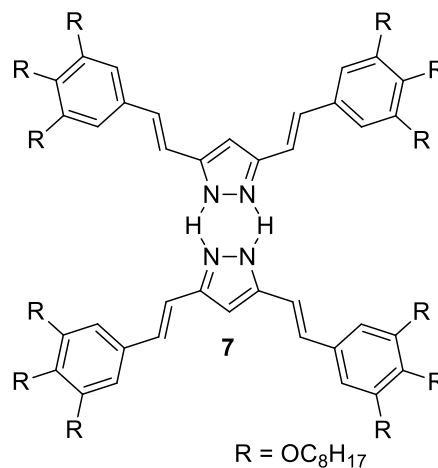
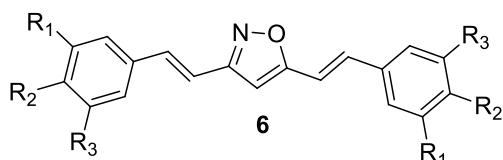
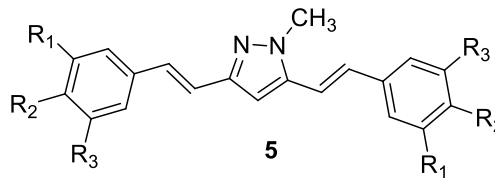
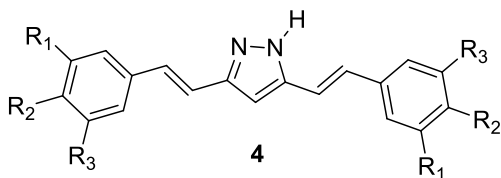
β -Diketones are key precursors for the synthesis of various five-membered heterocyclic and metallomesogenic derivatives. The heterocyclic core units have been used to generate mesogenic materials in the past decades. The presence of heterocyclic aromatic core unit in thermotropic liquid crystalline compounds causes significant impact on lateral or longitudinal dipole moment, polarisability and electronic nature of the molecules. Incorporation of polarisable heteroatoms such as N, O and S gives considerable changes in the mesomorphic and physical properties [21]. These factors can significantly influence the type of mesophases, phase transition temperature, dielectric and other physical properties of the mesogens. Therefore, a large number of bent core liquid crystals have been derived from various heterocyclic cores [22–32].

Numerous bent-core mesogens and metallomesogens have been synthesized from β -diketone key intermediates. In 1992, Serrano et al. reported the synthesis and liquid crystalline properties of symmetrical bis-(4-alkoxyphenyl)-pyrazole (**1**), -isoxazoles (**2**) and -thallium (II) (**3**) complexes derived from β -diketone which exhibit smectic phases over broad temperature [21,33]. Pyrazole and isoxazole derivatives directly linked with aryl group containing monoalkoxy terminal chain per phenyl ring exhibit SmA and SmC mesophases; whereas each aromatic ring substituted with two alkoxy chains per phenyl ring of pyrazole, isoxazole and thallium (II) complex does not show any liquid crystalline behaviour [33]. They also reported metallomesogens derived from pyrazole and β -diketone exhibiting columnar and lamellar phases [34].



1a, 2a, 3a, R = OC₈H₁₇
1b, 2b, 3b, R = OC₁₀H₂₁

Similar methodologies have been applied to prepare a variety of symmetrical and unsymmetrical isoxazole- based LCs [31,32]. Recently, Krówczyński et al. reported synthesis and mesomorphic characterisation of curcumin analogue of pyrazole (**4**), *N*-methylpyrazole (**5**) and isoxazole (**6**) derivatives [35].



4a; 5a; 6a. $R_1 = H$, $R_2 = OC_8H_{17}$, $R_3 = H$

4b; 5b; 6b. $R_1 = H$, $R_2 = OC_8H_{17}$, $R_3 = OCH_3$

4c; 5c; 6c. $R_1 = H$, $R_2 = OC_8H_{17}$, $R_3 = OC_8H_{17}$

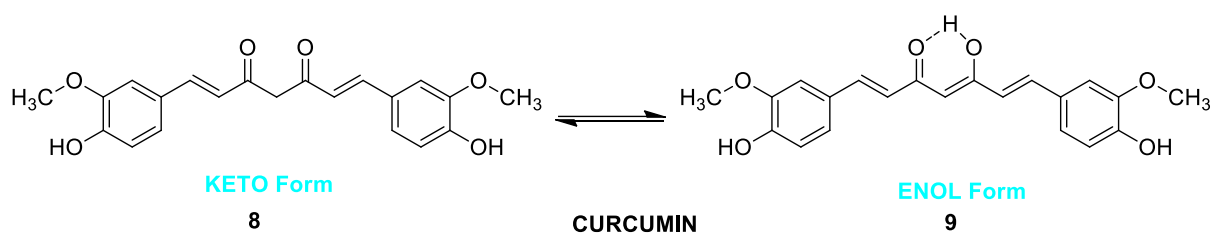
4d; 5d; 6d. $R_1 = OC_8H_{17}$, $R_2 = OC_8H_{17}$, $R_3 = OC_8H_{17}$

4e; 5e; 6e. $R_1 = H$, $R_2 = OC^*(H)(CH_3)C_6H_{13}$, $R_3 = H$

All the compounds in the series contain mono-, di- and tri substituted alkoxy chains at ortho, meta and para position of phenyl group. These alkoxy substituted rings are connected to central heterocyclic ring with ethylene spacer. For pyrazole or isoxazole derivatives containing one octyloxy chain at para position of each phenyl rings of elongated molecules exhibit lamellar (SmA, SmC) and nematic phases. XRD results confirm the formation of pyrazole dimer (**7**) that can be established by N-H-N hydrogen bonds. The compound exhibits Col_{hd} phase.

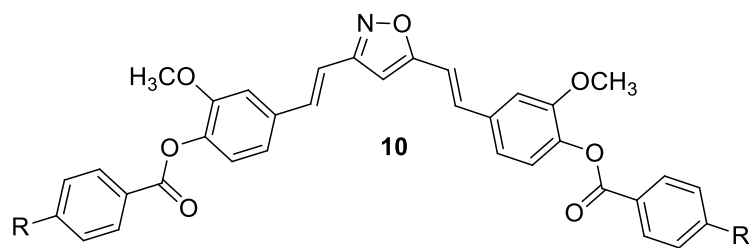
This chapter deals with the synthesis and mesomorphic properties of BC LCs obtained from naturally available curcumin. Curcumin is a natural medicinal compound and member of *Zingiberaceae* family, which can be isolated from the rhizome of *Curcuma longa L.* Curcumin is a highly pleiotropic molecule, which was first discovered for its biological activity in 1949 [36]. It is a symmetric molecule, also known as diferuloylmethane. The IUPAC name of curcumin is (1E,6E)-1,7-bis(4-hydroxy-3-methoxyphenyl)-1,6-heptadiene-3,5-dione. Curcumin belongs to the family of β -diketone, it retains three chemical entities in its structure: two aromatic ring

systems containing *o*-methoxy phenolic groups, connected by an ethylene spacer between guaiacol and an α,β -unsaturated β -diketone moiety, which is entrenched by stable six-membered cyclic keto-enol form through hydrogen bonding **8** & **9**. The keto-enol tautomerization present in curcumin is able to form different types of isomers depending on medium [37]. The chemistry of α,β -unsaturated β -diketone group can be further extended by cyclization to generate heterocyclic ring structure and the two phenyl rings having a free hydroxyl group at the para position to the ethylene spacer can be further modified through simple esterification with various acid derivatives.



2.2 Objective

Literature search revealed that most of the isoxazole derivatives are three-ring structures in which the central isoxazole unit is flanked by two substituted phenyl rings. Such three ring systems are not favourable for forming BC LCs [38]. However, they can be made five membered ring structures by attaching appropriately substituted phenyl groups on each side, which are most common molecular structures of BC LCs. The bent-core liquid crystals derived from curcumin having extended side wing on both side with ester linking group are not known in the literature. Therefore, the main objective of the present work is to synthesize novel BC LCs derived from isoxazole ring, evaluate their mesomorphic properties and establish structure-property relationship in these novel materials. The molecular structures **10a–10e** were designed to accomplish novel BC LCs.



10a: R = OC₆H₁₃

10b: R = OC₈H₁₇

10c: R = OC₁₀H₂₁

10d: R = OC₁₂H₂₅

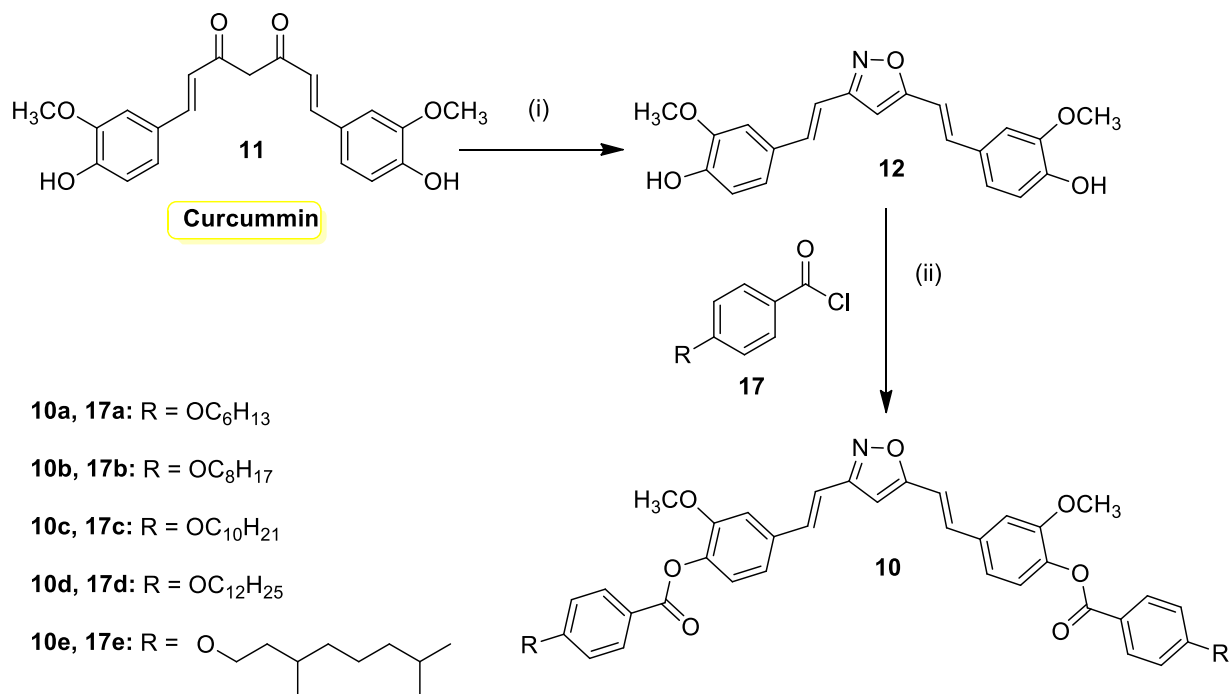
10e: R =

2.3 Results and discussion

2.3.1 Synthesis

The investigated mesogenic compounds were designed and synthesised as shown in **Scheme 1**. Condensation of β -diketone of curcumin **11** with hydroxylamine hydrochloride in presence of absolute ethanol and catalytic amount of glacial acetic acid under reflux condition furnished the cyclized isoxazole intermediate **12** in about 70% yield. Final isoxazole based mesogenic compounds were obtained by simple esterification reaction of intermediate isoxazole compound **12** with various 4-*n*-alkoxy benzoyl chlorides **17a–17e** in presence of catalytic amount of dry pyridine and anhydrous dichloromethane solvent. The intermediate acid chlorides (**17a–17e**) were synthesised from well known reported synthetic procedure.

Esterification of 4-hydroxy benzoic acid **13** in presence of absolute ethanol and catalytic amount of con. H₂SO₄ under reflux condition affords ester product **14**. O-alkylation of ethyl 4-hydroxybenzoate **14** with various alkyl bromide gives compound **15**. Hydrolysis of compound **15** gives corresponding acid derivative **16**, which on treating with oxalyl chloride in presence of catalytic amount of DMF gives 4-*n*-alkoxy benzoyl chloride derivatives (**17a–17e**). Five derivatives with varying number of terminal alkyl chains, including one branched alkyl chain was synthesised. The chemical structure of the all intermediate and final BC LCs was confirmed through spectral and elemental analysis and details of synthetic procedure are given in the experimental section. The mesogenic properties of all the isoxazole based BC LCs were investigated using POM, DSC and XRD studies.



Scheme 1. Synthesis of final BC mesogenic compounds. (i) NH₂OH.HCl, absolute EtOH, cat. CH₃COOH, 16 h, reflux, 70%; (ii) 4-*n*-alkoxybenzoyl chloride, cat. pyridine, anhydrous DCM, 24 h, r.t., 60%; (iii) Cat. Con. H₂SO₄, absolute EtOH, reflux, 85%; (iv) alkyl bromide, anhyd. K₂CO₃, dry DMF, reflux, 24 h; (v) NaOH, toluene/water, reflux, 6 h; (vi) oxalyl chloride, cat. DMF, DCM, r.t. 3 h.

2.3.2 Density functional theory calculations

Density functional theory based quantum chemical calculations have been performed in gaseous phase using Gaussian 16 computational package at the level of 6-311 G(d) basis set, Becke's three-parameter functional and Lee-Yang-Parr correlation functional (B3LYP) was employed to calculate molecular parameters such as bend angle and molecular length. The internal coordinates of the molecular system, which is used as input for Gaussian 16 computational program was generated by the Gauss View 06 program [39]. The absence of any imaginary frequency in the calculated vibrational frequencies ensures that the optimized geometry corresponds to a true energy minimum. DFT computational calculations revealed the energy and the length of fully extended stable bent-core mesogens. As a representative example in the series, the compound **10d** was carried out for DFT studies. The optimized energy of fully extended phenyl ring with dodecyloxy alkyl chain was found to be -3025.87 a.u and length of the molecules is 60.73 Å is shown in **Figure 1**. The dihedral angles between central and first phenyl rings with stilbene linkage, the first and second phenyl rings with ester linkage, the central and third phenyl rings with stilbene linkage and between the third and fourth phenyl rings with ester linkage are 178.56° , 175.88° , 178.55° and 173.29° , respectively, represents the coplanarity of the phenyl rings in the molecule. The DFT analysis shows that the bending angle is approximately 154.62° .

2.3.3 Thermal behaviour

The mesomorphic properties of all the novel mesogens (**10a–10e**) were investigated by POM and DSC studies. The phase transition temperature and corresponding enthalpy of phase transition for all the compounds (**10a–10e**) are summarized in **Table 1**. The onset temperature is given in $^\circ\text{C}$ and enthalpy of phase transition presented in parenthesis (ΔH in kJ mol^{-1}). All the bent-core mesogens exhibit enantiotropic mesophase with wide temperature range. The compounds **10a–10c** and **10e** show nematic phase on both heating and cooling scans, whereas compound **10d** having dodecyloxy terminal chain exhibit smectic C phase at lower temperature along with N phase at higher temperature.

Table 1. Thermal data of all the bent-core mesogens (**10a–10e**).

Compound	Phase transition (onset (°C) [ΔH (kJ mol ⁻¹)])
10a	Cr 163.8 [53.5] N 262.2 [1.3] I
10b	Cr 148.7 [66.2] N 259.7 [1.4] I
10c	Cr 125.1 [56.0] N 248.3 [0.8] I
10d	Cr 118.4 [45.7] SmC 168.0 [0.9] N 231.8 [1.5] I
10e	Cr 151.4 [48.9] N 208.3 [1.1] I

The liquid crystalline textures of all the compounds were viewed under POM with cross polarisers which reveal characteristic defect textures. The microscopic textures were recorded by placing small amount of sample on clean normal glass slide and cover with cover slip. The compounds **10a–10c** and **10e** exhibit enantiotropic nematic phase only, while compound **10d** shows SmC phase at lower temperature along with N phase at higher temperature on both heating and cooling scan. Upon heating under POM, the bent-core compound **10a** melts at around 164 °C and become isotropic liquid at 263 °C. The nematic droplets observed on slow cooling from isotropic liquid. The compound **10b** goes to isotropic liquid at 260 °C and upon slow cooling shows nematic droplets with two and four point brushes of nematic textures. The next higher homologous compound **10c** exhibits phase transition from crystalline phase to nematic phase at 125 °C and become isotropic liquid at 249 °C. Nematic textures were observed upon cooling from the isotropic phase. Similarly, compound **10e** having branched alkyl chain exhibits phase transition from crystal to nematic phase at 152 °C and nematic phase to isotropic phase at 209 °C. The two and four point brushes of nematic textures were observed under POM upon slow cooling from the isotropic liquid. The higher homolog **10d** exhibits enantiotropic mesophase. Upon cooling from the isotropic melt, typical schlieren textures of the nematic phase were observed. Nematic droplets were observed during early growing stage on cooling from the isotropic liquid. The POM textures of nematic phase recorded at 225 °C, as shown in **Figure 2a** & **2b**, viewed at 200 × magnifications. The dark area corresponds to isotropic liquid. Typical

schlieren texture is photographed at 178 °C on cooling from isotropic phase, as shown in **Figure 2c & 2d**, 100 × magnifications. Similar two and four point brushes of nematic textures were observed for all other bent-core mesogens. On further cooling from isotropic liquid to 168 °C, there is a significant change in texture from nematic schlieren texture to fan-like texture of smectic phase observed for this compound **10d**. To investigate the nature of this smectic phase, we used commercial available polyimide-coated cell (Instec Inc.) having 9 µm cell gap for planar alignment of the sample in the LC phases. The sample was filled uniformly in the LC cell at isotropic temperature. The sample, upon slow cooling from the nematic phase to lower temperature, shows significant changes in the texture, focal conic fan-like texture of smectic phase as shown in **Figure 3**. The early growing stage of SmC phase was photographed at 158 °C, viewed at 200 × magnifications as shown in **Figure 3a & 3b** and further cooling to down to 142 °C shows fully grown textures of smectic phase as shown in **Figure 3c & 3d**, viewed at 100 × magnifications. The dark brush pattern in the fan region of the texture appears at an angle with respect to the layer normal indicating a synclinal smectic C phase. Using polarised optical microscopy, the tilt angle of the molecules with respect to the layer normal was estimated to be about 50°, which agrees very well with the XRD investigations. Moreover, polarisation measurements using the triangular wave voltage technique indicate the absence of spontaneous polarizations in the layers. Thus, the smectic phase observed in compound **10d** is characterized as a calamitic (rod like) smectic C-type phase possibly due to the large bend angle in these molecules. Any light or thermal isomerisation involving carbon–carbon double bonds *cis–trans* isomerisation was also not observed.

The thermal behaviour of all the bent-core mesogens (**10a–10e**) were further investigated using DSC measurements on both heating and cooling scan rate of 5 °C min⁻¹ and recorded under a nitrogen atmosphere. The phase transition temperatures obtained for all the mesogens in DSC agree very well with POM observations. The bent-core mesogens **10a–10c** and **10e** exhibit exclusively two types of endothermic phase transition from crystalline phase to nematic phase at lower temperature and nematic phase to isotropic phase transition at higher temperature. However, compound **10d** shows an additional transition in between these two transitions, which confirms the stability of the enantiotropic smectic C phase between the nematic and crystal phase. The compound **10a** shows enantiotropic nematic phase over broad temperature. On heating, the onset temperature at 163.8 °C, with corresponding enthalpy change

(ΔH) at 53.5 kJ mol⁻¹ is constituted crystal to N phase at lower temperature and the onset temperature at 162.2 °C along with lower phase transition enthalpy value 1.3 kJ mol⁻¹ shows N phase to isotropic phase transition. The compound **10b** exhibits crystal to N phase at 147.7 °C ($\Delta H = 66.2$ kJ mol⁻¹) and N phase to isotropic phase transition at 148.7 °C ($\Delta H = 66.2$ kJ mol⁻¹). On other hand, the compound **10c** shows Cr to N phase at lower temperature 125.1 °C ($\Delta H = 56.0$ kJ mol⁻¹) and N phase to isotropic liquid at high temperature 248.3 °C ($\Delta H = 0.8$ kJ mol⁻¹). Similarly, compound **10e**, substituted with branched alkyl chain exhibits Cr to N phase at 151.4 °C ($\Delta H = 48.9$ kJ mol⁻¹) and N phase to isotropic temperature at 208.3 °C ($\Delta H = 1.1$ kJ mol⁻¹) respectively. A representative DSC thermogram obtained for compounds **10e** is shown in **Figure 4**. On both heating and cooling scan, the higher homologous compound **10d** in the series exhibits additional enantiotropic SmC phase transition in between crystalline phase and N phase respectively. The compound **10d** displayed Cr to SmC phase at 118.4 °C ($\Delta H = 45.7$ kJ mol⁻¹), SmC to N phase and N phase to isotropic phase at 168 °C ($\Delta H = 0.9$ kJ mol⁻¹), 231.8 °C ($\Delta H = 1.5$ kJ mol⁻¹) respectively as shown in **Figure 4**.

It is noticed that, all the bent-core mesogens (**10a–10e**) becomes crystalline phase upon keeping at room temperature for a few hours. The DSC measurements reveals the isotropic temperature of all the bent core mesogens are in range between 200 °C and 270 °C and a significant reduction of isotropic temperature could be achieved by using branched alkyl chains. The compound **10e** having branched alkyl chains exhibits isotropic temperature at 210 °C, which is 40 °C lower than corresponding straight alkyl chain derivative **10c** having equal number of carbon atoms.

A plot of transition temperature as a function of terminal alkyl chain derivatives is shown in **Figure 6**. From the graph, it can be clearly seen that melting point and nematic to isotropic phase transition temperatures of bent-core mesogens **10a–10d** decreases with increasing number of carbon atoms in the terminal alkyl chains. However, the compound **10e** with terminal branched chain shows random decrease in the isotropic temperature.

2.3.4 X-ray diffraction studies

In order to investigate the mesophase structure and hence supramolecular organisation of novel BC mesogens, X-ray diffraction studies are performed for all the compounds. As representative example, the XRD patterns obtained for compound **10d** in the nematic phase at 180 °C and SmC phase at 135 °C are shown in **Figure 7** and **8** respectively. The XRD profile recorded for compound **10d** in the nematic phase at 180 °C shows two significant characteristic peaks, a diffuse peak at small angle regime and another diffuse peak at wide angle region at $d = 4.54 \text{ \AA}$ typical of the nematic phase as shown in **Figure 7**. Similarly, the XRD pattern obtained for compound **10d** in the SmC phase at 135 °C is shown in **Figure 8**. From the XRD graph, two sharp peaks in the small angle regime with d -spacings 38.4 \AA (d_1) and 19.1 \AA (d_2) were observed along with diffuse wide-angle peak at 4.54 \AA . The two sharp peaks in the small-angle region are in the ratio of 1:1/2 in the wave number reveals the lamellar smectic-like packing of molecules in the mesophase. The first order layer spacing $d_1 = 38.4 \text{ \AA}$ in smectic phase is smaller than of the molecular length $l = 60.73 \text{ \AA}$, obtained by DFT calculations with terminal chains all in *trans* conformations and bend-angle is 154.62° . This suggested tilted organization of the molecules. The tilt angle, estimated from first order layer spacing and molecular length, using the relation $\cos\theta = d/l$ was found to be 51° , which agrees with POM textural observations.

2.4 Thermogravimetric analysis

The thermal stability of all the bent-core mesogens was investigated by thermogravimetric analysis. All the samples (**10a–10e**) were subjected to heat scan of $10 \text{ }^\circ\text{C min}^{-1}$ under a nitrogen atmosphere. All the mesogenic compounds show no weight loss till about $320 \text{ }^\circ\text{C}$ as shown in **Figure 9**. All the compounds initiate weight loss at about $350\text{--}435 \text{ }^\circ\text{C}$ and decomposes at $500 \text{ }^\circ\text{C}$. The decomposition temperatures for all the compounds were much higher than isotropic temperature. It concludes that all the mesogenic compounds possess good thermal stability.

2.5 Conclusions

In conclusion, we have prepared and characterized BC LCs derived from naturally occurring inexpensive curcumin. From DFT study, the bent-angle in these compounds was estimated to be around 155°. The lower homologous in the series show enantiotropic nematic phase over broad temperature range. XRD investigation suggested that a higher homologous exhibits tilted smectic C phase with fairly large tilt angle of 51° along with the nematic phase at high temperature. All the compounds show good thermal stability.

2.6 Experimental section

Curcumin is purchased from commercial source. The intermediate 4-*n*-alkoxybenzoyl chloride (**17a–17e**) was synthesised by following reported procedure published elsewhere.

2.6.1 General information

All the chemicals and reagents were AR-grade quality and purchased from Sigma-Aldrich and Spectrochem. The solvents used in reactions were dried and distilled using standard protocols prior to use. The monitoring, completion of the reactions and purity of all the compounds were primarily determined by thin layered chromatography (TLC, Merck make). The intermediate and final compounds were purified by column chromatography using silica gel 100–200 mesh for column chromatography as stationary phase. The molecular structure and purity of all compounds were established with the aid of data access from spectroscopic and elemental analysis methods. FT-IR spectra were recorded using Shimadzu – 8400 in Nujol liquid paraffin; only major peaks were reported in cm^{-1} (wave number). ^1H NMR were recorded on Bruker machine at 500 MHz and ^{13}C NMR at 125 MHz using deuterated chloroform (CDCl_3) as a solvent and chemical shifts are given in ppm relative to TMS as an internal standard (CDCl_3 : ^1H NMR $\delta = 7.23$ ppm; ^{13}C NMR = 77.0 ppm). The patterns (splitting or multiplicity) of the ^1H NMR signals are represented as s = singlet, d = doublet, t = triplet, m = multiplet and coupling constant are mentioned in Hz. Elemental analysis was carried out using Elementar Vario MICRO Select instrument. The microscopic textures were recorded on sample placed between ordinary glass slide using Olympus BX51 polarised optical microscope attached with a digital camera

(Olympus, Tokyo, Japan) in conjunction with Mettler FP82HT hot stage controlled by Mettler FP90 central processor. The phase transition temperature and associated enthalpy values for all the liquid crystalline compounds using 2–4 mg of samples were determined by METTLER TOLEDO DSC 3 STAR^e system with PC system operating on STAR^e software. Prior to the use, the instrument was calibrated using pure indium and zinc. DSC traces were recorded at scan rate of 5 °C min⁻¹ under continuous flow of nitrogen gas. X-ray diffraction studies were performed on powder samples in Lindemann capillaries with Cu K α ($\lambda = 1.54060 \text{ \AA}$) radiation using DY 1042-Empyrean (PANalytical) X-ray diffractometer comprising a programmable divergence slit and PIXcel 3D detector. Thermal stability of mesogens was obtained by using TGA 4000 thermogravimetric analysis instrument.

Synthesis of 4,4'-((1e,1'e)-isoxazole-3,5-diylbis(ethene-2,1-diyl))bis(2-methoxyphenol) (12)

In a two-neck round bottom flask containing curcumin **11** (2g, 5.42 mmol) in absolute ethanol (50 mL) was added catalytic amount of glacial acetic acid (1 mL). To this added hydroxylamine hydrochloride (3.99 g, 57.54 mmol) at room temperature. The resulted reaction mixture was refluxed for 8 hours. After completion of reaction, the solvent was removed completely under vacuum. The crude reaction mixture was quenched with ice cold water, then extracted with ethyl acetate (3 \times 40 mL) and washed with brine solution (1 \times 10 mL). The combined extracts were dried over Na₂SO₄ and concentrated under vacuum. The crude product was purified through column chromatography using silica gel (hexane/ethyl acetate 8:2) to afford cyclized intermediate isoxazole **12** as an off-white solid. Yield: 80%. m.p. 172 °C; IR (film) ν_{max} : 3498, 2955, 2926, 2854, 1643, 1633, 1606, 1573, 1512, 1462, 1454, 1433, 1377, 1269, 1234, 1211, 1155, 1118, 1039, 964, 825, 800, 732 cm⁻¹. ¹H NMR (500 MHz, CDCl₃): $\delta = 7.3$ – 6.8 (10 H, m); 6.42 (1 H, s); 5.79 (1 H, s); 5.77 (1 H, s); 3.96 (3 H, s); 3.95 ppm (3 H, s). ¹³C NMR (125 MHz, CDCl₃): $\delta = 168.5, 162.1, 146.9, 146.8, 146.8, 146.7, 135.6, 134.8, 128.7, 128.5, 128.2, 121.6, 115.8, 114.7, 113.8, 110.9, 108.7, 108.2, 97.6, 55.9, 55.9$ ppm; elemental analysis: C₂₁H₁₉NO₅; calculated: C, 69.03; H, 5.24; N, 3.83 %; found: C, 69.14; H, 5.50; N, 3.96. ¹H NMR and ¹³C NMR are presented in **Figure 10**.

Synthesis of ((1*e*,1'*e*)-isoxazole-3,5-diylbis(ethene-2,1-diyl))bis(2-methoxy-4,1-phenylene) bis(4-alkoxybenzoate) (10)

All the mesogenic compounds were synthesised by esterification reaction between 4,4'-((1*e*,1'*e*)-isoxazole-3,5-diylbis(ethene-2,1-diyl))bis(2-methoxyphenol) (**12**) with 4-*n*-alkoxybenzoyl chloride (**17a–17e**) in presence of catalytic amount of anhydrous pyridine and dichloromethane solvent. The general method is described as follows.

To a stirring solution of isoxazole **12** (0.53g, 1.45 mmol) in dry DCM (30 mL) solvent was added catalytic amount of pyridine (1 mL) at room temperature. To this, added drop wise solution of 4-*n*-alkoxybenzoyl chloride (**17a–17e**) (3.62 mmol) in dry DCM (15 mL) at 0 °C. The resulted reaction mixture was kept stirring at room temperature for 24 hours. At the end of the reaction, ice cold water (200 mL) was added and the solution was extracted with DCM (3 × 50 mL). The combined extracts were dried over Na₂SO₄ and concentrated under vacuum. The crude compound was purified by column chromatography using silica gel (hexane/dichloromethane 1:1). Further, recrystallization of pure compound with chloroform: hexane (1:9) gives white colour solid in about 60% yield.

Compound 10a. IR (film) ν_{\max} : 2955, 2924, 2852, 1730, 1643, 1604, 1510, 1454, 1377, 1313, 1249, 1203, 1161, 1118, 1064, 962, 846 cm⁻¹. ¹H NMR (500 MHz, CDCl₃): δ = 8.08 (4 H, d, *J* = 8.5 Hz), 7.3–6.9 (14 H, m), 6.44 (1 H, s), 3.98 (4 H, t, *J* = 6.5 Hz), 3.81 (6 H, s), 1.75 (4 H, m), 1.42–1.18 (12 H, m), 0.85 ppm (6 H, t, *J* = 6.5 Hz); ¹³C NMR (125 MHz, CDCl₃): δ = 167.2, 163.4, 162.5, 160.9, 150.7, 140, 134.2, 133.7, 131.4, 122.5, 120.2, 119.1, 115.2, 113.3, 112.1, 109.8, 97.5, 67.3, 55, 30.5, 28, 24.6, 21.5, 12.9 ppm; elemental analysis: C₄₇H₅₁NO₉; calculated: C, 72.94; H, 6.64; N, 1.80; % found: C, 72.69; H, 6.39; N, 1.82.

Compound 10b. IR (film) ν_{\max} : 2953, 2922, 2852, 1732, 1604, 1514, 1462, 1454, 1377, 1298, 1251, 1203, 1163, 1120, 1064, 935, 846 cm⁻¹. ¹H NMR (500 MHz, CDCl₃): δ = 8.16 (4 H, d, *J* = 8.5 Hz), 7.4–7.0 (14 H, m), 6.51 (1 H, s), 4.06 (4 H, t, *J* = 6.5 Hz), 3.88 (6 H, s), 1.75 (4 H, m), 1.49–1.25 (20 H, m), 0.89 ppm (6 H, t, *J* = 6.5 Hz); ¹³C NMR (125 MHz, CDCl₃): δ = 168.2, 164.4, 163.6, 161.9, 151.8, 141, 135.2, 134.7, 134.4, 132.4, 123.5, 121.2, 120.1, 116.2, 114.3,

113.1, 110.8, 110.3, 98.5, 68.3, 56, 31.8, 29.3, 26, 22.6, 14.1 ppm; elemental analysis: $C_{51}H_{59}NO_9$; calculated: C, 73.80; H, 7.16; N, 1.68; % found: C, 73.62; H, 6.83; N, 1.79. 1H NMR and ^{13}C NMR are presented in **Figure 11**.

Compound 10c. IR (film) ν_{max} : 2955, 2924, 2854, 1735, 1604, 1512, 1462, 1454, 1377, 1296, 1255, 1201, 1163, 1120, 1078, 936, 846 cm^{-1} . 1H NMR (500 MHz, $CDCl_3$): δ = 8.16 (4 H, d, J = 8.5 Hz), 7.39–6.93 (14 H, m), 6.51 (1 H, s), 4.06 (4 H, t, J = 6.5 Hz), 3.88 (6 H, s), 1.75 (4 H, m), 1.49–1.25 (28 H, m), 0.89 ppm (6 H, t, J = 6.5 Hz); ^{13}C NMR (125 MHz, $CDCl_3$): δ = 168.2, 164.4, 163.5, 161.9, 151.7, 141, 135.2, 134.7, 134.4, 132.4, 123.5, 121.2, 120.1, 116.2, 114.3, 113.1, 110.7, 110.3, 98.57, 68.3, 56, 31.9, 29.5, 29.3, 29.1, 25.9, 22.6, 14.1 ppm; elemental analysis: $C_{55}H_{67}NO_9$; calculated: C, 74.55; H, 7.62; N, 1.58; % found: C, 74.76; H, 7.74; N, 1.62. 1H NMR and ^{13}C NMR are presented in **Figure 12**.

Compound 10d. IR (film) ν_{max} : 2955, 2924, 2852, 1730, 1647, 1606, 1505, 1456, 1419, 1377, 1259, 1205, 1163, 1120, 1064, 962, 842 cm^{-1} . 1H NMR (500 MHz, $CDCl_3$): δ = 8.16 (4 H, d, J = 8.5 Hz), 7.39–6.93 (14 H, m), 6.51 (1 H, s), 4.05 (4 H, t, J = 6.5 Hz), 3.88 (6 H, s), 1.82 (4 H, m), 1.49–1.25 (36 H, m), 0.89 ppm (6 H, d, J = 6.5 Hz); ^{13}C NMR (125 MHz, $CDCl_3$): δ = 168.2, 164.4, 163.3, 161.9, 151.8, 141, 135.2, 134.7, 134.5, 132.4, 123.5, 121.2, 120.1, 116.2, 114.3, 113.1, 110.8, 110.3, 98.5, 68.3, 56, 31.9, 29.7, 29.6, 29.5, 29.3, 29.1, 26, 22.7, 14.1; elemental analysis: $C_{59}H_{75}NO_9$; calculated: C, 75.21; H, 8.02; N, 1.48; % found: C, 75.40; H, 7.85; N, 1.53.

Compound 10e: IR (film) ν_{max} : 2955, 2924, 2852, 1730, 1726, 1604, 1512, 1462, 1454, 1377, 1315, 1253, 1163, 1120, 1062, 962, 846 cm^{-1} . 1H NMR: (500 MHz, $CDCl_3$) δ = 8.16 (4 H, d, J = 8.5 Hz), 7.38–6.92 (14 H, m), 6.51 (1 H, s), 4.06 (4 H, m), 3.88 (6 H, s), 1.86–1.15 (20 H, m), 0.96 (6 H, t, J = 6.5 Hz), 0.88 ppm (12 H, t, J = 6.5 Hz); ^{13}C NMR (500 MHz, $CDCl_3$): δ = 168.2, 164.4, 163.5, 161.9, 151.8, 141, 135.2, 134.7, 134.4, 132.4, 123.5, 121.3, 120.1, 116.2, 113.1, 110.8, 110.3, 98.5, 56, 39.2, 37.2, 36, 29.8, 27.9, 24.6, 22.7, 19.6 ppm; elemental analysis: $C_{55}H_{67}NO_9$; calculated: C, 74.55; H, 7.62; N, 1.58; % found: C, 74.35; H, 7.67; N, 1.67.

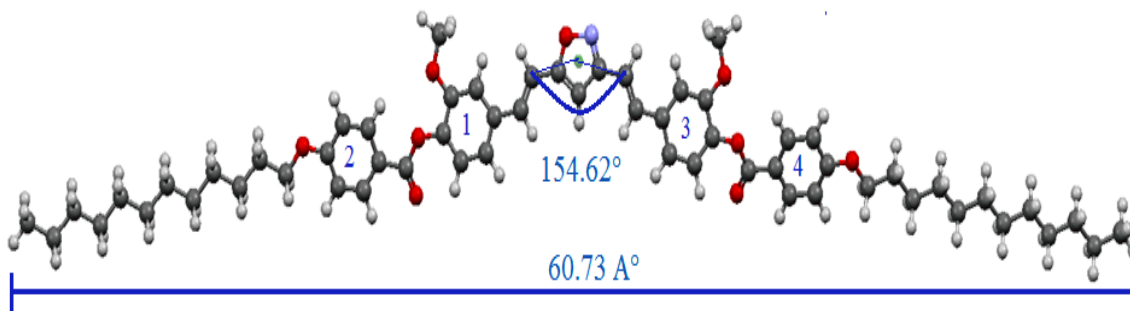


Figure 1. DFT optimized molecular structure (ball and stick model) of compound **10d**.

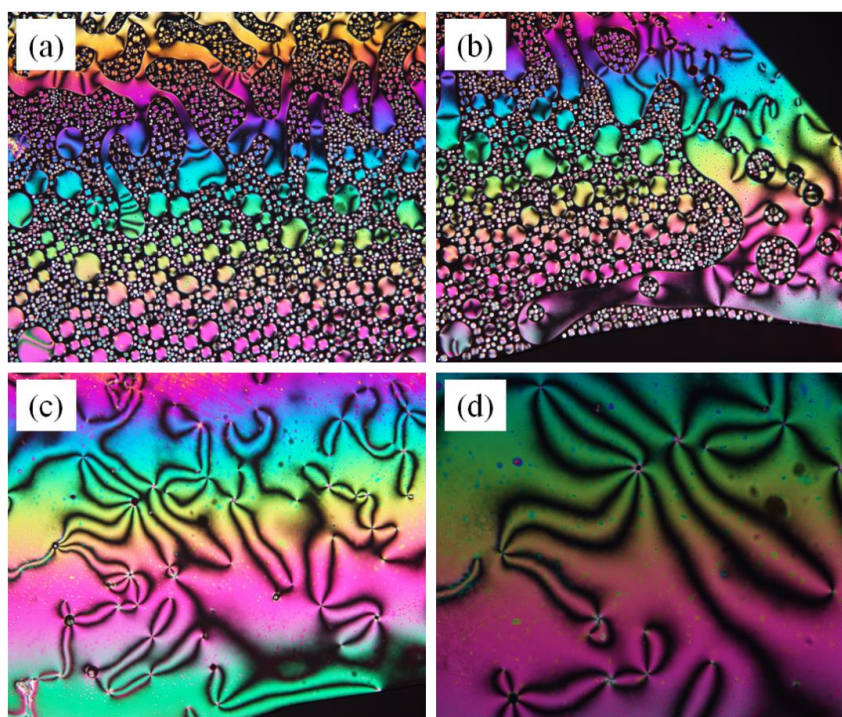


Figure 2. POM textures of compound **10d**: (a) and (b) nematic droplets observed during early growing stage after cooling from isotropic liquid, recorded at 225 °C (dark area are isotropic liquid), (c) and (d) complete nematic texture after further cooling to 178 °C. Sample were sandwiched between untreated glass slides and viewed through crossed polarizers.

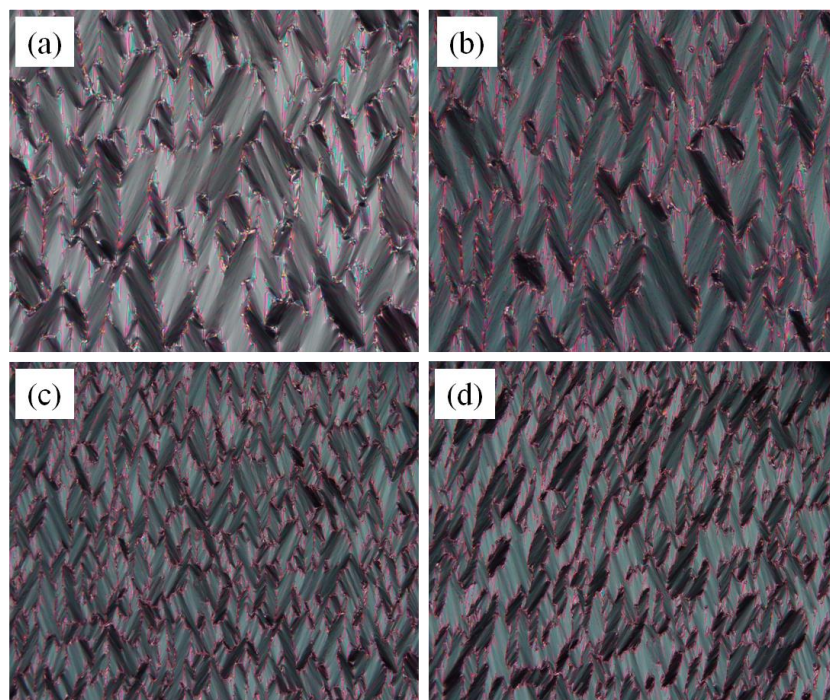


Figure 3. POM textures of compound **10d** shows SmC phase. Sandwiched between 9 μm polyimide-coated cell and viewed through cross-polariser, cooling from nematic phase. (a) and (b) early growing stage of SmC phase at 158 $^{\circ}\text{C}$. (c) and (d) complete texture at 142 $^{\circ}\text{C}$.

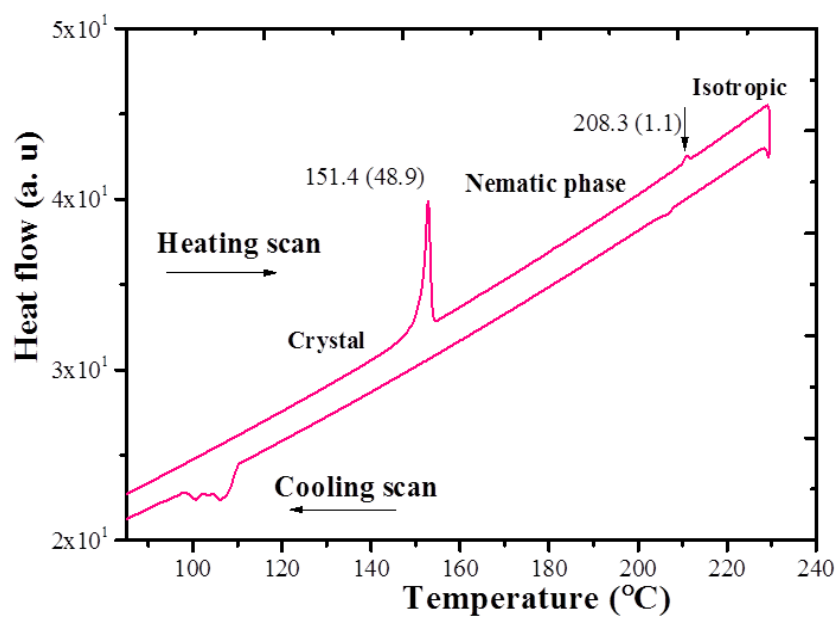


Figure 4. DSC thermogram of compound **10e**.

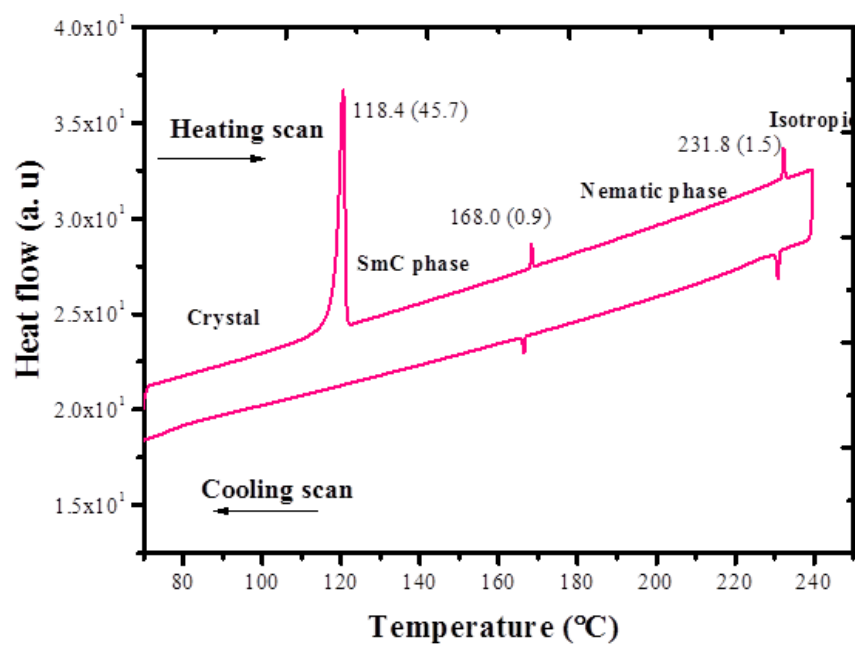


Figure 5. DSC thermogram of compound 10d.

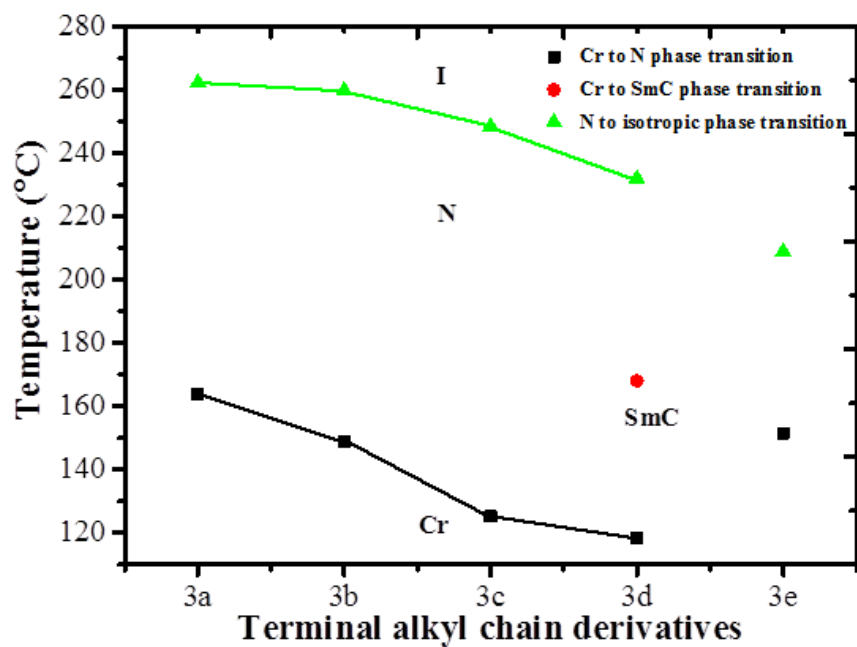


Figure 6. Graphical presentation of the thermal behaviour of compounds 10a–10e.

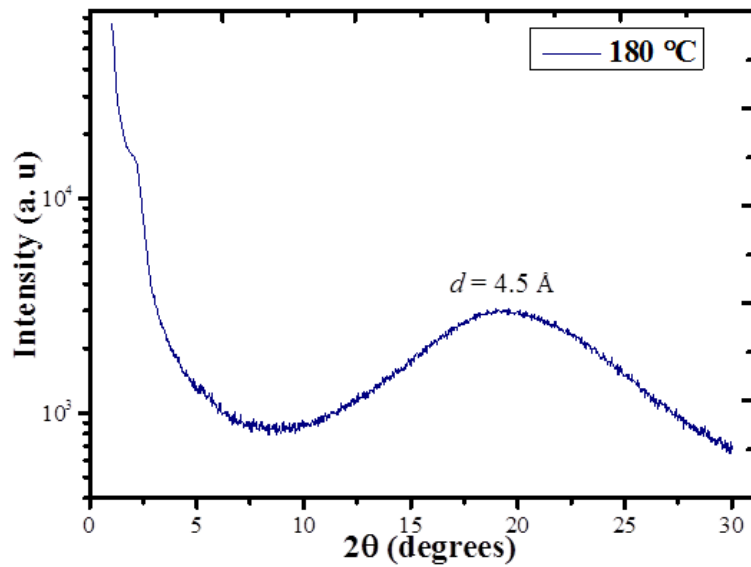


Figure 7. The XRD pattern obtained for compound **10d** at 180 °C in the nematic phase.

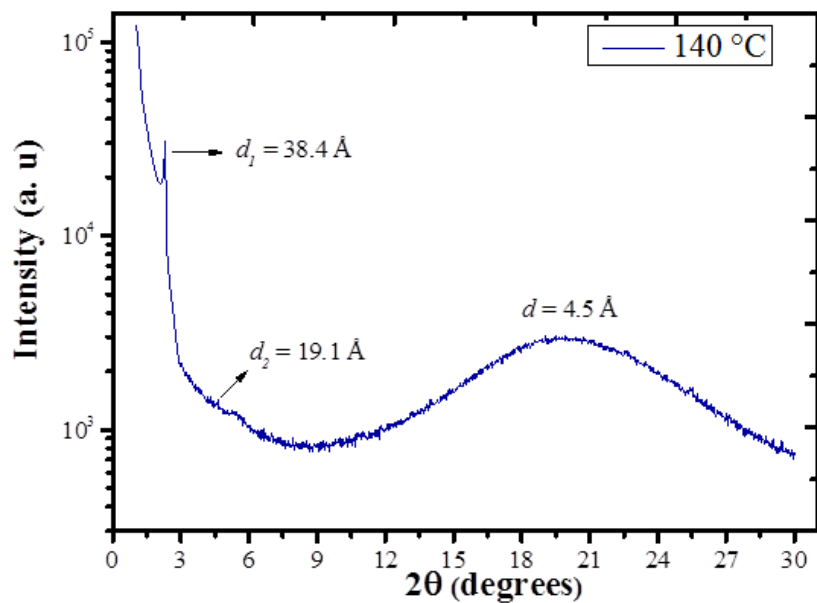


Figure 8. The XRD pattern obtained for compound **10d** at 140 °C in the SmC phase.

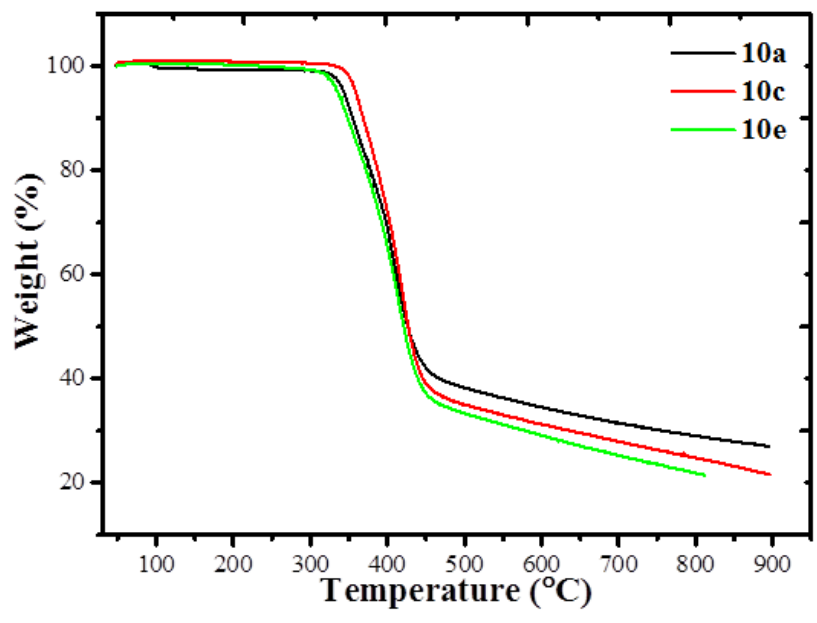


Figure 9. Thermogravimetric studies of **10a**, **10c** and **10e** compounds.

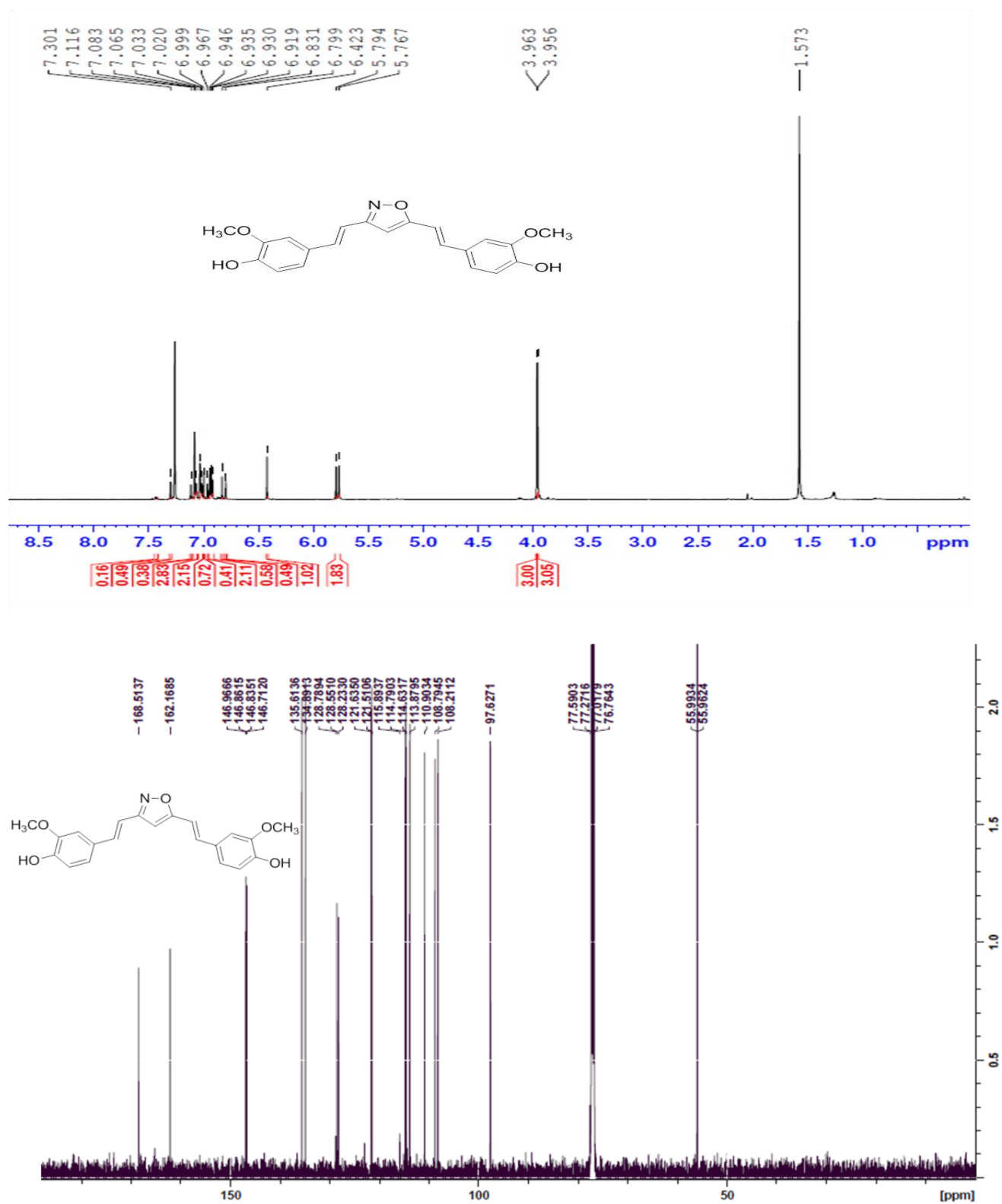


Figure 10. ¹H and ¹³C NMR spectrum of compound 12.

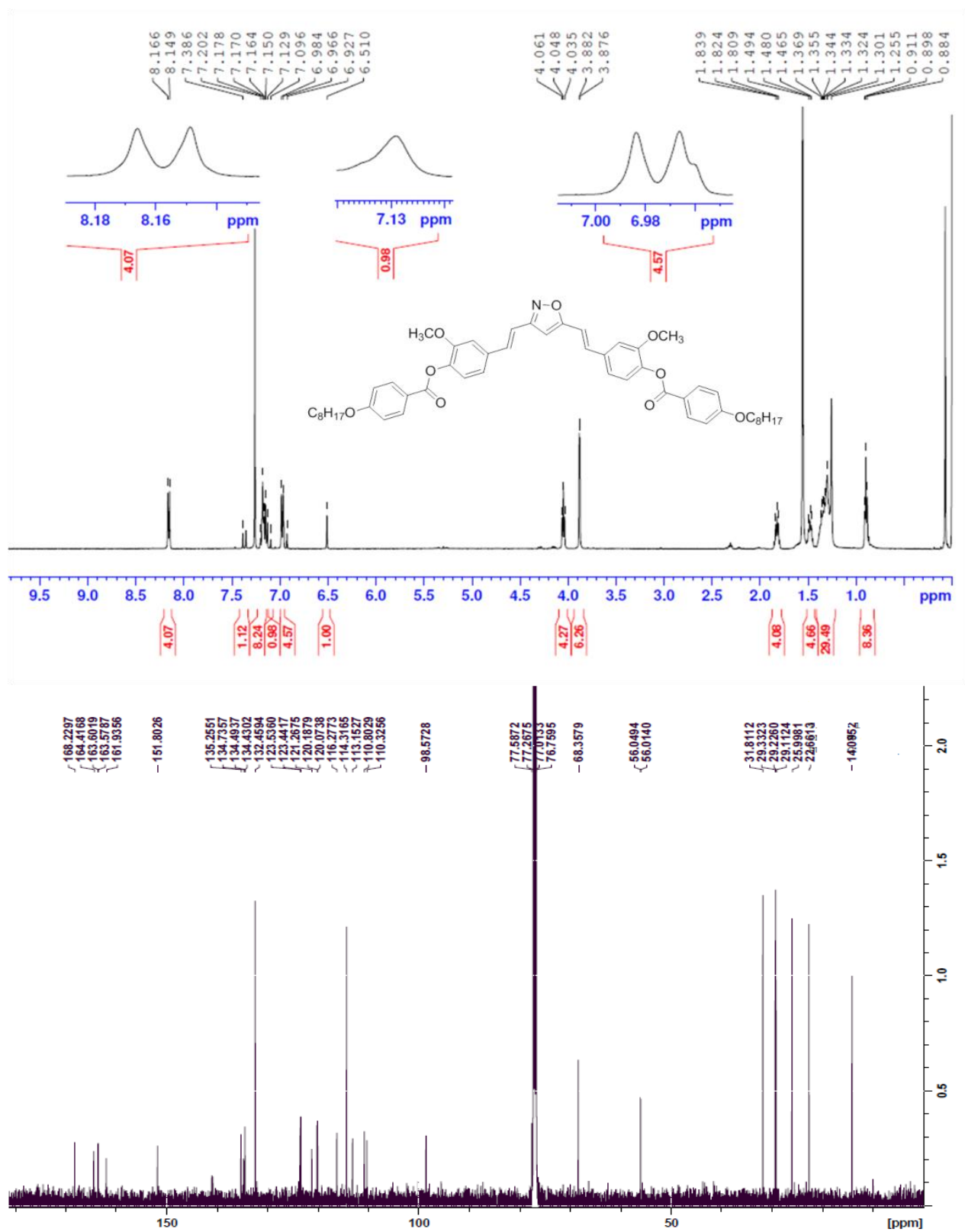


Figure 11. ¹H and ¹³C NMR spectrum of compound **10b**.

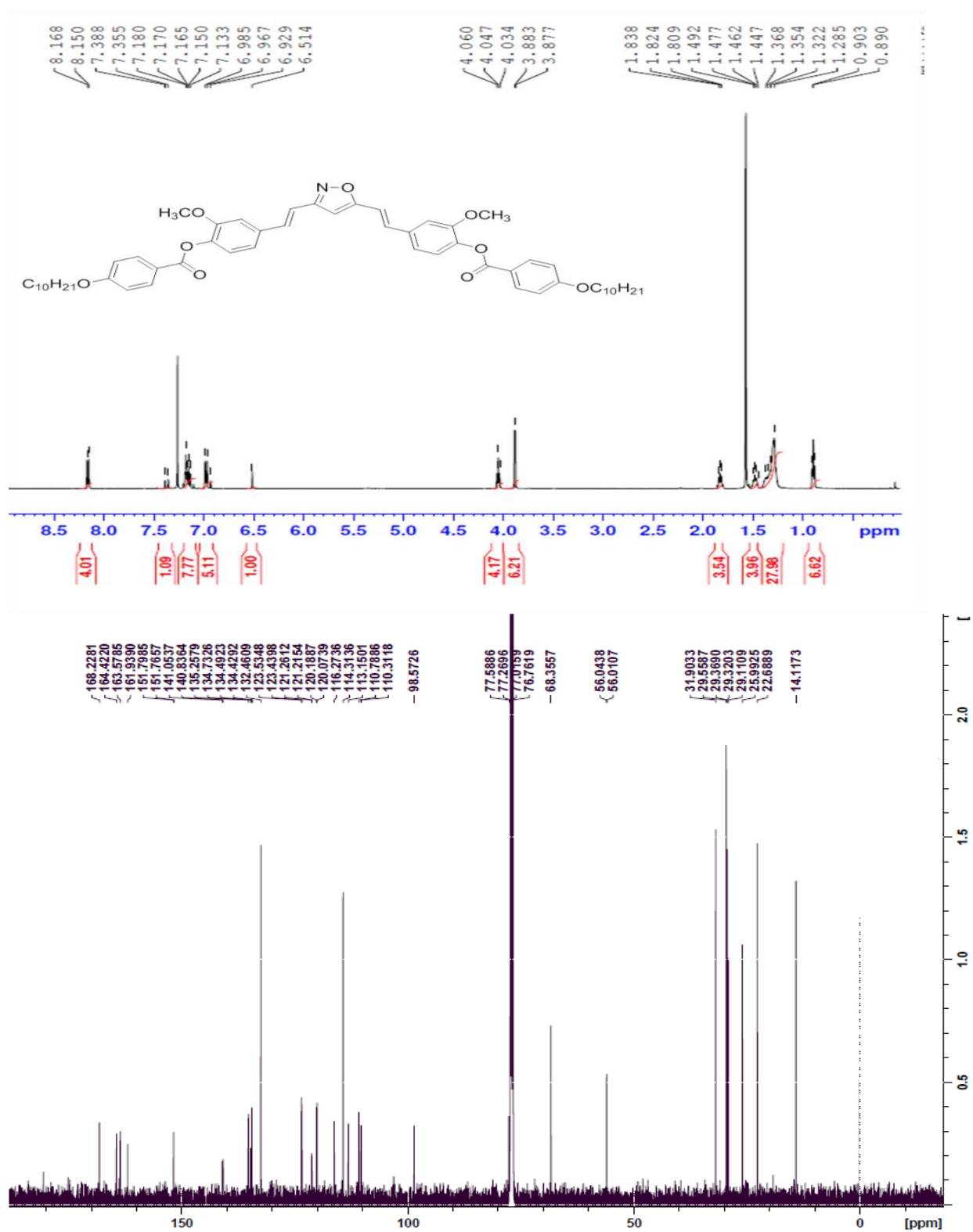


Figure 12. ¹H and ¹³C NMR spectrum of compound **10c**.

References

- [1] (a) Vorländer D, Fuchs K, Katscher E. E. *Ber. Dtsch. Chem Ges.*, **1929**, 62, 2381–2386; (b) D. Vorländer and A. Apel. *Ber. Dtsch. Chem. Ges.*, **1932**, 65, 1101
- [2] (a) Matsunaga Y, Miyamoto S. *Mol. Cryst. Liq. Cryst.*, **1993**, 237, 311–317; (b) Matsuzaki H, Matsunaga Y. *Liq. Cryst.*, **1993**, 14, 105–120.
- [3] (a) Niori T, Sekine T, Watanabe J, et al. *J. Mater. Chem.*, **1996**, 6, 1231–1233; (b) Niori T, Sekine T, Watanabe J, et al. *Mol. Cryst. Liq. Cryst. Sci. Technol.*, **1997**, 301, 337–342.
- [4] (a) Link D. R, Natale G, Shao R, et al. *Science.*, **1997**, 278, 1924–1927; (b) Heppke G, Moro D. *Science.*, **1998**, 279, 1872.
- [5] Weissflog W, Lischka C. H, Benne I, Schare T, et al. In Proceedings of the European Conference on Liquid Crystals, Science and Technology, Zaopane: Poland, **1997**, March 3–8, pp 126–132.
- [6] (a) Pelzl G, Diele S, Weissflog W. *Adv Mater.*, **1999**, 11, 707–724; (b) Tschierske C, Dantlgraber G. *Pramana.*, **2003**, 61, 455–481; (c) Ros M. B, Serrano J. L, Fuente M. R, et al. *J. Mater. Chem.*, **2005**, 15, 5093–5098
- [7] (a) Takezoe H, Takanishi Y. *Jpn. J. Appl. Phys.*, **2006**, 45, 597–625; (b) Reddy A. R, Tschierske C. *J. Mater. Chem.*, **2006**, 16, 907–961; (c) Weissflog W, Murthy S. N. H, Diele S, et al. *Phil. Trans. R. Soc. A.*, **2006**, 364, 2657–2679.
- [8] (a) Etxebarria J, Ros M. B. *J. Mater. Chem.*, **2008**, 18, 2919–2926; (b) Goodby J. W, Saez I. M, Cowling S. J, et al. *Angew. Chem. Int. Ed.*, **2008**, 47, 2754–2787; (c) Lin S-C, Ho R-M, Chang C-Y, et al. *Chemistry – Eur J.*, **2012**, 18, 9091–9098; (d) Eremin A, Jáklí A. *Soft. Matt.*, **2012**, 9, 615–637.
- [9] (a) Shen D, Diele S, Wirt I, Tschierske C. *Chem. Commun.*, **1998**, 2573–2574; (b) Shen D, Pegenau A, Diele S, Wirth I, Tschierske C. *J. Am. Chem. Soc.*, **2000**, 122, 1593–1601; (c) Takanishi Y, Takezoe H, Fukuda A. *Phys. Rev. B.*, **1992**, 45, 7684–7689.
- [10] (a) Takanishi Y, Takezoe H, Fukuda A. et al. *J. Mater. Chem.*, **1992**, 2, 71–73; (b) Takanishi Y, Toshimitsu M, Nakata M. et al. *Phys. Rev. E.*, **2006**, 74, 051703-1–051703-10.; (c) Takezoe H. *Top. Curr. Chem.*, **2012**, 318, 303–330.

- [11] (a) Görtz V, Goodby J. W, *Chem. Commun.*, **2005**, 3262; (b) Lehmann M, Köhn C, Kresse H, Vakhovskaya Z, *Chem. Commun.* 2008, 1768; (c) Martin P. J, Bruce D. W, *Liq. Cryst.* 2007, **34**, 767.
- [12] (a) Choi S.-W, Kang S, Takanishi Y, Ishikawa K, et al. *Chirality.*, 2007, **19**, 250; (b) Apreutesei D, Mehl G. H, *J. Mater. Chem.*, **2007**, 17, 4711; (c) Southern C. D, Brimicombe P. D, Siemianowski S. D, Jaradat S, et al. *Eur. Phys. Lett.*, **2008**, 82, 56001.
- [13] (a) Xiang Y, Goodby J. W, Görtz V, Gleeson H. F. *Appl. Phys. Lett.*, **2009**, 94, 193507; (b) Shanker G, Prehm M, Nagaraj M, et al. *ChemPhysChem.*, **2014**, **15**, 1323–1335; (c) Han J. *J. Mater. Chem. C.*, **2013**, 1, 7779–7797.
- [14] (a) Lehmann M, Seltmann J, Auer A. A, et al. *J. Mater. Chem.*, **2009**, 19, 1978–1988; (b) Campbell N. L, Duffy W. L, Thomas G. I, et al. *J. Mater. Chem.*, **2002**, 12, 2706–2721; (c) Seltmann J, Marini A, Mennucci B, et al. *Chem. Mater.*, **2011**, 23, 2630–2636.
- [15] (a) Gleeson H, Kaur S, Gortz V, et al. *ChemPhysChem.*, **2014**, 15, 1251–1260; (b) Jakli A. *Liq. Cryst. Rev.*, **2013**, 1, 65–82; (c) Gortz V. *Liq. Cryst. Today.*, **2010**, 19, 37–48.
- [16] (a) Shen D, Diele S, Pelzl G, et al. *J. Mater. Chem.*, **1999**, 9, 661–672; (b) Luckhurst G. *Angew. Chem. Int. Ed.*, **2005**, 44, 2834–2836; (c) Dingemans T, Madsen L, Francescangeli O, et al. *Liq. Cryst.*, **2013**, 40, 1655–1677; (d) Weissflog W, Baumeister U, Tamba M-G, et al. *Soft Matter.*, **2012**, 8, 2671–2685.
- [17] (a) Weissflog W, Baumeister U. *Liq. Cryst.*, **2013**, 40, 959–967; (b) Alaasar M, Tschierske C, Prehm M. *Liq. Cryst.*, **2011**, 38, 925–934; (c) Matraszek J, Mieczkowski J, Szydłowska J, et al. *Liq Cryst.*, **2000**, 27, 429–436.
- [18] Upadhyaya K, Gude V, Mohiuddin G, et al. *Beilstein J Org Chem.*, **2013**, 9, 26–35; (b) Debnath S, Mohiuddin G, Turlapati S, et al. *Dyes Pigments.*, **2013**, 99, 447–455; (c) Metrangolo P, Prasang C, Resnati G, et al. *Chem. Commun.*, **2006**, 3290–3292.
- [19] Lee SK, Li X, Kang S, et al. *J. Mater. Chem.*, **2009**, 19, 4517–4522; (b) Wang H, Zheng Z, Shen D. *Liq Cryst.*, **2012**, 39, 99–103; (c) Dingemans T.J, Samulski E.T. *Liq. Cryst.*, **2000**, 27, 131–136.
- [20] (a) Apreutesei D, Mehl GH. *J. Mater. Chem.*, 2007, 17, 4711–4715; (b) Speetjens F, Lindborg J, Tauscher T, LaFemina N. et. al. *J. Mater. Chem.*, **2012**, 22, 22558–22564; (c) Kozhevnikov VN, Whitwood AC, Bruce DW. *Chem. Commun.* **2007**, 3826–3828.

- [21] (a) Silfirski P. *Acta. Biochim. Pol.*, **2012**, 59, 201–212; (b) Serrano J. L, Sierra T. Metallomesogens, synthesis, properties and applications. Serrano JL, editor. Chapter 3. Weinheim: Wiley-VCH Verlag GmbH; **1996**.
- [22] (a) Lai C. K, Ke Y, Chien-Shen J. S, et al. *Liq. Cryst.*, **2002**, 29, 915–920; (b) Mayoral M. J, Ovejero P, Campo J. A, Heras J. V, et al. *Dalton. Trans.*, **2008**, 6912–6924; (c) Cavero E, Uriel S, Romero P, Serrano J. L, et al. *J. Am. Chem. Soc.*, **2008**, 129, 11608–21161.
- [23] (a) Gimnez R, Elduque A, Lopez J. A, Barbera J, et al. *Inorg. Chem.*, **2006**, 45, 10363–10370; (b) Torralba M. C, Campo J. A, Heras J. V, Bruce D. W, et al. *Dalton. Trans.*, **2006**, 3918–3926; (c) Torralba M. C, Cano M, Campo J. A, Heras J. V, et al. *Inorg. Chem. Commun.*, **2006**, 9, 1271–1275.
- [24] (a) Torralba M. C, Cano M, Campo J. A, Heras J. V, et al. *J. Organomet. Chem.*, **2006**, 691, 765–778; (b) Rasika D. H. V, Diyabalanage H. V. K. *Polyhedron.*, **2006**, 15, 1655–1661; (c) Li Y-L, Lee G-H, Lai C-K tetrahedron. **2015**, 71, 5296–5307.
- [25] (a) Mohamed A. A, Perez L. M, Fackler J. P. *J. Inorg. Chim. Acta.*, **2005**, 358, 1657–1662; (b) Soria L, Ovejero P, Cano M, Campo J. A. et al. *Dyes. Pig.*, **2014**, 110, 159–168; (c) Cuerva C, Campo J. A, Ovejero P, Torres M. R, et al. *Dalton. Trans.*, **2014**, 43, 8849–8860.
- [26] (a) Kishiura A, Yamashita T, Aida T. *J. Am. Chem. Soc.*, **2005**, 127, 179–183; (b) Gimnez R, Manrique A. B, Uriel S, Barbera J, et al. *Chem. Commun.*, **2004**, 2064–2065; (c) Vieira A. A, Bryk F. R, Conte G. et al. *Tetrahedron Lett.*, **2009**, 50, 905–908.
- [27] (a) Brown D. H, Styring P. *Liq. Cryst.*, **2003**, 30, 23–30; (b) Bezborodov V. S, Kauhanka N. N, Lapanik V. I. *Liq. Cryst.*, **2003**, 30, 579–583; (c) Seed, A. *Chem. Soc. Rev.* 2007, **36**, 2046–2069.
- [28] (a) Picken S. J, Dingemans T. J, Madsen L. A, Francescangeli O, et al. *Liq. Cryst.*, **2012**, 39, 19–21; (b) Prajapati A. K, Modi V. *Liq. Cryst.*, **2011**, 38, 191–199; (c) Bates M. A. *Chem. Phys. Lett.*, **2007**, 437, 189–192.
- [29] (a) Acharya B. R, Primak A, Dingemans T. J, Samulski E. T, et al. *Pramana- J. Phys.*, **2003**, 61, 231–237; (b) Lin H. Y, Kuo H. M, Wen S. G, Sheu H. S, et al. *Tetrahedron*. 2012, **68**, 6231–6239; (c) Chen M. C, Lee S. C. et al. *Tetrahedron*. **2009**, 65, 9460–9467.

- [30] (a) Chou S. Y, Chen C. J, Tsai S. L, Sheu H. S, et al. *Tetrahedron.*, **2009**, 65, 1130–1139; (b) Shen W. C, Wang Y. J, Cheng K. L, Lee G. H, et al. *Tetrahedron.*, **2006**, 62, 8035–8044; (c) Lu L. Y, Kuo H. et al. *Tetrahedron.*, **2014**, 70, 5999–6011.
- [31] (a) Fritsch L, Merlo A. A. *ChemistrySelect.*, **2016**, 1, 23–29; (b) Bartulin J, Martinez R, Gallardo H, et al. *Mol. Cryst. Liq. Cryst.*, **1993**, 225, 175–182; (c) Gallardo H, Bryk F. R, Vieira A. A, et al. *Liq. Cryst.*, **2009**, 839–845; (d) Tanaka M, Haino T, Ideta K, Kubo K, et al. *Tetrahedron.*, **2007**, 63, 652–665.
- [32] (a) Silva L, Gallardo H, Magnago R. F, Begnini I. K. *Mol. Cryst. Liq. Cryst.*, **2005**, 432, 1–13; (b) Haino T, Tanaka M, Ideta K, Kubo K, et al. *Tetrahedron.* 2004, **45**, 2277–2279; (c) Gallardo H, Zucco C, Silva, U. D. *Mol. Cryst. Liq. Cryst.*, **2002**, 373, 181–190; (d) Iglesias R, Serrano J. L, Sierra T. *Liq. Cryst.*, **1997**, 22, 37–46; (e) Kuo H. M, Tsai S. L, Lee G. H, Sheu H. S, et al. *Tetrahedron.*, **2013**, 69, 618–626.
- [33] Barbera J, Cativiela C, Serrano J. L, et al. *Liq Cryst.*, **1992**, 11, 887–897.
- [34] (a) Beltrán E, Cavero E, Barberá J, Serrano J. L, et al. *Chem. Eur. J.*, **2009**, 15, 9017–9023; (b) Barberá J, Giménez R, Serrano J. L. *Chem. Mater.*, **2000**, 12, 481–489.
- [35] Krówczyński A, Zep A, Kuć K, et al. *Liq. Cryst.*, **2014**, 41, 685–693.
- [36] (a) Sharma R. A, Gescher A. J, Steward W. P. *Eur. J. Cancer.*, **2005**, 41, 1955–1968; (b) Schraufstatter E, Bernt H. *Nature.*, **1949**, 164, 456; (c) Aggarwal B.B, Kumar A, Bharti A.C. *Anticancer Res.*, **2003**, 23, 363–398.
- [37] (a) Weissflog W. *Liq. Cryst.*, **2011**, 38, 1081–1083; (b) Weissflog W, Baumeister U, Tamba M-G, et al. *Soft Matter.*, **2012**, 8, 2671–2685.
- [38] (a) Wilken R, Veena S. M, Wang M. B, etc al. *Mol. Cancer.*, **2011**, 10, 1–19; (b) Venkata R. E. Sudheer P. *Indian J. Pharm. Sci.*, **2011**, 73, 262–270; (c) Grykiewicz G, Silfirski P. *Acta. Biochim. Pol.*, **2012**, 59, 201–212; (d) Esatbeyoglu T, Huebbe P, Ernst I. M. A, Chin D, et al. *Angew. Chem. Int. Ed.*, **2012**, 51, 5308–5332.
- [39] Frisch M. J. et al., Gaussian 16, Gaussian, Inc., Wallingford, CT, 2017

Chapter 3

Novel EDOT- based bent-core and hockey stick mesogens

3.1 Part A. Synthesis and characterisation of EDOT-based bent-core liquid crystals containing alkyne-linkage

3.2 Part B. Synthesis and characterisation of EDOT-based bent-core liquid crystals containing Schiff-base linkage

3.3 Part C. Synthesis, characterization and physical studies of EDOT based bent-core and hockey-stick like liquid crystals

3.1 Part A. Synthesis and characterisation of EDOT-based bent-core liquid crystals containing alkyne-linkage

3.1.1 Introduction

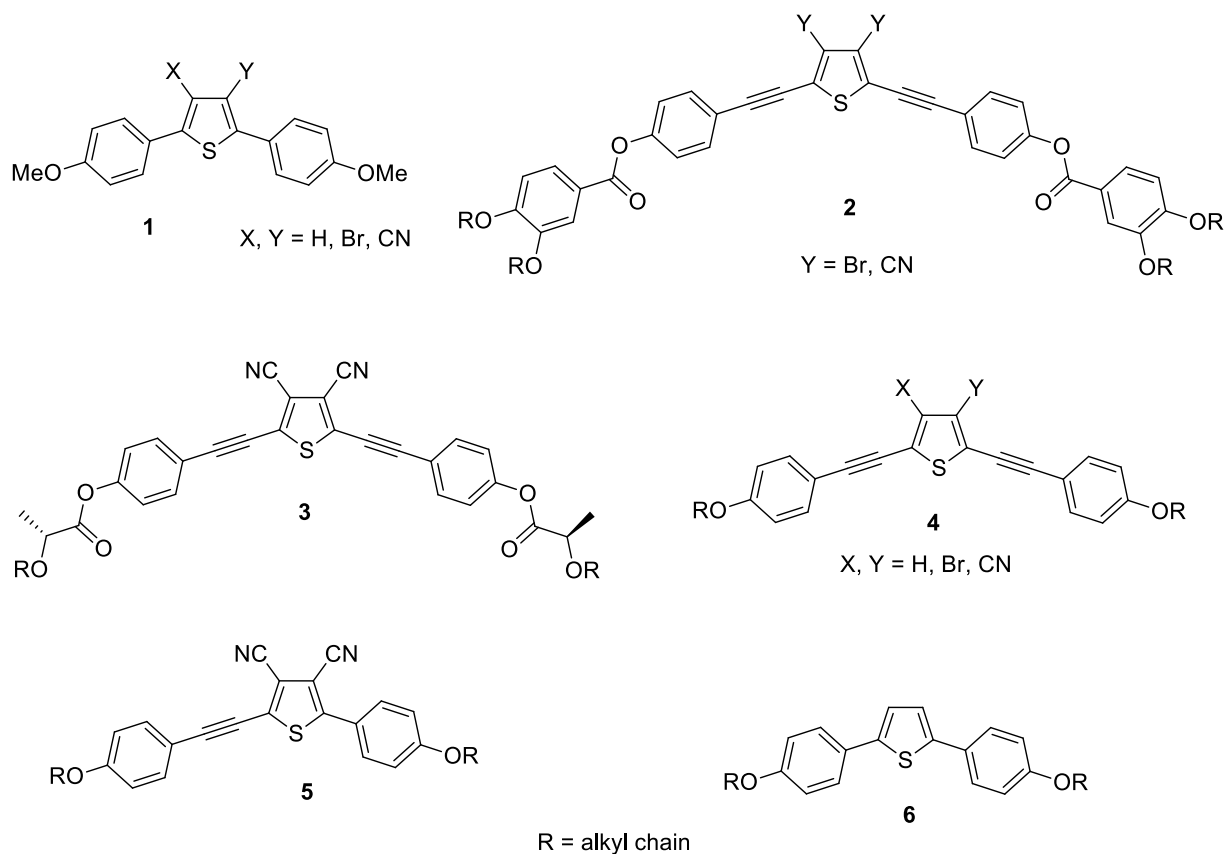
Mesogenic shape anisotropy, central unit, connecting groups and flexible alkyl chains are contemporary approaches to the design and synthesis of thermotropic bent-core liquid crystals. Even a slight variation in the molecular structure and intermolecular interactions may lead to dramatic change on liquid crystalline properties of respective mesogens. Such remarkable changes were most often observed in the case of bent-core mesogens unlike liquid crystals of rod-like molecules [1–3]. The molecular shape anisotropy of BC mesogens with no C_∞ symmetry along the molecular axis leads to a directed packing of the molecules within layers, which exhibit unique smectic phases (B1....B7). These phases have not been realized in normal calamitic LCs. Hence, BC LCs have become subject of considerable research interest to understand the structural mesophase property relationship in these intriguing materials [1–4].

The first observation of ferroelectric switching of achiral BC LCs in 1996 has led to very intense research activities in the LC field. Over the past two decades, several hundred bent-core molecules have been synthesized with fairly different molecular structure, not only to understand the basic structure property relationship but also with aim to investigate precise functional properties. Bent-shaped compounds provide access to mesophase with polar order and supramolecular chirality despite the molecules are achiral [4,5]. The design of novel thermotropic BC LCs for advanced functional materials is a challenging task for a chemist to optimise basic modification of the structural properties for various applications [6]. Numerous bent core mesogens have been derived from polycyclic aromatic cores such as resorcinol, isophthalic acid, 3-aminobenzoic acid, 3-aminophenol, 3-aminobenzaldehyde, 3-hydroxybenzaldehyde, 3-hydroxybenzoic acid and naphthalene [7–11]. The bent angle in these molecules is typically around 120°–130°.

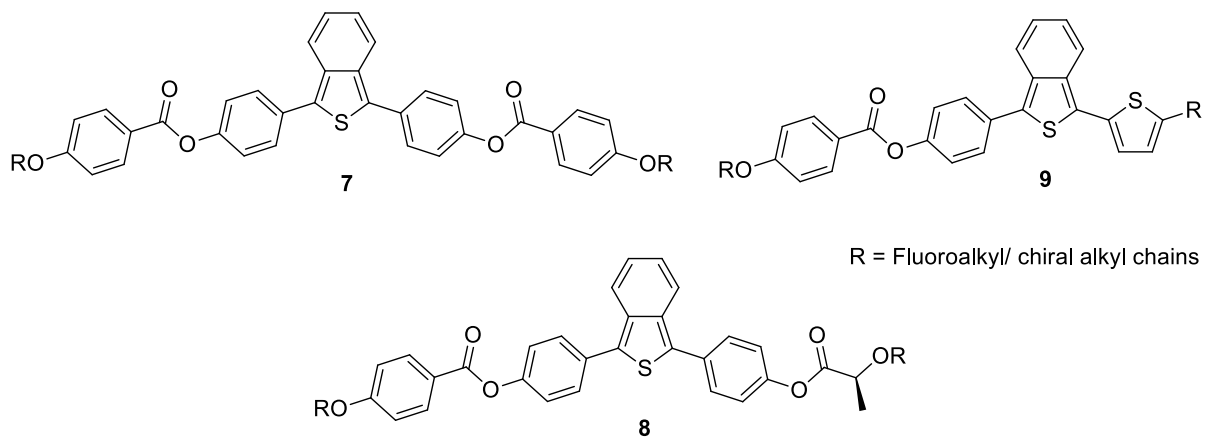
BC LCs have also been synthesised from various heteroaromatic central cores. These heterocyclic compounds have advantages over polycyclic aromatic cores due to the presence of heteroatoms such as N, O, S which causes significant effects on polarity, polarisability, molecular structure which in turns influence the type of mesophase, phase transition temperature, dielectric constant, bent angle, etc. In recent years, BC mesogens were derived from central heterocyclic aromatic core units [12–16], whose optimal bent is usually found around 130–157°, which is a borderline between rod-like and banana LCs. Due to the large bent angle, which prevent the compact packing commonly observed in typical BC LCs, these compounds mostly show nematic and nonpolar smectic phases. The major disadvantage of BC LCs based on five membered heteroaromatic compounds is their high isotropic temperatures, which make them difficult for detail investigations and technological applications. The design of novel thermotropic heteroaromatic five membered BC LCs for cutting edge useful materials is important task to optimize basic modification of the structural properties for different applications. Therefore, it is of incredible significance to seek novel heterocyclic bent-core units which significantly help to contribute to physical parameters such as increased lateral dipole moments, optical anisotropy, elevation of negative dielectric anisotropy, reduction in the melting point, fast switching response, and stability of the mesophase, which promote advancement in technologically promising materials [6–16].

In 1999, Swager's research group synthesized a series of BC LCs derived from 2,5-disubstituted thiophene central ring (1–5). They investigated the effect of bend angle, lateral dipole moment, chirality, and molecular symmetry on liquid crystalline properties of mesogens derived from central thiophene core [17]. All the mesogens exhibit stable nematic and SmC phases over broad temperature range.

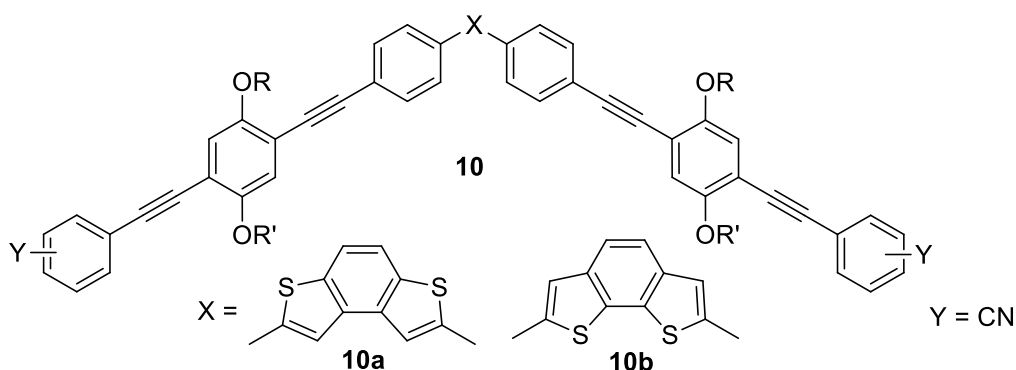
Later, Kelly et al reported the three membered 2,5-disubstituted thiophene based BC LCs, (6) which exhibit enantiotropic nematic phase over broad temperature range [18]. Afterwards, several number of thiophene-based bent core mesogens have been synthesised and studied for their physical properties [19].



Recently, Gorecka et al. introduced the novel benzothiophene central core (**7–9**). The mesogens were modified with fluoroalkyl and/or chiral terminal chains to induce stability of chiral mesophases. The bend angle in these compounds was calculated to be around 140° . These mesogens exhibit nematic, SmA and SmC phases, which are similar to the phases observed for rod-like mesogens [20].



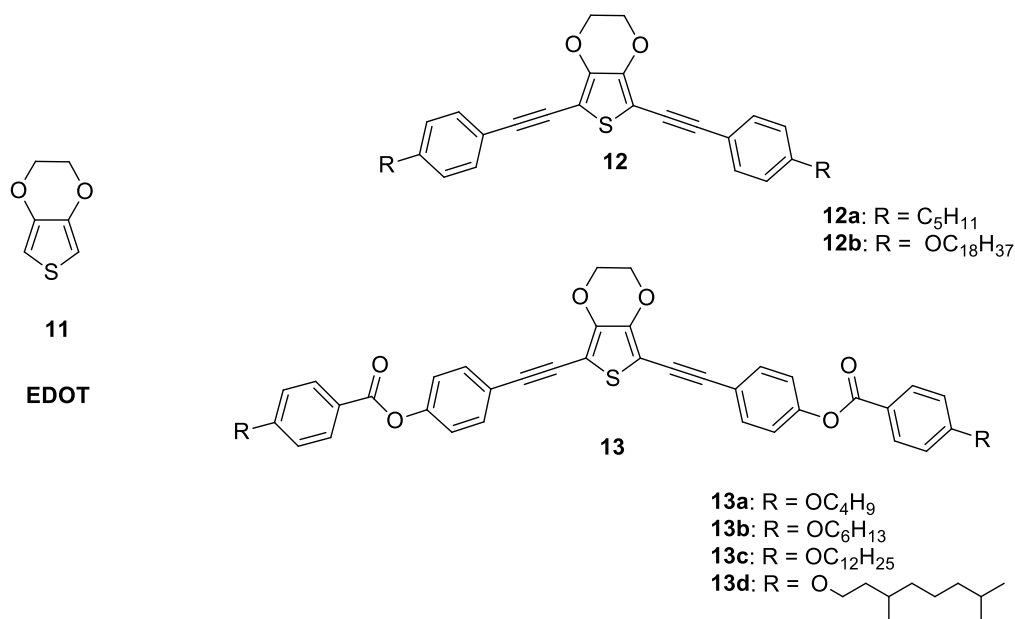
Lehmann et al. reported two series of benzodithiophene-based shape-persistent V-shaped mesogens **10** with the “magic bent angle” of compound **10a** is falling around 109°, and the larger bent-angle of the compound **10b** around 134°. Both these compounds show nematic phase [21]. Recently, the observation of biaxial nematic (N_b) phase has been claimed for some BC LCs; though the topic is still under investigations [22–24]. The BC LCs have been extensively studied for various physical properties such as dielectric properties, optical properties, rheological and elastic properties, ferroelectric and antiferroelectric properties, and so on [25].



In order to gain fresh insight into structure-mesophase property relationship of heteroaromatic based BC LCs, we have discovered that 3,4-ethylenedioxythiophene (**EDOT**) can be utilized as a heterocyclic central unit for the synthesis of thermotropic BC LCs. EDOT is a thiophene based heterocyclic electron-rich monomer compound and key precursor to numerous conducting polymer materials. EDOT acts as incredible contender for assorted building blocks of π -electron conjugated functional materials. It undergoes rapid polymerisation at ambient conditions, slowly turns to dark colour and these conducting polymers find applications in fabrication of various kinds of electronic and optoelectronic devices such as field-effect transistors, photovoltaic devices, non-linear optical materials, light-emitting diodes etc [26,27].

3.1.2 Objective

Extensive literature search reveals that any BC LC derived from EDOT has so far not been realized. In the first part of this chapter, we report for the first time, the synthesis and mesomorphic properties of BC LCs derived from EDOT central unit. We have used alkyne spacers for the synthesis of EDOT based BC LCs **12** and **13**.



3.1.3 Results and discussion

3.1.3.1 Density functional theory calculations

The novel BC molecules obtained from EDOT were designed as shown in **Scheme 1**. Gaussian-09 program package was utilized to carry out density functional theory calculations at the Becke's three parameter functional and Lee, Yang and Parr correlation functional (B3LYP) [29]. The 6-311G (d) basis set was used for ground state geometry optimization for C, H, S atoms. The internal coordinates of the system, which is used as input for the Gaussian-09 program was produced by the Gauss View 4.1 program.

The absence of any imaginary frequency in the calculated vibrational frequencies ensures that the optimized geometry corresponds to a true energy minimum. From the DFT calculations, the energy and the length of fully extended three-ring compound **12b** is found to be -2629.37 a.u. and 58.74 \AA , respectively. These values for five-ring BC LCs **13c** were -3328.47 a.u. and 59.94 \AA , respectively. The DFT calculations demonstrate that the bending angle is approximately 154.68° in three-ring compound **12b** and 152.17° in five-ring compound **13c** as shown in **Figure 1**.

3.1.3.2 Synthesis

At first, we designed and synthesised EDOT based three-ring bent-core molecules as shown in **Scheme 1**, where the central EDOT core is connected between alkyl or alkoxy-substituted phenyl rings. These compounds were found to be non-LC, which is not much surprising as three-ring structures are usually not conducive for BC LCs [28]. To enhance the length: width proportion, we added one phenyl ring on each side to create five-ring structure. The additional rings were coupled *via* ester bridge on both wings as shown in **Scheme 1**. The 2,5-disubstituted EDOT with acetylene linkage groups promotes greater stability of mesophase and provides a moderate bent angle in between $152\text{--}155^\circ$ depending on substitution. We synthesised four five ring EDOT derivatives, including one racemic mixture of branched alkoxy chain derivative. All the homologous derivatives display nematic phase only. All the compounds were synthesised by following general synthetic pathway as shown in **Scheme 1**. Bromination of EDOT **11** using *N*-bromosuccinimide gives 2,5-dibrominated EDOT **14** (DBEDOT) as the key intermediate for the synthesis of three- and five-ring derivatives. DBEDOT is highly unstable at room temperature and hence material was stored at 0°C . Sonogashira C–C bond coupling reaction of 4-alkyl phenylacetylene (**15a**) or 4-alkoxy phenylacetylene (**15b**) with DBEDOT **14** in the presence of $\text{PdCl}_2(\text{PPh}_3)_2$ and CuI in anhydrous triethylamine solvent offered three membered heteroaromatic bent-core non-mesogenic compound (**12a–12b**). Here, we optimised the best condition for coupling reaction.

Similarly, the Sonogashira coupling reaction between 4-iodophenol **16** and trimethylsilylacetylene gives coupled product **17**. Typical condensation reaction between 4-((trimethylsilyl)ethynyl)phenol (**17**) and 4-alkoxy benzoic acid in the presence of DCC and

4-alkoxybenzoic acid, DCC, cat. DMAP, DCM, 48 h, RT; (v) TBAF, THF, 8 h, RT; (vi) 4-ethynylphenyl-4-alkoxybenzoate, PdCl₂(PPh₃)₂, CuI, TEA, 24 h, 72 °C.

3.1.3.3 Thermal properties

The thermal properties of all the liquid crystalline compounds were primarily investigated by POM. The exact phase transition temperatures along with enthalpy change values recorded from DSC measurements are tabulated in **Table 1**. The onset temperatures are reported in °C and relative enthalpy changes (kJ mol⁻¹) are given in parentheses. The mesophase texture of all the compounds is recorded by using small amount of sample placed on clean glass slide and covered with cover slip and viewed under optical microscope with crossed polarizers. The three-ring compounds (**12a–12b**) derived from EDOT central unit did not show any liquid crystalline properties and therefore, not studied further. All the five membered mesogens (**13a–13d**) exhibit enantiotropic nematic phase over broad temperature which display characteristic defect textures with two and four-point brushes, upon cooling from the isotropic phase (**Figure 2**).

Table 1. Phase transition temperature (onset in DSC °C) and enthalpies (kJ mol⁻¹, in parentheses) of EDOT derivatives **12a–12b** and **13a–13d** (on heating cycle & cooling scan). * phase transition temperature observed in POM.

Compound	Phase transition, onset temperature (°C); (ΔH , kJ mol ⁻¹)	
	<i>heating scan</i>	<i>cooling scan</i>
12a	Cr 109.9 [55.3] I	I 61 [-89.6] Cr
12b	Cr 102.7 [94.8] I	I 86.7 [-113.5] Cr
13a	Cr 179.6 N 301.5 I*	I 295 N 156 Cr*
13b	Cr 163.7 N 286.4 I*	I 279 N 139 Cr*
13c	Cr 109.7 [81.5] N 215.6 [1.6] I	I 214.5 [-1.3] N 96.4 [-74.3] Cr
13d	Cr 108.8 [30.3] N 190.1 [1.3] I	I 189 [-1.2] N 63.2 [-43.2] Cr

Upon heating under POM, the five membered compound **13a** melts at 179 °C and goes to the isotropic liquid at 302 °C. Similarly, compound **13b** transferred to isotropic liquid at 287 °C and the nematic droplets were observed on cooling from the isotropic phase. Compound **13c** melts at about 110 °C and transferred to isotropic liquid at about 216 °C. On slow cooling from the isotropic liquid, schlieren texture appears at 208 °C and it crystallized out at 88 °C. Upon slow cooling from the isotropic melt, nematic droplets were observed at 216 °C, dark area are isotropic liquid as shown in **Figure 2**. Typical schlieren texture (**Figure 2c & 2d**) was photographed at 202 °C on cooling from isotropic phase. Similarly, nematic textures were observed for all other derivatives. The compound **13d** having decyloxy alkyl chain with methyl group branching at 3 and 7 positions cleared to isotropic liquid phase at 191 °C. Upon slow cooling, typical schlieren texture having 2- and 4- brushes appeared at about 182 °C, reflects the existence of nematic liquid crystalline phase.

DSC measurements were carried out to examine the phase transition temperatures. All the compounds were subjected to heating and cooling scan at 5 °C per minute under nitrogen atmosphere. The phase transition temperatures obtained from DSC data were in good agreement with POM observations. All the five-membered mesogens (**13a–13d**) exhibit two types endothermic phase transition from crystalline phase to nematic phase at lower temperature and nematic phase to isotropic phase at higher temperature as shown in **Table 1**. A representative and typical DSC thermogram obtained for compound **13c** is depicted in **Figure 3**. All the derivatives crystallize out after few hours at room temperature. Among all the five ring compounds, compound **13d** display lowest melting and isotropization temperature. This is primarily attributed to lowering the van der Waals interactions due to steric hindrance of branched methyl groups. The branching of the alkoxy chain does not alter the mesophase properties but rather significantly affect the melting and isotropisation temperatures and stability of mesophase. The detailed explanation of the impact of branched alkoxy chain on mesogenic compounds of the single component system has been well documented in the literature [**30–31**].

3.1.3.4 X-ray diffraction studies

For quantitative mesophase characterisation of novel five membered BC mesogens, X-ray diffraction studies using unoriented samples filled in Lindemann capillaries were carried out. The XRD scattering patterns observed for compounds **13b–13d** were quite similar on both heating and cooling scans. XRD of compound **13a** could not be taken due to its very high isotropic temperature. As a representative example, XRD measurement conducted on compound **13d** at 150 °C on cooling run in the nematic phase, is presented in **Figure 4**. It is observed that all the compounds exhibit two peaks in the liquid crystalline phase; a diffuse scattering peak at small angle regime and a diffuse scattering in the wide angle region with a maximum at $d = 4.41$ Å. This indicated the absence of any smectic layers or columnar structures in their mesophase.

3.1.4 Photophysical properties

We have further carried out photophysical properties of the newly synthesised compounds using Perkin-Elmer UV-Vis-lambda 35 double beam spectrophotometer absorption spectra. The UV absorption properties of compounds (**13a–13d**) were studied in a very dilute solution using arbitrary concentration of chloroform solvent to obtain information on absorption maxima. All the compounds exhibit maximum absorption band at $\lambda_{\text{max}} = 366$ nm which corresponds to $n \rightarrow \pi^*$ transition. Similar, maximum absorption band at $\lambda_{\text{max}} = 267$ nm is attributed to the $\pi \rightarrow \pi^*$ transitions as shown in **Figure 5 (a)**. Emission spectra of all the mesogens were recorded using FluoroMax-4 (Horiba Jobin Yvon) Spectrofluorometer. The emission spectra were recorded in very dilute chloroform solution and the compounds are excited at $\lambda_{\text{ex}} = 340$ nm. The compounds (**13a–13d**) exhibit strong emission maximum at 425 nm and 405 nm as shown in **Figure 5 (b)**. No apparent changes are seen by increasing number of methylene units of alkoxy chain. The absorption and fluorescence properties could be ascribed because of the extended π -conjugation in all the molecules.

3.1.5 Raman spectroscopy

The structure of novel bent core mesogens was further contemplated by Raman spectroscopy. Raman spectra were recorded with Horiba Jobin Yvon T6400 Micro Raman using a He–Ne Laser operating at $\lambda = 632.8$ nm instrument. The laser power at 1.8 mW was kept constant throughout measurements. Spectral data were acquired at an optical resolution of $50 \times$ objective lens and accumulated at 10 seconds to obtain data with a sufficiently high signal-to-noise ratio. All the liquid crystalline samples are placed in a clean glass slide and covered with cover slip. The Raman shift recorded in the range between 400 and 2600 cm^{-1} at room temperature. The Raman spectra (**Figure 6**) clearly indicates the typical Raman bands at lower regions at $443\text{--}1297\text{ cm}^{-1}$ which corresponding to aliphatic chains and aromatic rings. The intense peaks at $1454\text{--}1602\text{ cm}^{-1}$ correspond to EDOT containing a heteroaromatic ring. The prominent peaks at 1712 cm^{-1} and 2198 cm^{-1} are responsible for ester and acetylene linking groups in the mesogenic derivatives (**13a–13d**) respectively.

3.1.6 Thermogravimetric analysis

The thermal stability of all the liquid crystalline compounds was checked using TGA 4000 thermogravimetric analysis instrument. All the samples (**12a–12b** & **13a–13d**) are subjected to heat scan of $10\text{ }^{\circ}\text{C min}^{-1}$ under a nitrogen atmosphere. The solid samples exhibit no weight loss in the temperature range $300\text{--}330\text{ }^{\circ}\text{C}$. All the compounds initiated weight loss at $335\text{--}350\text{ }^{\circ}\text{C}$ and whole process complete at about $520\text{ }^{\circ}\text{C}$ as shown in **Figure 7**. The decomposition temperature in these compounds is much higher than the isotropic temperature. It reveals that all the mesogenic derivatives possess excellent thermal stability.

3.1.7 Conclusions

In conclusion, we have discovered that EDOT acts as a central core for the synthesis of bent-core mesogens. The bent angle of these molecules is $152\text{--}155^{\circ}$. All the mesogenic compounds display enantiotropic nematic phase over wide temperature range. EDOT based three-ring compounds do not exhibit any liquid crystalline phase; however, by increasing side

wing with phenyl group, mesomorphism can be induced. The nematic phase of all the compounds has been investigated by polarised optical microscopy, differential scanning calorimetry. The nematic phase structure of representative compounds was established with X-ray diffraction studies. The use of branched alkoxy chains reduces isotropic temperature significantly. The electron rich nature of EDOT based BC LCs may putative candidates for electro-optical applications.

3.1.8 Experimental section

3.1.8.1 General information

The general information has been explained in **chapter 2**. The intermediate compound **1** ethynyl-4-pentylbenzene (**15a**) was procured from commercial source and characterised before use. The compounds 1-ethynyl-4-(octadecyloxy)benzene (**15b**) and 4-((trimethylsilyl) ethynyl)phenol (**17**) were prepared by following the method described in literature [32].

3.1.8.2 General procedure for the synthesis of intermediates and final compounds.

Synthesis of 5,7-dibromo-2,3-dihydro-thieno[3,4-b][1,4]dioxine (DBEDOT) (14):

In a two neck flask containing **EDOT 11** (2.0 g, 14.06 mmol) was added a solution of 40 mL anhydrous THF/glacial acetic acid (1:1) at room temperature under stirring. To the above reaction mixture, *N*-bromosuccinimide (5.25 g, 29.54 mmol) was added in small portions at room temperature in the presence of argon atmosphere. The reaction mixture was further allowed to stirring for additional 4 to 5 hours until deep-blue colour appeared. The completion of the reaction was monitored by TLC. After completion, the reaction mixture was poured into crushed ice under vigorous stirring to get white precipitate which was filtered off. The crude solid was washed with an excess of water and dried under high vacuum. Recrystallization of the crude product from cold methanol gives desired pure white colour needles of DBEDOT **14**. Yield: 70%, m.p: 97–98 °C. IR: (film) ν_{\max} : 2951, 2926, 2852, 1514, 1454, 1373, 900, 690 cm^{-1} ; ^1H

NMR (500 MHz, CDCl₃): δ = 4.27 ppm (s, 4H); ¹³C NMR (125 MHz, CDCl₃): δ = 139.71, 85.54, 64.96 ppm; elemental analysis: C₆H₄Br₂O₂S; calculated (%): C 24.02, H 1.34, S 10.66; found: C 24.12, H 1.42, S 10.58. The ¹H and ¹³C NMR spectra are shown in **Figure 8**.

Synthesis of 5,7-bis((4-alkyl or alkoxy phenyl)ethynyl)-2,3-dihydrothieno[3,4-b][1,4] dioxine (12a–12b)

In a deoxygenated three-necked flask containing stirring solution of DBEDOT **14** (0.25 g, 0.833 mmol) in 30 mL anhydrous triethylamine solvent was added PdCl₂(PPh₃)₂ (0.011 g, 0.016 mmol) and CuI (0.075 g, 0.041 mmol) at room temperature for 10 min under argon atmosphere. To this, added 1-ethynyl-4-pentylbenzene (0.43 g, 2.50 mmol) (**15a**) or 1-ethynyl-4-(octadecyloxy)benzene (**15b**) (0.92 g, 2.50 mmol) in 10 mL anhydrous triethylamine solvent. The resulting reaction mixture was heated to 72 °C for 24 hours. The reaction was monitoring by TLC. After completion of reaction, the reaction mixture allowed to cooling at room temperature and diluted with excess of diethyl ether and filtered through celite pad. The filtrate was then extracted with diethyl ether (3 × 20 mL). The combined extracts were dried over Na₂SO₄ and concentrated under vacuum. The crude compound was purified by column chromatography using silica gel (dichloromethane/n-hexane 2:8). Recrystallisation of the pure product with ethanol gives yellow colour solid **12a–12b** in about 60% yield. A representative ¹H and ¹³C NMR spectra of compound **12b** is shown in **Figure 9**.

2,3-dihydro-5,7-bis(2-(4-pentylphenyl)ethynyl)thieno[3,4-b][1,4]dioxine (12a). Yield: 62 %. IR (film) ν_{max} : 2914, 2852, 2189, 1607, 1454, 1377 cm⁻¹; ¹H NMR (500 MHz, CDCl₃): δ = 7.42 (d, J = 7 Hz, 4H), 7.14 (d, J = 7 Hz, 4H), 4.31 (s, 4H), 2.60 (t, J = 7 Hz, 4H), 1.62–1.59 (m, 4H), 1.31 (br, 8H), 0.88 ppm (m, 6H); ¹³C NMR (125 MHz, CDCl₃): δ = 143.77, 142.94, 131.45, 128.44, 119.89, 99.83, 97.04, 79.08, 64.85, 35.91, 31.44, 30.88, 22.52, 14.02 ppm; elemental analysis: C₃₂H₃₄O₂S; calculated (%): C 79.63, H 7.09, S 6.62; found: C 79.51, H 7.21, S 6.69.

2,3-dihydro-5,7-bis(2-(4-(octadecyloxy)phenyl)ethynyl)thieno[3,4-b][1,4]dioxine (12b). Yield: 65 %. IR (film) ν_{\max} : 2918, 2852, 2200, 1605, 1462, 1378 cm^{-1} ; ^1H NMR (500 MHz, CDCl_3): δ = 7.44 (d, J = 8 Hz, 4H), 6.84 (d, J = 8 Hz, 4H), 4.31 (s, 4H), 3.95 (br, 4H), 1.79–1.76 (m, 4H), 1.44 (br, 4H), 1.34–1.25 (m, 56H), 0.87 ppm (m, 6H); ^{13}C NMR (125 MHz, CDCl_3): δ = 159.46, 142.72, 133.07, 114.59, 114.50, 99.78, 96.85, 78.29, 68.10, 64.85, 31.94, 29.71, 29.67, 29.60, 29.58, 29.39, 29.38, 29.20, 26.02, 22.71, 14.13 ppm; elemental analysis: $\text{C}_{58}\text{H}_{86}\text{O}_4\text{S}$; calculated (%): C 79.22, H 9.84, S 3.63; found: C 79.05, H 9.75, S 3.51. ^1H and ^{13}C NMR spectra are shown in **Figure 9**.

Synthesis of 4-((trimethylsilyl)ethynyl)phenyl-4-alkoxybenzoate (18a–18d).

All the intermediate derivatives were obtained by condensation reaction of 4-alkoxybenzoic acids with 4-((trimethylsilyl)ethynyl) phenol **17** in presence of DCC and catalytic amount of DMAP in dry DCM solvent. The general procedure is described as follows:

In a two neck-flask containing compound **17** (5 g, 26.27 mmol), 4-alkoxybenzoic acid (28.90 mmol) and catalytic amount of DMAP (0.32 g, 2.62 mmol) was dissolved in dry DCM solvent (50 mL) under argon. To this above solution, DCC (10.84 g, 52.54 mmol) in 30 mL of dry DCM was added. The resulting mixture was stirred at room temperature for 48 hours. At the end of reaction, the precipitated *N,N'*-dicyclohexylurea (DCU) was removed by filtration and the filtrate was washed with excess of water and then extracted with DCM (3 \times 75 mL). The combined extracts were dried over Na_2SO_4 and concentrated under vacuum. The solid residue was purified by column chromatography using silica gel (*n*-hexane/ethyl acetate 8:2) to afford white solid **18a–18d**.

Compound 18a. (Yield: 5.48 g, 57 %). IR (film) ν_{\max} : 2924, 2918, 2852, 2158, 1730, 1606, 1454 cm^{-1} ; ^1H NMR (500 MHz, CDCl_3): δ = 8.11 (d, J = 8.5 Hz, 2H), 7.51 (d, J = 8 Hz, 2H), 7.15 (d, J = 8 Hz, 2H), 6.96 (d, J = 8.5 Hz, 2H), 4.052 (t, J = 6 Hz, 2H), 1.95–1.92 (m, 2H), 1.70–1.68 (m, 2H), 0.98 (br, 3H), 0.25 ppm (s, 9H); ^{13}C NMR (125 MHz, CDCl_3): δ = 164,

163.72, 133.18, 132.34, 121.81, 114.40, 105.10, 94.25, 68.09, 34.01, 31.18, 25.67, 24.98, 19.23, 13.83 ppm; elemental analysis: C₂₂H₂₆O₃Si; calculated (%): C 72.09, H 7.14; found: C 72.20, H 7.28.

Compound 18b. (Yield: 6.21 g, 60 %). IR (film) ν_{\max} : 2960, 2923, 2856, 2161, 1725, 1604, 1455 cm⁻¹; ¹H NMR (500 MHz, CDCl₃): δ = 8.11 (d, *J* = 8 Hz, 2H), 7.72 (d, *J* = 8 Hz, 2H), 7.15 (d, *J* = 8.5 Hz, 2H), 6.96 (d, *J* = 8.5 Hz, 2H), 4.04 (t, *J* = 6 Hz, 2H), 1.81 (br, 2H), 1.47 (br, 2H), 1.33–1.29 (m, 4H), 0.89 (br, 3H), 0.24 ppm (s, 9H); ¹³C NMR (125 MHz, CDCl₃): δ = 164.58, 163.72, 151, 138.47, 133.15, 132.33, 124.05, 121.78, 114.37, 89.63, 68.38, 31.80, 29.32, 29.21, 29.09, 25.98, 22.65, 14 ppm; elemental analysis: C₂₄H₃₀O₃Si; calculated (%): C 73.05, H 7.65; found: C 73.24, H 7.81.

Compound 18c. (Yield: 7.5 g, 60 %). IR (film) ν_{\max} : 2951, 2924, 2854, 2156, 1728, 1606, 1454 cm⁻¹; ¹H NMR (500 MHz, CDCl₃): δ = 8.11 (d, *J* = 8.5 Hz, 2H), 7.51 (d, *J* = 8 Hz, 2H), 7.15 (d, *J* = 8 Hz, 2H), 6.96 (d, *J* = 8.5 Hz, 2H), 4.03 (t, *J* = 6 Hz, 2H), 1.80 (br, 2H), 1.47 (br, 2H), 1.36–1.26 (m, 16H), 0.88 (br, 3H), 0.25 ppm (s, 9H); ¹³C NMR (125 MHz, CDCl₃): δ = 164.61, 163.71, 151.16, 133.18, 132.34, 121.81, 121.35, 120.69, 114.4, 104.43, 94.25, 68.41, 31.93, 29.73, 29.58, 29.39, 29.34, 29.14, 26.02, 22.71, 14.13 ppm; elemental analysis: C₃₀H₄₂O₃Si; calculated (%): C 75.26, H 8.83; found: C 75.38, H 8.93.

Compound 18d. (Yield: 6.51 g, 55 %). IR (film) ν_{\max} : 2953, 2928, 2852, 2121, 1714, 1604, 1449 cm⁻¹; ¹H NMR (500 MHz, CDCl₃): δ = 8.12 (d, *J* = 8 Hz, 2H), 7.51 (d, *J* = 8 Hz, 2H), 7.15 (d, *J* = 8 Hz, 2H), 6.96 (d, *J* = 8 Hz, 2H), 4.07 (t, *J* = 6.5 Hz, 2H), 1.87–1.84 (m, 1H), 1.68 (br, 2H), 1.64–1.16 (m, 8H), 0.95 (d, *J* = 6.5 Hz, 3H), 0.87 (d, *J* = 6 Hz, 6H), 0.25 ppm (s, 9H); ¹³C NMR (125 MHz, CDCl₃): δ = 164.62, 163.67, 151.13, 133.18, 132.34, 121.82, 114.39, 104.40, 94.24, 66.73, 39.26, 37.29, 36.03, 29.86, 29.74, 28.01, 25.50, 24.69, 22.74, 22.64, 19.68, 13 ppm; elemental analysis: C₂₈H₃₈O₃Si; calculated (%): C 74.62, H 8.49; found: C 74.78, H 8.63.

Synthesis of 4-ethynylphenyl-4-alkoxybenzoate (19a–19d).

The desilylation of compounds **18a–18d** was carried out using TBAF in dry THF solvent at room temperature. Hence, all the compounds are synthesized by following general procedure:

A solution of TBAF (12.15 mmol) in dry THF (20 mL) was added to a stirring solution of compounds **18a–18d** (10.13 mmol) in THF (40 mL) at room temperature under argon. The reaction mixture was kept stirring at room temperature for 8 hours. At the end of reaction, ice cold water was added and the reaction mixture was extracted with diethyl ether (3 × 50 mL). The combined organic layers were dried over Na₂SO₄ and the solvent was evaporating under vacuum. The crude product was purified by column chromatography using silica gel (*n*-hexane/ethyl acetate 9:1) to give white colour solid **19a–19d** in about 75–80 % yield.

Compound 19a. IR (film) ν_{\max} : 2953, 2924, 2854, 2110, 1730, 1604, 1454 cm⁻¹; ¹H NMR (500 MHz, CDCl₃): δ = 8.12 (d, *J* = 8.5 Hz, 2H), 7.54 (d, *J* = 8 Hz, 2H), 7.18 (d, *J* = 8 Hz, 2H), 6.97 (d, *J* = 8.5 Hz, 2H), 4.04 (t, *J* = 6 Hz, 2H), 3.07 (s, 1H), 1.82–1.79 (m, 2H), 1.53–1.50 (m, 2H), 0.99 ppm (t, *J* = 7.5 Hz, 3H); ¹³C NMR (125 MHz, CDCl₃): δ = 164.57, 163.71, 151.38, 133.34, 132.32, 121.94, 119.60, 114.37, 82.98, 68.05, 31.13, 19.9, 13.79 ppm; elemental analysis: C₁₉H₁₈O₃; calculated (%): C 77.53, H 6.15; found: C 77.48, H 6.11.

Compound 19b. IR (film) ν_{\max} : 2956, 2928, 2858, 1922, 1727, 1606, 1454 cm⁻¹; ¹H NMR (500 MHz, CDCl₃): δ = 8.12 (d, *J* = 7.5 Hz, 2H), 7.54 (d, *J* = 7.5 Hz, 2H), 7.17 (d, *J* = 7.5 Hz, 2H), 6.96 (d, *J* = 7.5 Hz, 2H), 4.04 (t, *J* = 6 Hz, 2H), 3.07 (s, 1H), 1.83–1.80 (m, 2H), 1.48 (br, 2H), 1.35 (br, 4H), 0.91 ppm (t, *J* = 7.5 Hz, 3H); ¹³C NMR (125 MHz, CDCl₃): δ = 164.60, 163.71, 151.37, 133.36, 132.34, 131.58, 122.15, 121.21, 119.60, 114.22, 82.99, 68.3, 31.56, 29.08, 25.67, 22.60, 14.03 ppm; elemental analysis: C₂₁H₂₂O₃; calculated: C 78.23, H 6.87; found: C 78.31, H 6.93.

Compound 19c. IR (film) ν_{\max} : 2953, 2924, 2852, 1921, 1728, 1604, 1454 cm^{-1} ; ^1H NMR (500 MHz, CDCl_3): δ = 8.12 (d, J = 8 Hz, 2H), 7.54 (d, J = 7.5 Hz, 2H), 7.17 (d, J = 7.5 Hz, 2H), 6.96 (d, J = 8 Hz, 2H), 4.04 (t, J = 6 Hz, 2H), 3.07 (s, 1H), 1.83–1.80 (m, 2H), 1.47–1.45 (m, 2H), 1.41–1.27 (m, 16H), 0.86 ppm (t, J = 6.5 Hz, 3H); ^{13}C NMR (125 MHz, CDCl_3): δ = 164.57, 163.72, 151.39, 133.34, 132.33, 121.94, 121.24, 119.60, 114.38, 82.99, 68.39, 31.89, 29.55, 29.35, 29.30, 29.10, 25.98, 22.67, 14.09 ppm; elemental analysis: $\text{C}_{27}\text{H}_{34}\text{O}_3$; calculated (%): C 79.76, H 8.42; found: C 79.68, H 8.51.

Compound 19d. IR (film) ν_{\max} : 2953, 2924, 2852, 2112, 1741, 1606, 1462 cm^{-1} ; ^1H NMR (500 MHz, CDCl_3): δ = 8.12 (d, J = 7.5 Hz, 2H), 7.54 (d, J = 7.5 Hz, 2H), 7.17 (d, J = 7.5 Hz, 2H), 6.97 (d, J = 7.5 Hz, 2H), 4.07 (t, J = 6.5 Hz, 2H), 3.07 (s, 1H), 1.88–1.84 (m, 1H), 1.68–1.58 (m, 2H), 1.35–1.16 (m, 7H), 0.96 (d, J = 6 Hz, 3H), 0.87 ppm (d, J = 6 Hz, 6H); ^{13}C NMR (125 MHz, CDCl_3): δ = 164.59, 163.67, 151.35, 133.35, 132.33, 121.95, 121.20, 119.58, 114.37, 82.97, 66.71, 39.23, 37.26, 36, 29.83, 27.98, 24.65, 22.70, 22.60, 19.64 ppm; elemental analysis: $\text{C}_{25}\text{H}_{30}\text{O}_3$; calculated (%): C 79.33, H 7.98; found: C 79.43, H, 7.91.

Synthesis of five membered BC mesogenic compounds (13a–13d).

All the mesogenic derivatives prepared by Sonogashira C–C coupling reaction between DBEDOT **14** and 4-ethynylphenyl-4-alkoxybenzoate (**19a–19d**) in presence of $\text{PdCl}_2(\text{PPh}_3)_2$ and CuI in anhydrous TEA solvent. The general method is described as follows:

DBEDOT **14** (0.22 g, 0.73 mmol) were dissolved in 30 mL of anhydrous triethylamine solvent. To this solution was added $\text{PdCl}_2(\text{PPh}_3)_2$ (0.020 g, 0.02 mmol) and CuI (0.011 g, 0.05 mmol) under argon atmosphere. The reaction mixture was allowed to stir under argon for 10 min. To the above reaction mixture, 4-ethynylphenyl-4-alkoxybenzoate (**19a–19d**) (2.20 mmol) was added under argon flow. The resulting reaction mixture was heated to 72 °C for 24 hours. After cooling to room temperature, the reaction mixture was diluted with diethyl ether and filtered through celite pad. The filtrate was washed with excess of water and then extracted with diethyl ether (3 × 20 mL). The combined extracts were dried over Na_2SO_4 and solvent was

evaporated under vacuum. The residue was purified by column chromatography using silica gel (*n*-hexane/dichloromethane 9:1). Recrystallisation of the pure product with isopropyl alcohol affords yellow colour solid **13a–13d** in about 55–60 % yield. A representative example of ^1H and ^{13}C NMR spectra is shown in **Figure 10 & 11** respectively.

Mesogenic compound 13a. IR (film) ν_{max} : 2918, 2897, 2850, 2198, 1730, 1600, 1454, 1377 cm^{-1} ; ^1H NMR (500 MHz, CDCl_3): δ = 8.12 (d, J = 8.5 Hz, 4 H), 7.57 (d, J = 8.5 Hz, 4 H), 7.20 (d, J = 8.5 Hz, 4 H), 6.97 (d, J = 8.5 Hz, 4 H), 4.33 (s, 4 H), 4.05 (t, J = 6.5 Hz, 4 H), 1.84–1.78 (m, 4 H), 1.51–1.48 (m, 4 H), 0.99 ppm (t, J = 7 Hz, 6 H); ^{13}C NMR (125 MHz, CDCl_3): δ = 164.60, 163.69, 151.17, 143.24, 132.69, 132.34, 121.97, 121.25, 120.24, 114.36, 99.78, 96.20, 68.04, 64.87, 31.13, 19.20, 13.83 ppm; elemental analysis: $\text{C}_{44}\text{H}_{38}\text{O}_8\text{S}$; calculated (%): C 72.71, H 5.26, S 4.40; found: C 72.73, H 5.31, S 4.47. ^1H and ^{13}C NMR spectra are shown in **Figure 10**.

Mesogenic compound 13b. IR (film) ν_{max} : 2920, 2852, 2196, 1740, 1606, 1444, 1379 cm^{-1} ; ^1H NMR (500 MHz, CDCl_3): δ = 8.13 (d, J = 8 Hz, 4 H), 7.57 (d, J = 7.5 Hz, 4 H), 7.20 (d, J = 7.5 Hz, 4 H), 6.97 (d, J = 8 Hz, 4 H), 4.33 (s, 4 H), 4.04 (t, J = 6.5 Hz, 4 H), 1.83–1.80 (m, 4 H), 1.48 (br, 4 H), 1.36–1.35 (m, 8 H), 0.92 ppm (br, 6 H); ^{13}C NMR (125 MHz, CDCl_3): δ = 164.61, 163.69, 151.17, 143.24, 132.70, 132.34, 121.97, 121.25, 120.24, 114.36, 99.78, 96.21, 79.78, 68.37, 64.87, 31.56, 29.07, 25.67, 22.60, 14.04 ppm; elemental analysis: $\text{C}_{48}\text{H}_{46}\text{O}_8\text{S}$; calculated (%): C 73.63, H 5.91, S 4.08; found: C 73.69, H 5.88, S 4.13.

Mesogenic compound 13c. IR (film) ν_{max} : 2924, 2852, 2204, 1730, 1604, 1454, 1377 cm^{-1} ; ^1H NMR (500 MHz, CDCl_3): δ = 8.12 (d, J = 8.5 Hz, 4 H), 7.57 (d, J = 8.5 Hz, 4 H), 7.20 (d, J = 8.5 Hz, 4 H), 6.96 (d, J = 8.5 Hz, 4 H), 4.33 (s, 4 H), 4.04 (t, J = 6.5 Hz, 4 H), 1.84–1.79 (m, 4 H), 1.48–1.46 (m, 4 H), 1.36–1.27 (m, 32 H), 0.88 ppm (br, 6 H); ^{13}C NMR (125 MHz, CDCl_3): δ = 164.60, 163.69, 151.18, 143.24, 132.69, 132.33, 121.96, 121.25, 120.24, 114.37, 99.79, 96.21, 79.78, 68.38, 64.87, 31.93, 29.67, 29.64, 29.60, 29.57, 29.36, 29.10, 25.99, 22.70, 14.13 ppm; elemental analysis: $\text{C}_{60}\text{H}_{70}\text{O}_8\text{S}$; calculated (%): C 75.75, H 7.41, S 3.36; found: C 75.68, H, 7.50, S 3.32. The ^1H and ^{13}C NMR spectra are shown in **Figure 11**.

Mesogenic compound 13d. IR (film) ν_{\max} : 2920, 2854, 2220, 2198, 1737, 1726, 1604, 1454, 1361, 1255 cm^{-1} ; ^1H NMR (500 MHz, CDCl_3): δ = 8.13 (d, J = 8 Hz, 4 H), 7.57 (d, J = 8 Hz, 4 H), 7.20 (d, J = 8 Hz, 4 H), 6.97 (d, J = 8 Hz, 4 H), 4.33 (s, 4 H), 4.07 (t, J = 6.5 Hz, 4 H), 1.69 (br, 2 H), 1.66–1.60 (m, 8 H), 1.35–1.16 (m, 10 H), 0.96 (d, J = 6 Hz, 6 H), 0.87 ppm (d, J = 6 Hz, 12 H); ^{13}C NMR (125 MHz, CDCl_3): δ = 164.60, 163.67, 151.18, 143.25, 132.69, 132.34, 121.97, 121.26, 120.25, 114.38, 99.79, 96.20, 79.78, 66.72, 64.87, 39.23, 37.27, 36.01, 29.84, 29.71, 27.98, 24.66, 22.66, 19.65 ppm; elemental analysis: $\text{C}_{56}\text{H}_{62}\text{O}_8\text{S}$; calculated: C 75.14, H 6.97, S 3.57; found: C 75.19, H 6.94, S 3.62.

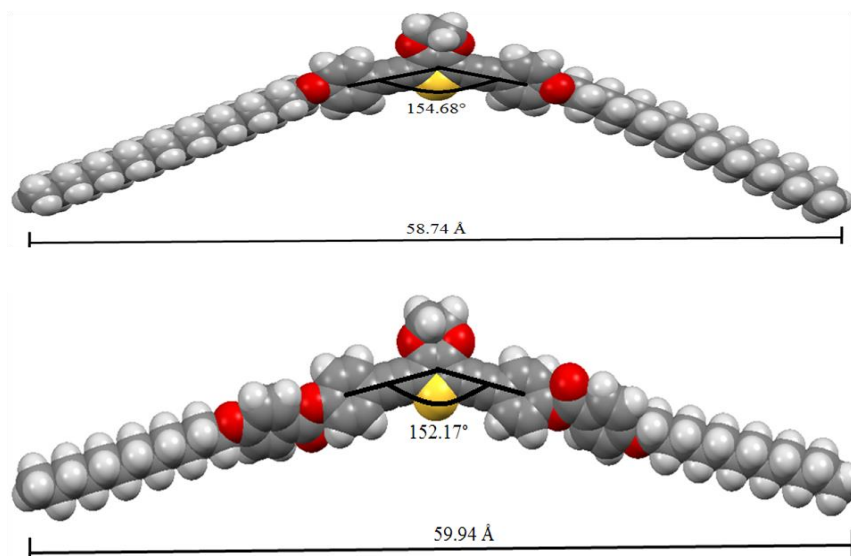


Figure 1. The DFT optimised molecular structure of three-ring compound (**12b**) and five-ring compound (**13c**). The bent angles are 154.68° (**12b**) and 152.17° (**13c**) respectively.

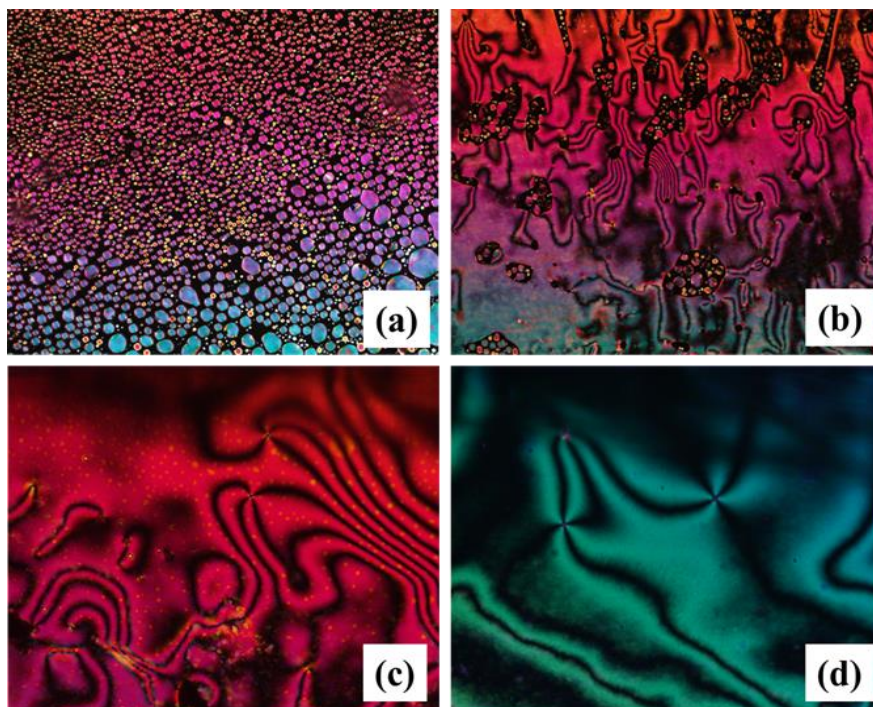


Figure 2. POM textures of compound **13c**: (a) nematic droplets observed during the early growing stage after cooling from the isotropic liquid at 216 °C (dark area are isotropic liquid), (b) further growing of nematic texture on cooling to 212 °C, viewed at 100 × magnifications. (c) and (d) complete nematic texture on further cooling to 202 °C, viewed at 200 × magnifications.

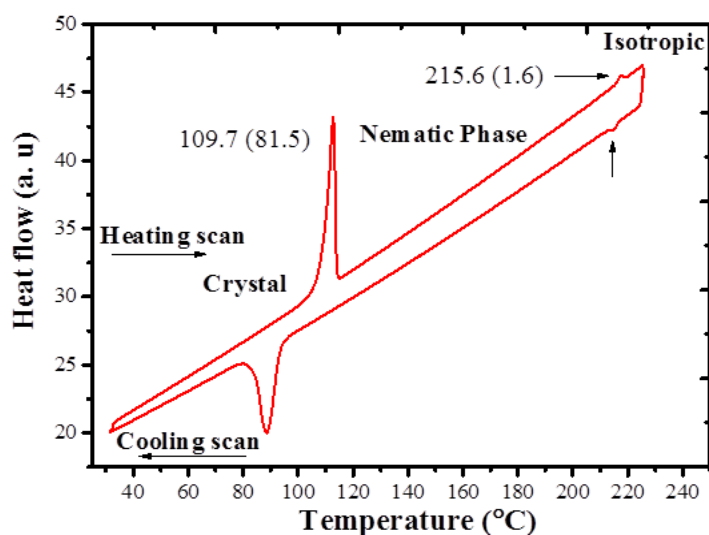


Figure 3. DSC thermogram obtained for the **13c** derivative showing phase transitions on heating and cooling cycles at a scan rate of 5 °C min⁻¹.

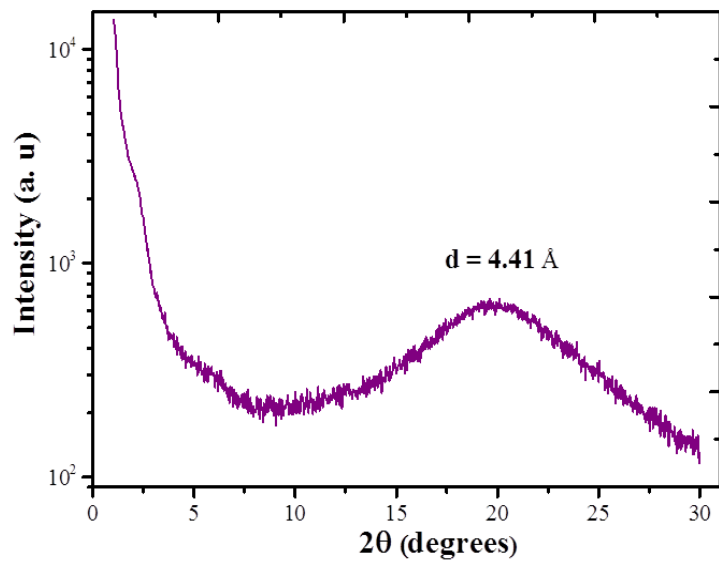


Figure 4. XRD diffraction pattern obtained for compound **13d** in the nematic phase at 150 °C (on cooling scan).

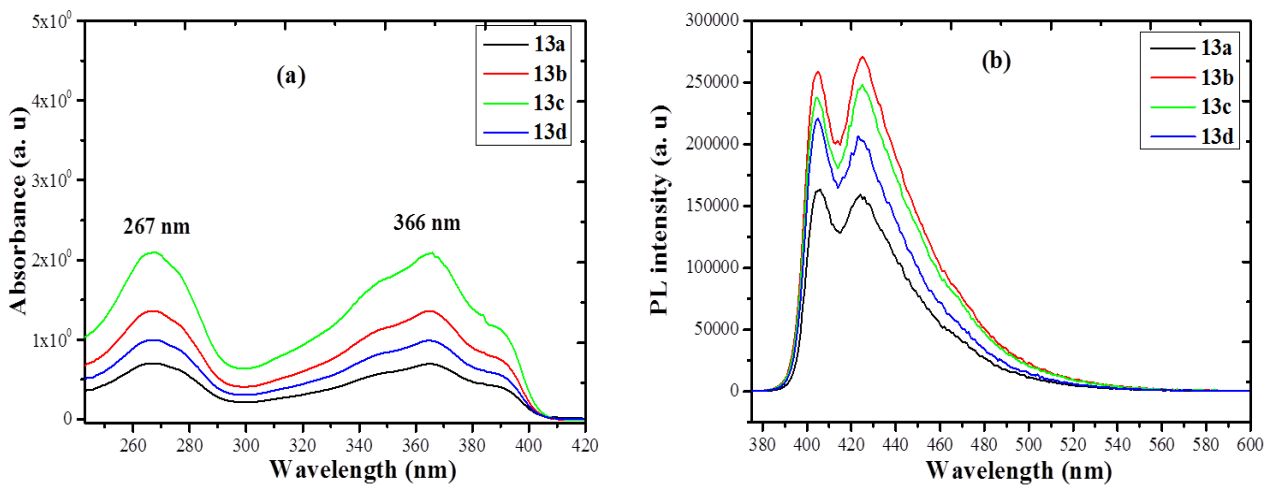


Figure 5. (a) The UV-Vis absorption spectra and (b) fluorescence emission spectra ($\lambda_{\text{ex}} = 340$ nm) of **13a–13d** mesogens.

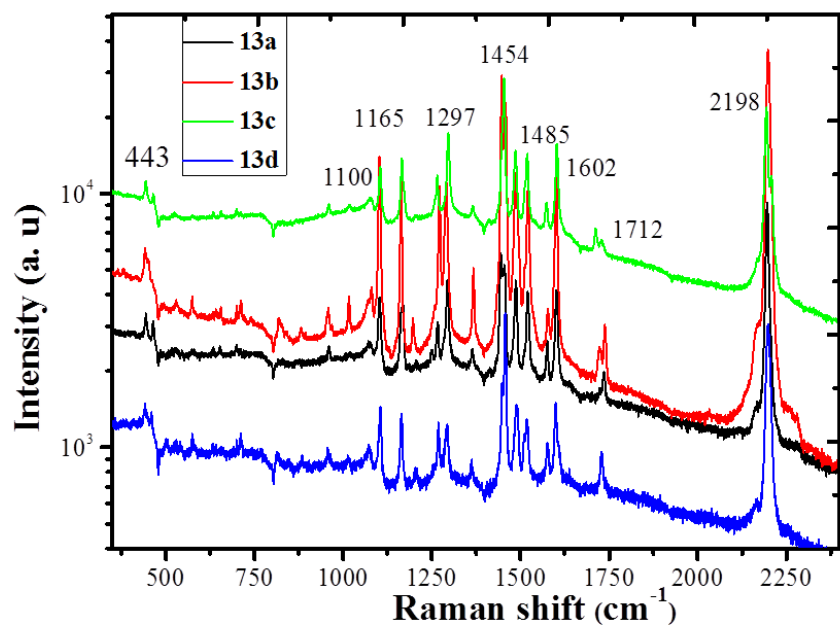


Figure 6. Raman spectrum of mesogenic compounds (**13a–13d**) over the range 400–2600 cm^{-1} at 298 K.

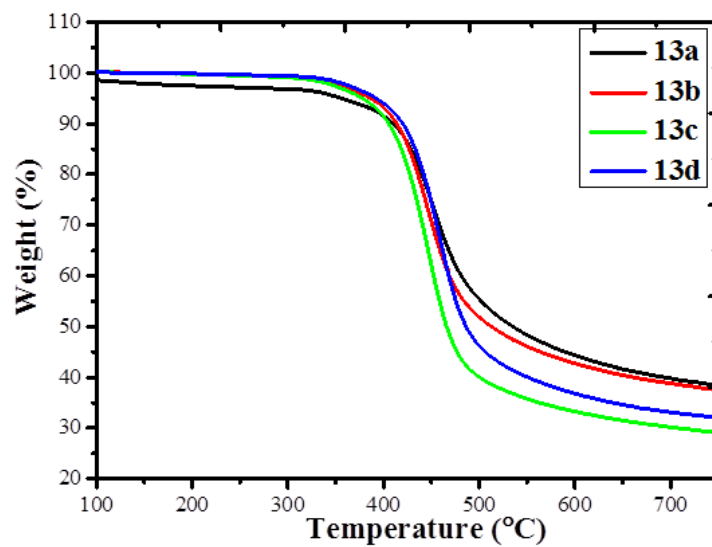


Figure 7. Thermogravimetric analysis of compounds **13a–13d** respectively

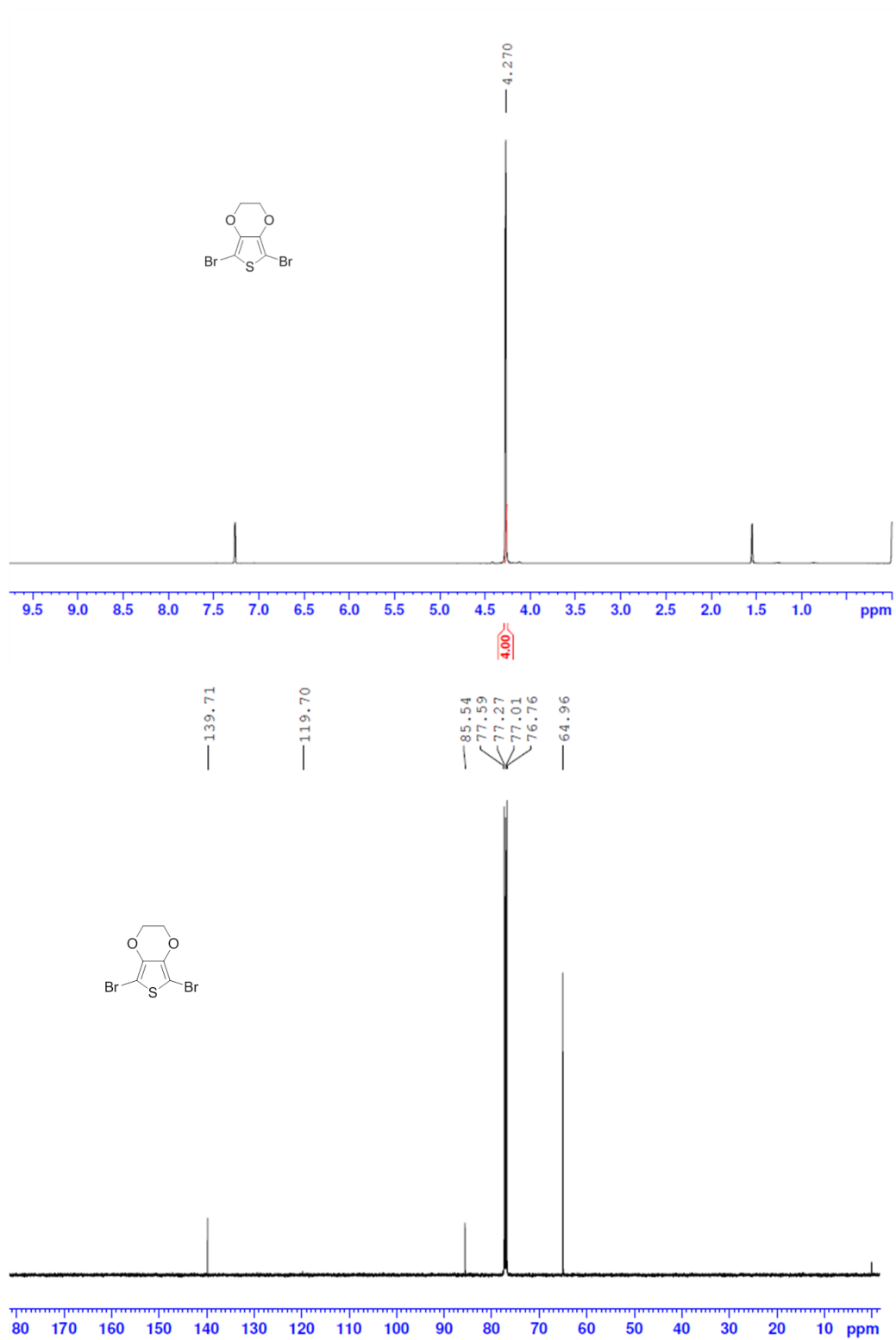


Figure 8. ^1H and ^{13}C NMR of compound DBEDOT 14.

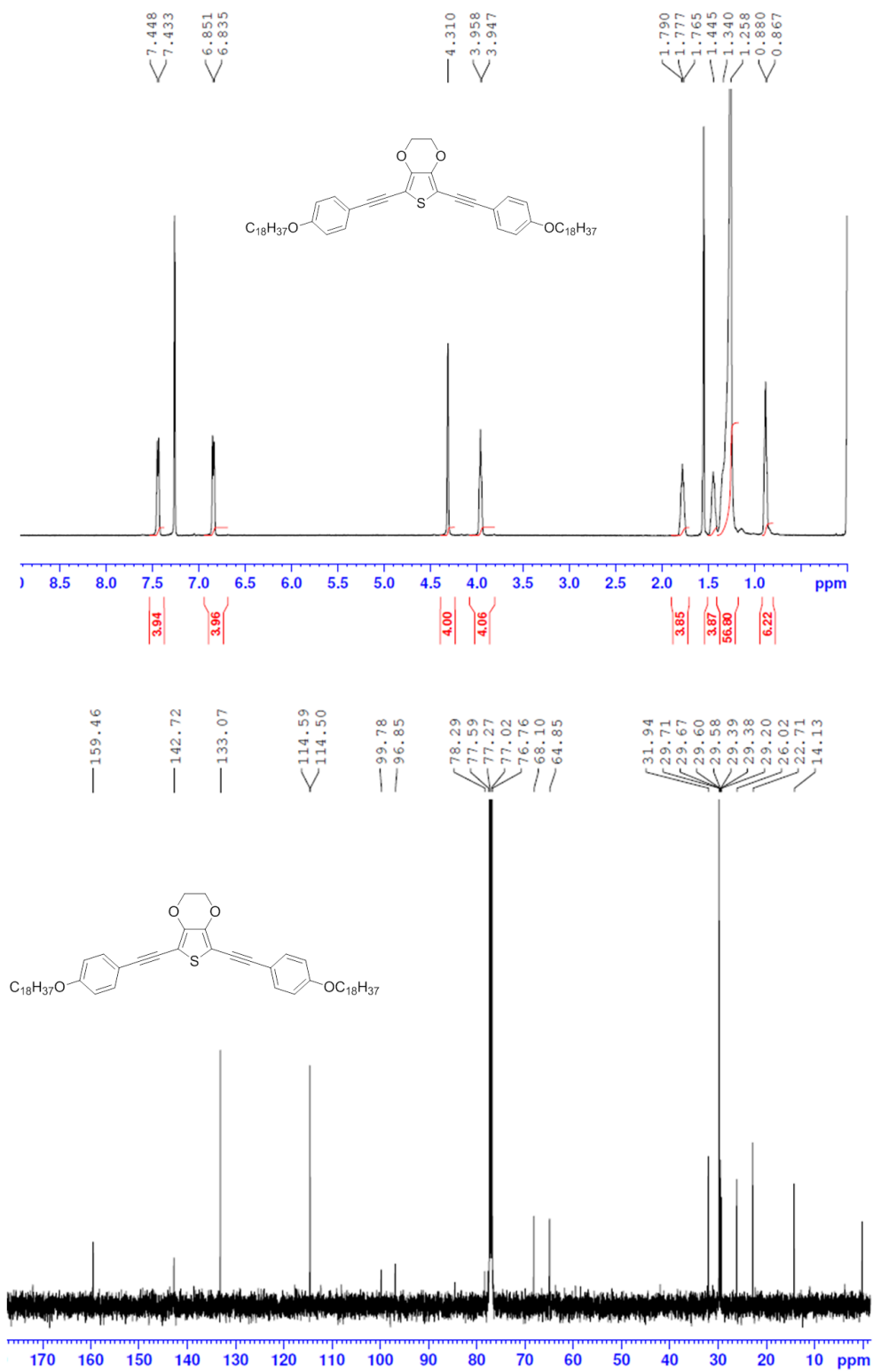


Figure 9. ¹H and ¹³C NMR of compound 12b.

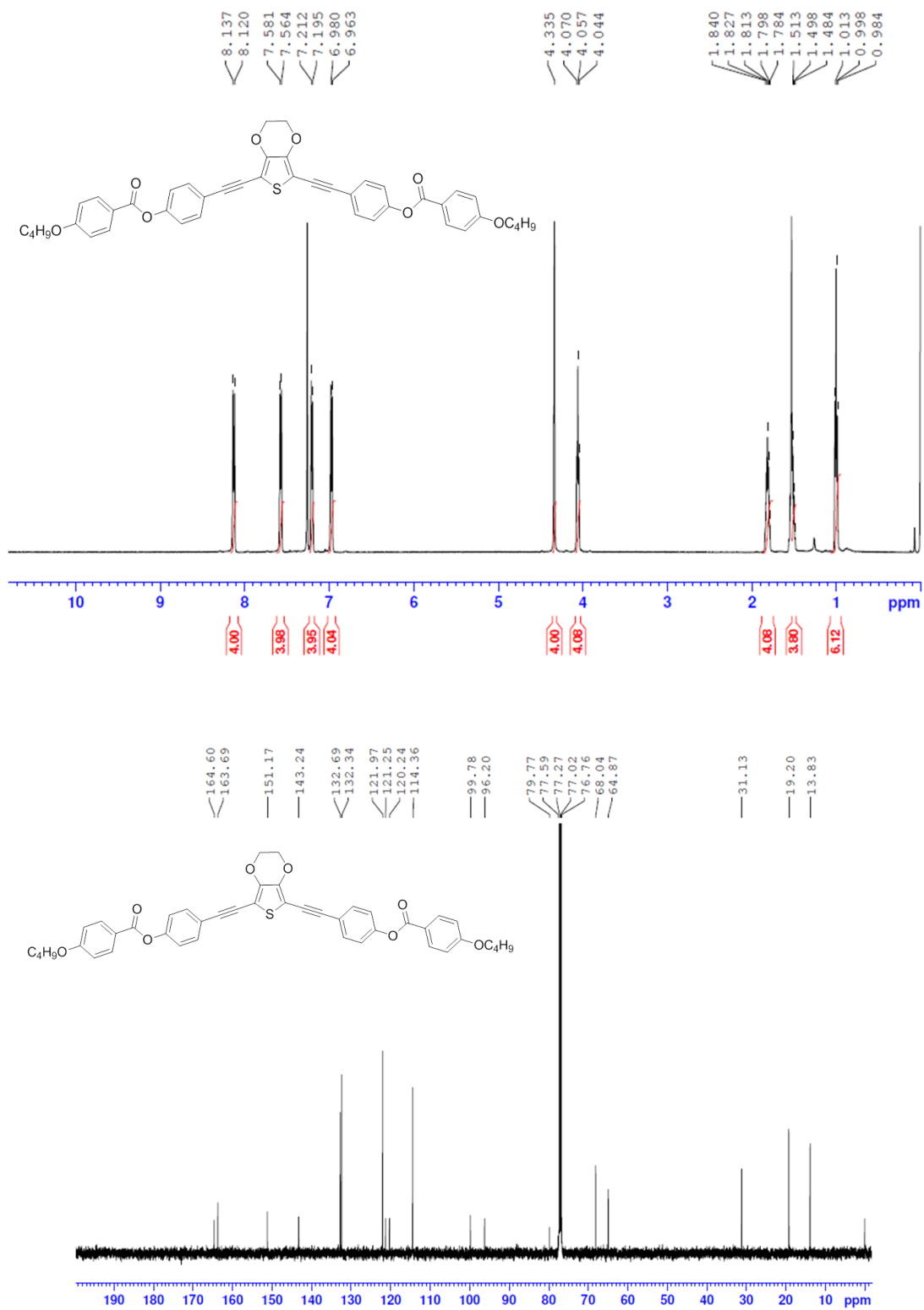


Figure 10. ¹H and ¹³C NMR of compound 13a.

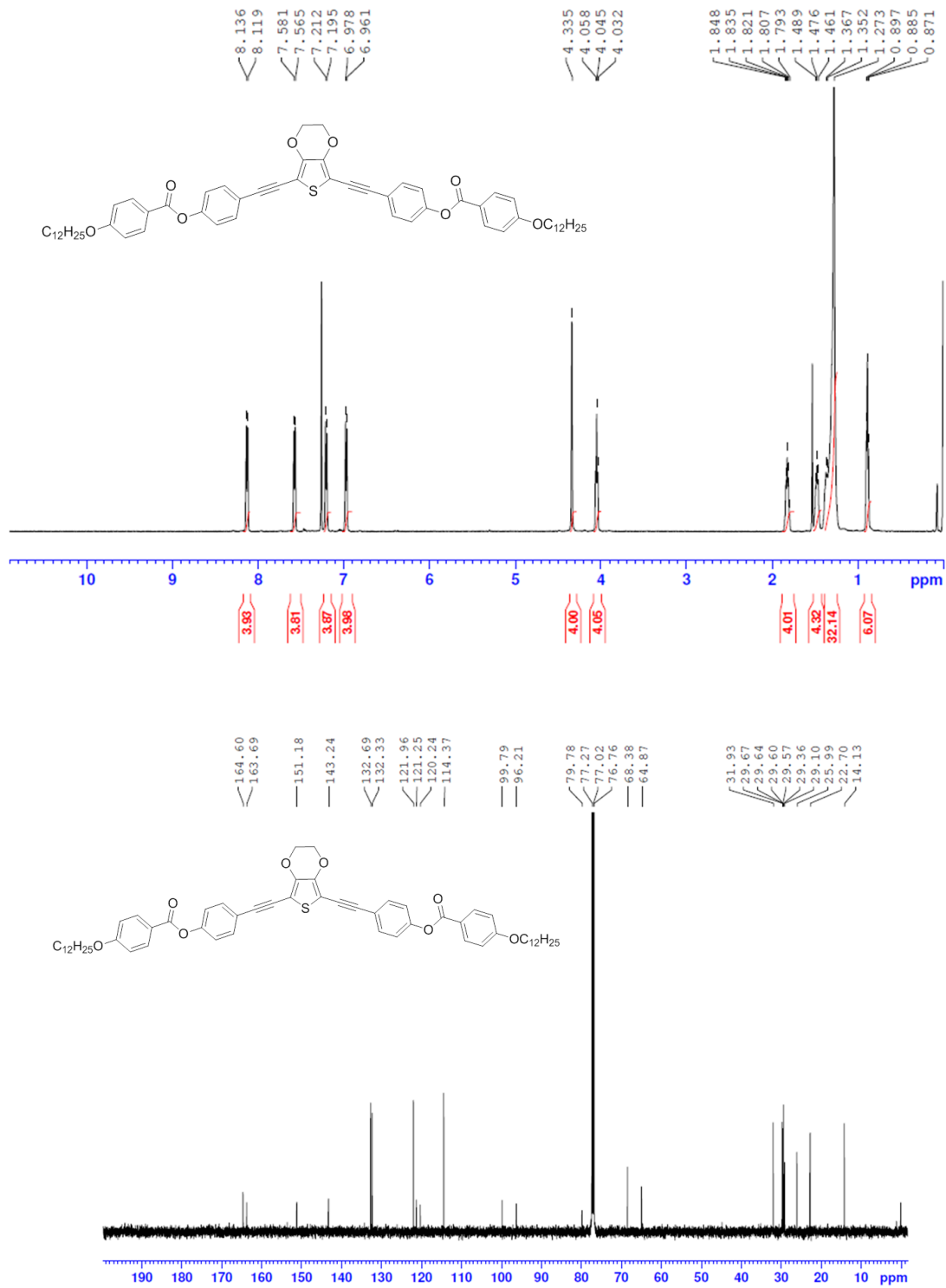


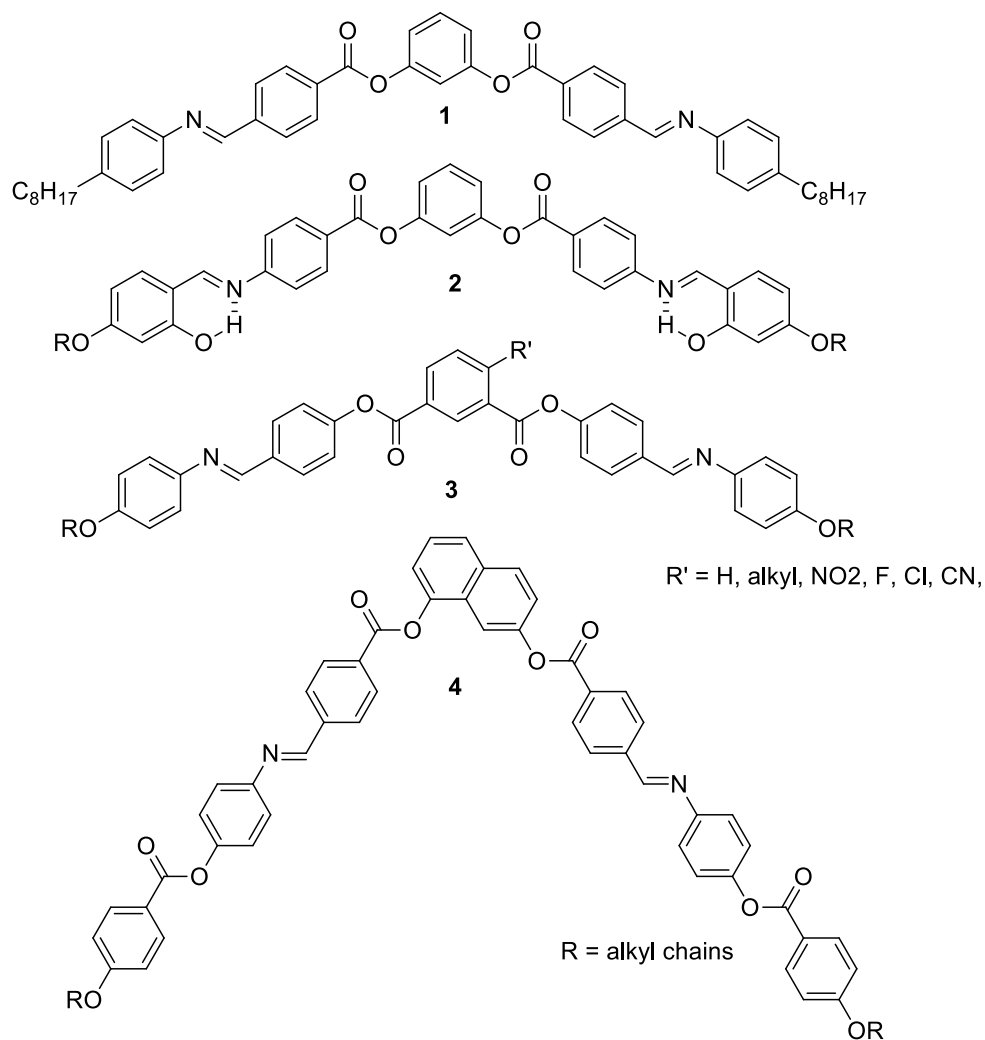
Figure 11. ¹H and ¹³C NMR of compound 13c.

3.2 Part B. Synthesis and characterisation of EDOT-based bent-core liquid crystals containing Schiff-base linkage

3.2.1 Introduction

The designing of BC LCs rely upon number of structural modification, in particular, the selection of linking group that connects central aromatic core to rod-like peripheral wing. Systematic investigations have been carried out to study the effects of type and direction of linking groups on the mesomorphic properties of BC LCs [33]. In general, ester (-COO-) and imine (-CH=N-) linking groups are most often used in BC LCs due to their thermal stability, solubility and flexibility. A number of other linking groups such as azo, amide, thioester, double and triple carbon bonds etc., have also been used. Among all the linking groups, imine based Schiff-base (SB) linking group is extensively used. Schiff-bases are well known organic imine compounds that have been recognized long time ago [34]. The applications of SBs were extended to many fields of chemistry including organic synthesis, analytical chemistry, coordination chemistry and biological sciences etc. Schiff-base compounds have been extensively studied in liquid crystal field.

In 1996 Niori et al. [35], reinvestigated the mesomorphic behaviour of 1,3-phenylene-bis-[4-(4-n-octylphenylimino)methyl]benzoates **1** banana-shaped Schiff's base derivatives originally synthesized by Matsunaga et al. [36]. Their studies revealed the unique features of ferroelectric switching in these molecules, although the constituent mesogens are achiral. Later, numerous Schiff-base containing BC LCs have been synthesised to explore their exotic mesophase behavior [1,37]. The structural modification of Schiff-base BC LCs can be achieved by introducing lateral substitution of functional groups such as F, Cl, CN, NO₂, OH, and CH₃ (**2–4**) into central aromatic core to attain interesting mesomorphic properties and reduction of phase transition temperatures [38–40]. The main disadvantage of SBs containing BC LCs is their chemical and photophysical instability, which reduces their potential use in electro-optical display applications [41–43]. However, several efforts have been made to prepare highly stable SB liquid crystals.

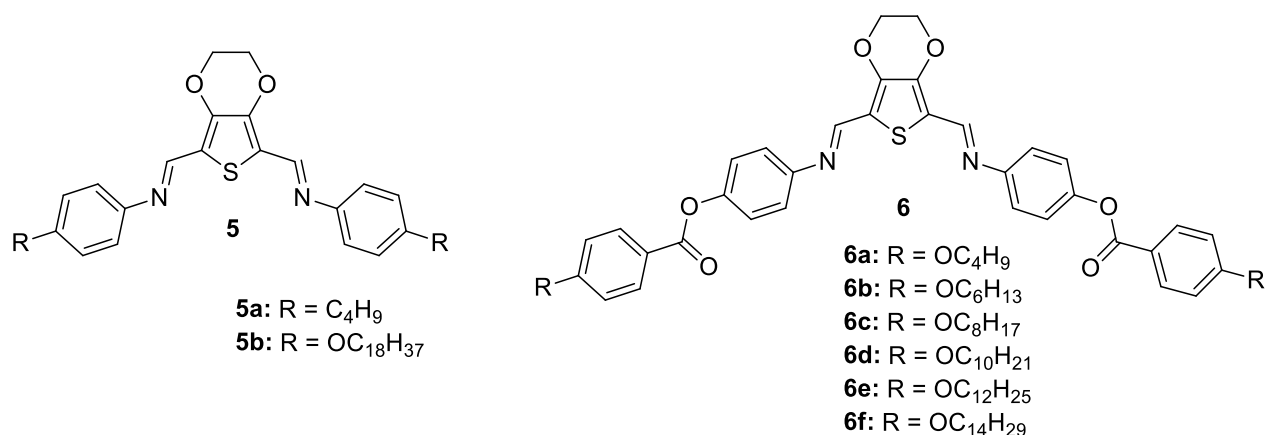


The SB containing BC LCs exhibit rich mesomorphism and interesting electro-optical properties [13,17,19,44–48]. The incorporation of imine linkage for the designing of heteroaromatic BC LCs may abundantly increase optical anisotropy, devaluation in melting point, elevation of a negative dielectric anisotropy, reduction of viscosity and fast switching response, which makes them highly technological important materials [18,19].

3.2.2 Objective

It is essential to understand the structure property relationship and self assembly of novel Schiff-base containing heteroaromatic EDOT based BC LCs. Extensive literature search reveals that any Schiff base bearing EDOT based BC LCs has not been reported so far. In the part B of

this chapter, we report for the first time, the synthesis and characterization of Schiff-base containing BC LC **6** derived from EDOT central unit.



3.2.3 Results and discussion

3.2.3.1 Density functional theory calculations

Gaussian-09 program package was employed to carry out DFT calculations at the Becke's three-parameter functional and Lee, Yang and Parr correlation functional (B3LYP). The 6-311 G(d) basis set was used for ground-state geometry optimisation for C, H, N and S atoms. The internal coordinates of the system, which is used as input for Gaussian -09 program was generated by the Gauss View 4.1 program [29]. The absence of any imaginary frequency in the calculated vibrational frequencies ensures that the optimized geometry corresponds to a true energy minimum.

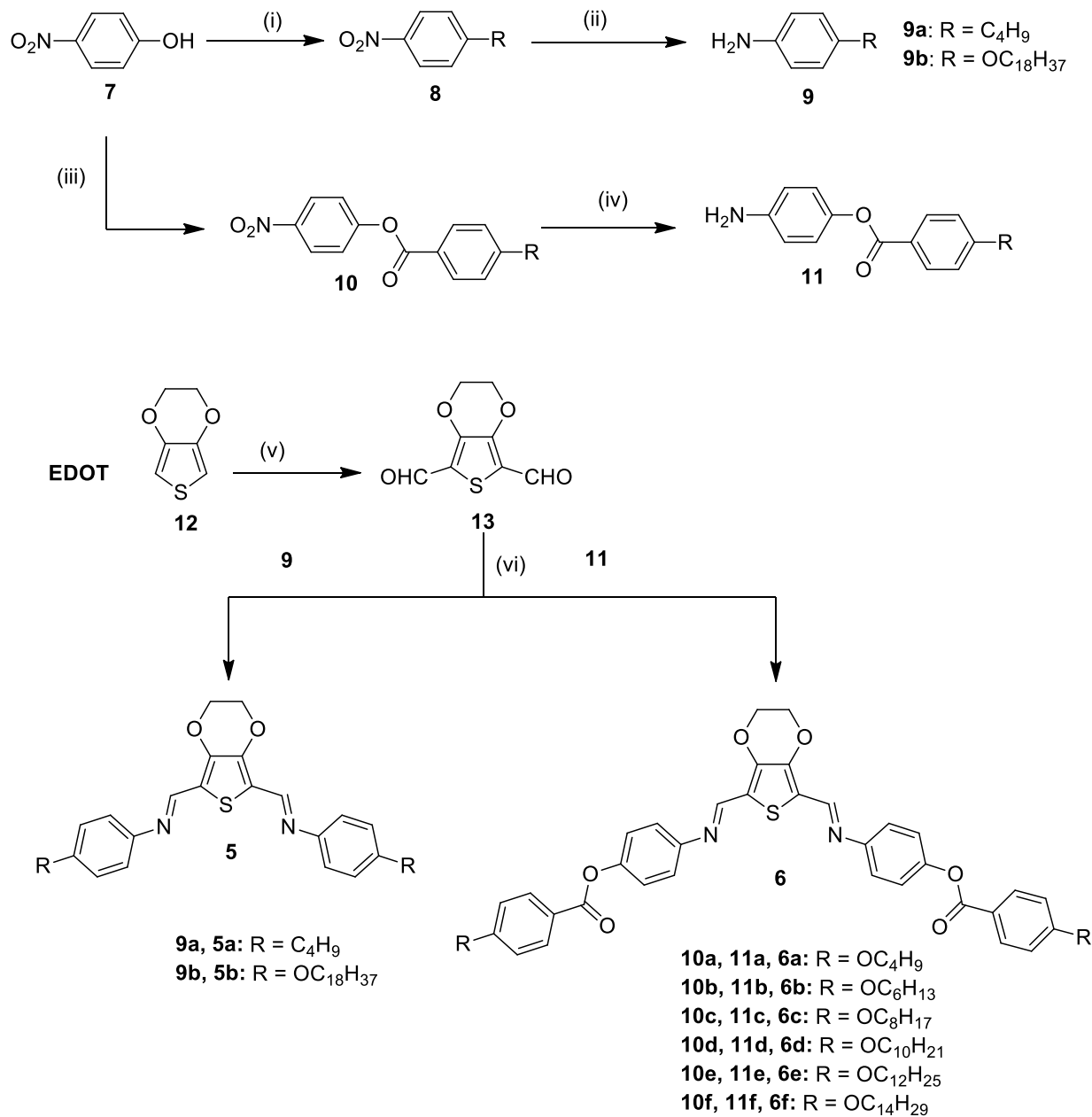
From the DFT calculations, the energy and the length of fully extended Schiff base containing three-ring compound **5b** were found to be $-6814984.61 \text{ kJ mol}^{-1}$ and 60.83 \AA and for five-ring compound **6f** these were, $-9242837.16 \text{ kJ mol}^{-1}$ and 64.57 \AA respectively, as shown in **Figure 1**. The dihedral angle between central EDOT and phenyl ring with imine linkage is 159.35° in three-ring compound **5b** while in five-ring compound **6f**, the dihedral angles between central EDOT and first phenyl ring with imine linkage, the first and second phenyl ring with ester linkage are 156.97° and 146.22° , respectively, reflecting the absence of coplanarity of the

phenyl rings in the molecule. The DFT optimized analysis shows that the bending angle is approximately 167.17° in three-ring compound **5b** and 153.39° in five-ring compound **6f** respectively.

3.2.3.2 Synthesis

Initially, we designed and synthesized three-ring Schiff base compounds as shown in **Scheme 1**, where central EDOT is flanked between two phenyl rings via imine linkage. These three-ring compounds were found to be non-liquid crystalline (**5a–5b**), which is not much surprising as three-ring structures are usually not useful for the construction of BC LCs [28]. To increase length: width ratio, we extended the structure with one more phenyl ring on each side by ester linkage to generate five-membered BC LCs bearing Schiff base as shown in **Scheme 1**. The 2,5-disubstituted EDOT with imine linkage exhibits the bent-angle of around 155° . To understand the structure–property relationship and to develop novel BC LCs of EDOT central unit, we prepared six novel derivatives in which EDOT was converted into EDOT-2,5-dialdehyde as the key intermediate for the synthesis of Schiff base containing three- and five-ring compounds. The influence of terminal chains on mesophase transition temperatures is studied by varying the length of the flexible alkyl chains. All the five-membered mesogens in the series (**6a–6f**) were found to exhibit enantiotropic mesophase behaviour. Higher homologous of the series show nematic phase along with smectic C phase at lower temperature.

The synthesis of novel Schiff base containing BC LCs is shown in **Scheme 1**. Lithiation of EDOT **12** with *n*-butyl lithium (*n*-BuLi) in dry THF followed by quenching with DMF produces EDOT-2,5-dialdehyde **13** as a key intermediate for the synthesis of three- and five-ring Schiff base compounds. Compound **9a** was purchased from commercial source. O-alkylation of 4-nitrophenol **7** with 1-bromooctadecane gives compound **8b**. Reduction of compound **8b** with hydrogen gas in presence of palladium on carbon catalyst at room temperature gives 4-(octadecyloxy) aniline **9b**. Reaction of 4-butylaniline or 4-(octadecyloxy)aniline (**8a–8b**) with EDOT-2,5-dialdehyde **13** in presence of catalytic amount of glacial acetic acid in absolute ethanol under reflux temperature gives Schiff base containing three-ring BC non-mesogenic derivatives **5a–5b**.



Scheme 1. Syntheses of EDOT-based BC LCs. (i) 1-bromooctadecane, K₂CO₃, dry. DMF, 80 °C 12 h; (ii) 10% Pd/C, (1:1) EtOH:THF, r.t, 6 h; (iii) 4-alkoxybenzoic acid, DCC, DMAP, DCM, r.t, 12 h; (iv) 10% Pd/C, (1:1) EtOH:THF, r.t, 6 h; (v) *n*-BuLi (1.6 M), dry DMF, dry THF, -78 °C, 2 h; (vi) 3-4 drops of glacial acetic acid, EtOH, reflux, 4 h.

Condensation reaction of 4-nitrophenol **7** with 4-alkoxy benzoic acids in presence of DCC and catalytic amount of DMAP affords compounds **10a–10f**, which yield key intermediates **11** on reduction. Finally, the Schiff base containing five membered mesogenic derivatives (**6a–6f**) were obtained by the reaction of compound **11a–11f** with EDOT-2,5-dialdehyde **13**. Detailed synthetic procedure and characterisation of all intermediate and final compounds are described in the experimental section.

3.2.3.3 Mesomorphic properties

The thermotropic mesophase behaviour of all novel compounds was primarily investigated by POM. The exact temperature of phase transition and associated enthalpy values were determined by DSC and are summarised in **Table 1**. The onset temperatures are given in °C and the numbers in parentheses indicate the transition enthalpy in kJ mol⁻¹.

The Schiff base containing three-ring compounds **5a** and **5b** did not show any liquid crystalline properties and was not studied further. Lower homologous of the series **6a–6f** exhibit exclusively the nematic phase with wide temperature range, while compounds **6e** and **6f** with alkoxy dodecane and tetradecane chains display enantiotropic nematic phase at higher temperature, followed by appearance of SmC phase at lower temperature. All the mesogenic compounds when observed under cross polarisers upon cooling from isotropic melt, display characteristic defect textures with two- and four-point brushes for nematic mesophase (**Figure 2**). The thermal behaviour of all the mesogenic (**6a–6f**) compounds was also investigated with DSC measurements on heating and subsequent cooling scan rate of 10 °C min⁻¹ under nitrogen atmosphere. The phase transition temperatures obtained in DSC agree very well with POM observation. The compounds **6a–6d** exhibit exclusively enantiotropic nematic phase over wide temperature. These compounds display two types of endothermic transition from crystal to nematic phase at lower temperature and nematic to isotropic transition at higher temperature as shown in **Table 1**. However, compound **6e–6f** shows an additional transition in between these two transitions on heating and cooling scan, which confirms the presence of enantiotropic SmC phase between the nematic and crystal phases. Representative DSC thermographs of **6e** are presented in **Figure 3**.

Table 1. Phase transition temperature (onset in DSC, °C) and enthalpies (kJ mol⁻¹, in parentheses) of Schiff base EDOT derivatives **5a–5b** and **6a–6f** (on heating scan & cooling scan). * phase transition temperature observed in POM.

Compounds	Phase transition (onset (°C) [ΔH (kJ mol ⁻¹)])	
	<i>heating scan</i>	<i>cooling scan</i>
5a	Cr 149.7 [33.1] I	I 130.2 [-19.3] Cr
5b	Cr 129.4 [35.4] I	I 114.5 [-6.3] Cr
6a	Cr 176 N 295 I *	I 292 N 148 Cr *
6b	Cr 163.7 [26.5] N 273.1 [2.0] I	I 266.2 [-0.9] N 127.1 [-17.9] Cr
6c	Cr ₁ 158.8 [2.3] Cr ₂ 166.2 [18.4] N 245.3 [1.2] I	I 244.7 [-1.4] N 160.8 [-23.6] Cr
6d	Cr ₁ 159.2 [4.7] Cr ₂ 175.2 [42.5] N 229.7 [1.7] I	I 225.6 [-1.3] N 160.6 [-28.3] Cr
6e	Cr ₁ 143.2 [1.7] Cr ₂ 169.0 [18.5] SmC 176.3 [0.3] N 209.8 [0.9] I	I 206.8 [-1.0] N 172.1 [-0.4] SmC 160.2 [-15.1] Cr
6f	Cr ₁ 139.6 [1.4] Cr ₂ 165.8 [14.7] SmC 198.3 [1.6] N 201.0 [1.3] I	I 200.1 [-1.6] N 197.4 [-1.7] SmC 151.5 [-2.9] Cr

Compound **6a** melts at 176 °C and become isotropic liquid at 295 °C. The microscopic textures were recorded for compound **6a** as shown in **Figure 2**. The early growing nematic droplets observed on cooling from isotropic liquid at 291 °C as shown in **Figure 2a**. Typical schlieren textures were photographed at 280 °C on further cooling from the isotropic melt as shown in **Figure 2b**. Similar nematic textures were observed for all other derivatives. Upon heating compound **6b** melts at 163.7 °C along with phase transition enthalpy 26.5 kJ mol⁻¹ and become isotropic liquid at 273.1 °C with $\Delta H = 2$ kJ mol⁻¹. Under POM, nematic droplets were observed on slow cooling from isotropic melts. On heating, compound **6c** melts at 158.8 °C ($\Delta H = 2.3$ kJ mol⁻¹) and endure with crystal-crystal transition at 166.2 °C ($\Delta H = 18.4$ kJ mol⁻¹) and become isotropic liquid at 245.3 °C along with phase transition enthalpy 1.2 kJ mol⁻¹. Upon slow cooling from isotropic liquid show nematic phase observed under POM. Similarly, compound **6d**

goes through crystal-crystal transition and melts to nematic phase at 175.2 °C ($\Delta H = 42.5 \text{ kJ mol}^{-1}$) and become isotropic liquid at 229.7 °C ($\Delta H = 1.7 \text{ kJ mol}^{-1}$). Nematic phase obtained upon slow cooling from isotropic liquid observed under POM.

On the other hand, compounds **6e** and **6f** show significant changes in texture from schlieren texture to fan-like texture of smectic phase at low temperature (**Figure 2**). To investigate the nature of this smectic phase, we used commercial polyimide-coated cell (Instec Inc.) having 9 μm thickness for planar alignment of the sample in the LC phases. The compounds **6e** and **6f** was filled uniformly in the LC cell at isotropic temperature. Upon cooling from the nematic phase to lower temperature, shows a focal conic fan-like texture of smectic phase as shown in **Figure 2c** and **2d** respectively. The compound **6e** melts to smectic phase at 169.0 °C ($\Delta H = 18.5 \text{ kJ mol}^{-1}$) and transition from smectic phase to nematic phase at 176.3 °C ($\Delta H = 0.3 \text{ kJ mol}^{-1}$) and become isotropic liquid at 209.8 °C ($\Delta H = 0.9 \text{ kJ mol}^{-1}$) (**Figure 3**). Under POM, the textural changes observed for nematic to smectic phase transition at 176 °C. Similarly, compound **6f** goes through crystal-crystal transition at 139.6 °C ($\Delta H = 1.4 \text{ kJ mol}^{-1}$) and melts to smectic phase at 165.8 °C ($\Delta H = 14.7 \text{ kJ mol}^{-1}$) and transition from smectic phase to nematic phase at 198.3 °C ($\Delta H = 1.6 \text{ kJ mol}^{-1}$) and become isotropic liquid at 201.0 °C ($\Delta H = 1.3 \text{ kJ mol}^{-1}$). Under POM, appearances of nematic texture at higher temperature followed by smectic phase texture at low temperature were observed upon slow cooling from the isotropic liquid. POM textures of smectic phase of compound **6f** are shown in **Figure 2c & 2d**. The early growing stage of SmC phase at 197 °C, viewed at 100 \times magnifications. **Figure 2c & 2d** represents fully grown textures at 181 °C, viewed at 200 \times magnifications. The dark brush in the smectic phase region appears at angles with respect to layer normal revealed the synclincic smectic C phase. Using POM the calculated tilt angle of molecule with respect to the layer normal is nearly 45°, which is in good agreement with XRD results, discussed later. The polarization measurement using triangular wave voltage technique determines that absence of spontaneous polarization in these layers. Therefore, smectic C phase observed for the compounds **6e–6f** represents calamitic smectic C type phase due to large bent angles in these molecules.

The graphical representation of thermal data is presented in **Figure 4**, where Y axis represents transition temperature and X axis represents compounds **6a–6f**. As can be seen, both crystalline state to nematic phase and nematic–isotropic temperatures exhibit a smooth falling

tendency with increasing number of carbon atoms in the terminal alkoxy chain compounds **6a–6f**. However, compounds **6e–6f** display increasing smectic C phase range with increasing length of terminal alkyl chain and decreasing nematic phase. This decrease in melting and clearing temperature could be due to the lowering of van der Waals interactions between aromatic cores and higher degree of flexibility of the terminal chains.

3.2.3.4 X-ray scattering measurements

The mesophase structures of novel Schiff base BC LCs were further confirmed by X-ray diffraction studies of unoriented samples filled in Lindemann capillaries. The XRD pattern was observed for the compounds **6c–6f** on both heating and cooling scans. The XRD of compounds **6a–6d** could not be taken due to their very high isotropic temperature. A representative and typical diffraction pattern obtained for compound **6f** at 201 °C in the nematic phase and at 183 °C for the smectic C phase are shown in **Figure 5a & 5b**, respectively. The XRD pattern of compound **6f** at 201 °C shows a diffuse peak at a small angle region and a diffuse wide-angle maxima at $d = 4.62$ Å typical of the nematic phase (**Figure 5a**). Similarly, the XRD pattern at 183 °C in the smectic C phase region is shown in **Figure 5b**. Two sharp reflections in the small angle regime with d -spacings of 46.95 Å and 23.52 Å were observed. These peaks in the small-angle region are in the ratio of 1:2 of wave number indicating the lamellar smectic-like packing of the molecules in the layers with layer spacing as 46.95 Å. The diffuse peak at wide angle region at 4.76 Å indicates a fluid-like correlation of the molecules in the layers. The layer spacing of 46.95 Å in the smectic C phase is smaller than the molecular length of 64.57 Å, indicating the tilted organisation of the molecules in the layers. The tilt angle estimated from the layer spacing and the molecular length is found to be about 45° at 182 °C, which endorses with tilt angle measured using POM observations in the smectic C phase.

3.2.4 Raman spectroscopy

The structure of novel banana liquid crystals was further examined by Raman spectroscopy. Raman spectra were recorded with Horiba Jobin Yvon T6400 Micro Raman using

a He–Ne Laser operating at $\lambda = 632.8$ nm. The laser power at 1.8 mW was kept constant throughout measurements. Spectral data were obtained at an optical resolution of $50 \times$ objective lens and accumulated at 10 seconds to obtain data with a sufficiently high signal-to-noise ratio. All solid samples (**6a–6f**) were placed in a normal glass slide and covered with a coverslip. The Raman shift recorded in the range between 400 and 2000 cm^{-1} at room temperature. The Raman spectra (**Figure 6**) clearly indicated the typical Raman bands at lower regions at 443–1350 cm^{-1} which corresponding to aliphatic chains and aromatic rings. The intense peaks at 140–1600 cm^{-1} corresponds to EDOT containing a heteroaromatic ring. The prominent peaks at 1712 cm^{-1} are responsible for ester linking groups in the mesogenic derivatives respectively.

3.2.5 Thermogravimetric analysis

The thermal stability of all the liquid crystalline compounds was checked using TGA 4000 thermogravimetric analysis instrument. All the samples **6a–6f** were subject to heat scan of 10 $^{\circ}\text{C min}^{-1}$ under a nitrogen atmosphere. The solid samples exhibit no weight loss in the temperature range 310–340 $^{\circ}\text{C}$. All the compounds initiated weight loss at 340–360 $^{\circ}\text{C}$ and whole process was completed at about 530 $^{\circ}\text{C}$ as shown in **Figure 7**. The decomposition temperature in these compounds is much higher than the isotropic temperature. It revealed that all the mesogenic derivatives possess good thermal stability.

3.2.6 Conclusions

A new series of BC LCs bearing Schiff base derived from EDOT central unit was synthesized and characterized. EDOT based three ring Schiff-base compounds found to be non-mesogenic, while five ring Schiff-base compounds exhibit liquid crystalline phases. The bent angle of five membered ring is 154 $^{\circ}$. The lower homologous compounds exhibit wide range enantiotropic nematic phase, while higher homologous displays a tilted smectic C phase with fairly large tilt angle of 45 $^{\circ}$ in addition to a nematic phase at higher temperature.

3.2.7 Experimental section

3.2.7.1 General methods

The general methods are described in the previous **chapter 2**.

3.2.7.2 General procedure for the synthesis of intermediates and final compounds

All the compounds were synthesised by simple straightforward reaction conditions. The intermediate compound **9a** was purchased from commercial source.

Synthesis of 1-nitro-4-(octadecyloxy) benzene (8b): To a stirring solution of 4-nitrophenol **7** (1 g, 7.18 mmol) and anhydrous potassium carbonate (1.98 g, 14.37 mmol) in dry DMF (25 mL) was added 1-bromooctadecane (2.4 g, 7.18 mmol). The reaction mixture was refluxed for 8 hours. After cooling to room temperature, ice cold water was added under vigorous stirring and the solid was filtered off. The crude compound was dried under high vacuum and recrystallization from ethanol gives pure white crystals **8b**. Yield: 80%. IR (film) ν_{\max} : 2918, 2850, 1606, 1504, 1454, 1377, 1348 cm^{-1} ; ^1H NMR (500 MHz, CDCl_3): δ = 8.19 (d, 2 H, J = 8 Hz), 6.93 (d, 2 H, J = 8 Hz), 4.04 (t, 2 H, J = 6 Hz), 1.84–1.79 (m, 2 H), 1.47–1.43 (m, 2 H), 1.35–1.25 (m, 28 H), 0.89 ppm (t, 3 H, J = 6.5 Hz); ^{13}C NMR (125 MHz, CDCl_3): δ = 164.26, 141.32, 125.92, 114.40, 68.91, 31.93, 29.70, 29.67, 29.65, 29.57, 29.53, 29.37, 29.31, 28.97, 25.91, 22.70, 14.12 ppm; elemental analysis: $\text{C}_{24}\text{H}_{41}\text{NO}_3$; calculated (%): C 73.61, H 10.54, N 3.57; found: C 73.72, H 10.61, N 3.66.

Synthesis of 4-(octadecyloxy) aniline (9b): 1-nitro-4-(octadecyloxy)benzene **8b** (0.5 g, 1.38 mmol) and 10 % palladium on charcoal (100 mg) was placed in single necked round bottom flask along with 20 mL mixture of ethanol: THF (1:1) solvent. The reaction mixture was stirred at room temperature in presence of hydrogen atmosphere for 6 hours. After completion, the reaction mixture was filtered through celite pad and filtrate was concentrated under reduced pressure to give crude product. In order to remove trace amount of palladium content, the crude product was passed through neutral alumina and recrystallization from *n*-heptane affords white

colour solid **9b**. Yield: 85%. IR (film) ν_{\max} : 3387, 3169, 2953, 2922, 2850, 1592, 1518, 1462, 1377 cm^{-1} ; ^1H NMR (500 MHz, CDCl_3): δ = 6.73 (d, 2 H, J = 8 Hz), 6.63 (d, 2 H, J = 8 Hz), 3.87 (t, 2 H, J = 6.5 Hz), 3.40 (br, 2 H), 1.76–1.70 (m, 2 H), 1.43–1.39 (m, 2 H), 1.29–1.25 (m, 27 H), 0.88 ppm (t, 3 H, J = 6.5 Hz); ^{13}C NMR (125 MHz, CDCl_3): δ = 152.38, 139.78, 116.43, 115.69, 68.74, 31.93, 29.70, 29.67, 29.61, 29.60, 29.44, 29.37, 26.08, 22.70, 14.12 ppm; elemental analysis: $\text{C}_{24}\text{H}_{43}\text{NO}$; calculated (%): C 79.71, H 11.97, N 3.87 found: C 79.78, H 12.01, N 3.91. ^1H and ^{13}C NMR are shown in **Figure 8**.

Synthesis of 4-nitrophenyl-4-alkoxybenzoate (10a–10f)

In a two neck-flask containing 4-nitrophenol **7** (2 g, 14.37 mmol), 4-alkoxybenzoic acid (14.37 mmol) and catalytic amount of DMAP (0.17 g, 1.43 mmol) was added dry DCM solvent (50 mL) under argon at room temperature. After stirring for 10 minutes, DCC (4.42 g, 21.56 mmol) in 15 mL of dry DCM was added. The resulting mixture was stirred at room temperature for 24 hours. At the end of reaction, the precipitated DCU was removed by filtration and the filtrate was washed with 5% KOH solution and followed by washing with excess of distilled water and then extracted with DCM (3 \times 75 mL). The combined extracts were dried over Na_2SO_4 and concentrated under vacuum. Recrystallisation of crude compound with isopropyl alcohol affords yellow colour solid (**10a–10f**). Yield: 55–65 %. A representative ^1H and ^{13}C NMR spectra of compounds **10a** and **10d** are shown in **Figure 9** and **10** respectively.

Compound 10a. IR (film) ν_{\max} : 2922, 2914, 2854, 1735, 1606, 1529, 1454, 1377, 1348 cm^{-1} ; ^1H NMR (500 MHz, CDCl_3): δ = 8.31 (d, 2 H, J = 8.5 Hz), 8.13 (d, 2 H, J = 8.5 Hz), 7.40 (d, 2 H, J = 8.5 Hz), 6.99 (d, 2 H, J = 8.5 Hz), 4.06 (t, 2 H, J = 6.5 Hz), 1.82 (br, 2 H), 1.51 (br, 2 H), 1.0 ppm (t, 3 H, J = 7 Hz); ^{13}C NMR (125 MHz, CDCl_3): δ = 164.09, 163.97, 156, 145.28, 132.53, 125.22, 122.67, 120.44, 114.54, 68.14, 31.11, 19.19, 13.80 ppm; elemental analysis: $\text{C}_{17}\text{H}_{17}\text{NO}_5$; calculated (%): C 64.75, H 5.42, N 4.44; found: C 64.81, H 5.49, N 4.52.

Compound 10b. IR (film) ν_{\max} : 2920, 2912, 2854, 1743, 1606, 1514, 1454, 1377, 1344 cm^{-1} ; ^1H NMR (500 MHz, CDCl_3): δ = 8.31 (d, 2 H, J = 8.5 Hz), 8.13 (d, 2 H, J = 8 Hz), 7.40 (d, 2 H, J = 8.5 Hz), 6.99 (d, 2 H, J = 8 Hz), 4.058 (d, 2 H, J = 6.5 Hz), 1.84–1.81 (m, 2 H), 1.49–1.47 (m, 2 H), 1.36 (br, 4 H), 0.92 ppm (t, 3 H, J = 6 Hz); ^{13}C NMR (125 MHz, CDCl_3): δ = 164.08, 163.98, 155.99, 145.27, 132.52, 125.22, 122.68, 120.41, 114.53, 68.46, 31.54, 29.04, 25.65, 22.59, 14.02 ppm; elemental analysis: $\text{C}_{19}\text{H}_{21}\text{NO}_5$; calculated (%): C 66.46, H 6.15, N 4.07; found: C 66.55, H 6.23, N 4.15.

Compound 10c. IR (film) ν_{\max} : 2955, 2920, 2910, 1732, 1608, 1525, 1456, 1377, 1350 cm^{-1} ; ^1H NMR (500 MHz, CDCl_3): δ = 8.31 (d, 2 H, J = 8 Hz), 8.13 (d, 2 H, J = 8 Hz), 7.40 (d, 2 H, J = 8 Hz), 6.98 (d, 2 H, J = 8 Hz), 4.05 (t, 2 H, J = 6.5 Hz), 1.85–1.80 (m, 2 H), 1.49–1.45 (m, 2 H), 1.37–1.32 (m, 8 H), 0.88 ppm (t, 3 H, J = 6.5 Hz); ^{13}C NMR (125 MHz, CDCl_3): δ = 164.09, 163.97, 156, 145.28, 132.52, 125.22, 122.67, 120.44, 114.54, 68.47, 31.89, 29.55, 29.35, 29.31, 29.07, 25.97, 22.68, 14.10 ppm; elemental analysis: $\text{C}_{21}\text{H}_{25}\text{NO}_5$; calculated (%): C 67.90, H 6.77, N 3.76; found: C 67.95, H 6.84, N 3.81.

Compound 10d. IR (film) ν_{\max} : 2920, 2910, 2852, 1732, 1608, 1525, 1456, 1377, 1350 cm^{-1} ; ^1H NMR (500 MHz, CDCl_3): δ = 8.32 (d, 2 H, J = 8 Hz), 8.13 (d, 2 H, J = 8 Hz), 7.40 (d, 2 H, J = 8 Hz), 6.99 (d, 2 H, J = 8 Hz), 4.05 (t, 2 H, J = 6.5 Hz), 1.82 (br, 2 H), 1.47 (br, 2 H), 1.37–1.28 (m, 12 H), 0.88 ppm (t, 3 H, J = 6.5 Hz); ^{13}C NMR (125 MHz, CDCl_3): δ = 164.09, 163.97, 156, 145.28, 132.52, 125.22, 122.67, 120.44, 114.54, 68.47, 31.89, 29.55, 29.35, 29.31, 29.07, 25.97, 22.68, 14.10 ppm; elemental analysis: $\text{C}_{23}\text{H}_{29}\text{NO}_5$; calculated (%): C 69.09, H 7.31, N 3.50; found: C 69.16, H 7.36, N 3.54.

Compound 10e. IR (film) ν_{\max} : 2926, 2918, 2852, 1732, 1609, 1527, 1454, 1377, 1351 cm^{-1} ; ^1H NMR (500 MHz, CDCl_3): δ = 8.32 (d, 2 H, J = 7.5 Hz), 8.13 (d, 2 H, J = 7 Hz), 7.40 (d, 2 H, J = 7.5 Hz), 6.99 (d, 2 H, J = 7 Hz), 4.05 (t, 2 H, J = 6.5 Hz), 1.82 (br, 2 H), 1.47 (br, 2 H), 1.36–1.27 (m, 16 H), 0.88 ppm (t, 3 H, J = 6.5 Hz); ^{13}C NMR (125 MHz, CDCl_3): δ = 164.09,

163.97, 156, 145.29, 132.52, 125.22, 122.67, 120.44, 114.54, 68.47, 31.92, 29.65, 29.59, 29.55, 29.35, 29.07, 25.97, 22.69, 14.11 ppm; elemental analysis: C₂₅H₃₃NO₅; calculated (%): C 70.17, H 7.77, N 3.27; found: C 70.10, H 7.82, N 3.35.

Compound 10f. IR (film) ν_{\max} : 2956, 2914, 2852, 1732, 1608, 1525, 1454, 1377, 1350 cm⁻¹; ¹H NMR (500 MHz, CDCl₃): δ = 8.32 (d, 2 H, J = 8.5 Hz), 8.13 (d, 2 H, J = 8.5 Hz), 7.40 (d, 2 H, J = 8.5 Hz), 6.99 (d, 2 H, J = 8.5 Hz), 4.05 (t, 2 H, J = 6.5 Hz), 1.82 (br, 2 H), 1.47 (br, 2 H), 1.36–1.26 (m, 20 H), 0.88 ppm (t, 3 H, J = 6.5 Hz); ¹³C NMR (125 MHz, CDCl₃): δ = 164.10, 163.97, 156.21, 145.29, 132.52, 125.22, 122.67, 114.54, 68.47, 31.93, 29.69, 29.65, 29.58, 29.55, 29.35, 29.07, 25.97, 22.69, 14.11 ppm; elemental analysis: C₂₄H₄₃NO; calculated (%): C 71.18, H 8.17, N 3.07; found: C 71.23, H 8.24, N 3.12.

Synthesis of 4-aminophenyl-4-alkoxybenzoate (11a–11f)

Palladium on carbon (10% Pd/C) (0.1 g) was added to a vigorous stirring solution of 5 mL mixture of THF: EtOH (1:1) solvent containing nitro compound **10a–10f** (0.2 g). The reaction was stirring under hydrogen atmosphere at room temperature for 8 hours. After completion of reaction, the resulting reaction mixture was filtered through celite pad and filtrate was concentrated completely under vacuum. In order to remove trace palladium content, the residue was passed through column chromatography using neutral alumina (*n*-hexane/ethyl acetate 1:1). Recrystallisation of crude compound with *n*-heptane gives pure white solid **11a–11f** in about 90 % yield. A representative ¹H and ¹³C NMR spectra of compounds **11b** and **11e** are shown in **Figure 11** and **12** respectively.

Compound 11a. IR (film) ν_{\max} : 3452, 3365, 2955, 2924, 2854, 1712, 1606, 1514, 1454, 1377 cm⁻¹; ¹H NMR (500 MHz, CDCl₃): δ = 8.11 (d, 2 H, J = 8.5 Hz), 6.95 (m, 4 H), 6.70 (d, 2 H, J = 8 Hz), 4.04 (t, 2 H, J = 6.5 Hz), 3.64 (s, 2 H), 1.80 (br, 2 H), 1.51 (m, 2 H), 0.98 ppm (t, 3 H, J = 6.5 Hz); ¹³C NMR (125 MHz, CDCl₃): δ = 165.49, 163.38, 144.06, 143.27, 132.16,

122.38, 121.89, 115.70, 114.22, 67.98, 31.15, 19.20, 13.81 ppm; elemental analysis: C₁₇H₁₉NO₃; calculated (%): C 71.55, H 6.70, N 4.90; found: C 71.52, H 6.76, N 4.94.

Compound 11b. IR (film) ν_{\max} : 3402, 3294, 2953, 2922, 2854, 1724, 1606, 1514, 1454, 1377 cm⁻¹; ¹H NMR (500 MHz, CDCl₃): δ = 8.11 (d, 2 H, J = 8.5 Hz), 6.96 (m, 4 H), 6.70 (d, 2 H, J = 8 Hz), 4.03 (t, 2 H, J = 6.5 Hz), 3.64 (s, 2 H), 1.84–1.81 (m, 2 H), 1.49–1.46 (m, 2 H), 1.35 (br, 4 H), 0.91 ppm (t, 3 H, J = 6.5 Hz); ¹³C NMR (125 MHz, CDCl₃): δ = 165.52, 163.38, 144.07, 143.25, 132.18, 122.29, 121.84, 115.71, 114.22, 68.30, 31.56, 29.08, 25.67, 22.60, 14.04 ppm; elemental analysis: C₁₉H₂₃NO₃; calculated (%): C 72.81, H 7.39, N 4.46; found: C 72.86, N 7.46, N 4.51.

Compound 11c. IR (film) ν_{\max} : 3464, 3373, 2955, 2920, 2852, 1714, 1604, 1510, 1456, 1375 cm⁻¹; ¹H NMR (500 MHz, CDCl₃): δ = 8.11 (d, 2 H, J = 8 Hz), 6.96 (m, 4 H), 6.70 (d, 2 H, J = 8 Hz), 4.03 (t, 2 H, J = 6.5 Hz), 3.64 (s, 2 H), 1.82–1.80 (m, 2 H), 1.48–1.44 (m, 2 H), 1.34–1.29 (m, 8 H), 0.90 ppm (t, 3 H, J = 6.5 Hz); ¹³C NMR (500 MHz, CDCl₃): δ = 165.51, 163.38, 144.07, 143.26, 132.17, 122.38, 121.86, 115.70, 114.23, 68.31, 31.81, 29.33, 29.22, 29.11, 25.99, 22.66, 14.10 ppm; elemental analysis: C₂₁H₂₇NO₃; calculated (%): C 73.87, H 7.96, N 4.10; found: C 73.91, H 8.01, N 4.15.

Compound 11d. IR (film) ν_{\max} : 3406, 3302, 2920, 2852, 1714, 1606, 1510, 1456, 1377 cm⁻¹; ¹H NMR (500 MHz, CDCl₃): δ = 8.11 (d, 2 H, J = 8 Hz), 6.96 (m, 4 H), 6.70 (d, 2 H, J = 8 Hz), 4.03 (t, 2 H, J = 6.5 Hz), 3.64 (s, 2 H), 1.81 (br, 2 H), 1.46 (br, 2 H), 1.36–1.28 (m, 12 H), 0.88 ppm (t, 3 H, J = 6.5 Hz); ¹³C NMR (125 MHz, CDCl₃): δ = 165.49, 163.38, 144.07, 143.28, 132.16, 122.38, 121.89, 115.69, 114.23, 68.31, 31.89, 29.55, 29.36, 29.31, 29.11, 25.98, 22.68, 14.10 ppm; elemental analysis: C₂₃H₃₁NO₃; calculated (%): C 74.76, H 8.44, N 3.78; Found: C 75.01, H 8.49, N 3.83.

Compound 11e. IR (film) ν_{\max} : 3458, 3369, 2928, 2912, 2850, 1714, 1604, 1514, 1454, 1377 cm^{-1} ; ^1H NMR (500 MHz, CDCl_3): δ = 8.11 (d, 2 H, J = 7.5 Hz), 6.96 (m, 4 H), 6.70 (d, 2 H, J = 7.5 Hz), 4.03 (t, 2 H, J = 6.5 Hz), 3.64 (s, 2 H), 1.81 (br, 2 H), 1.46 (br, 2 H), 1.35–1.27 (m, 16 H), 0.88 ppm (t, 3 H, J = 6.5 Hz); ^{13}C NMR (125 MHz, CDCl_3): δ = 165.50, 163.39, 144.07, 143.27, 132.17, 122.38, 121.88, 115.70, 114.23, 68.32, 31.93, 29.66, 29.64, 29.59, 29.56, 29.36, 29.12, 25.99, 22.69, 14.12 ppm; elemental analysis: $\text{C}_{25}\text{H}_{35}\text{NO}_3$; calculated (%): C 75.53, H 8.86, N 3.52; found: C 75.59, H 8.93, N 3.57.

Compound 11f. IR (film) ν_{\max} : 3423, 3331, 2908, 2897, 2872, 1730, 1606, 1512, 1454, 1377 cm^{-1} ; ^1H NMR (500 MHz, CDCl_3): δ = 8.11 (d, 2 H, J = 8 Hz), 6.96 (m, 4 H), 6.70 (d, 2 H, J = 8 Hz), 4.03 (t, 2 H, J = 6.5 Hz), 3.64 (s, 2 H), 1.81 (br, 2 H), 1.46 (br, 2 H), 1.35–1.26 (m, 19 H), 0.88 ppm (t, 3 H, J = 6.5 Hz); ^{13}C NMR (125 MHz, CDCl_3): δ = 165.49, 163.39, 144.06, 143.28, 132.16, 122.38, 115.69, 114.23, 68.31, 31.93, 29.69, 29.65, 29.59, 29.55, 29.36, 29.11, 25.99, 22.69, 14.11 ppm; elemental analysis: $\text{C}_{27}\text{H}_{39}\text{NO}_3$; calculated (%): C 76.19, H 9.22, N 3.28; found: C 76.24, H 9.28, N 3.34.

Synthesis of 2,3-dihydrothieno[3,4-*b*][1,4]dioxine-5,7-dicarbaldehyde (13)

1.6 M solution of *n*-butyl lithium (29 mL) was added dropwise to a stirring solution of EDOT **12** (3 g, 0.021 mol) in dry THF (50 mL) at -78 °C under N_2 atmosphere. After addition, the reaction mixture was slowly raised to temperature to 0 °C and stirred same at temperature for 30 minutes. Again the reaction mixture was recooled to -78 °C and quenched with dry DMF (3.5 mL). The reaction mixture was stirred at room temperature for 2 hours. The resulting reaction mixture was poured in to crushed ice containing HCl (pH = 4). The brown colour solid precipitated out and filtered off, washed with excess of water and dried *in vacuo*. Recrystallisation of crude product with cold methanol gives brown colour solid **13**. Yield: 75%. IR (film) ν_{\max} : 2955, 2924, 2854, 1666, 1614, 1504, 1454, 1375 cm^{-1} ; ^1H NMR (500 MHz, CDCl_3): δ = 10.04 (s, 2 H), 4.46 (s, 4 H); ^{13}C NMR (125 MHz, CDCl_3): 180.94, 147.15, 124.16, 65.15; elemental analysis: $\text{C}_8\text{H}_6\text{O}_4\text{S}$; calculated (%): C 48.48, H 3.04, S 16.14; found: C 48.51, H 3.06, S 16.14. ^1H and ^{13}C NMR are shown in **Figure 13**.

Synthesis of final compounds 5a–5b and 6a–6f.

The condensation reaction between 4-alkoxy aniline or 4-aminophenyl-4-alkoxybenzoate with EDOT-2,5-dialdehyde **13** gives Schiff base mesogenic derivatives. The general method described as follows.

3,4-Ethylenedioxythiophene-3,5-dicarboxyaldehyde **13** (0.2 g, 0.86 mmol) and 4-alkoxyaniline (**9a–9b**) or 4-aminophenyl 4-alkoxybenzoate (**11a–11f**) (3.47 mmol) was dissolved in 20 mL of absolute ethanol and few drops of glacial acetic acid was added. The reaction mixture was refluxed for 4 hours in presence on nitrogen atmosphere. After completion of reaction, the solid was filtered off and crude solid was purified by repeated recrystallization from isopropyl alcohol gives pure yellow coloured compounds **5a–5b** and **6a–6f**. Yield: 75–85 %. Representative ^1H and ^{13}C NMR spectra of compounds **5a** and **6c** are shown in **Figure 14** and **15** respectively.

Compound 5a. IR (film) ν_{max} : 2953, 2918, 2852, 1614, 1516, 1462, 1377 cm^{-1} ; ^1H NMR (500 MHz, CDCl_3): δ = 8.61 (s, 2 H), 7.16 (m, 8 H), 4.36 (s, 4 H), 2.61 (t, 4 H, $J = 7$ Hz), 1.62–1.59 (m, 4 H), 1.38–1.34 (m, 4 H), 0.94 ppm (t, 3 H, $J = 6.5$ Hz); ^{13}C NMR (125 MHz, CDCl_3): 149.01, 148.11, 143.61, 141.20, 129.07, 121.16, 121.01, 65.09, 35.23, 33.67, 22.34, 13.96 ppm. elemental analysis: $\text{C}_{28}\text{H}_{32}\text{N}_2\text{O}_2\text{S}$; calculated (%): C 73.01, H 6.99, N 6.07, S 6.94; found: C 73.07, H 7.04, N 6.11, S 6.97.

Compound 5b. IR (film) ν_{max} : 2953, 2918, 2852, 1614, 1516, 1462, 1377 cm^{-1} ; ^1H NMR (500 MHz, CDCl_3): δ = 8.61 (s, 2 H), 7.17 (d, 2 H, $J = 8$ Hz), 6.89 (d, 2 H, $J = 8$ Hz), 4.36 (s, 4 H), 3.96 (t, 4 H, $J = 6.5$ Hz), 1.79–1.75 (m, 4 H), 1.46–1.42 (m, 4 H), 1.35–.25 (m, 54 H), 0.89 ppm (br, 6 H); ^{13}C NMR (125 MHz, CDCl_3): 158.04, 146.71, 122.52, 114.93, 68.30, 65.08, 31.93, 29.70, 29.67, 29.61, 29.59, 29.42, 29.37, 29.31, 26.06, 22.70, 14.12 ppm; elemental analysis: $\text{C}_{56}\text{H}_{88}\text{N}_2\text{O}_4\text{S}$; calculated (%): C 75.96, H 10.0, N 3.16, S 3.61; found: C 75.99, H 10.04, N 3.19, S 3.63.

Compound 6a. IR (film) ν_{\max} : 2918, 2906, 2852, 1716, 1606, 1508, 1454, 1377 cm^{-1} ; ^1H NMR (500 MHz, CDCl_3): δ = 8.63 (s, 2 H), 8.14 (d, 4 H, J = 8.5 Hz), 7.29 (d, 4 H, J = 8 Hz), 7.21 (d, 4 H, J = 8 Hz), 6.97 (d, 4 H, J = 8.5 Hz), 4.39 (s, 4 H), 4.05 (t, 4 H, J = 6.5 Hz), 1.82–1.80 (m, 4 H), 1.51 (br, 4 H), 1.0 ppm (t, 6 H, J = 7.5 Hz); ^{13}C NMR (125 MHz, CDCl_3): 165.03, 163.58, 149.42, 148.97, 148.93, 143.97, 132.29, 122.39, 122.16, 121.53, 121.05, 114.31, 68.02, 65.13, 31.15, 19.20, 13.82 ppm. elemental analysis: $\text{C}_{42}\text{H}_{40}\text{N}_2\text{O}_8\text{S}$; calculated (%): C 68.83, H 5.49, N 3.82, S 4.36; found: C 68.87, H 5.54, N 3.84, S 4.39.

Compound 6b. IR (film) ν_{\max} : 2928, 2854, 1722, 1604, 1510, 1454, 1377 cm^{-1} ; ^1H NMR (500 MHz, CDCl_3): δ = 8.63 (s, 2 H), 8.14 (d, 4 H, J = 8 Hz), 7.29 (d, 4 H, J = 8.5 Hz), 7.21 (d, 4 H, J = 8 Hz), 6.97 (d, 4 H, J = 8.5 Hz), 4.39 (s, 4 H), 4.05 (t, 4 H, J = 6.5 Hz), 1.84–1.81 (m, 4 H), 1.48 (br, 4 H), 1.36 (br, 8 H), 0.92 ppm (br, 6 H); ^{13}C NMR (125 MHz, CDCl_3): 165.02, 163.58, 149.42, 148.96, 143.97, 132.29, 122.38, 122.16, 114.32, 68.35, 65.13, 31.55, 29.08, 25.67, 22.59, 14.02 pm; elemental analysis: $\text{C}_{46}\text{H}_{48}\text{N}_2\text{O}_8\text{S}$; calculated (%): C 70.03, H 9.95, N 3.54, S 4.05; found: C 70.09, H 9.99, N 3.57, S 4.07.

Compound 6c. IR (film) ν_{\max} : 2955, 2924, 2854, 1716, 1604, 1508, 1456, 1363 cm^{-1} ; ^1H NMR (500 MHz, CDCl_3): δ = 8.63 (s, 2 H), 8.14 (d, 4 H, J = 8 Hz), 7.29 (d, 4 H, J = 8 Hz), 7.21 (d, 4 H, J = 8 Hz), 6.97 (d, 4 H, J = 8 Hz), 4.39 (s, 4 H), 4.04 (t, 4 H, J = 6.5 Hz), 1.83–1.81 (m, 4 H), 1.48–1.46 (m, 4H), 1.34–1.30 (m, 16 H), 0.89 ppm (m, 6H); ^{13}C NMR (125 MHz, CDCl_3): 165.03, 163.57, 149.41, 148.97, 148.93, 143.98, 132.29, 122.39, 122.17, 121.51, 121.04, 114.31, 68.35, 65.13, 31.81, 29.34, 29.23, 29.11, 26, 22.66, 14.11 ppm; elemental analysis: $\text{C}_{50}\text{H}_{56}\text{N}_2\text{O}_8\text{S}$; calculated (%): C 71.06, H 6.67, N 3.31, S 3.78; found: C 71.10, H 6.69, N 3.33, S 3.80.

Compound 6d. IR (film) ν_{\max} : 2953, 2922, 2852, 1714, 1606, 1508, 1454, 1365 cm^{-1} ; ^1H NMR (500 MHz, CDCl_3): δ = 8.63 (s, 2 H), 8.14 (d, 4 H, J = 8 Hz), 7.29 (d, 4 H, J = 8 Hz), 7.21 (d, 4 H, J = 8 Hz), 6.97 (d, 4 H, J = 8 Hz), 4.39 (s, 4 H), 4.04 (t, 4 H, J = 6.5 Hz), 1.83–1.81 (m,

4 H), 1.49–1.46 (m, 4 H), 1.37–1.28 (m, 24 H), 0.90 ppm (br, 6 H); ^{13}C NMR (125 MHz, CDCl_3): 165.01, 163.58, 149.43, 148.94, 143.97, 132.29, 122.38, 122.15, 121.54, 121.06, 114.33, 68.36, 65.13, 31.90, 29.56, 29.36, 29.31, 29.11, 25.99, 22.68, 14.11 ppm; elemental analysis: $\text{C}_{54}\text{H}_{64}\text{N}_2\text{O}_8\text{S}$; calculated (%): C 71.97, H 7.15, N 3.10, S 3.55; found: C 72.01, H 7.18, N 3.13, S 3.56.

Compound 6e. IR (film) ν_{max} : 2924, 2852, 1730, 1604, 1510, 1454, 1363 cm^{-1} ; ^1H NMR (500 MHz, CDCl_3): δ = 8.63 (s, 2 H), 8.14 (d, 4 H, J = 8 Hz), 7.29 (d, 4 H, J = 8 Hz), 7.21 (d, 4 H, J = 8 Hz), 6.97 (d, 4 H, J = 8 Hz), 4.39 (s, 4 H), 4.04 (t, 4H, J = 6 Hz), 1.83–1.80 (m, 4 H), 1.47 (br, 4 H), 1.36–1.27 (m, 32 H), 0.88 ppm (t, 6 H, J = 6 Hz); ^{13}C NMR (125 MHz, CDCl_3): 165.01, 163.58, 149.43, 148.94, 143.96, 132.28, 122.38, 122.15, 121.55, 121.07, 114.33, 68.36, 65.13, 31.92, 29.66, 29.63, 29.59, 29.56, 29.36, 29.35, 29.11, 25.99, 22.69, 14.11 ppm; elemental analysis: $\text{C}_{58}\text{H}_{72}\text{N}_2\text{O}_8\text{S}$; calculated (%): C 72.77, H 7.57, N 2.92, S 3.34; found: C 72.81, H 7.61, N 2.95, S 3.37.

Compound 6f. IR (film) ν_{max} : 2955, 2924, 2854, 1732, 1604, 1510, 1454, 1377 cm^{-1} ; ^1H NMR (500 MHz, CDCl_3): δ = 8.63 (s, 2 H), 8.14 (d, 4 H, J = 8 Hz), 7.29 (d, 4 H, J = 8 Hz), 7.21 (d, 4 H, J = 8 Hz), 6.97 (d, 4 H, J = 8 Hz), 4.39 (s, 4 H), 4.04 (t, 4 H, J = 6 Hz), 1.83–1.81 (m, 4 H), 1.36–1.26 (m, 42 H), 0.88 ppm (t, 6 H, J = 6 Hz); ^{13}C NMR (125 MHz, CDCl_3): 165, 163.58, 148.97, 148.93, 143.97, 132.29, 122.39, 122.16, 114.32, 68.36, 65.13, 31.93, 29.70, 29.67, 29.60, 29.57, 29.37, 29.11, 25.99, 22.70, 14.12 ppm; elemental analysis: $\text{C}_{62}\text{H}_{80}\text{N}_2\text{O}_8\text{S}$; calculated (%): C 73.48, H 7.94, N 2.76, S 3.15; found: C 73.52, H 7.97, N 2.79, S 3.19.

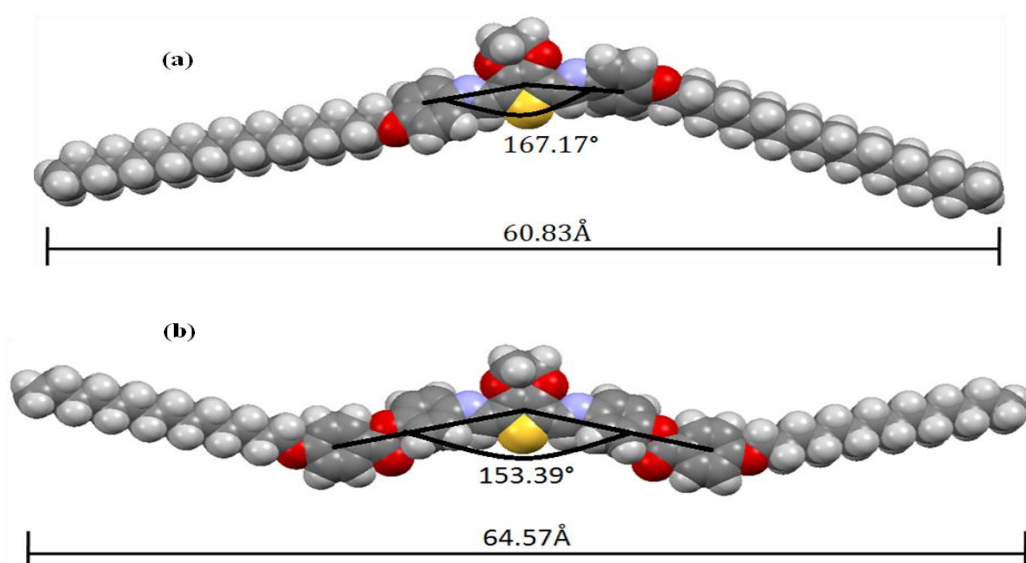


Figure 1. DFT optimized structures. (a) The molecular structure of three-ring compound **5b** and (b) five-ring compound **6f** optimized at DFT level. The bent angles are 167.17° (**5b**) and 153.39° (**6f**), respectively. The dihedral angles reveal that the phenyl rings are out-of-plane.

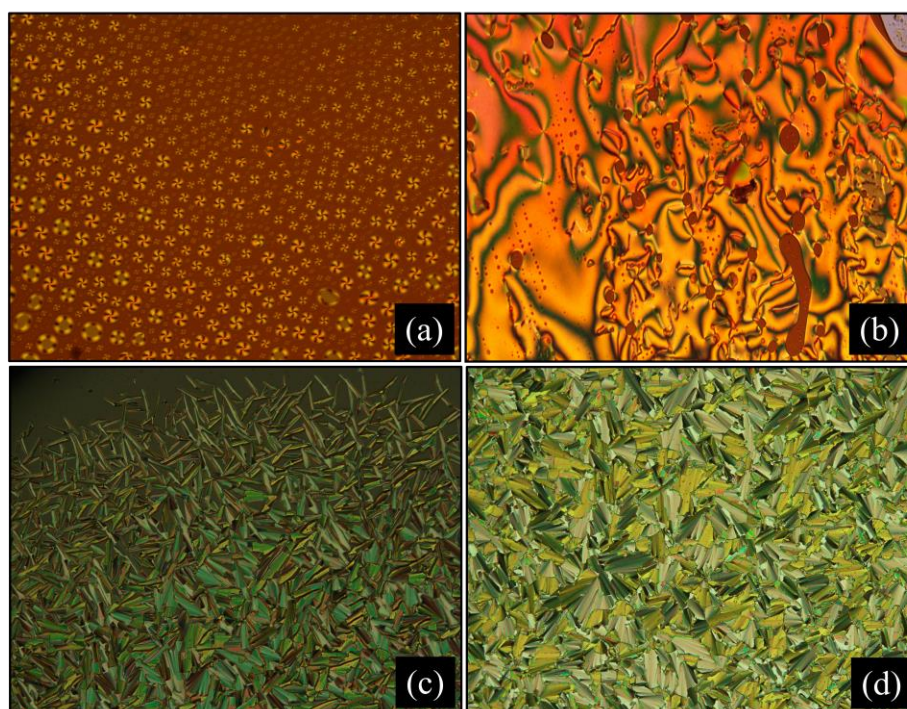


Figure 2. POM textures, for compound **6a**: (a) nematic droplets observed during the early growing stage after cooling from the isotropic liquid at 291°C, viewed at 100 × magnifications, (b) growing of nematic texture on further cooling to 282°C, viewed at 200 × magnifications, for compound **6f**: (c) early growing stage of SmC phase at 197°C, viewed at 100 × magnification, (d) SmC texture at 181°C, viewed at 200 × magnifications. The smectic C phase was observed in a 9 μm polyimide-coated LC cell for planar alignment of the sample and viewed through cross-polariser on cooling from nematic phase.

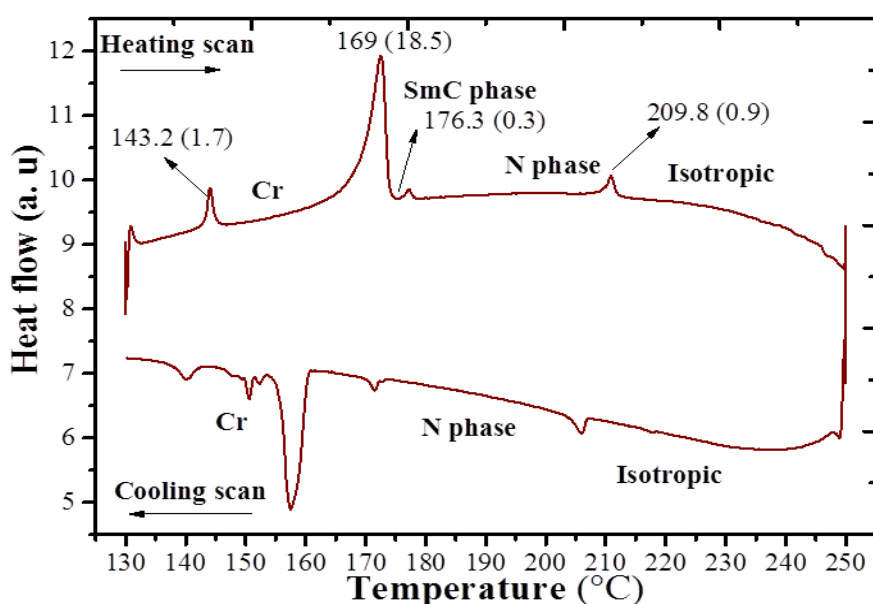


Figure 3. DSC thermograms obtained for the compound **6e** derivative showing phase transitions on heating and cooling cycles at a scan rate of 10°C min⁻¹.

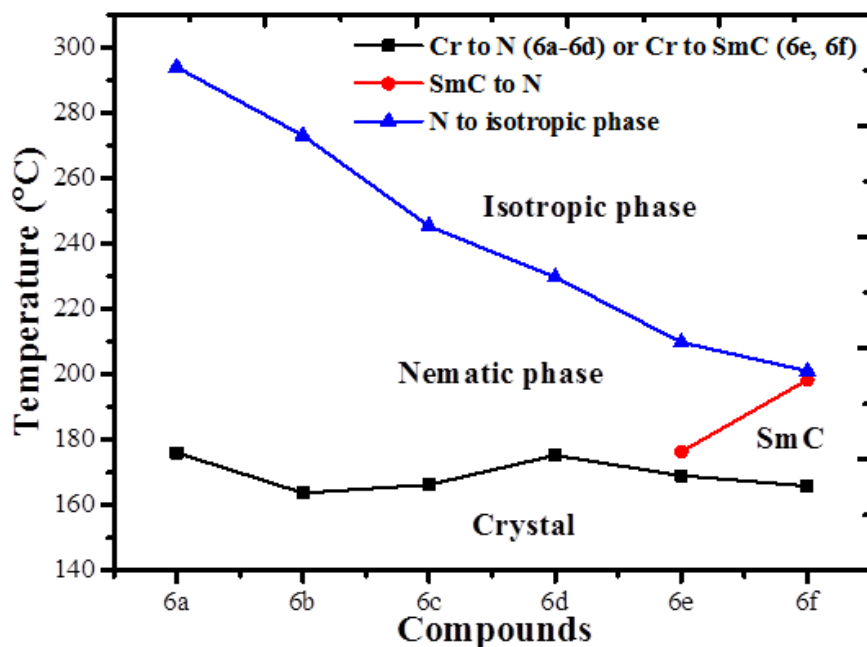


Figure 4. Graphical presentation of the thermal behaviour of compounds **6a–6f**.

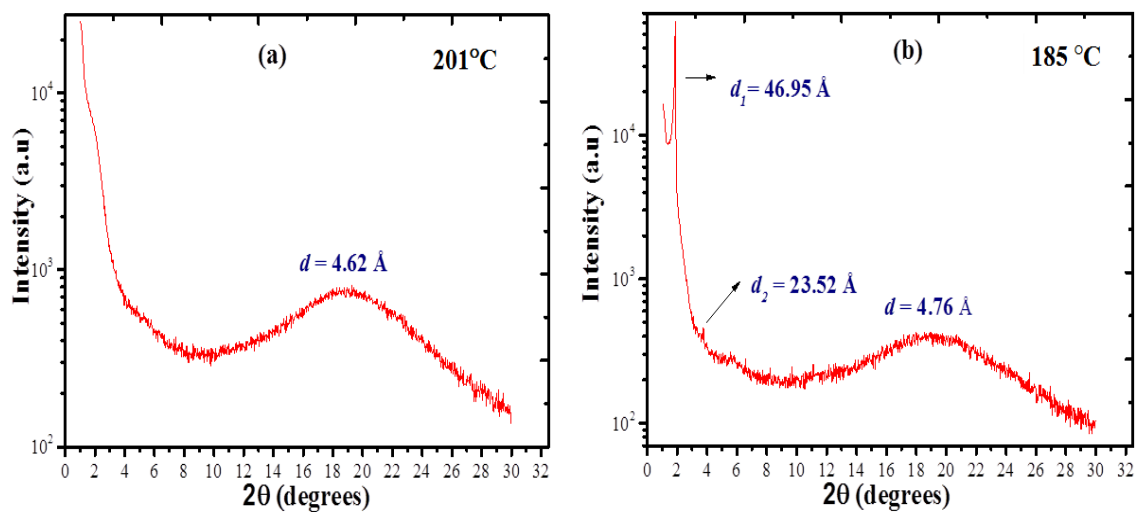


Figure 5. XRD patterns of compound **6f**: (a) nematic phase at 201°C; (b) smectic C phase at 183 °C.

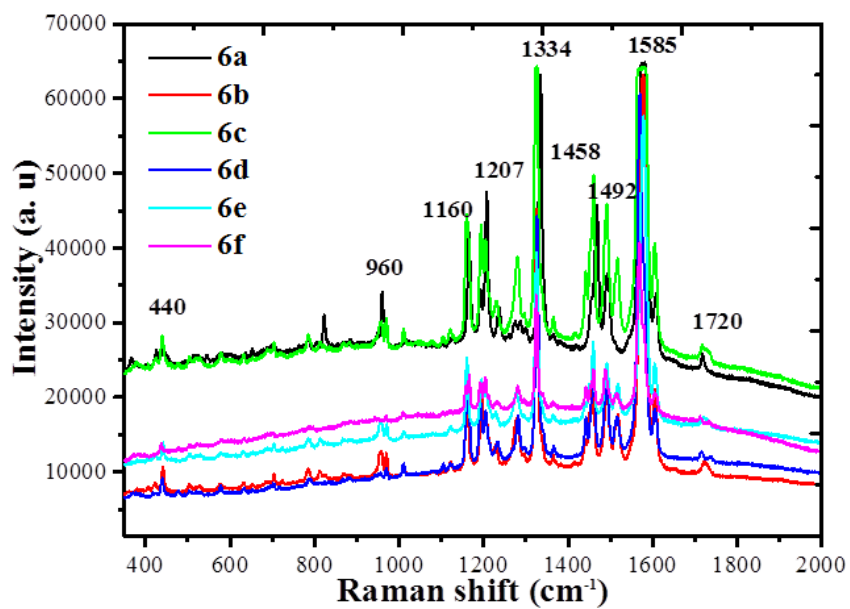


Figure 6. Raman spectrum of mesogenic compounds **6a–6f** over the range 450–2000 cm^{-1} at 298 K.

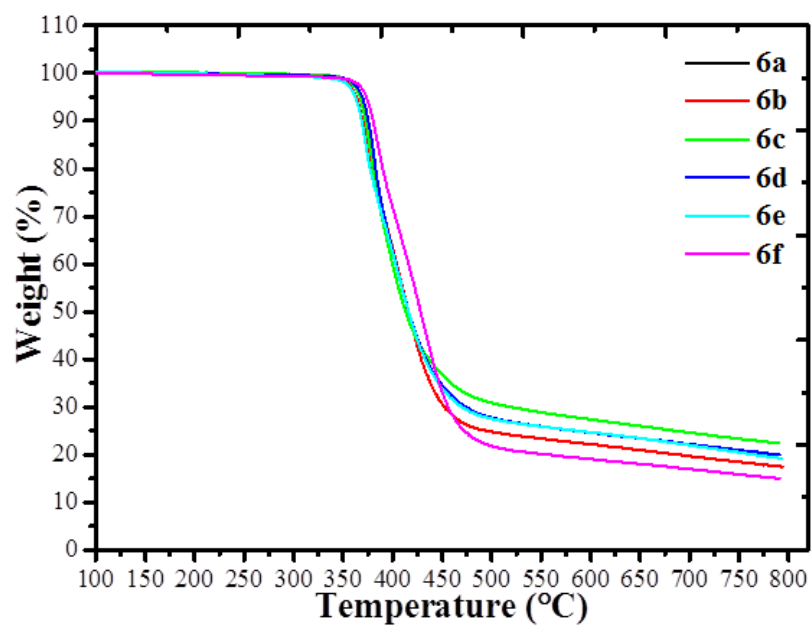


Figure 7. Thermogravimetric analysis of compounds **6a–6f**, respectively.

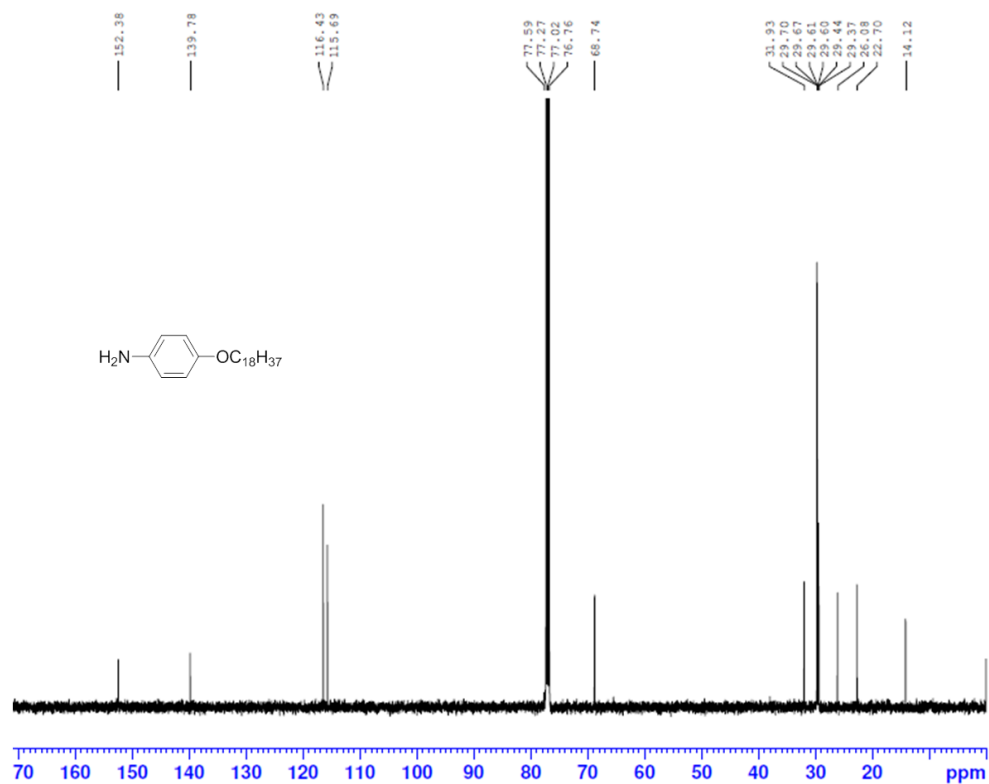
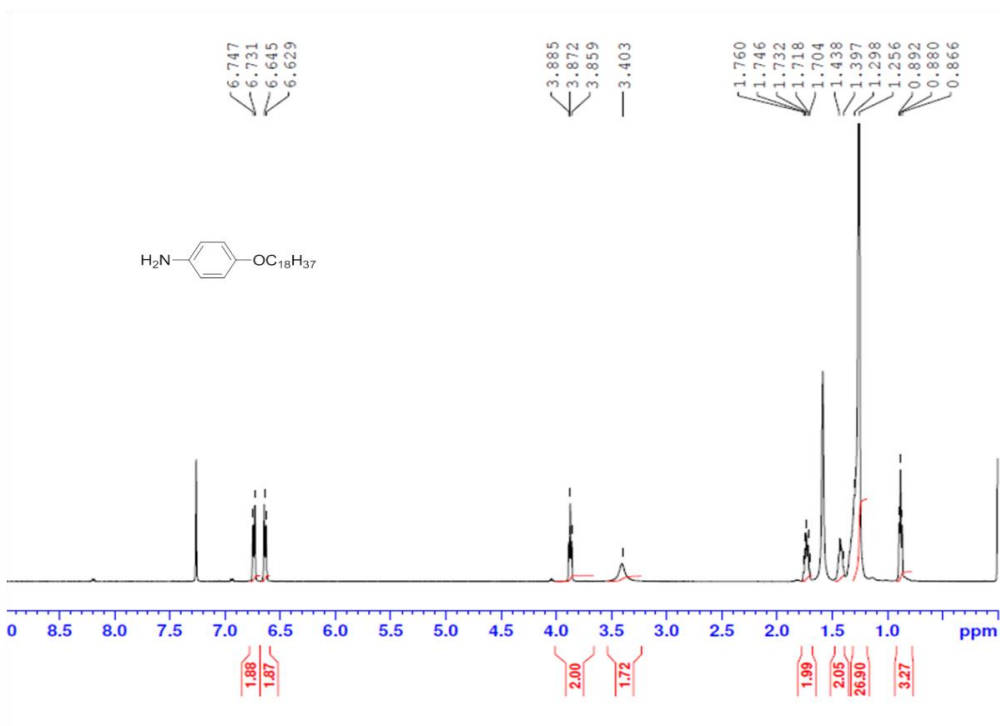


Figure 8. ¹H and ¹³C NMR of compound **9b**.

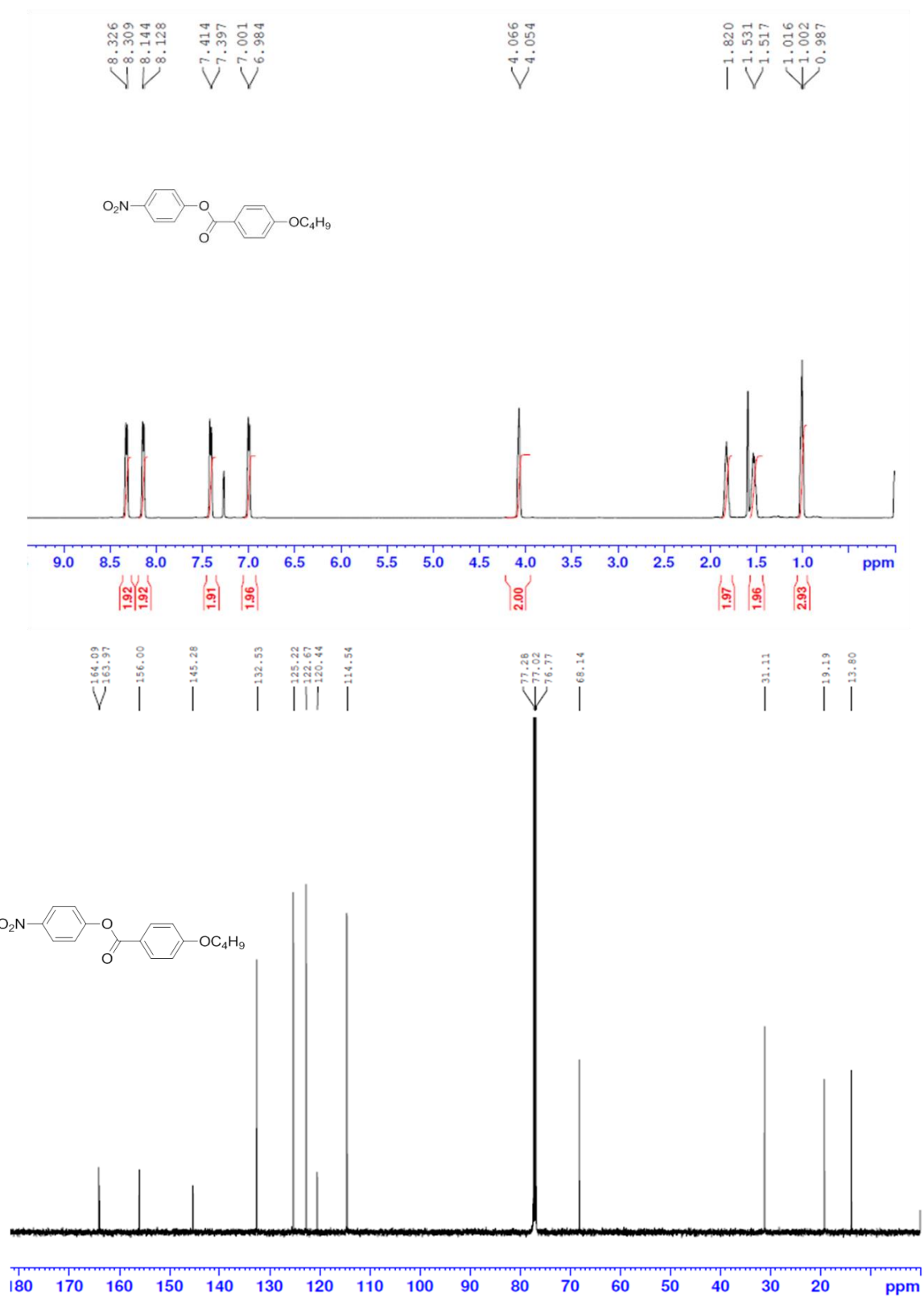


Figure 9. ¹H and ¹³C NMR of compound 10a.

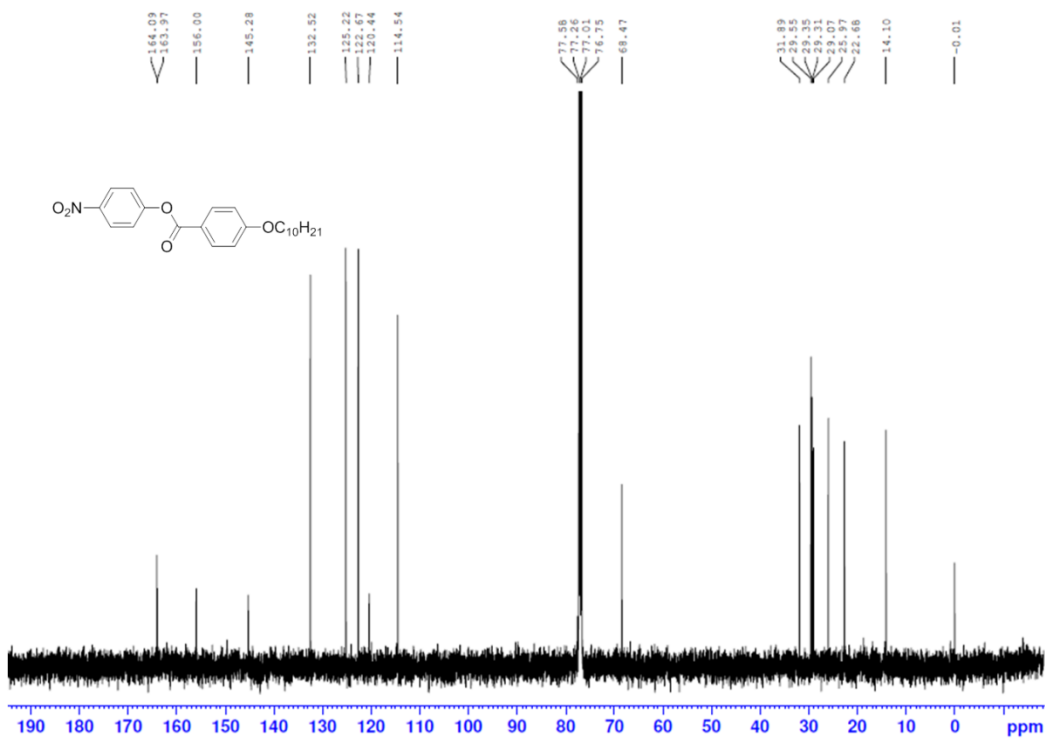
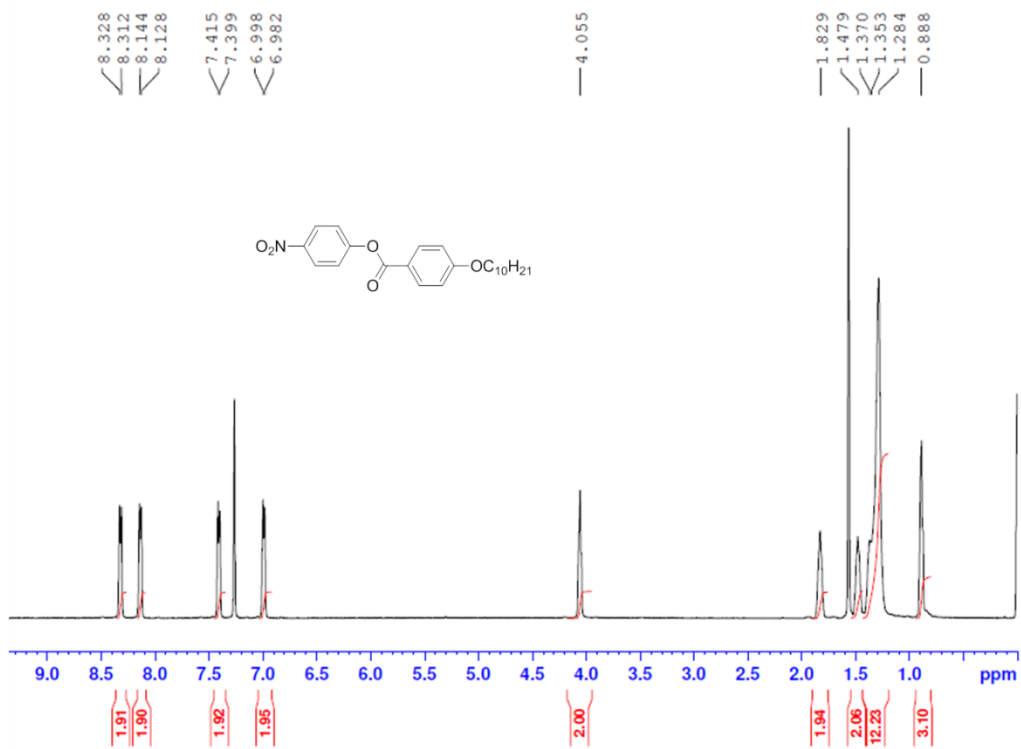


Figure 10. ¹H and ¹³C NMR of compound 10d.

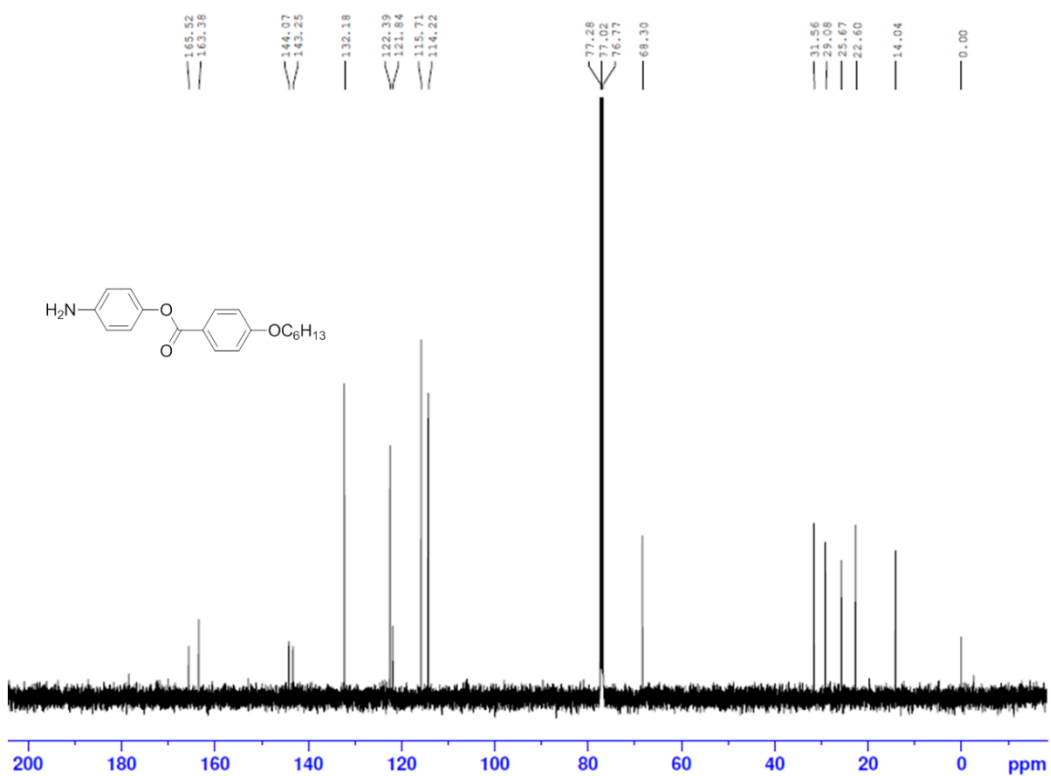
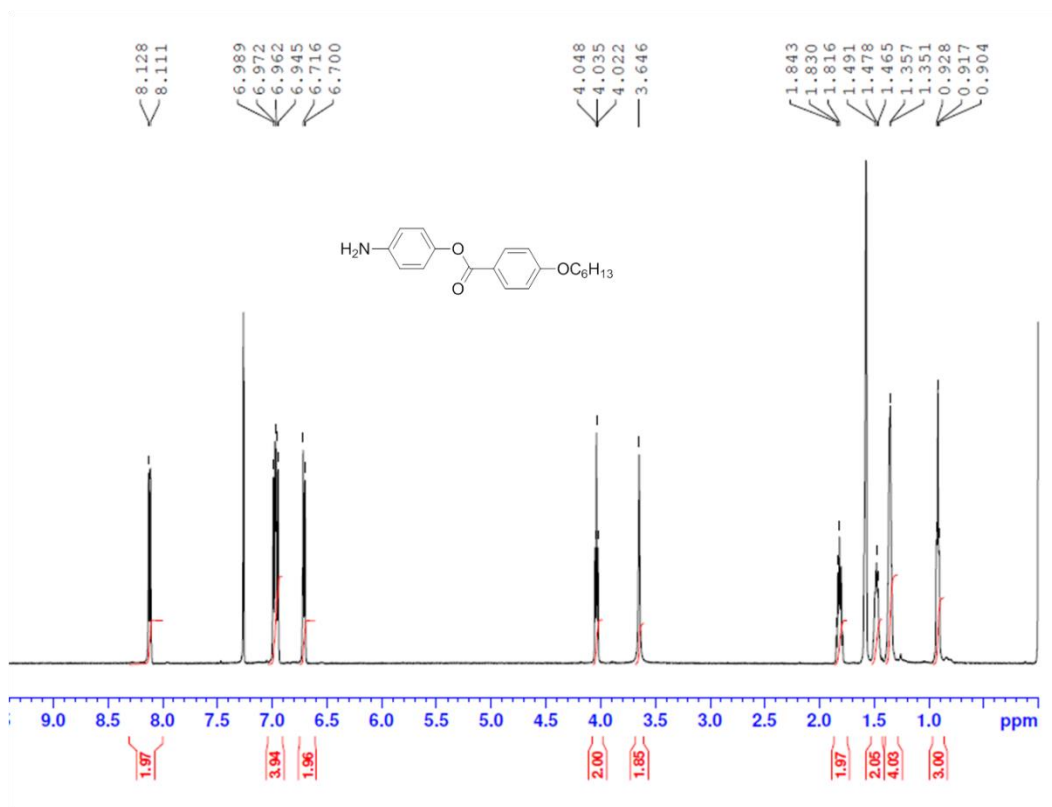


Figure 11. ¹H and ¹³C NMR of compound **11b**.

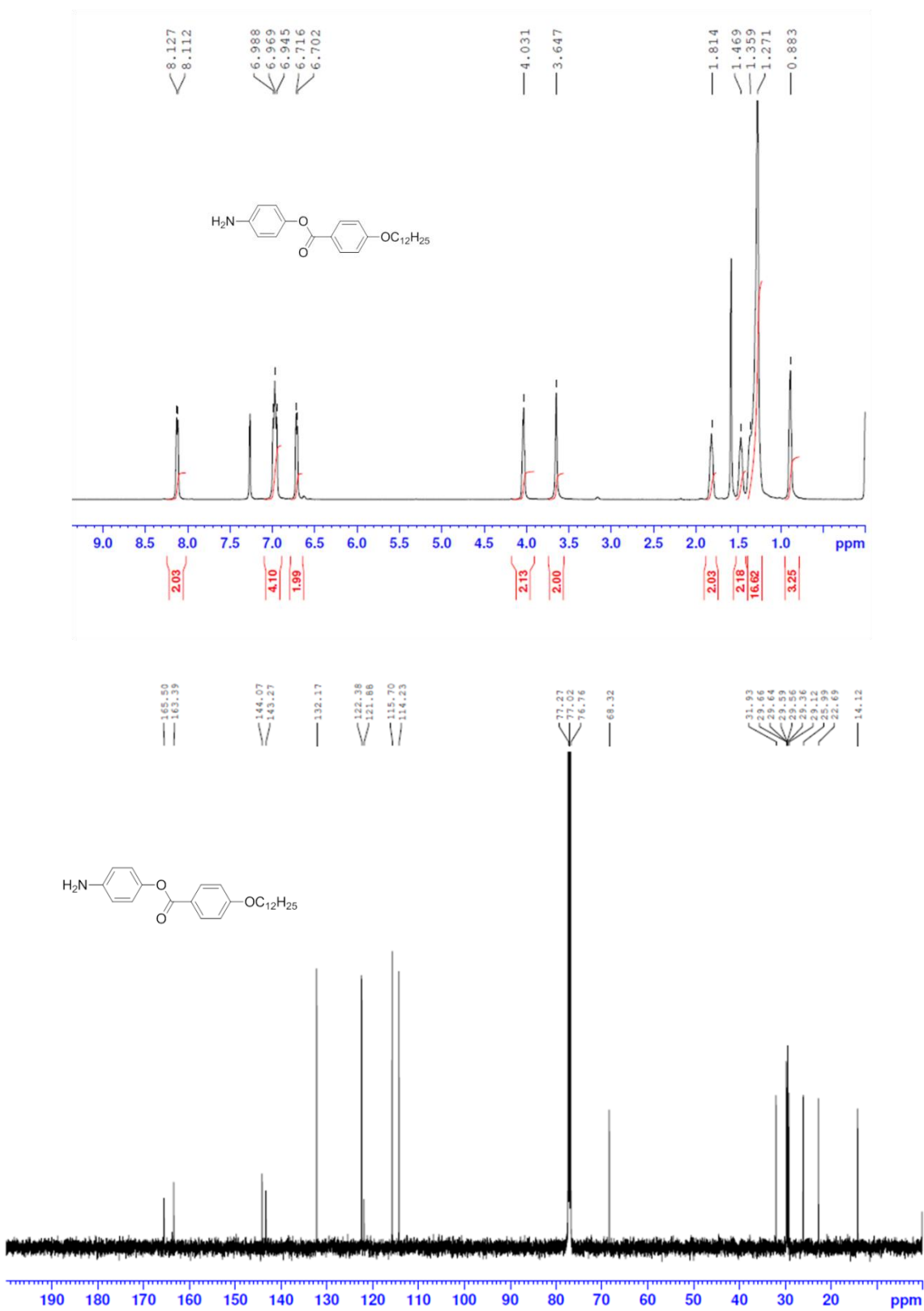


Figure 12. ¹H and ¹³C NMR of compound 11e.

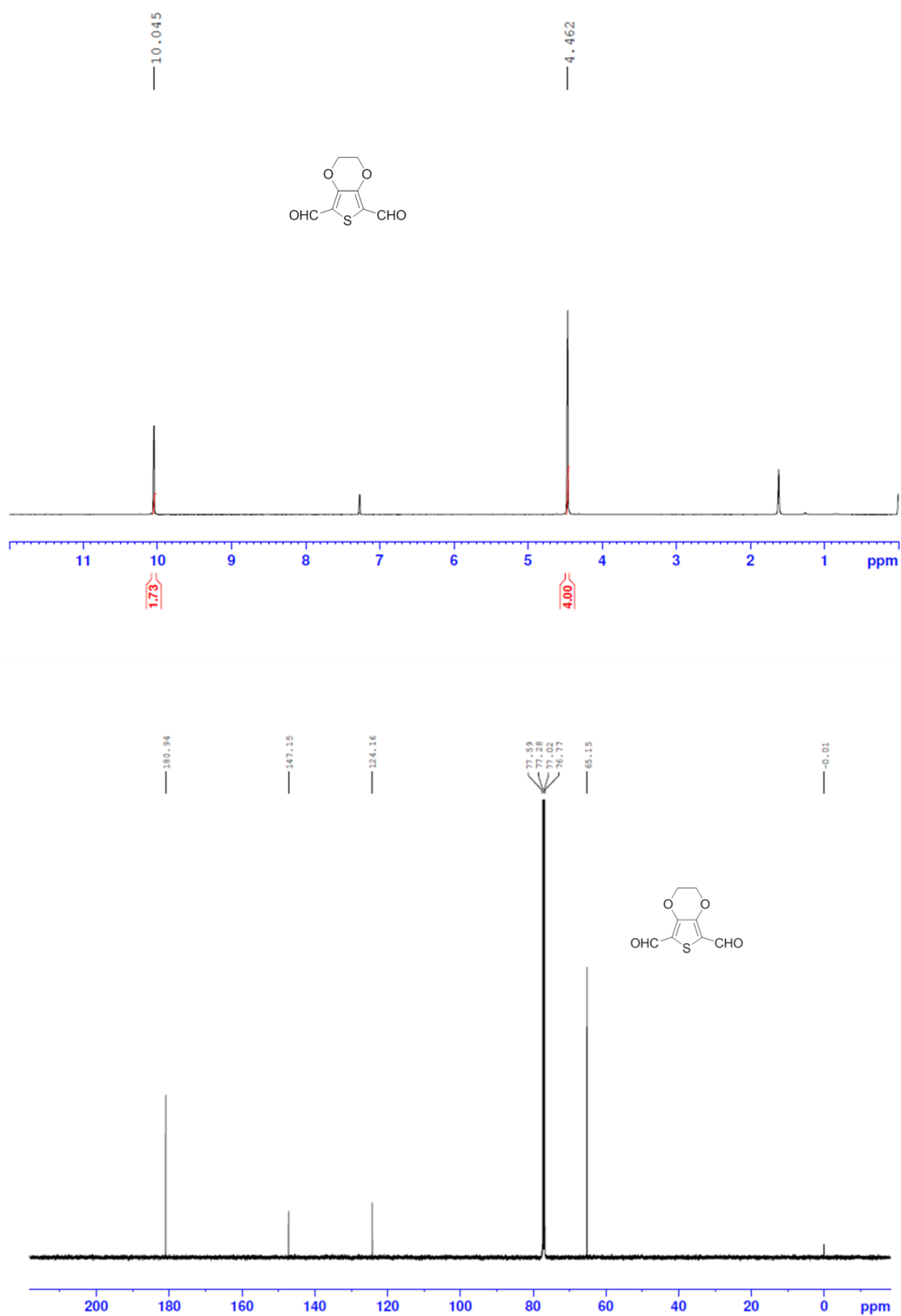


Figure 13. ¹H and ¹³C NMR of compound 13.

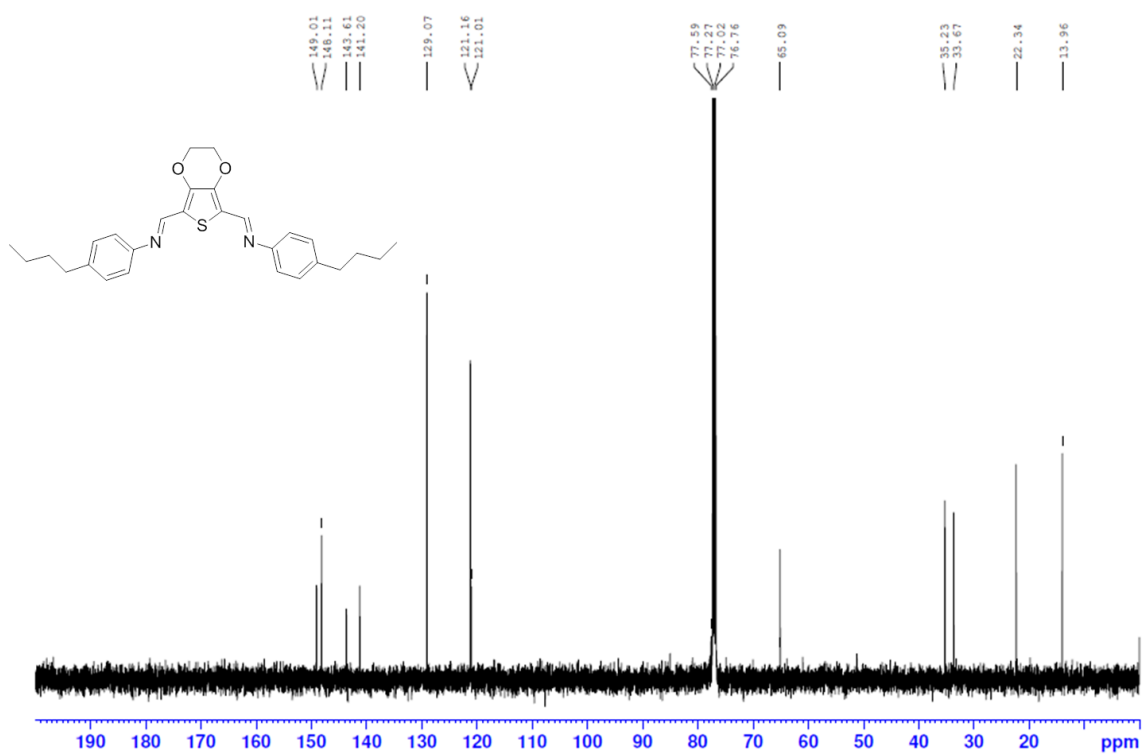
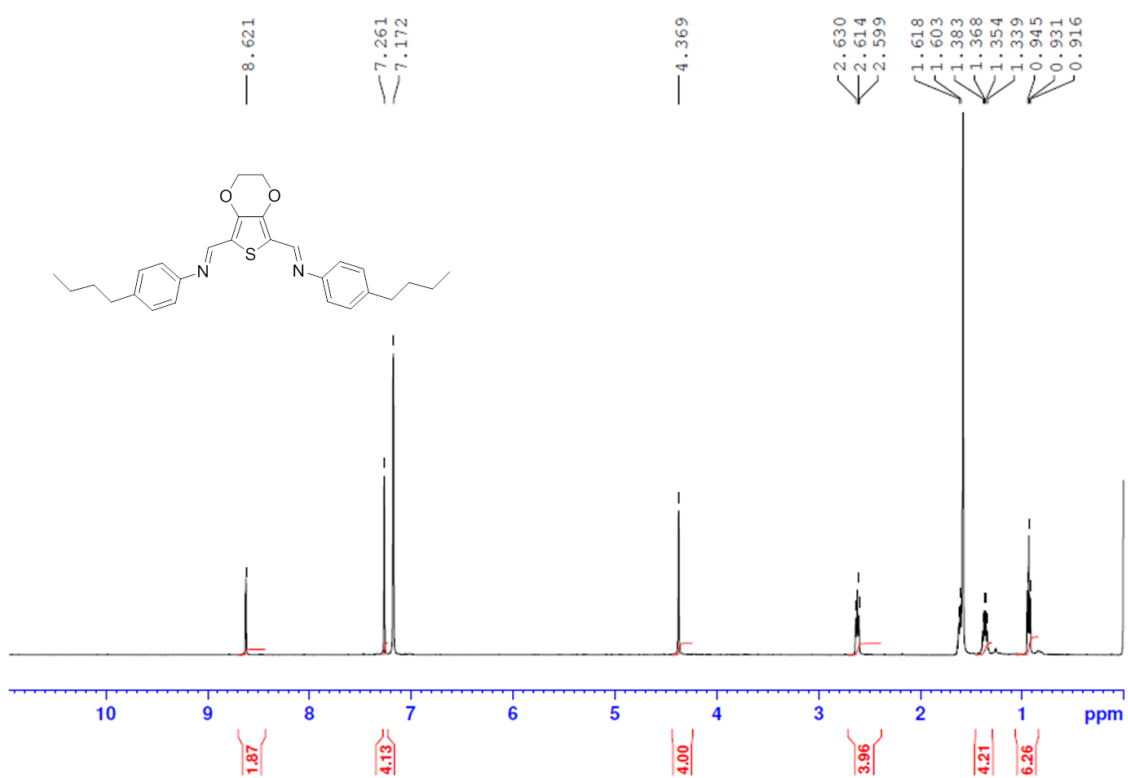


Figure 14. ^1H and ^{13}C NMR of compound 5a.

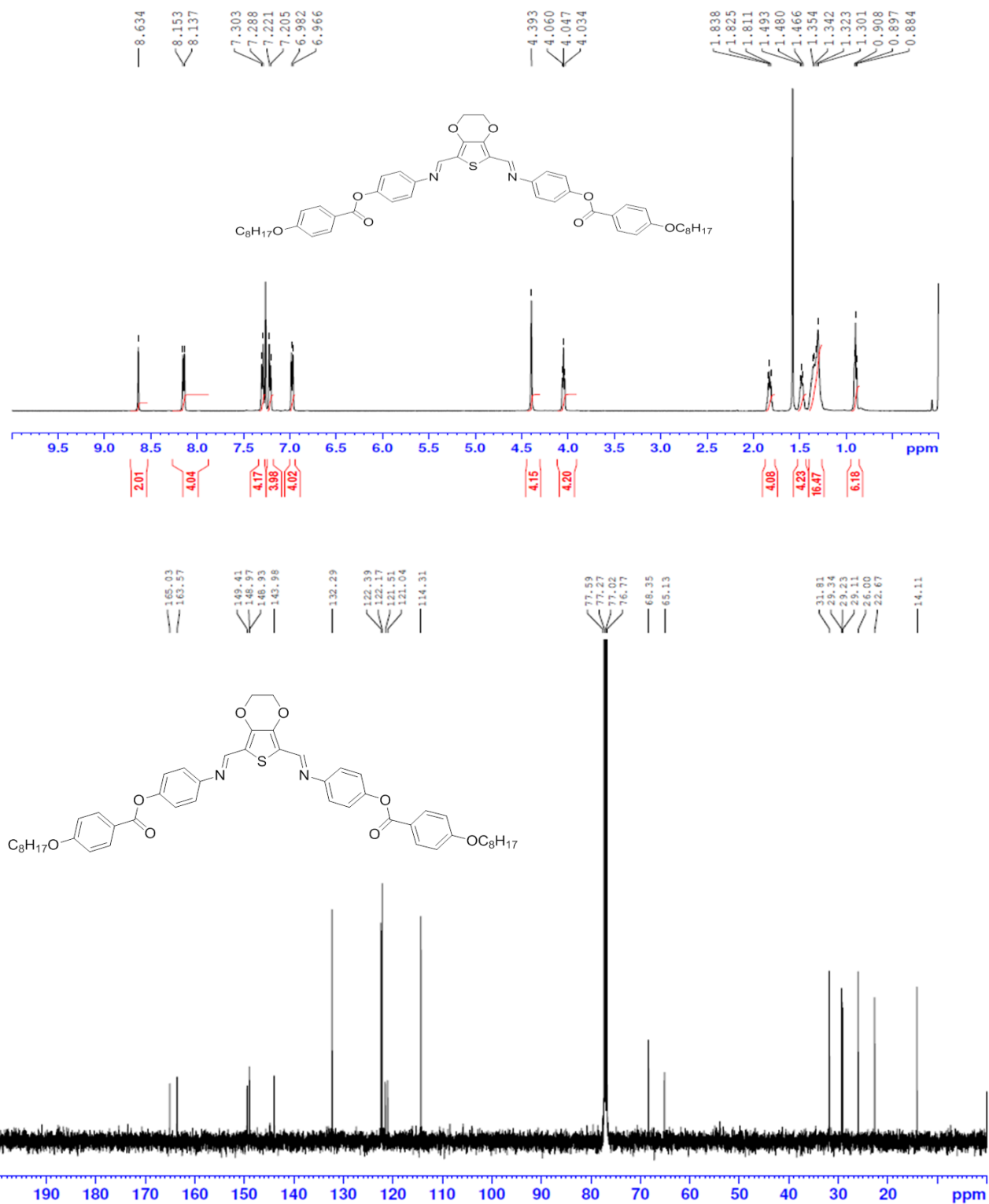


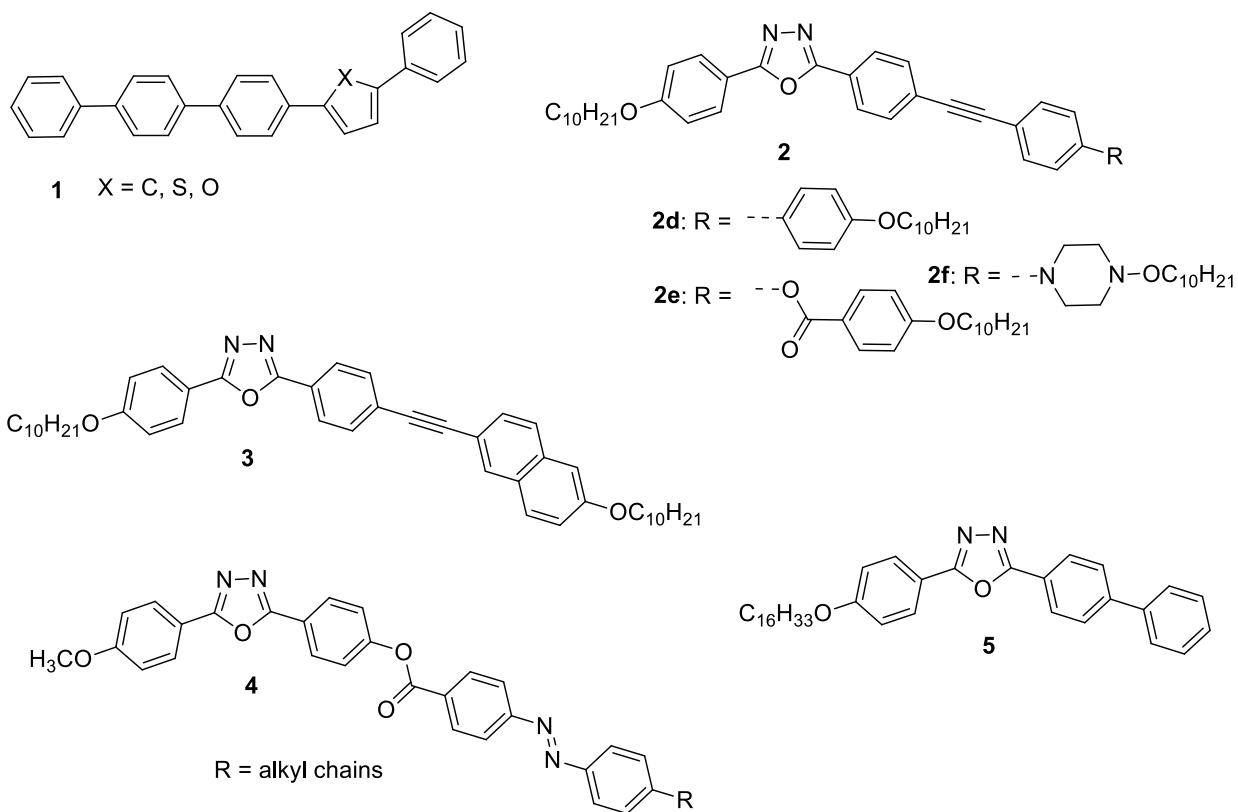
Figure 15. ¹H and ¹³C NMR of compound **6c**.

3.3 Part C. Synthesis, characterization and physical studies of EDOT based bent-core and hockey-stick like liquid crystals

3.3.1 Introduction

The designing of thermotropic liquid crystals involves appropriate selection of different building blocks of rigid cores, spacers and terminal flexible aliphatic chains [49]. Thus, it is significantly important to optimize the molecular structure without losing its liquid crystallinity. Eventually, the molecular shape plays significant role in the self-assembly of LC phases. In addition to research on BC LCs [50,51], recently, significant efforts have been made to change the molecular shape of BC LCs to produce a special kind of nonsymmetrical liquid crystals called “hockey-stick” liquid crystals. Hockey-stick shape compounds are structurally intermediate between rod-like mesogens and true bent core liquid crystals. The asymmetric shape anisotropy of the molecules often results in unusual mesomorphic properties occurring between bent core and calamitic mesogens. Such molecules commonly exhibit nematic and smectic phases with fairly low temperatures. In this regard, hockey stick shape molecules paid focal attention to understand the fresh insight into the structure mesophase properties relationship in these intriguing molecules [52,53].

In 2001, Samulski et al. investigated the structural variation of hockey stick and bent shape liquid crystals derived from *p*- quinquphenyl core (**1**) which exhibit enantiotropic mesophase over broad range. The nonlinearity of mesogens reduces the melting transition temperature [52a]. Gallardo et al. prepared several hockey-stick mesogens derived from 1,3,4-oxadiazole heterocyclic core using Sonagashira coupling reaction (**2** & **3**) and they exhibit very good photophysical properties [54]. Similarly, Scutaru and co-workers have also synthesised hockey-stick liquid crystals from 2,5-asymmetric disubstituted 1,3,4-oxadiazole derivatives containing azo and ester linkage groups **4** and investigated their mesomorphic properties [55].

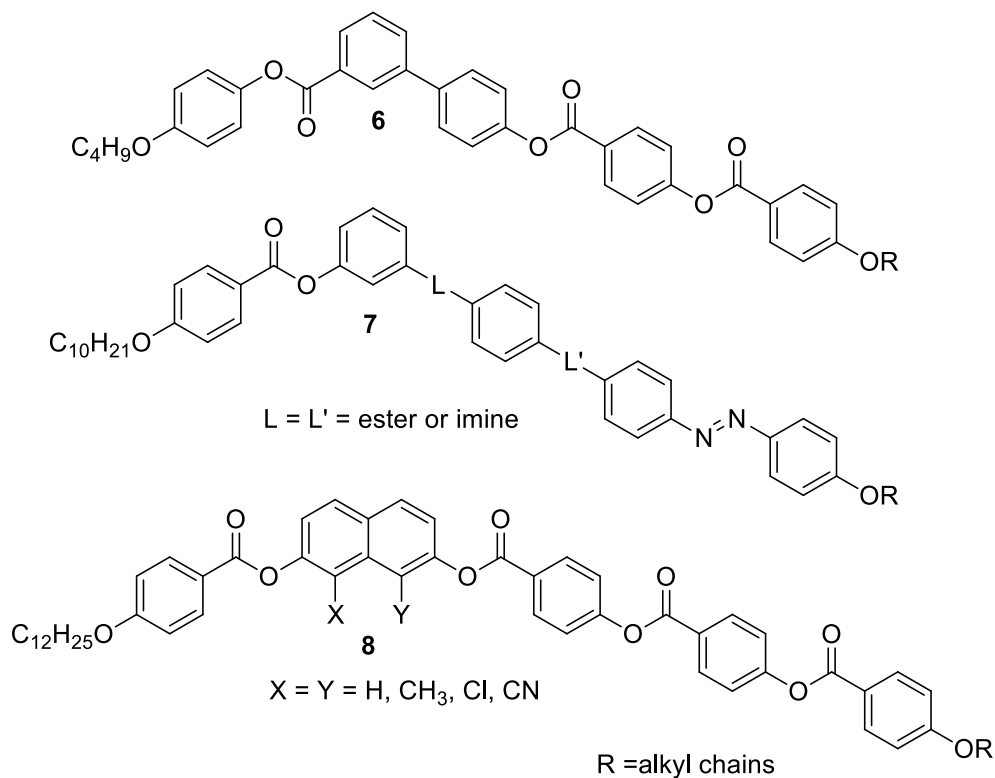


Subsequently, Clark et al. observed the random grain boundary (RGB) phase below the SmA phase of hockey stick molecules synthesised from 1,3,4-oxadiazole central heterocyclic core **5**. They also observed that the RGB phase is a self-assembly of randomly oriented blocks of smectic layers which was observed using freeze-fracture transmission electron microscopy and such arrangement is different from dark, chiral conglomerate phases of bent-core mesogens [56].

Later, Sadashiva and co-workers synthesised a series of five membered hockey stick compounds derived from central benzene core and studied their liquid crystalline properties **6**. All the synthesized compounds exhibit smectic and nematic phases [57]. The compound with heptyloxy chain was further studied for birefringence, dielectric constant, splay, bend elastic constant and rotational viscosity in the nematic phase by Dhar et al. [58].

Recently, Prasad et al. prepared several five membered hockey-stick compounds derived from central 1,3 di-substituted phenyl ring bearing azo linking group **7**. They investigated the

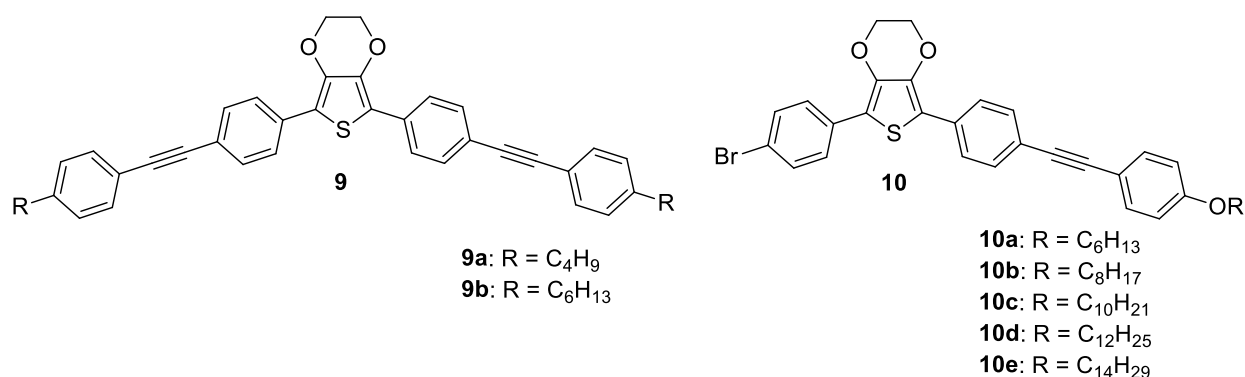
effect of different types of linkages (ester or imine) and their direction of linking groups on the mesomorphic properties [59]. They also observed N, SmA, SmC, SmX and B1 phases.



Svoboda et al. prepared novel hockey-stick liquid crystals derived from lateral substitution (methyl, chloro and cyano groups) of naphthalene central core **8** and exhibit nematic and smectic phases over broad temperature. They investigated dielectric and switching properties [60]. Later, several research groups have reported the synthesis of novel achiral hockey stick-shaped mesogens and studied their mesomorphic and physical properties [61–67].

3.3.2 Objective

In the part A and part B of this chapter, we have presented the synthesis and characterization of a number of novel BC LCs derived from EDOT. Literature search reveals that any hockey stick liquid crystal derived from central EDOT core has not yet been synthesised. In this last part of chapter, we aimed to deals with the synthesis and mesomorphic characterization of some new five membered BC (**9a–9b**) and hockey-stick LCs (**10a–10e**) derived from EDOT central unit.



3.3.3 Results and discussion

3.3.3.1 Density functional theory calculations

Density functional theory based quantum chemical calculations has been performed in gaseous phase to calculate the related molecular parameters such as, bend angle, molecular length, dihedral angle etc., using Gaussian 16 computational package at the level of 6-311 G(d) basis set, Becke's three-parameter functional and Lee-Yang-Parr correlation functional (B3LYP). The internal coordinates of the molecular system, which is used as input for Gaussian 16 computational program was generated by the Gauss View 06 program [29].

The absences of any imaginary frequency in the calculated vibrational frequencies ensure that the optimized geometry corresponds to a true energy minimum. DFT computational calculations reveal the energy and the length of fully extended bent-core mesogen **9b** to be – 6,113,866.99 kJ mol⁻¹ and 40.64 Å respectively (**Figure 1a**). The dihedral angle between first

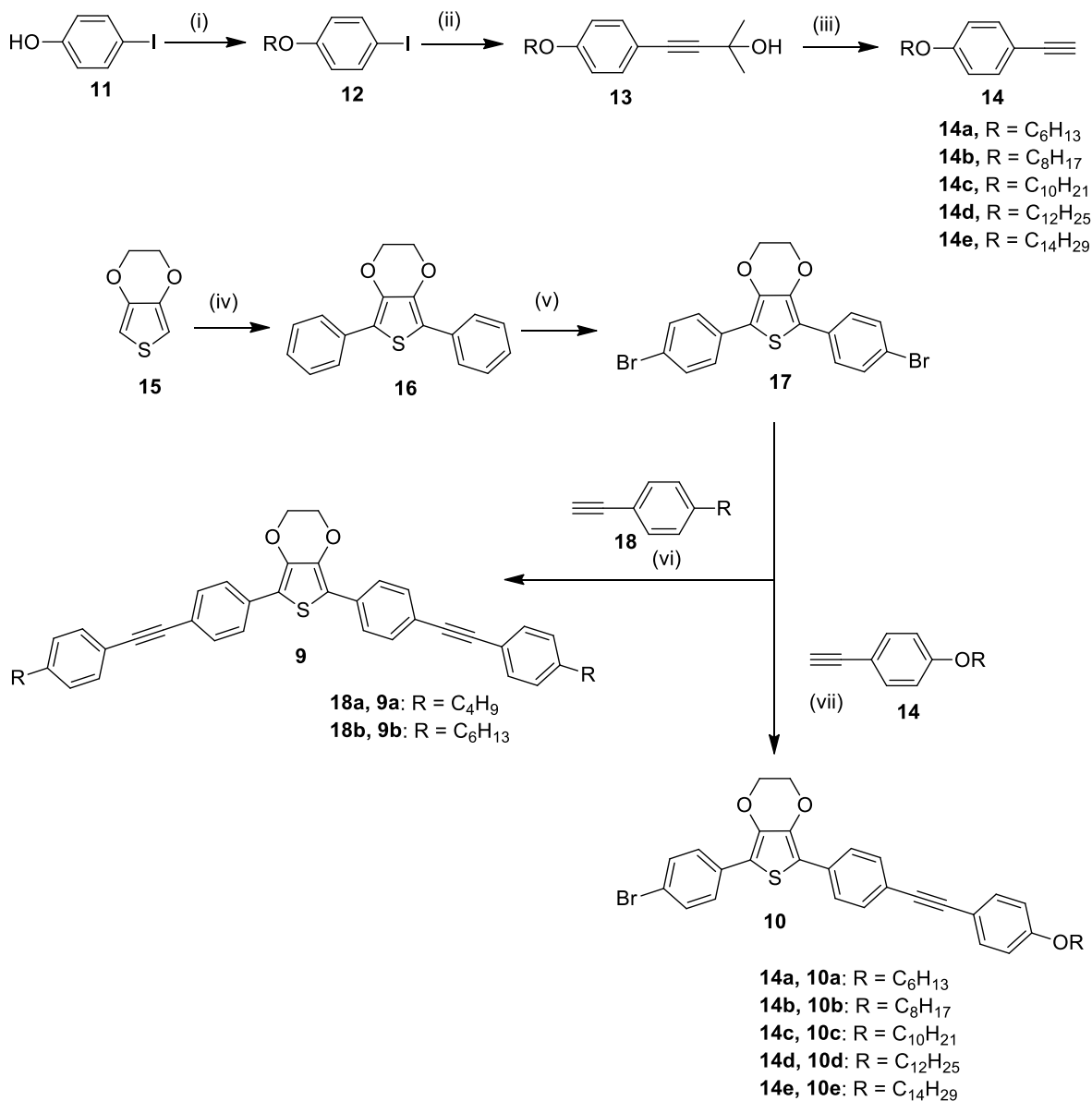
phenyl ring and second phenyl ring with acetylene ring, the central EDOT core and first phenyl ring is $\sim 180^\circ$ and $\sim 170^\circ$, respectively. Similarly, the energy and length of fully extended hockey-stick shaped mesogen **10d** were found to be $-12,260,268.33 \text{ kJ mol}^{-1}$ and 35.45 \AA respectively, (**Figure 1b**). The dihedral angle between first *p*-bromo-phenyl ring and central EDOT core, the second phenyl ring and central EDOT core, second phenyl ring and third phenyl ring with acetylene linkage is $\sim 170^\circ$, 170° and 179.2° , respectively. The bending angle or bent angle (θ) is calculated by $(\theta) = (\theta_1 + \theta_2)/2$ as shown in **Figure 1**. The DFT computational analysis (**Table 1**) indicate that, the bend angle is 151.5° in bent-core mesogens **9b** and 152.2° in hockey-stick like mesogens **10d** respectively [61].

Table 1. The DFT quantum chemical calculations data of representative bent-core and hockey-stick like mesogens (**9b** and **10d**).

Comp ounds	Selected bond length (\AA)	Selected dihedral angle ($^\circ$)	Selected bond angle ($^\circ$)	Bent angle ($^\circ$)
9b	1.47 (O6-C7; O9-C8)	Ring 1-Ring 2 = 180.0	C1-S5-C4 = 91.7	151.5 $^\circ$
	1.40 (O9-C3; O6-C2)	Ring 2-Ring 3 = 170.6	C2-O6-C7 = 114.2	
	1.83 (C4-S5; C1-S5)	Ring 3-Ring 4 = 170.6	C3-O9-C8 = 114.2	
	1.22(C22 \equiv C24; C23 \equiv C25)	Ring 4-Ring 5 = 179.8		
10d	1.95 (C19-Br23)	Ring 1-Ring 2 = 169.7	C1-S5-C4 = 91.6	152.2 $^\circ$
	1.47 (O6-C7; O9-C8)	Ring 2-Ring 3 = 170.0	C2-O6-C7 = 114.2	
	1.40 (O9-C3; O6-C2)	Ring 3-Ring 4 = 179.2	C3-O9-C8 = 114.2	
	1.83 (C4-S5; C1-S5)			
	1.22 (C22 \equiv C24)			
	1.39 (C28-O31)			

3.3.3.2 Synthesis

The synthesis of these BC and hockey-stick LCs is shown in **Scheme 1**



Scheme 1. Synthesis of novel BC and hockey-stick compounds: (i) alkyl halide, anhydrous K₂CO₃, dry DMF, reflux, 24 h; (ii) 2-methyl-3-butyn-2-ol, PdCl₂(PPh₃)₂, CuI, TEA, reflux, 24 h; (iii) NaOH, toluene, reflux, 3 h; (iv) bromobenzene, Pd(OAc)₂, PPh₃, Cs₂CO₃, toluene, 110 °C,

24 h; (v) Br₂, dry. DCM, 6 h, r.t; (vi) 1-ethynyl-4-alkylbenzene, PdCl₂(PPh₃)₂, CuI, TEA, reflux, 24 h; (vii) 1-ethynyl-4-alkoxybenzene, PdCl₂(PPh₃)₂, CuI, TEA, reflux, 24 h.

Compounds **18a** and **18b** were purchased from a commercial source. O-alkylation of 4-iodophenol **11** with an alkyl halide in the presence of dry potassium carbonate and dry DMF solvent under reflux condition gives 1-alkoxy-4-iodobenzene **12**. Sonogashira coupling reaction between compound **12** with 2-methyl-3-butyn-2-ol in the presence of palladium and copper catalyst gives compound **13**. The intermediate compound **14** was obtained by refluxing compound **13** with sodium hydroxide in toluene solvent. The palladium-catalyzed C–H bond arylation [68] of EDOT **15** with bromobenzene gives diarylated EDOT **16** in good yield which on bromination gives the key intermediate compound **17**. The final compounds were obtained by the Sonogashira coupling reaction between key intermediated compounds **17** with 4-alkyl or 4-alkoxy phenylacetylene (**18** and **14**) in good yield.

3.3.3.3 Mesomorphic properties

The thermal behaviour of all the synthesised compounds was first investigated by polarised optical microscopy. The exact phase transition temperature and associated enthalpy values were determined by DSC on heating and cooling scans and the thermal behaviour is summarized in the **Table 2**. The onset temperatures are given in °C and the numbers in parentheses indicate the transition enthalpy in kJ mol⁻¹. The five membered bent core compounds **9a–9b** exhibit wide range enantiotropic nematic phase along with SmA for **9b** compound at lower temperature. Similarly, homologous series of compounds with hockey-stick like molecules **10a–10e** exhibit exclusively wide range enantiotropic nematic phase along with SmA phase for longer alkyl chain compounds, respectively. The mesophase textures of all the liquid crystalline compounds were viewed under optical microscopy with crossed polarisers which display characteristic defect textures. The microscopic textures were recorded by placing small amount of compounds on a normal glass slide and covered with a cover slip.

Table 2. Phase transition temperature (peak in DSC, °C, on heating and cooling scan) and enthalpy of phase transition (kJ mol^{-1}) of bent-core and hockey-stick like molecules. (**9a–9b** & **10a–10e**).

Compounds	Phase transition (peak temperature (°C); (ΔH , kJ mol^{-1}))	
	<i>second heating scan</i>	<i>second cooling scan</i>
9a	Cr 181.3 (68.2) N 249.5 (1.7) I	I 233 (-1.4) N 170 (-24.1) Cr
9b	Cr₁ 135 (4.4) Cr₂ 143.4 (22.0) SmA 191.3 (0.1) N 257.9 (0.6) I	I 256.4 (-0.6) N 188.9 (-0.3) SmA 122.5 (-24.3) Cr₂ 78.6 (-2.7) Cr₁
10a	Cr 159.2 (34.9) N 190.8 (0.3) I	I 189.8 (-0.3) N 129.9 (-31.2) Cr
10b	Cr 146.1 (40.4) N 180.3 (0.3) I	I 179.7 (-0.3) N 131.4 (-38.2) Cr
10c	Cr₁ 137.4 (6.6) Cr₂ 144.9 (37.4) N 171.8 (0.4) I	I 171.3 (-0.4) N 121.2 (-41.6) Cr
10d	Cr₁ 81.6 (8.5) Cr₂ 133.8 (39.8) SmA 153 (0.3) N 163.9 (0.4) I	I 163.2 (-0.4) N 152.2 (-0.3) SmA 104.7 (-35.0) Cr
10e	Cr 129 (52.0) SmA 154.5 (1.8) I	I 153.6 (-1.5) SmA 112.6 (-53.3) Cr

Five membered bent core compound **9a** exhibits exclusively enantiotropic nematic phase over wide temperature range. The early growing nematic droplets and four brush nematic textures of compounds **9a** are shown in **Figure 2a** and **2b** respectively. Compound **9b** shows SmA phase along with a nematic phase at lower temperature. To investigate the nature of smectic phase, we used polyimide-coated cells with approximately 9 μm thickness for planer alignment in the mesophase. The compound **9b** was filled uniformly in the LC cell at isotropic temperature. Upon slow cooling from the nematic phase, focal conic texture of smectic A phase appears as shown in **Figure 2c**. The series of compounds in hockey-stick like molecules **10a–10e** display enantiotropic nematic phase with broad temperature range followed by the appearance of SmA phase at a lower temperature for compounds **10d** as shown in **Figure 2d**. Compound **10e** exhibits an enantiotropic SmA phase only. Compound **9a** melts at 182 °C and become isotropic

liquid at 250 °C; the nematic texture observed on slow cooling from the isotropic liquid (**Figure 2a & 2b**). Compound **9b** melts at 143 °C to a SmA phase but prior to that it exhibits a crystal-crystal transition at 135 °C. On further heating it shows a nematic phase at about 192 °C that goes to the isotropic phase at 258 °C. The nematic droplets were observed on slow cooling from the isotropic liquid and SmA phase observed at 172 °C (**Figure 2c**) which crystallizes at 122 °C. The hockey-stick like compound **10a** melts at 159 °C and become isotropic liquid at 191 °C. The nematic phase was observed on slow cooling from the isotropic liquid. The next homologous of the series, **10b**, becomes isotropic liquid at 180 °C and the nematic phase texture was observed on cooling from isotropic liquid. Upon heating, compound **10c** endures with the crystal-crystal transition at 137 °C and melts at 145 °C to a nematic phase that becomes clear liquid at 172 °C. Nematic droplets were observed on slow cooling from the isotropic melt. Compounds **10d** and **10e** show significant changes in texture from schlieren texture to the fan-like texture of smectic phase at low temperature. Compound **10d** goes through crystal- crystal transition at 82 °C and melts at 134 °C and becomes isotropic liquid at 164 °C. On slow cooling, the nematic phase appears at about 163 °C that changes to a SmA phase at 152 °C (**Figure 2d**). Compound **10e** melts at about 129 °C and transforms to the isotropic liquid at 155 °C. On cooling, SmA phase appears at about 153 °C that crystallises at 112 °C.

The thermal behaviour of all the mesogenic compounds were also further investigated with DSC measurements on both heating and cooling scan rate of 10 °C min⁻¹ and recorded under a nitrogen atmosphere. The phase transition temperatures obtained in DSC agree very well with POM observations. The bent core compound **9a** exhibits solely enantiotropic nematic phase over broad temperature range with two types of endothermic phase transition. The peak temperature at 181.3 °C, with phase transition enthalpy 68.2 kJ mol⁻¹ is attributed to crystalline phase to N phase at lower temperature and the peak at 249.5 °C ($\Delta H = 1.7$ kJ mol⁻¹) corresponds N phase to isotropic phase transition at higher temperature. However, compound **9b** exhibited Cr to SmA phase at lower temperature 143.4 °C ($\Delta H = 22.0$ kJ mol⁻¹), weak phase transition from SmA to N phase at 191.3 °C ($\Delta H = 0.1$ kJ mol⁻¹) and N phase to isotropic phase transition at 257.9 °C ($\Delta H = 0.6$ kJ mol⁻¹). Similarly, hockey-stick compounds **10a–10c** shows two types of endothermic phase transition from crystal to nematic phase at a lower temperature and nematic phase to isotropic phase at higher temperature. The compound **10a** shows Cr to N phase at 159.2

°C ($\Delta H = 34.9 \text{ kJ mol}^{-1}$) and N phase to isotropic phase at 190.8 °C ($\Delta H = 0.3 \text{ kJ mol}^{-1}$). For the compound **10b** and **10c** exhibited N phase at 146.1 °C ($\Delta H = 40.4 \text{ kJ mol}^{-1}$) and 144.9 °C ($\Delta H = 37.4 \text{ kJ mol}^{-1}$) and transition from N phase to isotropic phase at 180.3 °C ($\Delta H = 0.3 \text{ kJ mol}^{-1}$), 171.8 °C ($\Delta H = 0.4 \text{ kJ mol}^{-1}$). However, on heating and cooling scans, compounds **10d** exhibit additional enantiotropic SmA phase transition in between crystalline phase and nematic phase respectively. The compound **10d** displayed Cr to SmA phase at 133.8 °C ($\Delta H = 39.8 \text{ kJ mol}^{-1}$), SmA to N phase and N phase to isotropic phase at 153 °C ($\Delta H = 0.3 \text{ kJ mol}^{-1}$), 163.9 °C ($\Delta H = 0.4 \text{ kJ mol}^{-1}$). Similarly, compound **10e** exhibited two types of endothermic phase transition from crystal to SmA phase at 129 °C, with transition enthalpy 52.0 kJ mol^{-1} and SmA phase to isotropic phase transition at 154.5 °C ($\Delta H = 1.8 \text{ kJ mol}^{-1}$) respectively. As representative example, the DSC of compound **10d** is shown in **Figure 3**.

3.3.3.4 X-ray scattering measurements

The liquid crystalline behaviour of both the novel BC LCs (**9a–9b**) and hockey-stick liquid crystals (**10a–10e**) was further examined by X-ray scattering studies of unoriented samples filled in Lindemann capillaries. A representative and typical diffraction pattern obtained for BC compound **9b** at 210 °C in the nematic phase and at 160 °C for the SmA phase are shown in **Figure 4 (a)** and **(b)**, respectively. The XRD pattern for nematic phase at 210 °C shows diffuse peak at small angle region and a diffuse wide angle maxima at $d = 4.48 \text{ \AA}$, which corresponds to typical nematic phase as shown in **Figure 4 (a)**. However, the XRD pattern at 160 °C shows a sharp reflection in the small angle regime with d - spacings 37.37 \AA as shown in the **Figure 4 (b)**. Based on POM observation and calculated molecular length (35.45 \AA), this phase was deduced as a SmA phase. The diffuse peak at wide angle maxima at 4.46 \AA responsible for fluid like correlation of the molecules in the layers.

3.3.4 Photophysical properties

The photophysical properties of novel compounds were investigated by Perkin-Elmer UV-Vis lambda 35 double-beam spectrometer absorption spectra. The UV absorption properties

of all the compounds (**9a–9b** & **10a–10e**) were studied in anhydrous chloroform solvent (10^{-5} M) recorded at room temperature to know absorption maxima as presented in **Figure 5 (a)** and the values are summarized in **Table 3**. The bent-core compounds (**9a–9b**) exhibit maximum absorption band at $\lambda_{\text{max}} = 392$ nm. Similarly, hockey-stick compounds (**10a–10e**) exhibit maximum absorption at $\lambda_{\text{max}} = 375–378$ nm. The highly delocalized electronic systems and $\pi \rightarrow \pi^*$ transitions in the heteroaromatic portion (central EDOT), phenyl rings and acetylene linking group, and high molar absorption coefficient ($\epsilon = 6.5–11.2 \times 10^6 \text{ Lmol}^{-1}\text{cm}^{-1}$) attributed to the high absorption in these compounds. Generally, the extent of light absorption and intensity of peak in the absorption spectrum largely depends on the number of molecules that absorb light of a given wavelength. It is also known that extended conjugation in bent-core mesogens (**9a–9b**) causes bathochromic shift (longer wavelength) with respect to hockey-stick like liquid crystalline compounds (**10a–10e**).

Table 3. Photophysical properties of the bent-core and hockey-stick like mesogens recorded in the anhydrous chloroform (10^{-5} M) solution.

Compounds	Absorption $\lambda_{\text{abs}}/\text{nm}$ ($\epsilon/10^6 \text{ Lmol}^{-1}\text{cm}^{-1}$)	Emission $\lambda_{\text{em}}/\text{nm}$
9a	392 (11.2)	442, 463
9b	392 (9.1)	443, 464
10a	377 (6.5)	423, 441
10b	375 (8.2)	419, 441
10c	378 (6.6)	418, 440
10d	377 (11.1)	421, 441
10e	376 (7.1)	419, 441

Photoluminescence spectra of all the mesogens (**9a–9b** & **10a–10e**) were recorded using a spectrofluorometer (Fluorolog-3, Horiba Jobin Yvon), the emission spectra were recorded with a slit size of 2 nm in dilute anhydrous chloroform solution at room temperature and all the

compounds are excited at $\lambda_{\text{ex}} = 390$ nm. The bent-core mesogens (**9a–9b**) exhibit strong dual emission bands at 442 nm and 464 nm along with negligible shoulder peak at 490 nm as shown in **Figure 5 (b)** and **Table 3**. Similarly, emission spectra of hockey-stick compounds (**10a–10e**) exhibits strong dual emission bands at 418–423 nm and 440 nm along with shoulder peak at 468 nm. The photoluminescence mechanism of bent-core mesogens (**9a–9b**) and hockey-stick compounds (**10a–10e**) involves two strong stable emission bands and one shoulder emission peak which attributed to the electronic transition from lowest unoccupied molecular orbital (LUMO) to the highest occupied molecular orbital (HOMO) and occupied molecular orbitals below HOMO (H-1, H-2) respectively. No appreciable changes were observed on increasing number of methylene group in the terminal chains.

3.3.5 Raman spectroscopy

The molecular structures of novel liquid crystalline compounds (**9a–9b** & **10a–10e**) were further investigated by Raman spectroscopy. Raman spectra were recorded using Horiba Jobin Yvon T6400 Micro Raman using He–Ne laser operating at $\lambda = 632.8$ nm. The laser power at 1.8 mW was kept constant throughout measurement. The Raman spectral data obtained at an optical resolution of $50 \times$ objective lenses and accumulated at 10 s to obtained data with sufficiently high signal-to-noise ratio at room temperature as shown in **Figure 6**. All the solid samples were placed in a normal glass slide and covered with a cover slip. Theoretical Raman values were compared with experimentally obtained values are represented in **Table 4**. The peaks at lower regions at $919\text{--}1193\text{ cm}^{-1}$, correspond to aliphatic chains vibrations. The intense peak at 1142 cm^{-1} is for the central heteroaromatic EDOT ring ν (C–S). The vibrational peaks at $1437\text{--}1597\text{ cm}^{-1}$ are obtained for aromatic and hetero aromatic rings. The intense prominent vibrational peak at 2213 cm^{-1} is responsible for alkyne linking group in all the mesogenic derivatives. All experimentally obtained Raman shift (wave numbers, cm^{-1}) values were matching with the respective functional groups as shown in **Table 4**.

Table 4. Comparison of experimental Raman shift values of all the mesogens (**9a–9b** and **10a–10e**) with theoretical Raman shift values.

Compounds	Theoretical Raman shift (cm ⁻¹)	Experimental Raman shift (cm ⁻¹)	Functional group/vibration
	800–950	919	ν (C-O-C)
9a–9b	1080–1100	1142	ν (C-S) aromatic
&	1060–1150	1193	ν (C-O-C) asym
10a–10e	1450–1505	1437, 1476	ν (C-C) aromatic
	1550–1610	1597	ν (C-C) hetero ring
	2100–2250	2213	ν (C≡ C)

3.3.6 Thermogravimetric analysis

The thermal stability of all the liquid crystalline compounds was investigated by thermogravimetric analysis. All the samples (**9a–9b** and **10a–10e**) are subjected to heat scan of 10 °C min⁻¹ under a nitrogen atmosphere. All the mesogenic compounds show no weight loss till about 350 °C as shown in **Figure 7**. The five membered bent core compounds **9a–9b** initiate weight loss at about 380 °C–400 °C and decompose at 520 °C. Similarly, hockey-stick like compounds **10a–10e** initiates weight loss at about 350 °C and the whole process was completed at about 500 °C. The decomposition temperature of hockey-stick like compounds decreases with increasing terminal alkyl chain length. The thermal stability of five membered bent core compounds was higher than hockey-stick like compounds. The decomposition temperatures for all the compounds were much higher than isotropic temperature. It concludes that all the mesogenic compounds possess good thermal stability.

3.3.7 Nonlinear optical transmission measurements

Liquid crystals are known to exhibit large optical nonlinearities which have been the subject of considerable research interest in recent years, from both experimental and theoretical point of view. Since LC molecules typically have extended delocalized π -electrons and geometrical configuration, they are believed to be potential source of fast and large nonlinearities. In this open aperture Z-scan technique (**Figure 8**), the transmission of all the samples is measured as a function of the input laser fluence. For varying the laser fluence the beam was focused using a plano-convex lens of 9.5 cm focal length, and the transmission was measured at different positions (z-axis) with respect to the beam focus. All the compounds were dissolved in anhydrous chloroform solvent and taken in a 1 mm path length cuvette to have linear transmission of 89% at 532 nm excitation wavelength. The samples experiences different fluences at different z, with a maximum at the focal point ($z = 0$). The laser pulse energy was 100 μ J and the transmitted energy was measured using a pyro electric energy detector (Laser probe, RJP-735). A curve can be obtained by plotting the normalized transmittance, T_{norm} (where the linear transmission is taken as unity) with z position, which is called the Z scan curve as shown in **Figure 9**.

For a spatially filtered Gaussian beam, the fluence ($F_{in}(z)$) at any position z can be obtained from the relation,

$$F_{in}(z) = 4(\ln 2)^{\frac{1}{2}} E_{in} / \pi^{\frac{3}{2}} \omega(z)^2$$

Where the beam radius $\omega(z)$ is given by

$$\omega(z) = \omega_0 \left(1 + \left(\frac{z}{z_0} \right)^2 \right)^{\frac{1}{2}}$$

ω_0 is the focal spot size and z_0 is the Rayleigh length given by $z_0 = \pi \omega_0^2 / \lambda$. We find that the nonlinear transmission has contributions from both reverse saturable absorption (RSA, sometimes referred to as effective two-photon absorption (2PA) in literature) and saturable absorption (SA). [69] The nonlinear absorption coefficient is given by,

$$\alpha(I) = \frac{\alpha_0}{1 + \frac{I}{I_s}} + \beta I$$

Where I_s is the saturation intensity (in W/m^2) and β is the reverse saturable absorption coefficient (in m/W). I_s and β can be obtained by numerically fitting the pulse propagation equation to the measured transmission data. The obtained values are tabulated in **Table 5**. The presence high electron conjugation imparts nonlinear optical properties to these molecules. This can be attributed due to strong dipole moment and polarization of the molecules.

$$\frac{dI}{dx} = - \left[\frac{\alpha_0}{1 + \frac{I}{I_s}} + \beta I \right] I$$

Table 5. RSA coefficient (β) and saturation intensity (I_s) calculated for the samples from the data given in **Figure 9**.

Compounds	Liner Transmission (%)	Beta (β) ($\times 10^{-11}$ m/W)	I_s ($\times 10^{11}$ W/ m^2)	Omega zero (ω_0) ($\times 10^{-6}$ m)	Energy (μ J)
9a	89	5.6	9.8	22	100
9b	89	3.3	58	20	100
10a	89	1.9	45	19	100
10b	89	1.3	50	22	100
10c	89	2.3	50	18	100
10d	89	1.5	25	20	100
10e	89	1.5	9	22	100

We believe that the two photon absorption observed in the present samples originates from excited state absorption. In bent-core mesogens (**9a–9b**), the acetylene ($-\text{C}\equiv\text{C}-$) linking group acts as the conjugating spacer between central heteroaromatic EDOT ring and phenyl group with flexible alkoxy chain entities. These compounds are expected to be higher extended delocalized π -electronic conjugation and geometrical shape of the molecules, which further enhance the high nonlinearities. Similarly, unsymmetrical molecular structure and electron acceptor bromo group at one end of the molecule and electron donor ability of phenyl acetylene group through central heteroaromatic EDOT in hockey-stick like liquid crystals (**10a–10e**) enhance the nonlinear optical properties.

3.3.8 Conclusions

Two new series of BC and hockey-stick like liquid crystals from central EDOT core were synthesized and characterized. The BC LCs exhibit wide range of enantiotropic nematic phase for lower homologous and SmA phase for higher homologous at lower temperature. Similarly, hockey-stick compounds exhibit wide range enantiotropic nematic phase for lower homologous, while SmA phase obtained from higher homologous at lower temperature respectively. DFT calculations revealed that the bent angle of these compounds is around 151° – 153° . All the compounds exhibit strong photoluminescence in chloroform solvent under excitation wavelength of 390 nm. The presence of extended delocalized π -electron conjugations in these novel mesogens exhibit large optical nonlinear properties which make them potential candidates for technological applications.

3.3.9 Experimental section

3.3.9.1 General procedure for the synthesis of intermediate and final compounds

The compounds 1-alkoxy-4-iodobenzene, 4-(4-alkoxyphenyl)-2-methylbut-3-yn-2-ol and 1-ethynyl-4-alkoxybenzene were synthesised as reported [70] and confirmed by spectral and elemental analysis.

Synthesis of 5,7-Diphenyl-2,3-dihydrothieno[3,4-b][1,4]dioxine (16)

In a two neck-flak containing Pd(OAc)₂ (5 mol %), PPh₃ (10 mol %) ligand, Cs₂CO₃ (2.4 mmol) in toluene solvent (50 mL) was added EDOT (**15**) (1.0 mmol) and bromobenzene (2.2 mmol) under argon atmosphere. The reaction mixture was heated at 110 °C for 24 h under argon. After completion of the reaction, the reaction mixture was cooled to room temperature, an excess of water was added. The aqueous layer was extracted with ethyl acetate (3× 100 mL) and the combined organic layers were dried over Na₂SO₄ and concentrated under vacuum. The crude compound was further purified by column chromatography using silica gel (*n*-hexane/ ethyl acetate 9:1) gives desired pure product. Recrystallization of the pure compound with a mixture of DCM: hexane (1:9) gives light green solid **16**. Yield: 75 %. IR (film) ν_{\max} : 2912, 2872, 2852, 1597, 1518, 1454, 1359 cm⁻¹; ¹H NMR (500 MHz, CDCl₃): δ = 7.76–7.73 (m, 4 H), 7.38–7.34 (m, 4 H), 7.24–7.19 (m, 2 H), 4.34 ppm (s, 4 H); ¹³C NMR (125 MHz, CDCl₃): δ = 138.61, 132.96, 128.65, 126.62, 126.11.15.39, 64.59 ppm; elemental analysis: C₁₈H₁₄O₂S; calculated (%): C 73.44, H 4.78, S 10.87; found: C 73.51, H 4.84, S 10.91.

Synthesis of 5,7-bis(4-bromophenyl)-2,3-dihydrothieno[3,4-b][1,4]dioxine (17)

A solution of bromine (5.43 g, 33.97 mmol) in dry chloroform (20 mL) was added drop wise to a stirring solution of compound **16** (5g, 16.98 mmol) in dry chloroform (75 mL) at 0 °C, and slowly allowed to room temperature. The resulting reaction mixture was stirred for 6 h at room temperature. After completion of the reaction, the reaction mixture was successfully washed with 3% aqueous NaOH, saturated NaHSO₃ and excess of water. The aqueous layer was extracted with chloroform (3 × 75 mL) and the combined organic layers were dried over Na₂SO₄ and concentrated under vacuum. The crude compound was purified from column chromatography using silica gel (*n*-hexane/ ethyl acetate 8:2) gives desired pure compound **17**.

Recrystallization of pure compound from hexane afford off-white solid. Yield: 90 %. IR (film) ν_{\max} : 2922, 2911, 2854, 1591, 1454, 1373, 1085 cm^{-1} ; ^1H NMR (500 MHz, CDCl_3): δ = 7.60 (d, J = 8.8 Hz, 4 H), 7.48 (d, J = 8.8 Hz, 4 H), 4.36 ppm (s, 4 H); ^{13}C NMR (125 MHz, CDCl_3): δ = 138.97, 131.72, 127.49, 120.35, 114.50, 64.58 ppm; elemental analysis: $\text{C}_{18}\text{H}_{14}\text{O}_2\text{S}$; calculated (%): C 47.81, H 2.67, S 7.07; found: C 47.86, H 2.71, S 7.11. ^1H and ^{13}C NMR is shown in **Figure 10**.

Synthesis of final bent core (9a–9b) and hockey-stick (10a–10e) mesogenic compounds.

All the mesogenic derivatives were prepared by Sonogashira C–C coupling reaction between 5,7-bis(4-bromophenyl)-2,3-dihydrothieno[3,4-*b*][1,4]dioxine **17** with 1-ethynyl-4-alkylbenzene or 1-ethynyl-4-alkoxybenzene in the presence of $\text{PdCl}_2(\text{PPh}_3)_2$ and CuI in anhydrous triethylamine solvent. The general method is described as follows. A representative ^1H and ^{13}C NMR spectra is shown in **Figure 11, 12** and **13**.

In a three-neck flask, deoxygenated solution of compound **17** (1 eq), $\text{PdCl}_2(\text{PPh}_3)_2$ (0.04 eq) and CuI (0.05 eq) in 75 mL anhydrous triethylamine solvent was allowed to stir at room temperature under argon atmosphere for 10 minutes. To this, added 1-ethynyl-4-alkylbenzene (2.5 eq) or 1-ethynyl-4-alkoxybenzene (2.5 eq) in triethylamine (50 mL) solvent. The resulted reaction mixture was heated 72 °C for 24 h. After cooled to room temperature, the reaction mixture was diluted with diethyl ether and filtered through celite bed. The filtrate was then extracted with diethyl ether (3 × 100 mL). The combined organic layers were dried over Na_2SO_4 and concentrated under vacuum. The crude compound was purified through silica gel (*n*-hexane/ethyl acetate 7:3) gives desired pure compound. Recrystallization of pure compound with cold ethanol gives pale green colour compound. Yield: 55–60 %.

5,7-bis(4-((4-butylphenyl)ethynyl)phenyl)-2,3-dihydrothieno[3,4-*b*][1,4]dioxine (9a): IR (film) ν_{\max} : 2953, 2926, 2852, 2210, 1606, 1541, 1454, 1354, 1120, 1082 cm^{-1} ; ^1H NMR (500 MHz, CDCl_3): δ = 7.73 (d, J = 8 Hz, 4 H), 7.51 (d, J = 8 Hz, 4 H), 7.44 (d, J = 8 Hz, 4 H), 7.16 (d, J = 8 Hz, 4 H), 4.36 (s, 4 H), 2.62 (t, J = 7.5 Hz, 4 H), 1.63–1.58 (m, 4 H), 1.39–1.32 (m, 4 H), 0.93

ppm (t, $J = 7$ Hz, 6 H); ^{13}C NMR (125 MHz, CDCl_3): $\delta = 143.38, 139.23, 132.57, 131.77, 131.50, 128.48, 125.72, 121.49, 120.46, 115.56, 90.39, 89, 64.60, 35.61, 33.38, 22.31, 13.91$ ppm; elemental analysis: $\text{C}_{42}\text{H}_{38}\text{O}_2\text{S}$; calculated (%): C 83.13, H 6.30, S 5.27; found: C 83.20, H 6.38, S 5.31. ^1H NMR and ^{13}C NMR spectrum showed in **Figure 11**.

5,7-bis(4-((4-hexylphenyl)ethynyl)phenyl)-2,3-dihydrothieno[3,4-b][1,4]dioxine (9b): IR (film) ν_{max} : 2955, 2924, 2852, 2220, 1604, 1577, 1454, 1361, 1222, 1082 cm^{-1} ; ^1H NMR (500 MHz, CDCl_3): $\delta = 7.73$ (d, $J = 8$ Hz, 4 H), 7.51 (d, $J = 8$ Hz, 4 H), 7.45 (d, $J = 8$ Hz, 4 H), 7.16 (d, $J = 8$ Hz, 4 H), 4.39 (s, 4 H), 2.61 (t, $J = 7.5$ Hz, 4 H), 1.64–1.58 (m, 4 H), 1.36–1.25 (m, 12 H), 0.88 ppm (t, $J = 6$ Hz, 6 H); ^{13}C NMR (125 MHz, CDCl_3): $\delta = 143.43, 139.22, 132.57, 131.77, 131.49, 128.47, 125.72, 121.49, 120.44, 115.56, 90.39, 88.99, 64.60, 35.92, 31.69, 31.19, 28.91, 22.58, 14.06$ ppm; elemental analysis: $\text{C}_{46}\text{H}_{46}\text{O}_2\text{S}$; calculated (%): C 83.34, H 6.98, S 4.82; found: C 83.39, H 7.03, S 4.89.

5-(4-bromophenyl)-7-(4-((4-(hexyloxy)phenyl)ethynyl)phenyl)-2,3-dihydrothieno[3,4-b][1,4]dioxine (10a): IR (film) ν_{max} : 2955, 2924, 2854, 2206, 1604, 1519, 1454, 1377, 1249, 1085 cm^{-1} ; ^1H NMR (500 MHz, CDCl_3): $\delta = 7.71$ (d, $J = 8$ Hz, 2 H), 7.61 (d, $J = 8.5$ Hz, 2 H), 7.50–7.45 (m, 6 H), 6.86 (d, $J = 8.5$ Hz, 2 H), 4.37 (s, 4 H), 3.97 (t, $J = 6.5$ Hz, 2 H), 1.81–1.75 (m, 2 H), 1.49–1.43 (m, 6 H), 0.91 ppm (t, $J = 6.5$ Hz, 3 H); ^{13}C NMR (125 MHz, CDCl_3): $\delta = 159.26, 139.11, 139.03, 133.01, 132.31, 131.81, 131.70, 131.66, 127.50, 125.71, 121.71, 120.30, 115.37, 115.16, 114.67, 114.57, 90.31, 88.21, 68.11, 64.59, 31.57, 29.17, 25.69, 22.58, 14.01$ ppm; elemental analysis: $\text{C}_{32}\text{H}_{29}\text{BrO}_3\text{S}$; calculated (%): C 67.01, H 5.09, S 5.57; found: C 67.09, H 5.14, S 5.61. ^1H NMR and ^{13}C NMR spectrum showed in showed in **Figure 12**.

5-(4-bromophenyl)-7-(4-((4-(octyloxy)phenyl)ethynyl)phenyl)-2,3-dihydrothieno[3,4-b][1,4]dioxine (10b): IR (film) ν_{max} : 2953, 2922, 2852, 2210, 1608, 1521, 1454, 1359, 1255, 1085 cm^{-1} ; ^1H NMR (500 MHz, CDCl_3): $\delta = 7.71$ (d, $J = 8.5$ Hz, 2 H), 7.62 (d, $J = 8.5$ Hz, 2 H), 7.50–7.45 (m, 6 H), 6.86 (d, $J = 9$ Hz, 2 H), 4.38 (s, 4 H), 3.97 (t, $J = 6.5$ Hz, 2 H), 1.81–1.76 (m, 2 H),

1.47–1.42 (m, 2 H), 1.34–1.25 (m, 8 H), 0.89 ppm (t, $J = 6.5$ Hz, 3 H); ^{13}C NMR (125 MHz, CDCl_3): $\delta = 159.26, 139.03, 139, 133.01, 132.31, 131.70, 131.66, 127.50, 125.71, 121.68, 120.30, 115.40, 115.15, 114.68, 114.57, 90.30, 88.21, 68.12, 64.59, 31.80, 29.20, 26.02, 22.64, 14.07$ ppm; elemental analysis: $\text{C}_{34}\text{H}_{33}\text{BrO}_3\text{S}$; calculated (%): C 67.88, H 5.52, S 5.31; found: C 67.92, H 5.59, S 5.35.

5-(4-bromophenyl)-7-(4-((4-(decyloxy)phenyl)ethynyl)phenyl)-2,3-dihydrothieno[3,4-*b*][1,4]dioxine (10c): IR (film) ν_{max} : 2953, 2924, 2852, 2212, 1606, 1541, 1454, 1377, 1253, 1084 cm^{-1} ; ^1H NMR (500 MHz, CDCl_3): $\delta = 7.71$ (d, $J = 8.5$ Hz, 2 H), 7.61 (d, $J = 8.5$ Hz, 2 H), 7.49–7.44 (m, 6 H), 6.86 (d, $J = 8.5$ Hz, 2 H), 4.36 (s, 4 H), 3.96 (t, $J = 6.5$ Hz, 2 H), 1.81–1.75 (m, 2 H), 1.48–1.42 (m, 2 H), 1.34–1.27 (m, 12 H), 0.88 ppm (t, $J = 7$ Hz, 3 H); ^{13}C NMR (125 MHz, CDCl_3): $\delta = 159.26, 139.11, 139.03, 133.01, 132.31, 131.81, 131.70, 131.66, 127.50, 125.70, 121.71, 120.30, 115.37, 114.67, 114.57, 90.32, 88.22, 68.12, 64.58, 31.90, 29.57, 29.55, 29.31, 29.21, 26.02, 22.68, 14.10$ ppm; elemental analysis: $\text{C}_{36}\text{H}_{37}\text{BrO}_3\text{S}$; calculated (%): C 68.67, H 5.91, S 5.08; found: C 68.72, H 5.96, S 5.13.

5-(4-bromophenyl)-7-(4-((4-(dodecyloxy)phenyl)ethynyl)phenyl)-2,3-dihydrothieno[3,4-*b*][1,4]dioxine (10d): IR (film) ν_{max} : 2953, 2922, 2852, 2210, 1608, 1519, 1438, 1377, 1247, 1085 cm^{-1} ; ^1H NMR (500 MHz, CDCl_3): $\delta = 7.71$ (d, $J = 8$ Hz, 2 H), 7.61 (d, $J = 8.5$ Hz, 2 H), 7.50–7.44 (m, 6 H), 6.86 (d, $J = 8.5$ Hz, 2 H), 4.37 (s, 4 H), 3.96 (t, $J = 6.5$ Hz, 2 H), 1.81–1.75 (m, 2 H), 1.48–1.42 (m, 2 H), 1.35–1.26 (m, 18 H), 0.88 ppm (t, $J = 7$ Hz, 3 H); ^{13}C NMR (125 MHz, CDCl_3): $\delta = 159.26, 139.10, 139.03, 133.01, 132.30, 131.81, 131.70, 131.65, 127.50, 125.70, 121.71, 120.30, 115.15, 114.67, 114.57, 90.31, 88.21, 68.12, 64.58, 31.91, 30.89, 29.65, 29.63, 29.56, 29.38, 29.34, 29.20, 26.01, 22.68, 14.09$ ppm; elemental analysis: $\text{C}_{38}\text{H}_{41}\text{BrO}_3\text{S}$; calculated (%): C 69.39, H 6.27, S 4.86; found: C 69.45, H 6.32, S 4.92.

5-(4-bromophenyl)-7-(4-((4-(tetradecyloxy)phenyl)ethynyl)phenyl)-2,3-dihydrothieno[3,4-*b*][1,4]dioxine (10e): IR (film) ν_{max} : 2955, 2920, 2852, 2214, 1606, 1508, 1454, 1377, 1242,

1082 cm^{-1} ; ^1H NMR (500 MHz, CDCl_3): δ = 7.64 (d, J = 8 Hz, 2 H), 7.54 (d, J = 8.5 Hz, 2 H), 7.42–7.37 (m, 6 H), 6.79 (d, J = 8.5 Hz, 2 H), 4.29 (s, 4 H), 3.89 (t, J = 6.5 Hz, 2 H), 1.73–1.68 (m, 2 H), 1.48 (br, 2 H), 1.39–1.35 (m, 2 H), 1.27–1.19 (m, 22 H), 0.81 ppm (t, J = 6.5 Hz, 3 H); ^{13}C NMR (125 MHz, CDCl_3): δ = 158.25, 138.10, 138.02, 132, 131.29, 130.80, 130.69, 130.64, 126.48, 126.69, 120.70, 119.28, 114.36, 114.14, 113.66, 113.56, 89.31, 87.20, 67.10, 63.57, 30.91, 28.67, 28.66, 28.64, 28.58, 28.55, 28.37, 28.34, 28.20, 25.01, 21.67, 13.09 ppm; elemental analysis: $\text{C}_{40}\text{H}_{45}\text{BrO}_3\text{S}$; calculated (%): C 70.06, H 6.60, S 4.66; found: C 70.11, H 6.64, S 4.72. ^1H NMR and ^{13}C NMR spectrum showed in showed in **Figure 13**.

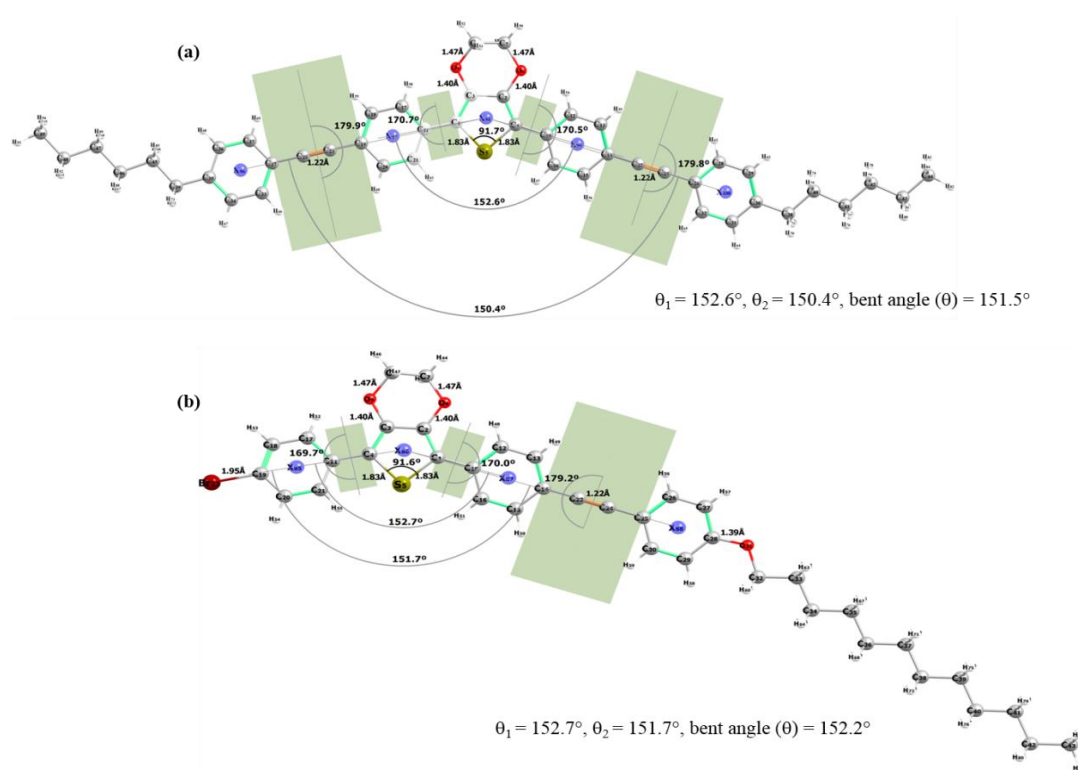


Figure 1. DFT optimized molecular structures: (a) bent-core mesogen **9b** and (b) hockey-stick like mesogen **10d**. The bent angles are 151.5° and 152.2° respectively.

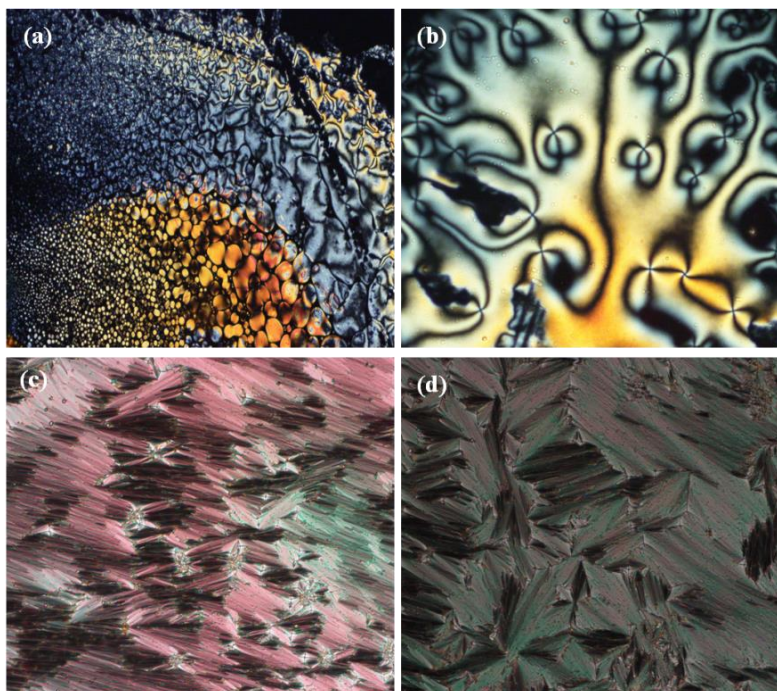


Figure 2. POM textures, for compounds **9a**: (a) early growing nematic droplets after cooling from the isotropic liquid at 233 °C, (b) growing of nematic schlieren texture on further cooling to 198 °C, for compounds **9b**: (c) SmA focal conic texture observed at 172 °C, for compounds **10d**: (d) SmA texture observed at 152 °C. All the POM textures were viewed at 200 × magnifications.

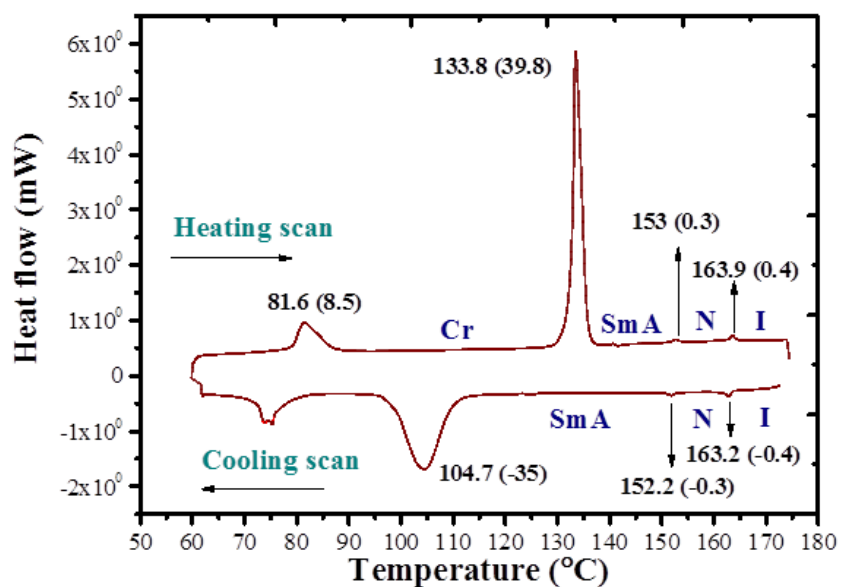


Figure 3. DSC thermograms obtained for the hockey-stick mesogen **10d** showing phase transitions on heating and cooling cycles at a scan rate of $10\text{ }^{\circ}\text{C min}^{-1}$. Vertical arrow indicates phase transition point.

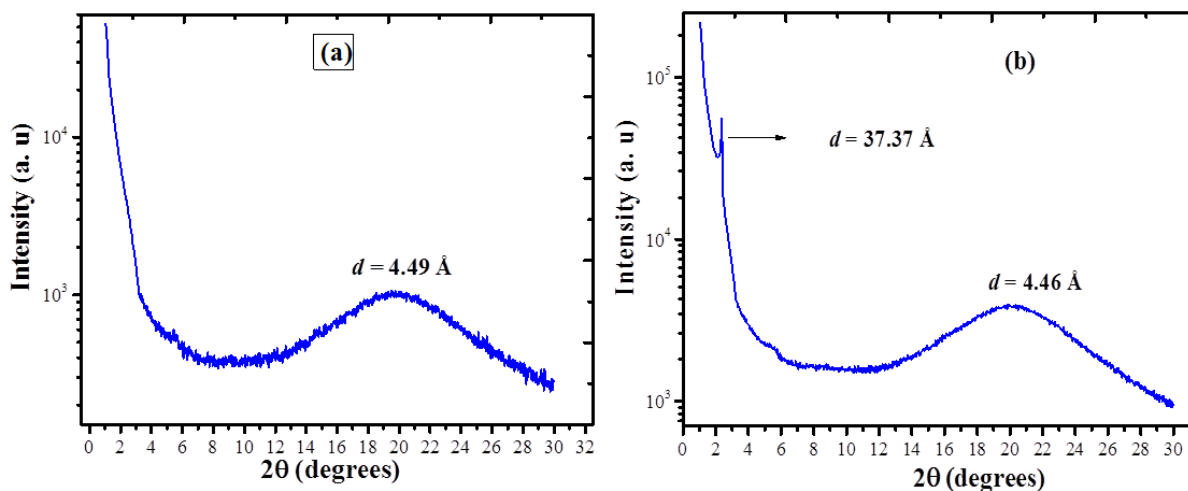


Figure 4. XRD patterns recorded for BC LCs compound **9b** on cooling from isotropic temperature: (a) nematic phase at 210 °C; (b) smectic A phase at 160 °C respectively.

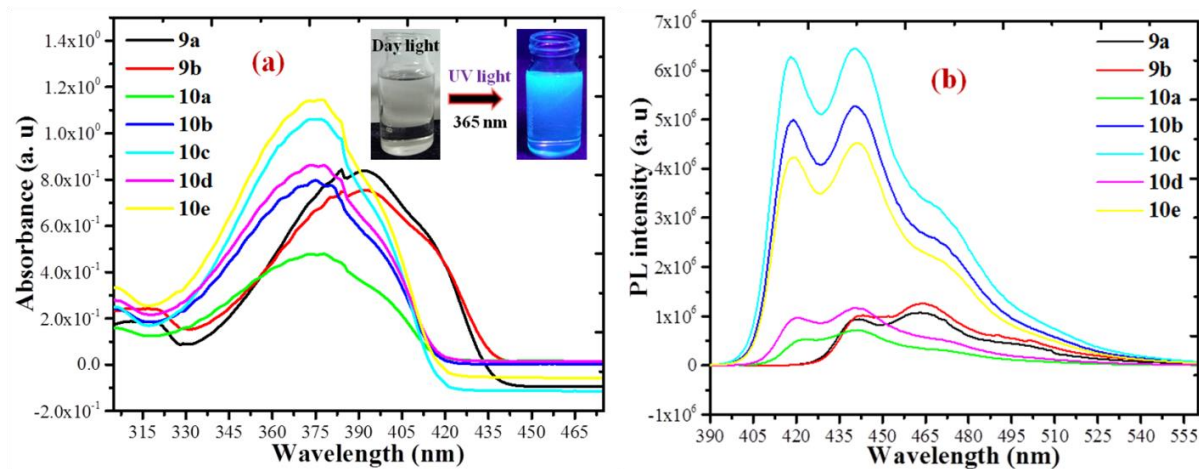


Figure 5. (a) UV-Visible absorption spectrum, (b) fluorescence emission spectrum of all the novel mesogens.

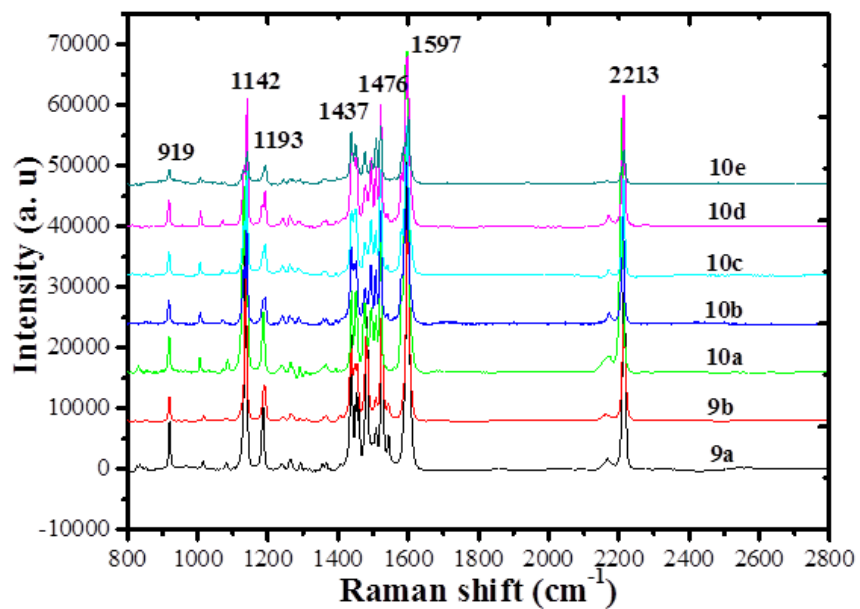


Figure 6. Raman data of all the mesogenic compounds (**9a–9b**) and (**10a–10e**).

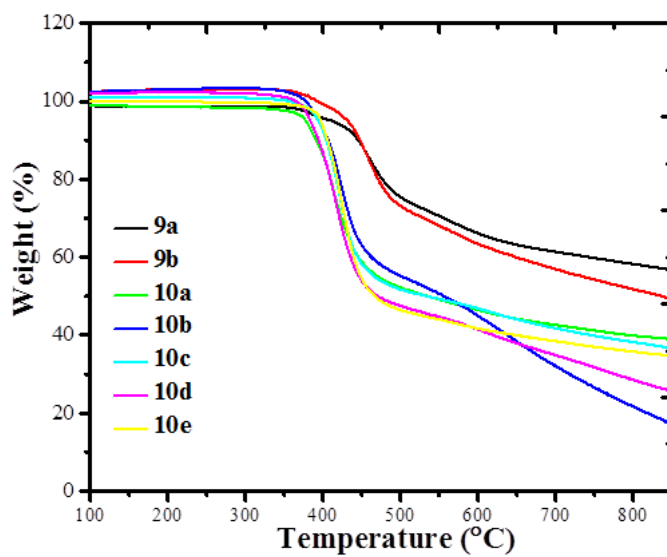


Figure 7. The thermogravimetric analysis of compounds **9a–9b** and **10a–10e**.

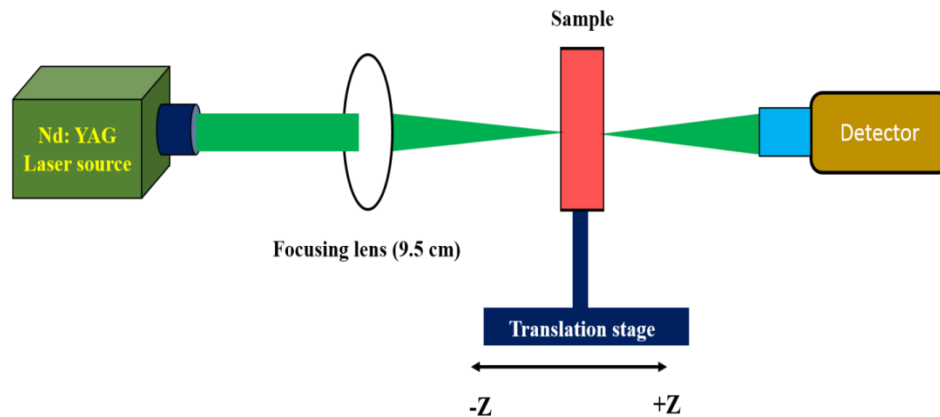


Figure 8. Schematic illustration of the open aperture Z-scan setup used for nonlinear transmission measurements.

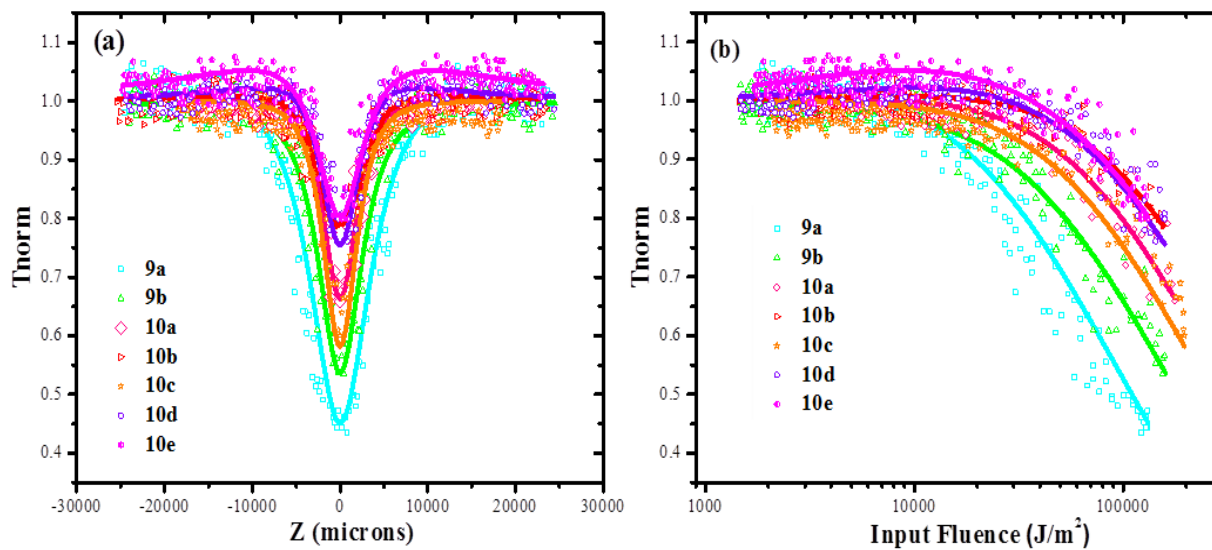


Figure 9. (a) Z-scan measurement of novel mesogenic compounds (**9a–9b**) and (**10a–10e**) respectively. The experimental measurements were carried out at room temperature with very high dilute anhydrous chloroform solvent. (b) Normalized transmission as a function of input laser fluence, calculated from open aperture Z-scan measurements recorded at laser pulse energy of 100 micro Joules respectively.

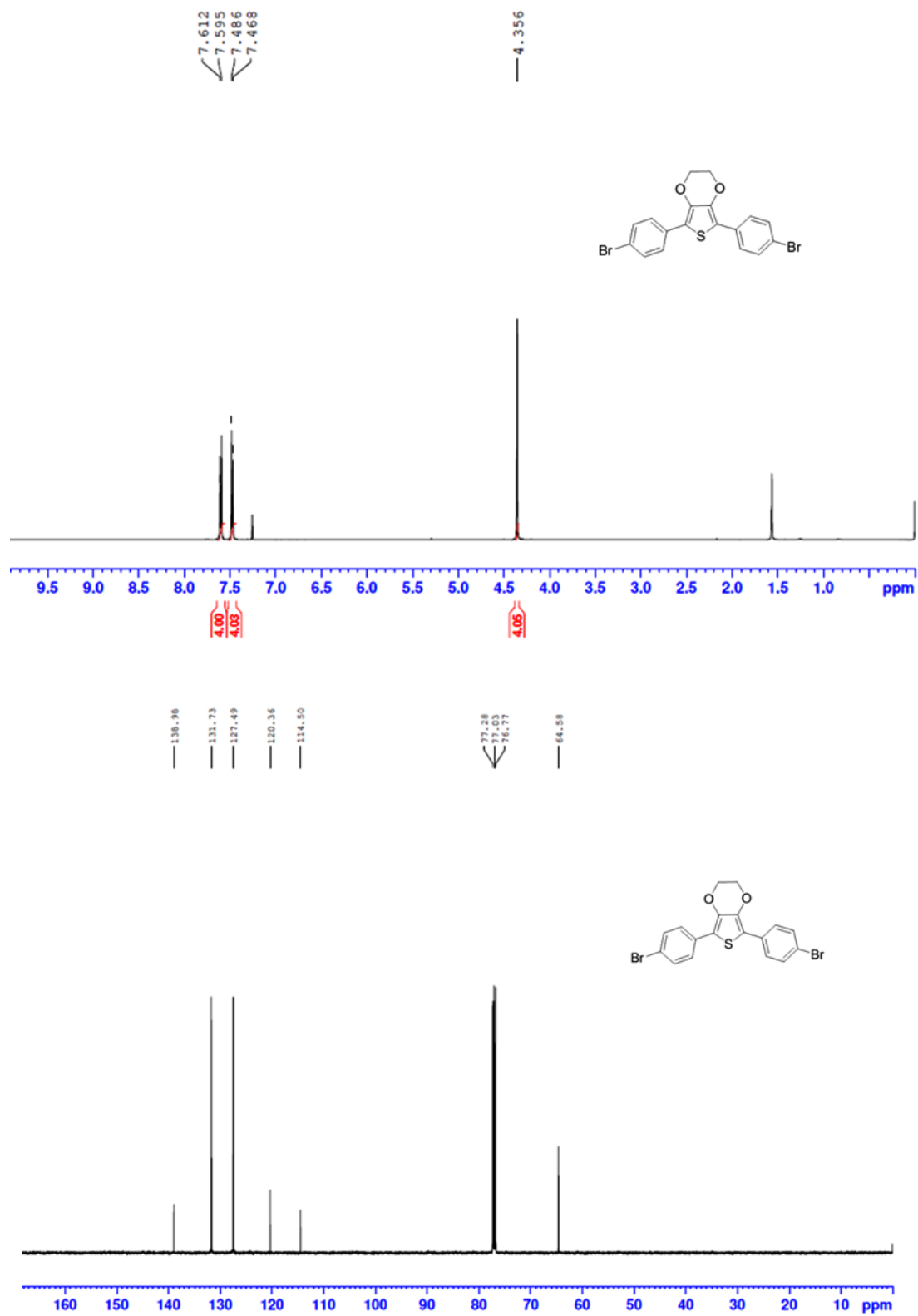


Figure 10. The ^1H and ^{13}C NMR of compound 17.

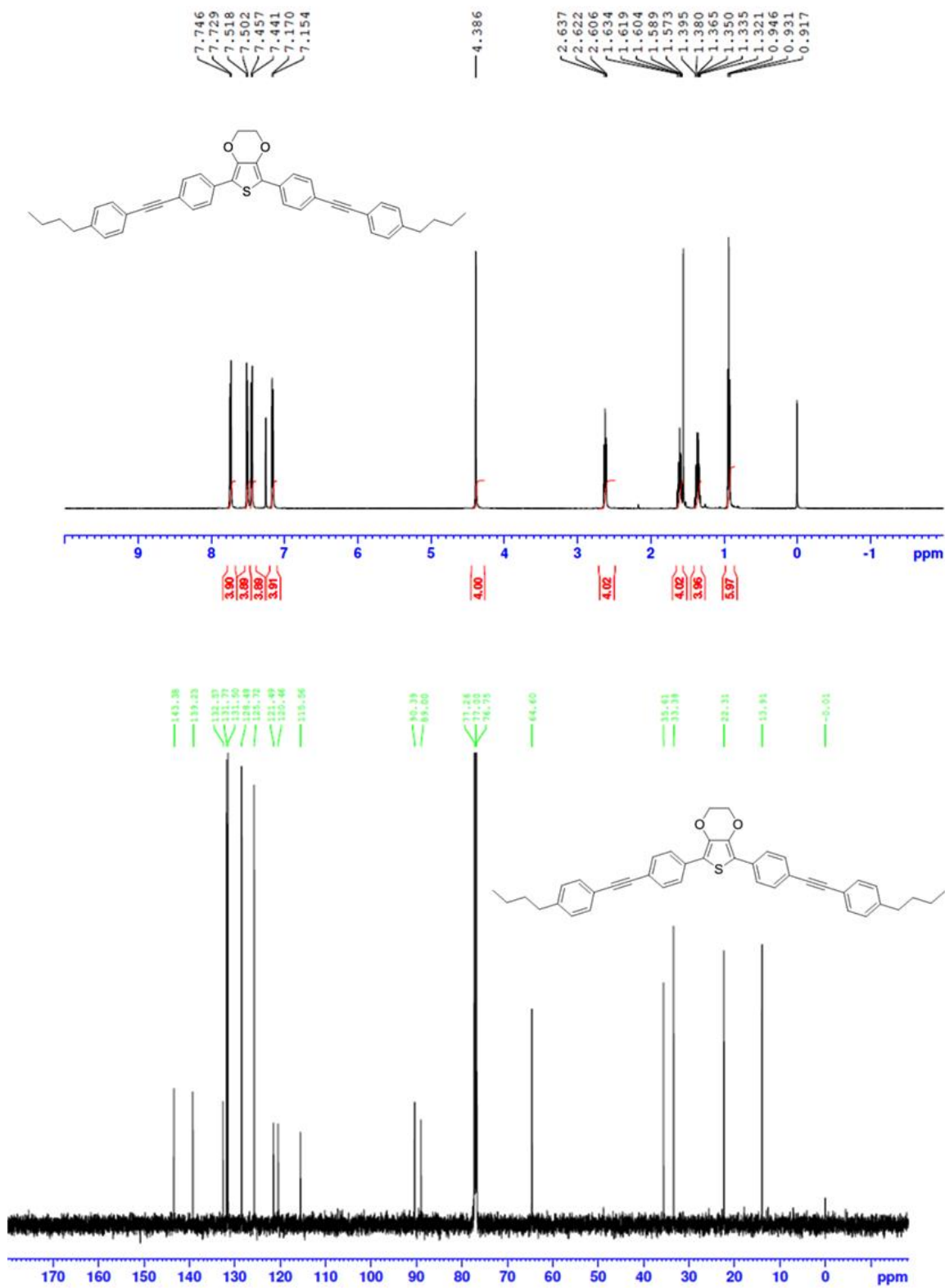


Figure 11. The ¹H and ¹³C NMR of compound 9a.

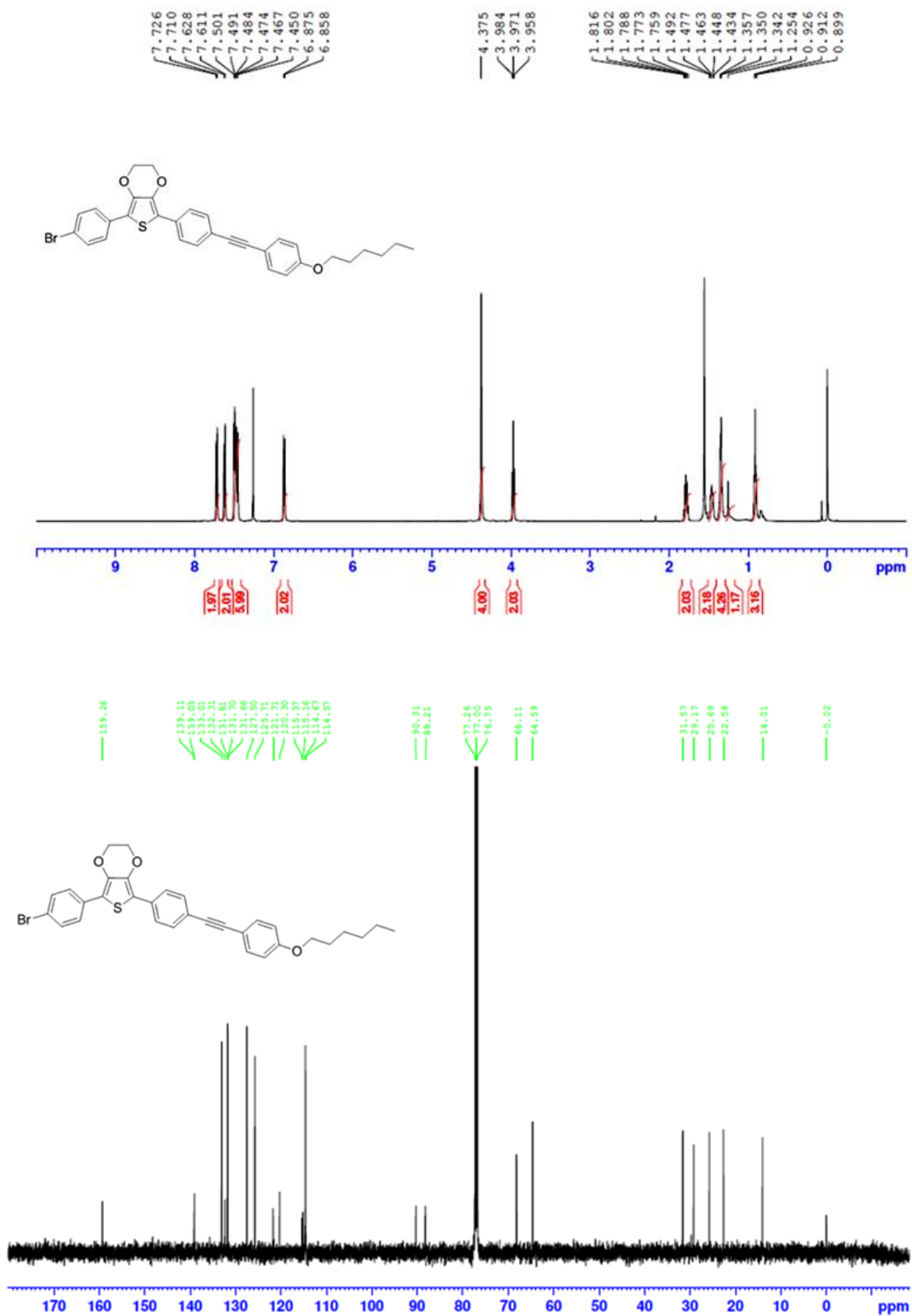


Figure 12. The ¹H and ¹³C NMR of compound 10a.

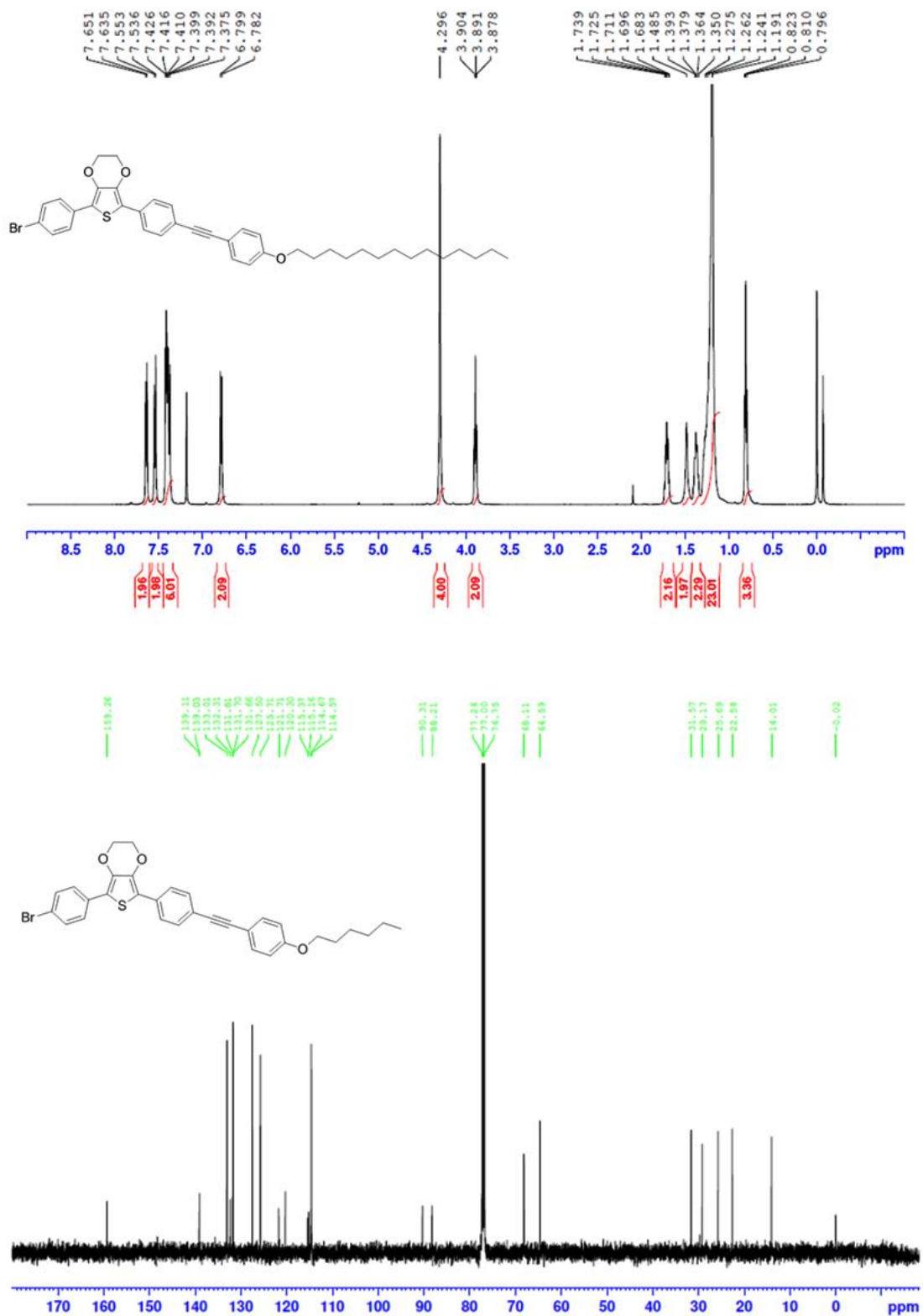


Figure 13. The ¹H and ¹³C NMR of compound 10e.

References

- [1] (a) Pelzl G, Diele S, Weissflog W. *Adv. Mater.*, **1999**, 11, 707; (b) Reddy R.A, Tschierske C. *J. Mater. Chem.*, **2006**, 16, 907; (c) Takezoe H, Takanishi Y. *Jpn. J. Appl. Phys.*, **2006**, 45, 597; (d) Prasad V, Kang S.-W, Kumar S. *J. Mater. Chem.*, **2003**, 13, 1259.
- [2] (a) Prasad V, Kang S.-W, Suresh K. A. et. al. *J. Am. Chem. Soc.*, **2005**, 127, 17224; (b) Prasad V, Kang S.-W, Qi X. et. al. *J. Mater. Chem.*, **2004**, 14, 1495; (c) Folcia C.L, Alonso I, Ortega J. et. al. *Chem. Mater.*, **2006**, 18, 4617; (d) Pintre I. C, Gimeno N, Serrano J. L, et. al. *J. Mater. Chem.*, **2007**, 17, 2219.
- [3] (a) Etxebarria J, Ros M. B, *J. Mater. Chem.*, **2008**, 18, 2919; (b) Prasad V, Jakli A, *Liq. Cryst.*, **2004**, 31, 473; (c) Link DR, Natale G, Shao R, et al. *Science.*, 1997;278:1924–1927.
- [4] (a) Tschierske C, Dantlgraber G. *Pramana.*, **2003**, 61, 455–481; (b) Ros MB, Serrano JL, Fuente MR, et al. *J. Mater. Chem.*, **2005**, 15, 5093–5098; (c) Weissflog W, Murthy SNH, Diele S, et al. *Phil. Trans. R Soc A.*, 2006, 364, 2657–2679.
- [5] (a) Goodby JW, Saez IM, Cowling SJ, et al. *Angew. Chem. Int. Ed.*, **2008**, 47, 2754–2787; (b) Lin S-C, Ho R-M, Chang C-Y, et al. *Chemistry – Eur J.*, **2012**, 18, 9091–9098; (c) Eremin A, Jakli A. *Soft Matt.*, **2012**, 9, 615–637.
- [6] (a) Goodby JW, Bruce DW, Hird M, et al. *J. Mater. Chem.*, **2001**, 11, 2631–2636; (b) Kumar S, Gowda AN. *Liq. Cryst. Rev.*, **2015**, 3, 99–145.
- [7] (a) Zygadło K, Dardas D, Nowicka K, et al. *Mol. Cryst. Liq. Cryst.*, **2009**, 509, 283–291; (b) Shanavas A, Sathiyaraj S, Chandramohan A, et al. *J. Mol. Struct.*, **2013**, 1038, 126–133; (c) Yelamaggad CV, Mathews M, Nagamani SA, et al. *J. Mater. Chem.*, **2007**, 17, 284–298; (d) Kovalenko L, Schroder MW, Reddy RA, et al. *Liq. Cryst.*, **2005**, 32, 857–865.
- [8] (a) Lee C-K, Kwon S-S, Zin W-C, et al. *Liq. Cryst.*, **2003**, 30, 415–421; (b) Kwon S-S, Kim T-S, Lee C-K, et al. *Liq. Cryst.*, **2006**, 33, 1005–1014; (c) Weissflog W, Lischka CH, Diele S, et al. *Mol. Cryst. Liq. Cryst.*, **1999**, 333, 203–235; (d) Alaasar M, Prehm M, Tschierske C. *Liq. Cryst.*, **2014**, 41, 126–136.

- [9] (a) Paul MK, Kalita G, Laskar AR, et al. *J. Mol. Struct.*, **2013**, 1049, 78–89; (b) Mathews M, Kang S, Kumar S, et al. *Liq. Cryst.*, **2011**, 38, 31–40; (c) Begum N, Turlapati S, Debnath S, et al. *Liq. Cryst.*, **2013**, 40, 1105–1115; (d) Metrangolo P, Prasang C, Resnati G, et al. *Chem. Commun.*, **2006**, 3290–3292.
- [10] (a) Reddy RA, Sadashiva BK, Raghunathan VA. *Chem. Mater.*, **2004**, 16, 4050–4062; (b) Murthy HNS, Sadashiva BK. *Liq. Cryst.*, **2004**, 31, 1347–1356; (c) Reddy RA, Sadashiva BK. *J. Mater. Chem.*, **2004**, 14, 1936–1947; (d) Rahman ML, Asik J, Kumar S, et al. *Liq. Cryst.*, **2008**, 35, 1263–1270.
- [11] (a) Kohout M, Svoboda J, Novotna V, et al. *J. Mater. Chem.*, **2009**, 19, 3153–3160; (b) Kozmik V, Kuchar M, Svoboda J, et al. *Liq. Cryst.*, **2005**, 32, 1151–1160; (c) Choi E-J, Seo Y-H, Park S-B, et al. *J. Mater. Chem C.*, **2013**, 1, 451–455.
- [12] (a) Wang H, Zheng Z, Shen D. *Liq. Cryst.*, **2012**, 39, 99–103; (b) Wang L, Yu L, Xiao X, et al. *Liq. Cryst.*, **2012**, 39, 629–638; (c) Dingemans TJ, Samulski ET. *Liq. Cryst.*, **2000**, 27, 131–136; (d) Belaisaoui A, Cowling SJ, Goodby JW. *Liq. Cryst.*, **2013**, 40, 421–427.
- [13] (a) Speetjens F, Lindborg J, Tauscher T, et al. *J. Mater. Chem.*, **2012**, 22, 22558–22564; (b) Kang S, Saito Y, Watanabe N, et al. *J. Phys. Chem B.*, **2006**, 110, 5205–5214; (c) Lehmann M, Kohn C, Kresse H, et al. *Chem. Commun.*, **2008**, 1768–1770; (d) Cristiano R, Ely F, Gallardo H. *Liq. Cryst.*, **2005**, 32, 15–25.
- [14] (a) Shanker G, Prehm M, Nagaraj M, et al. *ChemPhysChem.*, **2014**, 15, 1323–1335; (b) Han J. *J. Mater. Chem C.*, **2013**, 1, 7779–7797; (c) Han J, Chui SS-Y, Che C-M. *Chem. Asian. J.*, **2006**, 1, 814–825; (d) Torgova SI, Karamysheva LA, Geivandova TA, et al. *Mol. Cryst. Liq. Cryst.*, **2001**, 365, 99–106.
- [15] (a) Seltmann J, Marini A, Mennucci B, et al. *Chem. Mater.*, **2011**, 23, 2630–2636; (b) Seltmann J, Muller K, Klein S, et al. *Chem. Commun.*, **2011**, 47, 6680–6682; (c) Kozhevnikov VN, Whitwood AC, Bruce DW. *Chem. Commun.*, **2007**, 3826–3828 (d) Goodby JW, Bruce DW, Hird M, et al. *J. Mater. Chem.* **2001**, 11, 2631–2636.
- [16] (a) Aldred MP, Vlachos P, Dong D, et al. *Liq. Cryst.*, **2005**, 32, 951–965; (b) Belmar J, Parra ML, Zúñiga C, et al. *Liq. Cryst.*, **1999**, 26, 389–396; (c) Parra ML, Elgueta EY, Ulloa JA, et al. *Liq. Cryst.*, **2012**, 39, 917–925.

- [17] (a) Kishikawa K, Harris MC, Swager TM. *Chem. Mater.*, 1999, **11**, 867–871; (b) Paraskos AJ, Swager TM. *Chem. Mater.*, **2002**, 14, 4543–4549; (c) Eichhorn SH, Paraskos AJ, Kishikawa K, Swager TM. *J. Am. Chem. Soc.*, **2002**, 124, 12742.
- [18] Campbell NL, Duffy WL, Thomas GI, et al. *J. Mater. Chem.*, **2002**, 12, 2706–2721.
- [19] (a) Herman J, Chojnowska O, Harmata P, et al. *Liq. Cryst.*, **2014**, 41, 1647–1652; (b) Funahashi M, Kato T. *Liq. Cryst.*, **2015**, 42, 909–917; (c) Kovářová A, Kohout M, Svoboda J, et al. *Liq. Cryst.*, **2014**, 41, 1730–1718; (d) Zhang W, He W, Di C, et al. *Liq. Cryst.*, **2016**, 43, 524–534; (e) Vaupotic N, Szydłowska J, Salamonczyk M, et al. *Phys. Rev. E.*, **2009**, 80, 030701/1–4.
- [20] (a) Kovářová A, Svoboda J, Novotná V, Glogarová M, et al. *Liq. Cryst.*, **2010**, 37, 1501–1513; (b) Vaupotic N, Szydłowska J, Salamonczyk M, et al. *Phys. Rev. E.*, 2009, 80, 030701-1–4.
- [21] Seltmann J, Muller K, Klein S, et al. *Chem Commun.*, **2011**, 47, 6680–6682.
- [22] (a) Luckhurst GR, Sluckin TJ, editors. *Biaxial nematic liquid crystals: theory, simulation and experiment*. West Sussex: Wiley; **2015**. (b) Madsen L, Dingemans T, Nakata M, et al. *Phys. Rev. Lett.*, **2004**, 92(14), 145505-1–4; (c) Acharya B, Primak A, Kumar S. *Phys. Rev. Lett.*, **2004**, 92(14):145506-1–4; (d) Luckhurst G. *Angew. Chem. Int. Ed.*, **2005**, 44, 2834–2836.
- [23] (a) Mettout B. *Phys. Rev. E.*, **2005**, 72, 031706-1–6; (b) Kim Y-K, Majumdar M, Senyuk B, et al. *Soft Matter.*, **2012**, 8, 8880–8890; (c) Dingemans T, Madsen L, Francescangeli O, et al. *Liq Cryst.*, **2013**, 40, 1655–1677; (d) Nguyen H, Rouillon J, Marcerou J, et al. *Mol. Cryst. Liq. Cryst.*, **1999**, 328, 177–184.
- [24] (a) Subala S, Sundar S, Tamilenthil V, et al. *Recent Res Sci Technol.*, **2011**, 3, 120–124; (b) Zygodlo K, Dardas D, Nowicka K, et al. *Mol. Cryst. Liq. Cryst.*, **2009**, 509, 283–291; (c) Shanavas A, Sathiyaraj S, Chandramohan A, et al. *J. Mol. Struct.*, **2013**, 1038, 126–133.
- [25] (a) Gleeson H, Kaur S, Gortz V, et al. *ChemPhysChem.*, **2014**, 15, 1251–1260; (b) Jakli A. *Liq. Cryst. Rev.*, **2013**, 1, 65–82; (c) Gortz V. *Liq. Cryst. Today.*, **2010**, 19, 37–48.

- [26] (a) Dimitrakopoulos CD, Malenfant PRL. *Adv. Mater.*, **2002**, 14, 99–117; (b) Hulvat JF, Stupp SI. *Angew. Chem. Int. Ed.*, **2003**, 42, 778–781; (c) De Bettignies R, Nicolas Y, Blanchard P, et al. *Adv. Mater.*, **2003**, 15, 1939–1943.
- [27] (a) Wohrle D, Meissner D. *Adv. Mater.*, **1991**, 3, 129–138; (b) Mitschke U, Bäuerle P. *J. Mater. Chem.*, **2000**, 10, 1471–1507.
- [28] (a) Weissflog W. *Liq. Cryst.*, **2011**, 38, 1081–1083; (b) Weissflog W, Baumeister U, Tamba MG, et al. *Soft Matter*, **2012**, 8, 2671–2685.
- [29] (a) Dziembowska T, Szafran M, Jagodzińska E, et al. *J. Spectrochim Acta Part A*, **2003**, 59, 2175–2189. (b) Dennington IIR, Keith T, Millam J, et al. Gauss view 03. Shawnee Mission (KS): Semichem, Inc; **2003**.
- [30] (a) Collard DM, Cp L. *J. Am. Chem. Soc.*, **1991**, 113, 8577–8583; (b) Schouten PG, Van Der Pol JF, Zwikker JW, et al. *Mol. Cryst. Liq. Cryst.*, **1991**, 195, 291–305; (c) Ohta K, Watanabe T, Hasebe H, et al. *Mol. Cryst. Liq. Cryst.*, **1991**, 196, 13–26; (d) Ohta K, Morizumi Y, Ema H, et al. *Mol. Cryst. Liq. Cryst.*, **1991**, 208, 55–63.
- [31] (a) Schouten PG, Warman JM, De Haas MP, et al. *J. Am. Chem. Soc.*, 1994, 116, 6880–6894; (b) Glebowska A, Vita F, Francescangeli O, et al. *Liq. Cryst.*, **2015**, 42, 829–839; (c) Takezoe H, Araoka F. *Liq. Cryst.*, **2014**, 41, 393–401.
- [32] (a) Rampon DS, Rodembusch FS, Juliana M. F. M. et. al. *J. Mater. Chem.*, **2010**, 20, 715–722; (b) Ho M-S, Hsu C-S. *Liq. Cryst.*, **2010**, 37, 293–301.
- [33] (a) Thisayukta J, Nakayama Y, Watanabe J. *Liq. Cryst.*, **2000**, 27, 1129–1135; (b) Pintre IC, Gimeno N, Serrano JL, Ros MB, et. al. *J. Mater. Chem.*, **2007**, 17, 2219–2227; (c) Yang P, Lin HC. *Liq. Cryst.*, **2006**, 33, 587–603; (d) Lee SK, Kang S, Tokita M, Watanabe J. *Liq. Cryst.*, **2010**, 37, 593–598; (e) Folcia CL, Alonso I, Ortega J, Etxebarria, J. et. al. *Chem. Mater.*, **2006**, 18, 4617–4626.
- [34] Schiff H, Liebigs J. *Ann. Chem.*, **1864**, 131, 118–119
- [35] Niori T, Sekine T, Watanabe J. et. al. *J. Mater. Chem.*, **1996**, 6, 1231–1233.
- [36] Akutagawa T, Matsunaga Y, Yasuhara K. *Liq. Cryst.*, **1994**, 17, 659–666.
- [37] (a) Kim H, Yi Y, Chen D, et. al. *Soft Matter*, **2013**, 9, 2793–2797; (b) Merlo A.A, Gallardo H, Taylor TR, Kroin T. *Mol. Cryst. Liq. Cryst.*, **1994**, 250, 31–39.

- [38] (a) Weissflog W, Nadasi H, Dunemann U, et. al. *J. Mater. Chem.*, **2001**, 11, 2748; (b) Dunemann U, Schroeder MW, Reddy AR, et. al. *J. Mater. Chem.*, **2005**, 15, 4051; (c) Pelzl G, Diele S, Grande S, et. al. *Liq. Cryst.*, **1999**, 26, 401.
- [39] (a) Weissflog W, Lischka C, Diele S, et. al. *Mol. Cryst. Liq. Cryst.*, **1999**, 328, 101; (b) Diele S, Grande S, Kruth H, et. al. *Ferroelectrics*, **1998**, 212, 169; (c) Pelzl G, Diele S, Jakli A, et. al. *Liq. Cryst.*, **1999**, 26, 135; (d) Weissflog W, Kovalenko L, Wirth I, et. al. *Liq. Cryst.*, **2000**, 27, 677.
- [40] (a) Weissflog W, Lischka C, Benne T, Scharf T, et. al. *Proc. SPIE—Int. Soc. Opt. Eng.*, **1998**, 3319, 14; (b) Wirth I, Diele S, Eremin A, et. al. *J. Mater. Chem.*, **2001**, 11, 1642.
- [41] Demus D, Goodby JW, Gray GW, Spiess H.-W, Vill V (ed.), *Handbook of Liquid Crystals*, Wiley-VCH, Weinheim, **1998**, Vol. 2B.
- [42] Goodby JW, Collings PJ, Kato T, et. al. *Handbook of Liquid Crystals: Fundamentals*, Wiley-VCH, Weinheim, Germany, **2014**, vol. 1.
- [43] Toyne KJ, Gray GW (ed), *Thermotropic Liquid Crystals*, Wiley: Chichester, UK, **1987**, 28–63.
- [44] (a) Matraszek J, Mieczkowski J, Szydłowska J, et al. *Liq. Cryst.*, **2000**, 27, 429–436; (b) Wirth I, Diele S, Eremin A, et al. *J. Mater. Chem.*, **2001**, 11, 1642–1650; (c) Mathews M, Zola RS, Yang D-K, et al. *J. Mater. Chem.*, **2011**, 21, 2098–2103; (d) Niori T, Yamamoto J, Yokoyama H. *Mol. Cryst. Liq. Cryst.*, **2004**, 409, 475–482.
- [45] (a) Lee SK, Li X, Kang S, et al. *J. Mater. Chem.*, **2009**, 19, 4517–4522; (b) Schroder MW, Pelzl G, Dunemann U, et al. *Liq. Cryst.*, **2004**, 31, 633–637.
- [46] (a) Chiang I-H, Long C-J, Lin H-C, et. al. *ACS Appl. Mater. Inter.*, **2014**, 6, 228–235; (b) Subrao M, Potukuchi DM, Ramachandra GS, et. al. *Beilstein J. Org. Chem.*, **2015**, 11, 233–241; (c) Shanker G, Prehm M, Tschierske C. *Beilstein J. Org. Chem.*, **2012**, 8, 472–485; (d) Hariprasad S, Srinivasa H. T. *Liq. Cryst.*, **2015**, 42, 1612–1620.
- [47] (a) Kiryanov AA, Seed AJ, Sampson P. *Tetrahedron Lett.*, **2001**, 42, 8797–8800; (b) Kozmlk V, Hodík T, Svoboda J, et. al. *Liq. Cryst.*, **2016**, 43, 839–852; (c) Giroto E, Bechtold I.H, Gallardo H. *Liq. Cryst.*, **2015**, 42, 1798–1807.

- [48] (a) Seed AJ, Tietz JI, Gipson RM, et. al. *Liq. Cryst.*, **2015**, 42, 918–927; (b) Kovarova A, Kohout M, Svoboda J, et. al. *Liq. Cryst.* **2014**, 41, 1703–1718; (c) Lai LL, Wang CH, Hsien WP, et. al. *Mol. Cryst. Liq. Cryst.*, **1996**, 287, 177–181.
- [49] Demus D, Goodby JW, Gray G, et. al. *Low Molecular Weight Liquid Crystals*. Wiley-VCH: Weinheim; New York, **1998**; Vol. 2A
- [50] (a) Niori T, Sekine T, Watanabe J, et. al. *Mol. Cryst. liq. Cryst.*, **1997**, 337, 301; (b) Sekine T, Takanashi Y, Niori T, et. al. *Jnp. J. appl. Phys.*, **1997**, 1, 1201; (c) Shen D, Diele S, Pelzl G, et. al. *J. Mater. Chem.*, **1999**, 9, 661; (d) Shreenivasa HN, Murthy, Sadashiva BK. *Liq. Cryst.*, **2004**, 31, 567.
- [51] Walba DM. *Science.*, **1995**, 270, 250.
- [52] (a) Dingemans TJ, Murthy NS, Samulski ET, et. al. *J. Phys. Chem. B.*, **2001**, 105, 8845; (b) Das B, Grande S, Weissflog W. et. al. *Liq. Cryst.*, **2003**, 30, 529; (c) Stannarius R, Li J, Weissflog W. *Phys. Rev. Lett.*, **2003**, 90, 025502.
- [53] (a) Wu J, Okamoto H, Akenaka S. *Chem. Lett.*, **2001**, 2, 116–117; (b) Hird M, Goodby JW, Gough N. et. al. *J. Mater. Chem.*, **2001**, 11, 2732–2742; (c) Yu FC, Yu LJ. *Chem. Mater.*, **2006**, 18, 5410–5420, (d) Yu FC, Yu LJ. *Liq. Cryst.*, **2008**, 35, 799–813, (e) Enz E, Tandel SF, Dabrowski R. et. al. *J. Mater. Chem.*, **2009**, 19, 2950–2957.
- [54] Cristiano R, Vieira AA, Ely F, Gallardo H. *Liq. Cryst.*, **2006**, 33, 381.
- [55] Cioanca ER, Epure EL, Carlescu J, et. al. *Mol. Cryst. Liq. Cryst.*, **2011**, 537, 51
- [56] Dong CH, Wang H, Li M, et. al. *Soft Matter.*, **2014**, 10, 9105.
- [57] Radhika S, Srinivasa HT, Sadashiva BK. *Liq. Cryst.*, **2011**, 38, 785
- [58] Sathyanarayana P, Radhika S, Sadashiva BK, et. al. *Soft Matter.*, **2012**, 8, 2322
- [59] Monika M, Prasad V, Nagaveni NG. *Liq. Cryst.*, **2015**, 42, 1–16
- [60] Novatna V, Zurek J, Kozmik V, et. al. *Liq. Cryst.*, **2008**, 35, 1023
- [61] (a) Gallardo H, Cristiano R, Vieira AA, et. al. *Liq. Cryst.*, **2008**, 35, 857; (b) Sarkar G, Das MK, Paul R, et. al. *Phase. Transitions.*, **2009**, 82, 433; (c) Tavares A, Ritter MS, Ursula B, et. al. *Liq. Cryst.*, **2010**, 37, 159
- [62] (a) Deb R, Nath RK, Paul MK, et. al. *J. Mater. Chem.*, **2010**, 20, 7332; (b) Chakraborty A, Das B, Das MK, et. al. *Liq. Cryst.*, **2011**, 38, 1085; (c) Paul MK, Nath RK, Moths B, et. al. *Phase. Transitions.*, **2012**, 85, 1070.

- [63] (a) Upadhyaya K, Gude V, Mohiuddin G, et. al. *J. Org. Chem.*, **2013**, 9, 26; (b) Chakraborty L, Chakraborty N, Sarkar DD, et. al. *J. Mater. Chem. C.*, **2013**, 1, 1562; (c) Belaisaoui A, Cowling SJ, Goodby JW. *Liq. Cryst.*, **2013**, 40, 822.
- [64] (a) Novoyna V, Glogarova M, Kozmik V, et. al. *Soft. Matter.*, **2013**, 9, 647; (b) Paul MK, Saha SK, Singh YD, et. al. *Liq. Cryst.*, **2014**, 41, 1367; (c) Choi E-J, Park K-M, Kim D-Y, et. al. *Liq. Cryst.*, **2016**, 43, 1597.
- [65] (a) Alaasar M, Poppe S, Tschierske C. *Liq. Cryst.*, **2017**, 44, 729; (b) Kapuscinski S, Wojciechowska A, Urbanaik K, et. al. *Liq. Cryst.*, **2017**, 44, 1093; (c) Alaasar M, Poppe S, Kerzig C, et. al. *J. Mater. Chem. C.*, **2017**, 5, 8454
- [66] (a) Saha SK, Deb J, Sarkar U, et. al. *Liq. Cryst.*, **2017**, 44, 2203; (b) kim M-H, Nam Y-K, Choi E-J. *J. Information. Display.*, **2017**, 18, 31; (c) Patranabish S, Mohiuddin G, Begum N, Laskar AR, et. al. *J. Mol. Liq.*, **2018**, 257, 144; (d) Weissflog W, Nauman G, Kosata B, et. al. *J. Mater. Chem.*, **2005**, 15, 4328.
- [67] (a) Prasad V, Rao DSS, Prasad SK. *Liq. Cryst.*, **2001**, 28, 643; (b) Nagaveni NG, Roy A, Prasad V. *J. Mater. Chem.*, **2012**, 22, 8948; (c) Nagaveni NG, Prasad V. *Liq. Cryst.*, **2013**, 86, 1227; (d) Reddy RA, Baumeister U, Chao LJ, et. al. *Soft Matter.*, **2010**, 6, 3883
- [68] Liu C.-Y, Zhao H, Yu H.-h. *Org. Lett.*, **2011**, 13, 4068
- [69] (a) Krishnan SAR, Weissflog W, Pelzl G, et. al. *Phys. Chem. Chem. Phys.*, **2006**, 8, 1170; (b) Sutherland RL, in *Handbook of Nonlinear Optics*, Dekker, New York, 2nd ed. **1996**; (c) Philip R, Kumar GR, Sandhyarani N, et. al. *Phys. Rev. B.*, **2000**, 62, 13160.
- [70] Arakawa Y, Nakajima S, Ishige R, et. al. *J. Mater. Chem.*, **2012**, 22, 8394.

Chapter 4

Phenazine fused triphenylene discotic liquid crystals

4.1 Part A. Synthesis, characterization and charge transport properties of thiol-substituted phenazine fused triphenylene supramolecular systems

4.2 Part B. Alkyl and alkoxy-phenylacetylene containing phenazine fused triphenylene discotic liquid crystals

4.3 Part C. Monomeric ester containing phenazine fused triphenylene discotic liquid crystals

4.4 Part D. Synthesis, mesomorphic and photophysical properties of π - extended dibenzophenazine based discotic liquid crystals

4.1 Part A. Synthesis, characterization and charge transport properties of thiol-substituted phenazine fused triphenylene supramolecular systems

4.1.1 Introduction

Most of the DLCs are derived from polycyclic aromatic cores such as benzene, naphthalene, phenanthrene, pyrene, perylene, triphenylene, anthraquinone (AQ), phthalocyanine (Pc), decacylene, hexabenzocoronene (HBC), and so on. Among all, triphenylene is the most extensively studied discotic core known in the literature. Triphenylene, as the name indicates is a trimer of phenyl (benzene) units where three benzene rings are fused to form a central fourth ring. The potential of TP as a novel core for DLCs was recognized by Billard et al. in 1978 [1], just after the discovery of DLCs derived from benzene hexa-*n*-alkanoates by Chandrasekhar et al. in the year 1977 [2]. TP derivatives are thermally as well as chemically stable, their chemistry is fairly accessible, and they show rich mesomorphism at elevated temperature as well as at ambient temperature. Their one-dimensional charge and energy migration properties offer tremendous potential applications. Accordingly, they have been described as ‘*the workhorses*’ in the field of discotics [3]. Appropriately functionalized TP derivatives are known for hole-transporting properties and their charge carrier mobility is ranged from $10^{-5} \text{ cm}^2 \text{ V}^{-1} \text{ s}^{-1}$ to $10^{-1} \text{ cm}^2 \text{ V}^{-1} \text{ s}^{-1}$ in the highly ordered columnar phase [4]. The electron rich nature of TP derivatives are typically known as hole transport materials and are suitable for doping with electron acceptors to serve as a *p*-type semiconductor. Recently, TP based DLCs have been widely used to disperse various zero-dimensional (0-D), one-dimensional (1-D) and two-dimensional (2-D) metallic, semiconducting and carbon nanoparticles, and so formed nanocomposites have been studied for various physical properties [5–13]. The TP-based DLCs find interesting applications such as 1D conductor, photoconductors, photovoltaic solar cells, gas sensors, so on. The nature of alkyl chains on the aromatic TP and substitutions in the core unit significantly influence the phase behaviour and physical properties. Till date, TP remained the focus of considerable attention of LC scientists, and extensive research work is continuously going on. Thus TP remains the ‘*Drosophila of discotic liquid crystal*’ which has received one of the potential

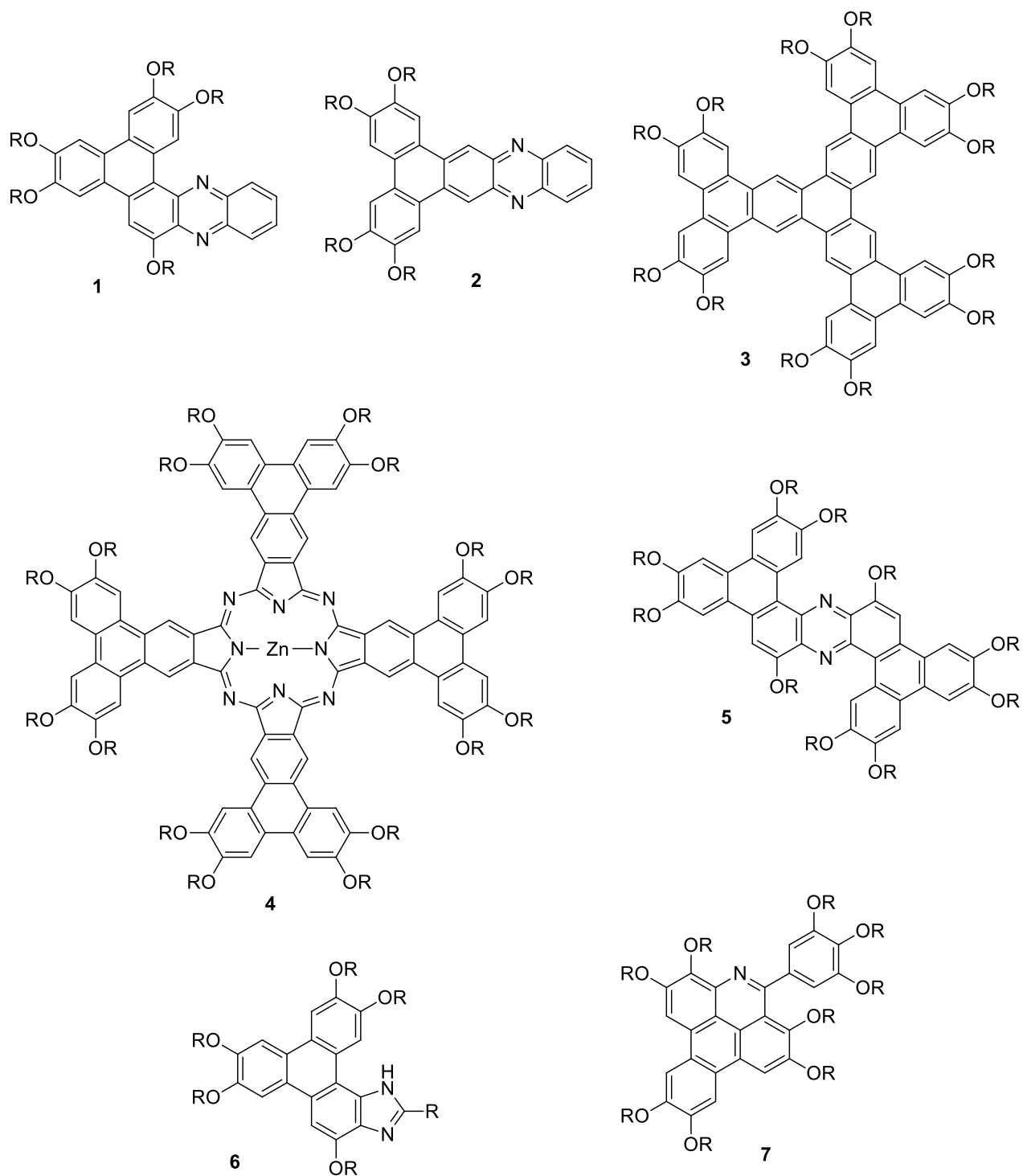
materials in the class of discotic LCs. The chemical and physical properties of TP DLCs have been well documented in several reviews and book chapters, for example, Ref [14,15,16–25].

Extension of triphenylene core is expected to demonstrate significant changes on mesomorphic properties along with their electronic properties. Such supramolecular macrocyclic compounds are anticipated to exhibit columnar mesomorphic phases over a broad temperature range with better electronic properties [29–28]. Commonly, triphenylene derivatives having less than six alkoxy chains are non mesomorphic; however, the mesophase can be induced by substituting functional groups in the periphery [29]. Several research groups followed the concept of reducing overall symmetry of the mesogens, with the idea that such molecules may self-organize distinctly in the mesophase and eventually exhibit different physical properties. There are many ways to reduce the symmetry of mesogens, such as, asymmetric substitution of alkyl chains or substitution of functional groups or substitution of alkyl chains using ester, ether or amine linking groups. In 1999, Kumar et al. have made initial attempt to extended triphenylene discotic core by fusing 1,2-phenylenediamine with triphenylene-diquinone to produce phenanthro[a]phenazine (1) and phenanthro[b]phenazine (2) based heteroaromatic DLCs [30].

Subsequently, Mullen group reported Suzuki coupling reaction between hexabromotriphenylene with 3,4-dialkoxyphenylboronic acid gives extended TP derivatives (3) [31]. Later, Cammidge et al. reported triphenylenophthalocyanines macrocyclic DLCs (4) which exhibit columnar phase over broad temperature [32]. They also reported electron rich character of triphenylene twin linking through electron deficient pyrazine ring (5) that represents a donor-acceptor-donor framework with wide range mesomorphic properties [33]. Our group reported the synthesis of heterocyclic imidazole ring fused TP core (6) that exhibits columnar mesophase over broad temperature range [34].

Yang and co-workers have prepared DLCs based on the triphenylene-bodipy dyads and investigated their photophysical properties. These mesogens exhibited strong fluorescence properties along with a high quantum yields in solution and weak fluorescence in film. They have also reported triphenylene-perylene-triphenylene discotic triads with bay substituents which exhibit Col_h phase over a broad temperature range [35]. Recently, novel annulated triphenylene

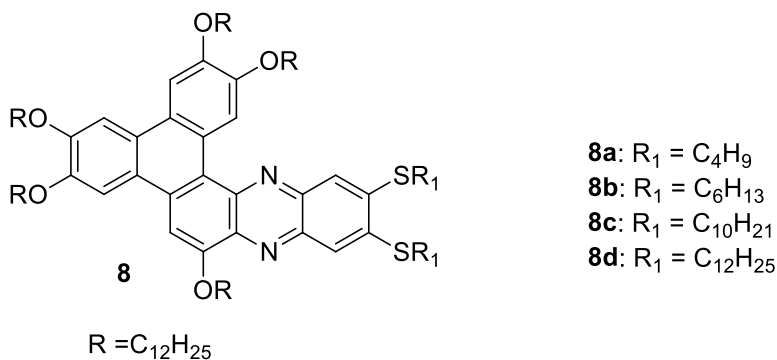
based heteroaromatic DLCs (**7**) using Pictet-Spengler cyclization reaction was reported from our group [36].



R = alkyl chains

4.1.2 Objective

Discotic liquid crystals are well known for their one-dimensional electron, ion or energy transport properties. The designing of triphenylene discotic core fused with phenazine heterocyclic ring may results novel hybrid materials with interesting physical properties. The presence of polar and coloured nature of phenazine heterocyclic core along with the mesomorphic character of triphenylene derivatives can show supramolecular framework systems suitable for molecular electronic device applications. We envisioned that, the incorporation of phenazine moiety in TP discotic core would enhance π -electron conjugation and induces a wide mesophase along with high charge carrier properties. The aim of this work is to prepare novel extended triphenylene based phenazine heterocyclic discotic liquid crystals tethered with alkanethiols and alkoxy chains (**8**) and investigate their mesomorphic, photophysical and charge transport properties.

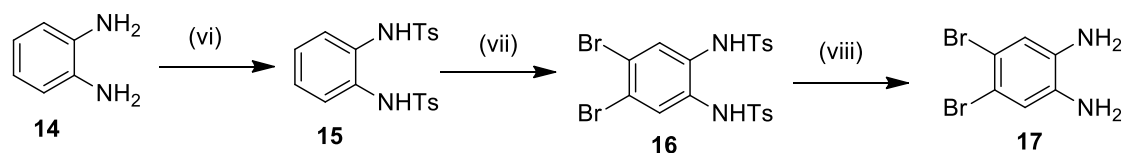
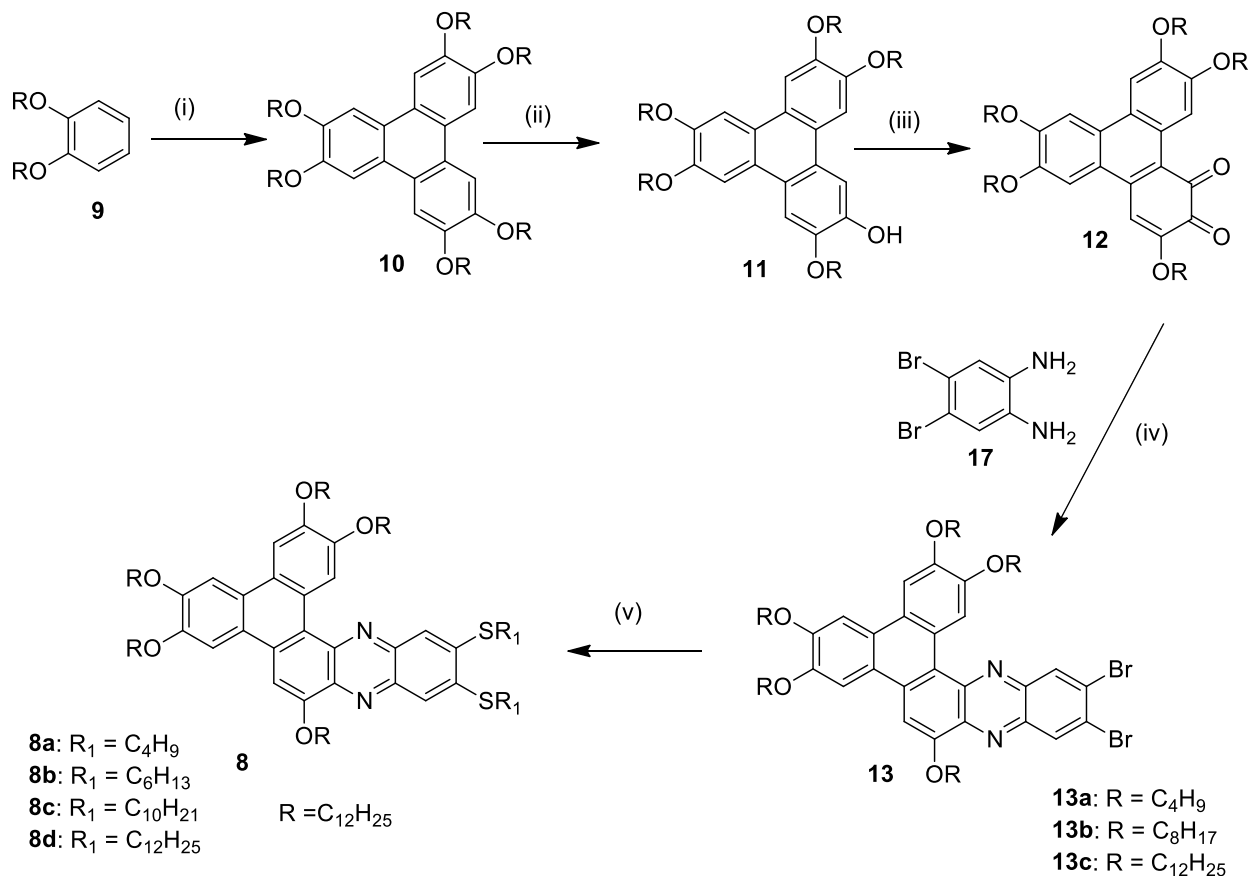


4.1.3 Results and discussion

4.1.3.1 Synthesis

The intermediates and final discotic mesogens were synthesized by following route as shown in **Scheme 1**. The monohydroxytriphenylene **11** was synthesised by following reported procedure [37]. Oxidation of the 2-hydroxy-3,6,7,10,11-pentakis(alkyloxy) triphenylene **11** with ceric ammonium nitrate gives 3,6,7,10,11-pentakis(alkyloxy)triphenylene-1,2-diones **12** [38].

The intermediate 4,5-dibromobenzene-1,2-diamine **17** compound was synthesized following a reported procedure [39] and it was condensed with triphenylene-1,2-diquinone **12** in presence of glacial acetic acid in toluene (7:3) under reflux condition to afford intermediate 9,10-dibromo-2,3,6,14,15-pentaalkoxyphenanthro [9, 10-a]phenazine compounds (**13a–13c**).



Scheme 1. (i) FeCl_3 , CH_2Cl_2 , r.t., 30 min; (ii) catechol boron bromide, CH_2Cl_2 , r.t., 24 h; (iii) CAN, CH_3CN , r.t., 30 min; (iv) CH_3COOH : toluene (7:3), reflux, 6 h; (v) alkanethiol, Cs_2CO_3 ,

DMAC, reflux, 24 h; (vi) *p*-TosCl, pyridine, r.t, 24 h; (vii) Br₂, NaOAc, acetic acid, 110 °C, 3 h; (viii) Con. H₂SO₄, 110 °C, 15 min.

Further, reaction of alkanethiols with intermediate mesogenic compound **13c** in presence of cesium carbonate under reflux condition produces the desired extended phenazine based triphenylene mesogenic derivatives (**8a–8d**). All the intermediates and final compounds were purified by column chromatography, followed by recrystallization with appropriate solvent and well characterized using spectral and elemental analysis as given in the experimental part.

4.1.3.2 Thermal properties

Thermotropic liquid crystalline properties of all the intermediates and final triphenylene based phenazine derivatives (**13a–13c** & **8a–8d**) are summarized in **Table 1**. The phase transition temperature (peak temperature in °C) and associated enthalpy (kJ mol⁻¹) values obtained from the heating and subsequent cooling cycles of respective mesogens were determined by DSC at the scan rate of 10 °C min⁻¹ under nitrogen atmosphere. The columnar textures of all the mesogens were observed using POM under crossed polarizers, display the characteristic of hexagonal columnar mesophase as shown in **Figure 1**. The compound **13a** exclusively shows enantiotropic columnar phase. The peak temperature at 154.4 °C is due to crystalline-columnar phase transition with the enthalpy of phase transition of 32.42 kJ mol⁻¹, whereas the peak temperature at 315.3 °C with lower enthalpy value ($\Delta H = 11.21$ kJ mol⁻¹) corresponds to Col_h to isotropic phase transition. On slow cooling under POM, the microscopic observation of dendritic textures revealed the formation of hexagonal columnar mesophase at 312.9 °C. The crystallization was confirmed by the moderate appearance of small needle like domains into liquid crystal texture upon cooling to room temperature. As a representative example, polarized optical micrograph of compound **13a** obtained on cooling from the isotropic liquid at about 245 °C is shown in **Figure 1a**. Similarly, compounds **13b** and **13c** exhibit Cr to Col_h phase at 94.8 °C ($\Delta H = 40.65$ kJ mol⁻¹) and 81.3 °C ($\Delta H = 48.90$ kJ mol⁻¹), respectively and Col_h to isotropic liquid at 265.4 °C ($\Delta H = 8.46$ kJ mol⁻¹) and 232 °C ($\Delta H = 7.90$ kJ mol⁻¹)

respectively. A representative DSC thermogram of intermediate compound **13c** is shown in **Figure 2**. Under POM, compound **13b** showed appearance of columnar texture at 263 °C, on cooling from isotropic phase. On the other hand, compound **13c** show a similar textural transition during the cooling from isotropic phase (232 °C) to room temperature.

Table 1. Phase transition temperature (peak in DSC °C) and enthalpies (kJ mol⁻¹, in parentheses) of all the mesogens **13a–13c** and **8a–8d** (on heating and cooling cycle).

Compound	Phase transition peak temperature (°C); (ΔH , [kJ mol ⁻¹])	
	<i>second heating scan</i>	<i>second cooling scan</i>
13a	Cr 154.4 [32.42] Col _h 315.3 [11.21] I	I 312.9 [-11.61] Col _h 55.2 [-18.10] Cr
13b	Cr 94.8 [40.65] Col _h 265.4 [8.46] I	I 263 [-8.16] Col _h 13.5 [-31.88] Cr
13c	Cr 81.3 [48.90] Col _h 232 [7.90] I	I 228.9 [-7.62] Col _h 17.2 [-51.58] Cr
8a	Cr 55.1 [36.60] Col _h 172 [6.49] I	I 170.3 [-6.24] Col _h 17.4 [-38.83] Cr
8b	Cr 45.7 [47.36] Col _h 176.4 [6.66] I	I 174.7 [-6.17] Col _h 19 [-45.49] Cr
8c	Cr ₁ 44.2 [10.95] Cr ₂ 73 [20.16] Col _h 167.1 [5.38] I	I 163.2 [-5.66] Col _h 23.6 [-38.39] Cr
8d	Cr ₁ 34.5 [6.11] Cr ₂ 74.1 [25.83] Col _h 165.1 [6.72] I	I 163.5 [-6.52] Col _h 35.7 [-36.04] Cr

Similar trend of enantiotropic phase transition is also observed for the final mesogenic derivatives (**8a–8d**). The compounds **8a** and **8b** show two endothermic phase transition temperatures from Cr to Col_h at 55.1 °C ($\Delta H = 36.60$ kJ mol⁻¹) and 45.7 °C ($\Delta H = 47.36$ kJ mol⁻¹), respectively and Col_h phase to isotropic phase at 172 °C ($\Delta H = 6.49$ kJ mol⁻¹) (**Figure 2**) and 176.4 °C ($\Delta H = 6.66$ kJ mol⁻¹) respectively. On cooling under POM, compound **8a** showed the appearance of columnar phase at 170.3 °C which transferred to crystalline phase at 17.4 °C. Representative DSC thermogram of **8a** is shown in **Figure 2**. On the other hand, compound **8b**

observed under the POM exhibit mesophase at 174.7 °C and retain Col_h phase upto 19 °C (on cooling). Compound **8c** undergoes crystal-crystal transition at 44.2 °C ($\Delta H = 10.95 \text{ kJ mol}^{-1}$) and melt to Col_h phase at 73 °C ($\Delta H = 20.16 \text{ kJ mol}^{-1}$) and become isotropic liquid at 167.1 °C ($\Delta H = 5.38 \text{ kJ mol}^{-1}$). Under POM, compound **8c** showed the formation of columnar phase texture at 163.2 °C and transferred to crystalline phase at 23.6 °C (on cooling). Similarly, on heating compound **8d** display crystal-crystal transition at 34.5 °C ($\Delta H = 6.11 \text{ kJ mol}^{-1}$) and become melting to Col_h phase at 74.1 °C with enthalpy change ($\Delta H = 25.83 \text{ kJ mol}^{-1}$), which goes to isotropic phase at 165.1 °C ($\Delta H = 6.72 \text{ kJ mol}^{-1}$). Compound **8d**, on slow cooling from isotropic liquid exhibit typical texture of Col_h phase at 163.5 °C as shown in **Figure 1b**, viewed at 200 × magnifications. POM and DSC studies reveal the presence of mesophase structure, while self-assembly of hexagonal columnar phase has been investigated by X-ray diffraction studies. It is noticed that the extended phenazine core with flexible alkanethiol substituted derivatives (**8a–8d**) exhibit a lower isotropic temperature in comparison to intermediate dibrominated phenazine compounds (**13a–13c**) owing to the more number of flexible alkyl chains surrounded around the discotic core.

4.1.3.3 X-ray diffraction studies

In order to understand the mesophase structure along with the supramolecular self-assembly of all the novel mesogens, X-ray diffraction experiments were performed using liquid crystalline samples filled in Lindemann capillaries. X-ray diffraction patterns recorded for all the mesogens (**13a–13c** and **8a–8d**) in the columnar mesophase on both heating and cooling scans are shown in **Table 2** and **Figure 3**. All the mesogenic compounds **13a–13c** and **8a–8d** showed increasing order of diffraction angle, the *d*-spacing's of the first reflection (lowest angle and highest intensity) to the second one are in the ratio of 1:1/√3:1/2:1/7. These values corresponding to those expected from two dimensional hexagonal lattice and relatively broad peak in the wide angle regime corresponding to the liquid like packing of the molten aliphatic chains. The distance between neighbouring columns was calculated by using the relation $a = d_{10}/(\cos 30^\circ)$, where d_{10} is the spacing of highest intensity peak in the small angle region (**Table 2**).

A representative and typical XRD pattern obtained for compound **13a** and **8d** on heating scan is shown in **Figure 3**. The XRD pattern of compound **13a** at 175 °C during heating in columnar phase is shown in **Figure 3a**. In the small angle region three peaks were observed, one very strong and other two weak peaks of d -spacing $d_1 = 16.65 \text{ \AA}$, $d_2 = 9.59 \text{ \AA}$ and $d_3 = 6.27 \text{ \AA}$ values and respective lattice constant ($a = 19.22$) are in good agreement with the hexagonal columnar phase. The broad peak at wide angle region $d = 4.32 \text{ \AA}$ corresponds to liquid like packing of molten aliphatic chains and the sharp peak at 3.61 \AA corresponds to core–core distance describes ordered hexagonal columnar phase. The intercolumnar distance is found to be 19.22 \AA , which is less than higher homologous derivatives **13b** and **8c**. Similarly, X-ray diffraction pattern obtained for alkanethiol substituted compound **8d** upon heating in columnar phase at 100 °C is shown in **Figure 3b**. In the small angle region four prominent peaks observed, one sharp peak of d - spacing values $d_1 = 26.74 \text{ \AA}$ and corresponding three weak peaks at $d_2 = 15.37 \text{ \AA}$, $d_3 = 13.35 \text{ \AA}$ and $d_4 = 10.10 \text{ \AA}$, along with lattice constant $a = 30.87$, suggesting the formation of hexagonal columnar phase. The broad halo peak in the wide angle region at 4.59 \AA shows liquid like arrangement of flexible chains and a weak peak at further wide angle region at 3.64 \AA is analogous to the distance between cores in the columns. The intercolumnar distance for **8d** is found to be 30.87 \AA , which is higher than the corresponding lower homologous compounds (**8a–8c**) in the series. It is evident that the increase in the number of alkyl chain length, the width of the cylindrical columns framed by the discotic molecules also increases. All the above properties obey well known supramolecular order of Col_h phase in which the disc like aromatic cores stack on top of other to form columns surrounding by the flexible molten aliphatic chains. These columns self assembled themselves in a two-dimensional hexagonal lattice. The above futures confirmed that all the mesogenic derivatives (**13a–13c** & **8a–8d**) are self-assembled in the hexagonal columnar fashion in their liquid crystal phase.

Table 2. X-ray data of all the mesogens (**13a–13c** & **8a–8d**). I_C = Intercolumnar distance, C–C = Core-Core separation, R_L = Alkyl- chain length.

Compound/ Temperatur e (°C)	2θ (degrees)	d -spacing's, observed (calculated) Å	Phase/ lattice constant	Col_h para meter	Miller indices	R_L (Å)	C–C (Å)	I_C (Å)
13a/ 175	5.30	16.65 (16.64)	Col_h	1	100			
	9.21	9.59 (9.60)	$a = 19.22$	$1/\sqrt{3}$	110	4.32	3.61	19.22
	14.09	6.27 (6.29)		$1/\sqrt{7}$	210			
13b/ 200	3.70	20.52 (20.51)	Col_h	1	100			
	7.42	11.90 (11.84)	$a = 23.69$	$1/\sqrt{3}$	110	4.51	3.65	23.69
	11.39	7.75 (7.75)		$1/\sqrt{7}$	210			
13c/ 140	3.72	23.69 (23.68)	Col_h	1	100			
	6.43	13.75 (13.67)	$a = 27.35$	$1/\sqrt{3}$	110	4.62	3.66	27.35
8a/ 100	3.59	24.58 (24.57)	Col_h	1	100			
	6.22	14.19 (14.18)	$a = 28.38$	$1/\sqrt{3}$	110	4.50	3.55	28.38
	7.19	12.28 (12.28)		$1/2$	200			
8b/ 75	3.51	25.14 (25.13)	Col_h	1	100			
	6.08	14.52 (14.50)	$a = 29.02$	$1/\sqrt{3}$	110	4.62	3.56	29.03
	7.03	12.56 (12.56)		$1/2$	200			
8c/ 130	3.36	26.27 (26.26)	Col_h	1	100			
	5.72	15.46 (15.16)	$a = 30.33$	$1/\sqrt{3}$	110	4.57	3.60	30.33
	6.58	13.41 (13.13)		$1/2$	200			
8d/ 100	3.30	26.74 (26.73)	Col_h	1	100			
	5.72	15.37 (15.42)	$a = 30.87$	$1/\sqrt{3}$	110	4.59	3.64	30.87
	6.61	13.35 (13.36)		$1/2$	200			
	8.74	10.10 (10.10)		$1/\sqrt{7}$	210			

4.1.4 Photophysical properties

The novel π -extended discotic mesogens (**13a–13c** & **8a–8d**) show strong light absorption and photo induced light emission, as measured by UV-Vis absorption and photoluminescence studies. The UV absorption properties were studied in a very dilute solution in anhydrous chloroform solvent recorded at ambient temperature to know absorption maxima as presented in **Figure 4**. The details of absorption bands have been summarized in **Table 3**. All the mesogens display absorption bands below 600 nm. The intermediate phenazine derivatives (**13a–13c**) exhibit absorption at $\lambda_{\text{max}} = 257\text{--}473$ nm and molar absorption coefficient (ϵ) $1.34\text{--}3.94$ L mol⁻¹ cm⁻¹, which corresponds to $n\rightarrow\pi^*$ and $\pi\rightarrow\pi^*$ electronic transitions as shown in **Figure 4a**. Similarly, alkanethiol substituted phenazine derivatives show maximum absorption bands at $\lambda_{\text{max}} = 260\text{--}469$ nm and corresponding molar absorption coefficient ($\epsilon = 2.48\text{--}4.18$ L mol⁻¹ cm⁻¹), which are responsible for $n\rightarrow\pi^*$ and $\pi\rightarrow\pi^*$ electronic transitions as shown in **Figure 4b**. The intermediate dibrominated compounds (**13a–13c**) are red shifted with increased intensity to a longer wavelength ($\lambda_{\text{max}} = 473$ nm) in comparison with alkanethiol substituted phenazine derivative ($\lambda_{\text{max}} = 465$ nm). This may be attributed to extended π -conjugation along with electro-negativity effect of bromo functional groups present in the heteroaromatic phenazine ring on molecular structure of discotic mesogen. Extension of π -conjugation frame work in the novel mesogens (**13a–13c** & **8a–8d**) causes bathochromic shift (longer wavelength) with respect to triphenylene derivatives.

Similarly, photoluminescence spectra of all the mesogens (**13a–13c** & **8a–8d**) were recorded using dilute solution of anhydrous chloroform solvent at room temperature and all the compounds were excited at $\lambda_{\text{ex}} = 460$ nm as shown in **Figure 4c** and **4d**. The intermediate dibrominated phenazine derivatives (**13a–13c**), exhibit strong emission at $659\text{--}663$ nm (**Table 3**). Similarly, final phenazine derivatives exhibit fluorescence emission at $620\text{--}622$ nm. No apparent changes were seen upon increasing the number of methylene groups in the terminal chains.

Table 3. Photophysical properties of intermediate and final DLCs (**13a–13c** & **8a–8d**) recorded in anhydrous chloroform (10^{-5} M) solution.

Compound	Absorption, $\lambda_{\text{abs}}/\text{nm}$ ($\epsilon/10^7 \text{ L mol}^{-1} \text{ cm}^{-1}$)	Emission, $\lambda_{\text{em}}/\text{nm}$
13a	257 (0.72), 290 (0.82), 314 (0.88), 352 (0.99), 476 (1.34)	661
13b	258 (1.38), 289 (1.55), 315 (1.69), 352 (1.89), 476 (2.55)	659
13c	258 (2.13), 289 (2.39), 316 (2.62), 352 (2.91), 476 (3.94)	663
8a	260 (2.32), 293 (2.61), 352 (3.14), 469 (4.18)	622
8b	261 (1.38), 292 (1.54), 352 (1.86), 468 (2.48)	621
8c	261 (1.54), 294 (1.73), 352 (2.08), 468 (2.76)	622
8d	260 (2.04), 293 (2.30), 352 (2.77), 469 (3.69)	620

4.1.5 Density functional theory calculations

The quantum mechanical calculations and molecular properties were determined computationally using DFT calculations. Gaussian 16 program package was employed to carry out DFT calculations at the Lee-Yang-Parr correlation functional (B3LYP) by using 6–311G (d) basis set to obtain the information related to molecular conformation and frontier molecular orbitals (FMOs) of the discotic mesogen [40]. The internal coordinates of the molecular system, which are used as an input for the Gaussian 16 computational program, were generated by the Gauss View 06 program. The energy minimized molecular structure of representative final discotic mesogen (**8b**) is shown in **Figure 5a**, whereas the contours of highest occupied molecular orbital (HOMO) and lowest unoccupied molecular orbital (LUMO) is depicted in **Figure 5b**. The HOMO and LUMO energy levels of the compound **8b** are at -5.32 and -2.46 eV respectively. The theoretically calculated energy gap (ΔE_{gap}) is found to be 2.86 eV. FMOs and difference in their energies provide information on the length of extended conjugation and band gap level in these novel discotic mesogens. The calculated HOMO and LUMO energy levels for the phenazine fused discotic mesogens were further illustrated to confirm the charge transfer from donor (triphenylene core) to the acceptor (phenazine core) in the excited state [33].

4.1.6 Thermogravimetric analysis

Thermal stability of all novel intermediate and final discotic mesogens (**13a–13c** & **8a–8d**) was investigated by using thermogravimetric analysis. All the samples were subject to heat scan of $10\text{ }^{\circ}\text{C min}^{-1}$ under nitrogen atmosphere as shown in **Figure 6**. The intermediate compounds (**13a–13c**) show no weight loss till $345\text{ }^{\circ}\text{C}$ (**Figure 6a**) and final mesogenic compounds (**8a–8d**) exhibit thermal stability without weight loss until $325\text{ }^{\circ}\text{C}$ (**Figure 6b**). Upon further increasing temperature, intermediate and final compounds initiated weight loss around $353\text{ }^{\circ}\text{C}$ – $375\text{ }^{\circ}\text{C}$ (**13a–13c**) and $344\text{ }^{\circ}\text{C}$ – $355\text{ }^{\circ}\text{C}$ (**8a–8d**), respectively. All the compounds decompose completely at $520\text{ }^{\circ}\text{C}$ – $540\text{ }^{\circ}\text{C}$. The thermal stability of all the compounds is much higher than their isotropic temperature. However, the thermal stability of intermediate compounds was higher than the final discotic mesogens. Hence, all the compounds are thermally stable over a broad temperature range.

4.1.7 Charge carrier mobility

We examined the charge carrier mobility of a representative compound **8b** using the time of flight method. First, the LC sample was filled in the ITO cell with cell gap of $9.2\text{ }\mu\text{m}$ and then excited by Nd:YAG pulsed laser having excitation wavelength of 355 nm and 5 ns pulse width. The generation of charge carriers was examined by applying the bias of 90 to 150 V (**Figure 7 & 8**). The transit time (τ) of charge carriers was obtained by the transient photocurrent curve. The induced charge displacement was recorded by a digital oscilloscope (Agilent, DSO 1012A) connected to a current amplifier Keithley 428.

In general, the mobility (μ) is calculated using the formula; $\mu = d^2 / \tau.V$, where τ is the transient time obtained by photocurrent curves, V is the applied voltage and d is the thickness of ITO cell. We adopted more precise method to calculate mobility in which, we first plotted a curve between transient time and inverse of voltage i.e. $\tau = \left(\frac{d^2}{\mu} \right) \left[\frac{1}{V} \right]$. In this relation the value of slope is equivalent to d^2/μ . Then, mobility is calculated using the formula; $\mu = d^2/\text{slope}$. The charge carrier mobility as a function of temperature is plotted in **Figure 9**.

We observed that compound **8b** exhibits charge transport having hole mobility in the order of $10^{-4} \text{ cm}^2\text{V}^{-1}\text{s}^{-1}$ in discotic hexagonal columnar phase which is comparable to recently reported articles [41]. In the present investigation, discotic material (**8b**) exhibited *p*-type (hole) charge transport due to large triphenylene core whereas charge transport due to electron associated to small phenazine was not fairly detected. Another reason for the absence of electron charge transport could be the trapping of electron by space charges or oxygen vacancies in the material. Usually, the value of charge mobility is invariant of temperature for a particular mesophase regime[41d], however, Kato *et al.* have shown the temperature dependent nature of mobility but physical mechanism behind this characteristic is not discussed [42]. We found that the charge carrier mobility increases with increasing temperature following a power law [43].

$$\mu(T) = CT^n \text{ -----(1)}$$

Where *C* and *n* are an arbitrary constant and an exponent, respectively.

In general, the temperature dependent mobility of single crystalline materials follows the power law [44] having negative value of exponent, *n*, varies between 0.5 to 3. For disordered mesogenic system, its value can be larger than 3. As mobility versus temperature curves are fitted well in the power law (eqn. 1), which signifies that the columnar molecular assembly is unidirectionally oriented and π -stacked columnar molecular assembly gradually grows as a function of temperature.

Current-voltage (I–V) characteristics of compound **8b** as a function of voltage at different temperatures, ranging from 70 to 170 °C, were carried out using Keysight B2902A Precision Source/Measure Unit (SMU). During the measurement, the temperature of ITO cell was maintained with an accuracy of ± 0.1 °C using the Linkam TMS 93 hot plate. The current versus voltage (I–V) curves follow Ohmic behavior for a region of low voltages from –10 to +10V [44]. The charge-transport in the investigated LC system is due to the donor-acceptor mechanism of charge carriers between phenazine and triphenylene moieties. The variation of current on the temperature scale also follows the power law as shown in **Figure 10**, which is in good agreement with the aforementioned temperature dependent behavior of mobility. This material is quite

suitable for charge transportation at high temperatures and potential applications in the high temperature electronic devices and photovoltaics [45].

Relative permittivity of discotic mesogen **8b** as a function of temperature was evaluated at 3kHz using a HP4284 Impedance/Gain-Phase Analyzer. In **Figure 11** shows that relative permittivity increases with the decrease in temperature which is attributed to the thermally fluctuating π -stacked columnar molecular assembly of discotic mesogens.

4.1.8 Conclusions

The phenazine fused triphenylene discotic core containing alkanethiols and alkoxy chains have been successfully synthesised and characterised. These π -extended intermediate dibrominated phenazine derivatives and final alkanethiols containing phenazine fused TP derivatives self organize into hexagonal columnar mesophase over a broad temperature range. The mesomorphic properties of all the compounds were confirmed by POM and DSC. Hexagonal columnar structure of the liquid crystalline compounds was further confirmed by X-ray diffraction studies. All these phenazine derivatives exhibit excellent photophysical properties in anhydrous chloroform solvent. Charge carrier mobility of representative compound (**8b**) was measured by the ToF techniques, which reveals that compound (**8b**) exhibits *p*-type mobility of order $10^{-4} \text{ cm}^2 \text{ V}^{-1} \text{ s}^{-1}$. The mobility of charge carriers increases with increase in temperature following to a power law. This behavior of synthesized LC material is similar to single crystalline materials. The current-voltage characteristics follow ohmic behavior. The π -extended phenazine fused triphenylene based columnar DLCs may play a significant role in organic optoelectronic devices and solar cells applications.

4.1.8 Experimental section

4.1.8.1 General procedure for synthesis of intermediate and final compounds

The general materials and methods have been explained in **chapter 2**. The intermediate compounds 3,6,7,10,11-pentakis(alkyloxy)triphenylene-1,2-diones **12** and 4,5-dibromobenzene-

1,2-diamine **17** were synthesized as reported [37,38] and confirmed by spectral and elemental analysis.

Synthesis of 13,14-dibromo-2,3,6,7,10-pentaalkoxyphenanthro[9,10-a]phenazine (13):

Compound **12** (1 equiv) and 4,5-dibromobenzene-1,2-diamine **17** (1.1 equiv) were dissolved in a mixture of glacial acetic acid and toluene solvent (7:3) under stirring. The reaction mixture was refluxed under nitrogen atmosphere for 6 h. After completion of reaction, the reaction mixture was cooled to room temperature and poured into ice water, extracted with dichloromethane. The combined extracts were dried over Na₂SO₄ and solvent was evaporated under vacuum. The residue was purified by column chromatography using silica gel (*n*-hexane/dichloromethane 8:2). Recrystallization of the pure product with ethanol affords red colour solid **13a–13c** in about 80% yield. A representative example of ¹H and ¹³C NMR are shown in **Figure 12**.

13,14-dibromo-2,3,6,7,10-pentabutoxyphenanthro[9,10-a]phenazine (13a): IR (film) ν_{\max} : 2949.26, 2926.11, 2853.60, 1622.19, 1537.32, 1454.38, 1377.22, 1338.64, 1263.42, 1182.40, 1080.17, 833.28, 721.40, 667.39 cm⁻¹; ¹H NMR (500 MHz, CDCl₃): δ = 10.52 (s, 1H), 8.67 (s, 1H), 8.46 (s, 1H), 7.93 (s, 1H), 7.86–7.84 (m, 3H), 4.42 (t, 2H, *J* = 6.5 Hz), 4.34 (t, 2H, *J* = 7 Hz), 4.26–4.20 (m, 6H), 2.10–2.0 (m, 4H), 1.98–1.89 (m, 6H), 1.66–1.55 (m, 10H), 1.07–1.04 ppm (m, 15H); ¹³C NMR (125 MHz, CDCl₃): δ = 151.11, 150.96, 149.26, 148.66, 148, 144.78, 139.34, 138.62, 137.52, 133.36, 132.65, 130.54, 126.68, 126.35, 125.63, 124.54, 124.25, 122.20, 117.38, 112.17, 107.68, 105.74, 105.53, 105.26, 69.39, 69.11, 68.91, 68.77, 68.63, 31.54, 31.42, 31.40, 30.89, 19.46, 19.44, 14.18, 14.11, 14.07, 14.03 ppm; elemental analysis: C₄₄H₅₂Br₂N₂O₅, calculated: C, 62.26; H, 6.16; N, 3.29. % found: C, 62.37; H, 6.28; N, 3.39.

13,14-dibromo-2,3,6,7,10-pentakis(octyloxy)phenanthro[9,10-a]phenazine (13b): IR (film) ν_{\max} : 2953.12, 2922.25, 2852.81, 1624.12, 1535.39, 1456.30, 1377.22, 1338.64, 1261.49, 1182.40, 1082.10, 833.28, 721.40 cm⁻¹; ¹H NMR (500 MHz, CDCl₃): δ = 10.28 (s, 1H), 8.40 (s, 1H), 8.01 (s, 1H), 7.58–7.46 (m, 4H), 4.16–4.07 (m, 10H), 2.0–1.91 (m, 10H), 1.41–1.27 (m,

50H), 0.84 (m, 15H); ^{13}C NMR (125 MHz, CDCl_3): $\delta = 151, 150.89, 149.16, 148.57, 147.85, 144.72, 139.22, 138.53, 137.41, 133.31, 132.66, 130.66, 126.60, 126.26, 125.56, 124.50, 124.13, 122.10, 117.22, 111.99, 107.54, 105.59, 105.39, 105.09, 69.65, 69.41, 69.16, 69.01, 68.84, 31.95, 29.76, 29.72, 29.66, 29.62, 29.54, 29.46, 29.10, 26.37, 26.31, 26.28, 22.81, 22.76, 14.16$ ppm; elemental analysis: $\text{C}_{64}\text{H}_{92}\text{Br}_2\text{N}_2\text{O}_5$, calculated: C, 68.07; H, 8.20; N, 2.47. % found: C, 68.21; H, 8.31; N, 2.58.

13,14-dibromo-2,3,6,7,10-pentakis(dodecyloxy)phenanthro[9,10-a]phenazine (13c): IR (film) ν_{max} : 2955.04, 2920.32, 2852.81, 1620.26, 1535.39, 1454.38, 1377.22, 1340.57, 1261.49, 1161.19, 1082.10, 831.35, 721.40 cm^{-1} ; ^1H NMR (500 MHz, CDCl_3): $\delta = 10.40$ (s, 1H), 8.57 (s, 1H), 8.23 (s, 1H), 7.74–7.67 (m, 4H), 4.33 (t, $J = 7$ Hz, 2H), 4.27–4.22 (m, 8H), 2.12–1.97 (m, 10H), 1.63–1.62 (m, 10H), 1.47–1.29 (m, 80H), 0.88 ppm (t, $J = 6.5$ Hz, 15 H); ^{13}C NMR (125 MHz, CDCl_3): $\delta = 151.15, 150.99, 149.28, 148.67, 147.99, 144.87, 139.44, 138.69, 137.58, 133.44, 132.74, 130.62, 126.75, 126.49, 125.75, 124.59, 124.29, 122.24, 117.44, 112.12, 107.73, 105.83, 105.61, 105.27, 69.75, 69.50, 69.29, 69.08, 68.91, 31.97, 29.87, 29.84, 29.81, 29.75, 29.70, 29.66, 29.60, 29.56, 29.44, 29.07, 26.35, 26.32, 26.30, 26.28, 22.73, 14.14$ ppm; elemental analysis: $\text{C}_{84}\text{H}_{132}\text{Br}_2\text{N}_2\text{O}_5$, calculated: C, 71.56; H, 9.42; N, 1.98. % found: C, 71.67, H, 9.53, N, 2.09. ^1H NMR and ^{13}C NMR spectra are shown in the **Figure 12**.

Synthesis of 13,14-bis(alkylthio)-2,3,6,7,10-pentaalkoxyphenanthro[9,10-a]phenazine (8):

To a stirring solution of compound **13c** (1 equiv) and anhydrous cesium carbonate (5 equiv) in dry *N,N*-dimethylacetamide (DMAc) was added alkanethiol (2.2 equiv). The reaction mixture was refluxed for 24 h. After cooling to room temperature, ice cold water was added under vigorous stirring and the formed solid was filtered off. The crude solid was dissolved in chloroform solvent, dried over Na_2SO_4 and solvent was evaporated. The residue was purified by column chromatography using silica gel (*n*-hexane/dichloromethane 9:1) which affords red solid. Recrystallization of the pure product with cold ethanol gives red colour solid (**8a–8d**) in about 60% yield. A representative example of ^1H and ^{13}C NMR are shown in **Figure 13 & 14** respectively.

13,14-bis(butylthio)-2,3,6,7,10-pentakis(dodecyloxy)phenanthro[9,10-a]phenazine (8a): IR (film) ν_{\max} : 2953.12, 2920.32, 2906.82, 1631.83, 1454.38, 1377.22, 1263.42, 1035.81, 833.28, 721.40 cm^{-1} ; ^1H NMR (500 MHz, CDCl_3): δ = 10.59 (s, 1H), 7.97 (s, 1H), 7.88–7.80 (m, 5H), 4.42 (t, J = 6.5 Hz, 2H), 4.35 (t, J = 5.5 Hz, 2H), 3.12–3.07 (m, 4H), 2.10–2.07 (br, 2H), 1.96–1.86 (m, 9H), 1.79–1.74 (m, 5H), 1.61–1.51 (14H), 1.36–1.19 (84H), 0.93 (t, J = 7.5 Hz, 6H), 0.79 ppm (br, 15H); ^{13}C NMR (125 MHz, CDCl_3): δ = 150.63, 149.72, 148.27, 147.76, 147.02, 142.90, 140.87, 140.59, 138.48, 137.65, 135.55, 128.97, 125.53, 123.97, 123.52, 122.79, 122.33, 121.79, 117.25, 111.54, 107.12, 105.71, 104.86, 103.55, 68.88, 68.81, 68.41, 68.24, 67.55, 32.03, 31.97, 30.92, 29.21, 29.12, 28.74, 28.70, 28.69, 28.62, 28.59, 28.56, 28.51, 28.38, 27.93, 25.56, 25.23, 21.68, 21.34, 21.33, 12.73 ppm; elemental analysis: $\text{C}_{92}\text{H}_{150}\text{N}_2\text{O}_5\text{S}_2$, calculated: C, 77.36; H, 10.57; N, 1.96; S, 4.48. % found: C, 77.52, H, 10.70, N, 2.07, S, 4.59.

13,14-bis(hexylthio)-2,3,6,7,10-pentakis(dodecyloxy)phenanthro[9,10-a]phenazine (8b): IR (film) ν_{\max} : 2955.04, 2924.18, 2852.81, 1620.26, 1458.23, 1377.22, 1261.49, 1080.17, 844.85, 771.55 cm^{-1} ; ^1H NMR (500 MHz, CDCl_3): δ = 10.63 (s, 1H), 8.02 (s, 1H), 7.95 (s, 1H), 7.90–7.87 (m, 4H), 4.46 (t, J = 6.5 Hz, 2H), 4.39 (t, J = 6 Hz, 2H), 4.24–4.19 (m, 6H), 3.14–3.09 (m, 4H), 2.12–2.10 (m, 2H), 1.98–1.88 (m, 10H), 1.80 (br, 4H), 1.52–1.20 (m, 100H), 0.84 ppm (br, 21H); ^{13}C NMR (125 MHz, CDCl_3): δ = 150.73, 149.79, 148.34, 147.83, 147.10, 142.97, 141.03, 140.68, 138.57, 137.79, 135.68, 129.04, 125.61, 123.99, 123.58, 122.91, 122.35, 121.86, 117.35, 111.55, 107.23, 105.82, 104.98, 103.68, 68.95, 68.86, 68.51, 68.30, 67.59, 32.40, 32.31, 30.92, 30.46, 30.38, 28.74, 28.70, 28.68, 28.59, 28.56, 28.53, 28.49, 28.37, 27.92, 27.85, 27.15, 27.07, 25.55, 25.22, 25.20, 21.68, 21.55, 13.09 ppm; elemental analysis: $\text{C}_{96}\text{H}_{158}\text{N}_2\text{O}_5\text{S}_2$; calculated: C, 77.67, H, 10.71, N, 1.88, S, 4.31. % found: C, 77.78, H, 10.81, N, 1.98, S, 4.25. ^1H NMR and ^{13}C NMR spectra are shown in **Figure 13**.

13,14-bis(decylthio)-2,3,6,7,10-pentakis(dodecyloxy)phenanthro[9,10-a]phenazine (8c): IR (film) ν_{\max} : 2953.12, 2920.32, 2852.81, 1622.19, 1454.38, 1377.22, 1261.49, 1080.17, 833.28, 773.48 cm^{-1} ; ^1H NMR (500 MHz, CDCl_3): δ = 10.63 (s, 1H), 8.02 (s, 1H), 7.94 (s, 1H), 7.90–7.87 (m, 4H), 4.46 (t, J = 6.5 Hz, 2H), 4.38 (t, J = 5.5 Hz, 2H), 4.24–4.19 (m, 6H), 3.13 (m, 4H), 2.12–2.09 (m, 2H), 1.99–1.79 (m, 10H), 1.56–1.20 (br, 120H), 0.80 ppm (br, 21H); ^{13}C NMR (125 MHz, CDCl_3): δ = 150.71, 149.79, 148.33, 147.83, 147.09, 142.96, 141.04, 140.70, 138.57,

137.77, 135.65, 129.03, 125.61, 123.99, 123.58, 122.88, 122.32, 121.86, 117.34, 111.55, 107.23, 105.81, 104.97, 103.66, 68.94, 68.86, 68.50, 68.30, 67.59, 32.40, 32.32, 30.92, 30.88, 28.77, 28.73, 28.68, 28.59, 28.56, 28.49, 28.38, 28.36, 28.33, 28.31, 28.25, 28.21, 28.19, 27.91, 27.19, 27.11, 25.56, 25.22, 25.20, 21.68, 13.10 ppm; elemental analysis: C₁₀₄H₁₇₄N₂O₅S₂; calculated: C, 78.23; H, 10.97; N, 1.75; S, 4. % found: C, 78.38; H, 11.09; N, 1.86; S, 4.12.

13,14-bis(dodecylthio)-2,3,6,7,10-pentakis(dodecyloxy)phenanthro[9,10-a]phenazine (8d): IR (film) ν_{\max} : 2953.12, 2924.18, 2854.74, 1620.26, 1458.23, 1377.22, 1261.49, 1080.17, 846.78, 721.40 cm⁻¹; ¹H NMR (500 MHz, CDCl₃): δ = 10.59 (s, 1H), 7.94 (s, 1H), 7.84–7.81 (m, 4H), 7.77 (s, 1H), 4.40 (t, *J* = 7Hz, 2H), 4.34 (t, *J* = 6Hz, 2H), 4.21–4.16 (m, 6H), 3.10–3.04 (m, 4H), 2.11–2.05 (m, 2H), 1.96–1.88 (m, 8H), 1.78 (br, 4H), 1.77–1.19 (br, 126H), 0.80 ppm (br, 21H); ¹³C NMR (125 MHz, CDCl₃): δ = 150.59, 149.69, 148.26, 147.73, 146.98, 142.89, 140.85, 140.58, 138.42, 137.61, 135.50, 128.94, 125.52, 123.99, 123.48, 122.72, 122.25, 121.78, 117.19, 111.51, 107.11, 105.69, 107.84, 103.51, 68.86, 68.80, 68.38, 68.23, 67.51, 32.36, 32.29, 30.93, 28.80, 28.76, 28.72, 28.70, 28.68, 28.65, 28.64, 28.61, 28.54, 28.41, 28.39, 28.36, 28.30, 28.25, 28.22, 27.94, 27.18, 27.11, 25.60, 25.26, 25.24, 25.23, 25.21, 21.68, 13.09 ppm; elemental analysis: C₁₀₈H₁₈₂N₂O₅S₂; calculated: C, 78.48, H, 11.08, N, 1.69, S, 3.87. % found: C, 78.56, H, 11.18, N, 1.85, S, 4.01. ¹H NMR and ¹³C NMR spectra are shown in **Figure 14**.

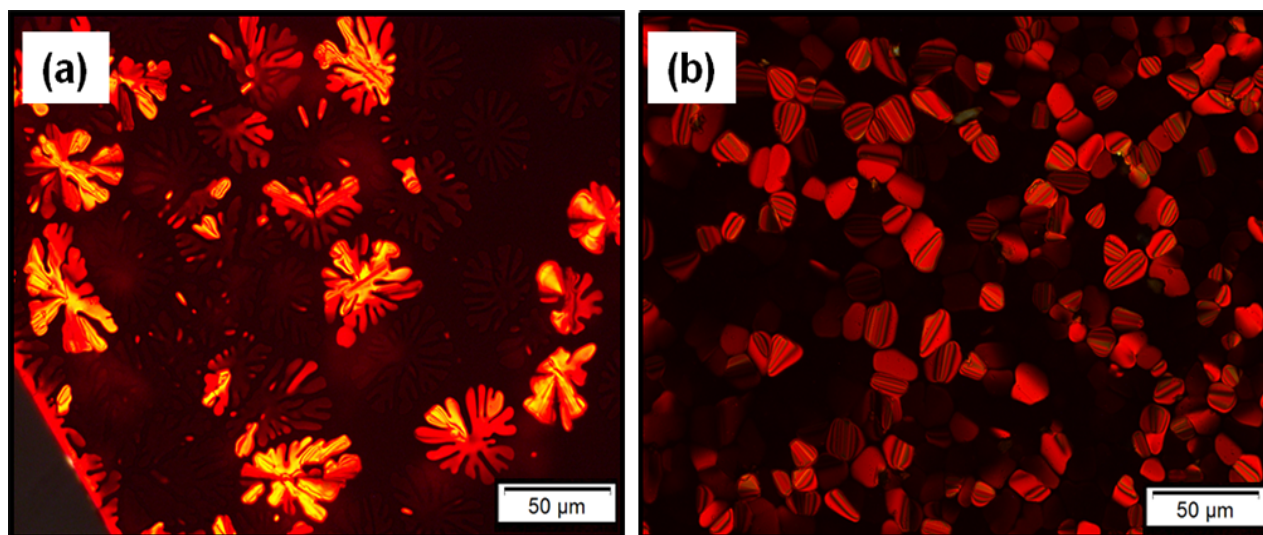


Figure 1. Polarized optical micrographs taken in hexagonal columnar phase. (a) Compound **13a** at 245 °C, viewed at 200 × magnifications. (b) Compound **8d** at 110 °C on cooling from isotropic liquid, viewed at 200 × magnifications.

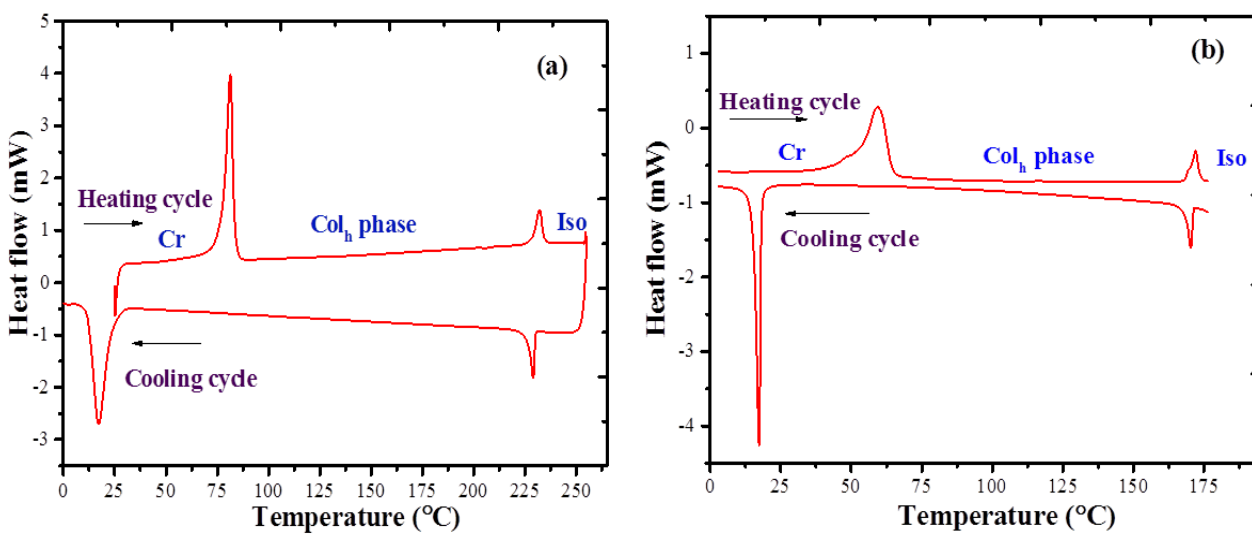


Figure 2. DSC thermogram of (a) **13c** and (b) **8a** on heating and cooling cycles (scan rate 10 °C min⁻¹).

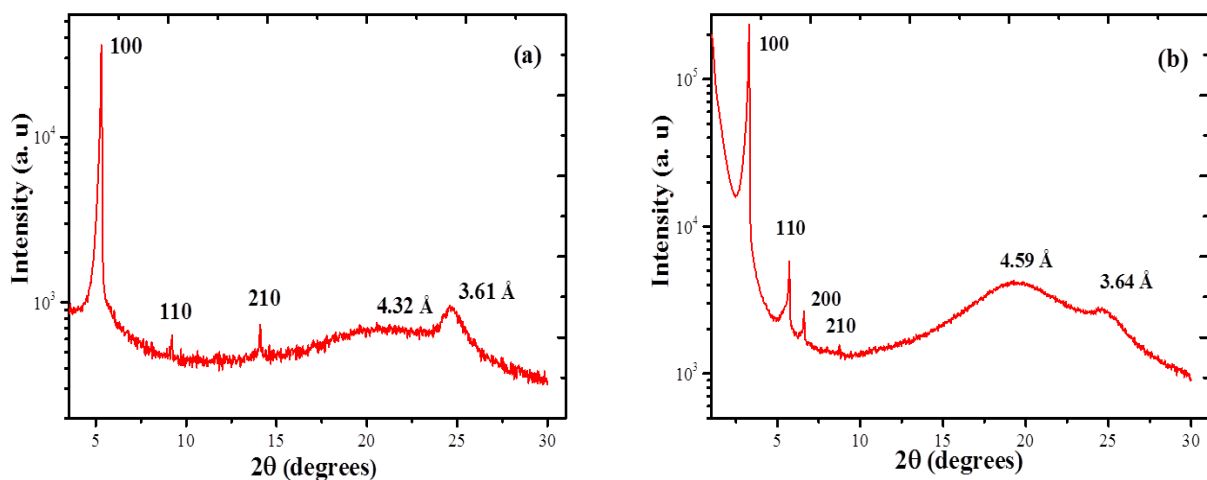


Figure 3. The intensity profile of the X-ray pattern exhibited by (a) **13a** at 175 °C and (b) **8d** at 100 °C respectively

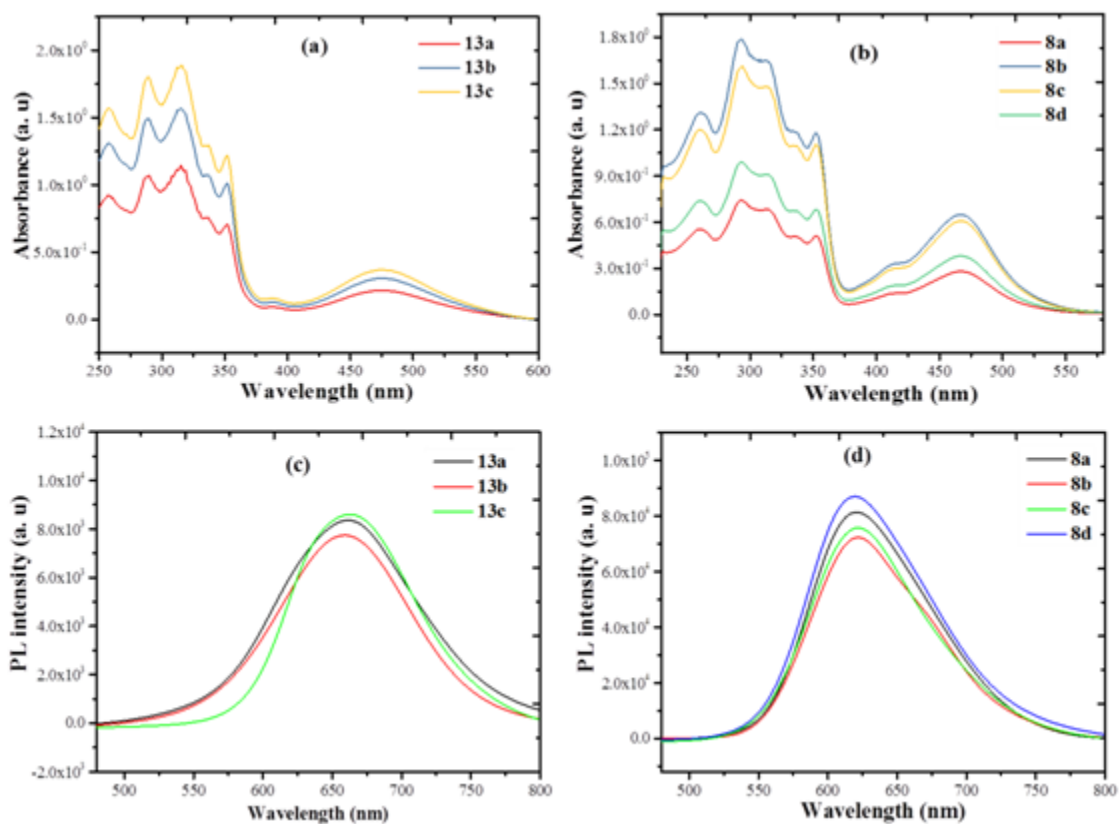


Figure 4. (a) and (b) UV-Visible absorption spectra, (c) and (d) fluorescence spectra of all the mesogens (**13a–13c** & **8a–8d**).

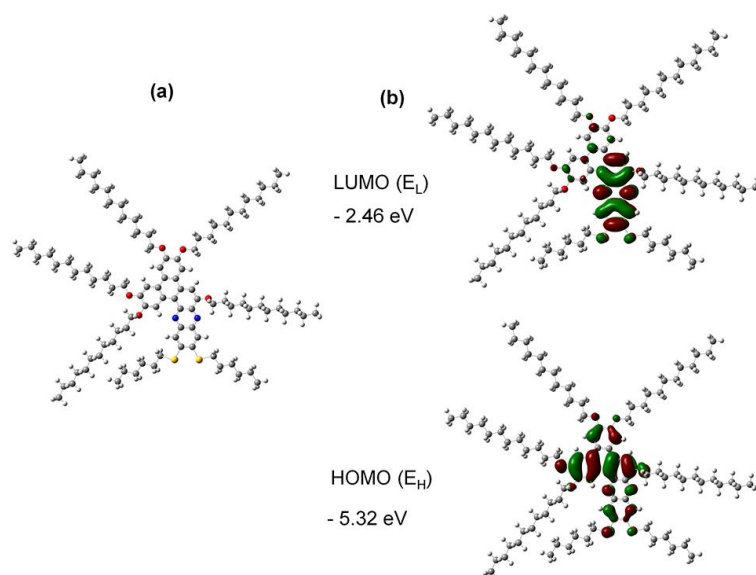


Figure 5. (a) Optimized molecular structure of compound **8b**. (b) HOMO and LUMO frontier molecular orbital of **8b** at the B3LYP/6.311G (d) level. E_H and E_L represents energies of highest occupied molecular orbital (HOMO) and the lowest unoccupied molecular orbital (LUMO).

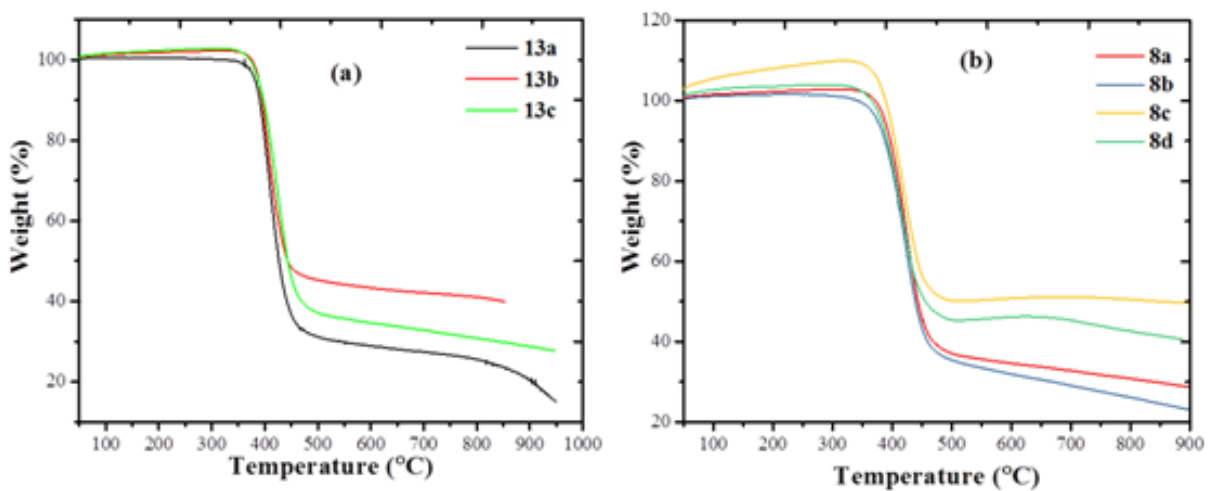


Figure 6. Thermogravimetric analysis of intermediate (**13a–13c**) and final discotic mesogens (**8a–8d**).

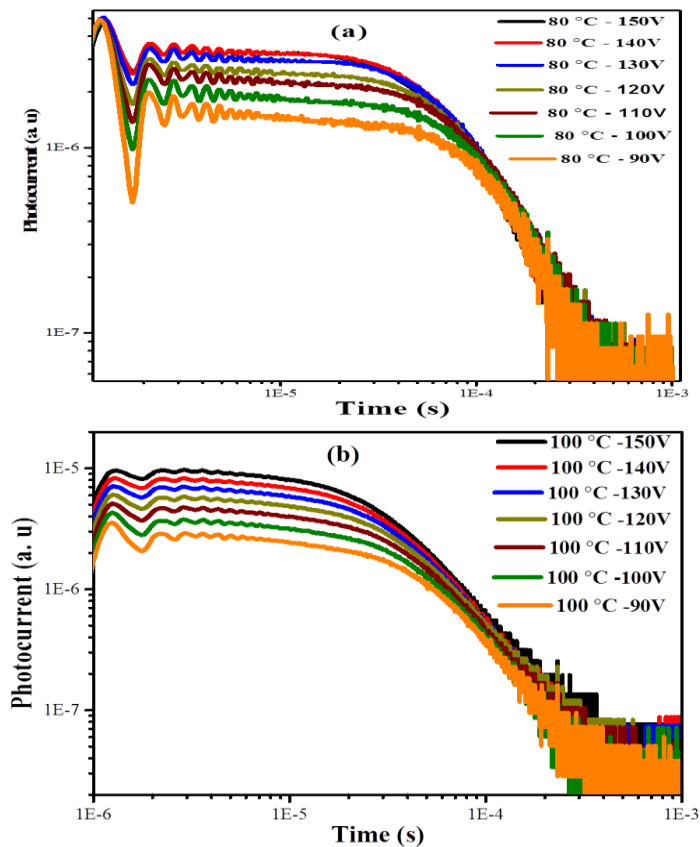


Figure 7. Transient photocurrent curves of compound **8b** at (a) 80 °C and (b) 100 °C with the variation of voltage from +90 to +150V.

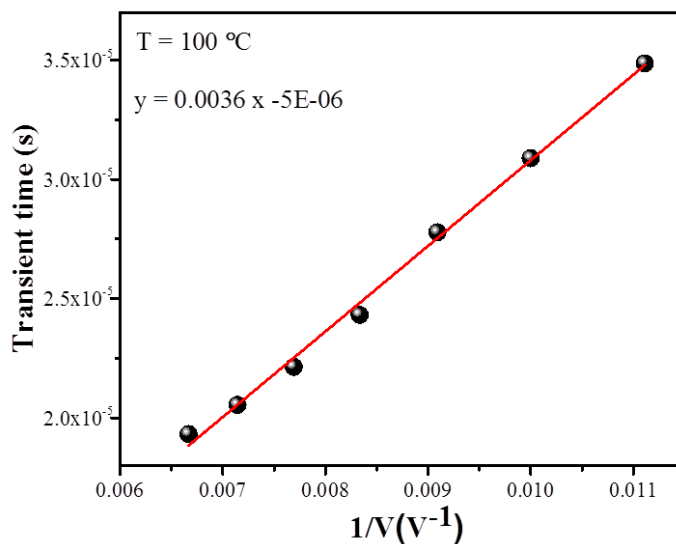


Figure 8. Transient time versus inverse of voltage curve was linearly fitted to get slope of curve.

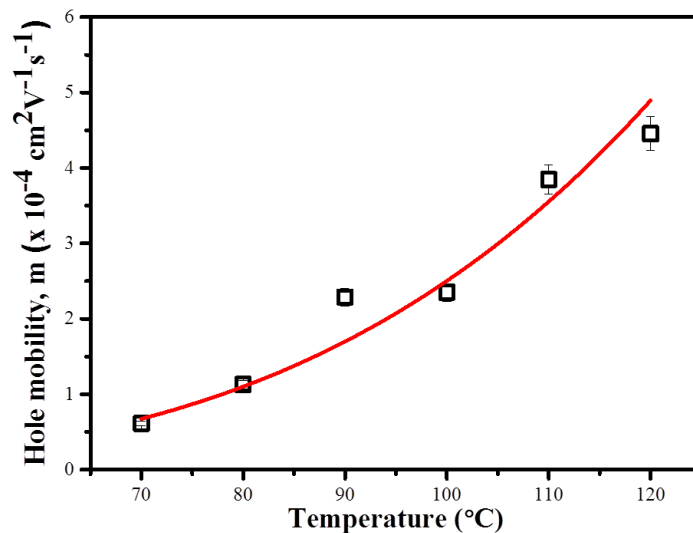


Figure 9. Hole mobility of compound **8b** as a function of temperature. The solid line shows the fitting of experimental data by using equation 1. The values of exponent n and arbitrary constant C are found to be 3.6 and 1.09×10^{-11} , respectively.

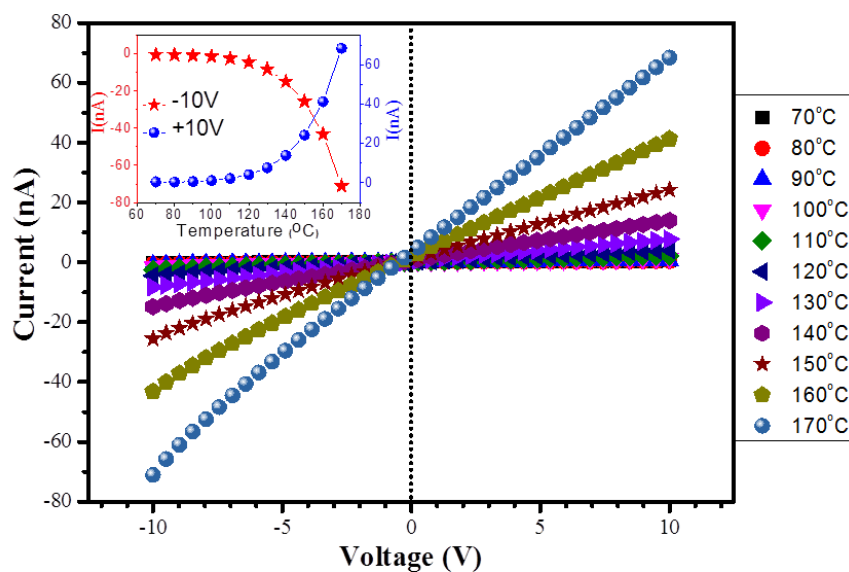


Figure 10. Current–voltage (I–V) characteristics of compound **8b** as a function of voltage for the temperature range of 70 to 170 °C. Inset shows the variation of current at ± 10 V as a function of temperature. I–V measurement was performed on 9.2 μm thick ITO cell.

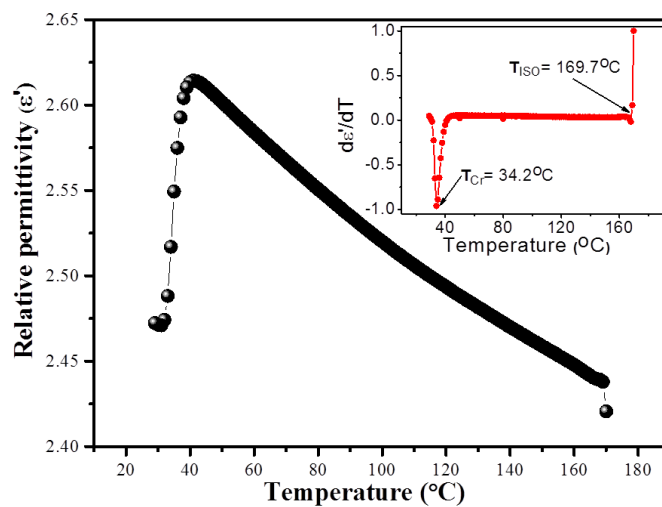


Figure 11. Relative permittivity of compound **8b** as a function of temperature evaluated at 3kHz in cooling cycle. Inset shows the derivative of relative permittivity with respect to temperature ($d\epsilon'/dT$) as a function of temperature to examine the phase transition by dielectric spectroscopy. Dielectric spectroscopy was performed on 9.2 μm thick ITO cell.

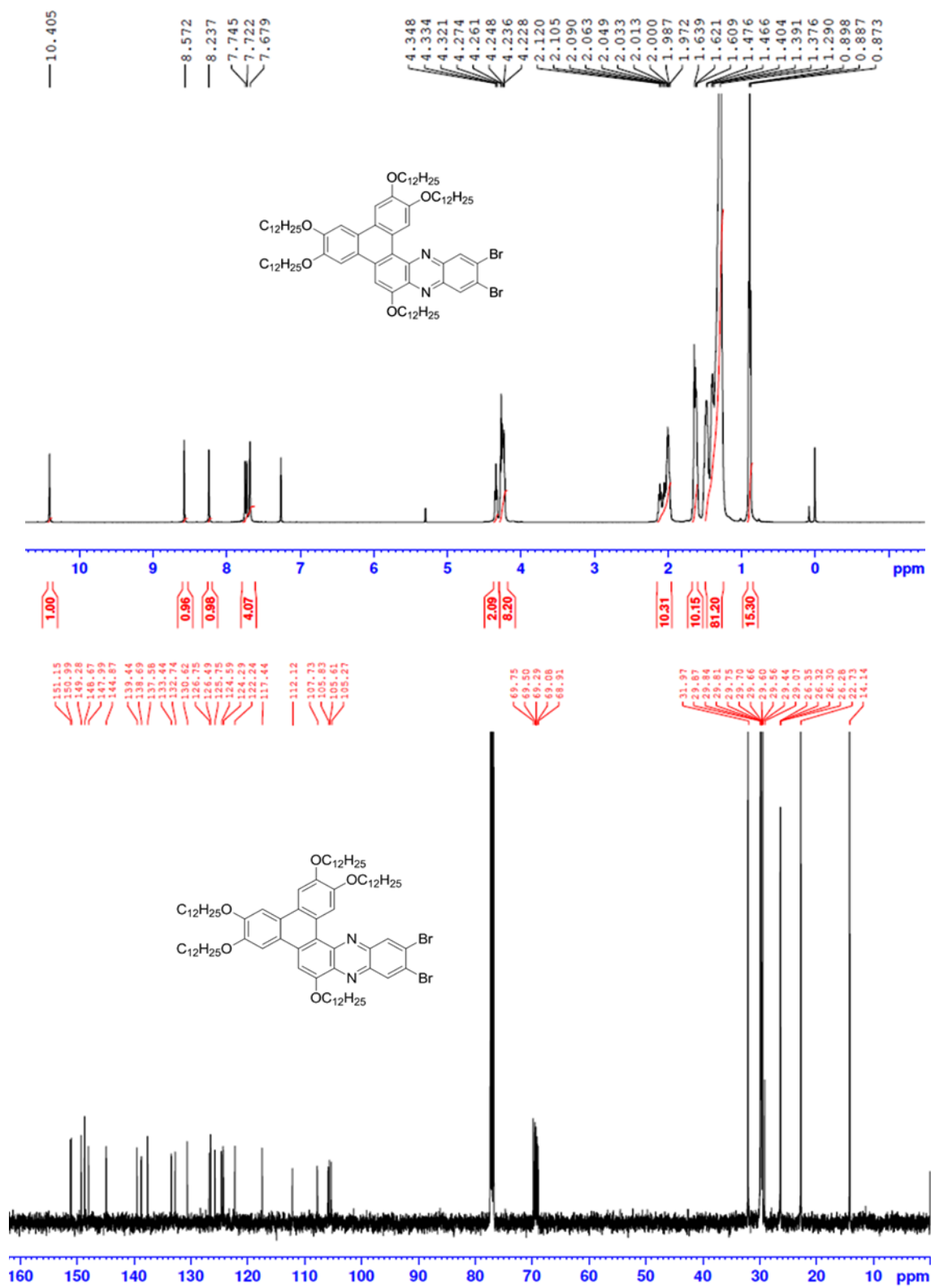


Figure 12. ¹H and ¹³C NMR of compound 13c.

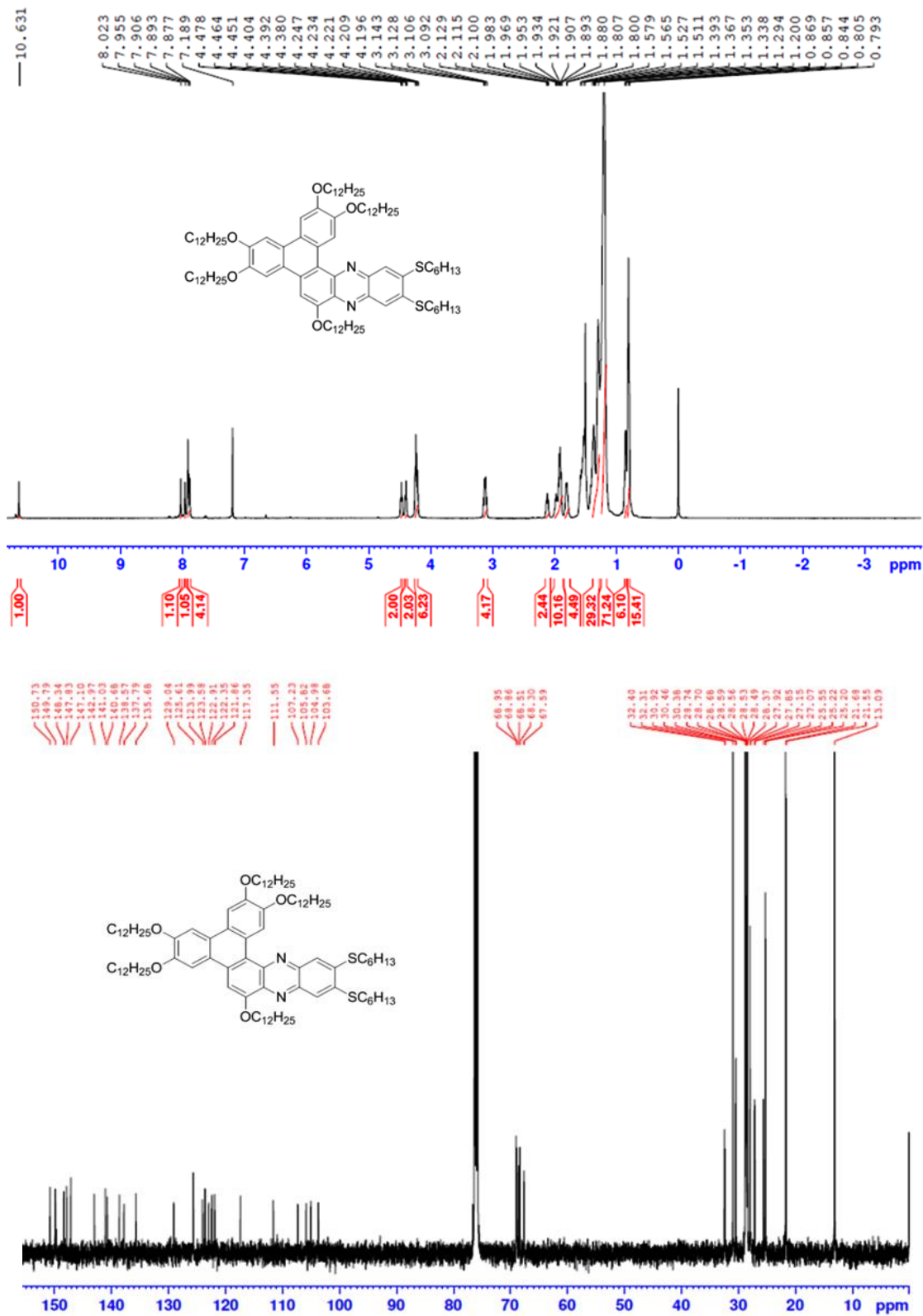


Figure 13. ¹H and ¹³C NMR of compound 8b.

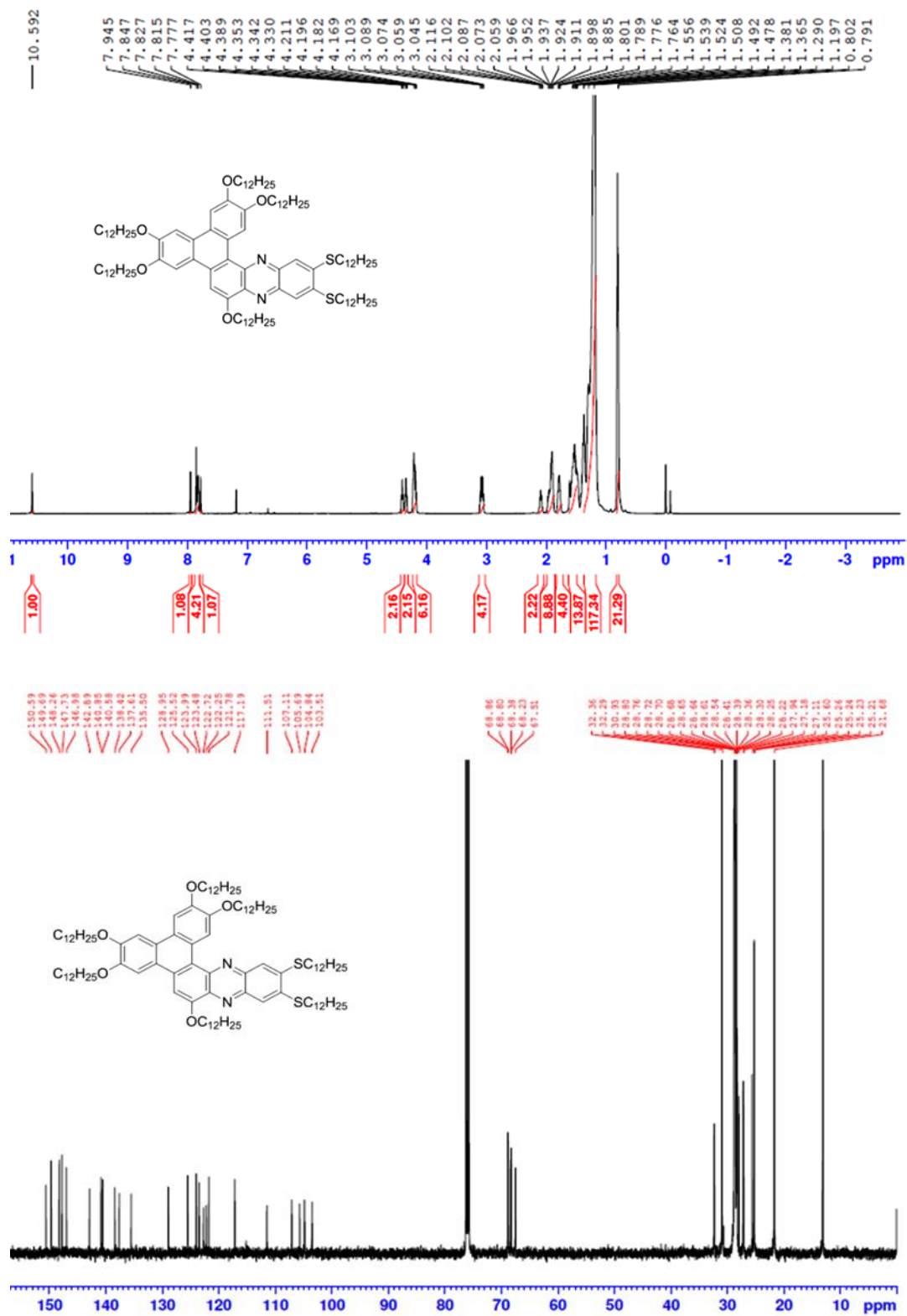


Figure 14. ¹H and ¹³C NMR of compound 8d.

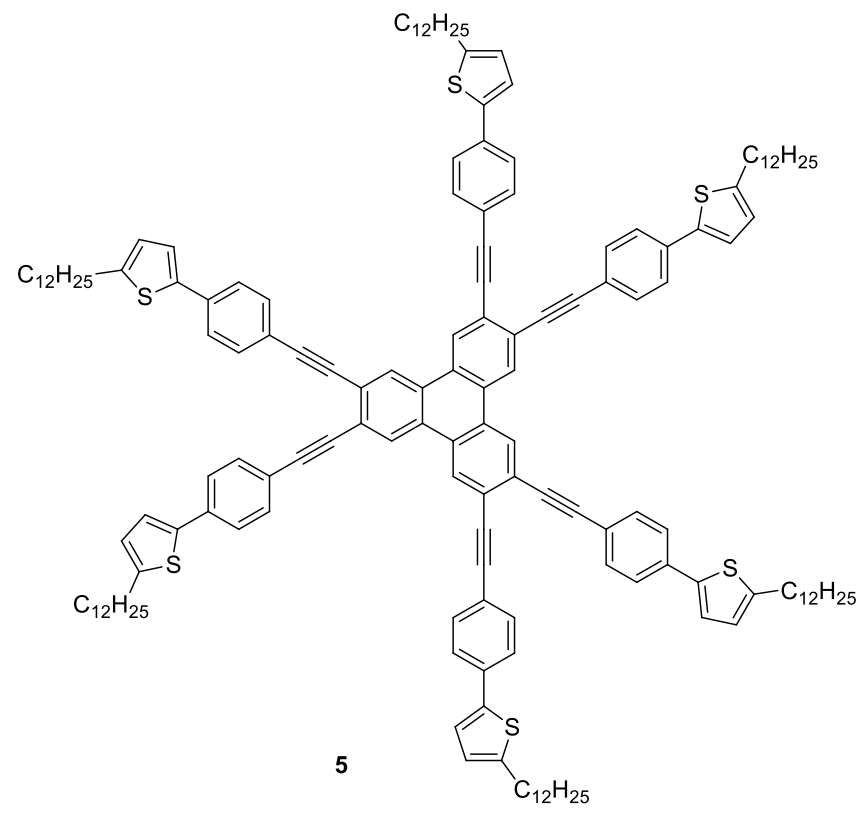
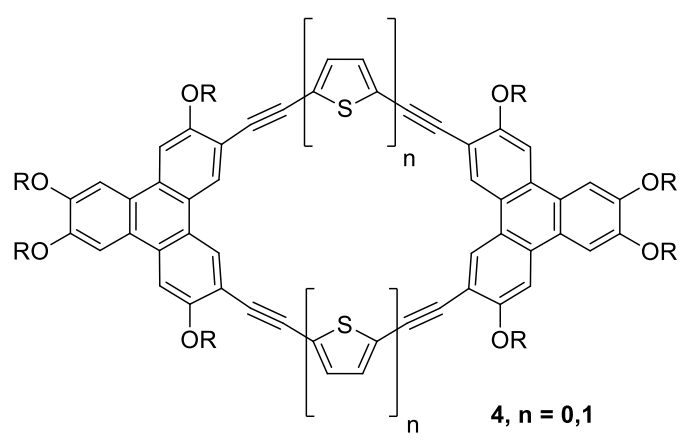
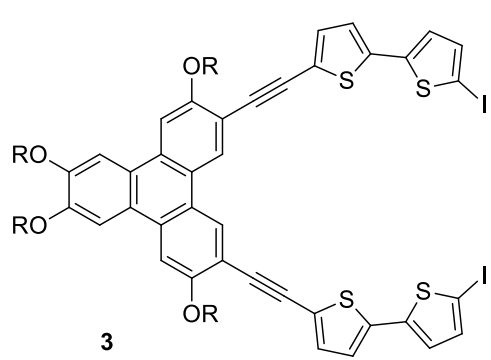
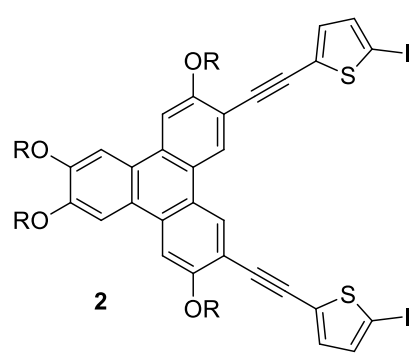
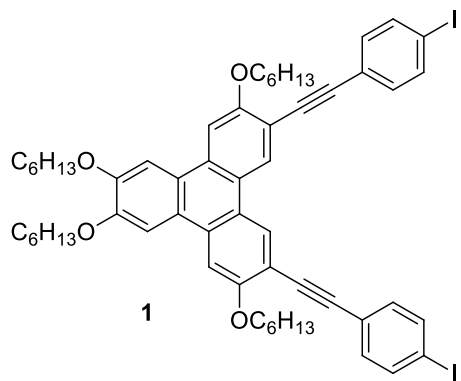
4.2 Part B. Alkyl and alkoxy phenylacetylene containing phenazine fused triphenylene discotic liquid crystals

4.2.1 Introduction

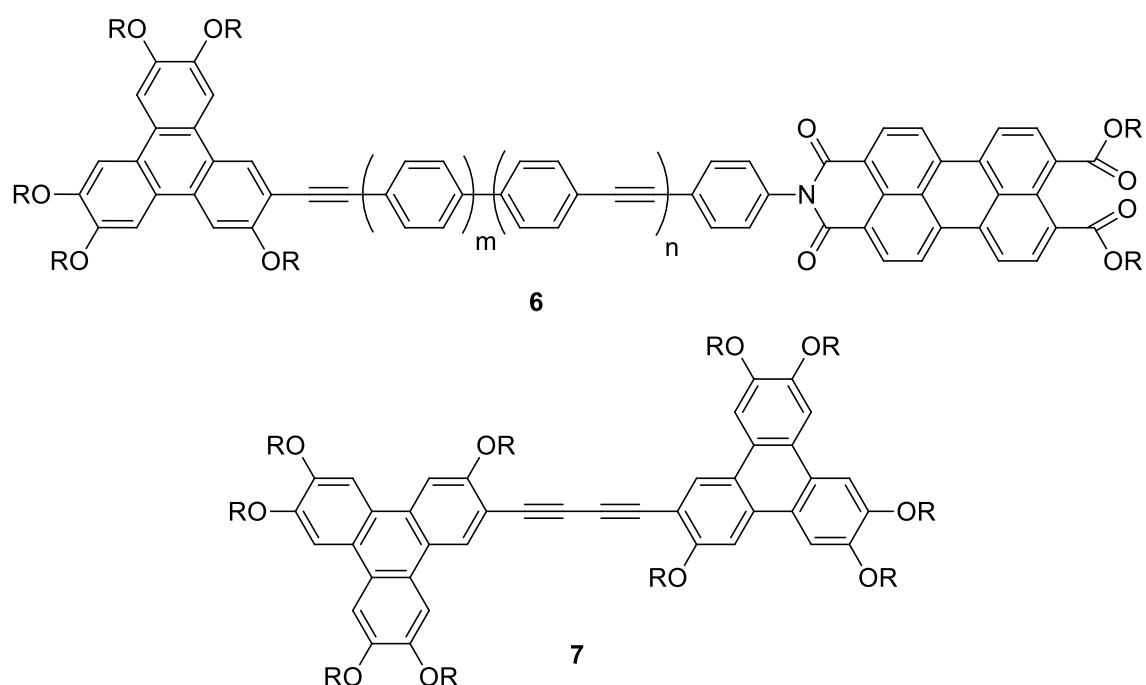
The DLCs derived from triphenylene core represents widely studied class of mesogens exhibit ordered columnar phases. Research over past decades demonstrate the potential use of these and related materials in semiconductor device applications [14,15,16–25]. The hexasubstituted TP discotic mesogens have been examined significantly due to formation of ordered columnar mesophases, which are of interest for one-dimensional charge (electron or ion) transport and also they have been used optical compensating films to enlarge wide viewing angle in optoelectronic devices. In this contest, the structure-property relationships of TP DLCs have been extensively explore for their considerable technological point of view.

The molecular shape anisotropy is among the key important which determines the self-assembly of mesogens into mesomorphic properties. The extension of TP discotic core significantly changes the liquid crystalline behaviour and electronic properties. Such extended discotic core gives large π -conjugated aromatic systems, which may enhance the high charge carrier mobility in the columnar phase. Several research groups attempted to extend TP discotic core via acetylene linkage [26–36].

Zhang et al. prepared a new class of twinned discotic TP connected via π -conjugated thiophene bridge produce macrocyclic compound (1–4). The electron-rich TP DLCs twins exhibit stable discotic nematic phase and are potential materials for optoelectronic applications [22a]. Similarly, Choi et al reported extended TP discotic core with π -conjugated thiophene bridge (5) which shows columnar phase and low band gap energy ($E_g = 2.53$ eV) [22b].



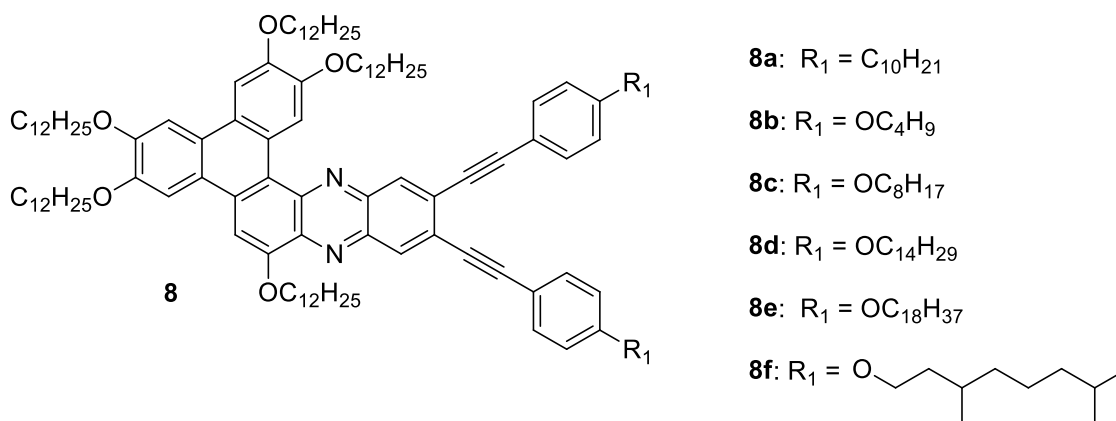
Recently, Wang et al. reported the donor-acceptor dyads having triphenylene (donor) – perylene monoimide dihexyl ester (acceptor) (**6**) connected through ethynylphenyl bridges which exhibits broad Col_h phase. These extended π -conjugation in aforementioned compound results an intramolecular photo-induced electronic charge transfer between the donor and acceptor units [46]. Kumar et al. synthesised the first examples of triphenylene dimers discotic mesogens linked via rigid π -conjugated diacetylene spacers (**7**), which shows discotic nematic phase over broad temperature range [47].



4.2.2 Objective

The aim of this work is to prepare alkyl and alkoxy phenylacetylene containing phenazine fused triphenylene DLCs (**8a–8f**) with enhanced π -electron conjugation. These are obtained by the condensation reaction of triphenylene-1,2-diquinone with 1,2-diamino-4,5-dibromobenzene, followed by Sonogashira C–C coupling reaction with 4-alkyl phenylacetylene or 4-alkoxy phenylacetylene. All the novel compounds were characterised using spectral and elemental analysis. The liquid crystalline behaviour of all the compounds was investigated by

POM and DSC. The mesophase structure of all the mesogens were characterised using XRD. Further, the photophysical and nonlinear optical studies were also investigated for all the mesogens.



4.2.3 Results and discussion

4.2.3.1 Synthesis

The synthesis of π -extended phenazine fused triphenylene discotic liquid crystals is shown in **Scheme 1**. The intermediate monohydroxytriphenylene **19** was prepared following reported procedure starting from catechol [37]. Its oxidation with CAN produces 3,6,7,10,11-pentakis(dodecyloxy)triphenylene-1,2-diones **20** [38]. The another intermediate compound 4,5-dibromobenzene-1,2-diamine **12** was synthesized using a reported procedure [39]. Its condensed with triphenylene-1,2-diquinone in glacial acetic acid: toluene solvent under reflux condition gives 13,14-dibromo-2,3,6,7,10-pentakis(dodecyloxy)phenanthro [9,10-a]phenazine discotic mesogen **21**. Sonogashira C–C bond coupling reaction of 4-alkyl phenylacetylene or 4-alkoxy phenylacetylene **16** [63] with mesogenic compound **21** in the presence of bis(triphenylphosphine)palladium(II) dichloride and copper(I) iodide in anhydrous triethylamine solvent offered final discotic liquid crystal compounds (**8a–8f**). All the compounds are well characterized from their spectral and elemental analysis (see experimental part).

Scheme 1. (i) *p*-TOSCl, pyridine, r.t, 24 h; (ii) Br₂, NaOAc, acetic acid, 110 °C, 3 h; (iii) Con. H₂SO₄, 110 °C, 15 min; (iv) alkyl halide, anhydrous K₂CO₃, dry DMF, reflux, 12 h; (v) 2-methyl-3-butyn-2-ol, PdCl₂(PPh₃)₂, CuI, TEA, reflux, 12 h; (vi) NaOH, toluene, reflux, 3 h; (vii) FeCl₃, CH₂Cl₂, r.t, 30 min; (viii) catechol boron bromide, CH₂Cl₂, r.t, 24 h; (ix) CAN, CH₃CN, r.t, 30 min; (x) acetic acid: toluene (7:3), reflux, 6 h; (xi) 4-alkyl-phenylacetylene or 4-alkoxy phenylacetylene, PdCl₂(PPh₃)₂, CuI, TEA, reflux, 24 h.

4.2.3.2 Mesomorphic properties

The thermotropic liquid crystalline behaviour of all the synthesised compounds (**8a–8f**) was first viewed using optical microscopy with cross polarisers which display characteristic defect texture of columnar phase. The exact phase transition temperature (peak temperature in °C) and associated enthalpy values (kJ mol⁻¹) were investigated with the help of DSC measurement on both heating and subsequent cooling scans with a scan rate of 10 °C min⁻¹ and recorded under nitrogen atmosphere. The phase transition temperature of all mesogens agrees very well with POM observations, as summarized in **Table 1**.

Table 1. Phase behaviour of discotic mesogens (**8a–8f**).

Compound	Phase transition (peak temperature (°C); (ΔH , [kJ mol ⁻¹]))	
	<i>second heating scan</i>	<i>second cooling scan</i>
8a	Cr 37.2 [44.0] Col _h 217 [3.2] I	I 209.3 [-3.1] Col _h 12.2 [-38.3] Cr
8b	Cr 64.8 [50.0] Col _h 231.7 [2.1] I	I 224.4 [-2.2] Col _h 27.3 [-39.5] Cr
8c	Cr 49.9 [42.9] Col _h 228.5 [4.0] I	I 221.7 [-2.5] Col _h 21.2 [-41.1] Cr
8d	Cr 49.0 [39.5] Col _h 163.6 [2.3] I	I 162.2 [-2.2] Col _h 23.3 [-42.7] Cr
8e	Cr 69.5 [79.1] Col _h 139.4 [0.6] I	I 135.1 [-0.7] Col _h 37.1 [-71.6] Cr
8f	Cr 40.9 [45.3] Col _h 200.3 [2.7] I	I 196.9 [-2.6] Col _h 19.6 [-41.9] Cr

All the mesogens exhibit wide range of enantiotropic hexagonal columnar mesophase with two types of endothermic phase transition from crystal to Col_h phase at lower temperature and Col_h phase to isotropic phase at higher temperature and they retain columnar phase up to room temperature upon cooling from the isotropic liquid. The first compound in the series **8a**, with mixed alkyl and alkoxy chains, melts at 37.2 °C with phase transition enthalpy 44 kJ mol⁻¹ to Col_h phase and transition from Col_h phase to isotropic phase at 217 °C ($\Delta H = 3.2$ kJ mol⁻¹). Upon slow cooling from isotropic liquid under POM, the texture of Col_h phase was observed as shown in **Figure 1a**. As a representative example of DSC thermogram of compound **8a** is shown in **Figure 2**. The compound **8b** with alkoxy chains in the phenylacetylene part melts to Col_h at 64.8 °C ($\Delta H = 50$ kJ mol⁻¹) and Col_h to isotropic liquid at 231.7 °C with corresponding heat transition ($\Delta H = 2.1$ kJ mol⁻¹). Columnar textures were observed upon cooling from the isotropic liquid at 224.4 °C. On the other hand, compounds **8c** and **8d** exhibit phase transition from crystalline phase to columnar phase at 49.9 °C ($\Delta H = 42.9$ kJ mol⁻¹) and 49 °C ($\Delta H = 39.5$ kJ mol⁻¹) respectively, and the peak temperature at 228.5 °C ($\Delta H = 4.0$ kJ mol⁻¹) and 163.6 °C ($\Delta H = 2.3$ kJ mol⁻¹) attributed to Col_h to isotropic phase transition. Under POM, the compound **8c** exhibits mesophase texture at 221.7 °C (on cooling) as shown in **Figure 1b**. The compounds **8d** exhibits similar mesophase texture observed under POM upon cooling from isotropic liquid. Similarly, compound **8e** transformed to Col_h phase at 69.5 °C ($\Delta H = 79.1$ kJ mol⁻¹) and Col_h to isotropic phase at 139.4 °C ($\Delta H = 0.6$ kJ mol⁻¹) at higher temperature. The compound **8f** with branched alkoxy chain show similar behaviour, peak temperature at 40.9 °C, with enthalpy change at 45.3 kJ mol⁻¹ characteristic for Cr to Col_h phase and Col_h to isotropic liquid at 200.3 °C ($\Delta H = 2.7$ kJ mol⁻¹). Upon cooling under POM, the mesophase texture appeared at 135.1 °C (**8e**) and 196.9 °C (**8f**) respectively.

4.2.3.3 Thermogravimetric analysis

Thermal stability of all the discotic mesogens (**8a–8f**) was measured using thermogravimetric analysis. All the compounds were subjected to heat scan of 10 °C min⁻¹ under a nitrogen atmosphere. All the compounds were found stable up to 365–375 °C depending on the alkyl chain length as shown in **Figure 3**. All the compounds initiated weight loss at 385 °C–400

°C and decomposed at 480 °C. The decomposition temperature of the mesogens was much higher than the isotropic temperature. It is inferred that all the compounds possess good thermal stability over broad temperature.

4.2.3.4 X-ray scattering measurements

In order to understand the mesophase structure of all the novel mesogens, X-ray diffraction experiments were carried out using LC samples filled in Lindemann capillaries. X-ray diffraction patterns are recorded for all the mesogens (**8a–8f**) on both heating and subsequent cooling scans as shown in **Table 2** and a representative example is shown in **Figure 4**. All the mesogenic compounds **8a–8f** showed increasing order of diffraction angle. The d -spacing of the first reflection in the small angle region to the second one is in the ratio of $1:1/\sqrt{3}:1/2:1/\sqrt{7}$. These values corresponding to those obtained from two-dimensional hexagonal lattice and relatively broad peaks in the wide angle regime corresponding to the liquid like packing of the molten aliphatic chains and core-core separation. The intercolumnar distance, a , calculated by using the relation $a = d_{10}/(\cos 30^\circ)$, where d_{10} is the spacing corresponding to the strongest peak in the small angle region (**Table 2**). As a representative and typical XRD pattern obtained for compound **8a** (on heating scan) and **8d** (on cooling scan) are shown in **Figure 4**. The XRD pattern of compound **8a** at 100 °C on heating in the columnar phase as shown in **Figure 4a** and respective lattice parameters were tabulated in **Table 2**. In the small angle region four peaks being observed, one very strong and other three weak peaks of d -spacing $d_1 = 28.26 \text{ \AA}$, $d_2 = 16.24 \text{ \AA}$, $d_3 = 14.07 \text{ \AA}$ and $d_4 = 10.64 \text{ \AA}$ respectively, values are in agreement with the hexagonal columnar lattice. The broad peak at wide angle region $d = 4.65 \text{ \AA}$ corresponds to liquid like packing of molten aliphatic chains and the intercolumnar distance is found to be 32.63 \AA respectively (**Figure 4a**). Similarly, X-ray diffraction pattern obtained for compound **8d** in the columnar phase at 70 °C on cooling from the isotropic liquid as shown in **Figure 4b**. The compound **8d** shows similar reflections in the small angle regime with d -spacing $d_1 = 30.04 \text{ \AA}$, $d_2 = 17.24 \text{ \AA}$ and $d_3 = 14.95 \text{ \AA}$. The broad peak in wide angle regime at 4.66 \AA corresponds to a flexible alkyl chain length and the core-core gap is 3.54 \AA . It is evident that with an increase in the number of alkyl chain length, the width of the columns obtained from discotic mesogens also increases. Similar X-ray diffraction patterns were obtained for all other compounds.

Table 2. XRD data of all the discotic mesogens (**8a–8f**). I_C = Intercolumnar distance, C–C = Core-core separation, R_L = Alkyl- chain length.

Compound	Temperature (°C)	2θ (degrees)	d - spacings (Å)	Col_h Parameter	Miller indices	R_L (Å)	C–C (Å)	I_C (Å)
8a	100	3.12	28.26	1	100			
		5.43	16.24	$1/\sqrt{3}$	110			
		6.273	14.07	1/2	200	4.65	3.51	32.63
		8.29	10.64	$1/\sqrt{7}$	210			
8b	122	3.56	24.73	1	100			
		6.19	14.25	$1/\sqrt{3}$	110	4.50	3.61	28.67
		7.14	12.36	1/2	200			
8c	70	3.25	27.12	1	100			
		5.61	15.71	$1/\sqrt{3}$	110	4.49	3.52	31.40
		6.50	13.51	1/2	200			
8d	70	2.93	30.04	1	100			
		5.11	17.24	$1/\sqrt{3}$	110	4.66	3.54	34.68
		5.90	14.95	1/2	200			
8e	85	2.91	30.23	1	100			
		5.03	17.51	$1/\sqrt{3}$	110	4.62	3.55	34.97
		5.80	15.24	1/2	200			
8f	65	3.12	28.28	1	100			
		5.43	16.25	$1/\sqrt{3}$	110	4.60	3.48	32.65
		6.24	14.13	1/2	200			
		8.26	10.65	$1/\sqrt{7}$	210			

The above results further confirmed that all the mesogenic derivatives are self-assembled in the hexagonal columnar fashion in their liquid crystal phase as shown in graphical model **Figure 5**.

4.2.4 Photophysical properties

The photophysical properties of all the novel discotic mesogens were investigated by a Perkin-Elmer UV-Vis lambda 35 double-beam spectrometer and photoluminescence spectra using spectrofluorometer (Fluorolog-3, Horiba Jobin Yvon). The UV-absorption properties of all the liquid crystalline compounds (**8a–8f**) were studied in anhydrous chloroform solvent (10^{-5} M) recorded at room temperature to determine absorption maxima as presented in **Figure 6a** and the respective absorption values are summarized in **Table 3**. From UV absorption spectra it is clearly indicated that the appearance of new red shifted peak at 487 nm is obtained from the π -extension of triphenylene ring. The compound **8a** having 4-alkyl phenylacetylene chains show maximum absorption (λ_{\max}) bands at 482 nm and 368 nm which corresponds to $n \rightarrow \pi^*$ and $\pi \rightarrow \pi^*$ transitions of triphenylene ring containing extended 4-alkyl phenylacetylene fused phenazine derivative. The less intense peaks at 313 nm, 217 nm may be because of $\pi \rightarrow \pi^*$ transitions of aromatic benzene rings (**Figure 6a**). The alkoxy chain compounds **8b–8f** exhibit similar kind of absorption behaviour with λ_{\max} corresponds to $n \rightarrow \pi^*$ transitions at 485–487 nm and $\pi \rightarrow \pi^*$ transition at 374 nm along with negligible shoulder peak around 360 nm.

Similarly, compounds **8d**, **8e** and **8f** with longer alkyl chain length show λ_{\max} corresponds to $n \rightarrow \pi^*$ transitions at 485–487 nm and $\pi \rightarrow \pi^*$ transition at 370–374 nm along with negligible shoulder peak around 360 nm. The less intense peaks at around 297 nm and 270 nm correspond to $\pi \rightarrow \pi^*$ transitions of benzene ring. The high molar absorption coefficients ($\epsilon = 4.6\text{--}5.8 \times 10^6$ L mol $^{-1}$ cm $^{-1}$) attributed to the good photophysical absorption properties in this novel mesogens.

Photoluminescence spectra of all the mesogens (**8a–8f**) were recorded in anhydrous chloroform solvent (**Figure 6b**). The emission spectra were recorded using a slit size of 2 nm in dilute anhydrous chloroform solution at room temperature and all the compounds were excited at

$\lambda_{\text{max}} = 490$ nm. All the mesogens exhibits strong emission band at 657–663 nm. A stokes shift in the range of 286–295 nm observed for all the mesogens (**Table 3**).

Table 3. Photophysical properties of discotic mesogens recorded using anhydrous chloroform (10^{-5} M).

Compound	Absorption $\lambda_{\text{abs}}/\text{nm}$ ($\epsilon/10^6 \text{ L mol}^{-1} \text{ cm}^{-1}$)	Emission/ nm
8a	277, 313, 368, 482 (5.3)	663
8b	270, 300, 370, 485 (4.6)	661
8c	270, 296, 371, 486 (5.7)	657
8d	270, 297, 360, 374, 486 (5.8)	663
8e	270, 297, 360, 374, 487 (5.7)	660
8f	271, 297, 359, 374, 485 (5.3)	660

4.2.5 Nonlinear optical studies

Nonlinear optical studies of all the discotic mesogens (**8a–8f**) are carried out by utilizing the open aperture Z-scan technique using a frequency doubled Nd:YAG laser (Minilite I, Continuum) providing linearly polarized Gaussian of 5 ns pulse width at 532 nm wavelength. The experimental setup consists of the laser source, focusing lens, a 1 mm quartz cuvette containing sample (which is fixed on a stepper motor controlled translation stage) and a pyroelectric detector.

The laser light is focused using a lens of focal length 9.5 cm along the z axis. All the discotic mesogens (**8a–8f**) were dissolved in anhydrous chloroform solvent, which is kept between the focusing lens and the detector and moved along the z axis, in order to change the laser fluence. The transmitted energy is then measured using the pyroelectric detector (Laser probe, RJP-735). The open aperture Z-scans obtained are shown in **Figure 7**.

The fluence of the laser beam, which is a function of position with respect to the focal point, is given by

$$F_{in}(z) = 4(\ln 2)^{\frac{1}{2}} E_{in} / \pi^{\frac{3}{2}} \omega(z)^2 \dots\dots\dots(1)$$

Where E_{in} is input energy (3 μ J) and $(z) = \omega_0(1 + (\frac{z}{z_0})^2)^{\frac{1}{2}}$, ω_0 is the radius of the laser beam at the focus, and z_0 is the Rayleigh length given by $z_0 = \pi\omega_0^2/\lambda$.

The normalized transmittance (T_{norm}) vs. position graph is plotted to obtain the Z-scan curve. The pulse propagation equation is given by

$$\frac{dI}{dx} = - \left[\frac{\alpha_0}{1 + \frac{I}{I_s}} + \beta I \right] I \dots\dots\dots(2)$$

With $\alpha(I)$ being the net nonlinear absorption coefficient,

$$\alpha(I) = \frac{\alpha_0}{1 + \frac{I}{I_s}} + \beta I \dots\dots\dots(3)$$

where I_s is the saturation intensity (in W/m^2) and β is the reverse saturable absorption coefficient (in m/W). These parameters can be obtained by numerically fitting the measured nonlinear transmission data to equation 2.

The calculated values of I_s and β are given in **Table 4**. While doing the numerical calculations, we noticed that though RSA [48] dominates the nonlinearity, SA [49], which is not very obvious from the measured Z-scan curves, is also present in the system and should be accounted by including, I_s in the calculation for getting good fits. The high NLO response of

discotic mesogens arises due to extended conjugation. The donor ability of symmetrical π -extended phenylacetylene groups through alkyne spacer and heteroaromatic phenazine acceptor ring enhance the intramolecular delocalization of π -electrons, which are responsible for high nonlinear properties in these materials. These high NLO materials are subject of numerous investigations of photonic applications like optical switches and optical limiters etc [50].

Table 4: β and I_s values calculated for the samples (8a–8f)

Compounds	Linear transmittance	$\beta \times 10^{-11}$ m/W	$I_s \times 10^{-11}$ W/m ²
8a	0.57	96	25
8b	0.69	36	50
8c	0.57	72	32
8d	0.69	41	28
8e	0.62	61	55
8f	0.69	34	45

4.2.6 Conclusions

A new class of triphenylene based discotic liquid crystals were synthesised using Sonogashira coupling reaction between alkoxy phenylacetylene or alkyl phenylacetylene with intermediate dibrominated phenazine fused triphenylene. All the extended mesogens were self-assembled into hexagonal columnar mesophase over wide temperature and retains liquid crystalline properties upto room temperature upon cooling from isotropic liquid. The liquid crystalline properties were investigated using POM, DSC. The mesophase structure of all the mesogens were investigated using XRD studies. All the extended discotic compounds exhibit strong photoluminescence properties in the anhydrous chloroform solvent. The π -extended

heteroaromatic triphenylene discotic mesogens enhance nonlinear optical properties and are suitable for materials for electro-optical applications.

4.2.7 Experimental section

4.2.7.1. General procedure for the synthesis of final compounds

The compounds 4,5-dibromobenzene-1,2-diamine **12** [39], 1-ethynyl-4-alkoxybenzene **16** and 13,14-dibromo-2,3,6,7,10-pentapropoxyphenanthro[9,10-a]phenazine [51] were synthesized as reported and confirmed by spectral and elemental analysis.

Synthesis of 13,14-bis(2-(4-decylphenyl)ethynyl)-2,3,6,7,10-pentakis(dodecyloxy) phenanthro[9,10-a]phenazine (8a) and 13,14-bis(2-(4-alkoxyphenyl)ethynyl)-2,3,6,7,10-penta(alkoxy) phenanthro[9,10-a]phenazine (8b–8f).

To a stirring solution of compound **21** (0.5 g, 1 eq.) in triethylamine (40 mL) solvent was added PdCl₂(PPh₃)₂ (0.06 eq.) and CuI (0.07 eq.) under argon atmosphere. The resulting reaction mixture was allowed to stir for 10 minutes under argon at room temperature. To this, 1-decyl-4-ethynylbenzene or 1-ethynyl-4-alkoxybenzene (2.6 eq.) was added under argon flow. The resulting reaction mixture was heated to 72 °C for 24 h. After completion of reaction, the reaction mixture was allowed to cool to room temperature and diluted with diethyl ether, followed by filtered through celite pad. The filtrate was washed with excess of water and extracted with diethyl ether (3 × 40 mL). The combined extracts were dried over Na₂SO₄ and solvent was evaporated under vacuum. The residue was purified by column chromatography using silica gel (*n*-hexane/dichloromethane 9:1). Recrystallisation of the pure product with absolute ethanol affords dark red color solid (**8a–8f**) in about 65–70% yield. A representative ¹H and ¹³C NMR spectra is shown in **Figure 8 & 9** respectively.

Mesogenic compound 8a: IR (film) ν_{\max} = 2951, 2922, 2852, 2216, 1624, 1516, 1456, 1375, 1261, 1163, 1080 cm⁻¹; ¹H NMR (500 MHz, CDCl₃): δ = 10.72 (s, 1H), 8.53 (s, 1H), 8.33 (s,

1H), 7.94–7.88 (m, 4H), 7.57 (d, $J = 6.5$ Hz, 4H), 7.21 (d, $J = 6.5$ Hz, 4H), 4.46 (m, 4H), 4.30–4.27 (m, 6H), 2.65 (t, $J = 7$ Hz, 4H), 2.16–2.10 (m, 4H), 2.0–1.96 (m, 6H), 1.69 (m, 8H), 1.66–1.63 (m, 4H), 1.49–1.20 (m, 108 H), 0.88–0.83 ppm (m, 21H); ^{13}C NMR (125 MHz, CDCl_3): $\delta = 149.83, 148.24, 147.63, 146.94, 143.89, 143.07, 142.98, 138.89, 138.11, 136.49, 131.58, 130.91, 129.40, 127.52, 125.69, 123.88, 123.33, 121.44, 119.27, 111.43, 106.86, 104.99, 104.40, 95.21, 86.64, 68.72, 68.54, 68.34, 68.08, 67.91, 35.04, 30.94, 30.30, 28.78, 28.73, 28.68, 28.65, 28.55, 28.41, 28.35, 28.12, 25.31, 25.27, 25.17, 21.69, 13.10$ ppm; elemental analysis: $\text{C}_{120}\text{H}_{182}\text{N}_2\text{O}_5$; calculated (%): C 83.18, H 10.59, N 1.62; found: C 83.26, H 10.64, N 1.68.

Mesogenic compound 8b: IR (film) $\nu_{\text{max}} = 2924, 2893, 2852, 2208, 1606, 1510, 1454, 1377, 1249, 1163, 1078$ cm^{-1} ; ^1H NMR (500 MHz, CDCl_3): $\delta = 10.70$ (s, 1H), 8.47 (s, 1H), 8.24 (s, 1H), 7.86–7.83 (m, 4H), 7.58 (br, 4H), 6.90 (br, 4H), 4.43 (m, 4H), 4.30–4.24 (m, 6H), 4.01 (t, $J = 6.5$ Hz, 4H), 2.16–2.11 (m, 4H), 2.09–1.97 (br, 6H), 1.82–1.79 (m, 4H), 1.69–1.21 (m, 94H), 1.01 (t, $J = 7$ Hz, 6H), 0.88 ppm (br, 15H); ^{13}C NMR (125 MHz, CDCl_3) = 159.78, 159.71, 151.64, 150.91, 149.40, 148.76, 148.07, 144.97, 140.10, 139.31, 137.61, 133.48, 133.45, 132.32, 131.57, 130.54, 127.24, 126.80, 126.68, 125, 124.47, 122.65, 118.08, 114.64, 112.62, 108.62, 105.69, 96.36, 96.21, 87.07, 69.85, 69.67, 69.49, 69.21, 69.02, 67.83, 31.96, 31.29, 29.82, 29.79, 29.75, 29.73, 29.66, 29.62, 29.57, 29.54, 29.42, 29.21, 26.31, 26.27, 26.20, 22.71, 19.26, 14.12, 13.87 ppm; elemental analysis: $\text{C}_{108}\text{H}_{158}\text{N}_2\text{O}_7$; calculated (%): C 81.25, H 9.98, N 1.75; found: C 81.34, H 10.05, N 1.84.

Mesogenic compound 8c: IR (film) $\nu_{\text{max}} = 2956, 2924, 2852, 2206, 1606, 1510, 1454, 1377, 1249, 1163, 1078$ cm^{-1} ; ^1H NMR (500 MHz, CDCl_3): $\delta = 10.68$ (s, 1H), 8.44 (s, 1H), 8.20 (s, 1H), 7.84–7.81 (m, 4H), 7.58 (br, 4H), 6.90 (br, 4H), 4.41 (br, 4H), 4.28–4.23 (m, 6H), 3.99 (t, $J = 6$ Hz, 4H), 2.16–2.10 (m, 4H), 1.97 (br, 6H), 1.82 (t, $J = 6.5$ Hz, 4H), 1.68–1.58 (m, 12H), 1.49–1.21 (m, 98H), 0.90–0.84 ppm (m, 21H); ^{13}C NMR (125 MHz, CDCl_3) = 158.65, 158.58, 150.16, 149.56, 148.03, 147.39, 146.66, 143.62, 138.57, 137.82, 136.09, 132.46, 132.41, 131.03, 130.47, 129.15, 125.67, 125.41, 125.20, 123.80, 123.69, 123.06, 121.26, 94.95, 94.88, 68.49, 68.36, 68.06, 67.92, 67.77, 67.10, 30.97, 30.84, 28.97, 28.84, 28.77, 28.68, 28.64, 28.44, 28.42,

28.30, 28.27, 28.16, 25.37, 25.34, 25.30, 25.15, 25.09, 25.07, 21.71, 21.67, 13.11 ppm; elemental analysis: C₁₁₆H₁₇₄N₂O₇; calculated (%): C 81.54, H 10.26, N 1.64; found: C 81.74, H 10.41, N 1.79. ¹H NMR and ¹³C NMR spectra are shown in the **Figure 8**.

Mesogenic compound 8d: IR (film) ν_{\max} = 2956, 2906, 2895, 2210, 1606, 1529, 1454, 1377, 1249, 1161, 1078 cm⁻¹; ¹H NMR (500 MHz, CDCl₃): δ = 10.76 (s, 1H), 8.52 (s, 1H), 8.34 (s, 1H), 7.97–7.90 (m, 4H), 7.57 (br, 4H), 6.90 (d, J = 8 Hz, 4H), 4.50–4.46 (m, 4H), 4.32–4.26 (m, 6H), 4.0 (t, J = 6.5 Hz, 4 H), 2.18–2.10 (m, 4H), 2.0–1.96 (m 6H), 1.81 (t, J = 6.5 Hz, 4H), 1.71–1.20 (m, 110H), 0.88–0.85 ppm (m, 21H); ¹³C NMR (125 MHz, CDCl₃) = 158.66, 158.59, 151.22, 150.17, 149.59, 148.06, 147.42, 146.68, 143.63, 138.59, 138.21, 137.82, 136.10, 135.06, 132.46, 132.41, 131.01, 130.47, 129.69, 129.17, 127.81, 125.70, 125.44, 125.24, 123.82, 123.69, 123.09, 121.28, 116.54, 114.11, 113.54, 113.52, 113.04, 111.32, 106.51, 104.65, 104.14, 103.94, 94.99, 94.92, 86.17, 68.51, 68.39, 68.09, 67.94, 67.79, 67.11, 35.12, 33.30, 32.81, 30.97, 30.93, 29.29, 28.86, 28.84, 28.77, 28.71, 28.68, 28.67, 28.65, 28.52, 28.48, 28.46, 28.44, 28.37, 28.35, 28.32, 28.29, 28.23, 28.13, 25.37, 25.34, 25.30, 25.15, 25.10, 25.08, 21.71, 21.69, 13.11 ppm; elemental analysis: C₁₂₈H₁₉₈N₂O₇; calculated (%): C 81.91, H 10.63, N 1.49; found: C 82.29, H 10.74, N 1.83. ¹H NMR and ¹³C NMR spectra are shown in the **Figure 9**.

Mesogenic compound 8e: IR (film) ν_{\max} = 2955, 2918, 2850, 2210, 1606, 1514, 1454, 1377, 1259, 1161, 1074 cm⁻¹; ¹H NMR (500 MHz, CDCl₃): δ = 10.71 (s, 1H), 8.47 (s, 1H), 8.25 (s, 1H), 7.88–7.84 (m, 4H), 7.57 (br, 4H), 6.90 (d, J = 7.5 Hz, 4H), 4.44 (br, 4H), 4.30–4.25 (m, 6H), 3.99 (t, J = 6 Hz, 4H), 2.17–2.09 (m, 4H), 1.98 (br, 6H), 1.83–1.80 (m, 4H), 1.69–1.58 (m, 14H), 1.48–1.21 (m, 136H), 0.88–0.84 ppm (m, 21H); ¹³C NMR (125 MHz, CDCl₃) = 159.72, 151.66, 150.93, 149.41, 148.78, 148.10, 144.99, 140.12, 139.33, 137.63, 133.48, 133.45, 132.32, 131.57, 130.56, 127.27, 126.82, 126.71, 125.01, 124.49, 122.67, 118.11, 114.98, 114.65, 108.10, 105.73, 105.57, 96.39, 87.10, 69.86, 69.69, 69.52, 69.23, 69.04, 68.18, 31.96, 29.79, 29.73, 29.68, 29.66, 29.63, 29.57, 29.54, 29.48, 29.46, 29.42, 29.38, 29.28, 29.27, 26.31, 26.28, 26.21, 26.08, 22.71, 14.12 ppm; elemental analysis: C₁₃₆H₂₁₄N₂O₇; calculated (%): C 82.12, H 10.84, N 1.41; found: C 82.19, H 10.91, N 1.52.

Mesogenic compound 8f: IR (film) ν_{\max} = 2949, 2924, 2852, 2210, 1606, 1512, 1454, 1377, 1261, 1161, 1080 cm^{-1} ; ^1H NMR (500 MHz, CDCl_3): δ = 10.75 (s, 1H), 8.52 (s, 1H), 8.20 (s, 1H), 7.92 (m, 4H), 7.59–7.57 (m, 4H), 6.91 (d, J = 8.5 Hz, 4H), 4.48 (br, 4H), 4.32–4.27 (m, 6H), 4.03 (t, J = 6.5 Hz, 4H), 2.16–2.0 (m, 4H), 1.99–96 (m, 6H), 1.71–1.67 (m, 2H), 1.65–1.17 (m, 102H), 0.97 (d, J = 6.5Hz, 6H), 0.89–0.83 ppm (m, 33H); ^{13}C NMR (125 MHz, CDCl_3) = 159.76, 159.69, 151.58, 150.88, 149.35, 148.73, 148.04, 144.94, 140.06, 139.25, 137.54, 133.48, 133.45, 132.28, 131.58, 130.51, 127.19, 126.77, 126.65, 124.97, 124.44, 124.03, 123.49, 122.61, 118.02, 115.95, 115, 114.91, 114.65, 114.07, 112.57, 108, 106.19, 105.63, 105.45, 96.34, 96.20, 87.09, 69.82, 69.64, 69.45, 69.19, 69, 66.49, 39.27, 37.36, 37.34, 36.18, 31.96, 31.63, 29.92, 29.91, 29.83, 29.80, 29.78, 29.74, 29.71, 29.68, 29.64, 29.58, 29.55, 29.43, 29.13, 28.01, 26.32, 26.28, 26.20, 24.69, 22.72, 22.63, 19.68 ppm; elemental analysis: $\text{C}_{120}\text{H}_{182}\text{N}_2\text{O}_7$; calculated (%): C 81.67, H 10.40, N 1.59; found: C 82.05, H 10.72, N 1.81.

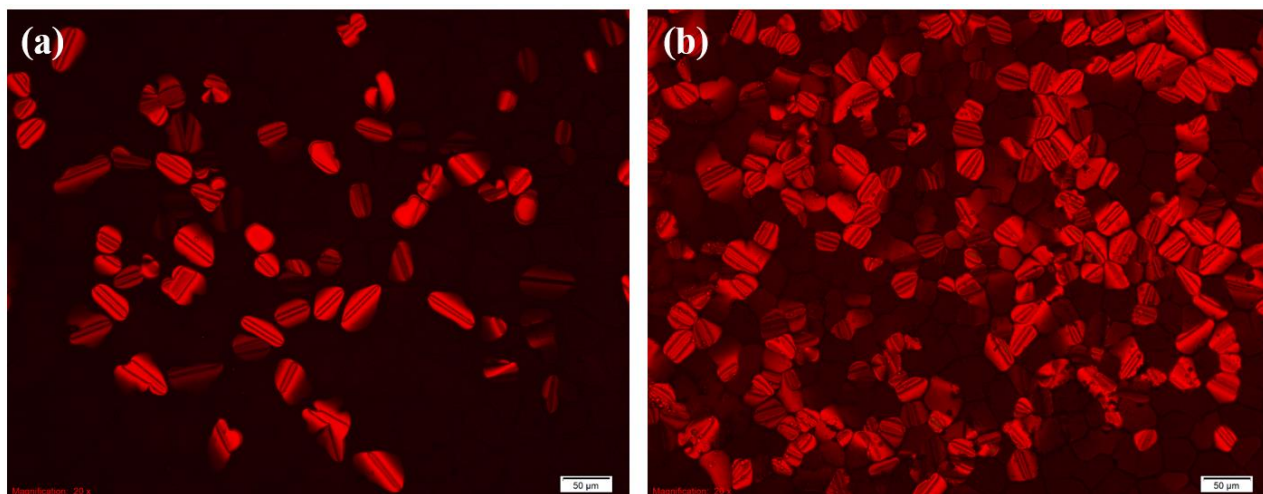


Figure 1. POM textures for compound **8a**, (a) early growing rectilinear defect texture of Col_h phase at 202 $^\circ\text{C}$, viewed at 100 \times magnifications; for compound **8c** (b) hexagonal columnar texture recorded at 114 $^\circ\text{C}$, viewed at 200 \times magnifications. Both POM images were recorded on slow cooling from the isotropic liquid.

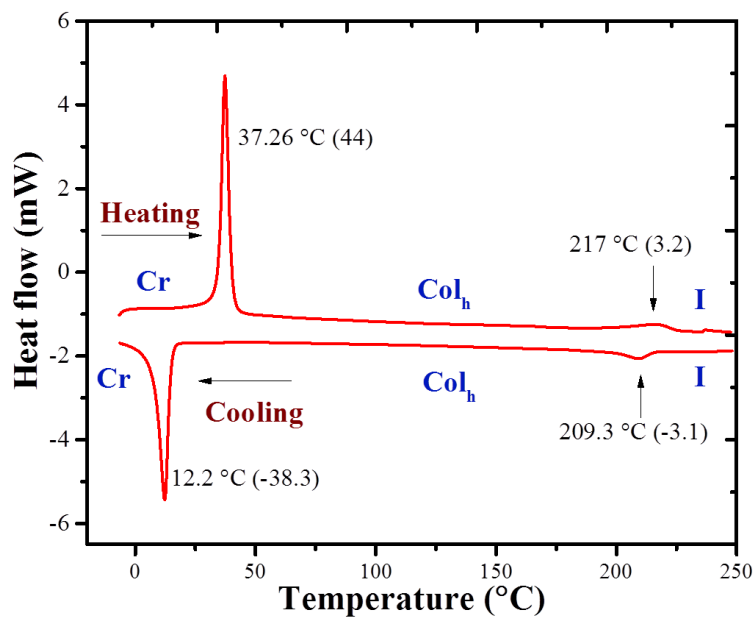


Figure 2. DSC thermogram of compound **8a** showing phase transitions on heating and cooling cycles at a scan rate of 10 °C min^{-1} . Vertical arrows indicate phase transition points.

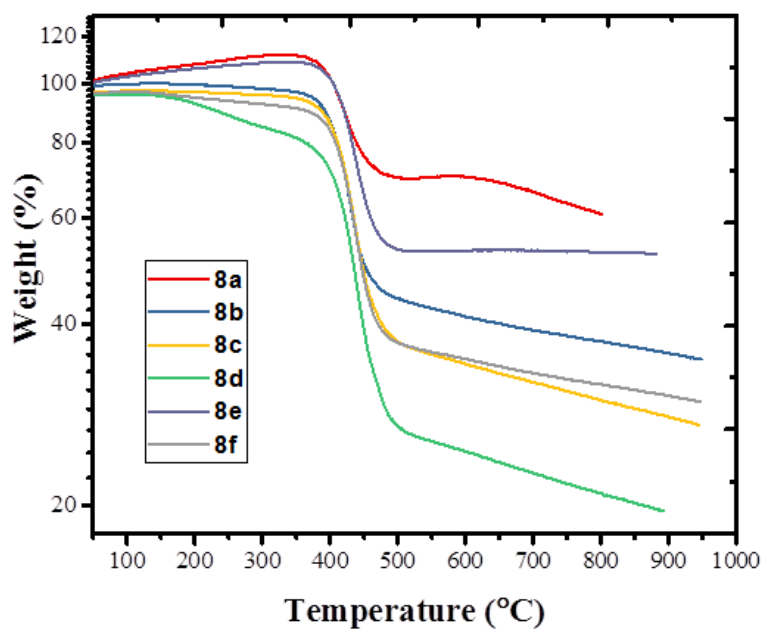


Figure 3. TGA analysis of discotic mesogens **8a–8f**

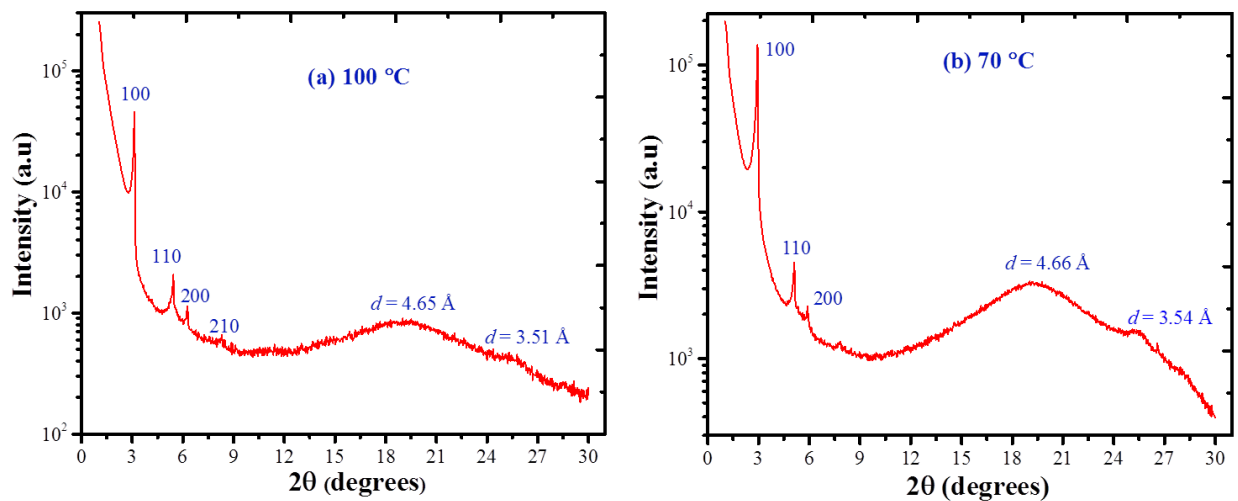


Figure 4. The intensity profile of the X-ray pattern: (a) **8a** at 100 °C (heating scan) and (b) **8d** at 70 °C (cooling scan) respectively.

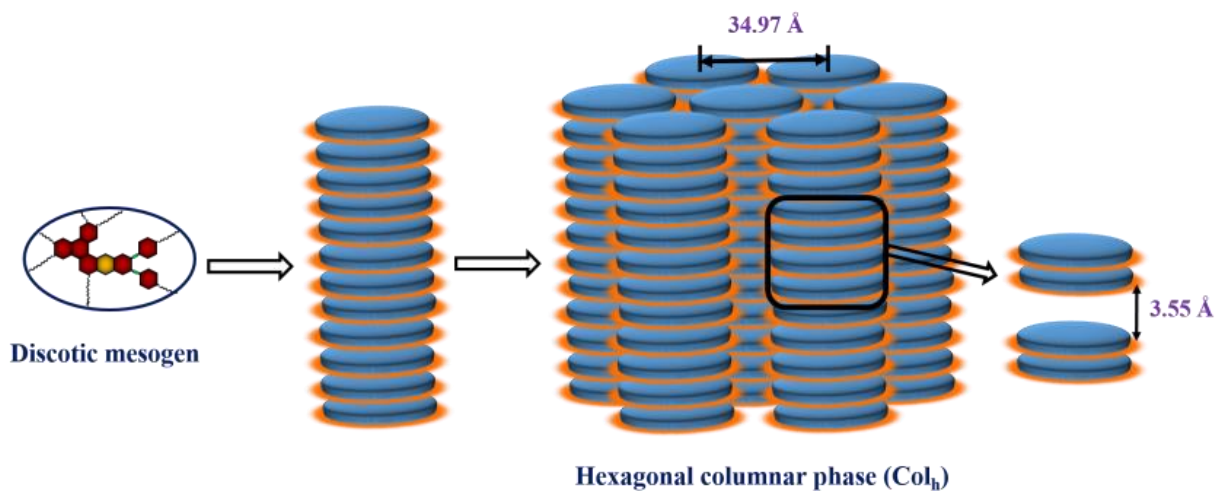


Figure 5. Schematic representation of self-assembly of hexagonal columnar phase obtained for the representative compound **8e**.

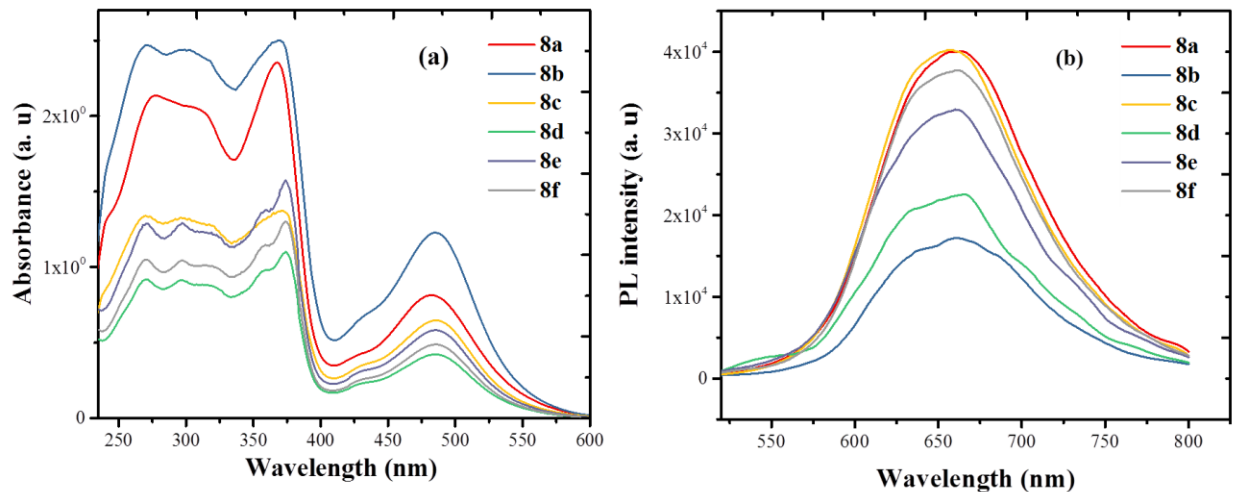


Figure 6. (a) UV-Visible absorption spectra and (b) fluorescence emission spectra of all the discotic mesogens (8a–8f).

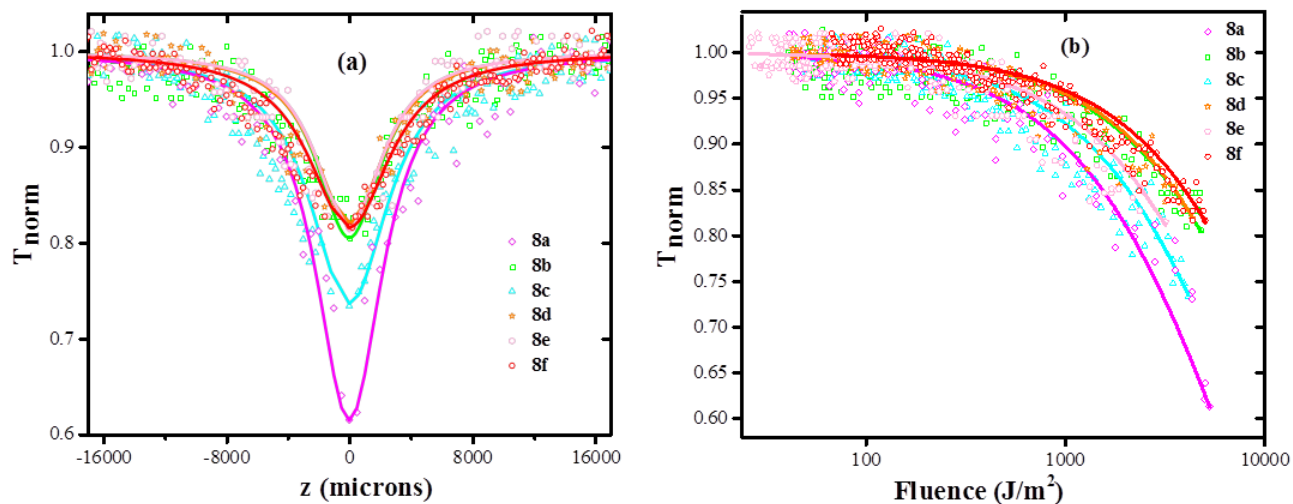


Figure 7. (a) Open aperture Z-scan measurements done at the laser pulse energy of 3 micro Joules, (b) Normalized transmission as a function of input laser fluence, calculated from the Z-scan data.

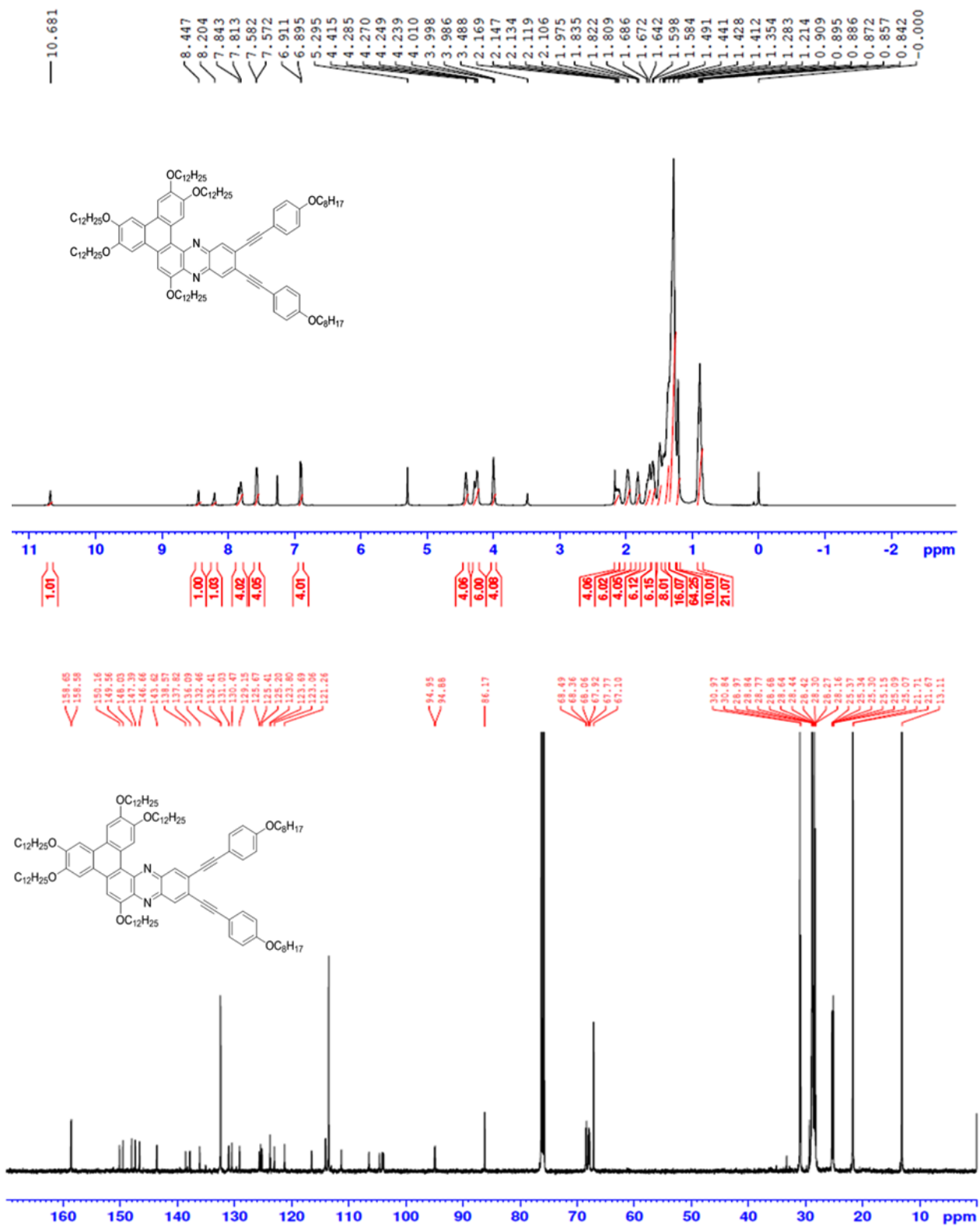


Figure 8. ¹H and ¹³C NMR spectra of compound **8c**.

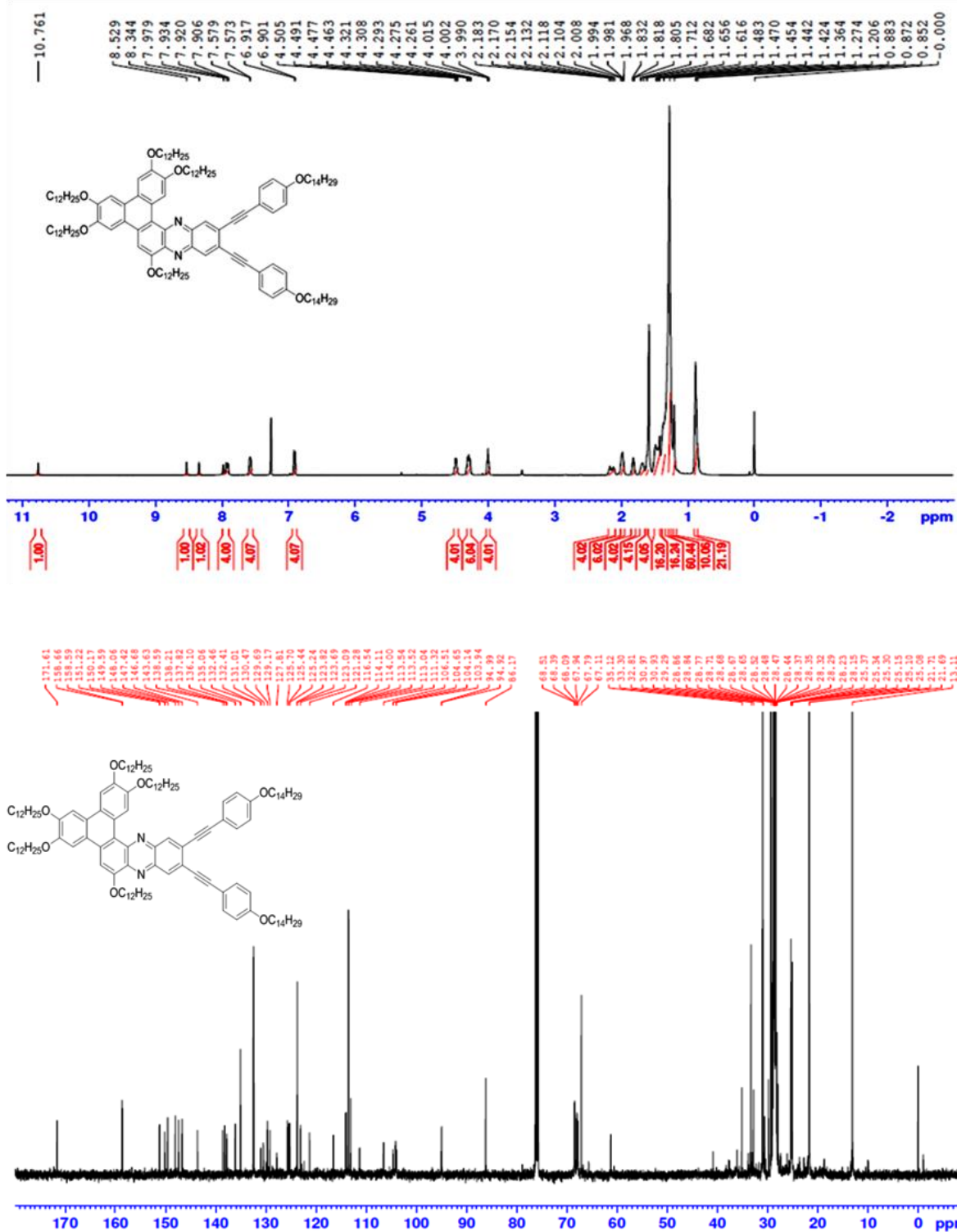


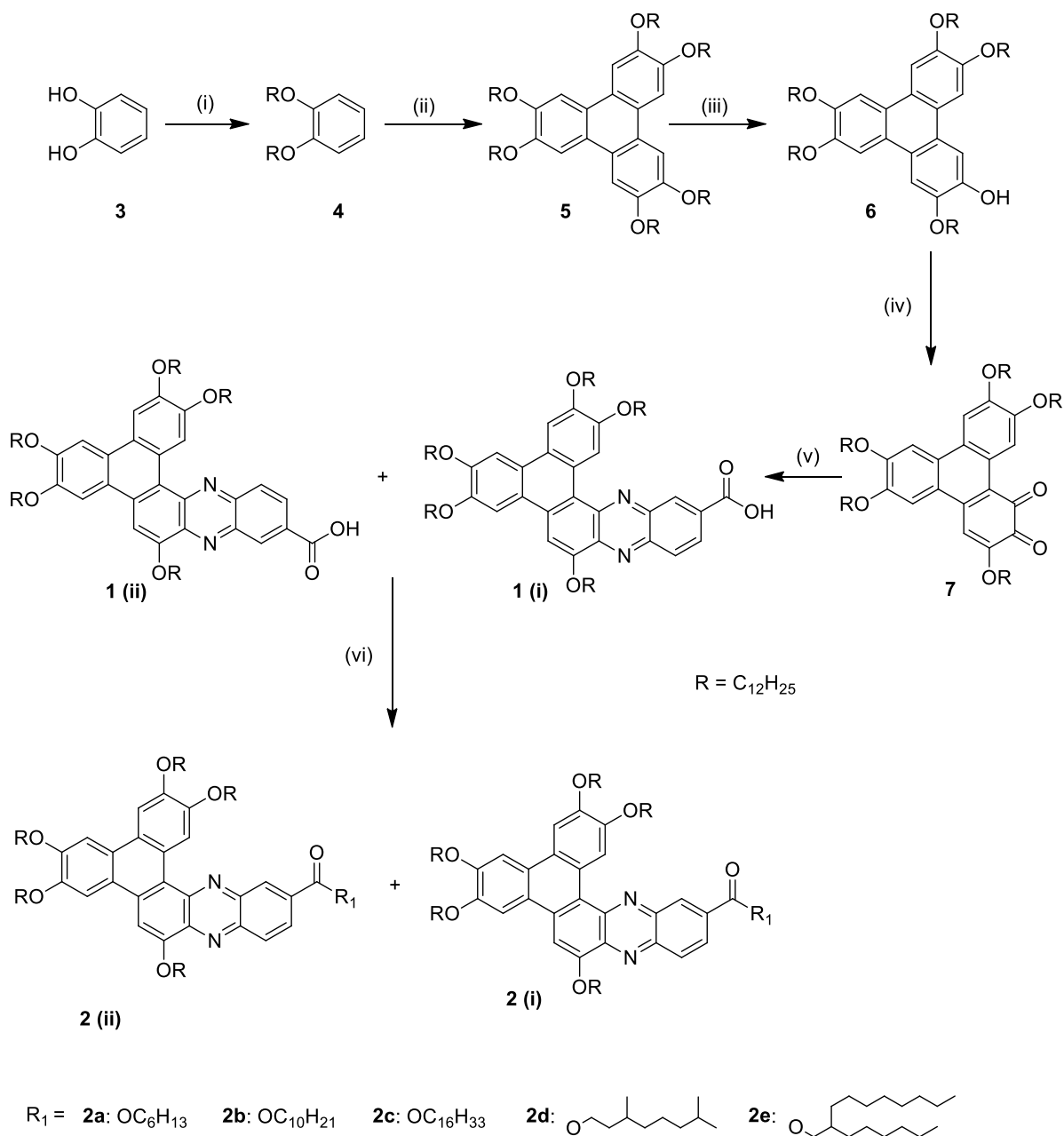
Figure 9. ¹H and ¹³C NMR spectra of compound 8d.

broad temperature range. We investigated the mesomorphic characterization, photophysical properties and nonlinear optical studies of these new monomeric acid and ester of TP DLCs.

4.3.2 Results and discussion

4.3.2.1. Synthesis

The synthesis of unsymmetrical monomeric ester containing phenazine fused triphenylene derivatives is shown in **Scheme 1**. The key intermediate 3,6,7,10,11-pentakis(alkyloxy)triphenylene-1,2-dione (**7**) was prepared from reported synthetic procedure as stated in the part A and characterised before proceeding to next step [**38**]. Further it was condensed with commercially available 3,4-diaminobenzoic acid in presence of glacial acetic acid and toluene (7:3) solvent medium under reflux condition to afford the corresponding intermediate inseparable acid derivatives 2,3,6,7,10- pentaalkoxyphenanthro[9,10-*a*]-14-carboxylic acid **1(i)** and its regioisomer, 2,3,6,7,10- pentaalkoxyphenanthro[9,10-*a*]-13-carboxylic acid **1(ii)**. This mixture is denominated as **1**. The esterification of **1** with aliphatic alcohols produces an inseparable mixture of final mesogenic ester derivatives **2(i)** and **2(ii)**, denominated as **2**. All the intermediate and final compounds were purified using column chromatography, followed by recrystallization using respective solvent to ensure high purity. The intermediate acid derivative **1** is sparingly soluble in organic solvent like chloroform and dichloromethane solvent. However, final compounds (**2a–2e**) were freely soluble in all chlorinated solvents.



Scheme 1: (i) alkyl halide, anhy. K₂CO₃, DMF, reflux, 24 h; (ii) anhy. FeCl₃, DCM, 15 min, r.t.; (iii) *B*-bromocatecholborane, DCM, 24 h, r.t.; (iv) ceric ammonium nitrate, acetonitrile, r. t, 30 min; (v) 3,4-diaminobenzoic acid, acetic acid: toluene (7:3), 100 °C, 8 h; (vi) alkyl alcohol, EDCI.HCl, HOBT, DMAP, DCM, 24 h, r.t.

4.3.2.2 Thermal properties

Thermotropic liquid crystalline textures of all the compounds (**1**, **2a–2e**) were investigated by POM under cross polarisers. The phase transition temperature (peak in °C) along with enthalpy of phase transition values (kJ mol^{-1}) were examined with help of DSC measurements on both heating and subsequent cooling with a scan rate of $10\text{ }^{\circ}\text{C min}^{-1}$, under nitrogen atmosphere and the thermal values were summarised in the **Table 1**.

Table 1. Phase transition temperature of all the mesogens **1** & **2a–2e** (both heating and cooling cycle).

Compound	Phase transition (peak temperature (°C); (ΔH , [kJ mol^{-1}]))	
	<i>second heating scan</i>	<i>second cooling scan</i>
1	Cr 95.3 [45.30] Col_r 237.4 [25.40] I	232.7 [-23.80] Col_r 84 [-30.53] Cr
2a	Cr₁ 46.4 [10.40] Cr₂ 68.0 [40.52] I Col_h 200.1 [4.31] I	I 197.1 [-4.41] Col_h 16.9 [-53.31] Cr
2b	Cr 71.1 [47.88] Col_h 207.2 [8.12] I	I 205.7 [-7.41] Col_h 22.6 [-47.45] Cr
2c	Cr 63.4 [46.17] Col_h 155.2 [1.12] I	I 154.1 [-2.52] Col_h 31.6 [-62.89] Cr
2d	Cr 69.7 [67.66] Col_h 191.7 [0.58] I	I 180.4 [-0.63] Col_h 21.8 [-57.55] Cr
2e	Cr 43.0 [54.61] Col_h 173.1 [8.31] I	I 171.4 [-7.96] Col_h 21 [-57.51] Cr

The intermediate acid derivative **1** exhibits enantiotropic **Col_r** phase over broad temperature. The DSC scan exhibits two types of endothermic phase transitions from **Cr** phase to **Col_r** at lower temperature and **Col_r** to isotropic phase at higher temperature. The peak temperature at 95.3 °C along with corresponding enthalpy of phase transition ($\Delta H = 45.30\text{ kJ mol}^{-1}$) is attributed to crystalline phase to **Col_r** phase transition while peak temperature at 237.4 °C ($\Delta H = 25.40\text{ kJ mol}^{-1}$) referred to **Col_r** phase to isotropic liquid. On slow cooling under POM,

appearance of microscopic texture at 232.7 °C revealed the existence of Col_r phase which crystallizes at 84 °C. The Col_r phase structure was confirmed by XRD investigations as discussed later.

Similarly, all the ester derivatives (**2a–2e**) exhibit two types of endothermic phase transition from Cr to Col_h at lower temperature and Col_h to isotropic phase at higher temperature. The Col_h phase retains till room temperature, upon cooling from the isotropic liquid. Compound **2a** exhibited crystal-crystal transition at 46.4 °C ($\Delta H = 10.40 \text{ kJ mol}^{-1}$) and melts to Col_h phase at 68 °C with enthalpy change ($\Delta H = 40.52 \text{ kJ mol}^{-1}$) and goes to isotropic liquid at 200.1 °C ($\Delta H = 4.31 \text{ kJ mol}^{-1}$). Upon cooling under POM, the appearance of rectilinear defect textures were observed which are characteristics of hexagonal columnar mesophase as shown in **Figure 1a**, viewed at 100 × magnifications. On the other hand, compounds **2b** and **2c** show Cr to Col_h phase at 71.1 °C ($\Delta H = 47.88 \text{ kJ mol}^{-1}$) and 63.4 °C ($\Delta H = 46.17 \text{ kJ mol}^{-1}$), respectively and phase transition from Col_h phase to isotropic phase at 207.2 °C ($\Delta H = 8.12 \text{ kJ mol}^{-1}$) and 155.2 °C ($\Delta H = 1.12 \text{ kJ mol}^{-1}$), respectively. Upon cooling under POM from isotropic phase, compounds **2b** and **2c** showed the appearance of Col_h texture at 205.7 °C and 154.1 °C respectively. Similarly, branched chain compounds **2d** and **2e** exhibit enantiotropic phase transition from Cr phase to Col_h phase at lower temperature 69.7 °C ($\Delta H = 67.66 \text{ kJ mol}^{-1}$) and 43 °C ($\Delta H = 54.61 \text{ kJ mol}^{-1}$) respectively, and phase transition from Col_h phase to isotropic phase at 191.7 °C ($\Delta H = 0.58 \text{ kJ mol}^{-1}$) and 173.1 °C ($\Delta H = 8.31 \text{ kJ mol}^{-1}$), respectively. Under POM, compound **2d** exhibits fan shaped texture with large domains, upon slow cooling from the isotropic liquid as shown in **Figure 1b**, viewed at 200 × magnifications. On the other hand, compound **2e** displayed the mesophase at 171.4 °C, upon cooling from isotropic liquid. Eventually, it is noticed that acid derivative show much higher isotropic temperature in comparison to ester derivatives which could be due to the formation of H-bonding [52]. As a representative DSC thermogram of compound **2b** is shown in **Figure 2**.

4.3.2.3 X-ray diffraction studies

The mesophase structures of acid and other ester derivatives (**1** & **2a–2e**), were investigated with the help of X-ray diffraction studies using unoriented liquid crystal samples

filled in Lindemann capillaries. The XRD data recorded in the columnar mesophase on both heating and cooling temperature and the values are summarised in **Table 2**. The XRD diffractogram obtained for acid compound **1** at 120 °C on cooling is shown in **Figure 3a** (**Table 2**). The compound **1** showed two strong reflections in the small angle region with high intensity and several additional weak reflections in the wide angle regions of low intensity (**Figure 3a**). In XRD pattern further affirm the *d*-spacings of first peak and third peak, second peak and fourth peaks are in the ratio of 1:1/2 owing to lamellar arrangement of discotic structure in two different directions. The two intense peaks located in the small angle region are most commonly detected for rectangular columnar phase. These reflections were characterised as (200), (110), (400), (020), (220) and (600) of a two-dimensional rectangular lattice with lattice spacing $a = 69.36 \text{ \AA}$ and $b = 29.47 \text{ \AA}$ respectively. In the wide angle region, a broad halo reflection around 4.76 \AA and shoulder peak at 3.63 \AA were observed that corresponds to average distance between alkyl chains (h_a) and core-core separation of columnar stacks. Similarly, XRD pattern obtained for ester derivatives (**2a–2e**) in the hexagonal columnar phase are shown in **Figure 3b** and **Table 2**. All the ester derivatives show ascending order of diffraction angle along with *d*-spacings of first reflection to the second is in the ratio of $1:1/\sqrt{3}:1/2:1/\sqrt{7}$ respectively. These diffraction values correspond to the two-dimensional hexagonal columnar phase. The broad halo peak at wide angle region corresponds to average distance between alkyl chains, along with shoulder peak show average distance between core-core separation. The intercolumnar distance (*a*) can be calculated by adopting the relation $a = d_{10}/(\cos 30^\circ)$, where d_{10} spacing corresponding to highest intensity peak in the small angle region (**Table 2**). As a representative the XRD diffractogram obtained for compound **2e** in the hexagonal columnar phase at 70 °C on cooling is shown in **Figure 3b**. The highest intensity peak in the small angle region show *d*-spacing of $d_1 = 25.68 \text{ \AA}$ and other three corresponding to a lower intensity was observed at $d_2 = 14.81 \text{ \AA}$, $d_3 = 12.85 \text{ \AA}$ and $d_4 = 9.70 \text{ \AA}$, respectively. All the values agree with hexagonal columnar lattice parameters. The broad halo peak in the wide angle region at approximately 4.52 \AA corresponds to average distance between alkyl chains. The prominent peak at 3.50 \AA was assigned to π - π stacking of aromatic discotic cores.

Table 2. XRD data of compounds **1** and **2a–2e**. I_C = Intercolumnar distance, C–C = Core-core separation, R_L = Alkyl- chain length.

Compound	Temperature (°C)	2 θ (degree s)	d -spacings/ Å observed (calculated)	Miller indexes	Phase (lattice constant)	R_L (Å)	C–C (Å)	I_C (Å)
1	120	2.63	33.65	200	Col_r $a = 69.36$ $b = 29.47$	4.76	3.63	31.32
		3.25	27.14	110				
		5.11	17.24 (17.34)	400				
		6.01	14.68 (14.73)	020				
		6.56	13.45 (13.56)	220				
		7.69	11.48 (11.56)	600				
		3.59	24.54 (24.53)	100				
2a	130	6.24	14.13 (14.16)	110	Col_h $a = 28.33$	4.64	3.55	28.33
		7.21	12.23 (12.26)	200				
		3.51	25.10 (25.09)	100				
		6.11	14.44 (14.48)	110				
2b	110	7.06	12.50 (12.54)	200	Col_h			
		9.34	9.45 (9.48)	210				
		3.33	26.48 (26.47)	100				
2c	110	5.77	15.28 (15.27)	110	Col_h $a = 30.57$	4.84	3.58	30.57
		6.66	13.24 (13.23)	200				
		8.71	10.14 (10.00)	210				
		3.51	25.41 (25.40)	100				
2d	85	6.11	14.50 (14.66)	110	Col_h $a = 29.34$	4.53	3.50	24.64
		7.06	12.57 (12.70)	200				
		3.43	25.68 (25.67)	100				
2e	70	5.95	14.81 (14.82)	110	Col_h $a = 29.65$	4.52	3.50	29.65
		6.87	12.85 (12.83)	200				
		9.10	9.70 (9.70)	210				

4.3.3 Photophysical properties

The photophysical properties of monomeric ester derivatives (**2a–2e**) were investigated by UV-Vis and photoluminescence spectroscopy in a very dilute solution as shown in **Figure 4** and data are presented in **Table 3**. Both absorption and emission spectra have been recorded by dissolving liquid crystalline compounds in anhydrous chloroform solvent and recorded at room temperature. Absorption spectra of all the monomeric ester derivatives were similar, irrespective of number of alkyl chains with maximum absorption bands located below 580 nm as shown in **Figure 4a**. The maximum absorption bands at 290, 312, 338, 352 nm, along with shoulder peaks at 240–275 nm is observed at shorter wavelengths is attributed due to $\pi \rightarrow \pi^*$ transition, while the intense peak at 474 nm corresponds to $n \rightarrow \pi^*$ transition at longer wavelength. The maximum absorption at longer wavelength may be due to extended π -conjugation of heteroaromatic structure causes increasing the intensity of absorption. The intensity of light absorption eventually relies upon number of molecules that absorb light at given wavelength, presumably causes bathochromic shift.

Table 3. Photophysical properties of monomeric ester derivatives (**2a–2e**)

Compound	Absorption $\lambda_{\text{abs}}/\text{nm}$	Molar absorption coefficient ($\epsilon/\text{L mol}^{-1} \text{cm}^{-1}$)	Emission $\lambda_{\text{em}}/\text{nm}$
2a	292, 312, 339, 352, 472	4.0714×10^6	661
2b	292, 312, 338, 352, 472	4.8422×10^6	658
2c	293, 312, 338, 352, 472	3.1202×10^6	659
2d	292, 311, 337, 352, 472	4.5197×10^6	659
2e	291, 311, 338, 352, 472	3.9871×10^6	660

Similarly, emission spectra of all the compounds (**2a–2e**) were obtained by dissolving compounds in anhydrous chloroform solvent and exciting the solution of all the compounds at $\lambda_{\text{ex}} = 474$ nm as shown in **Figure 4b**. The emission spectra of all the compounds shows strong emission band around 658–661 nm. There is no significant changes were observed on increasing number of alkyl chain length. The gelation and rheological properties of monomeric acid **1** is in progress.

4.3.4 Nonlinear optical transmission studies

Nonlinear optical transmission measurements were obtained by dissolving monomeric ester compounds (**2a–2e**) in anhydrous chloroform solvent taken in 1 mm cuvette were carried out using the open aperture Z-scan technique at an excitation wavelength of 532 nm. The samples were excited using 5 ns laser pulses generated from a frequency doubled Nd:YAG laser (Continuum Minilite I).

In our open aperture Z- scan experiment, the laser beam was focused using a plano-convex lens ($f = 10$ cm). The transmission was recorded at different positions with respect to the beam focus ($z = 0$). The samples experiences a different fluence at each position, with maximum fluence at the focus and linear transmission of the samples was fixed at 65% for the wavelength of 532 nm. The Z scans were measured for all the samples at laser pulse energy of 3 μJ are given in **Figure 5**. From the Z scan curve it is clear that the samples exhibit strong optical limiting property as the transmission decreases at higher laser fluences.

For a spatially Gaussian laser beam, the fluence ($F_{\text{in}}(z)$) at any position z can be obtained from the relation.

$$F_{\text{in}}(z) = 4(\ln 2)^{\frac{1}{2}} E_{\text{in}} / \pi^{\frac{3}{2}} \omega(z)^2 \text{-----} (1)$$

with the beam radius $\omega(z)$ given by

$$\omega(z) = \omega_0 \left(1 + \left(\frac{z}{z_0} \right)^2 \right)^{\frac{1}{2}} \text{-----} (2)$$

Where ω_0 is the focal spot radius, and z_0 is the Rayleigh length given by $z_0 = \pi\omega_0^2/\lambda$. We found that the nonlinear transmission has contributions from both excited state absorption (ESA) [48] and saturable absorption (SA) [49]. The net nonlinear absorption coefficient is given by,

$$\alpha(I) = \frac{\alpha_0}{(1+I/I_s)} + \beta I \quad \text{-----} \quad (3)$$

Where I_s is the saturation intensity (W/m^2) and β is the excited state absorption coefficient (m/W). I_s and β can be obtained by numerically fitting the light propagation equation to the measured transmission data:

$$\frac{dI}{dx} = - \left[\frac{\alpha_0}{(1+I/I_s)} + \beta I \right] I \quad \text{-----} \quad (4)$$

Where x is propagation distance through the sample. The obtained values are tabulated in **Table 4**.

Table 4. ESA coefficient (β) and saturation intensity (I_{sat}) calculated for the samples (**2a–2e**) from the data given in **Figure 5a** and **5b**.

Compounds	Laser pulse energy (μJ)	Sample linear Transmission (%)	Beta (β) ($\times 10^{-10} \text{ mW}^{-1}$)	I_{sat} ($\times 10^{11} \text{ Wm}^{-2}$)
2a	3	65	10.8	8.5
2b	3	65	10.2	6.0
2c	3	65	9.5	8.0
2d	3	65	9.4	8.5
2e	3	65	9.2	6.0

We have observed that excited state absorption and saturable absorption properties of the molecules exhibit high nonlinear optical properties. The delocalization of π electrons arises from extended π -conjugation in the triphenylene fused phenazine ester derivatives increases the nonlinear optical properties in these DLCs.

4.3.5 Conclusions

The synthesis and characterisation of five novel extended π -conjugated monomeric ester containing phenazine fused triphenylene discotic liquid crystals are reported. The intermediate acid derivative **1** exhibits a rectangular columnar phase over broad temperature range, while monomeric ester derivatives exhibit hexagonal columnar phase which remains stable till room temperature upon cooling from isotropic phase. All the ester derivatives exhibit strong photoluminescence properties in anhydrous chloroform solvent upon excitation at 474 nm. The π -extended conjugation in triphenylene fused phenazine based DLCs enhance the nonlinear optical properties. Such ordered supramolecular structures may find applications in various semiconducting devices.

4.3.6 Experimental section

4.3.6.1 General procedure for synthesis of intermediate and final compounds

The intermediate compound 3,6,7,10,11-pentakis(dodecyloxy)triphenylene-1,2-diones **7** were synthesised as reported previously and confirmed by spectral and elemental analysis [38]. The intermediate 3,4-diaminobenzoic acid obtained from commercial source. The compound **1** is not characterised by ^{13}C NMR due to insufficient solubility in CDCl_3 solvent.

Synthesis of 2,3,6,7,10-pentakis(dodecyloxy)phenanthro[9,10-a]phenazine-13-carboxylic acid (1)

Mixture of compound **7** (0.5 g, 1 equiv) and 3,4-diaminobenzoic acid (1.1 equiv) were dissolved in a mixture of glacial acetic acid: toluene solvent (7:3). The resulted reaction mixture was refluxed at 100 °C for 8 h. After completion of reaction, the reaction mixture was cooled to room temperature and subsequently quenched with ice cold water, extracted with dichloromethane (3 × 100 mL). The combined extracts were dried over Na₂SO₄ and solvent was evaporated under vacuum. The crude compound was purified by column chromatography using silica gel (*n*-hexane/dichloromethane 6:4). Recrystallisation of the pure product with ethanol affords red colour solid **1**. Yield: 80 %. IR (film) ν_{\max} : 2953.12, 2908.75, 2852.81, 1691.63, 1612.54, 1454.38, 1377.22, 1261.49, 1166.97, 1101.39 cm⁻¹; ¹H NMR (500 MHz, CDCl₃): δ = 10.57 (s, 1H), 8.84 (s, 1H), 8.26–8.17 (m, 2H), 7.75–7.58 (m, 4H), 4.42–4.34 (m, 4 H), 4.17–4.01 (m, 6H), 2.14–2.08 (m, 4H), 1.94–1.87 (m, 8H), 1.66–1.21 (m, 91H), 0.81 pm (m, 15H); elemental analysis: C₈₅H₁₃₄N₂O₇, calculated: C, 78.77; H, 10.42; N, 2.16, % found: C, 78.02; H, 10.59; N, 2.32. ¹H NMR spectra are shown in the **Figure 6**.

Synthesis of monomeric ester discotic mesogens (2a–2e)

All the mesogenic derivatives were prepared by esterification reaction between the intermediate acid compound **1** with various aliphatic alcohols. The general method is depicted as follows.

In a two neck-flask containing compound **1** (0.2 g, 0.154 mmol), alkyl alcohol (1.2 eq) and catalytic amount of DMAP (0.01 g, 0.07 mmol) was added dry DCM solvent (50 mL) under argon at room temperature. After stirring for 10 min, *N*-(3-dimethylaminopropyl)-*N'*-ethylcarbodiimide hydrochloride (EDC.HCl) (0.047 g, 0.30 mmol) and *N*-hydroxybenzotriazole (HOBt) (0.04 g, 0.26 mmol) was added. The resulting mixture was stirred at room temperature for 24 h. After completion of reaction, water was added and extracted with DCM (3 × 50 mL). The combined extracts were dried over Na₂SO₄ and concentrate under vacuum. The residue was purified by column chromatography using silica gel (*n*-hexane/dichloromethane 9:1). Recrystallisation of the pure product with ethanol affords red colour solid **2a–2e**. Yield: 80–90%.

Hexyl 2,3,6,7,10-pentakis(dodecyloxy)phenanthro[9,10-a]phenazine-13-carboxylate (2a): IR (film) ν_{\max} : 2951, 2918, 2852, 1716, 1560, 1518, 1454, 1377, 1340, 1263, 1182, 1071 cm^{-1} ; ^1H NMR (500 MHz, CDCl_3): δ = 10.70 (s, 1H), 8.95 (s, 1H), 8.41–8.35 (m, 2H), 8 (s, 1H), 7.89–7.86 (m, 3H), 4.44 (t, J = 6.5 Hz, 4H), 4.38 (t, J = 6.5 Hz, 2H), 4.25–4.19 (m, 6H), 2.12–2.11 (m, 4H), 2.09–2 (m, 6H), 1.93–1.77 (m, 2H), 1.60–1.16 (m, 96H), 0.86 (t, J = 6.5 Hz, 3H), 0.80 ppm (t, J = 6 Hz, 15H); ^{13}C NMR (125 MHz, CDCl_3): δ = 165.96, 151.58, 151.11, 149.62, 148.90, 148.34, 145.44, 141.70, 140.10, 138.37, 132.08, 131.78, 130.62, 130.17, 128.78, 127, 124.91, 124.68, 122.64, 118.16, 112.42, 108.17, 106.53, 106.34, 105.80, 69.96, 69.77, 69.64, 69.28, 68.90, 65.81, 31.95, 31.55, 29.77, 29.71, 29.69, 29.61, 29.57, 29.49, 29.41, 29.39, 29, 28.82, 26.33, 26.25, 25.77, 22.71, 22.61, 14.13 ppm; elemental analysis: $\text{C}_{91}\text{H}_{146}\text{N}_2\text{O}_7$, calculated: C, 79.19; H, 10.66; N, 2.03. % found: C, 79.28; H, 10.73; N, 1.99.

Decyl 2,3,6,7,10-pentakis(dodecyloxy)phenanthro[9,10-a]phenazine-13-carboxylate (2b): IR (film) ν_{\max} : 2955, 2924, 2852, 1718, 1618, 1518, 1454, 1377, 1313, 1263, 1168, 1070 cm^{-1} ; ^1H NMR (500 MHz, CDCl_3): δ = 10.69 (s, 1H), 8.93 (s, 1H), 8.38–8.36 (m, 2H), 7.97 (s, 1H), 7.87–7.84 (m, 3H), 4.43 (t, J = 6.5 Hz, 4H), 4.38 (t, J = 6.5 Hz, 2H), 4.23–4.19 (m, 6H), 2.10–2.01 (m, 2H), 1.93–1.89 (m, 2H), 1.89–1.78 (m, 8H), 1.62–1.57 (m, 13H), 1.54–1.16 (m, 91), 0.81–0.79 ppm (m, 18H); ^{13}C NMR (125 MHz, CDCl_3): δ = 165.94, 151.55, 151.09, 149.62, 148.89, 148.32, 145.43, 141.67, 140.07, 138.35, 132.08, 131.75, 130.59, 130.13, 128.75, 126.99, 124.92, 124.66, 122.63, 118.14, 112.44, 108.17, 106.54, 106.32, 105.80, 69.95, 69.77, 69.62, 69.27, 68.89, 65.80, 31.95, 31.91, 29.79, 29.76, 29.74, 29.71, 29.61, 29.57, 29.51, 29.41, 29.34, 29.01, 28.87, 26.33, 26.25, 26.09, 22.70, 14.11 ppm; elemental analysis: $\text{C}_{95}\text{H}_{154}\text{N}_2\text{O}_7$, calculated: C, 79.44; H, 10.81; N, 1.95. % found: C, 79.50; H, 10.87; N, 1.21.

Hexadecyl 2,3,6,7,10-pentakis(dodecyloxy)phenanthro[9,10-a]phenazine-13-carboxylate (2c): IR (film) ν_{\max} : 2956, 2918, 2852, 1718, 1616, 1518, 1454, 1377, 1338, 1263, 1182, 1078 cm^{-1} ; ^1H NMR (500 MHz, CDCl_3): δ = 10.66 (s, 1H), 8.89 (s, 1H), 8.38–8.33 (m, 2H), 7.91 (s, 1H), 7.84–7.81 (m, 3H), 4.41–4.36 (m, 6H), 4.23–4.16 (m, 6H), 2.10–2.08 (m, 2H), 2.03–2.0 (m, 2H), 1.93–1.90 (m, 6H), 1.81–1.57 (m, 2H), 1.58 (m, 8H), 1.37–1.16 (m, 108H), 0.79 ppm (t, J =

6 Hz, 18H); ^{13}C NMR (125 MHz, CDCl_3): δ = 165.93, 151.49, 151.04, 149.57, 148.83, 148.26, 145.39, 141.62, 140.01, 138.28, 132.06, 131.69, 130.55, 130.10, 128.71, 126.93, 124.90, 124.61, 122.58, 118.06, 112.38, 108.06, 106.44, 106.22, 105.70, 69.89, 69.73, 69.55, 69.23, 68.86, 65.80, 31.96, 29.81, 29.78, 29.73, 29.68, 29.64, 29.60, 29.53, 29.42, 29.38, 28.87, 26.35, 26.26, 26.10, 22.71, 14.13 ppm; elemental analysis: $\text{C}_{101}\text{H}_{166}\text{N}_2\text{O}_7$, calculated: C, 79.79; H, 11; N, 1.84 % found: C, 79.86; H, 11.05; N, 1.88. ^1H NMR and ^{13}C NMR spectra are shown in the **Figure 7**.

3,7-Dimethyloctyl 2,3,6,7,10-pentakis(dodecyloxy)phenanthro[9,10-a] phenazine-13-carboxylate (2d): IR (film) ν_{max} : 2951, 2924, 2852, 1716, 1618, 1518, 1454, 1377, 1313, 1263, 1182, 1078 cm^{-1} ; ^1H NMR (500 MHz, CDCl_3): δ = 10.71 (s, 1H), 8.96 (s, 1H), 8.41–8.35 (m, 2H), 8.02 (s, 1H), 7.90–7.87 (m, 3H), 4.46–4.42 (m, 6H), 4.24–4.19 (m, 6H), 2.11 (m, 2H), 2.02 (m, 2H), 1.93–1.89 (m, 6H), 1.62 (m, 6H), 1.59–1.16 (m, 96H), 0.80 ppm (m, 24H); ^{13}C NMR (125 MHz, CDCl_3): δ = 164.93, 150.57, 150.10, 148.62, 147.90, 147.34, 144.43, 139.10, 130.70, 129.15, 127.74, 126, 123.89, 68.95, 68.75, 68.63, 68.27, 67.88, 63.33, 38.23, 36.22, 34.71, 30.92, 29.11, 28.74, 28.72, 28.68, 28.66, 28.57, 28.53, 28.46, 28.37, 28.35, 27.97, 26.95, 25.30, 25.21, 23.64, 21.67, 21.58, 18.67, 13.09 ppm; elemental analysis: $\text{C}_{95}\text{H}_{154}\text{N}_2\text{O}_7$, calculated: C, 79.44; H, 10.81; N, 1.95 % found: C, 79.68; H, 10.93; N, 2.06.

2-Hexyldecyl 2,3,6,7,10-pentakis(dodecyloxy)phenanthro[9,10-a]phenazine-13-carboxylate (2e): IR (film) ν_{max} : 2953, 2924, 2852, 1720, 1614, 1514, 1454, 1377, 1303, 1263, 1182, 1078 cm^{-1} ; ^1H NMR (500 MHz, CDCl_3): δ = 10.79 (s, 1H), 9.07 (s, 1H), 8.52–8.45 (m, 2H), 8.15 (s, 1H), 8.01–7.99 (m, 3H), 4.59–4.54 (m, 4H), 4.40–4.30 (m, 6H), 4.23–4.20 (m, 2H), 2.11–2.08 (m, 2H), 2.03–1.90 (m, 7H), 1.69–1.26 (m, 116H), 0.91–0.94 ppm (m, 21H); ^{13}C NMR (125 MHz, CDCl_3): δ = 166.06, 151.58, 151.13, 149.64, 148.92, 148.40, 145.46, 141.72, 140.17, 138.38, 132.07, 131.88, 130.62, 130.21, 128.77, 127.03, 124.91, 124.71, 122.65, 118.21, 112.41, 108.20, 106.55, 106.37, 105.83, 69.98, 69.77, 69.66, 69.29, 68.88, 68.38, 37.55, 31.95, 31.91, 31.88, 31.45, 30.01, 29.79, 29.77, 29.71, 29.68, 29.64, 29.60, 29.56, 29.49, 29.41, 29.38, 29.34, 28.99, 26.82, 26.79, 26.40, 26.24, 22.71, 22.67, 14 ppm; elemental analysis: $\text{C}_{101}\text{H}_{166}\text{N}_2\text{O}_7$,

calculated: C, 79.79; H, 11; N, 1.84 % found: C, 79.91; H, 11.28; N, 1.96. ^1H NMR and ^{13}C NMR spectra are shown in the **Figure 8**.

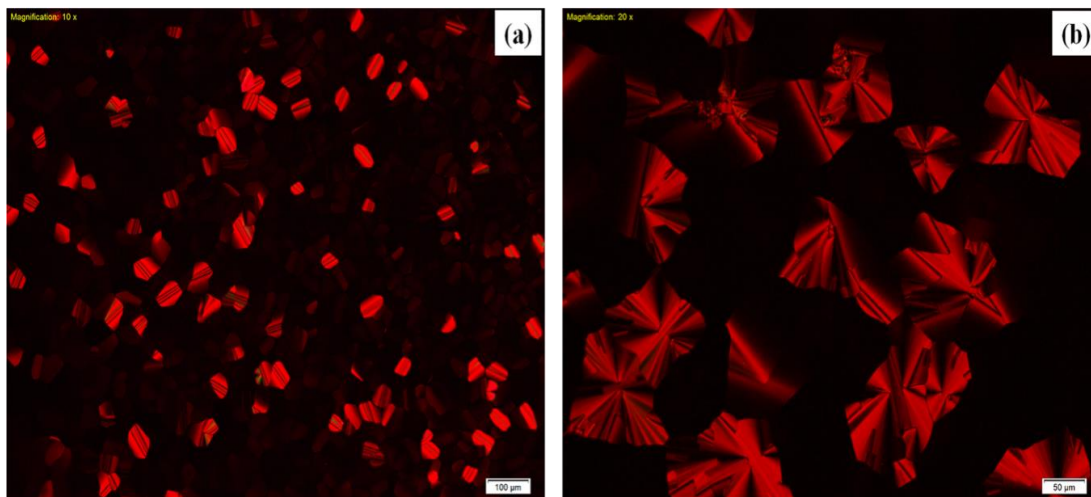


Figure 1. POM textures recorded in the hexagonal columnar phase, upon cooling from isotropic liquid. (a) Compound **2a** at 176 °C, viewed at 100 × magnifications, scale bar = 100 μm and (b) compound **2d** at 122 °C, and viewed at 200 × magnifications, scale bar = 50 μm respectively.

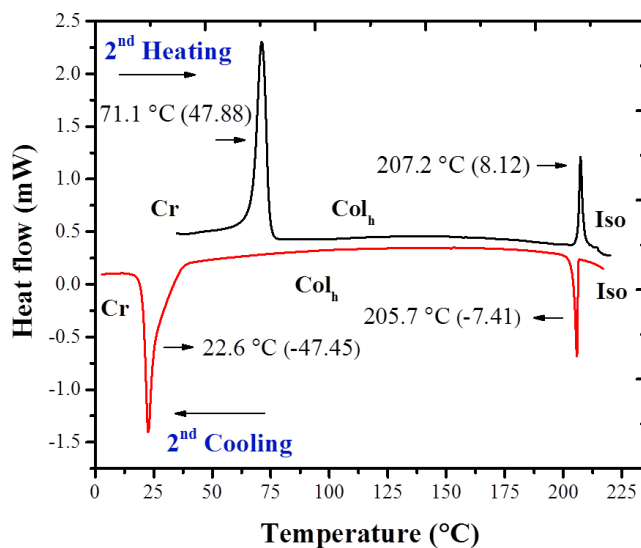


Figure 2. DSC thermogram obtained for compound **2b**.

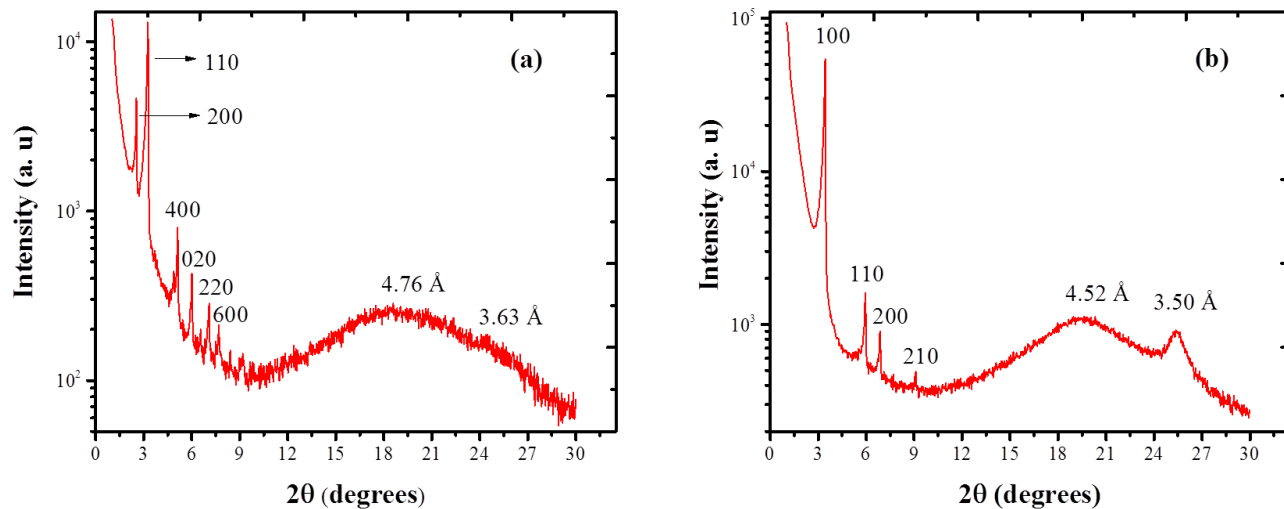


Figure 3. XRD diffractogram. (a) Acid derivative **1**, recorded at 120 °C on cooling in the Col_r phase. (b) Ester derivative **2e**, recorded at 70 °C on cooling in the Col_h phase.

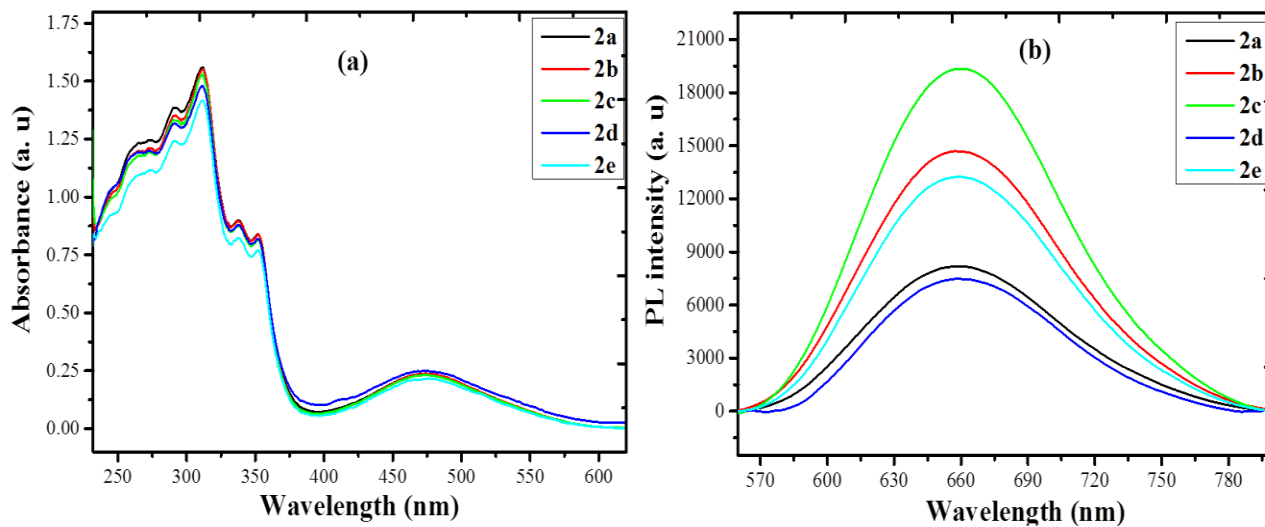


Figure 4. (a) UV-Visible absorption and (b) photoluminescence emission spectra of all the final compounds (**2a–2e**).

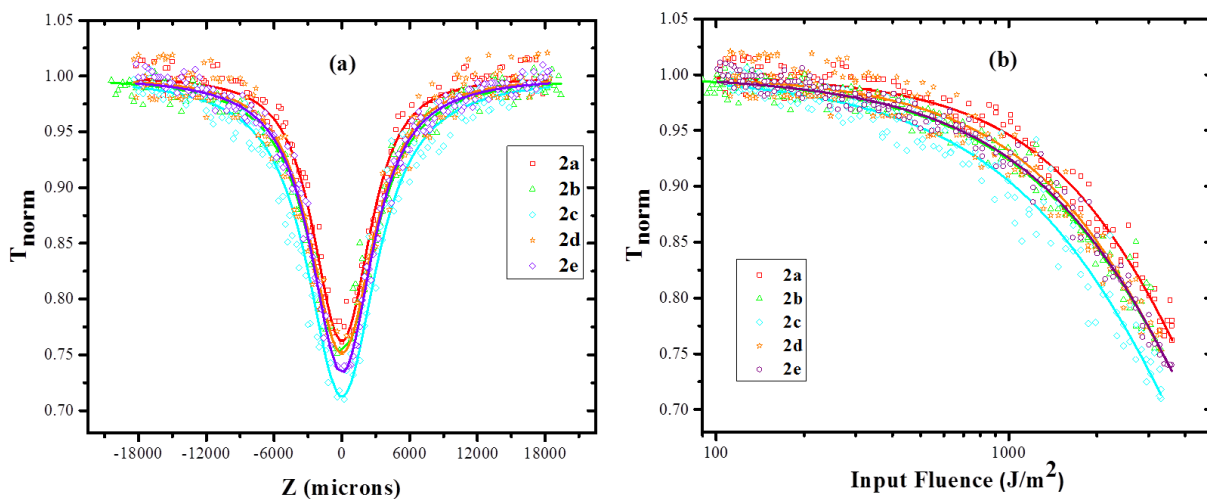


Figure 5. (a) Open aperture Z-scan curves for **2a–2e** compounds at energy of 3 μJ . Solid curves are numerical fits to the experimental data obtained using Eq. (4). (b) Normalized transmission as a function of input laser fluence, calculated from open aperture Z-scan measurements.

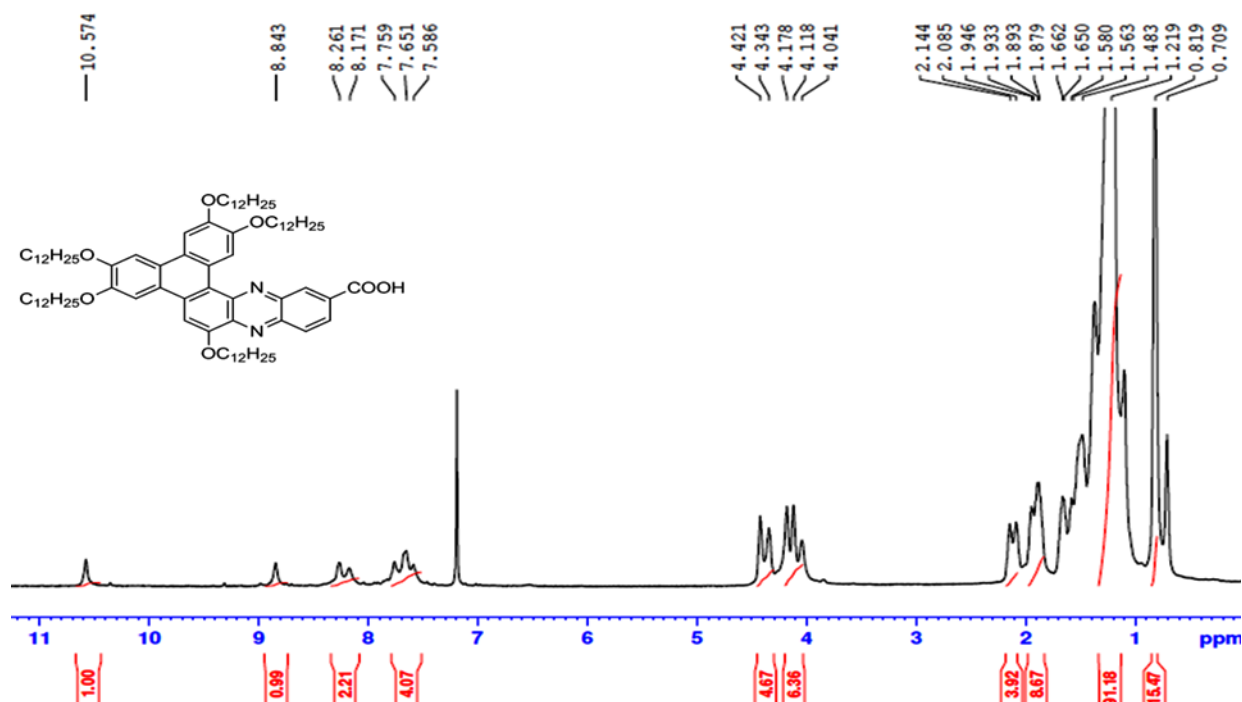


Figure 6. ^1H NMR of compound **1**.

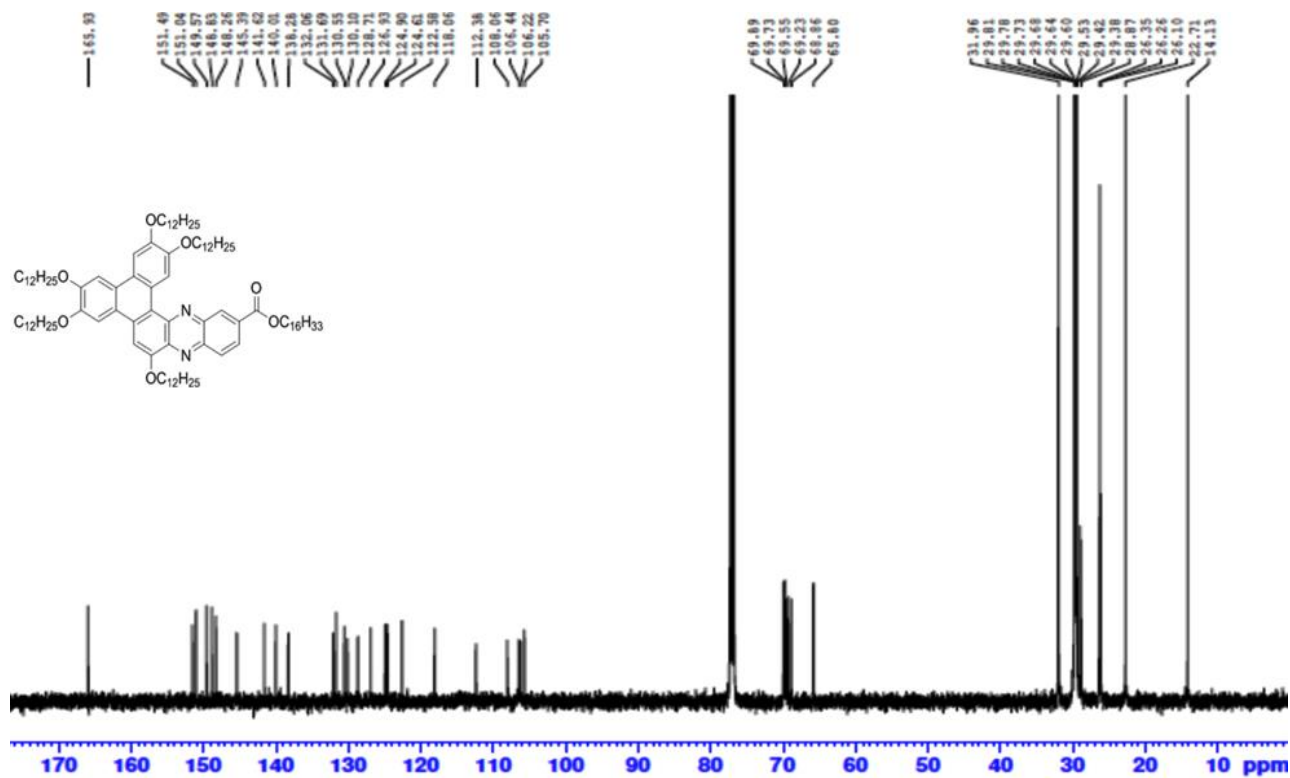
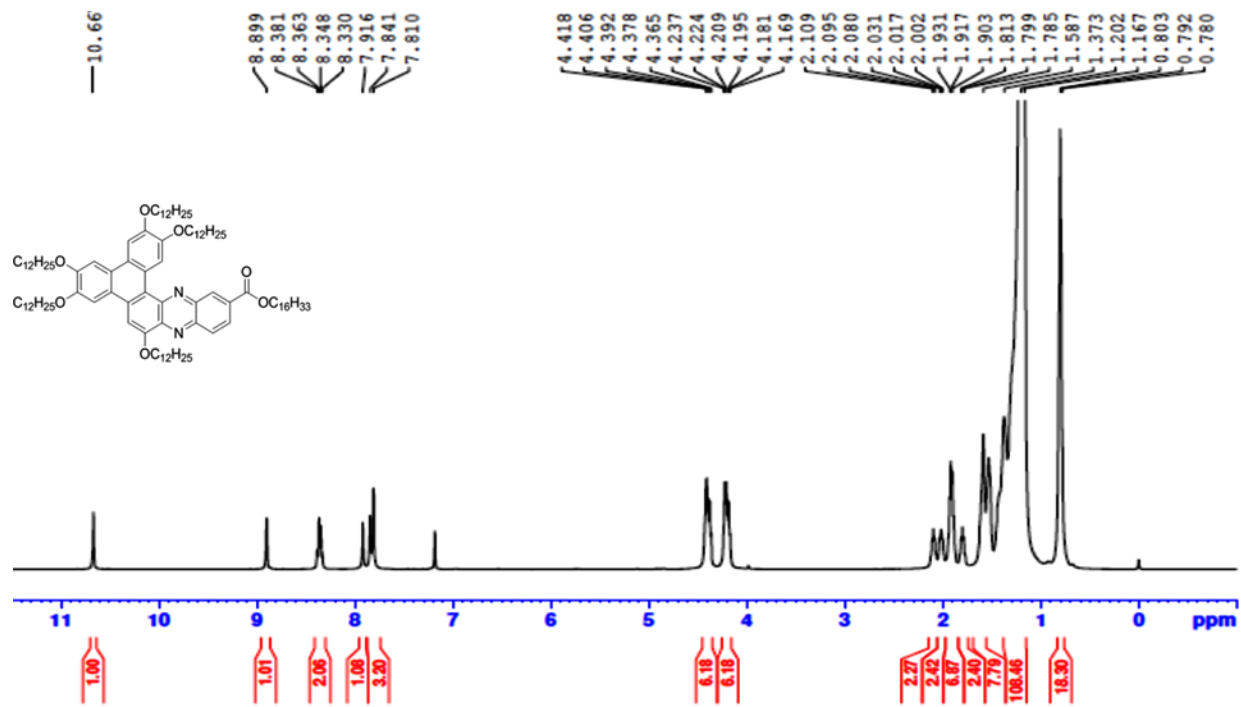


Figure 7. ¹H and ¹³C NMR of compound 2c.

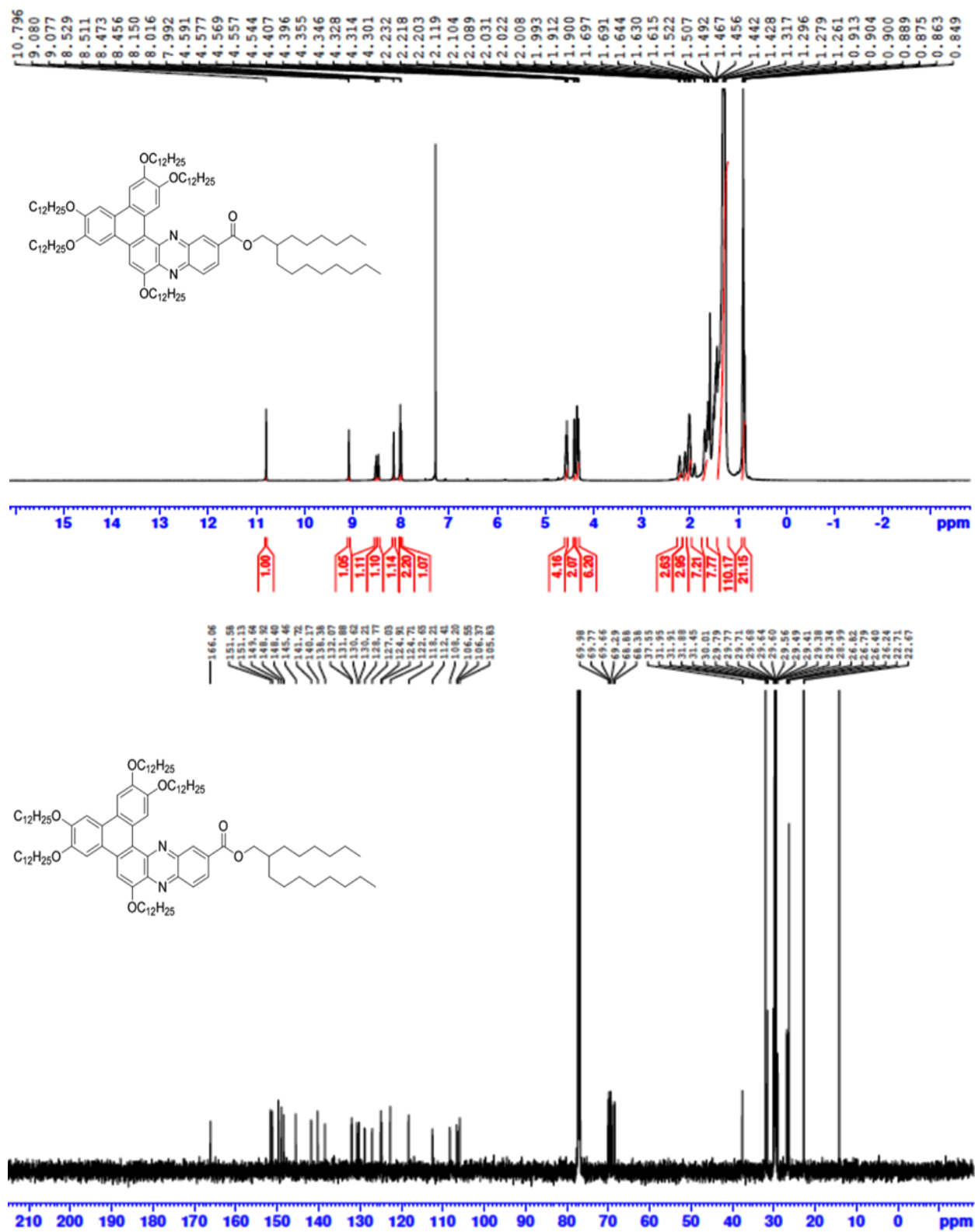
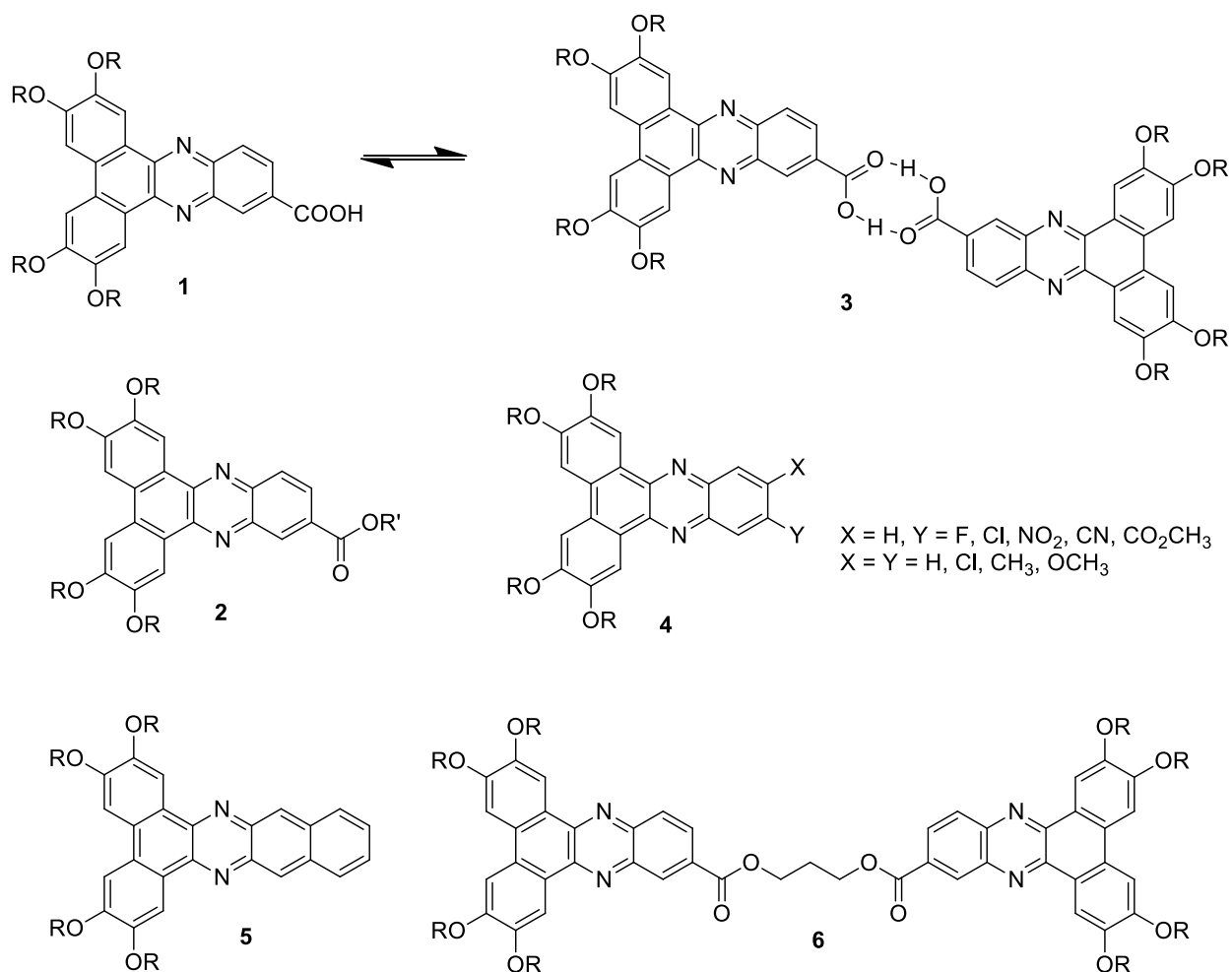


Figure 8. ¹H and ¹³C NMR of compound **2e**.

4.4 Part D. Synthesis, mesomorphic and photophysical properties of π -extended dibenzophenazine based discotic liquid crystals

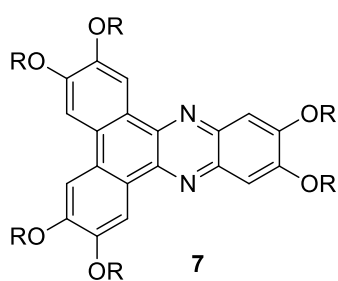
4.4.1 Introduction

Phenazine based heterocyclic compounds have found applications in material science and biological sciences [53]. A number of dibenzophenazine based DLCs have been prepared to understand structure–property relationship [52]. William et al. reported tetraalkoxy dibenzophenazine based discotic liquid crystals containing monomeric acid and ester derivatives (1 & 2). The acid derivatives form H-bonded elliptical shape dimer structure between two monomeric acid derivatives (3). These dimeric structures exhibit rich mesomorphic properties, displaying hexagonal, rectangular columnar and nematic phases over broad temperature range [52a]. The monomeric ester derivatives show only hexagonal columnar phase. The isotropic temperature of monomeric acid is much higher than corresponding ester derivatives; melting and clearing temperature decreases with increasing in alkyl chain length. They also prepared several tetraalkoxydibenzo[a,c]phenazine based DLCs containing electron donating and electron withdrawing functional groups present at the phenazine ring (4). Compounds with electron withdrawing functional groups (F, Cl, CN, CO₂CH₃) exhibit stable Col_h phase over broad temperature but phenazines containing electron donating groups do not show any liquid crystalline behaviour [52b]. The five ring systems are not liquid crystalline but the naphthalene derivatives 5 is mesomorphic. This implies that the large core size is favorable to form a columnar phase [52b]. Further, they also reported the detail investigation of position of functional groups such as acid, ester, nitro groups and mixed alkyl chains on mesomorphic properties of tetraalkoxydibenzo[a,c]phenazines [52c]. Recently, they successfully synthesised discotic mesogens derived from dibenzophenazine discotic dimer (6) linking through flexible alkyl chain to form double-decker architecture. The dimer exhibit folded conformation both in liquid crystal phase and solution [52d].

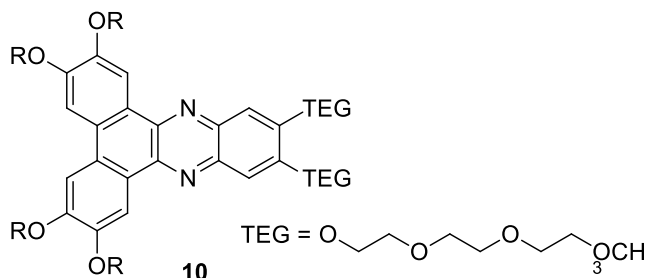
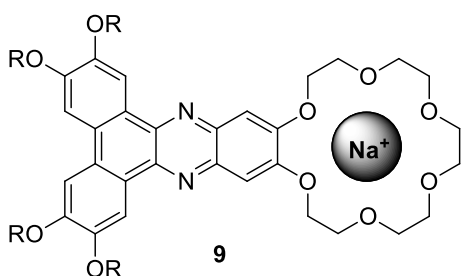
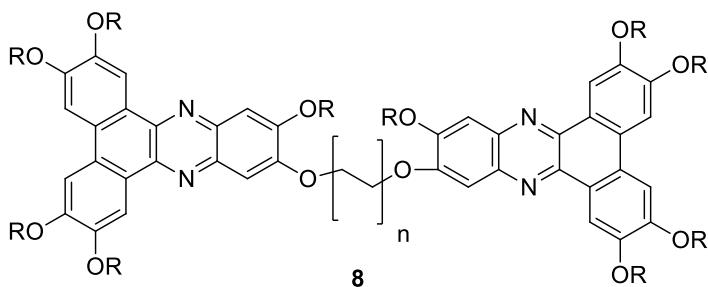


Ong and co-workers reported the synthesis and mesomorphic properties of hexaalkoxydibenzophenazine derivatives (**7**) which exhibit Col_h phase over broad temperature range [54a]. Further, dibenzophenazine based dimers (**8**) were synthesised, which exhibit folded conformation in the hexagonal columnar phase [54b]. They also reported tetraalkoxydibenzophenazines bearing lateral metal free crown ether which shows non-mesogenic behavior, however complexation with sodium metal crown ether exhibit rectangular columnar phase with C2mm symmetry (**9**) [54c]. Recently, they further demonstrated the hierarchical structure of tetraalkoxydibenzophenazines bearing amphiphilic chains (**10**) self assembles into 2-D hexagonal columnar phase. The compound **10** tends to align homeotropically on normal glass substrate over large area and could thus provide facile charge transfer path way perpendicular to substrate [54d].

Later, Paulina and co-workers investigated the gelation and photophysical properties of monomeric acid and corresponding monomeric methyl ester derivatives of dibenzophenazine (**1** & **2**, $R' = CH_3$) and diphenylquinoxaline based DLCs. The acid and ester derivatives of dibenzophenazine exhibit mesomorphic properties, however, acid and ester derivatives of diphenylquinoxaline do not form LC phase. The acid derivatives exhibit gelation properties in nonpolar solvents due to H-bonding [54e].

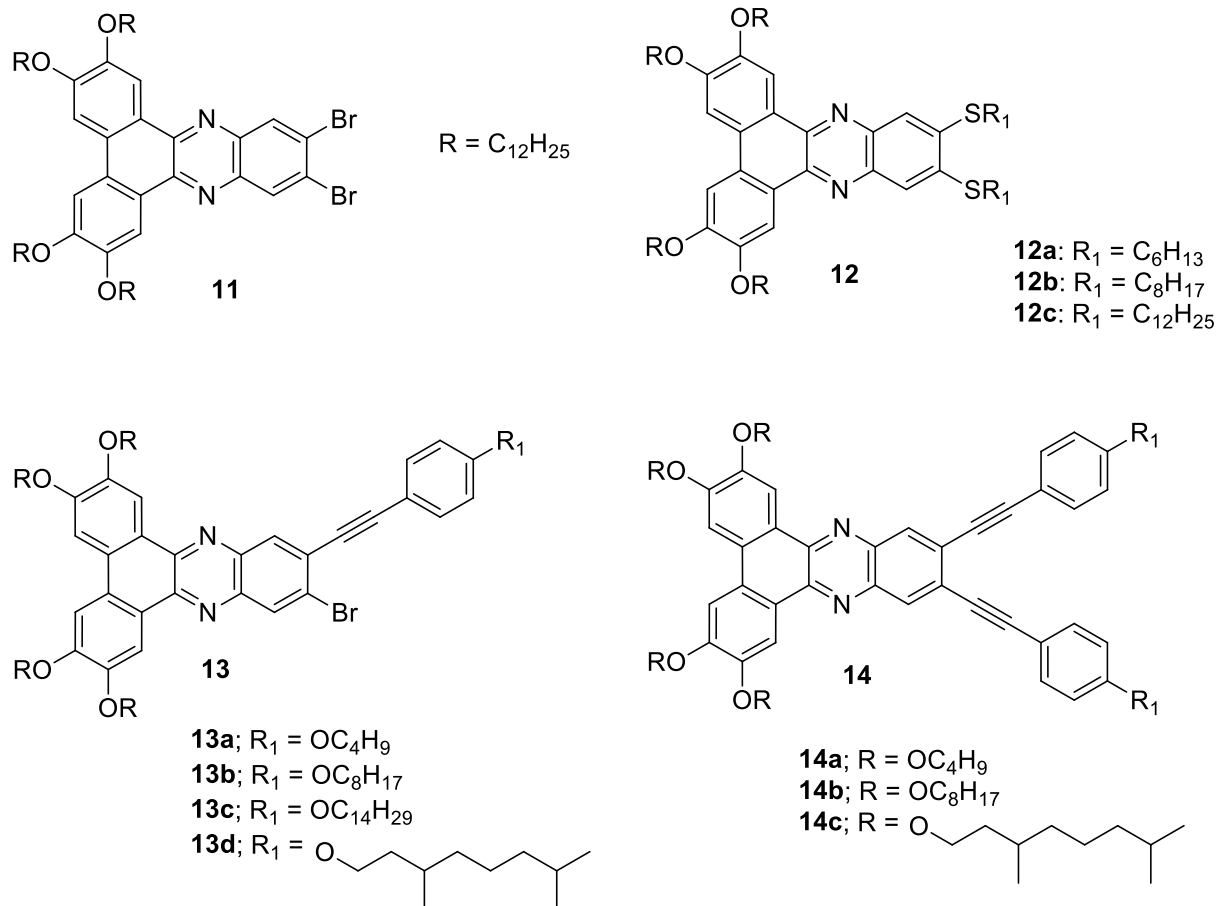


$R = C_nH_{2n+1}$ $n = 4, 6, 8, 10, 12$



4.4.2 Objective

In the last part of this chapter, we intend to prepare and characterize novel π -conjugated tetraalkoxydibenzophenazine based discotic mesogens tethered with dibromo (**11**), alkane thiols (**12**), mono phenylacetylene (**13**) and di phenylacetylene (**14**). This chapter presents the synthesis, characterization, mesomorphic and photophysical properties of these novel compounds.



4.4.3 Results and discussion

4.4.3.1 Synthesis

We designed and synthesised the dibenzophenazine based DLCs as shown in **Scheme 1**. The 1,2-bis(3,4-bis(dodecylperoxy)phenyl)ethane-1,2-dione intermediate **16** was synthesised following reported procedure [55] and it was condensed with 4,5-dibromobenzene-1,2-diamine **17** [39] in presence glacial acetic acid under reflux condition to afford tetraalkoxy substituted dibromoquinoxaline compound **4**. An intramolecular Scholl reaction was carried out in the presence of iron (III) chloride to furnish the tetraalkoxy substituted dibromo-dibenzophenazine key intermediate **11**. The reaction of alkane thiols with compound **11** in presence of cesium carbonate gives thiolated tetraalkoxydibenzo[a,c]phenazines (**12a–12c**) discotic liquid crystals. Further, Sonagashira coupling reaction of compound **11** with 4-alkoxy phenylacetylene [51a] in

All the intermediate and final compounds were purified from column chromatography and recrystallized from appropriate solvent to ensure maximum purity of the compounds. The molecular structures of all the compounds were characterized using IR, ^1H NMR and ^{13}C NMR and elemental analysis.

4.4.3.2 Thermal properties

Thermotropic liquid crystalline properties of all the intermediate and final dibenzophenazine DLCs derivatives are summarized in the **Table 1**. The phase transition temperature (peak temperature in $^{\circ}\text{C}$) and associated enthalpy (kJ mol^{-1}) values obtained from the heating and subsequent cooling cycles of respective mesogens were determined by DSC. The columnar textures of mesogens observed using the POM as shown in **Figure 1**.

The intermediate compound **11** was crystalline at room temperature and melts to mesophase at $103.1\text{ }^{\circ}\text{C}$ along with enthalpy of phase transition of 45.01 kJ mol^{-1} , which further transferred to isotropic liquid at $150.2\text{ }^{\circ}\text{C}$ ($\Delta H = 1.93\text{ kJ mol}^{-1}$). Upon cooling under POM, the appearance of dendritic texture revealed the formation of hexagonal columnar phase at $148.1\text{ }^{\circ}\text{C}$. The thiol substituted final mesogenic compounds (**12a–12c**) exhibit enantiotropic hexagonal columnar mesophase over broad temperature range. The compound **12a**, on heating melts at $55.1\text{ }^{\circ}\text{C}$ with phase transition enthalpy ($\Delta H = 62.55\text{ kJ mol}^{-1}$) to hexagonal columnar phase and become isotropic liquid at $121.1\text{ }^{\circ}\text{C}$ ($\Delta H = 5.01\text{ kJ mol}^{-1}$). On cooling from isotropic liquid, it exhibits Col_h phase transition at $118.4\text{ }^{\circ}\text{C}$ ($\Delta H = -4.85\text{ kJ mol}^{-1}$) in DSC scan and rectilinear defects texture was observed under POM. As a representative example of POM texture obtained for compound **12a** is shown in **Figure 1 (a)**. Further, compounds **12b** and **12c** also exhibit similar trends of phase transitions from crystalline phase to Col_h phase at $77.3\text{ }^{\circ}\text{C}$ ($\Delta H = 26.46\text{ kJ mol}^{-1}$) and $100.2\text{ }^{\circ}\text{C}$ ($\Delta H = 29.25\text{ kJ mol}^{-1}$) respectively and Col_h to isotropic liquid at $135.5\text{ }^{\circ}\text{C}$ ($\Delta H = 3.42\text{ kJ mol}^{-1}$) and $129.2\text{ }^{\circ}\text{C}$ ($\Delta H = 3.02\text{ kJ mol}^{-1}$) respectively. On cooling, Col_h phase transition was observed at $132.8\text{ }^{\circ}\text{C}$ ($\Delta H = -3.50\text{ kJ mol}^{-1}$) and $126.9\text{ }^{\circ}\text{C}$ ($\Delta H = -2.89\text{ kJ mol}^{-1}$) respectively. The DSC thermogram of representative compound **12c** is shown in **Figure 2a**.

Table 1. Phase transition temperature obtained from DSC (peak in DSC °C) and enthalpies (kJ mol⁻¹, in parentheses) of all the mesogens **11**, **12a–12c**, **13a–13d** and **14a–14c** (on heating and cooling cycle).

Compound	Phase transition (peak temperature (°C); (ΔH , [kJ mol ⁻¹]))	
	<i>second heating scan</i>	<i>second cooling scan</i>
11	Cr 103.1 [45.01] Col _h 150.2 [1.93] I	I 148.1 [-1.87] Col _h 74.1 [-42.29] Cr
12a	Cr 55.1 [62.55] Col _h 121.1 [5.01] I	I 118.4 [-4.85] Col _h 24.3 [-63.26] Cr
12b	Cr 77.3 [26.46] Col _h 135.5 [3.42] I	I 132.8 [-3.50] Col _h 45.32 [-27.27] Cr
12c	Cr 100.2 [29.25] Col _h 129.2 [3.02] I	I 126.9 [-2.89] Col _h 67.6 [-32.91] Cr
13a	Cr 73.7 [32.88] Col _h 174.7 [2.0] I	I 171.6 [-2.0] Col _h 9.7 [-18.12] Cr
13b	Cr 71.9 [25.63] Col _h 152.4 [0.92] I	I 148.9 [-0.96] Col _h 14.4 [-20.28] Cr
13c	Cr 79.6 [28.11] I	I 77.9 [-0.35] Col _h 39.6 [-29.38] Cr
13d	Cr 59.3 [25.33] Col _h 146.3 [1.18] I	I 143.4 [-1.14] Col _h 18.6 [-23.52] Cr
14a	Cr 82.1 [30.38] Col _h 181.1 [0.59] I	I 178.2 [-0.45] Col _h 55.4 [-32.38] Cr
14b	Cr 77.2 [29.37] Col _h 164.9 [0.94] I	I 161.5 [-0.89] Col _h 44.5 [-28.82] Cr
14c	Cr 60.1 [22.52] Col _h 158.9 [0.59] I	I 153.9 [-0.57] Col _h 30.5 [-21.72] Cr

The unsymmetrical substituted π -extended dibenzophenazine based DLCs (**13a–13d**) exhibit similar trends of phase transition from crystalline phase to Col_h at lower temperature and Col_h phase to isotropic phase at higher temperature. The compound **13a** melts to Col_h at 73.7 °C along with phase transition enthalpy 32.88 kJ mol⁻¹ and become isotropic liquid at 174.7 °C ($\Delta H = 2.0$ kJ mol⁻¹). The mesophase texture was observed upon slow cooling from isotropic liquid at 171.6 °C. As a representative example of POM texture obtained for compounds **13a** is shown in **Figure 1 (b)**. The compounds **13b** displayed similar phase transition from Cr to Col_h at 71.9 °C ($\Delta H = 25.63$ kJ mol⁻¹) and Col_h to isotropic phase at 152.4 °C ($\Delta H = 0.92$ kJ mol⁻¹). The appearance of columnar texture was observed under POM at 148.9 °C (on cooling) and become crystal phase at 14.4 °C. The higher homologous compound **13c** having tetradecane alkyl chain

show monotropic phase transition. Upon heating, compound **13c** directly transferred into isotropic phase at 79.6 °C ($\Delta H = 28.11 \text{ kJ mol}^{-1}$), however, upon cooling under POM exhibit dehydritic textures at 77.9 °C. The compound **13d** with branched alkyl chains displayed Cr to Col_h phase transition at 59.3 °C ($\Delta H = 25.33 \text{ kJ mol}^{-1}$), which become clear liquid at 146.3 °C ($\Delta H = 1.18 \text{ kJ mol}^{-1}$). On slow cooling from isotropic liquid under POM show appearance of dehydritic textures at 143.4 °C. On the other hand, the symmetrical substituted π -extended dibenzophenazine based DLCs (**14a–14c**) exhibit hexagonal columnar mesophase over broad temperature. The compounds **14a** and **14b** displayed Cr to Col_h phase at 82.1 °C ($\Delta H = 30.38 \text{ kJ mol}^{-1}$) and 77.2 °C ($\Delta H = 29.37 \text{ kJ mol}^{-1}$) respectively, which further transferred to isotropic liquid at 181.1 °C ($\Delta H = 0.59 \text{ kJ mol}^{-1}$) and 164.9 °C ($\Delta H = 0.94 \text{ kJ mol}^{-1}$) respectively. On slow cooling under POM exhibit appearance of columnar phase texture at 178.2 °C and 161.5 °C respectively. A representative DSC thermogram of compound **14b** is shown in **Figure 2(b)**. Similarly, the compound **14c** undergoes Cr to Col_h phase at 60.1 °C ($\Delta H = 22.52 \text{ kJ mol}^{-1}$) and become clear liquid at 158.9 °C ($\Delta H = 0.59 \text{ kJ mol}^{-1}$). On slow cooling under POM show the appearance of dehydritic textures at 153.9 °C and crystallize at around room temperature 30.5 °C.

4.4.3.4 X-ray diffraction measurements

The supramolecular self-assembly of dibenzophenazine based DLCs were investigated by X-ray diffraction studies using mesogenic compounds filled in a Lindemann capillaries. X-ray diffraction patterns were recorded for all the mesogens in the columnar mesophase on heating and cooling scan as shown in **Figure 3**. The diffraction parameters are summarized in **Table 2**. The mesogenic derivatives (**11**, **12a–12c**, **13a–13d** & **14a–14c**) exhibit increasing order of diffraction angle along with d -spacings of highest intensity peak in the small angle region to the second one are in the ratio of $1:1/\sqrt{3}:1/2$ respectively. These d -spacing values are obtained for the occurrence of hexagonal columnar phase. At wide angle regime, a diffuse peaks responsible for the packing arrangement of flexible molten aliphatic chains and a shoulder weak peak in the wide angle region is responsible for distance between discotic cores in the columns. The distance between adjacent columns in the mesophase was calculated using the relation $a = d_{10}/(\cos 30^\circ)$, where d_{10} is the d -spacing of highest intensity peak occurred in the small angle regime is shown

in **Table 2**. The XRD pattern obtained for intermediate compound **11** in the columnar phase is shown in **Figure 3a** (on heating). In the small angle region, three reflections were observed with corresponding d -spacings are $d_1 = 22.31 \text{ \AA}$, $d_2 = 12.81 \text{ \AA}$ and $d_3 = 11.34 \text{ \AA}$ observed with increasing order of diffraction angle. These values confirm the occurrence of two dimensional hexagonal columnar phase and the calculated lattice parameter, a , is found to be 25.76 \AA at $120 \text{ }^\circ\text{C}$ respectively. The broad halo peak ($d = 4.35 \text{ \AA}$) in the wide angle region obtained for the packing arrangement of molten aliphatic chains. The intercolumnar distance is estimated to be $a = 25.76 \text{ \AA}$ (**Figure 3a**) (**Table 2**). Similarly, the XRD pattern was recorded for alkyl thiol substituted tetraalkoxy dibenzophenazine DLCs (**12a–12c**). A representative and typical XRD pattern recorded for compound **12c** in the columnar phase at $90 \text{ }^\circ\text{C}$ upon cooling from isotropic liquid is shown in **Figure 3b**. The diffraction peaks observed in the small angle region with decreasing order of d -spacings $d_1 = 24.73 \text{ \AA}$, $d_2 = 14.33 \text{ \AA}$ and $d_3 = 12.41 \text{ \AA}$ along with lattice parameter $a = 28.55 \text{ \AA}$ corresponds to the two dimensional hexagonal columnar mesophase. The diffused peaks observed at wide angle region $d = 4.55 \text{ \AA}$ corresponding to the disordered packing of aliphatic chains and weak peak at $d = 3.46 \text{ \AA}$ corresponds to core-core separation. The distance between adjacent columns is found to be $a = 28.55 \text{ \AA}$ (**Table 2**). Similarly, the X-ray diffraction pattern observed for 4-alkoxy phenylacetylene substituted unsymmetrical tetraalkoxy dibenzophenazine DLCs (**13a–13d**). The representative X-ray diffraction pattern obtained for representative compound **13a** recorded at $120 \text{ }^\circ\text{C}$ in columnar phase upon cooling from isotropic liquid is shown in **Figure 3c**. The X-ray diffractogram shows several diffraction peaks in the small angle region with d -spacings of $d_1 = 23.51 \text{ \AA}$, $d_2 = 13.56 \text{ \AA}$ and $d_3 = 11.73 \text{ \AA}$ along with lattice parameter $a = 27.14 \text{ \AA}$ implies the occurrence of hexagonal columnar phase. The broad diffused peak at $d = 4.58 \text{ \AA}$ corresponds to packing arrangement of flexible aliphatic chains. The weak shoulder peak in wide angle region at $d = 3.47 \text{ \AA}$ is attributed to the core-core separation in the columns. The intercolumnar distance between neighbouring columns is found to be 27.14 \AA . Further, similar diffraction pattern observed for the symmetrical substituted 4-alkoxy phenylacetylene substituted tetraalkoxy dibenzophenazine DLCs (**14a–14c**). As a representative X-ray diffractogram recorded for **14c** compound at 110°C upon heating in the mesophase is shown in **Figure 3d**. In the small angle region three prominent diffraction peaks were observed with d - spacing's of $d_1 = 26.48 \text{ \AA}$, $d_2 = 15.28 \text{ \AA}$ and $d_3 = 13.25 \text{ \AA}$ along with lattice constant $a = 30.57 \text{ \AA}$ are expected from two dimensional hexagonal columnar phase. The

weak peak at wide angle regime with $d = 3.50 \text{ \AA}$ suggests the core-core separation in the columns. The intercolumnar distance between adjacent columns is estimated to be 30.57 \AA . From the above X-ray diffraction investigations reveals that, all the discotic mesogens (**11**, **12a–12c**, **13a–13d** & **14a–14c**) exhibit self-assembled hexagonal columnar mesophase structure where disc shape mesogens are stack on top of other to form columns surrounding by flexible aliphatic chains. It is apparent that the intercolumnar distance between adjacent columns varies depending on the central core structure and length of flexible chains.

Table 2. XRD data of discotic mesogens (**11**, **12a–12c**, **13a–13d** & **14a–14c**). a = on heating scan and b = on cooling scan, I_C = Intercolumnar distance, C–C = Core-core separation, R_L = Alkyl- chain length.

Compo und	Tempera ture ($^{\circ}\text{C}$) ^{a/b}	2θ (degre es)	d -spacings/ \AA observed (calculated)	Miller indexe s	Phase/ lattice constant	R_L (\AA)	C-C (\AA)	I_C (\AA)
11	120 ^a	3.96	22.31 (22.30)	100	Col_h	4.3	3.50	25.76
		6.90	12.81 (12.88)	110	$a = 25.76$			
		7.79	11.34 (11.15)	200				
12a	115 ^b	3.80	23.26 (23.25)	100	Col_h	4.47	3.48	26.85
		6.56	13.46 (13.42)	110	$a = 26.85$			
		7.58	11.66 (11.62)	200				
12b	85 ^a	3.70	23.91 (23.90)	100	Col_h	4.50	3.43	27.60
		6.40	13.79 (13.80)	110	$a = 27.60$			
		7.40	11.93 (11.95)	200				
12c	90 ^b	3.56	24.73 (24.72)	100	Col_h	4.55	3.46	28.55
		6.16	14.33 (14.27)	110	$a = 28.55$			
		7.11	12.41 (12.36)	200				

		3.75	23.51 (23.50)	100	Col _h				
13a	120 ^b	6.50	13.56 (13.57)	110	<i>a</i> = 27.14	4.58	3.47	27.14	
		7.53	11.73 (11.75)	200					
		3.67	24.06 (24.05)	100	Col _h				
13b	110 ^b	6.37	13.84 (13.89)	110	<i>a</i> = 27.78	4.40	3.48	27.78	
		7.35	12.03 (12.02)	200					
		3.59	24.55 (24.54)	100	Col _h	4.45	3.51	28.34	
13c	65 ^a	6.24	14.15 (14.17)	110	<i>a</i> = 28.34				
		7.21	12.24 (12.27)	200					
		3.59	24.60 (24.59)	100	Col _h				
13d	110 ^a	6.24	14.15 (14.20)	110	<i>a</i> = 28.40	4.63	3.46	28.40	
		7.21	12.24 (12.29)	200					
		3.56	24.73 (24.72)	100	Col _h				
14a	100 ^b	6.22	14.19 (14.27)	110	<i>a</i> = 28.55	4.52	3.50	28.55	
		7.19	12.27 (12.36)	200					
		3.41	25.87 (25.86)	100	Col _h				
14b	100 ^a	5.90	14.95 (14.93)	110	<i>a</i> = 29.87	4.65	3.48	29.87	
		6.82	12.94 (12.93)	200					
		3.33	26.48 (26.47)	100	Col _h				
14c	110 ^a	5.77	15.28 (15.28)	110	<i>a</i> = 30.57	4.84	3.50	30.57	
		6.66	13.25 (13.23)	200					

4.4.4 Photophysical properties

All the discotic mesogens (**12a–12c**, **13a–13d** & **14a–14c**) exhibit strong absorption and photo induced light emission properties. The UV-Vis absorption properties of all the mesogens were investigated in highly dilute solution (10^{-5} M) in chloroform solvent at ambient temperature to know absorption maxima as presented in **Figure 4** and corresponding absorption values are summarized in the **Table 3**. All the mesogens exhibit absorption bands below 465 nm. From

absorption spectra, it can be clearly seen that phenylacetylene substituted phenazine derivatives exhibit absorption at higher wavelength in comparison to alkylthiol derivatives. The observed red shift in the symmetrical and unsymmetrical phenylacetylene substituted phenazine derivatives can be attributed due to the presence of extended π -conjugation. The alkylthiol substituted phenazine (**12a–12c**) exhibit absorption bands at 451 nm, along with shoulder peak around 430 nm which corresponds to $n \rightarrow \pi^*$ and $\pi \rightarrow \pi^*$ transition. Similarly, the absorption bands were observed around 294–344 nm is attributed to the $\pi \rightarrow \pi^*$ transitions of aromatic rings. On the other hand, unsymmetrical substituted phenylacetylene derivatives (**13a–13d**) show bathochromic shift around 447 nm ($\epsilon = 1.98\text{--}3.77 \times 10^6 \text{ L mol}^{-1} \text{ cm}^{-1}$). Similarly, symmetrical substitution of 4-alkoxy phenylacetylene substituted phenazine derivatives (**14a–14c**) exhibit absorption at longer wavelength at 463nm with molar absorption coefficient ($\epsilon = 2.95\text{--}3.70 \times 10^6 \text{ L mol}^{-1} \text{ cm}^{-1}$) along with shoulder peak at 438 nm. Overall, the delocalization of π - electrons in symmetrical conjugated phenazine fused TP DLCs exhibit longer wavelength absorption along with high molar absorption coefficient.

Table 3. The photophysical properties of discotic mesogens (**12a–12c**, **13a–13d** & **14a–14c**) recorded in anhydrous chloroform solvent (10^{-5} M).

Compound	Absorption ($\lambda_{\text{max}}/\text{nm}$ ($\epsilon/10^6 \text{ L mol}^{-1} \text{ cm}^{-1}$))	Emission/nm
12a	294, 330, 344, 450 (2.0)	578
12b	297, 330, 344, 451 (2.35)	580
12c	296, 330, 344, 450 (2.77)	580
13a	295, 346, 447 (2.83)	601
13b	296, 346, 446 (1.98)	599
13c	296, 346, 446 (3.69)	597
13d	297, 346, 447 (3.77)	599
14a	301, 321, 359, 462 (3.70)	600
14b	300, 321, 359, 463 (3.41)	599
14c	301, 321, 359, 463 (2.95)	600

Similarly, photoluminescence emission spectra of all the mesogens (**12a–12c**, **13a–13d** & **14a–14c**) were recorded using dilute solution of anhydrous chloroform solvent at ambient temperature. The dilute solutions of discotic mesogens were excited at 450 nm and corresponding emission behaviour is shown in **Figure 4**. The thiol substituted discotic mesogens exhibit emission properties around 578–580 nm and symmetrical and unsymmetrical phenazine derivatives exhibit high emission properties around 597–600 nm respectively (**Table 3**).

4.4.5 Thermogravimetric analysis

The thermal studies of novel discotic mesogens were investigated by thermogravimetric analysis as shown in **Figure 5**. All the samples (**12a–12c**, **13a–13d** and **14a–14e**) were subjected to a heat scan of 10 °C min⁻¹ under a nitrogen atmosphere. The discotic mesogens (**12a–12c**) were thermally stable till 330 °C and initiated weight loss at about 330 °C –340 °C and decomposes at 485 °C. Similarly, symmetrical and unsymmetrical substituted phenazine discotic mesogens (**13a–13d** & **14a–14c**) were thermally stable upto 355 °C and initiated weight loss around 360–370 °C and decomposes at 510 °C. The decomposition temperature of π -extended discotic mesogens is greater than corresponding thiol substituted compounds. The results reveals that thermal stability of π - extended symmetrical an asymmetrical phenazine discotic (**13a–13d** & **14a–14c**) are high thermal stable in comparison with thiol substituted discotic mesogens (**12a–12c**) respectively (**Figure 5**). All the novel mesogens exhibit higher thermal stability than their isotropic temperature. This indicates that mesogens shows good thermal stability over broad temperature.

4.4.6 Conclusions

A number of novel dibenzophenazine discotic liquid crystals containing alkanethiols, alkoxy phenylacetylene and alkoxy chains are synthesized and characterised. All the mesogens self-assembled into hexagonal columnar phase. The mesomorphic properties were characterised using polarised optical microscopy and differential scanning calorimetry. The mesophase structure is investigated using X-ray diffraction method. All the π -extended mesogens exhibit

strong photoluminescence properties in the anhydrous chloroform solvent. The π -extended heteroaromatic discotic mesogens may play significant role in organic optoelectronic devices and solar cells applications.

4.4.7 Experimental section

The intermediate compounds 4,5-dibromobenzene-1,2-diamine (**17**) and 1-ethynyl-4-alkoxybenzene were synthesized as reported [**54,63b**] and confirmed by spectral and elemental analysis.

Synthesis of 1,2-bis(3,4-bis(dodecyloxy)phenyl)ethane-1,2-dione (16).

To a stirring suspension of anhydrous aluminum chloride (0.29g, 2.23 mmol) and 1,2-bis(dodecyloxy)benzene (2g, 4.47 mmol) in dry dichloromethane solvent (30 mL) was added drop wise solution of oxalyl chloride (0.34 g, 2.68 mmol) in dry dichloromethane solvent (10 mL) at 0 °C under nitrogen atmosphere. The resulting reaction mixture was stirred at the same temperature for 30 min and slowly allowed to reach room temperature and left for overnight. The reaction mixture was quenched into 1 M aqueous HCl solution and extracted with DCM solvent (3 × 20 mL). The combined extract was dried over Na₂SO₄ and concentrate under reduced pressure. The crude compound was purified by silica gel (*n*-hexane: ethyl acetate, 9:1) and recrystallization with ethanol gives pure compound **16** (Yield: 50 %). IR (film) ν_{\max} : 2918.40, 2906.82, 2852.81, 1664.62, 1583.61, 1462.09, 1377.2, 1265.35, 1074.39, 723.33 cm⁻¹; ¹H NMR (500 MHz, CDCl₃): δ = 7.56 (s, 1H), 7.42 (d, *J* = 8.5 Hz, 2H), 6.84 (d, *J* = 8 Hz, 2H), 4.05 (t, *J* = 6Hz, 8H), 1.83 (br, 8H), 1.46 (br, 8H), 1.35–1.26 (m, 64H), 0.88 ppm (t, *J* = 7Hz, 12H); ¹³C NMR (125 MHz, CDCl₃): δ = 193.78, 155.01, 149.33, 126.24, 126.09, 112.40, 111.65, 69.27, 69.14, 31.92, 29.70, 29.67, 29.65, 29.62, 29.58, 29.39, 29.36, 29.09, 28.94, 26, 25.93, 22.68, 14.10 ppm; elemental analysis: C₆₂H₁₀₆O₆, calculated: C, 78.59; H, 11.28. % found: C, 78.48; H, 11.09.

Synthesis of 2,3-bis(3,4-bis(dodecyloxy)phenyl)-6,7-dibromoquinoxaline (18).

Mixture of compound **16** (1g, 1.05 mmol) and 4,5-dibromobenzene-1,2-diamine **17** (0.28g, 1.06 mmol) were added glacial acetic acid solvent (20 mL) under nitrogen atmosphere. The resulting reaction mixture was refluxed for overnight. After completion of reaction, the reaction mixture was poured into ice cold water and extracted with DCM (3 × 20 mL). The organic layer was dried over Na₂SO₄ and concentrate under reduced pressure. The crude compound was purified by column chromatography using silica gel (*n*-hexane: ethyl acetate, 7:3) and recrystallization with ethanol gives pure compound **18**. Yield: 85 %. IR (film) ν_{\max} : 2949.26, 2920.32, 2899.11, 1600.97, 1518.03, 1454.38, 1377.22, 1269.20, 1139.7, 721.40 cm⁻¹; ¹H NMR (500 MHz, CDCl₃): δ = 8.42 (s, 1H), 7.08 (m, 4H), 6.82 (d, *J* = 8.5 Hz, 2H), 3.99 (t, *J* = 6.5Hz, 4H), 3.82 (t, *J* = 6.5Hz, 4H), 1.84–1.82 (m, 4H), 1.80–1.69 (m, 4H), 1.47–1.26 (m, 100H), 0.88 ppm (t, *J* = 6Hz, 15H); ¹³C NMR (125 MHz, CDCl₃): δ = 154.27, 150.33, 148.76, 140.23, 133, 131.06, 125.72, 122.92, 115.22, 113.06, 69.22, 69.18, 31.94, 31.80, 30.89, 30.04, 29.77, 29.71, 29.68, 29.66, 29.47, 29.43, 29.40, 29.38, 29.23, 29.15, 26.35, 26.04, 22.83, 22.70, 22.56, 14.11 ppm, elemental analysis: C₆₈H₁₀₈N₂Br₂O₆, calculated: C, 69.37; H, 9.25; N, 2.38. % found: C, 69.21; H, 9.05; N, 2.21.

Synthesis of 11,12-dibromo-2,3,6,7-tetrakis(dodecyloxy)dibenzo[a,c]phenazine (11).

To a stirring suspension of iron chloride (0.68g, 4.24 mmol) in dichloromethane solvent (20 mL) was added dropwise solution of compound **18** (1g, 0.84 mmol) in dichloromethane (10 mL) at 0 °C under nitrogen atmosphere and stirred at ambient temperature for 30 min. The reaction mixture was quenched with methanol and water. The resulting reaction mixture was extracted with dichloromethane (3 × 20 mL). The organic layer was dried over Na₂SO₄ and concentrated under reduced pressure. The crude compound was purified by column chromatography using silica gel (*n*-hexane: ethyl acetate, 7:3) gives desired compound **11**. Yield: 80 %. IR (film) ν_{\max} : 2926.11, 2914.54, 2895.25, 1606.76, 1454.38, 1377.22, 1271.13, 1168.90, 1072.46, 721.40 cm⁻¹; ¹H NMR (500 MHz, CDCl₃): δ = 8.45 (br, 4H), 7.49 (s, 2H), 4.15 (t, *J* = 6Hz, 8H), 1.90 (t, *J* = 6.5Hz, 8H), 1.61–1.52 (m, 8H), 1.38–1.20 (m, 64H), 0.80 ppm (t, *J* = 6.5Hz, 12H); ¹³C NMR (125 MHz, CDCl₃): δ = 152.09, 149.27, 142.36, 140.37, 132.89, 126.69, 124.79, 122.97, 108.55,

105.92, 69.46, 69.07, 31.95, 30.90, 29.78, 29.77, 29.75, 29.74, 29.71, 29.59, 29.40, 29.37, 26.24, 26.21, 22.70, 14.10 ppm, elemental analysis: C₆₈H₁₀₆N₂Br₂O₂, calculated: C, 69.49; H, 9.09; N, 2.38. % found: C, 69.37; H, 8.95; N, 2.26. ¹H and ¹³C NMR spectra are shown in the **Figure 6**.

Synthesis of 2,3,6,7-tetrakis(dodecyloxy)-11,12-bis(alkylthio)dibenzo[a,c]phenazine (12a–12c)

To a stirring solution of intermediate compound **11** (0.5 g, 1 equiv) and anhydrous cesium carbonate (5 equiv) in dry *N, N*-dimethylacetamide (DMAc) solvent (20 mL) was added alkanethiol (2.2 equiv). The resulting reaction mixture was refluxed for 24 h. After cooling to room temperature, ice cold water was added and extracted with dichloromethane solvent (3 × 20 mL). The combined extracts were dried over Na₂SO₄ and concentrated under reduced pressure gives crude compound. The residue was purified by column chromatography using silica gel (*n*-hexane/dichloromethane 9:1) which affords pure compound. Recrystallization of the pure product with cold ethanol gives final desired compound (**12a–12c**) in about 65% yield.

2,3,6,7-tetrakis(dodecyloxy)-11,12-bis(hexylthio)dibenzo[a,c]phenazine (12a): IR (film) ν_{\max} : 2953.12, 2922.25, 2852.81, 1608.69, 1508.38, 1454.38, 1377.22, 1271.13, 1166.97, 771.55 cm⁻¹; ¹H NMR (500 MHz, CDCl₃): δ = 8.63 (s, 2H), 7.90 (s, 2H), 7.62 (s, 2H), 4.25 (br, 4H), 4.18 (br, 4H), 3.11 (t, *J* = 7 Hz, 4H), 1.89 (br, 8H), 1.78 (m, 4H), 1.51 (br, 14H), 1.19 (br, 70H), 0.80 ppm (t, *J* = 6.5 Hz, 18H); ¹³C NMR (125 MHz, CDCl₃): δ = 151.58, 149.44, 141.12, 140.19, 140.03, 129.46, 126.65, 126.33, 124.28, 123.89, 108.53, 106.48, 69.65, 69.15, 33.42, 32.60, 31.94, 31.42, 31.38, 30.90, 30.01, 29.75, 29.71, 29.70, 29.55, 29.43, 29.39, 28.84, 28.70, 28.63, 28.25, 26.22, 26.18, 22.70, 22.55, 14.11, 14.04 ppm; elemental analysis: C₈₀H₁₃₂N₂O₄S₂, calculated: C, 76.87; H, 10.64; N, 2.24; S, 5.13, % found: C, 76.77; H, 10.56; N, 2.31; S, 4.91. ¹H and ¹³C NMR spectra are shown in the **Figure 7**.

2,3,6,7-tetrakis(dodecyloxy)-11,12-bis(octylthio)dibenzo[a,c]phenazine (12b): IR (film) ν_{\max} : 2953.12, 2920.32, 2852.81, 1608.69, 1504.53, 1462.09, 1377.22, 1271.13, 1166.97, 767.69 cm⁻¹; ¹H NMR (500 MHz, CDCl₃): δ = 8.65 (s, 2H), 7.92 (s, 2H), 2 (s, 2H), 4.27 (br, 4H), 4.19 (br, 4H), 3.13 (t, *J* = 7 Hz, 4H), 1.89 (br, 8H), 1.79 (m, 4H), 1.36 (br, 16H), 1.28–1.20 (m, 78H), 0.80

ppm (m, 18H); ^{13}C NMR (125 MHz, CDCl_3): δ = 151.61, 149.46, 141.17, 140.23, 140.07, 126.35, 124.34, 123.92, 108.56, 106.53, 69.66, 69.17, 33.45, 31.94, 31.82, 30.91, 29.75, 29.69, 29.54, 29.42, 29.39, 29.20, 29.19, 29.17, 28.29, 26.21, 26.18, 22.69, 14.11, 14.09 ppm; elemental analysis: $\text{C}_{84}\text{H}_{140}\text{N}_2\text{O}_4\text{S}_2$, calculated: C, 77.24; H, 10.80; N, 2.14; S, 4.91, % Found: C, 77.34; H, 10.96; N, 2.23; S, 5.06.

2,3,6,7-tetrakis(dodecyloxy)-11,12-bis(dodecylthio)dibenzo[a,c]phenazine (12c): IR (film) ν_{max} : 2953.12, 2918.40, 2850.88, 1608.69, 1510.31, 1462.09, 1377.22, 1271.13, 1166.97, 1074.39, 721.40 cm^{-1} ; ^1H NMR (500 MHz, CDCl_3): δ = 8.67 (s, 2H), 7.94 (s, 2H), 7.67 (s, 2H), 4.28 (br, 4H), 4.20 (br, 4H), 3.14 (t, J = 6.5 Hz, 4H), 1.89 (br, 8H), 1.81–1.78 (m, 4H), 1.36 (br, 14H), 1.28–1.99 (m, 94H), 0.80 ppm (br, 18H); ^{13}C NMR (125 MHz, CDCl_3): δ = 151.85, 151.60, 149.27, 141.83, 141.25, 140.58, 139.47, 132.06, 131.22, 130.39, 126.66, 126.16, 123.49, 108.59, 106.08, 69.52, 69.12, 69.03, 33.17, 29.78, 29.61, 29.41, 27.85, 22.71, 14.11 ppm; elemental analysis: $\text{C}_{92}\text{H}_{156}\text{N}_2\text{O}_4\text{S}_2$, calculated: C, 77.91; H, 11.09; N, 1.98; S, 4.52, % Found: C, 77.79; H, 11.25; N, 2.18; S, 4.65.

Synthesis of symmetrical and unsymmetrical dibenzophenazine based discotic mesogen (13a–13d & 14a–14c)

All the final discotic mesogens were obtained by Sonogashira C-C bond coupling reaction between 11,12-dibromo-2,3,6,7-tetrakis(dodecyloxy)dibenzo[a,c]phenazine (**11**) with 1-ethynyl-4-alkoxybenzene in the presence of $\text{PdCl}_2(\text{PPh}_3)_2$ and CuI in anhydrous triethylamine solvent. The general method is described as follows.

To a mixture of bis(triphenylphosphine) palladium dichloride ($\text{PdCl}_2(\text{PPh}_3)_2$) (0.04 eq.) and CuI (0.06 eq.) was added compound **11** (0.5 g, 1 eq.) in anhydrous triethylamine solvent under nitrogen atmosphere and allowed to stirring at room temperature for 10 mins. To the above reaction mixture, 1-ethynyl-4-(alkoxy)benzene (1.2 eq.) in anhydrous triethylamine was added under nitrogen flow. The resulting reaction mixture was heating to 75 °C for 24 h. The residue was diluted with diethyl ether and filtered through celite pad. The filtrate was washed with

excess of water and then extracted with diethyl ether (3×40 mL). The combined extracts were dried over Na_2SO_4 and concentrate under reduced pressure. The crude compound was purified by column chromatography using silica gel (hexane: ethylacetate 8:2) gives desired compound **13a–13d**. Similarly, symmetrical discotic mesogens (**14a–14c**) were obtained by using compound **11** (0.5g, 1 eq.), $\text{PdCl}_2(\text{PPh}_3)_2$ (0.08 eq.), CuI (0.09 eq.) and 1-ethynyl-4-(alkoxy)benzene (2.5 eq.) respectively.

11-bromo-12-((4-butoxyphenyl)ethynyl)-2,3,6,7-tetrakis(dodecyloxy)dibenzo[a,c] phenazine (13a): IR (film) ν_{max} : 2951.19, 2924.18, 2852.81, 2214.35, 1606.76, 1510.31, 1454.38, 1377.2, 1271.13, 1166.97, 773.48, 721.40 cm^{-1} ; ^1H NMR (500 MHz, CDCl_3): δ = 8.52–8.43 (m, 3 H), 8.34 (s, 1H), 7.61 (d, J = 8 Hz, 2H), 7.50 (d, J = 6 Hz, 2H), 6.95 (d, J = 8Hz, 2 H), 4.29–4.24 (br, 8 H), 4.03 (t, J = 5.5 Hz, 2 H), 2.0 (br, 8H), 1.83 (t, J = 6.5 Hz, 2H), 1.60–1.54 (m, 12 H), 1.46–1.30 (m, 62H), 1.03 (t, J = 6.5 Hz, 3H), 0.98 ppm (br, 12H); ^{13}C NMR (125 MHz, CDCl_3): δ = 159.82, 152, 151.89, 149.29, 149.25, 142.33, 142.04, 141.07, 139.95, 133.36, 132.70, 131.99, 126.70, 126.51, 125.88, 124.97, 123.28, 123.19, 114.68, 108.61, 106.05, 96.12, 87.13, 69.51, 69.08, 67.84, 31.95, 31.26, 29.78, 29.72, 29.60, 29.41, 26.24, 26.21, 22.70, 19.25, 14.11, 13.85 ppm; elemental analysis: $\text{C}_{80}\text{H}_{119}\text{N}_2\text{BrO}_5$, calculated: C, 75.73; H, 9.45; N, 2.21. % found: C, 75.66; H, 9.36, 2.29.

11-bromo-2,3,6,7-tetrakis(dodecyloxy)-12-((4-(octyloxy)phenyl)ethynyl)dibenzo [a,c] phenazine (13b): IR (film) ν_{max} : 2953.12, 2922.25, 2852.81, 2210.50, 1606.76, 1511.31, 1456.30, 1375.29, 1271.13, 1166.97, 771.55, 721.40 cm^{-1} ; ^1H NMR (500 MHz, CDCl_3): 8.38–8.33 (m, 3H), 8.22 (s, 1H), 7.58 (d, J = 7 Hz, 2H), 7.37 (br, 2H), 6.91 (d, J = 7 Hz, 2H), 4.21 (br, 8H), 3.99 (br, 2H), 1.96 (br, 8H), 1.81 (br, 2H), 1.61–1.28 (m, 94H), 0.86 ppm (br, 15H); ^{13}C NMR (125 MHz, CDCl_3): δ = 159.80, 151.89, 151.78, 149.15, 149.10, 142.16, 141.87, 140.95, 139.82, 133.35, 132.65, 131.92, 126.57, 126.38, 125.71, 124.82, 123.13, 123.03, 114.73, 114.68, 108.48, 105.81, 105.68, 87.17, 69.42, 69.38, 69.03, 68.17, 31.96, 31.84, 29.80, 29.74, 29.71, 29.65, 29.43, 29.26, 29.24, 26.27, 26.23, 26.06, 22.71, 22.68, 14.12 ppm; elemental analysis: $\text{C}_{84}\text{H}_{127}\text{N}_2\text{BrO}_5$, calculated: C, 76.15; H, 9.66; N, 2.11. % found: C, 76.26; H, 9.78, N, 2.23.

11-bromo-2,3,6,7-tetrakis(dodecyloxy)-12-((4-(tetradecyloxy)phenyl) ethynyl)dibenzo [a,c] phenazine (13c): IR (film) ν_{\max} : 2953.12, 2920.32, 2866.32, 2216.28, 1606.76, 1506.46, 1456.30, 1377.22, 1271.13, 1168.90, 771.55, 721.40 cm^{-1} ; ^1H NMR (500 MHz, CDCl_3): 8.53–8.49 (br, 2H), 8.43 (s, 1H), 8.34 (s, 1H), 7.58 (d, $J = 8$ Hz, 2H), 7.51 (s, 1H), 6.92 (d, $J = 8$ Hz, 2H), 4.25 (br, 8H), 3.99 (t, $J = 6$ Hz, 2H), 2.01–1.93 (m, 8H), 1.84–1.78 (m, 2H), 1.47–1.27 (m, 94H), 0.88 ppm (t, $J = 6.5$ Hz, 15H); ^{13}C NMR (125 MHz, CDCl_3): $\delta = 159.82, 152, 151.89, 149.25, 142.04, 141.07, 139.95, 133.36, 132.68, 131.98, 126.70, 126.50, 125.88, 124.98, 123.27, 123.19, 114.68, 114.68, 108.57, 106.06, 96.13, 87.13, 69.48, 69.07, 68.18, 31.95, 29.78, 29.72, 29.61, 29.41, 29.37, 29.23, 26.24, 26.05, 22.70, 14.11$ ppm; elemental analysis: $\text{C}_{90}\text{H}_{139}\text{N}_2\text{BrO}_5$, calculated: C, 76.72; H, 9.94; N, 1.99. % found: C, 76.84; H, 10.10; N, 2.13.

11-bromo-12-((4-((3,7-dimethyloctyl)oxy)phenyl)ethynyl)-2,3,6,7-tetrakis(dodecyloxy) dibenzo [a,c]phenazine (13d): IR (film) ν_{\max} : 2951.19, 2922.25, 2852.81, 2210.50, 1608.69, 1506.46, 1456.30, 1375.29, 1271.13, 1168.90, 771.55, 721.40 cm^{-1} ; ^1H NMR (500 MHz, CDCl_3): 8.40–8.23 (m, 3H), 8.23 (s, 1H), 7.51 (d, $J = 7.5$ Hz, 2H), 7.38 (br, 2H), 6.85 (d, $J = 7.5$ Hz, 2H), 4.16 (m, 8H), 3.97 (br, 2H), 1.90 (m, 8H), 1.53–1.20 (m, 82H), 0.90 (d, $J = 6$ Hz, 3H), 0.81 ppm (br, 18H); ^{13}C NMR (125 MHz, CDCl_3): $\delta = 159.80, 151.98, 151.87, 149.26, 149.22, 142.30, 142.01, 141.06, 139.93, 133.36, 132.69, 131.98, 126.68, 126.48, 125.85, 124.94, 126.26, 123.16, 114.69, 108.58, 106, 105.89, 96.11, 87.14, 69.49, 69.45, 69.07, 66.51, 39.27, 37.33, 36.15, 31.96, 29.90, 29.78, 29.75, 29.72, 29.62, 29.41, 27.99, 26.25, 26.21, 24.68, 22.71, 22.61, 19.67, 14.11$ ppm; elemental analysis: $\text{C}_{86}\text{H}_{131}\text{N}_2\text{BrO}_5$, calculated: C, 76.35; H, 9.76; N, 2.07. % found: C, 76.25; H, 9.64; N, 1.98. ^1H and ^{13}C NMR spectra are shown in the **Figure 8**.

11,12-bis((4-butoxyphenyl)ethynyl)-2,3,6,7-tetrakis(dodecyloxy)dibenzo[a,c]phenazine (14a): IR (film) ν_{\max} : 2955.04, 2922.25, 2852.81, 2216.28, 1606.76, 1506.46, 1456.30, 1377.22, 1269.20, 1168.90, 771.55, 721.40 cm^{-1} ; ^1H NMR (500 MHz, CDCl_3): 8.62 (br, 2H), 8.39 (br, 2H), 7.59 (d, $J = 8$ Hz, 6H), 6.93 (d, $J = 8$ Hz, 4H), 4.32–4.26 (m, 8H), 4.03 (t, $J = 6.5$ Hz, 4H), 1.99 (t, $J = 6$ Hz, 8H), 1.83 (t, $J = 6.5$ Hz, 4H), 1.63–1.30 (m, 77H), 1.03 (t, $J = 7$ Hz, 6H), 0.89 ppm (br, 12H); ^{13}C NMR (125 MHz, CDCl_3): $\delta = 159.61, 151.88, 149.36, 142.23, 140.73,$

133.34, 131.85, 126.57, 125.83, 123.59, 115.15, 114.65, 108.69, 106.23, 95.39, 87.20, 69.57, 69.10, 67.83, 31.94, 31.28, 29.77, 29.71, 29.58, 29.40, 26.20, 22.70, 19.25, 14.11, 13.85 ppm; elemental analysis: C₉₂H₁₃₂N₂O₆, calculated: C, 81.13; H, 9.77; N, 2.06. % found: C, 81.26; H, 9.86; N, 2.18.

2,3,6,7-tetrakis(dodecyloxy)-11,12-bis((4-(octyloxy)phenyl)ethynyl)dibenzo[a,c] phenazine

(14b): IR (film) ν_{\max} : 2953.12, 2924.18, 2852.81, 2208.57, 1606.76, 1507.16, 1456.30, 1377.22, 1247.99, 1168.90, 769.62, 721.40 cm⁻¹; ¹H NMR (500 MHz, CDCl₃): 8.56 (br, 2H), 8.33 (br, 2H), 7.57–7.52 (m, 6H), 6.90 (d, *J* = 7 Hz, 4H), 4.29–4.22 (m, 8H), 3.99 (br, 4H), 1.97 (br, 8H), 1.81 (br, 4H), 1.59–1.27 (m, 104H), 0.88 ppm (br, 18H); ¹³C NMR (125 MHz, CDCl₃): δ = 159.61, 151.83, 149.28, 142.15, 140.69, 133.33, 131.84, 126.54, 125.78, 123.50, 115.15, 114.65, 108.64, 106.14, 95.37, 87.21, 69.54, 69.09, 68.16, 31.95, 31.83, 29.77, 29.74, 29.72, 29.60, 29.40, 29.39, 29.25, 26.22, 26.20, 26.06, 22.70, 22.67, 14.10 ppm; elemental analysis: C₁₀₀H₁₄₈N₂O₆, calculated: C, 81.47; H, 10.12; N, 1.90. % found: C, 81.59; H, 10.23; N, 2.09. ¹H and ¹³C NMR spectra are shown in the **Figure 9**.

11,12-bis((4-((3,7-dimethyloctyl)oxy)phenyl)ethynyl)-2,3,6,7-tetrakis(dodecyloxy)dibenzo [a,c]

phenazine (14c): IR (film) ν_{\max} : 2953.12, 2920.32, 2852.81, 2218.21, 1606.76, 1506.11, 1456.30, 1377.22, 1246.06, 1168.90, 771.55, 721.40 cm⁻¹; ¹H NMR (500 MHz, CDCl₃): 8.44 (br, 2H), 8.25 (br, 2H), 7.57 (d, *J* = 7.5 Hz, 4H), 7.39 (br, 2H), 6.90 (d, *J* = 7.5 Hz, 4H), 4.26–4.19 (m, 8H), 4.03 (d, *J* = 5.5 Hz, 4H), 1.98–1.86 (m, 10H), 1.70–1.55 (m, 17H), 1.45–1.19 (m, 71H), 0.97 (m, 6H), 0.88 ppm (br, 24H); ¹³C NMR (125 MHz, CDCl₃): δ = 159.57, 151.72, 149.13, 141.96, 140.56, 133.34, 131.84, 126.41, 125.60, 123.33, 115.23, 114.65, 108.51, 105.84, 95.26, 87.29, 69.43, 69.05, 66.49, 39.28, 37.35, 36.20, 31.97, 29.92, 29.80, 29.74, 29.66, 29.48, 29.43, 28, 26.27, 26.23, 24.69, 22.72, 22.62, 19.68, 14.12 ppm; elemental analysis: C₁₀₄H₁₅₆N₂O₆, calculated: C, 81.62; H, 10.27; N, 1.83. % found: C, 81.88; H, 10.41, 2.01.

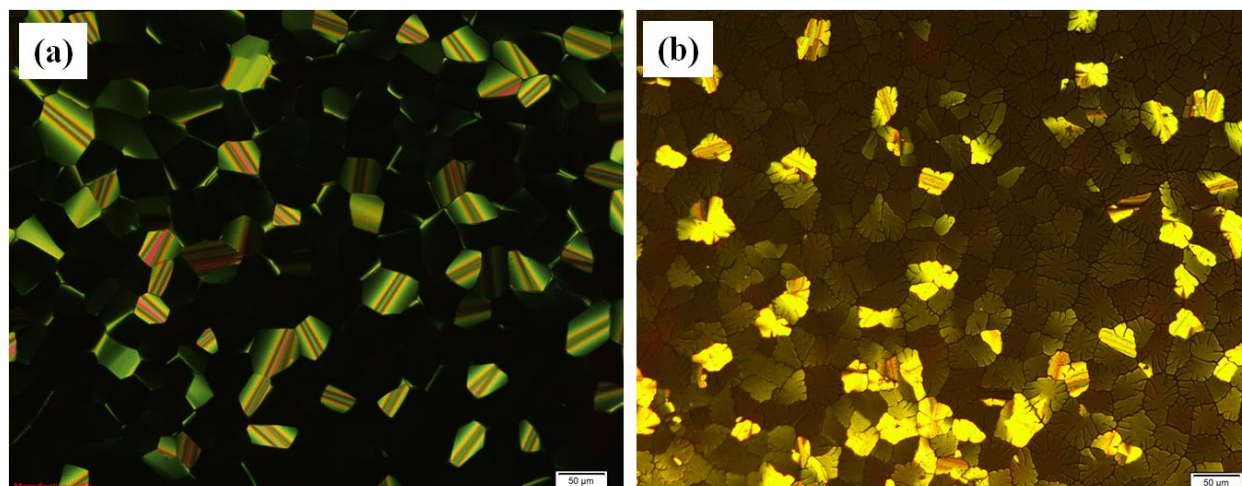


Figure 1. POM textures taken in hexagonal columnar phase, upon cooling from isotropic melt. (a) Compound **12a**, recorded at 109 °C, viewed at 200 × magnifications. (b) Compound **13a**, recorded at 157 °C, viewed at 200 × magnifications.

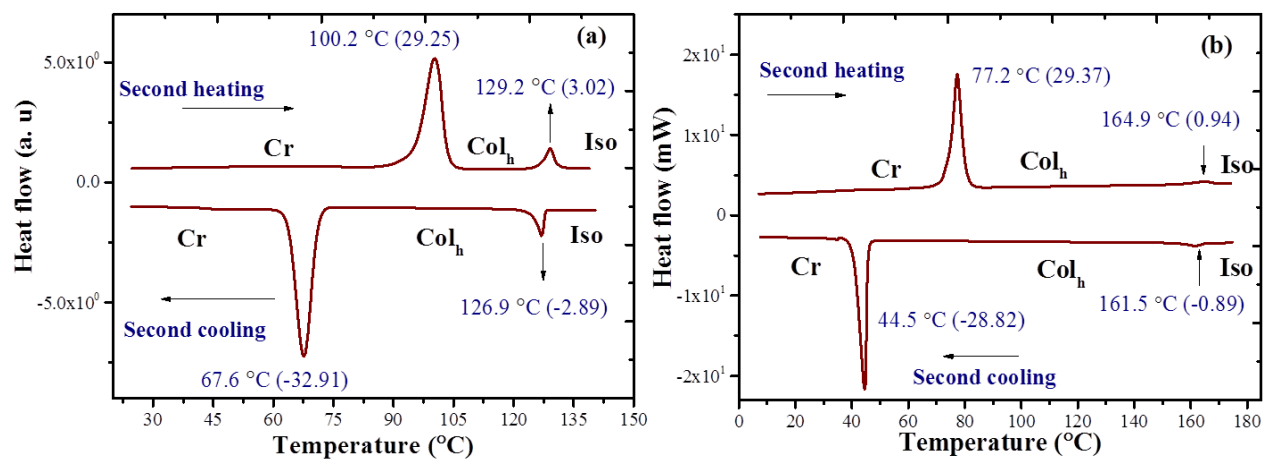


Figure 2. DSC thermograms of (a) compound **12c** and (b) compound **14b** respectively.

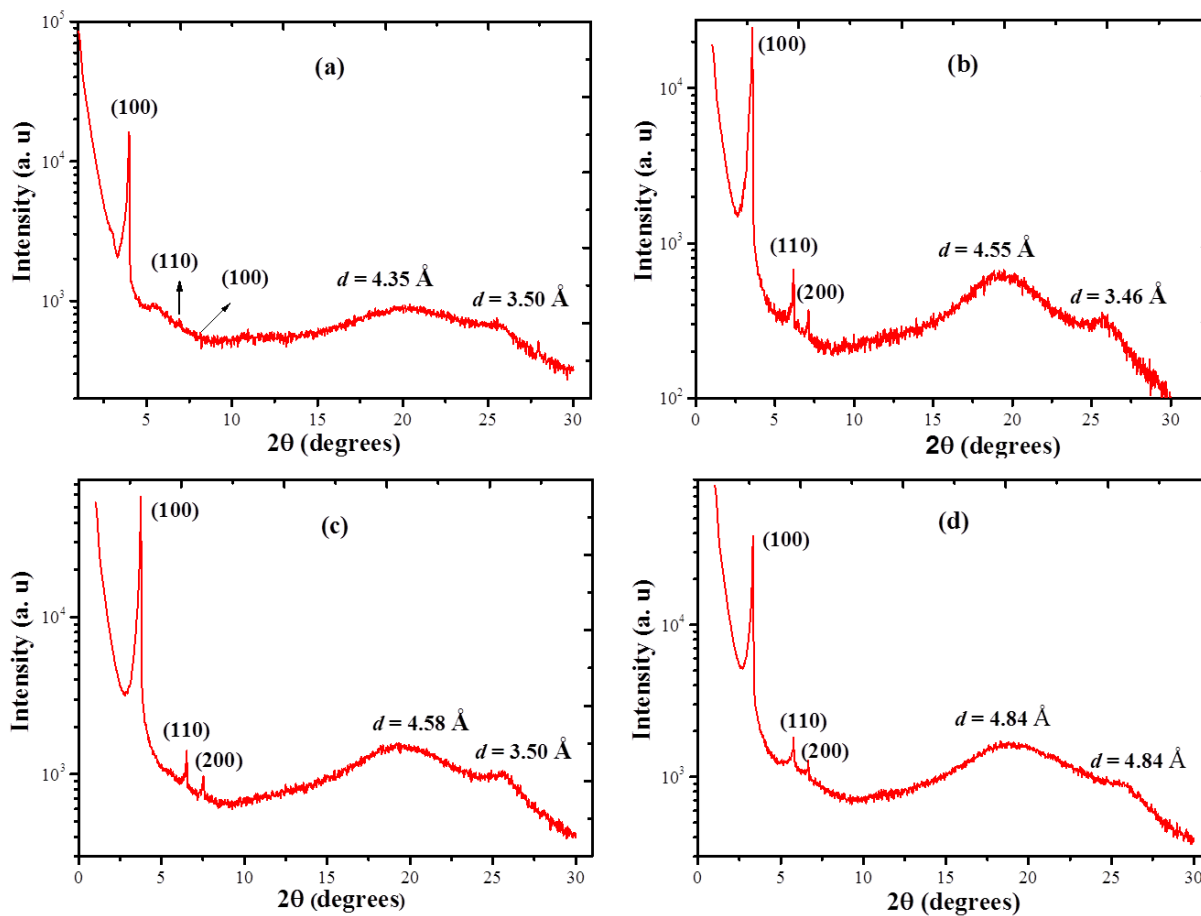


Figure 3. XRD profiles showing the intensity against the 2θ recorded in the Col_h phase. (a) Compound **11**, recorded at 120 °C, on heating scan. (b) Compound **12c**, recorded at 90 °C, on cooling scan. (c) Compound **13a**, recorded at 120 °C, on cooling scan. (d) Compound **14c**, recorded at 110 °C, on heating scan.

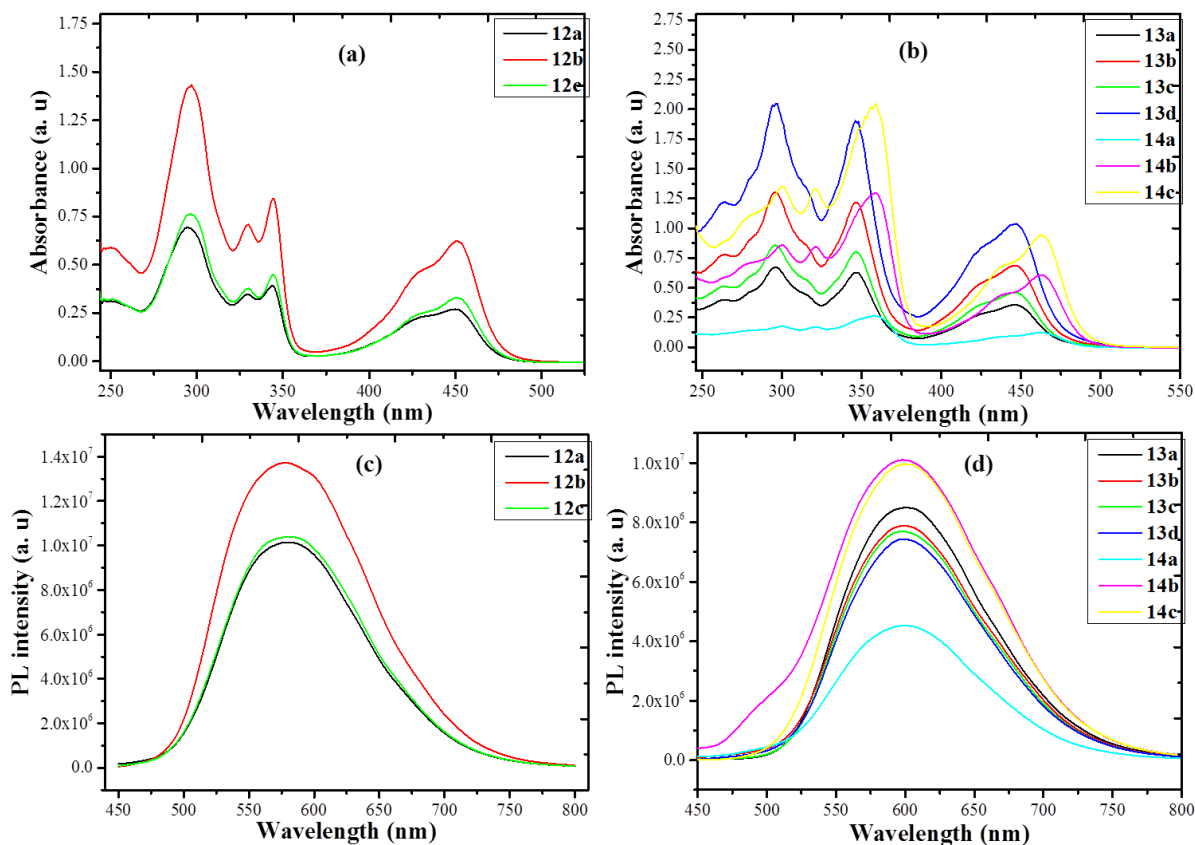


Figure 4. (a) and (b) UV-Vis absorption spectra; (c) and (d) photoluminescence emission spectra of all the discotic mesogens (12a–12c, 13a–13d & 14a–14c) respectively.

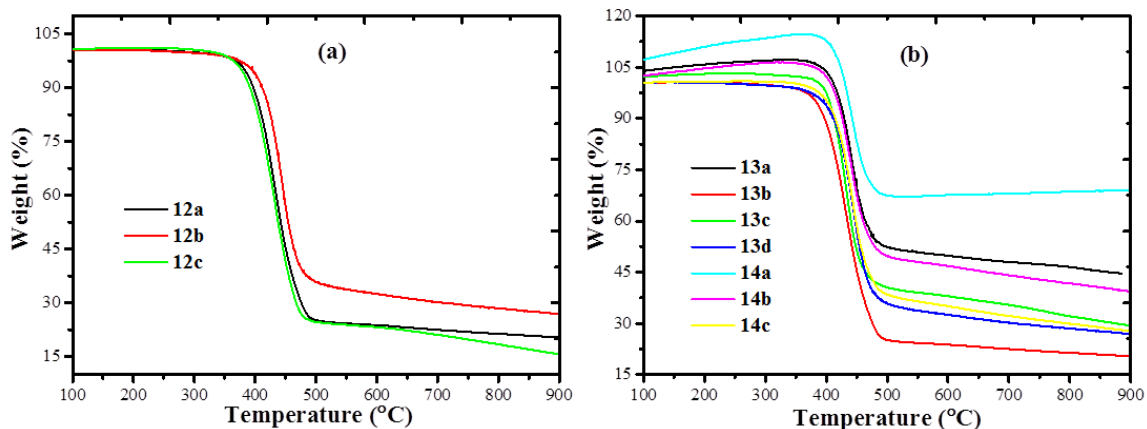


Figure 5. Thermogravimetric analysis: (a) compounds 12a–12c. (b) compounds 13a–13d & 14a–14c).

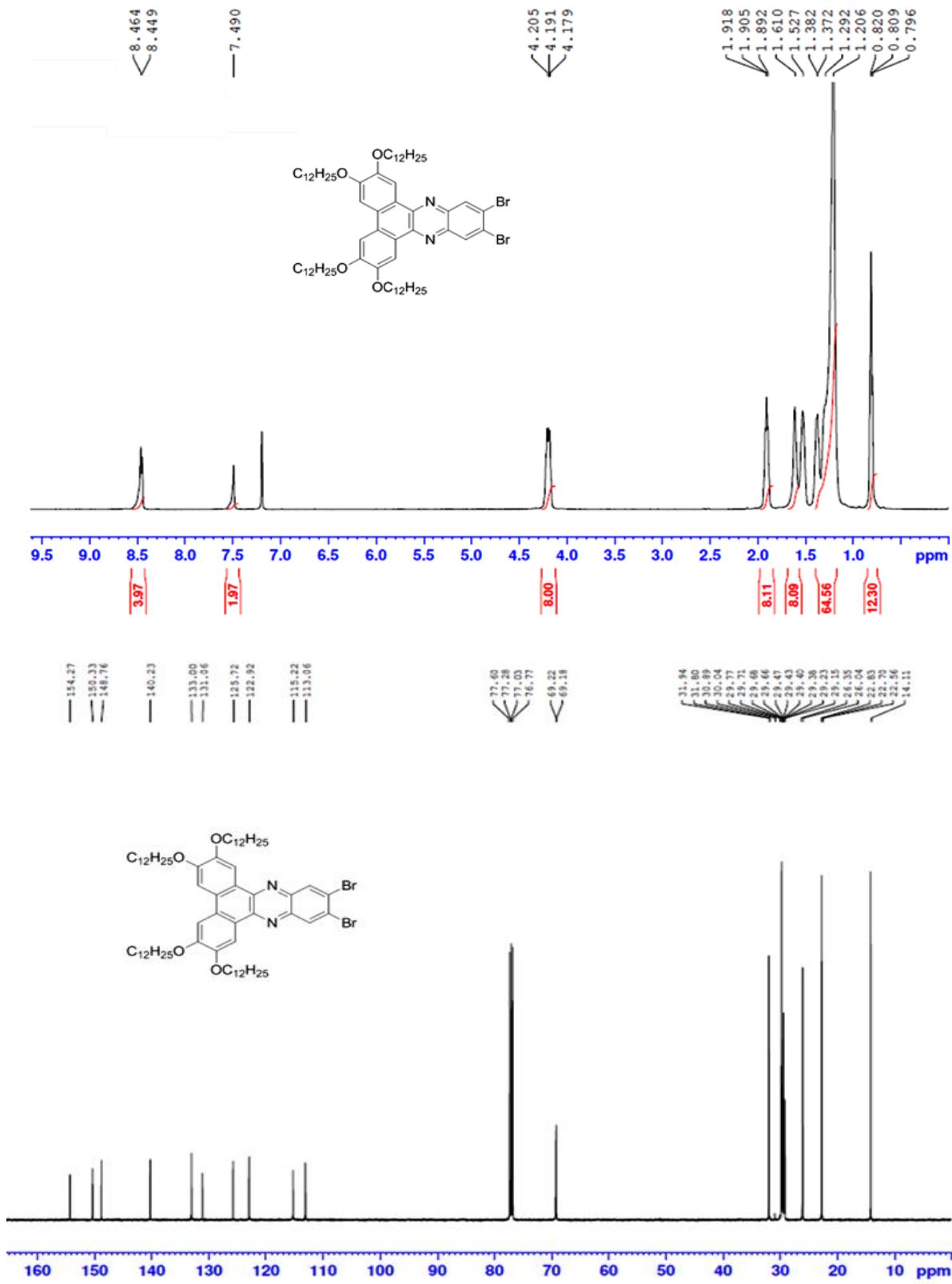


Figure 6. ¹H and ¹³C NMR spectra of compound 11.

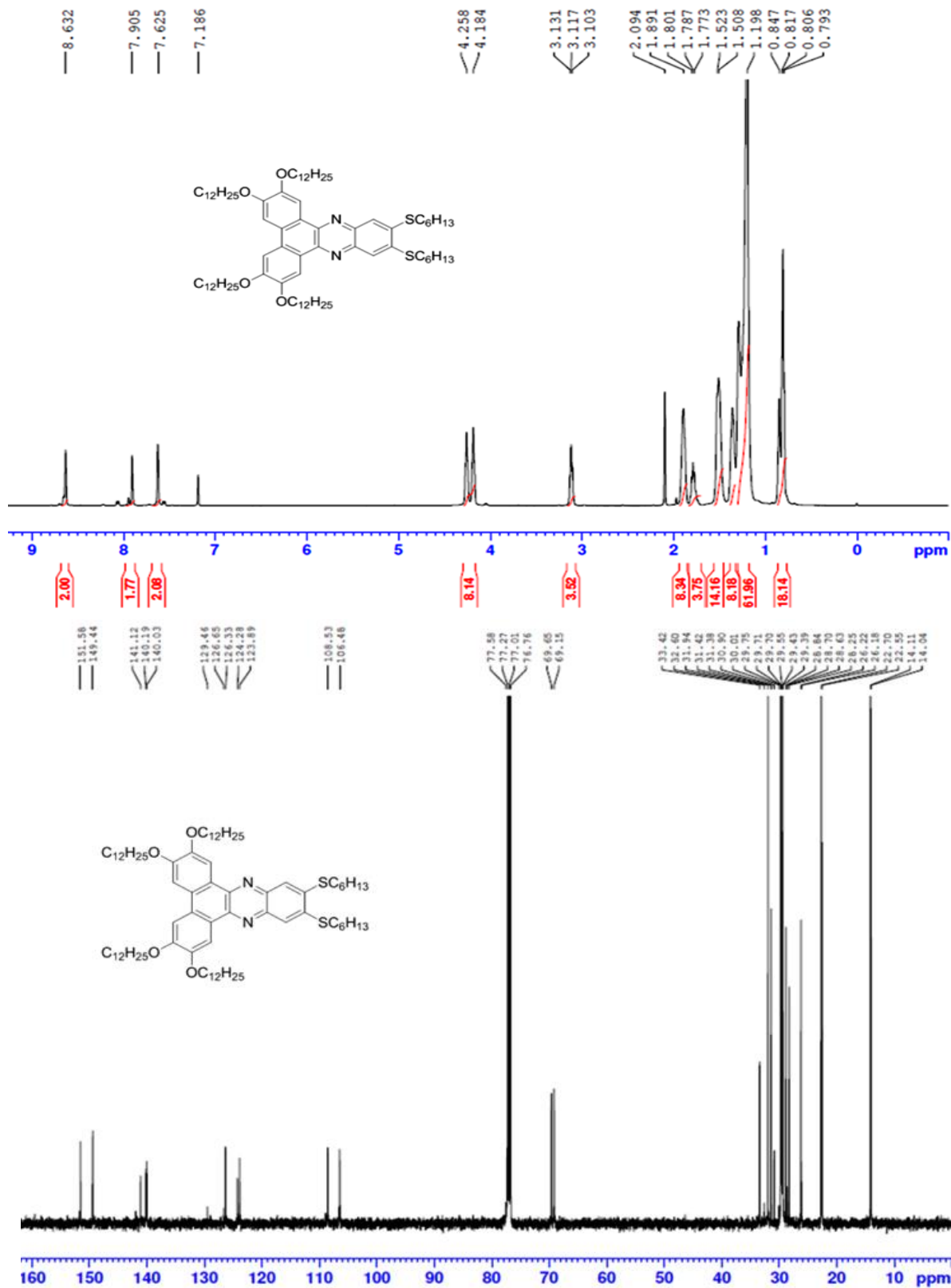


Figure 7. ¹H and ¹³C NMR spectra of compound 12a.

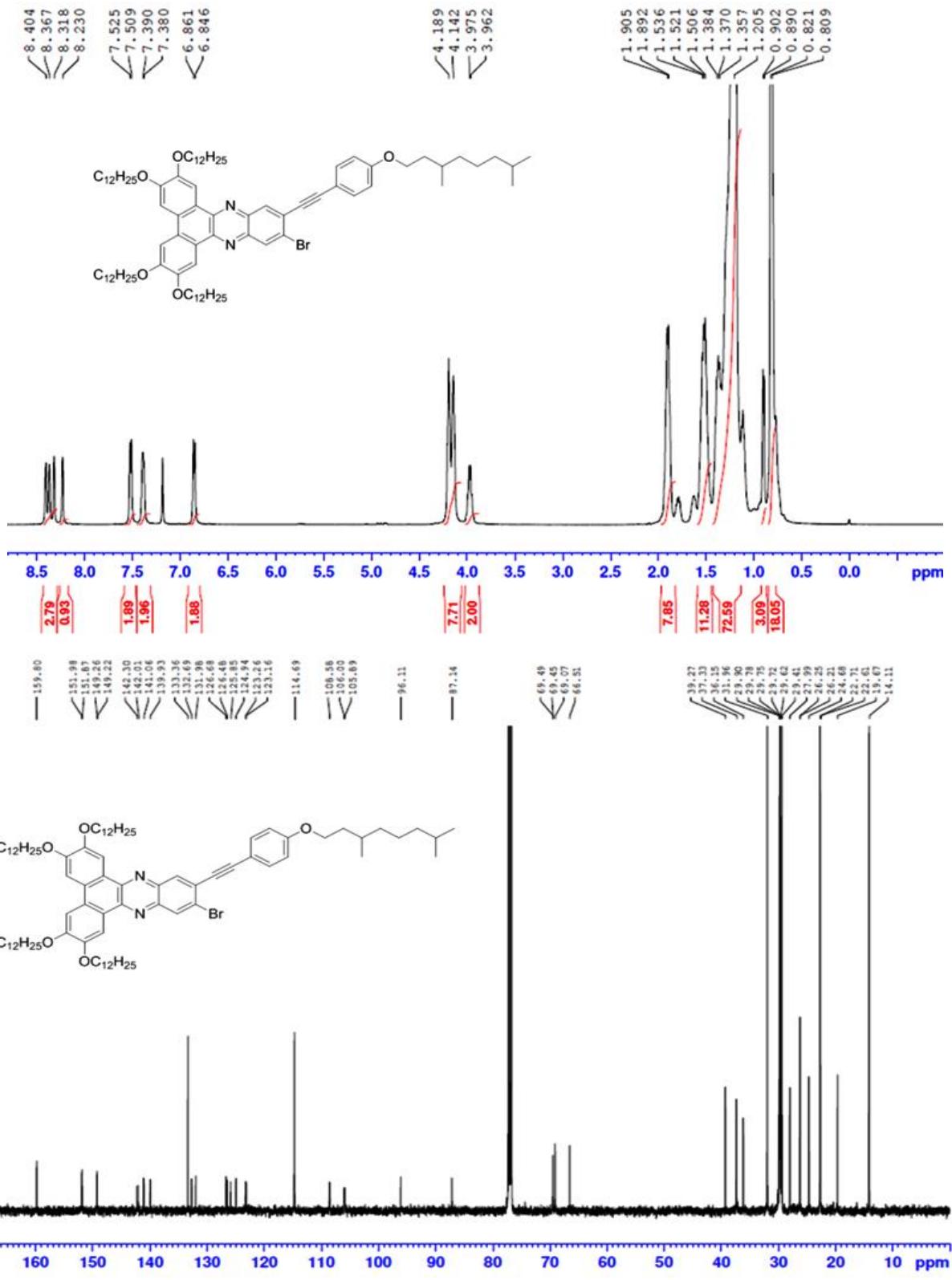


Figure 8. ¹H and ¹³C NMR spectra of compound 13d.

References

- [1] Billard J, Dubois JC, Tinh NH, et al. *Nouv. J. Chem.*, **1978**, 2, 535–540.
- [2] Chandrasekhar S, Sadashiva BK, Suresh KA. *Pramana*. **1977**, 9, 471–480.
- [3] Bushby RJ, Lozman OR. *Curr. Opin. Coll. Interface Sci.*, **2002**, 7, 343–354
- [4] (a) Simmerer J, Glusen B, Paulus W, et. Al. *Adv. Mater.*, **1996**, 8, 815–819
- [5] (a) Bisoyi HK, Kumar S. *Tetrahedron Lett.*, **2008**, 49, 3628–3631; (b) Kimura M, Moriyama M, Kishimoto K. *Liq. Cryst.*, **2007**, 34, 107–112; (c) Gupta SK, Raghunathan VA, Lakshminarayanan V, et. Al. *J. Phys. Chem. B.*, **2009**, 113, 12887–12895.
- [6] (a) Haverkate LA, Zbiri M, Johnson MR, et al. *J. Phys. Chem B.*, **2011**, 115, 13809; (b) Park JH, Kim KH, Park YW, et al. *Langmuir.*, **2015**, 31, 9432–9440; (c) Gayathri HN, Kumar B, Suresh KA, et al. *Phys. Chem. Chem. Phys.*, **2016**, 18, 12101–12107; (d) Kumar S, Laxminarayanan V. *Chem Commun.*, **2004**, 14, 1600–1601.
- [7] (a) Kumar S, Pal SK, Kumar PS, et al. *Soft Matter.*, **2007**, 3, 896–900; (b) Mishra M, Kumar S, Dhar R. *RSC Adv.*, **2014**, 4, 62404–62412; (b) Holt LA, Bushby RJ, Evans SD, et al. *J. Appl. Phys.*, **2008**, 103, 063712; (c) Supreet, Pratibha R, Kumar S, et al. *Liq. Cryst.*, **2014**, 41, 933–939; (d) Mishra M, Kumar S, Dhar R. *Thermochimica Acta.*, **2016**, 631, 59–70.
- [8] (a) Mukesh M, Kumar S, Dhar R. *Soft Materials.*, **2017**, 15, 34–44; (b) Yaduvanshi P, Kumar S, Dhar R. *Phase. Trans.*, **2015**, 88, 489–502; (c) Yaduvanshi P, Mishra A, Kumar S, et al. *J. Mol. Liq.*, **2015**, 208, 160–164; (d) Yaduvanshi P, Mishra A, Kumar S, et al. *Liq. Cryst.*, **2015**, 42, 1478–1489.
- [9] (a) Kumar S, Sagar LK. *Chem Commun.*, **2011**, 47, 12182–12184; (b) Kumar M, Kumar S. *RSC Adv.*, **2015**, 5, 1262–1267; (c) Zlateva G, Zhelev Z, Bakalova R, et al. *Inorg Chem.*, **2007**, 46, 6212–6214; (d) Wuister SF, Swart I, Driel FV, et al. *Nano Lett.*, **2003**, 3, 503–507.
- [10] (a) Lagerwall JPF, Scalia G. *Curr Appl Phys.*, **2012**, 12, 1387–1412; (b) Nealon GL, Greget R, Dominguez C, et al. *Beilstein J Org Chem.*, **2012**, 8, 349–370; (c) Stamatoiu O, Mirzaei J, Feng X, et al. *Top Curr Chem.*, **2012**, 318, 331–393.
- [11] (a) Umadevi S, Ganesh V, Hegmann T. *Nanoparticles: additives and building blocks for liquid crystal phases*. In: Goodby JW, Collings PJ, Kato T, et al., editors.

- Handbook of liquid crystals*. Vol. VI. Weinheim, Germany: Wiley-VCH; **2014**. p. 27–76; (b) Avinash BS, Lakshminarayanan V, Kumar S, et al. *Chem Commun.*, **2013**, 49, 978–980; (c) Kumar S, Bisoyi HK. *Angew Chem Int Ed.*, **2007**, 46, 1501–1503.
- [12] (a) Bisoyi HK, Kumar S. *J Mater Chem.*, **2008**, 18, 3032–3039; (b) Lee JJ, Yamaguchi A, Alam MA, et al. *Angew Chem Int Ed.*, **2012**, 51, 8490–8494; (c) Fukushima T, Kosaka A, Ishimura Y, et al. *Science.*, **2003**, 300, 2072–2074.
- [13] (a) Bajpai M, Yadav N, Kumar S, et al. *Liq Cryst.*, **2016**, 43, 305–313; (b) Bajpai M, Yadav N, Kumar S, et al. *Liq Cryst.*, **2016**, 43, 928–936; (c) Bajpai M, Yadav N, Kumar S, et al. *Liq Cryst.*, **2017**, 44, 379–386; (d) Shi Y, Tan L, Chen Y. *Appl Mater Interfaces.*, **2014**, 6, 17848–17856.
- [14] (a) Bushby RJ, Boden N. *Responses of Discotic Liquid Crystals to Mechanical, Magnetic, and Electrical Fields*. In *Handbook of Liquid Crystals*; Goodby, J. W., Collings, P. J., Kato, T., Tschierske, C., Gleeson, H. F., Raynes, P., Eds.; Wiley-VCH: Weinheim, **2014**; Vol. 5, pp 569–602; (b) Kumar S in *Chemistry of Discotic Liquid Crystals: From Monomers to Polymers*; Liquid Crystal Book Series; CRC Press, Taylor & Francis Group: Boca Raton, FL, **2011**; (c) Kumar S in *Design Concepts and Synthesis of Discotic Liquid Crystals*. In *Handbook of Liquid Crystals*; J. W. Goodby, P. J. Collings, T. Kato, C. Tschierske, H. F. Gleeson, P. Raynes, Wiley-VCH: Weinheim, **2014**; Vol. 4, pp 467–520;
- [15] (a) Boden N, Clements J, Movaghar B. Fluid Sensing Device Using Discotic Liquid Crystals; US006423272B1, 2002; (b) Heiney PA. *Structure and Physical Properties of Columnar Liquid Crystals*. In *Handbook of Liquid Crystals*; Goodby, J. W., Collings, P. J., Kato, T., Tschierske, C., Gleeson, H. F., Raynes, P., Eds.; Wiley-VCH: Weinheim, **2014**; Vol. 4, pp 521; (c) Pisula W, Mullen K. *Discotic Liquid Crystals as Organic Semiconductors*. In *Handbook of Liquid Crystals*; Goodby, J. W., Collings, P. J., Kato, T., Tschierske, C., Gleeson, H. F., Raynes, P., Eds.; Wiley-VCH: Weinheim, **2014**; Vol. 8, pp 627–674.
- [16] Adam DP, Schuhmacher J, Simmerer L, et. Al. *Adv. Mater.*, **1995**, 7, 276–280.
- [17] (a) Borner RC, Bushby RJ, Cammidge AN, et. Al. *Liq. Cryst.*, **2006**, 33, 1439–1448; (b) Morimoto K, Dohi T, Kita Y. *Eur. J. Org. Chem.*, **2013**, 2013, 1659–1662; (c) Wu H, Zhang C, Pu J, et. al. *Liq. Cryst.*, **2014**, 41, 1173–1178; (d)

- Kumar S, Manickam M. *Chem. Commun.*, **1998**, 1427-1428; (e) Schonherr H, Manickam M, Kumar S. *Langmuir.*, 2002, 18, 7082-7085.
- [18] (a) Kong X, He Z, Gopee H, et. al. *Tetrahedron Lett.*, **2011**, 52, 77–79; (b) Tanaka D, Ishiguro H, Shimizu Y, et. al. *J. Mater. Chem.*, **2012**, 22, 25065–25071; (c) Stackhouse PJ, Hird M. *Liq. Cryst.*, **2008**, 35, 597–607; (d) Zimmermann S, Wendorff J H, Weder C. *Chem. Mater.*, **2002**, 14, 2218-2223.
- [19] (a) Stackhouse PJ, Hird M. *Liq. Cryst.*, **2009**, 36, 953–965; (b) Varshney SK, Takezoe H, Prasad V, Rao DSS. *Mol. Cryst. Liq. Cryst.*, **2009**, 515, 16–38; (c) Cammidge AN, Gopee H. *Liq. Cryst.*, **2009**, 36, 809–816; (d) Cammidge AN, Gopee H, Patel H. *Tetrahedron Lett.*, **2009**, 50, 3513–3515.
- [20] (a) Cammidge AN, Beddall AR, Gopee H. *Tetrahedron Lett.*, **2007**, 48, 6700; (b) Varshney SK. *Liq. Cryst.*, **2013**, 40, 1477-1486; (c) Varshney SK, Yelamaggad CV, Takezoe H. *Liq. Cryst.*, **2007**, 34, 787-790; (d) Varshney SK, Nagayama H, Rao DSS, et. al. *Mol. Cryst. Liq. Cryst.*, **2010**, 528, 38–48.
- [21] (a) Mahoney SJ, Ahmida MM, Kayal H, et. al. *J. Mater. Chem.*, **2009**, 19, 9221–9232; (b) Kimura M, Hatanaka T, Nomoto H, et. al. *Chem. Mater.*, **2010**, 22, 5732–5738; (c) Yang F, Yuan J, Li C, et. al. *Liq. Cryst.*, **2014**, 41, 137–143; (d) Paraschiv I, Tomkinson A, Giesbers M, et. al. *Liq. Cryst.*, **2007**, 34, 1029–1038.
- [22] (a) Zhang L, Hughes DL, Cammidge AN. *J. Org. Chem.*, **2012**, 77, 4288–4297; (b) Hoang MH, Cho MJ, Kim KH, et. al. *Chem. Lett.*, **2010**, 39, 396–397; (c) Hoang MH, Cho MJ, Kim KH, et. al. *Thin Solid Films.*, **2009**, 518,501–506.
- [23] (a) Gopee H, Kong X, He Z, et. al. *J. Org. Chem.*, **2013**, 78, 9505–9511; (b) Kohmoto S, Mori E, Kishikawa K. *J. Am. Chem. Soc.*, **2007**, 129, 13364–13365; (c) Zhang L, Gopee H, Hughes DL, Cammidge AN. *Chem. Commun.*, **2010**, 46, 4255.
- [24] (a) Ichihara M, Suzuki H, Mohr B, et. al. *Liq. Cryst.*, **2007**, 34, 401–410; (b) Yelamaggad CV, Achalkumar AS, Rao DSS, et. al. *J. Mater. Chem.*, **2008**, 18, 3433–3437; (c) Gopee H, Cammidge AN, Oganessian VS. *Angew. Chem.*, **2013**, 125, 9085.
- [25] (a) Kong X, He Z, Gopee H, et. al. *Liq. Cryst.*, **2011**, 38, 943–955; (b) Gupta SK, Raghunathan VA, Kumar S. *New J. Chem.*, **2009**, 33, 112–118; (c) Varshney SK, Monobe H, Shimizu Y, Takezoe H, et. al. *Liq. Cryst.*, **2010**, 37, 607–615; (d) Varshney SK, Nagayama H, Prasad V, et. al. *Mol. Cryst. Liq. Cryst.*, **2010**, 517, 97–112.

- [26] (a) Pisula W, Feng X, Mullen K. *Chem. Mater.*, **2011**, 23, 554–567; (b) Gowda A, Kumar M, Kumar S, *Liq. Cryst.*, **2017**, 44, 1990–2017; (c) Kumar M, Gowda A, Kumar S, *Part. Part. Syst. Charact.*, **2017**, 34, 1700003/1–1700003/25; (d) van de Craats AM, Warman JM, *Adv. Mater.*, **2001**, 13, 130–133; (e) Voisin E, Williams VE. *Macromolecules.*, **2008**, 41, 2994–2997; (f) Ikeda M, Takeuchi M, Shinkai S. *Chem. Commun.*, **2003**, 1354–1355; (g) Luckhurst GR. *Nature.*, **2004**, 430, 413–414; (h) Luckhurst GR. *Angew. Chem. Int. Ed.*, **2005**, 44, 2834–2836..
- [27] (a) Kumar S, *Liq. Cryst.*, **2004**, 31, 1037–1059; (b) Kumar S, *Liq. Cryst.*, **2005**, 32, 1089–1113; (c) Cammidge AN, Chausson C, Gopee H, et. al. *Chem. Commun.* **2009**, 7375–7377.
- [28] (a) Cammidge AN, Bushby RJ. In *Handbook of Liquid Crystals*; D. Demus, J. W. Goodby, G. W. Gray, H.-W. Spiess, V. Vill, Eds.; Wiley-VCH: Weinheim, **1997**; Vol. 2, pp 693–748; (b) Zhang L, Gopee H, Hughes DL, et. al. *Chem. Commun.*, **2010**, 46, 4255–4257; (c) Zhang L, Hughes DL, Cammidge AN. *J. Org. Chem.*, **2012**, 77, 4288–4297; (d) Kong X, He Z, Zhang Y, et. al. *Org. Lett.*, **2011**, 13, 764–767.
- [29] (a) Kumar S, Schuhmacher P, Henderson P, et. al. *Mol. Cryst. Liq. Cryst. A.*, **1996**, 288, 211; (b) Henderson P, Kumar S, Rego JA, et. al. *J. Chem. Soc., Chem. Commun.*, **1995**, 1059; (b) Rego JA, Kumar S, Ringsdorf H, *Chem. Mater.*, **1996**, 8, 1402; (c) Rego JA, Kumar S, Dmochowski IJ, Ringsdorf H, *Chem. Commun.*, 196, 1031.
- [30] (a) Kumar S, Manickam M, *Liq. Cryst.*, **1999**, 26, 1097–1099; (b) Kumar S, Manickam M, *Mol. Cryst. Liq. Cryst.*, **2000**, 338, 175–179.
- [31] Yatabe T, Harbison MA, Brand JD, et. al. *J. Mater. Chem.*, **2000**, 10, 1519–1525.
- [32] Cammidge AN, Gopee H, *Chem. Commun.*, **2002**, 966–967
- [33] Xiao W, He Z, Remiro-Buenamañana S, et. al. *Org. Lett.*, **2015**, 17, 3286–3289.
- [34] Kumar S, Gupta SK, *Tetrahedron Lett.*, **2011**, 52, 5363–5367.
- [35] (a) Fang X, Guo H, Lin J, et. al. *Tetrahedron Lett.*, **2016**, 57, 4939–4943; (b) Guo H, Zhu M, Wang Z, et. al. *Tetrahedron Lett.*, **2016**, 57, 4191–4195
- [36] Vadivel M, Kumar IS, Swamynathan S, et. al. *ChemistrySelect.*, **2018**, 3, 8763
- [37] Kumar S, Manickam M, *Synthesis.*, 1998, 1119–1122.
- [38] Kumar S, Manickam M, Varshney SK, et. al. *J. Mater. Chem.*, **2000**, 10, 2483

- [39] Shao J, Chang J, Chi C, *Org. Biomol. Chem.*, **2012**, 10, 7045–7052.
- [40] Frisch MJ, Trucks GW, Schlegel HB, et. al. et al. Gaussian 16, Gaussian, Inc., Wallingford, CT, **2017**.
- [41] (a) Funatsu Y, Sonoda A, Funahashi M, *J. Mater. Chem. C.*, **2015**, 3, 1982–1993; (b) Feringan B, Romero P, Serrano JL, et. al. *J. Am. Chem. Soc.*, **2016**, 138, 12511–12518; (c) Zhang W, Zhang S, Zhang Z, et. al. *J. Phys. Chem B.*, **2017**, 121, 7519–7525; (d) Iino H, Hanna J.-I, Haarer D, *Phys. Rev. B.*, **2005**, 72, 193203/1–193203/4.
- [42] Gan KP, Yoshio M, Sugihara Y, Kato T, *Chem. Sci.*, **2018**, 9, 576–585.
- [43] Heck A, Kranz JJ, Elstner M, *J. Chem. Theory Comput.*, **2016**, 12, 3087–3096.
- [44] Eccher J, Faria GC, Bock H, et. al. *Appl. Mater. Interfaces.*, **2013**, 5, 11935
- [45] (a) Wohrle T, Wurzbach I, Kirres J, et. al. *Chem Rev.*, **2016**, 116, 1139–241; (b) Feng X, Marcon V, Pisula W, et. al. *Nat Mater.*, **2009**, 8, 421–6; (c) van de Craats AM, Warman JM, de Haas MR, et. al. *Adv Mater.*, **1996**, 8, 823–6; (d) Bushby RJ, Lozman OR, *Curr. Opin. Solid State Matter Sci.*, **2002**, 6, 569.
- [46] Kong X, Gong H, Liu P, et. al. *New J. Chem.*, **2018**, 42, 3211–3221
- [47] Kumar S, Varshney SK. *Org. Lett.*, **2002**, 4, 157
- [48] (a) Gowda A, Jacob L, Joy N, et. al. *New J Chem.*, **2018**, 42, 2047–2057; (b) Sutherland RL with contributions by D.G. McLean and S. Kirkpatrick, *Handbook of Nonlinear Optics*, second ed. New York, NY: Marcel Dekker, **2003**.
- [49] (a) Philip R, Kumar GR, Sandhyarani N, et. al. *Phys Rev B.*, **2000**, 62, 13160; (b) Rao SV, Nagasrinivas NKM, Rao DN, et. al. *Opt. Commun.*, **2000**, 182, 255.
- [50] Bredas JL, Adant C, Tackx P, et. al. *Chem Rev.*, **1994**, 94, 243–278
- [51] (a) Arakawa Y, Nakajima S, Ishige R, et. al. *J. Mater. Chem.*, **2012**, 22, 8394–8398; (b) Gowda A, Jacob L, Singh DP, et. al. *ChemistrySelect.*, **2018**, 3, 6551–6560.
- [52] (a) Foster EJ, Lavigueur C, Ke YC, et. al. *J. Mater. Chem.*, **2005**, 15, 4062–4068; (b) Foster EJ, Jones RB, Lavigueur C, et. al. *J. Am. Chem. Soc.*, **2006**, 128, 8569–8574; (c) Lavigueur C, Foster EJ, Williams VE, *J. Am. Chem. Soc.*, **2008**, 130, 11791; (d) Bozek KJA, Williams VE. *Soft Matter.*, **2014**, 10, 5749; (e) Lavigueur C, Foster EJ, Williams VE. *Liq. Cryst.*, **2007**, 34, 833–840.
- [53] (a) Krishnaiah M, de Almeida NR, Udumula V, et. al. *Eur. J. Med. Chem.*, **2018**, 143, 936–947; (b) Pierson LS, Pierson PA. *Appl. Microbiol. Biotechnol.*, **2010**, 86,

1659–1670; (c) Shaikh AM, Sharma BK, Chacko S, Kamble RM, *New J. Chem.*, **2017**, 41, 628–638.

[54] (a) Ong CW, Hwang JY, Tzeng M.-C, Liao S.-C, et. al. *J. Mater. Chem.*, **2007**, 17, 1785–1790; (b) Tzeng M.-C, Liao S.-C, Chang T.-H, et. al. *J. Mater. Chem.*, **2011**, 21, 1704–1712; (c) Ong CW, Yan CQ, Yeh M.-C, et. al. *Mol. Cryst. Liq. Cryst.*, **2015**, 610, 249–254; (d) Yeh M.-C, Su Y.-L, Tzeng M.-C, et. al. *Angew. Chem. Int. Ed.*, **2013**, 52, 1031–1034; (e) Szydłowska J, Krzyczkowska P, Salamonczyk M, et. al. *J. Mater. Chem. C.*, **2013**, 1, 6883.

[55] Lin K.-T, Lai CK. *Tetrahedron.*, **2016**, 72, 7579–7588.

Chapter 5

Self-assembly of metal nanoparticles in a metal-free phthalocyanine discotic liquid crystalline material

5.1 Introduction

Phthalocyanine is a two-dimensional symmetrical conjugated heterocyclic system in which four indole rings are fused through nitrogen atom and acts as a tetradentate ligand to form a macrocyclic molecule [1–3]. The cavity of phthalocyanine can accommodate various metal atoms. Delocalization of the π -electrons in the aromatic ring of phthalocyanine exhibits unconventional physical and chemical properties. Recently, phthalocyanines and metallo-phthalocyanines have been attracted considerable interest not only as dyes and pigments but also as macrocyclic building block materials for the construction of various advanced functional materials for electronic and optoelectronic devices [3]. The adaptability, functional capability, non-toxicity, easy processability and colored nature of the metal and metal free Pc derivatives make them suitable candidates for their use in electronic devices. Pc derivatives can behave as electron donor and electron acceptors with respect to other moieties in donor–acceptor molecular design. In addition to that, Pc derivatives can also find extensive wide range of applications in biological and biomedical sciences. The appropriate peripheral modification of Pc with flexible aliphatic chains not only enhances the solubility but also induces liquid crystallinity [4–10].

In 1982, Piechocki et al. reported the synthesis and columnar mesomorphic properties of Pc DLCs [11] and since then a large number (>400) of DLCs derived from Pc have been reported in the literature [12–18]. The Pc mesogens have been extensively studied for their broad physical properties such as charge transport, crystal structure, electron spin resonance, photophysical properties, nonlinear optical transmission, and magnetic properties etc [4–19]. Due to large macrocyclic core and good solubility, Pc derivatives exhibit aggregation in solution to form self-assembled fibers. Langmuir monolayers and Langmuir-Blodgett films of amphiphilic Pcs can be prepared and may be transferred on various substrates. These self-assembled monolayers can be visualized using STM on inert surface. The molecular structure of Pc DLCs enables strong nonlinear optical absorption properties in the visible and IR regions. Metal-free as well as metallo phthalocyanine (MPc) DLCs self-assemble into columnar stacks and provide efficient anisotropic electronic transport channels along the molecular columns [12–21].

The materials typically in the range of 1–100 nm size, at least in one-dimension, are commonly defined as nanomaterials. They are usually made of organic or inorganic materials

which demonstrate the characters quite different from those individual atoms or particles and from corresponding bulk materials [22]. A significant change in the electro-optical and biological properties has been observed when the size of material diminishes to one billionth of a meter. Nanomaterials have been widely investigated in different fields, for example, energy, computing, optics, catalysis, biomedical and biosensors [23–26]. In recent year, there has been huge development in the field of nanoscience and nanotechnology, because of our capability to visualize the nano-sized materials with the assistance of present day instruments, such as a FE-SEM, AFM, STM, and HR-TEM etc.

Nanoparticles are unique in their physical and chemical properties which depend on their size and shape [22]. A synergetic relation between anisotropic liquid crystalline compounds with excellent electronic properties of NPs may produce novel materials for electronic device applications. Recently, our group initiated the dispersion of alkanethiol-functionalized colloidal gold nanoparticles of small size in various DLCs such as hexahexylthiotriphenylene (HHTT), hexabutyloxytriphenylene (HAT4) and hexapentyloxytriphenylene (HAT5) [27]. Thermotropic behaviour of these discotic nanocomposites were investigated using POM, DSC and XRD studies, which reveals that the dispersion of NPs, in small amount, in DLCs does not affect the mesomorphic properties of DLCs. However, dispersion of larger amount leads to the aggregation of nanoparticles in the mesophase. The dispersion of AuNPs significantly increases the electrical conductivity of the system. Similarly, surface functionalization of AuNPs with triphenylene (TP-AuNPs) ligands were prepared and dispersed in TP-based DLCs such as hexaheptyloxytriphenylene (HAT7). Three composites (0.5, 1 & 3 wt% TP-AuNPs/HAT7) were prepared and all the composites show mesophase behaviour of classical columnar phase texture upon cooling from isotropic liquid. The clearing temperatures of all the composites were decreases, as expected, upon increasing TP-AuNPs dispersion. TEM studies reveal that these TP-functionalized AuNPs self-assembled into a hexagonal pattern on the surface. The electrical conductivity measurements were carried out while cooling form isotropic liquid for virgin HAT7 and 1 wt% TP-AuNP/HAT7 nanocomposite. There is dramatic increase in DC conductivity of the system by more than six orders of magnitude. This enrichment of the electrical conductivity could be because of the formation of charge transfer complex between electron rich TP DLCs and electron deficient AuNPs [27]. Holt et al. also reported an increase in the electrical conductivity (10^6) upon dispersion of organic functionalized AuNPs [28]. Similar properties

have also been observed when 1 wt% of a strong electron deficient molecule (TNF) was doped in TP DLCs [29].

Shen et al. reported the surface functionalization of AuNPs using TP DLCs and investigated the self assembly of NPs on the surface [30]. The triphenylene ligands self-assembled in a stripe-like arrangement over gold nanoparticles surface via π - π interactions. These nanocomposites provide a novel self-assembly structure for NPs and this linear 1D row in stripes have potential applications in electronic devices. Supreet et al. investigated thermal, electrical and optoelectronic properties of AuNPs dispersed mononitro-functionalized TP DLCs [31]. The dispersion of Au metal nanoparticles into the discotic columnar matrix decreases the orientational order parameter (S) and increases the relaxation time (τ). The effect of AuNPs dispersion on dielectric properties of DLCs was studied by Dhar et al. [32]. Different composites (0.2, 0.6 and 1.2 wt%) of AuNPs were dispersed in TP DLCs. Upon increasing the concentration of AuNPs in DLCs, the mesophase (Col_{hp}) to isotropic transition temperature decreases but crystal to mesophase transition does not alter much. However, a reduction in lattice parameter was observed.

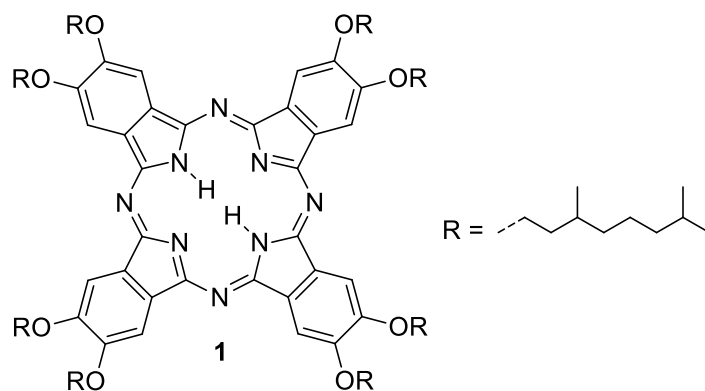
Yaduvanshi et al. [33] studied the effect of Ag NPs size on self-assembly of HAT4 DLCs. They prepared two composites (0.6 wt%) with Ag NPs of 6 nm and 100 nm size. The liquid crystalline property does not change upon dispersion of these NPs. The results reveal that, for 0.6 wt% AgNPs/HAT4 composites (6 nm size of AgNPs) increases the ionic conductivity along with relative permittivity and reduces the band gap energy of HAT4 DLCs from 4.2 eV to 3.3 eV. The increasing conductivity values observed owing to their better homeotropic alignment of small size NPs compare to 100 nm size of Ag NPs. For 0.6 wt% composite with 100 nm size of AgNPs shows maximum dielectric strength i.e. $\delta\epsilon_{\max} = 0.96$ at 130 °C with compare to pure HAT4 $\delta\epsilon_{\max} = 0.13$ at 138 °C.

Recently, Basova et al. investigated the dispersion of hexadecylamine capped gold nanoparticles (AuNP-HA) into nickel phthalocyanine DLCs (NiPcR4) [34]. Four composites (0.1, 1, 2 and 5 wt%) of AuNP-HA/NiPcR4 are prepared and studied for their thermal and electrical properties. The mesophase to isotropic transition temperature decrease upon increasing concentration of 0.1, 1, 2 and 5 wt% AuNPs respectively. Increase in conductivity of the system

by more than two orders of magnitude was also observed with increasing dopant (AuNPs) concentration. Doping of functionalized gold nanoparticles into the metal phthalocyanine liquid crystals improve the photosensitizers in photodynamic therapy, photophysical, photochemical and optical properties [34]. A combination of excellent electronic properties of nanomaterials at the nanoscale with the order and mobility of DLCs may produce advance functional materials and, therefore, evolution of their physical properties is currently a very active research field [35–43].

5.2 Objective

The main objectives of this work are; (i) synthesis and characterization of a novel metal free Pc DLC namely 2,3,9,10,16,17,23,24-octakis(3,7-dimethyloctoxy) phthalocyanine (**1**). (ii) synthesis and characterization of zero-dimensional gold and silver NPs; (iii) dispersion of these metallic NPs in the supramolecular order of Pc DLC and; (iv) characterization and physical studies of these nanocomposites.

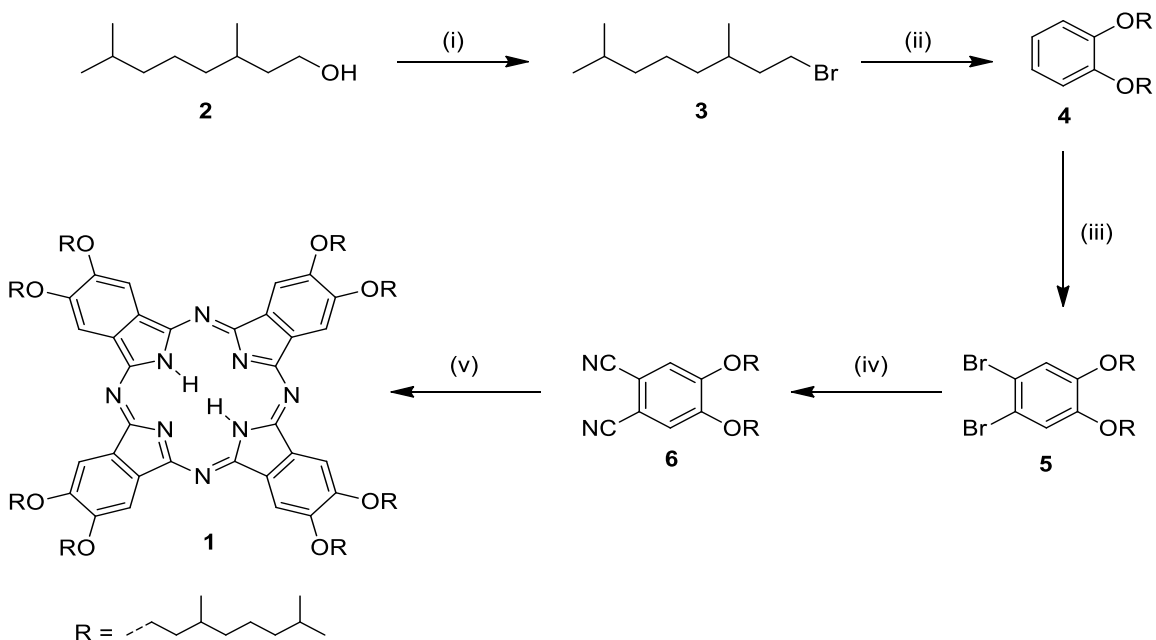


Metal-free 2,3,9,10,16,17,23,24-Octakis(3,7-dimethyloctoxy) phthalocyanine DLCs (Pc)

5.3 Results and discussion

5.3.1 Synthesis of 2,3,9,10,16,17,23,24-Octakis (3,7-dimethyloctoxy) phthalocyanine

Discotic liquid crystalline octaalkoxy substituted metal free phthalocyanine was reported earlier by Schouten et al, [4a] and as shown in **Scheme 1**. Following reported methodology, we have synthesized metal free phthalocyanine **1** containing octa alkoxy chains of eight carbon atoms with two branching methyl groups. All the intermediate compounds were synthesized following reported procedure and investigated with the help of spectral and elemental analysis.



Scheme 1. Synthesis of metal-free phthalocyanine DLCs: (i) PPh_3 , NBS, DCM, 24 h, r.t; (ii) Catechol, K_2CO_3 , DMSO, 85 °C, 16 h; (iii) Br_2 , DCM, 4 h, r.t; (iv) CuCN , NMP, 180 °C, 24 h; (v) DBN, abs. EtOH, reflux, 96 h.

5.3.2 Synthesis and characterization of alkanethiol-capped metal nanoparticles

We have synthesised the hexanethiol capped silver and gold nanoparticles by following reported procedure with slight modification. The detail synthetic methods are presented in the experimental section. These NPs were initially examined using UV-Vis spectrum in anhydrous

DCM solvent as shown in **Figure 2**. The surface plasmon resonance of nanoparticles is sensitive to the electronic and optical properties of the surface of nanoparticles and of the capping monolayer. Metal-nanoparticles stabilized by hexanethiol exhibit surface plasmon band at 436 nm and 544 nm for Ag and Au nanoparticles respectively, which is characteristic of surface plasmon band for Ag and Au NPs. The morphology of nanoparticles were characterized using HR-TEM and SEM. **Figure 3** shows HR-TEM images of the homogeneous size distribution of gold and silver nanoparticles. The average diameter of both Ag and Au NPs is about 2–4 nm. Both Ag and Au NPs were further characterized using SEM which reveals uniform size distribution of nanoparticles is shown in **Figure 4**.

5.3.3 Preparation of nanocomposites

Nanocomposites having weight percentage of 0.5 wt% and 3 wt% of MNPs in Pc were prepared by mixing two components in dry chloroform. For 0.5 wt% MNP/Pc composite, MNPs (0.5 mg) were taken in dry chloroform (5 mL) and sonicated for 1 hour at room temperature. To this solution, phthalocyanine derivative (99.5 mg) was added and the mixture was further sonicated for 1 hour to ensure homogeneous dispersion of nano composites. After that the solvent was removed by evaporation under N₂ flow at room temperature. For 3 wt% MNP/Pc composite, MNPs (3 mg) were dispersed in Pc-DLC (97 mg). Bulk composite can also be made by the dispersion of 1:1 ratio of MNP/Pc. In this case phase segregation can be seen when cooling from isotropic temperature. Two nanocomposites of Ag NPs and Au NPs (0.5 wt% and 3 wt%) were prepared by dispersing into metal free phthalocyanine DLCs.

5.3.4 Characterization of nanocomposites

5.3.4.1 Polarising optical microscopy studies

All the composites were found to be liquid crystalline in nature. Unlike the pure DLCs, doped composites cleared to isotropic state at much lower temperatures. **Figure 5** shows the typical POM textures for the composites 0.5 wt% MNPs/Pc and 3 wt% MNPs/Pc of silver and gold nanoparticles respectively. POM observations clearly indicate the homogeneous dispersion of metallic-nanoparticles in DLCs without any phase segregation. They show the texture of

hexagonal columnar mesophase upon cooling from the isotropic phase. If the weight percentage is increased to 5 wt%, a little aggregation of nanoparticles was seen under POM as shown in **Figure 6**.

5.3.4.2 Differential scanning calorimetry studies

The DSC traces were recorded for all the composites with heating and cooling scans at 5 °C min⁻¹ under nitrogen atmosphere. The DSC data of all the composites were presented in the **Table 1**. In all the Ag & Au nanocomposites, there is gradual decrease in mesophase to isotropic phase transition temperature with increasing concentration of MNPs as shown in **Figure 7**.

Upon heating, the pure Pc discotic exhibits phase transition from Col_h to isotropic liquid at 299.3 °C along with phase transition enthalpy (ΔH) of 2.5 J g⁻¹. On slow cooling, isotropic liquid to Col_h phase transition appeared at 292.2 °C with $\Delta H = -2.1$ J g⁻¹. Similarly, upon heating, the 0.5 wt% Ag/Pc and 3 wt% Ag/Pc nanocomposites exhibit phase transition from Col_h phase to isotropic phase at 297.2 °C ($\Delta H = 1.8$ J g⁻¹) and 295.7 °C ($\Delta H = 1.0$ J g⁻¹) respectively. Upon cooling, both the composites (0.5 wt% Ag/Pc and 3 wt% Ag/Pc) transferred to Col_h phase at 292.5 °C ($\Delta H = -1.5$ J g⁻¹) and 294.8 °C ($\Delta H = -1.3$ J g⁻¹) respectively. On the other hand, the 0.5 wt% Au/Pc and 3 wt% Au/Pc nanocomposites show Col_h phase to isotropic phase at 292.7 °C ($\Delta H = 2.2$ J g⁻¹) and 288.8 °C ($\Delta H = 1.1$ J g⁻¹) respectively. On cooling from isotropic liquid, Col_h phase transition appeared at 288.9 °C ($\Delta H = -2.8$ J g⁻¹) and 285.9 °C ($\Delta H = -1.1$ J g⁻¹) respectively. In all the nanocomposites, the isotropic temperature shifted to lower value compared to undoped phthalocyanine. Pure Pc and its nanocomposites were semisolid at room temperature and do not show any clear melting transition. They display columnar hexagonal mesophase upon cooling from isotropic phase down to room temperature. It is noticed that, the phase transition enthalpy of 0.5 wt% Ag composites was 1.8 J g⁻¹ that decreases to 1.0 J g⁻¹ in 3 wt% Ag composite. Similarly the enthalpy of 0.5 wt% Au composite was 2.2 J g⁻¹ which decreases to 1.1 J g⁻¹ in 3 wt% Au composite. The dispersion of MNPs in the columnar mesophase decreases the overall order of the mesophase and thus decreases the enthalpy of the phase transition.

Table 1. Phase transition temperature (peak temperature in DSC °C) and enthalpies (J g⁻¹, in parentheses) of pure phthalocyanine and its nanocomposites.

Compound	Phase transition (peak (°C) [ΔH (J g ⁻¹)])	
	<i>heating</i>	<i>cooling</i>
Pc	Col_h 299.3 [2.5] I	I 292.2 [-2.1] Col_h
0.5 wt% Ag/Pc	Col_h 297.2 [1.8] I	I 292.5 [-1.5] Col_h
3 wt% Ag/Pc	Col_h 295.7 [1.0] I	I 294.8 [-1.3] Col_h
0.5 wt% Au/Pc	Col_h 292.7 [2.2] I	I 288.9 [-2.8] Col_h
3 wt% Au/Pc	Col_h 288.8 [1.1] I	I 285.9 [-1.1] Col_h

5.3.4.3 Small angle X-ray scattering studies

In order to investigate the mesophase behaviour and self-assembly of nanomaterials in columnar phase, small angle X-ray scattering experiment was performed using mesogens filled in Lindemann capillaries. SAXS patterns of pure Pc and its nanocomposites were recorded at room temperature and are shown in **Figure 8a** and **Figure 8b**, respectively. All the mesogens (Pc and nanocomposites) show increasing order of the typical Bragg diffractions angle (lowest angle to highest intensity) in the order of 1: $1/\sqrt{3}$: $1/\sqrt{7}$: $1/\sqrt{9}$ which are responsible for the existence of two dimensional hexagonal columnar phase.

These patterns can be assigned to the Miller indices (100), (110), (210) and (300) respectively, reflection of a 2-D hexagonal lattice. The wide angle region displays, a halo at 4.81 Å for flexible alkyl chains and another sharp peak for core-core separation at 3.34 Å. The core-core separation is found to be same in all the composites as well in pure Pc. The above results confirmed that all four nanocomposites are self-assembled in the columnar hexagonal fashion in their liquid crystal phase and columnar hexagonal order of discotics is not affected on dispersion of metal nanoparticles. Crystal data and Miller indices for all the composites are presented in **Table 2**.

Table 2. XRD data of nano composites.

Composites	2θ (degrees)	d -spacing (Å)	Col_h parameter	Miller indices	Alkyl- chain (Å)	Core-Core separation (Å)
Pc	3.24	27.30	1	100	4.81	3.34
	5.61	15.77	$1/\sqrt{3}$	110		
	8.58	10.32	$1/\sqrt{7}$	210		
	9.72	9.09	$1/\sqrt{9}$	300		
0.5 wt% Au/Pc	3.26	27.11	1	100	4.82	3.34
	5.62	15.71	$1/\sqrt{3}$	110		
	8.59	10.26	$1/\sqrt{7}$	210		
	9.70	9.11	$1/\sqrt{9}$	300		
3 wt% Au/Pc	3.22	27.50	1	100	4.84	3.34
	5.54	15.93	$1/\sqrt{3}$	110		
	8.51	10.38	$1/\sqrt{7}$	210		
	9.63	9.16	$1/\sqrt{9}$	300		
0.5 wt% Ag/Pc	3.27	26.98	1	100	4.84	3.34
	5.64	15.87	$1/\sqrt{3}$	110		
	8.76	10.09	$1/\sqrt{7}$	210		
	9.75	9.06	$1/\sqrt{9}$	300		
3 wt% Ag/Pc	3.30	26.82	1	100	4.84	3.34
	5.74	15.4	$1/\sqrt{3}$	110		
	8.73	10.11	$1/\sqrt{7}$	210		
	9.9	8.93	$1/\sqrt{9}$	300		

5.3.4.4 FE-SEM and absorption studies

The self-assembly of nanoparticles in phthalocyanine discotic liquid crystals is further investigated by FE-SEM. A very dilute solution of nanocomposites in anhydrous chloroform was drop casted on ITO coated glass substrate for FE-SEM measurements and images are shown in **Figure 9**, which clearly show the uniform distribution of metal nanoparticles in Pc system at room temperature. The absorption properties of Pc and its composites were measured using UV-visible spectroscopy using arbitrary concentration of anhydrous chloroform solvent at room temperature. There are two intense strong absorption bands; one is in UV region between 250–350 nm called B-band (Soret) and another intense band in visible part of spectrum between 650–710 nm called Q-band. The splitting of Q-band in 664 nm and 701 nm is expected due to D_{2h} symmetry. All the derivatives show similar splitting of Q-bands. These intense bands are responsible for $\pi \rightarrow \pi^*$ transitions. The absorption spectra of all the composites are also shown in **Figure 10**. All the composites show the characteristics absorption peaks of Pc and no additional absorption peaks of MNPs were observed. This could be because of the very small concentrations of metal nanoparticles in DLC.

5.3.5 DC conductivity measurements

The temperature dependent DC conductivity measurements of the pure metal-free phthalocyanine compound and its Ag & Au nanocomposites were measured to examine the effect of dispersion of metal nanoparticles on the electrical properties of Pc-DLC. The pure Pc DLC compound is liquid crystalline at room temperature and goes to the isotropic phase at about 300 °C. The DC conductivity with respect to the temperature of pure PC compound is very low and in the order of 10^{-10} S/m at room temperature and same at 300 °C. The conductivity plots are depicted in **Figure 11** which show the variation in the conductivity of nanocomposites of Pc-DLCs with temperature. The nanocomposites doped with Ag and Au nanoparticles show significant enhancement in the conductivity to the order of two to four. It is observed that the electrical conductivity of 0.5 wt% Ag/Pc is 2.88×10^{-9} S/m and in 3 wt% Ag/Pc it is 6.96×10^{-9} S/m at 60 °C, as the temperature increases there is a shift in conductivity of order of 4 for both composites of silver nanoparticles and it is 1.42×10^{-5} S/m and 5.29×10^{-5} S/m, for the same composites at 300 °C (**Figure 11a**). The shift of the conductivity with the doping of gold

nanoparticles is also similar to the silver nanoparticles. In 0.5 wt% Au/Pc it is 4.03×10^{-9} S/m and in 3 wt% Ag/Pc it is 1.09×10^{-8} S/m. At higher temperature it is 5.5×10^{-6} S/m and 1.35×10^{-5} S/m for the composites 0.5 wt% Au/Pc and 3 wt% Au/Pc respectively (**Figure 11b**). This enrichment to the conductivity of nanocomposites can be corroborated due to the formation of electron donor-acceptor interaction between electron rich metal free phthalocyanine and the metallic nanoparticles. A graphical representation of spherical MNPs dispersed randomly in the columnar phase is presented in **Figure 12**. The overall conductivity in these systems is probably the sum of electronic and ionic conductivities. At lower temperature, where the mesophase is more ordered, electronic conductivity dominates while at higher temperature ionic conductivity plays a major role. The increase in conductivity with increase in temperature could be due to high ionic or NPs mobility at higher temperatures. These results are in accordance to previously published results on gold NPs and CdSe and CdTe QDs doped DLCs [27–41].

5.3.6 Thermogravimetric analysis

The thermal stability of the pure Pc and its nanocomposites was further examined using thermogravimetric analysis. The nanocomposites and phthalocyanine were subjected to a heat rate of $10 \text{ }^\circ\text{C min}^{-1}$ under nitrogen atmosphere. All the composites start decomposing at about $350 \text{ }^\circ\text{C}$ and completely decomposed at $500 \text{ }^\circ\text{C}$ as shown in **Figure 13**. The thermogravimetric analysis reveals that decomposition temperatures of all nanocomposites are higher than isotropic temperature and all the nanocomposites were stable up to $350 \text{ }^\circ\text{C}$ under inert atmosphere.

5.3.7 Nonlinear optical transmission measurements

The nonlinear optical transmission of pure Pc DLCs and its nanocomposites were studied using the open aperture Z-scan technique at the wavelength of 532 nm using 5 ns laser pulses obtained from a frequency doubled Nd:YAG laser (Minilite I, Continuum). The laser output was spatially filtered to obtain a nearly perfect Gaussian beam profile.

In the experiment, the laser beam was focused using a plano-convex lens of 10.8 cm focal length. The sample to be measured was taken in a 1 mm path length quartz cuvette and translated along the axis of the laser beam (z-axis) by means of a stepper motor controlled linear translation

stage. The experimental set up is represented in chapter 3C. All the samples were prepared in anhydrous chloroform solvent to have a linear transmission of 75% at 532 nm. By fixing the input laser pulse energy (E) at a suitable value (5 μJ in the present case) and translating the sample along the laser beam through the focal point, the incident laser fluence (F_{in}(z)) seen by the sample was varied. Maximum fluence is at the focal point, and it reduces as a Lorentzian function to either side (i. e., for z > 0 and z < 0). The transmitted energy for different sample positions (z) with respect to the focus was measured using a pyro electric energy detector (Laser probe, RJP-735). Z-scan curves were obtained by plotting the normalized energy transmittance T_{norm} (where the linear transmission is taken as unity) against the sample positions (inset of **Figure 14**). We note that for a spatially Gaussian Beam, the fluence (F_{in}(z)) at any position z can be calculated from the expression

$$F_{in}(z) = 4 (\ln 2)^{1/2} E_{in} / \pi^{3/2} \omega(z)^2 \dots\dots\dots (1)$$

where the beam radius ω(z) is given by

$$\omega(z) = \omega_0 (1 + (z/z_0)^2)^{1/2} \dots\dots\dots (2)$$

Here ω₀ is the focal spot radius and z₀ = πω₀²/λ is the Rayleigh range. T_{norm} can now be plotted as a function of F_{in}(z), as shown in **Figure 14**.

We note that the net nonlinear transmission, in the present case can have contributions from reverse saturable absorption (RSA, sometimes referred to as *effective* two-photon absorption in literature) and saturable absorption [44]. The nonlinear absorption coefficient can then be written in the form

$$\alpha(I) = \frac{\alpha_0}{1 + I/I_s} + \beta I \dots\dots\dots (3)$$

where I_s is the saturation intensity (in W/m²) and β is the RSA coefficient (in m/W). The corresponding pulse propagation equation is given by

$$\frac{dI}{dx} = - \left[\frac{\alpha_0}{1 + \left(\frac{I}{I_s}\right)} + \beta I \right] I \dots\dots\dots (4)$$

which can be fitted to the nonlinear transmission data shown in **Figure 14** (here x is the propagation distance within the sample). Values of I_s and β can be obtained from the numerical fit. The calculated values of I_s and β are given in **Table 3**. By comparing with literature values available for various NLO materials [44] it can be seen that the β values are quite high.

We ran one more set of Z-scans at a higher laser pulse energy of 15 micro Joules to determine the optical limiting thresholds (fluence at which T_{norm} drops to 0.5) of the samples (**Figure 15**). The estimated values are given in **Table 4**. T_{norm} drops to low values (≈ 0.25) in the focal region in **Figure 15**, revealing strong optical limiting in the samples.

Table 3. RSA coefficient (β) and saturation intensity (I_s) calculated for the samples from the data given in **Figure 14**.

Sample name	Laser pulse Energy (μJ)	β ($\times 10^{-10}$ m/W)	I_{sat} ($\times 10^{10}$ W/m ²)
Pc	5	1.6	45
Pc + 0.5 wt% Ag NPs	5	3.0	26
Pc + 0.5 wt% Au NPs	5	2.5	25
Pc + 3 wt% Ag NPs	5	2.7	27
Pc + 3 wt% Au NPs	5	5.0	50

Table 4. Optical limiting thresholds estimated for the samples from **Figure 15**.

Sample name	Laser pulse Energy (μJ)	Threshold Fluence ($\times 10^4 \text{ J/m}^2$)
Pc	15	0.98
Pc + 0.5 wt% Ag NPs	15	1.01
Pc + 0. wt5% Au NPs	15	1.17
Pc + 3 wt% Ag NPs	15	0.99
Pc + 3 wt% Au NPs	15	0.82

5.3.8 Conclusions

In conclusions, we have observed that the dispersion of metal nanoparticles (Ag and Au) in metal free phthalocyanine DLCs results in higher conductivity and nonlinear transmission properties compared to the pure compound. The POM, DSC and SAXS studies reveal that the doping of MNPs into discotic liquid crystals does not disturb the nature of mesophase with different concentration variations, except for a minor shift in the transition temperature. Hybrid composites of these liquid crystals possess high conductivity compared to pure DLC. The doping of metal nanoparticles into Pc liquid crystals leads to an enhancement of the nonlinear optical absorption response. Between Au and Ag NPs doping, Au NPs result in a higher enhancement. The enhanced conductivity and NLO properties make MNPs doped Pc DLC a potential candidate for optoelectronics and photonics applications.

5.3.9 Experimental section

5.3.9.1 Materials and methods

Silver-nitrate (AgNO_3), gold-chloride trihydrate ($\text{HAuCl}_4 \cdot 3\text{H}_2\text{O}$), *n*-hexanethiol, sodium borohydride (NaBH_4), tetra-octylammonium bromide (TOAB), acetone, toluene, dichloromethane and absolute ethanol are used for the synthesis of MNPs having AR-grade quality and purchased from Sigma-Aldrich. The synthesis of metal nanoparticles was carried out using deionized (DI) water. The solvents were dried using standard protocol. Absorption spectra were recorded on a Perkin Elmer UV-Vis-lambda 353 double beam-spectrophotometer. The exact size distribution and morphology of MNPs/Pc were estimated using SEM ZEISS Ultra-plus (40-98). FE-SEM and HR-TEM images were collected using JEOL microscope with an operating voltage of 200 kV. Sample (1 mg) was dissolved in 10 cm^3 chloroform and sonicated for 30 min. A drop of the sample was deposited on the copper grid and allowed to dry for 3 hour before TEM characterization. The decomposition temperature of all nano-composite and pure phthalocyanine was carried out using TGA 4000 thermogravimetric analysis instrument. Measurements of the DC conductivity was carried out using a DC voltage source (0.5 V), Keithley Picometer (modal 480) along with a temperature controller. The general methods used for characterisation of metal free phthalocyanines DLCs are depicted in the Chapter 2.

5.3.9.2 Synthesis of metal free phthalocyanine DLC

The compound **6** (1.97 g, 4.47 mmol) was dissolved in absolute ethanol (75 mL) and was added 1,5-diazabicyclo[4.3.0]non-5-ene (DBN) (0.61 g, 4.91 mmol). The reaction mixture was refluxed for 96 hours under dry nitrogen atmosphere. The reaction mixture was allowed to cool to room temperature and poured in to 500 mL of dry acetone. The crude solid was filtered and purified by column chromatography using silica gel (hexane/DCM 8:2). Recrystallisation of pure compound several times, with excess of cold acetone affords green colour metal free phthalocyanine **1**. Yield: 16 %; IR (film) ν_{max} : 3406, 2935, 2924, 2852, 1614, 1504, 1454, 1377, 1280, 1195, 1033, 721 cm^{-1} . ^1H NMR (500 MHz, CDCl_3): δ = 8.85 (br, 8H, s), 4.59 (br, 16H, s); 2.16 (br, 8 H, d), 1.89 (br, 16 H, s), 1.59–1.10 (br, 58 H, m), 1.10 (24 H, s), 0.91 ppm (48 H, d, J = 6Hz); ^{13}C NMR (125 MHz, CDCl_3): δ = 152.1, 130.5, 105.5, 68.0, 39.3, 37.6, 37.5, 36.4, 30.2, 28, 24.8, 22.7, 22.6, 19.8 ppm; elemental analysis: $\text{C}_{112}\text{H}_{178}\text{N}_8\text{O}_8$; calculated: C, 76.14; H, 10.16; N, 6.34; % found: C, 75.97; H, 10.29; N, 6.04. The IR, ^1H and ^{13}C NMR of compound **1** is shown in **Figure 1**.

5.3.9.3 Synthesis of metal nanoparticles

Synthesis of hexanethiol capped gold nanoparticles (AuNPs):

Gold nanoparticles capped with hexanethiol monolayer were prepared by following the reported procedure with some modification. Thus, a solution of tetra-octylammonium bromide (TOAB, 1.1 g) in toluene (65 mL) was added to stirring solution of 158 mg of $\text{HAuCl}_4 \cdot 3\text{H}_2\text{O}$ in 250 mL round-bottom flask and allowed to stirred for 30 minutes at room temperature. To this reaction mixture, *n*-hexanethiol (170 μL) was added and reaction was continuously stirred for 20 minutes and followed by a solution of freshly prepared NaBH_4 (450 mg) dissolved in water (5 mL) added slowly under vigorous stirring till the color of the solution become dark brown indicating the formation of the gold-nanoparticles. This reaction mixture was stirred for 24 hours at room temperature. Later, the organic phase was separated and evaporated in a rotary evaporator under high vacuum at room temperature. The crude material was mixed with absolute ethanol (50 mL) and centrifuged at 5000 rpm for 30 min to remove non-covalently bounded organic impurities. The resulting hexanethiol-protected AuNPs were re dissolved in dry dichloromethane (1 mL) and precipitated with absolute ethanol (10 mL). The centrifugation and redispersal process was repeated several times to get pure AuNPs. These gold-nanoparticles are well soluble in organic solvents like dichloromethane and chloroform. The average diameter of the gold nanoparticles is 2-4 nm.

Synthesis of hexanethiol capped silver nanoparticles (Ag NPs):

Neat *n*-hexanethiol (0.138g, 1.17 mmol) was added to a stirring solution of silver nitrate (0.2g, 1.176 mmol) in absolute ethanol (20 mL) at room temperature. A light yellow cloudy solution appeared during *n*-hexanethiol addition, which indicates the formation of silver thiolates. The reaction mixture was allowed to stirred for 1 hour at room temperature. To this reaction mixture a freshly prepared saturated solution of sodium borohydride (0.31 g, 8.23 mmol) in absolute ethanol (5 mL) was added to the dropwise under vigorous stirring at room temperature. After completion of sodium borohydride addition the reaction mixture turns dark brown in color and allowed to stirred further three hours at same temperature. The reaction mixture allowed to keep refrigerating overnight to get precipitation of nanoparticles and filtered through qualitative filter paper, washed with excess of acetone and followed by water to remove

water soluble impurities. The material was again washed with acetone and dried over night under vacuum to get fine powdered silver nanoparticles. These AgNPs are well soluble in dichloromethane and chloroform. The average diameter of the silver nanoparticles is 3–5 nm.

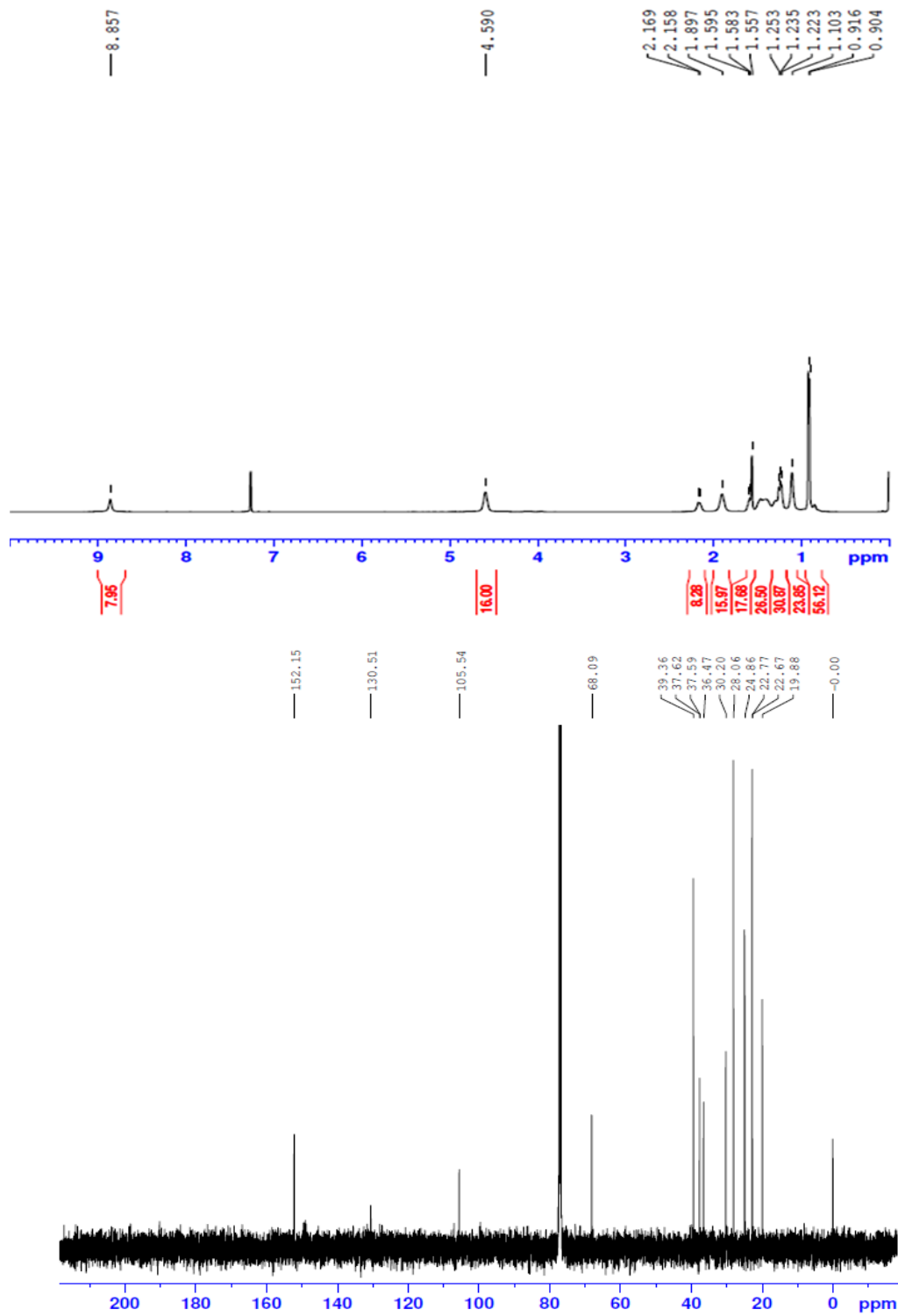


Figure 1. IR, ^1H NMR and ^{13}C NMR compound 1.

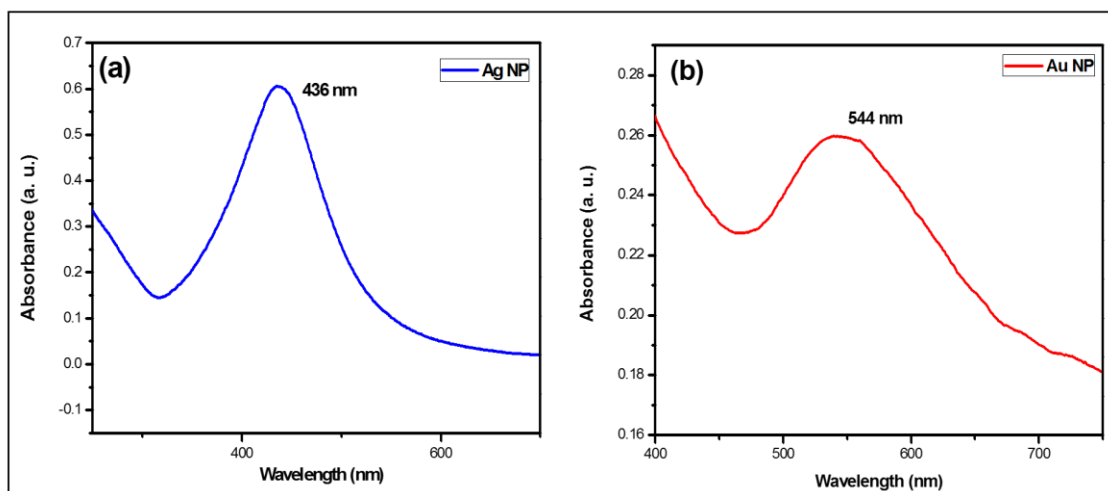


Figure 2. UV-Vis spectra of alkanethiol capped MNPs dichloromethane solvent: (a) Ag NPs; and (b) Au NPs.

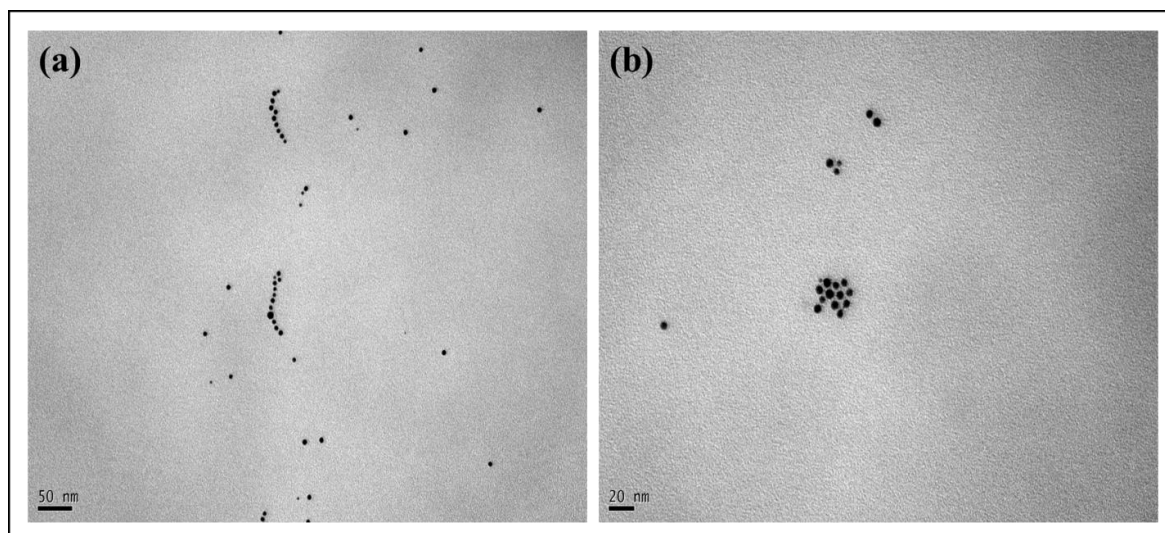


Figure 3. TEM image of (a) gold, and (b) silver nanoparticles with average diameter of 2-4 nm

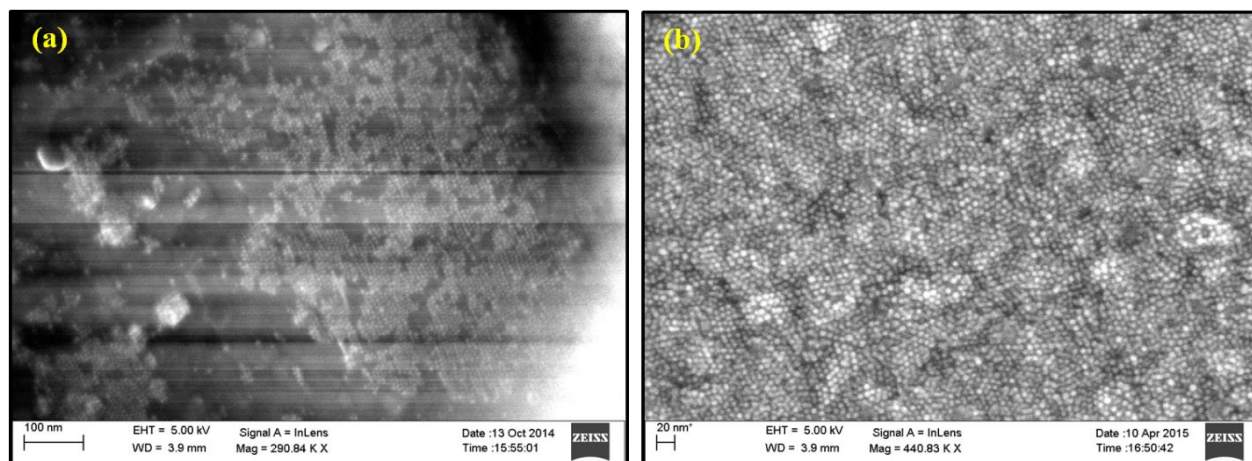


Figure 4. The SEM image of (a) gold and (b) silver nanoparticles.

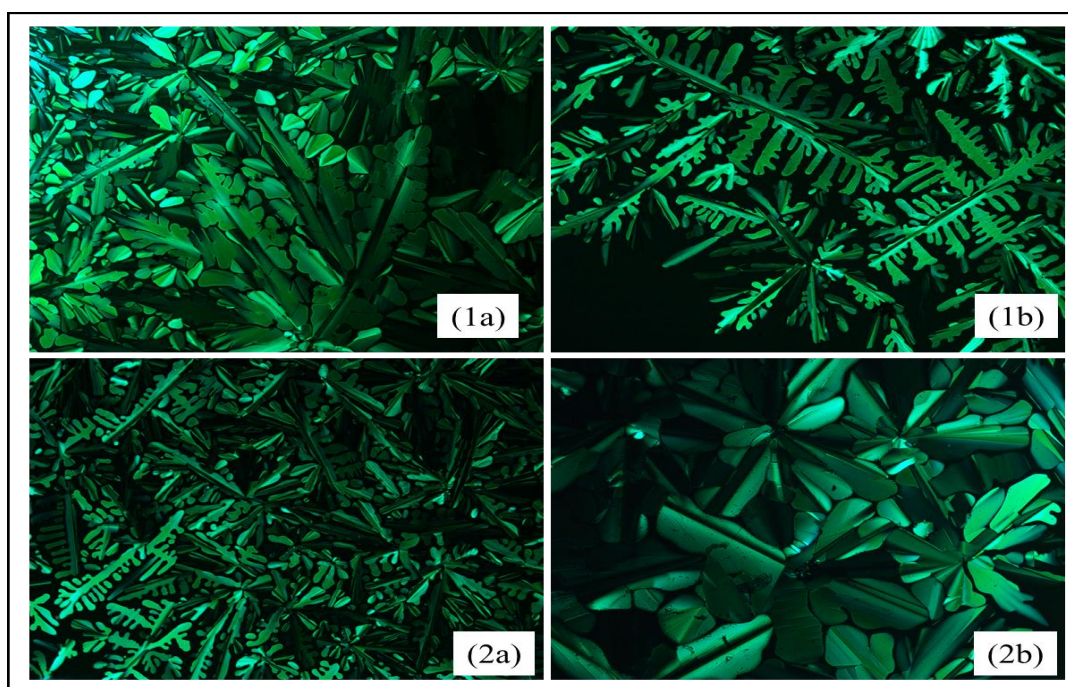


Figure 5. POM images of the columnar phase of Ag and Au NPs doped phthalocyanine. All the optical texture are viewed through cross-polariser upon cooling from isotropic temperature. **(1a)** 0.5 wt% Ag NPs /Pc composite, viewed at $200 \times$ magnifications, **(1b)** 3 wt% Ag NPs /Pc composite, viewed at $100 \times$ magnifications, **(2a)** 0.5 wt% Au NPs /Pc composite, viewed at $100 \times$ magnifications, **(2b)** 3 wt% Au NPs /Pc composite, viewed at $200 \times$ magnifications.

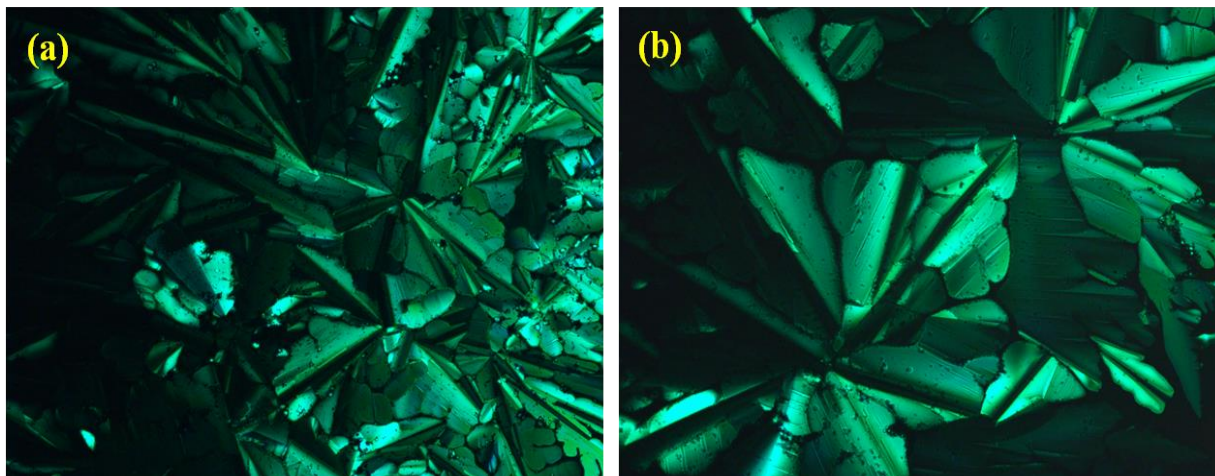


Figure 6. The POM images of small aggregates of metal nanoparticles. (a) 5 wt% Au/Pc; (b) 5 wt% Ag/Pc nano composites.

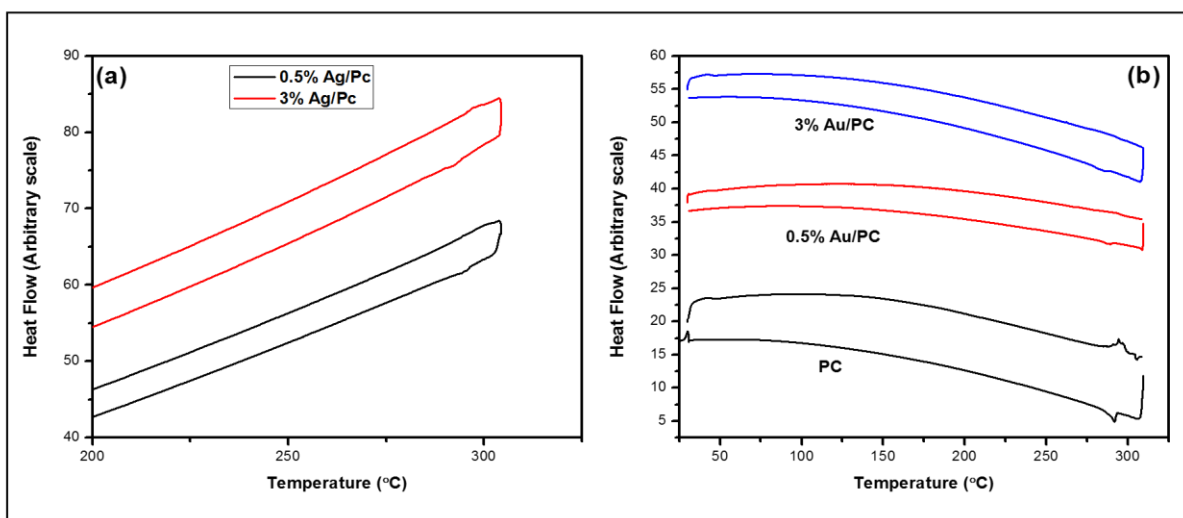


Figure 7. DSC plots for the Pc, 0.5 wt% MNPs/Pc and 3 wt% MNPs/Pc composites recorded at a rate of $5\text{ }^{\circ}\text{C min}^{-1}$. It is clear from the plots that phase transitions are not significantly changed after doping with MNPs: (a) Ag/Pc, and (b) Au/Pc nano composites.

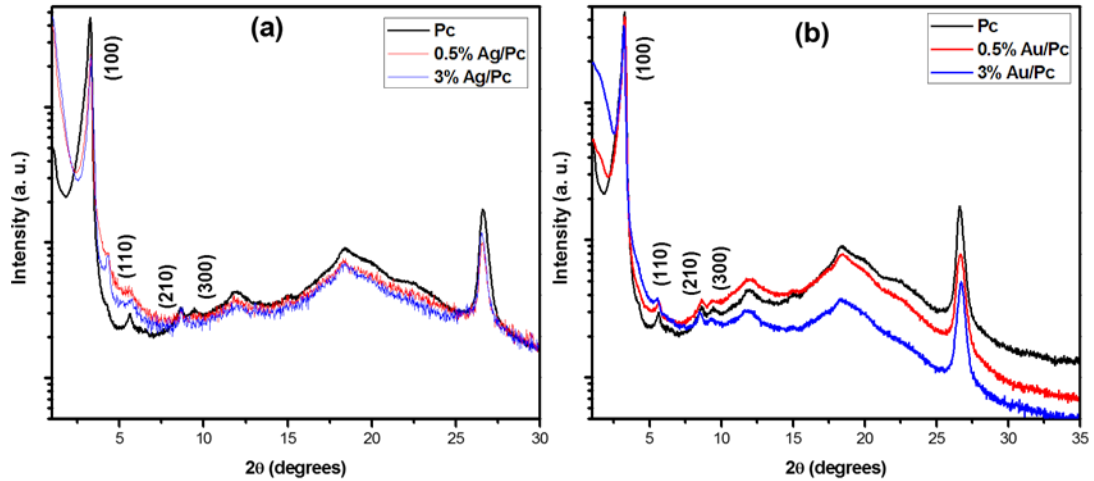


Figure 8. Intensity vs. 2θ plots for: (a) Pc, 0.5% Ag/Pc and 3% Ag/Pc, and (b) Pc, 0.5% Au/Pc and 3% Au/Pc (SAXS pattern was recorded at room temperature).

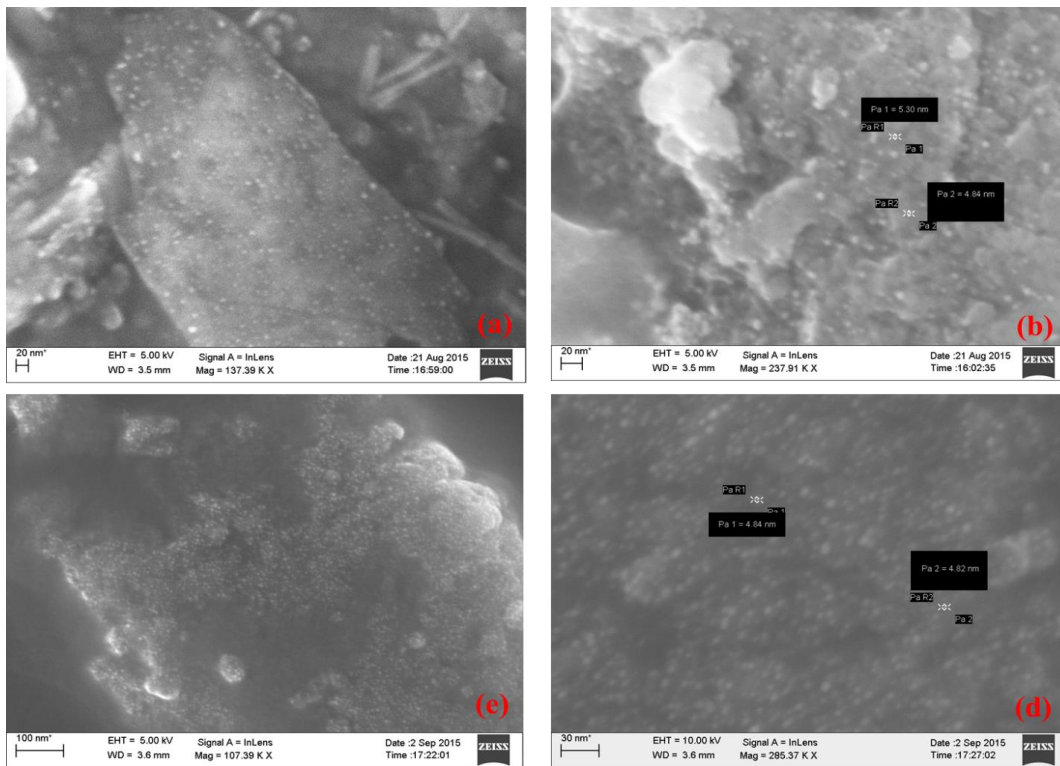


Figure 9. FE-SEM images of (a) 3 wt% Au/Pc and (c) 3 wt% Ag/Pc showing presence nanoparticles in composites; The expanded portion of showing the size distribution of nanoparticles (b) and (d).

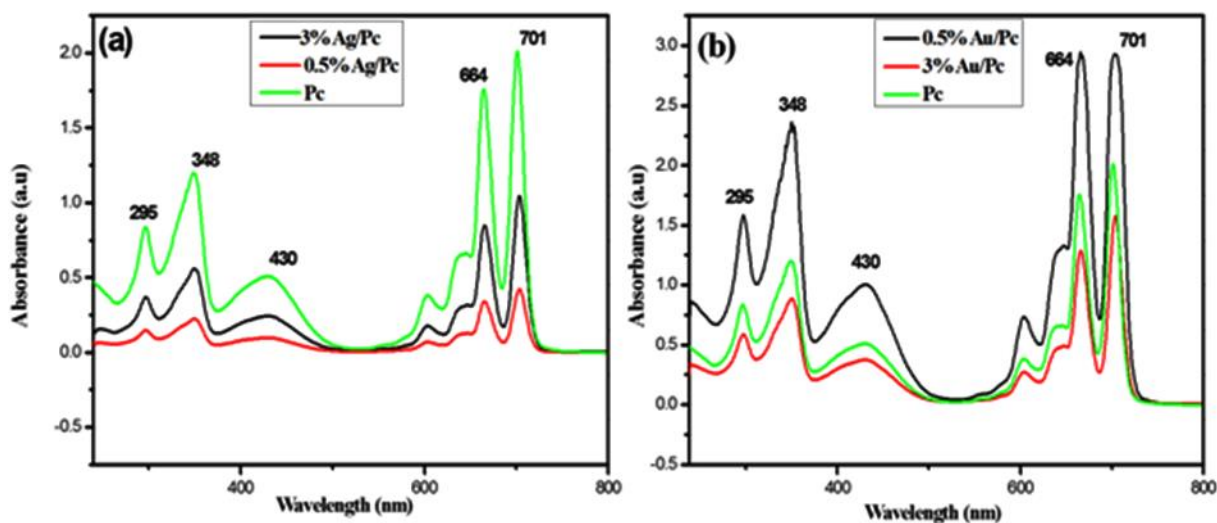


Figure 10. The UV-Visible spectroscopy of metal free-Phthalocyanine and nano composites recorded in chloroform solvent. (a) Ag/Pc composites, and (b) Au/Pc composites.

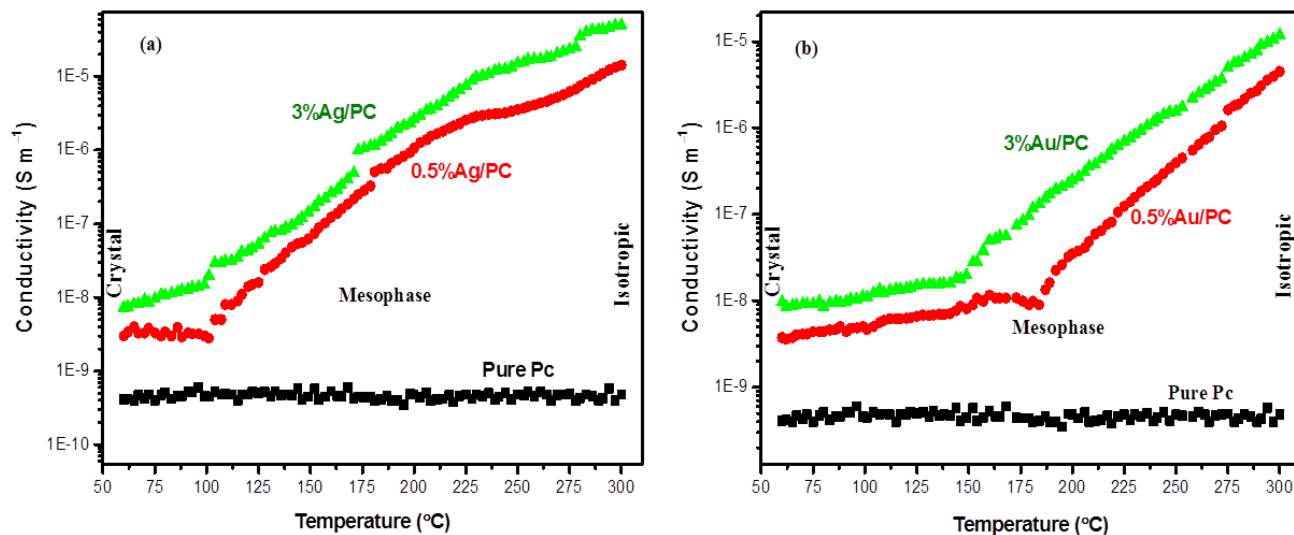


Figure 11. The DC conductivity values as a function of temperature for the undoped Pc (black), (a) 0.5% and 3% Ag/Pc, and 0.5% and 3% Au/Pc nanocomposites.

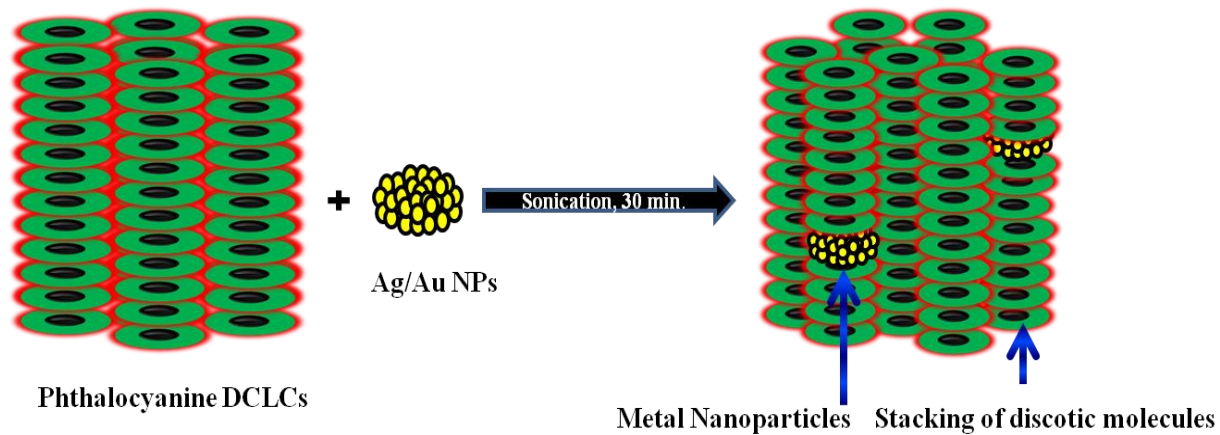


Figure 12. Schematic illustration of self-assembly of MNPs in a columnar matrix of discotic mesogen.

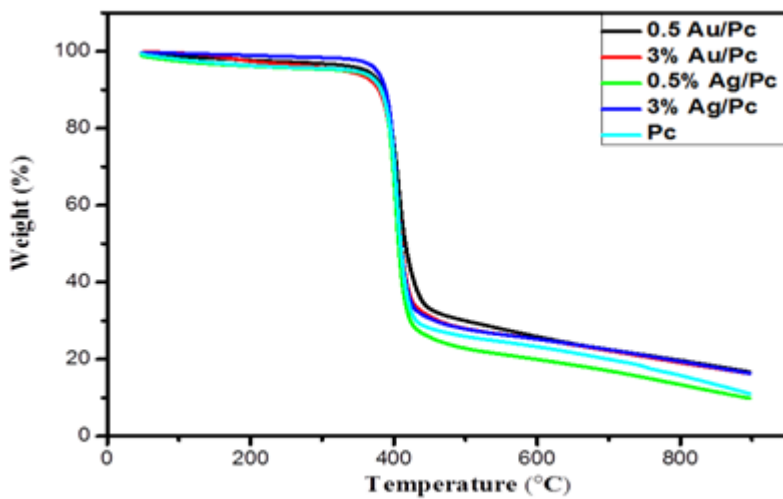


Figure 13. TGA thermograms of undoped phthalocyanine and nanocomposites.

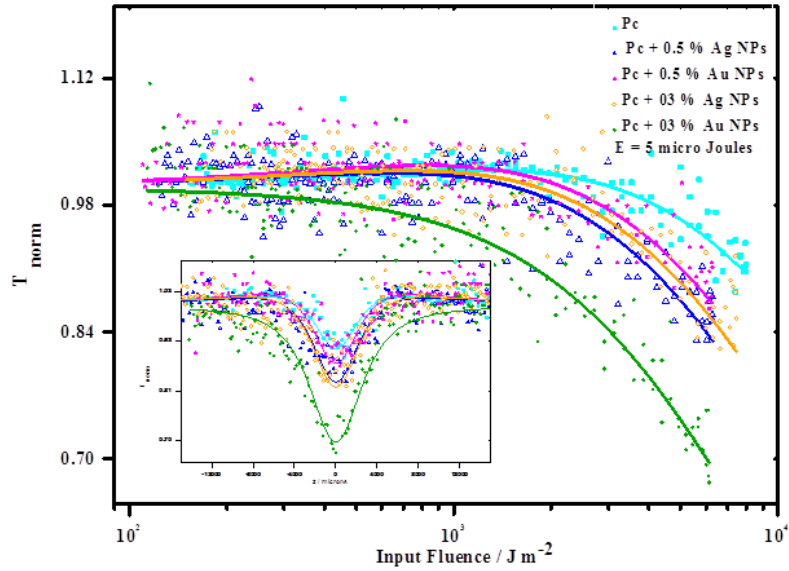


Figure 14. Normalized transmission as a function of input laser fluence, calculated from open aperture Z-scan measurements done at a laser pulse energy of 5 micro Joules. The Z-scans are given in the inset. Doping with metal nanoparticles enhances the nonlinear response of the Pc liquid crystal. Solid curves are numerical fits to the data using equation 4, from which the values of I_s and β are calculated.

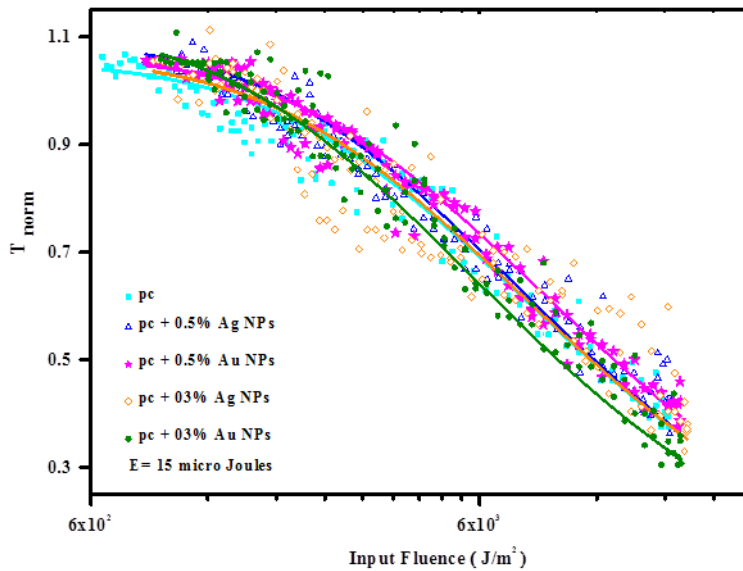


Figure 15. Normalized transmission as a function of input fluence, calculated from open aperture Z-scan measurements done at a laser pulse energy of 15 micro Joules. Optical limiting thresholds estimated from this data are given in **Table 4**.

References

- [1] Eichhorn H. *J. Porphyr. Phthalocyanines.*, **2000**, 4, 88–102; (b) van Nostrum C. F, Nolte R. J. M. *Chem. Commun.*, **1996**, 2385–2392; (c) Elemans JAAW, van Hameren R. Nolte R.J.M, Rowan A. E. *Adv. Mater.*, **2006**, 18, 1251–1266.
- [2] (a) Wöhrle D, Schnurpfeil G, Makarov S. G, Kazarin A. *Macroheterocycles.*, **2012**, 5, 191–202; (b) Hohnholza D, Steinbrecherb S, Hanacka M, *J. Mol. Structure.*, **2000**, 521, 231–237; (c) Ichihara M, Miida M, Mohr B. et al. *J. Porphyr. Phthalocyanines.*, **2006**, 10, 1145–1155; (d) Fernandez O, de la Torre G, Lazaro F. F, Barbera J. et al. *Chem. Mater.*, **1997**, 9, 3017–3022.
- [3] (a) Claessens C. G, Hahn U, Torres T. *Chem. Rec.*, **2008**, 8, 75–97; (b) de la Torre G, Vazquez P, Lopez F. A, Torres T. *J. Mater. Chem.*, **1998**, 8, 1671–1683; (c) de la Torre G, Vazquez P, Lopez F. A, Torres T. *Chem. Rev.*, **2004**, 104, 3723–3750.
- [4] (a) Schouten PG, Van Der Pol JF, Zwikker JW, Drenth W. et al. *Mol. Cryst. Liq. Cryst.*, **1991**, 195, 291–305; (b) Schouten PG, Warman JM, de Haas MP, van Nostrum CF. et al. *J. Am. Chem. Soc.*, **1994**, 116, 6880–6894; (c) Weber P, Guillon D, Skoulios A. *Liq. Cryst.*, **1991**, 9, 369–382; (d) Chambrier I, Cook MJ, Helliwell M, Powell AK. *J. Chem. Soc. Chem. Commun.*, **1992**, 444–445.
- [5] (a) Helliwell M, Deacon A, Moon KJ, Powell AK. et al. *Acta Cryst.*, **1997**, B53, 231–240; (b) Weber P, Guillon D, Skoulios A. *J. Phys. Chem.*, **1987**, 91, 2242–2243; (c) Andre JJ, Bernard M, Piechocki C, Simon J. *J. Phys. Chem.*, **1986**, 90, 1327–1330.
- [6] (a) Markovitsi D, Thi THT, Briois V. *J. Am. Chem. Soc.*, **1988**, 110, 2001–2002; (b) Markovitsi D, Lecuyer I. *Chem. Phys. Lett.*, **1988**, 149, 330–333; (c) Markovitsi D, Lecuyer I, Simon J. *J. Phys. Chem.*, **1991**, 95, 3620–3626; (d) Blasse G, Dirksen GJ, Meijerink A, van der Pol JF, Neeleman E, Drenth W. *Chem. Phys. Lett.*, **1989**, 154, 420–424.
- [7] (a) Belarbi Z, Sirlin C, Simon J, Andre JJ. *J. Phys. Chem.*, **1989**, 93, 8105–8110; (b) Schutte WJ, Rehbach MS, Sluyters JH. *J. Phys. Chem.*, **1993**, 97, 6069–6073; (c) Osburn EJ, Schmidt A, Chau LK, Chen SY, Smolenyak P. et al. *Adv. Mater.*, **1996**, 8, 926–928.

- [8] (a) Duzhko V, Singer KD. *J. Phys. Chem. C.*, **2007**, 111, 27–31; (b) Nalwa HS, Engel MK, Hanack M, Schultz H. *Appl. Organomet. Chem.*, **1996**, 10, 661–664; (c) Sato M, Takeuchi A, Yamada T, et. al. *Phys. Rev. E.*, **1997**, 56, R6264–R6266.
- [9] (a) Cook MJ, McKeown NB, Thomson AJ, Harrison KJ, et al. *Chem. Mater.*, **1989**, 1, 287–289; (b) Poynter RH, Cook MJ, Chesters MA, et. al. *Thin Solid Films.*, **1994**, 243, 346–350; (c) Kumaran N, Donley CL, Mendes SB, Armstrong NR. *J. Phys. Chem C.*, **2008**, 112, 4971–4977.
- [10] (a) Qiu X, Wang C, Zeng Q, Xu B, et. al. *J. Am. Chem. Soc.*, **2000**, 122, 5550–5556; (b) Mouthuy PO, Melinte S, Geerts YH, et. al. *Small.*, **2008**, 4, 728–732; (c) Tracz A, Makowski T, Masirek S, Pisula W, Geerts Y. H. *Nanotechnology.*, **2007**, 18, 485303.
- [11] Piechocki C, Simon J, Skoulios A, Guillon D. et al. *J. Am. Chem. Soc.*, **1982**, 104, 5245–5247
- [12] (a) Leznoff CC, Lever ABP. (eds.). *Phthalocyanines, Properties and Applications*, Vol. 2, VCH, New York, p. 226, **199**; (b) Ohta K, Jacquemin L, Sirlin C, et. al. *New J. Chem.*, **1988**, 12, 751–754; (c) Piechocki C, Simon J. *J. Chem. Soc. Chem. Commun.*, **1985**, 259–260.
- [13] (a) Knawby DM, Swager TM. *Chem. Mater.*, **1997**, 9, 535–538; (b) He N, Chen Y, Doyle J, Liu Y, Blau W. J. *Dyes Pigm.*, **2008**, 76, 569–573; (b) Piechocki C, Boulou JC, Simon J. *Mol. Cryst. Liq. Cryst.*, **1987**, 149, 115–120; (c) Guillon D, Weber P, Skoulios A, Piechocki C, Simon J. *Mol. Cryst. Liq. Cryst.*, **1985**, 130, 223–229.
- [14] (a) Hanack M, Beck A, Lehmann H. *Synthesis.*, **1987**, 703–705; (b) Sirlin C, Bosio L, Simon J. *Mol. Cryst. Liq. Cryst.*, **1988**, 155, 231–238; (c) Sirlin C, Bosio L, Simon J. *J. Chem. Soc. Chem. Commun.*, **1987**, 379–380.
- [15] (a) Cho I, Lim Y. *Mol. Cryst. Liq. Cryst.*, **1988**, 154, 9–26; (b) Sleven J. Mesomorphism and optical properties of peripherally substituted phthalocyanines; Influence of chain length, linking group and central metal ion, PhD thesis, The Katholieke Universiteit, Leuven, Belgium, **2002**; (c) Cho I, Lim Y. *Bull. Korean Chem. Soc.*, **1988**, 9, 98–101.
- [16] (a) van der Pol JF, Neeleman E, Zwikker JW. et. al. *Liq. Cryst.*, **2006**, 33, 1378–1387; (b) Sleven J, Cardinaels T, Binnemans K, et. al. *Liq. Cryst.*, **2003**, 30, 143–148; (c)

- Haisch P, Knecht S, Schlick U, Subramanian LR, Hanack M. *Mol. Cryst. Liq. Cryst.*, **1995**, 270, 7–16.
- [17] (a) Vacus J, Doppelt P, Simon J, Memetzidis G. *J. Mater. Chem.*, **1992**, 2, 1065–1068; (b) Sauer T, Wegner G. *Mol. Cryst. Liq. Cryst.*, **1998**, 162B, 97–118; (c) Severs LM, Underhill AE, Edwards D. et. al. *Mol. Cryst. Liq. Cryst.*, **1993**, 234, 235–240.
- [18] (a) Kimura M, Ueki H, Ohta K, Shirai H, Kobayashi N. *Langmuir.*, **2006**, 22, 5051–5056; (b) Nolte RJM, van der Pol JF, Neeleman E, Zwikker JW. et. al. *Liq. Cryst.*, **2006**, 33, 1373–1377.
- [19] (a) Belushkin AV, Cook MJ, Frezzato D. et. al. *Mol. Phys.*, **1998**, 93, 593–607; (b) Orti E, Bredas JL, Clarisse C. *J. Chem. Phys.*, **1990**, 92, 1228–1235.
- [20] (a) Cuellar EA, Marks TJ. *Inorg. Chem.*, **1981**, 20, 3766–3770; (b) Engel MK, Bassoul P, Bosio L, Lehmann H, Hanack M, Simon J. *Liq. Cryst.*, **1993**, 15, 709–722; (c) Adib Z. A, Clarkson GJ. et. al. *J. Mater. Chem.*, **1998**, 8, 2371–2378.
- [21] (a) Kimura M, Narikawa H, Ohta K. et. al. *Chem. Mater.*, **2002**, 14, 2711–2717; (b) Haisch P, Winter G, Hanack M. et. al. *Adv. Mater.*, **1997**, 9, 316–321; (c) Henari F, Davey A, Blau W, Haisch P, Hanack M. *J. Porphyr. Phthalocyanines.*, **1999**, 3, 331–338.
- [22] (a) Rao CNR, Muller A, Cheetham AK. *The chemistry of nanomaterials: synthesis, properties and applications*. John Wiley & Sons, **2006**; (b) Schmid G. *Clusters and Colloids, From Theory to Applications*; Wiley-VCH: Weinheim, Germany, **1994**.
- [23] (a) Daniel M.-C, Astruc D. *Chem. Rev.*, **2004**, 104, 293–346; (b) Burda C, Chen X, Narayanan R, El-Sayed MA. *Chem. Rev.*, **2005**, 105, 1025–1102.
- [24] (a) Wang Y, Herron N. *J. Phys. Chem.*, 1991, 95, 525–532; (b) Hamilton JF, Baetzold R. *Science*. **1979**, 205, 1213–1220; (c) Mansur HS, Grieser F, Marychurch MS, et. al. *J. Chem. Soc. Faraday. Trans.*, **1995**, 91, 665–672.
- [25] (a) Senapati S. Ph.D. Thesis. India: Biosynthesis and immobilization of nanoparticles and their applications; University of pune; **2005** pp. 1–57; (b) Klaus-Joerger T, Joerger R, Olsson E, Granqvist CG. *Trends. Biotechnol.*, **2001**, 19, 15–20; (c) Sastry M, Ahmad A, Khan MI, Kumar R. *Curr. Sci.*, **2003**, 85, 162–170; (d) Sylvestre JP, Kabashin AV, Sacher E, et. al. *J. Am. Chem. Soc.*, **2004**, 126, 7176–7177.

- [26] (a) Louis C, Pluchery O. (eds). *Gold Nanoparticles for Physics, Chemistry and Biology*. Imperial College Press, London, **2012**; (b) Zhao P, Li N, Astruc D. *Coordination Chem. Rev.*, **2013**, 257, 638–665.
- [27] (a) Kumar S, Lakshminarayanan V. *Chem. Commun.*, **2004**, 1600–1601; (b) Kumar S, Pal SK, Kumar PS, Lakshminarayanan V. *Soft Matter.*, **2007**, 3, 896–900.
- [28] Holt LA, Bushby RJ, Evans SD, Burgess A. et. al. *J. Appl. Phys.*, **2008**, 103, 063712.
- [29] Boden N, Bushby RJ, Clements J. *J. Chem. Phys.*, **1993**, 98, 5920–5931
- [30] Shen Z, Yamada M, Miyake M. *J. Am. Chem. Soc.*, **2007**, 129, 14271–14280.
- [31] Supreet, Pratibha R, Kumar S, Raina KK. *Liq. Cryst.*, **2014**, 41, 933–939.
- [32] Mishra M, Kumar S, Dhar R. *RSC Adv.*, **2014**, 4, 62404–62412
- [33] Yaduvanshi P, Mishra A, Kumar S, Dhar R. *Liq. Cryst.*, **2015**, 42, 1478–1489.
- [34] Basova TV, Parkhomenko RG, Igumenov IK. et. al. *Dyes Pigments.*, **2014**, 111, 58–63.
- [35] (a) Kumar S. *Nanoparticles in discotic liquid crystals*. In *Liquid Crystals with Nano- and Microparticles*; Lagerwall JPF, Scalia G. Eds.; World Scientific: Singapore, **2017**; Volume I & II, pp. 461–496; (b) Stamatoiu O, Mirzaei J, Feng X, Hegmann T. *Top. Curr. Chem.*, **2012**, 318, 331–393; (c) Nealon GL, Greget R, Dominguez C, Nagy ZT. et.al. *Beilstein J. Org. Chem.*, **2012**, 8, 349–370.
- [36] (a) Lagerwall JPF, Scalia G. *Current Appl. Phys.*, **2012**, 12, 1387–1412; (b) Kumar S, Sagar LK. *Chem. Commun.*, **2011**, 47, 12182–12184; (c) Kumar M, Kumar S. *RSC Adv.*, **2015**, 5, 1262–1267.
- [37] (a) Kumar S, Bisoyi HK. *Angew. Chem. Int. Ed.*, **2007**, 46, 1501–1503; (b) Bisoyi HK, Kumar S. *J. Mater. Chem.*, **2008**, 18, 3032–3039; (c) Shivanandareddy AB, Krishnamurthy S, Lakshminarayanan V, Kumar S. *Chem. Commun.*, **2014**, 50, 710–712.
- [38] Kanayama N, Tsutsumi O, Kanazawa A. et. al. *Chem. Commun.*, **2001**, 2640–2641, (b) In I, Jun YW, Kim YJ, Kim SY. *Chem. Commun.*, **2005**, 800–801; (c) Draper M, Saez IM, Cowling SJ. et al. *Adv. Funct. Mater.*, **2011**, 21, 1260–1278.
- [39] (a) Kumar M, Kumar S. *RSC Adv.*, **2015**, 5, 14871–14878; (b) Wojcik M, Lewandowski W, Matraszek J. et al. *Angew. Chem. Int. Ed.*, **2009**, 48, 5167–5169; (c) Wojcik M, Kolpaczynska M, Pocięcha D. et al. *Soft Matter.*, **2010**, 6, 5397–5400; (d) Zeng X, Liu F, Fowler AG. et al. *Adv. Mater.*, **2009**, 21, 1746–1750.

- [40] (a) Cseh L, Mehl GH. *J. Am. Chem. Soc.*, **2006**, 128, 13376–13377; (b) Cseh L, Mehl G. H. *J. Mater. Chem.*, **2007**, 17, 311–315; (c) Marx VM, Girgis H, Heiney PA, Hegmann T. *J. Mater. Chem.*, **2008**, 18, 2983–2994.
- [41] (a) Qi H, Hegmann T. *Liq. Cryst. Today.*, **2011**, 20, 102–114; (b) Vijayaraghavan D, Kumar S. *Mol. Cryst. Liq. Cryst.*, **2009**, 508, 101–114; (c) Mirzaei J, Reznikov M, Hegmann T. *J. Mater. Chem.*, **2012**, 22, 22350–22365.
- [42] (a) Huang Z, Huang L, Huang Y, He Y. et al. *Nanoscale.*, **2017**, 9, 15883–15894; (b) Hone DC, Walker PI, Evans-Gowing R. *Langmuir.*, **2002**, 18, 2985–2987; (c) de la Torre G, Claessens CG, Torres T. *Chem. Commun.*, **2007**, 2000–2015.
- [43] Nombona N, Maduray K, Antunes E, et al. *J. Photochem, Photobiology B: Biology.*, **2012**, 107, 35–44.
- [44] (a) Sutherland RL. *in Handbook of Nonlinear Optics*, Dekker, New York, 2nd ed. **1996**; (b) Philip R, Ravindra G, Kumar N, Sandhyarani, Pradeep T. *Phys. Rev. B.*, **2000**, 62, 13160–13166; (c) Claessens C, Blau W, Cook M. et al. *Monatshefte fuer Chemie.*, **2001**, 132, 3; (d) Sridharan K, Ollakkan MS, Philip R, Park T J. *Carbon.*, **2013**, 63, 263–273.

Chapter 6

6.1 Summary

In this chapter, we summarize some of the important results and conclusions obtained from this thesis work, which deals with **“Synthesis and Characterisation of Some Novel Banana and Discotic Liquid Crystals”**. Broadly, the research work that has been presented in this thesis can be classified as follows:

Chapter 1 is an introductory chapter and mainly deals with the classification of liquid crystals, discussion about bent-core mesogens and discotic liquid crystals. The molecular design of bent-core molecules and their mesophase structures have been addressed, there is also discussion about various mesophase structures of discotic molecules and the chemistry involved in synthesis of these molecules. The experimental techniques used for characterization of liquid crystalline properties have also been described. The potential applications of columnar mesophase formed by discotic molecules in organic electronics are discussed. This chapter also contains brief discussion about lyotropic liquid crystals. The following chapters elaborated the detail research work on bent-core liquid crystals, discotic liquid crystals and discotic nanocomposites.

Chapter 2 describes the synthesis of novel isoxazole based bent core liquid crystals derived from naturally occurring inexpensive curcumin as a starting precursor. The bent angle in these compounds is in between calamitic LCs and banana LCs. The liquid crystalline properties were investigated by POM and DSC. These derivatives exhibit enantiotropic mesophases. The detail mesophase structure of all the compounds were examined using an X-ray diffraction study, which reveals that the existence of nematic phase for lower homologous derivatives and smectic C phase for higher homologous along with nematic phase.

Chapter 3 presents the synthesis of some novel bent-core liquid crystals derived from EDOT central core and investigated their physical properties. Here, we adopted three different series of bent-core mesogens derived from EDOT. The first part of chapter deals with the synthesis of novel bent core mesogens via Sonagashira coupling reaction. EDOT containing the three ring compounds are not liquid crystalline, however by increasing side wing with phenyl group exhibit nematic phase over broad temperature. The bent angle of these molecules is around 152–155 °.

In the second part of this chapter, we focused on the synthesis and characterisation of novel Schiff base containing BC LCs derived from central EDOT core. The central EDOT connected between two phenyl rings via Schiff base does not show any liquid crystalline phase. Furthermore, to increase length: width ratio, we added one more phenyl ring on each side by ester linkage which gives five-membered BC LCs bearing Schiff base exhibiting wide range of mesophase. All the five membered Schiff base derivatives exhibit enantiotropic nematic phase for lower homologous and smectic C phase for longer chains along with nematic phase.

In the last part of this chapter, we presented the synthesis of some novel BC LCs and hockey-stick LCs and investigated their thermal, photophysical and nonlinear optical properties. All the compounds exhibit enantiotropic nematic phase for lower alkyl chains and smectic A phase for higher alkyl chains along with nematic phase. Both BC LCs and hockey stick mesogens exhibit good photophysical and nonlinear optical properties.

Chapter 4 describes the synthesis and characterisation of π -extended conjugation of phenazine fused triphenylene discotic liquid crystals in order to understand the structure mesophase relationship. Initial part of this chapter deals with novel extended triphenylene based phenazine heterocyclic DLCs containing alkanethiols and alkoxy chains. The intermediate dibrominated phenazine and final thiol substituted phenazine fused TP DLCs exhibit enantiotropic hexagonal columnar phase over broad temperature range. These phenazine derivatives exhibit good photophysical properties and charge carrier mobility.

Second part of this chapter deals with this synthesis, characterization of alkyl and alkoxy phenylacetylene containing phenazine fused extended triphenylene DLCs via Sonagashira coupling reaction. These extended mesogens exhibit wide range of enantiotropic hexagonal

columnar mesophase and retains liquid crystalline properties upto room temperature upon cooling from isotropic liquid. All the π -extended heteroaromatic triphenylene discotic mesogens enhance photophysical and nonlinear optical properties.

The third part of this chapter implies the synthesis, mesomorphic and optical properties of monomeric acid and corresponding ester derivatives of phenazine fused TP DLCs. POM and DSC analysis show that the monomeric acid and ester derivatives exhibit enantiotropic mesophase. X-ray investigation of intermediate acid derivative exhibit a rectangular columnar phase over broad temperature range, while all the monomeric ester derivatives exhibit hexagonal columnar phase which remains stable till room temperature upon cooling from the isotropic phase. Further gelation properties and rheological properties are in progress.

The last part of this chapter presents the synthesis and mesomorphic properties of dibenzophenazine based DLCs containing alkylthiol, symmetrical and unsymmetrical 4-alkoxy phenylacetylene derivatives. All the intermediate and final compounds exhibit hexagonal columnar phase over broad temperature and good photophysical properties in chloroform solvent.

Chapter 5 describes the incorporation of silver and gold nanoparticles in the supramolecular order of metal free phthalocyanine DLC. This was studied by POM, DSC, X-ray diffraction, FE-SEM and TEM. The doping of nanoparticles into hexagonal columnar phase of phthalocyanine DLC does not disturb the nature of mesophase with different concentration variations; except for a minor shift in the transition temperature is observed. These hybrid nanocomposite materials make themselves a potential candidate for devices like thin film transistors, LED's, and organic solar cells etc.

As final conclusions, it may be stated that the thesis deals with the synthesis and characterization of some novel bent core and discotic mesogenic materials using traditional as well as modern synthetic methods. We have also shown the metal nanoparticles dispersion into hexagonal columnar phase of discotic mesogens. These materials are extremely important for optoelectronics and photonics applications.

Some of the findings of this thesis have been published/communicated in the following international journals.

1. Synthesis and characterisation of novel isoxazole based banana liquid crystals from naturally occurring curcumin.
A. Gowda, A. Roy and S. Kumar. *Liq. Cryst.*, **2016**, 43, 175–182.
2. Self-Assembly of Silver and Gold Nanoparticles in a Metal-Free Phthalocyanine Liquid Crystalline Matrix: Structural, Thermal, Electrical and Nonlinear Optical Characterization.
A. Gowda, M. Kumar, A. R. Thomas, R. Philip and S. Kumar. *ChemistrySelect.*, **2016**, 1, 1361–1370.
3. Ethylenedioxythiophene as a novel central unit for bent-core liquid crystals.
A. Gowda and S. Kumar. *Liq. Cryst.*, **2016**, 43, 1721–1731.
4. Synthesis and mesomorphic properties of novel Schiff base liquid crystalline EDOT derivatives.
A. Gowda, A. Roy and S. Kumar. *J. Mol. Liq.*, **2016**, 225, 840–847.
5. Thermal and nonlinear optical studies of newly synthesized EDOT based bent-core and hockey-stick like liquid crystals.
A. Gowda, L. Jacob, N. Joy, R. Philip, Prathiba R and S. Kumar. *New J. Chem.*, **2018**, 42, 2047–2057.
6. Charge Transport in Novel Phenazine Fused Triphenylene Supramolecular Systems.
A. Gowda, L. Jacob, D. P. Singh, R. Douali, and S. Kumar. *ChemistrySelect.*, **2018**, 3, 6551–6560.
7. Synthesis, mesomorphic properties and nonlinear optical studies of alkyl and alkoxy phenylacetylene containing phenazine fused extended triphenylene discotic liquid crystal dyes.
A. Gowda, L. Jacob, A. Patra, A. George, R. Philip and S. Kumar. *Dyes and Pigment.*, **2019**, 160, 128–135.
8. Novel Phenazine Fused Triphenylene Discotic Liquid Crystals: Synthesis, Characterisation, Thermal, Optical and Nonlinear Optical Properties.
A. Gowda, L. Jacob, N. Joy, R. Philip and S. Kumar. *New J. Chem.*, **2018**. Accepted.
9. Dibenzophenazines based discotic liquid crystals: Synthesis, thermal and optical properties.

A. Gowda[†], L. Jacob[†] and Sandeep Kumar. (Manuscript under preparation, [†] Joint authors)

Article/review articles which are not included in this thesis:

10. The chemistry of bent-core molecules forming nematic liquid crystals
S. Kumar and **A. Gowda**. *Liq. Cryst. Rev.*, **2015**, 3, 99–145.
11. Discotic Liquid Crystals with Graphene: Supramolecular Self-assembly to Applications.
M. Kumar, **A. Gowda**, S. Kumar. *Part. Part. Syst. Charact.*, **2017**, 1700003.
12. Discotic liquid crystals derived from polycyclic aromatic cores: from the smallest benzene to the utmost graphene cores.
A. Gowda, M. Kumar, S. Kumar. *Liq. Cryst.*, **2017**, 44, 1990–2017.
13. Soft discotic matrix with 0-D silver nanoparticles: Impact on molecular ordering and conductivity.
S. Varshney, M. Kumar, **A. Gowda** and S. Kumar. *J. Mol. Liq.*, **2017**, 238, 290–295.
14. Silver nanodisks in soft discotic forest: Impact on self-assembly, conductivity and molecular packing.
M. Kumar, S. Varshney, **A. Gowda** and S. Kumar. *J. Mol. Liq.*, **2017**, 241, 666–674.
15. Trapping of inorganic nanowires in supramolecular organic nanoribbons.
A. B. Shivanandareddy, M. Kumar, **A. Gowda** & S Kumar. *J. Mol. Liq.*, **2017**, 244, 1–6.
16. Rapid Formation and Macroscopic Self-Assembly of Liquid-Crystalline, High-Mobility, Semiconducting Thienothiophene.
M. Pandey, **A. Gowda**, S. Nagamatsu, S. Kumar, W. Takashima, S. Hayase, and S. S. Pandey. *Adv. Mater. Interfaces.*, **2018**, 5, 1700875.
17. Recent Advances in Discotic Liquid Crystal-Assisted Nanoparticles.
A. Gowda and Sandeep Kumar. *Materials.*, **2018**, 11, 382.
18. Laser Beam Deflection Study of Diffusion in Bovine Serum Albumin and Green Synthesised Gold Nano-Particle-Conjugate.
N. P. Dhanya, **A. Gowda**, P. K. Bindu Sharmila, A. S. Shanu, and P. R. Sasikumar. *J. Bionanosci.*, **2018**, DOI: 10.1166/jbns.2018.1582. Accepted.